REGULATION OF SUBSTRATE METABOLISM AND RENIN-ANGIOTENSIN SYSTEM WITH DIETARY AND PHARMACOLOGICAL INTERVENTIONS: IMPLICATIONS FOR OBESITY AND RELATED DISORDERS

DANIEL PEREIRA DA EIRA

A DISSERTATION SUBMITTED TO THE FACULTY OF GRADUATE STUDIES IN PARTIAL FULFILLMENT OF THE REQUIREMENTS FOR THE DEGREE OF

DOCTOR OF PHILOSOPHY

GRADUATE PROGRAM IN KINESIOLOGY AND HEALTH SCIENCE

YORK UNIVERSITY

TORONTO, ONTARIO

MARCH 2024

Abstract

This dissertation investigates the effects of the ketogenic diet (KD) on adipose tissue (AT) metabolism and renin-angiotensin system (RAS) function and potential implications for other tissues, including lung, heart and skeletal muscle. In the first study, it was demonstrated that despite increasing fat mass, a KD enhanced energy-dissipating mechanisms in white AT (WAT) and brown AT (BAT) by upregulating the machinery for triacylglycerol recycling in white adipocytes and uncoupled fatty acid (FA) oxidation and UCP1 protein levels in the BAT. These effects could potentially be attributed to the shift to the counterregulatory RAS arm in WAT observed in study 2, which has been shown to produce beneficial metabolic effects. In study 3, the effect of the KD on RAS components was investigated in the context of the lung and heart, where an obesity-induced elevation in pulmonary inflammation could underlie an increase in angiotensin converting enzyme 2 (ACE2), the receptor for SARS-CoV-2 cellular infection. We observed that the obesogenic, high-fat sucrose-enriched (HFS) diet elevated the pulmonary content of this receptor, whereas the KD did not alter ACE2 levels. Moreover, the KD significantly suppressed inflammation, relative to the HFS group, in the lung. Because AT releases energy substrate for utilization in peripheral tissues, the KD also affects substrate preference and metabolism in skeletal muscle. To our knowledge, little has been done with respect the metabolic effects of a KD on muscles with distinct fiber-type compositions. Therefore, we assessed the effects of the KD on glucose, fat, and ketone metabolism in skeletal muscles. We observed that the KD increased fat oxidation and ketolytic capacity, when compared to the HFS group, in a fiber-type specific manner. However, irrespective of oxidative capacity, the KD preserved insulin-stimulated glucose metabolism, whereas the HFS diet suppressed this parameter. In our final study, we used a pharmacological intervention (the adiponectin mimetic ALY688) to alter AT glucose and fat

metabolism. Despite not altering glucose uptake in Epid or Sc Ing adipocytes, ALY688 significantly enhanced glucose oxidation. Together, these projects explore dietary and pharmacological interventions that alter the metabolic and endocrine roles of AT and investigate non-adipose tissues under KD conditions.

Acknowledgements

Dr. Rolando Ceddia: I would like to thank you for your relentless mentorship, your direct and honest approach, your friendship and for your support in every aspect of my journey. It has now been six years since I began working in your lab, and my development, both academic and personal, have been inspired by your passion, dedication, and personality. You have left a lasting impact on me, and I am truly grateful for having had the opportunity to learn from you. I take with me many valuable lessons that extend beyond the bench and that I can apply to my own life. Thank you also for reminding us that the work we do at the bench is something that we can apply in our day-to-day to improve our health and overall well-being.

Labmates: Shailee, Mateja, Aris, Diane, Isabel, Glen and Ish, thank you for sharing the good and less positive moments that science and research put us through. Your help throughout the various, tiring days of experiments is something that I will forever appreciate and cherish. Shailee, you were the best lab-partner. Thank you for putting up with my personality and for being a great friend.

Family: To my wife, you were with me throughout my entire graduate education. You listened when I had frustrations to vent, and you shared my successes with me. Even though you didn't understand any of the content in my presentations, you sat through them and nodded so that I could practice in front of someone. Thank you for your unconditional love and support. Without you, this process would have been significantly more difficult. Rosie, you were born about a year and a half before I completed my PhD. Despite taking away some hours of sleep, you brought me a joy that propelled me to the finish line, even through the most difficult of moments. I hope that, if you read dad's dissertation someday, you see this, and know how big of a role you played in helping me. Mom and dad, you shaped me into the man I am today. You came from nothing and gave me everything. I will never be able to repay you. Thank you.

Deus: Thank you for giving me strength and courage to overcome the obstacles in my life. Deia-me saude para ver os frutos do meu trabalho e para poder ver os meus filhos crescer.

Table of Contents

Table of Figures

Table of Tables

List of Abbreviations

aBAT	Aortic brown adipose tissue
ACAT1	Acetyl-CoA acetyltransferase 1
ACC	Acetyl-CoA carboxylase
ACE1	Angiotensin converting enzyme 1
ACE2	Angiotensin converting enzyme 2
AD	Alzheimer's disease
ADIPOAI	Anti-inflammation adiponectin
AdipoR1/R2	Adiponectin receptor 1/2
ADP	Adenosine diphosphate
Agt	Angiotensinogen
AMP	Adenosine monophosphate
AMPK	AMP-activated protein kinase
Ang-I/II	Angiotensin-I/II
aP2	Adipocyte P2
AR	AdipoRon
AT_1R	Angiotensin-II, type 1 receptor
AT_2R	Angiotensin-II, type 2 receptor
AT	Adipose tissue
ATGL	Adipose triglyceride lipase
ATP	Adenosine triphosphate
β3AdR	β3-adrenergic receptor
BAT	Brown adipose tissue
BDH1	βHB dehydrogenase 1
BHB/βHB	β-hydroxybutyrate
BMDM	Bone marrow-derived macrophages
BMI	Body mass index
BW	Body weight

CREB	cAMP response element-binding protein
CACT	Carnitine acylcarnitine translocase
C/EBP	CCAAT/enhancer-binding protein
CGI-58	Comparative gene identification-58
CLS	Crown-like structures
CPT	Carnitine palmitoyltransferase
Cr	Creatine
DAG	Diacylglycerol
DIO	Diet-induced obesity
DIT	Diet-induced thermogenesis
DNL	De novo lipogenesis
EDL	Extensor digitorum longus
Epid	Epididymal
Epit	Epitrochlearis
ETC	Electron transport chain
F-1,6-BP	Fructose-1,6-biphosphate
FA/FFA	Fatty acid/free fatty acid
FAT/CD36	Fatty acid transporter/cluster differentiation 36
FDG	Fluorodeoxyglucose
G3P	Glycerol-3-phosphate
G6P	Glucose-6-phosphate
GAPDH	Glyceraldehyde-3-phosphate dehydrogenase
GLUT4	Glucose transporter 4
GS	Glycogen synthase
GSK	Glycogen synthase kinase
GyK	Glycerol kinase
HbA1C	Glycated hemoglobin
HDL	High-density lipoprotein

HF/HFD	High-fat/high-fat diet
HFHS	High-fat, high sugar
HFS	High-fat, sucrose-enriched
HMGCL	HMG-CoA Lyase
HMGCS2	3-hydroxy-3-methylglutaryl-CoA synthase 2
HOMA-IR	Homeostatic model assessment-insulin resistance
HSL	Hormone sensitive lipase
iBAT	interscapular BAT
IL6/IL-1β	Interleukin-6/1β
ILC	Innate lymphoid cells
IRS	Insulin receptor substrate
Iso	Isoproterenol
IVGTT	Intravenous glucose tolerance test
KD	Ketogenic diet
KE	Ketone esters
KRBH	Krebs-Ringer bicarbonate HEPES buffer
JAK2	Janus kinase 2
kDa	kiloDaltons
LD	Lipid droplet
LepR	Leptin receptor
LPL	Lipoprotein lipase
LPS	Lipopolysaccharide
MAG	Monoacylglycerol
MAGL	Monoacylglycerol lipase
MAPK	Mitogen-activated protein kinase
MasR	Mas receptor
MCP-1	Monocyte chemotactic protein-1
MPC	Mitochondrial pyruvate carrier

MtDNA	Mitochondrial DNA
mTORC1	Mammalian target of rapamycin complex 1
$NADH_2$	Nicotinaminde adenine dinucleotide
NAFLD	Non-alcoholic fatty liver disease
NE	Norepinephrine
NEFA	Non-esterified fatty acid
Nox2	NADPH oxidase 2
NRF1	Nuclear respiratory factor 1
OLETF	Otsuka Long-Evans Tokushima Fatty
Oligo	Oligomycin
OXCT/OXCT1	3-oxoacid-CoA transferase 1
PCK	Phosphoenolpyruvate carboxykinase
PET	Positron emission tomography
PDH	Pyruvate dehydrogenase
PDHK4	Pyruvate dehydrogenase kinase 4
PDK1	Phosphoinositide-dependent kinase-1
PGC-1α	Peroxisome proliferator-activated receptor gamma co-activator 1a
PI3K	Phosphatidylinositol 3-kinase
PIP_2	Phosphatidylinositol diphosphate
PIP_3	Phosphatidylinositol triphosphate
PKA/C	Protein kinase A/C
PMF	Proton motive force
PPAR	Peroxisome proliferator-activated receptor
PRDM16	Pr-domain-containing protein 16
RAAS	Renin-angiotensin aldosterone system
RAS	Renin-angiotensin system
RNA	Ribonucleic acid
ROS	Reactive oxygen species

SARS	Severe acute respiratory syndrome
SC	Standard chow
Sc Ing	Subcutaneous inguinal
SNS	Sympathetic nervous system
SOCS3	Suppressor of cytokine signaling 3
Sol	Soleus
STAT3	Signal-transducer-and-activator-of-transcription 3
T2D	Type 2 Diabetes
TAG	Triacylglycerol
TCA	Tricarboxylic acid
TFAM	Mitochondrial transcription factor A
TH	Tyrosine hydroxylase
TMPRSS2	Transmembrane protease serine 2
TNFα	Tumour necrosis factor-α
UCP1	Uncoupling protein-1
Vc	Visceral
WAT	White adipose tissue

Chapter 1: Introduction

Obesity is a global issue, with increasing rates in developed and developing nations[1]. In the United States and Canada, specifically, obesity has risen significantly over the past decade, reaching over 40 and 27% of adults, respectively[2,3]. The onset of obesity has classically been attributed to positive energy balance, which is driven by inadequate physical activity and the overconsumption of energy-dense foods[4]. The result of these lifestyle behaviours is the expansion of adipose tissue (AT) mass that is characteristic of the obese phenotype[5]. However, it has become increasingly apparent that obesity-related metabolic disorders, including insulin resistance, are not just triggered by the volume of the AT[5]. Instead, it appears that adipocyte dysfunction is a crucial determinant for metabolic dysregulation and the development of systemic insulin resistance[5].

AT is classically recognized for its energy-storing properties[6]. However, the types of adipose tissue, their metabolic plasticities[4,7] and their endocrine capabilities highlight the robust physiological importance of this organ that extends beyond substrate storage and mobilization[4]. AT function is largely implicated by the type of AT, the depot and the conditions the AT is placed under[7–9]. In fact, two main forms of AT exist; white and brown (WAT and BAT)[6]. Each has its own distinct function and displays a plasticity to convert, to some extent, to the other[4,6]. Regardless, the preservation of WAT and BAT function appears to be crucial for the prevention of disease at the tissue and whole-body level[5,8]. In fact, the expansion of AT beyond its capacity to grow underlies impairment in its function[5], and is accompanied by inflammation[10] and ectopic lipid accumulation[11,12]. This leads to dysfunctional metabolic alterations in liver and skeletal muscle[11,12] and may contribute to the development of insulin resistance and Type 2 diabetes (T2D)[5]. In this context, researchers have attempted to identify interventions to preserve, and

potentially enhance AT function to prevent metabolic dysregulation and maintain proper whole-body glycaemic control.

One diet that has been proposed for its effectiveness in weight loss, compliance and induction of beneficial health outcomes has been the low-carbohydrate, high-fat ketogenic diet (KD)[13,14]. The consumption of a diet with an elevated fat content is controversial, particularly due to the general conception that it could cause dyslipidemia[14]. However, the KD has been consistently shown to improve blood lipid profile, as well as improve glycaemia and cause weight loss in obese subjects[14,15]. These effects highlight the importance and potential of this diet in reversing metabolic disorders and serving as a therapeutic intervention for obesity and T2D[14,15]. However, the impact of this diet on metabolic adaptations and the endocrine role of the AT is poorly understood. In this context, the focus of this dissertation was to investigate the effects of dietary interventions on glucose and fat metabolism in distinct adipose tissue depots, and the influence of dietary intervention on AT endocrine function. In addition to a dietary approach, this dissertation also contains studies regarding the effects of an adiponectin mimetic on AT metabolism. Adiponectin is an adipose-derived hormone that exerts beneficial metabolic effects in several tissues and has been proposed as a target for the management of obesity and T2D[16,17]. Moreover, FA released from AT are oxidized by numerous tissues, including skeletal muscles[4,18], prompting our investigation into the effects of dietary intervention on substrate metabolism in muscles with distinct fiber-type compositions. Collectively, these works will further our understanding of dietary and pharmacological interventions designed to manipulate AT metabolism. The main goal is to prevent obesity-induced dysfunctional alterations in adipose and non-adipose tissues and improve whole-body glycaemic control.

Chapter 2: Literature Review

2.1. Adipose Tissue (AT)

Two main forms of AT exist, white and brown (WAT and BAT, respectively)[4,6,7]. These distinct types of fat exhibit unique physiological roles; WAT stores and releases energy in response to varying stimuli, whereas BAT burns energy[19]. Moreover, several different depots of WAT and BAT exist in the body, varying slightly in their function and adaptive responses to different stimuli[7,20]. To better understand these differences, this dissertation will first review the structure and physiology of distinct AT depots and will summarize some key findings with respect to metabolic plasticity in these tissues.

2.1.1. Structure of White Adipose Tissue (WAT)

WAT is generally classified based on its localization in the body[19]. There are two main depots: visceral and subcutaneous (Sc) WAT, where the former is stored around organs and the latter is stored superficially, beneath the skin[19]. In humans, the Sc WAT depot makes up the majority of the total body fat[4] and is distributed widely across several anatomical regions (Figure 1), including the chest, axillary and gluteo-femoral regions[21,22], as well as in the lower trunk. Conversely, in rodents, Sc WAT contributes relatively less to the total WAT mass and is mainly localized in the inguinal, axillary, interscapular, cervical and subscapular regions[6]. Visceral fat is similarly distributed in humans and rodents, localized mainly to the omental, mesenteric, perirenal and gonadal regions[22]. However, visceral adipose tissue also exists surrounding major arteries in the trunk[6].

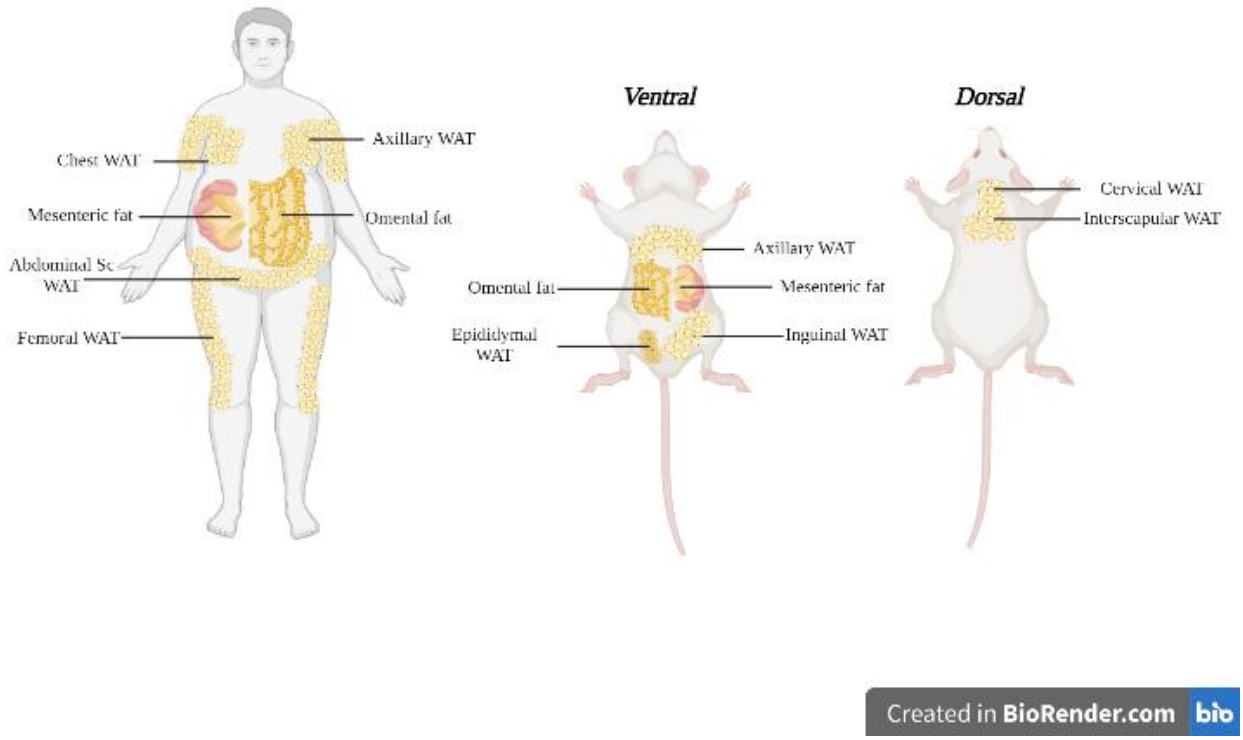

Figure 1: Subcutaneous white adipose tissue (Sc WAT) is widely distributed in the human, not specific to select anatomical regions. Conversely, in the rodent, Sc WAT is mainly found in the inguinal, interscapular and subscapular regions.

WAT is composed of a number of cells, including fibroblasts, vascular cells, and immune cells, as well as collagen, which contributes to the extracellular matrix[6]. However, the WAT cell, or white adipocyte, occupies the majority of the tissue's volume[23]. White adipocytes are derived from myogenic factor 5-negative precursor cells[24]. Differentiation of preadipocytes to mature adipocytes, or adipogenesis, is primarily mediated by peroxisome proliferator-activated receptors (PPARs), particularly PPARγ, which is the predominant PPAR in AT[25], as well as CCAAT/enhancer-binding protein (C/EBP)[25,26]. The PPARγ2 isoform has been extensively studied and shown to be highly expressed in differentiating adipocytes[25]. Remarkably, the induced expression of PPARγ in 3T3-NIH fibroblasts incubated with a PPAR-inducing agent upregulated the appearance of lipid-containing cells that were similar to adipocytes[25]. It also enhanced the expression of other adipogenic genes, including adipocyte P2 (aP2), lipoprotein lipase (LPL) and

PPARγ[25]. These effects were not observed in PPARα-expressing NIH 3T3 cells, reinforcing the importance of PPARγ for adipocytic differentiation[25].

Adipogenesis is one possible underlying mechanism for AT expansion, the other being hypertrophy[27]. Adipocyte hypertrophy most commonly explains the growth in fat mass in adults, and is linked to obesity-induced metabolic disorders[27]. Adipocyte growth is driven by the accumulation of fat in the lipid droplet (LD)[27] that composes ~90% of its intracellular volume[6]. This confers a spherical and unilocular appearance to the adipocyte[4,19]. Consequently, other intracellular components, including the nucleus and mitochondria are displaced to the periphery of the cell[4,6]. White adipocyte mitochondria are elongated in shape and contain randomly-oriented cristae[4]. The relatively low abundance of mitochondria in WAT underlies its inherently low oxidative capacity[4]. Instead, WAT is classically recognized as an energy reservoir[6], where it stores energy under post-prandial conditions and releases this energy under conditions of energy-demand[4].

2.1.2. Lipid Synthesis in Adipocytes

Lipid storage in adipocytes is largely regulated by insulin[28,29]. Upon binding to its receptor, insulin triggers the translocation of glucose transporter 4 (GLUT4) to the adipocyte's plasma membrane[30]. Briefly, this begins with the activation of receptor-associated tyrosine kinase, that autophosphorylates the receptor as well as its receptor substrates (insulin receptor substrate; IRS)[31]. Subsequently, phosphatidylinositol 3-kinase (PI3K) is activated to form phosphatidylinositol triphosphate (PIP_3) from phosphatidylinositol diphosphate (PIP_2)[31]. PIP_3 consequently recruits phosphoinositide-dependent kinase-1 (PDK1), which phosphorylates and activates Akt[31,32]. In turn, Akt phosphorylates AS160, which prompts the translocation of the intracellular GLUT4 vesicle to the plasma membrane[31,32]. This supports an influx of glucose into

the cell, whereby it can be processed, via glycolysis, into glycerol-3-phosphate (G3P), which serves as the backbone for triacylglycerol (TAG) synthesis[29,30]. In fact, almost half of the glucose that is imported into the cell under insulin-stimulated conditions is diverted to TAG synthesis[30] (Figure 1). G3P can also be derived from free glycerol that is phosphorylated by glycerol kinase (GyK)[7,33]. However, the content and activity of this enzyme is relatively low in WAT[7,33–35]. Conversely, the formation of new glycerol, or glyceroneogenesis, mediated by the enzyme phosphoenolpyruvate carboxykinase (PCK), may also provide G3P for fatty acid (FA) esterification[7].

The supply of FA for TAG synthesis is also promoted by insulin[28]. In fact, insulin stimulation enhances the expression and activity of LPL, a crucial enzyme for the hydrolysis of lipoprotein derived TAG[28]. These TAG are broken down into their glycerol backbone and free FAs (FFAs)[28]. Subsequently, the FFAs are imported into the cell via fatty acid transporter (FAT/CD36) and esterified to the glycerol backbone[29]. Moreover, the synthesis of new FAs, also known as de novo lipogenesis (DNL) also contributes to this FA pool[30]. Specifically, the influx of carbohydrate into the cell increases the expression of genes that upregulate DNL[30]. In adipocytes, this is mainly mediated by carbohydrate response element binding protein (CREBP)[30]. Thus, insulin supports lipid synthesis by increasing fat storage in adipocytes[28,30]. However, this insulin-mediated lipogenic effect is further propagated by insulin's suppression on TAG breakdown, also known as lipolysis[36].

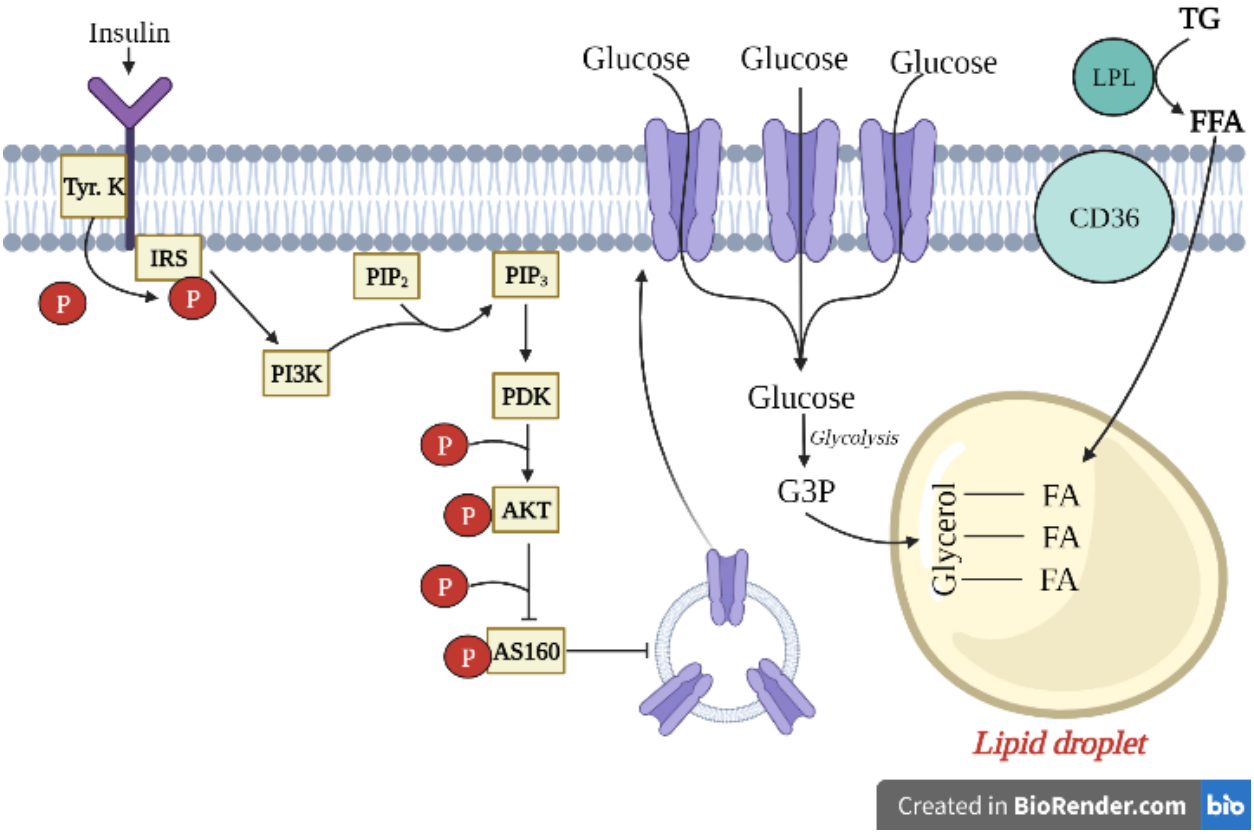

Figure 2: Schematic illustration of insulin-stimulated TAG synthesis. Insulin binds to its receptor, inducing autophosphorylation and the subsequent phosphorylation of insulin receptor substrates (IRS) by tyrosine kinase (Tyr. K). Subsequently, phosphatidylinositol 3-kinase is activated and phosphorylates phosphatidylinositol diphosphate (PIP_2) to phosphatidylinositol triphosphate (PIP_3). PIP_3 then activates phosphoinositide-dependent kinase-1 (PDK1) to phosphorylate AKT. The phosphorylation of AKT activates it, allowing it to phosphorylate and inhibit the action of AS160. This promotes GLUT4 vesicle translocation to the membrane, allowing glucose uptake to take place. This glucose is converted, through glycolysis, to glycerol-3-phosphate (G3P), which serves as the backbone for fatty acid (FA) esterification and triglyceride (TG) synthesis. FAs are imported into the cell by lipoprotein lipase (LPL)-mediated hydrolysis of circulating TG and FA transporter (CD36).

2.1.3. Lipolysis in Adipocytes

Unlike lipogenesis, lipolysis is the breakdown of the TAG molecule to glycerol and unesterified FA[28]. The release of these substrates occurs under conditions of energy demand and provides an energy source for other tissues[4]. Lipolysis is stimulated by catecholamines[28,37], namely norepinephrine (NE)[38]. Binding of catecholamines to the β3-adrenergic receptor (β3Adr), the most abundant of the β-adrenergic receptor isoforms in rodents[39], triggers a signaling cascade that

begins with the activation of adenylyl cyclase by a G-protein coupled receptor[37]. Subsequently, adenylyl cyclase increases the formation of cAMP, which, in turn, activates protein kinase A (PKA)[28,37]. PKA then phosphorylates LD-surrounding perilipin[28,40], which suppresses perilipin's protective function on the LD, exposing it to lipolytic enzymes[40,41]. Upon phosphorylation, perilipin also releases comparative gene identification-58 (CGI-58)[28]. CGI-58 binds to and activates adipose triglyceride lipase (ATGL), an enzyme that initiates TAG hydrolysis and gives rise to diacylglycerol (DAG)[28] and a single unesterified FA[7,40]. DAG is then broken down into monoacylglycerol (MAG) by hormone sensitive lipase (HSL), which is also activated by PKA phosphorylation[28]. HSL-mediated hydrolysis is highly dependent on perilipin-mediated translocation to the LD, where deficiency of perilipin significantly inhibits catecholamine-induced lipolysis[41]. The final hydrolysis step is catalyzed by MAG lipase (MAGL), releasing the remaining FA and the glycerol molecule[28] (Figure 3).

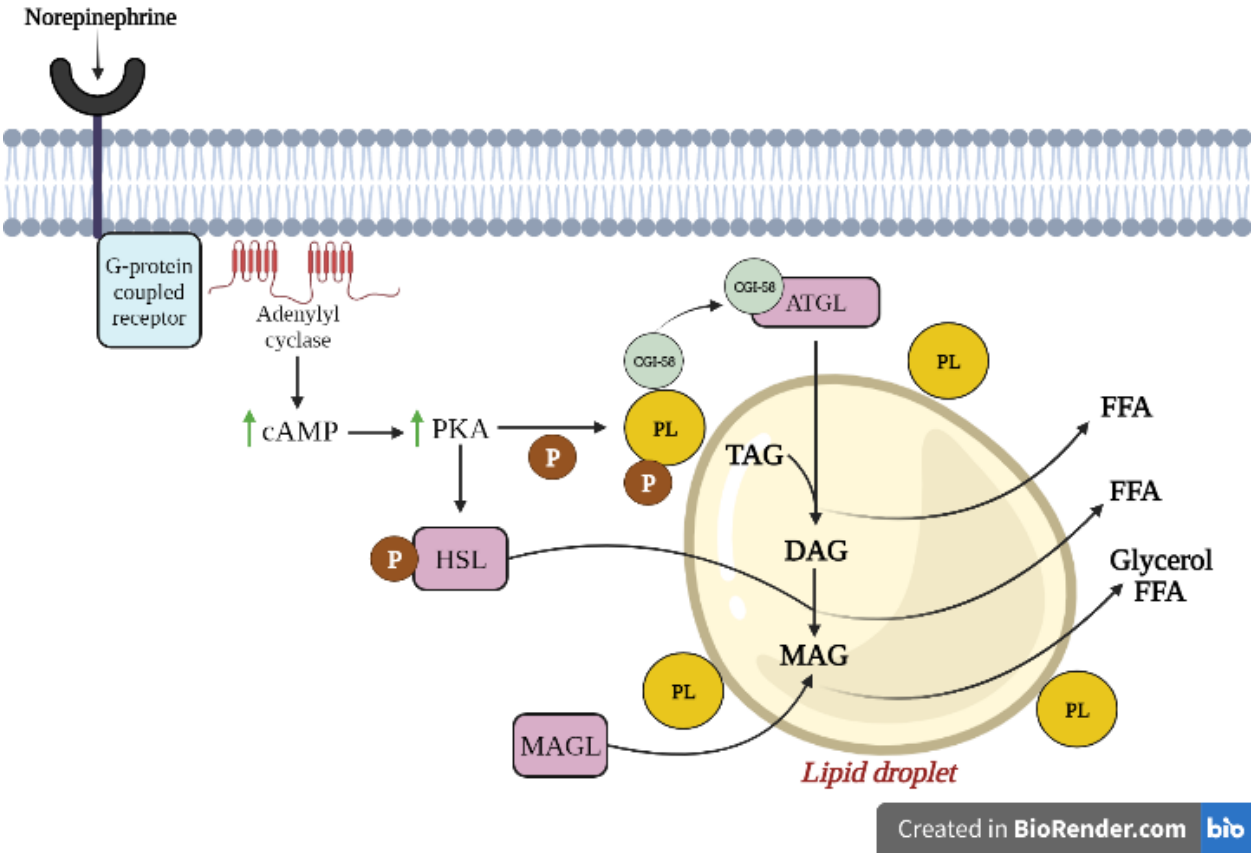

Figure 3: Schematic illustration of lipolytic signaling cascade. Binding of catecholamines to the β3-adrenergic receptor (β3Adr), triggers a signaling cascade that begins with the activation of adenylyl cyclase by a G-protein coupled receptor[37]. Subsequently, adenylyl cyclase increases the formation of cAMP, which, in turn, activates protein kinase A (PKA). PKA then phosphorylates lipid droplet (LD)-surrounding perilipin, which exposes the LD to lipolytic enzymes. Upon phosphorylation, perilipin also releases comparative gene identification-58 (CGI-58), which binds to and activates adipose triglyceride lipase (ATGL), the enzyme that initiates TAG hydrolysis and gives rise to diacylglycerol (DAG)[28], and a single unesterified FA[7,40]. DAG is then broken down into monoacylglycerol (MAG) by hormone sensitive lipase (HSL), which is also activated by PKA phosphorylation. The final hydrolysis step is catalyzed by MAG lipase (MAGL), whereby MAG is broken down into a remaining FA and glycerol molecule.

This lipolytic signaling cascade is inhibited by insulin, consequently favouring TAG synthesis over hydrolysis[28]. Specifically, insulin inhibits several components of the lipolytic signaling pathway to suppress TAG breakdown. For instance, activated AKT (pAKT) phosphorylates phosphodiesterase, which decreases cAMP and its ability to activate PKA[28]. Moreover, mammalian target of rapamycin complex (mTORC1), a factor that is activated with insulin stimulation, significantly suppresses ATGL expression[28]. Insulin signaling also inhibits

adenylyl cyclase[28]. Thus, insulin plays a prominent role in TAG synthesis by promoting lipogenesis and inhibiting lipolysis[28].

The intact regulation of lipolysis and lipogenesis are crucial WAT-mediated functions that become compromised under conditions of obesity[30,42]. In terms of lipolytic function, chronic HF-feeding increases basal lipolysis, but blunts the lipolytic response to catecholamines in visceral and subcutaneous adipocytes[43]. Additionally, insulin-stimulated FA import into the adipocyte, as well as lipogenesis are also significantly suppressed under conditions of DIO[43]. The underlying physiopathology for adipocyte dysfunction has been suggested to be the expansion in fat mass (adipocyte hypertrophy), as mentioned earlier in the review. Adipocytes possess an inherent ability to undergo hypertrophy under conditions of energy excess[27]. However, when the capacity of the adipocyte to grow is exceeded by chronic overfeeding, mechanical stress to the cell membrane and hypoxia take place and induce inflammation in the AT[5]. Inflammation, specifically, is one mechanism whereby adipocytes can become insulin resistance[5,44]. In this context, the expansion of fat mass by increasing adipocyte number, rather than cell size, is of interest for the mitigation of diet-induced AT dysfunction[27]. In line with this, attenuated PPARγ transcriptional activity has been demonstrated to exacerbate high-fat diet (HFD)- induced hypertrophy in white adipocytes, leading to an increase in circulating TAG and an enhancement in hepatic lipid storage[45]. Conversely, the application of a PPARγ-activating drug, such as thiazolidinediones, significantly reduces adipocyte size, and improves fasting glucose and TAG levels in the circulation[45]. Together, these findings point to an apparent link between adipocyte hypertrophy and dysfunction and support the notion that functional AT, rather than AT mass, is a critical determinant of whole-body metabolic health[5]. In addition to WAT, BAT also contributes to metabolic function and energy expenditure[46,47].

2.2. BAT and Uncoupled Oxidation

BAT differs from WAT in several morphological and functional features[4,7]. First, brown adipocytes are multilocular, rather than unilocular, in appearance and have a relatively higher abundance of mitochondria[19]. Additionally, brown adipocytes are highly vascularized and innervated[6]. In rodents, BAT is present mainly in the interscapular, aortic, perirenal regions, among others[38] (Figure 6). Functionally, BAT differs from WAT in that it is not naturally a storage-centric depot[4,7,8]. Rather, brown adipocytes burn energy and release it as heat[8,38]. This process is known as thermogenesis and it is driven by the elevated content of uncoupling protein-1 (UCP1) in BAT[38]. UCP1 uncouples substrate oxidation from adenosine triphosphate (ATP) synthesis[7,38]. This is achieved by UCP1-mediated proton leak and the dissipation of proton motive force (PMF) in the inter-mitochondrial membrane[48].

2.2.1. FA Oxidation and Oxidative Phosphorylation

Under normal conditions, FAs are brought into the mitochondria via the carnitine palmitoyltransferase (CPT) proteins[49]. Briefly, CPT1 replaces the coenzyme A (CoA) that is bound to the FA with L-carnitine[49]. Subsequently, carnitine acylcarnitine translocase (CACT) imports the acyl-carnitine into the mitochondrial matrix while simultaneously exporting carnitine[49]. The final step is catalyzed by CPTII, which exchanges the carnitine esterified to the FA with a CoA molecule, to regenerate acyl-CoA[49].

Once in the mitochondrial matrix, acyl-CoA is subjected to β-oxidation, which is the sequential cleavage of the long chain FA into two-carbon units (acetyl-CoA) and a progressively shorter FA chain[49]. The formation of acetyl-CoA from acyl-CoA involves the step-wise action of four enzymes: Acyl-CoA dehydrogenase, Enoyl-CoA hydratase, 3-L-hydroxyacyl-CoA and β-ketothiolase[49]. Acetyl-CoA enters the Krebs cycle and is combined with oxaloacetate to form citric

acid[50]. This reaction is catalyzed by citrate synthetase[50]. Aconitase converts citrate to cis-aconitate, then isocitrate[50]. Following this, α-ketoglutarate is formed from isocitrate via the enzyme isocitrate dehydrogenase, causing the release of a CO_2 molecule and nicotinaminde adenine dinucleotide ($NADH_2$)[50]. α-ketoglutarate is, in turn, decarboxylated by α-ketoglutarate dehydrogenase to form succinyl CoA[50,51], which is then converted to succinate by succinic thiokinase[50]. This reaction produces GTP from GDP[50]. The conversion of succinate to fumaric acid is catalyzed by succinate dehydrogenase and produces $FADH_2$[50]. From this point, fumaric acid is converted to malate, and then malate to oxaloacetate by fumarase and malate dehydrogenase, respectively[50]. The latter step forms an additional $NADH_2$ and an oxaloacetate that can recommence the Krebs Cycle with another acetyl-CoA[50].

The $NADH_2$ and $FADH_2$ produced in the Krebs cycle then donate electrons to the electron transport chain to drive oxidative phosphorylation[52]. This begins with $NADH_2$ and $FADH_2$ donating electrons to electron transport chain (ETC) complexes 1 and 2, respectively[52]. These electrons are sequentially transported to ubiquinone, Complex III, cytochrome C and Complex IV[52]. Electron transport ends with the transfer of electrons from Complex IV to O_2, forming H_2O. At complexes I, III and IV, electron transport is accompanied by the pumping of protons into the space between the outer and inner mitochondrial membranes, known as the intermembrane space[52]. The accumulation of protons in the intermembrane space generates a PMF that is dissipated through ATP Synthase (Complex V)[52]. Proton re-entry through Complex V into the mitochondrial matrix drives ATP synthesis, whereby adenosine diphosphate (ADP) is phosphorylated to form ATP[52] (Figure 4).

2.2.2. Glycolysis and Glucose Oxidation

Similar to FAs, glucose is processed in the Krebs cycle to generate intermediates for the ETC and, ultimately, ATP synthesis[53]. Upon entry into the cell, glucose is phosphorylated by hexokinase to form glucose-6-phospate (G6P), consuming ATP in the process[53,54]. Glucose phosphate isomerase then converts G6P to fructose-6-phosophate, which is phosphorylated by phosphofructokinase to fructose-1,6-biphosphate (F-1,6-BP), consuming a second ATP[53]. F-1,6-BP is, in turn, cleaved by aldolase into two, 3-carbon molecules: dihydroxyacetone phosphate (DHAP) and glyceraldehyde-3-phosphate[54]. DHAP can be converted to glyceraldehyde-3-phosphate by phosphotriose isomerase[50]. Consequently, two glyceraldehyde-3-phosphate molecules may by processed by glyceraldehyde-3-phosphate dehydrogenase (GAPDH) into 1,3-biphosphoglycerate, yielding two $NADH_2$ molecules. Phosphoglycerate then catalyzes the conversion of 1,3-biphosphoglycerate to 3-phosphoglycerate, making one ATP molecule from ADP for each of the 1,3-biphosphoglycerate molecules[53,54]. 3-phosphoglycerate is converted to 2-phosphoglycerate, and then phosphoenolpyruvate by phosphoglycerate and enolase, respectively[53,54]. Two additional ATP are generated from phosphoenolpyruvate being converted to pyruvate by pyruvate kinase[53,54]. To summarize, the consumption of two ATP in the early stages of glycolysis and the production of two ATP by each of the two trioses yields two net ATP produced in the glycolytic pathway[53].

Glucose metabolism proceeds past the glycolytic pathway with pyruvate[54]. Under anaerobic conditions[54], pyruvate is converted into lactate by the enzyme lactate dehydrogenase[55]. In contrast, aerobic conditions support pyruvate oxidation and the additional production of ATP in the ETC[54,55]. This is initiated by the import of pyruvate from the cytosol to the mitochondrial matrix where, subsequently, the pyruvate is decarboxylated by pyruvate dehydrogenase (PDH) to form acetyl-CoA, releasing a CO_2 molecule in the process[51,55]. Thereafter, the processing of

pyruvate-derived Acetyl-CoA in the Krebs Cycle occurs identical to FA-derived Acetyl-CoA[55], and allows for further ATP production from the original glucose molecule that was committed to glycolysis[55].

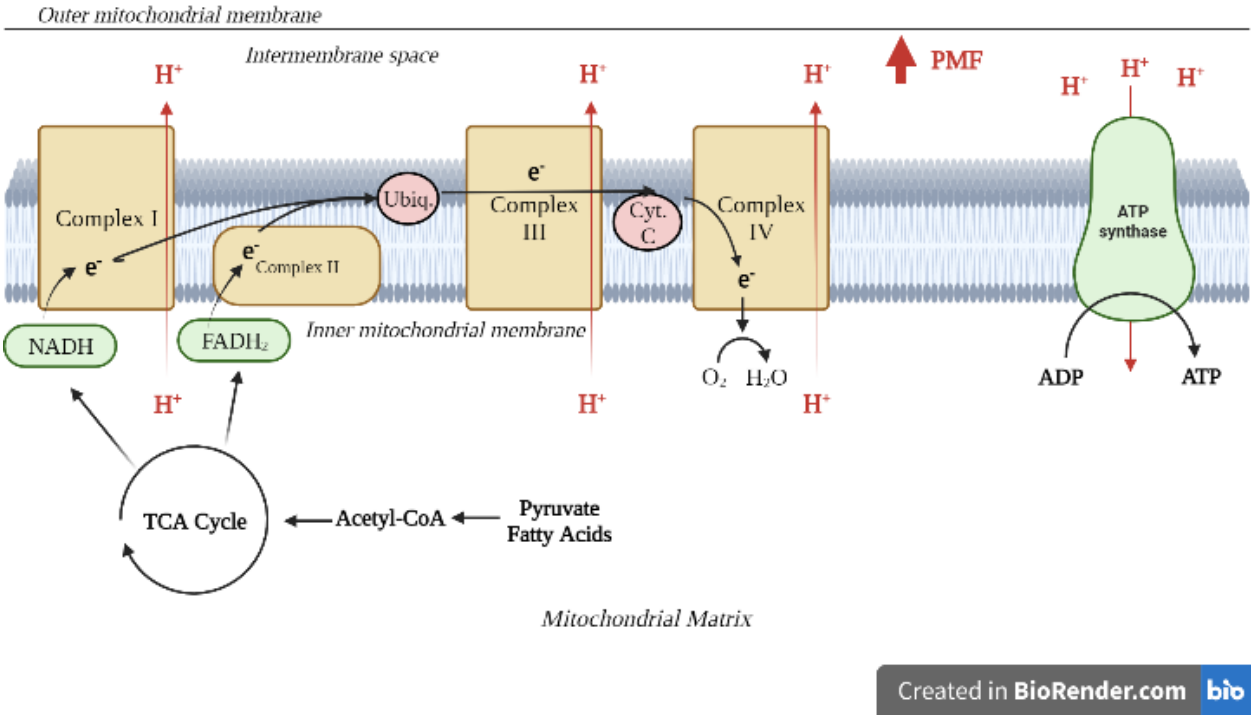

Figure 4: Schematic illustration of the electron transport chain (ETC). NADH and $FADH_2$ donate electrons to ETC complexes 1 and 2, respectively[52]. These electrons are sequentially transported to ubiquinone, Complex III, cytochrome C and Complex IV. Electron transport ends with the transfer of electrons from Complex IV to O_2, forming H_2O. At complexes I, III and IV, electron transport is accompanied by the pumping of protons into the intermembrane space[52]. The accumulation of protons in the intermembrane space generates a PMF that is dissipated through ATP Synthase (Complex V). Proton re-entry through Complex V into the mitochondrial matrix drives ATP synthesis, whereby adenosine diphosphate (ADP) is phosphorylated to form adenosine triphosphate (ATP).

2.2.3. Substrate Competition for Oxidation and the Randle Cycle

It is important to note that substrate preference for fuel production is a competitive dynamic between FA and glucose[56]. Under high-fat dietary conditions, metabolic substrate preference shifts to FAs[57]. In fact, FA infusion was shown to significantly attenuate glucose uptake in the legs of healthy males and shifted metabolism to fat[57]. The fat-induced attenuation in glucose metabolism can be attributed to impairments in the activities of several glycolytic enzymes, including PFK[58],

as well as PDH[56]. For instance, the increases in the concentrations of NADH and Acetyl-CoA relative to NAD^+ and CoA, respectively, suppress PDH activity[56], limiting the conversion of glucose-derived pyruvate to Acetyl-CoA[51,55]. Moreover, the consumption of a HFD has been shown to increase the gene expression of pyruvate dehydrogenase kinase 4 (PDHK4) in mouse skeletal muscle[59], which is also known to deactive PDH through phosphorylation[56,59]. The HFD-induced impairment in glucose metabolism was also observed in exercise-trained humans, who demonstrated glucose intolerance as well as attenuated contents of GLUT4 and IRS in skeletal muscle[60]. However, this metabolic shift may serve to spare glucose under conditions of lower dietary availability[56,61].

Fat oxidation is also impaired under conditions of elevated glucose metabolism[56,62]. With glycolysis and oxidation, the elevation in citrate levels leads to some citrate escape from the mitochondria[56]. This citrate can be converted back into its precursor molecules, oxaloacetate and acetyl-CoA[62]. The latter serves as a substrate for malonyl-CoA synthesis[56,62]. This conversion is catalyzed by acetyl-CoA carboxylase (ACC), and supplies malonyl-CoA for DNL[62,63]. Malonyl-CoA also has an inhibitory effect on CPT, significantly attenuating FA oxidation[62]. Importantly, the activation of AMP-activated protein kinase (AMPK), which is enhanced with FA availability[64] increases the phosphorylation and inhibition of ACC, disinhibiting CPT1 and enhancing FA oxidation[65]. Irrespective of the substrate preference for energy production, glucose and FA oxidation similarly contribute to the production of ATP through oxidative phosphorylation[52]. In BAT, thermogenesis is facilitated by the UCP1-mediated inhibition of oxidative phosphorylation[4].

2.2.4. UCP1-Dependent Thermogenesis

BAT-mediated thermogenesis is dependent on sympathetic nervous system activation[38]. In fact, denervation of the interscapular BAT (iBAT) depot, significantly impaired the diet-induced

elevation in BAT UCP1 in mice[66]. NE-mediated activation of the lipolytic signaling cascade culminates in the release of unesterified FA, which interact with UCP1 to activate it[38]. The mechanism underlying the FA-induced activation of UCP1 appears to be that FAs interfere with the inhibitory actions of purine nucleotides (including ATP, ADP, GTP and GDP) on UCP1[38,67]. Beyond UCP1 activation, several theories surrounding how FAs support proton leak exist[38]. As previously mentioned FAs and pyruvate are oxidized to produce intermediates in the ETC, where proton pumping into the intermembrane space generates a proton motive force that is essential for driving ATP synthesis[52,55]. UCP1 allows these protons to leak from the intermembrane space back into the mitochondrial matrix, dissipating the proton motive force and rendering the previous oxidation of energy substrates futile[4] (Figure 5). How FAs facilitate proton leak is still not fully understood, however distinct models exist to explain this mechanism, including FAs serving as allosteric activators, co-factors or shuttling machinery in UCP1[38]. Besides activating lipolysis, catecholaminergic stimulation also enhances the gene expression of UCP1 by activating transcription factors, including cAMP response element-binding protein (CREB)[38,68]. BAT thermogenesis plays distinct physiological roles, depending on the condition that mediates its activation.

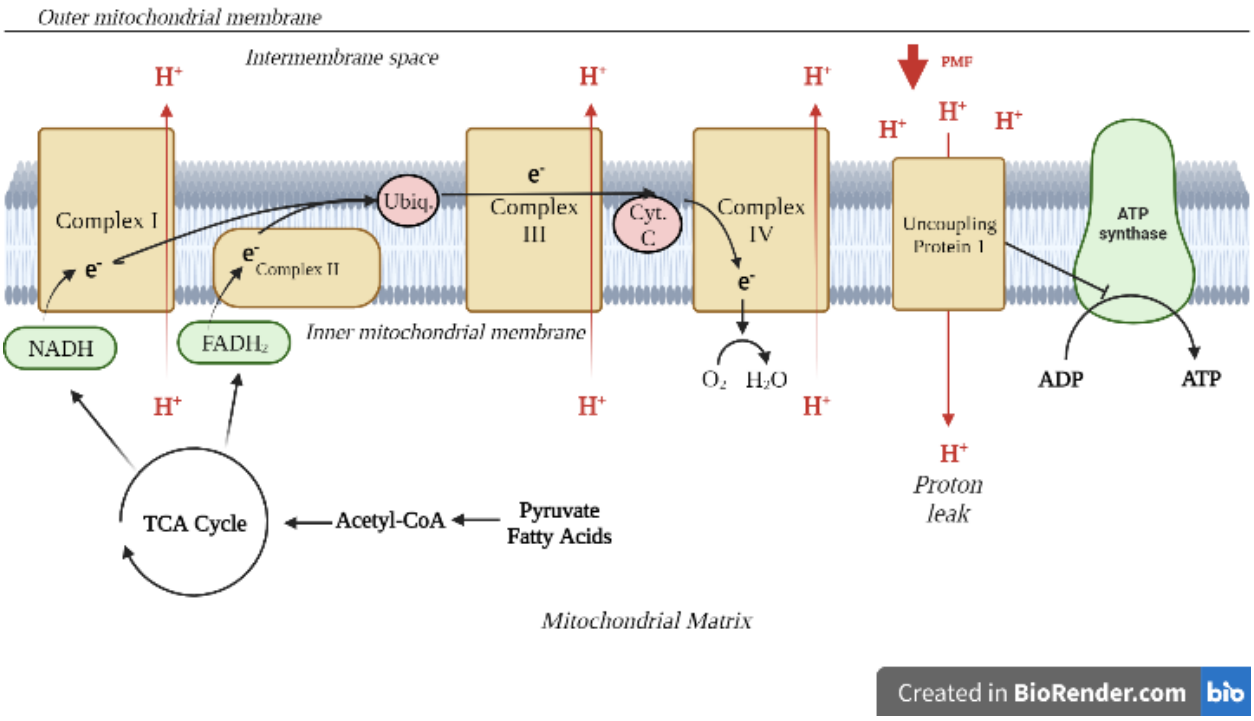

Figure 5: Schematic illustration of UCP1-mediated uncoupling. UCP1 allows protons to leak from the intermembrane space back into the mitochondrial matrix, dissipating the proton motive force and rendering the previous oxidation of energy substrates futile.

2.2.5. Cold-induced thermogenesis

With cold exposure, thermoregulatory mechanisms become activated to maintain core body temperature[38]. Acutely, heat production is achieved through shivering, whereas for non-shivering thermogenesis BAT is the major contributor and facilitates thermoregulation under conditions of chronic cold exposure[38]. In fact, rats housed at 4°C for one week displayed a significant elevation in BAT UCP1 content as well as the uncoupled oxidation of FAs in BAT adipocytes[7]. Consequently, despite increasing their food intake, cold-acclimated rats exhibited a significant attenuation in WAT mass[7]. In line with this, Wang et al. reported that cold-exposed mice displayed significantly enhanced glucose oxidation in BAT[69]. These effects could be attributed to cold-induced activation of the sympathetic nervous system (SNS)[69]. In fact, this group incubated differentiated primary brown adipocytes with a β3AdR agonist and observed an increase

in the activity of mitochondrial pyruvate carrier (MPC), which mediates the transport of pyruvate from the cytosol into the mitochondrion, whereby it can be processed in the Tricarboxylic acid (TCA) cycle[69]. This was reinforced with data showing that MPC inhibition significantly suppressed brown adipocyte oxygen consumption rate, body temperature in cold acclimated rats and glucose-mediated TCA cycle flux[69]. The propensity of BAT to metabolize glucose is promising from the perspective of whole-body glycaemic control. This is because activation of BAT can promote the oxidation of glucose[69], and, potentially increase clearance of this metabolite from the circulation. In fact, both glucose and FAs may be used as energy substrates in BAT. This is supported by observations that cold-induced metabolic adaptations in BAT can reverse deleterious effects caused by an obesogenic diet[70]. In fact, housing obese, cafeteria-fed rats at 4 °C significantly attenuated the diet-induced increase in body weight, reduced insulinemia and improved glucose tolerance[70]. Interestingly, this occurred despite the increased food intake observed in the cold-exposed, cafeteria diet-fed rats, when compared to the cafeteria diet-fed rats housed at 25 °C[70]. These effects were linked to the increase in brown adipocyte number, BAT mass and cytochrome oxidase activity[70]. It has recently been reported that the localization of mitochondria within the brown adipocyte also influences the functional outcome of the tissue[71]. Specifically, lipid-droplet associated mitochondria possess a lower FA-oxidizing capacity than cytoplasmic mitochondria in brown adipocytes. It appears that cold exposure induces a dissociation of mitochondria from the lipid droplet to the cytoplasm to support FA oxidation and thermogenesis. The role of the mitochondria, when bound to the lipid droplet, is instead to provide energy for TAG synthesis, which is supported by the enhanced ATP synthesizing capacity of these mitochondria in the brown adipocytes[71]. Thus, when assessing mitochondria in the brown fat as an indication of fat-burning capacity, it is crucial to first consider its localization.

Importantly, many rodent studies use temperatures for the control group that deviate from thermoneutrality[7,48,69]. This may be to accommodate more comfortable working conditions for laboratory and vivaria personnel[48]. Nevertheless, these temperatures typically fell below what is considered thermoneutral for mice and rats and may activate thermogenic responses in these animals[48]. Thus, the interpretation of cold-induced adaptations are relative to animals that, to some degree, are also subject to cold stress, which poses a limitation[48]. This was demonstrated by McKie et al. by housing mice at thermoneutrality and room temperature. They observed that room temperature conditions upregulated BAT UCP1 content and BAT mass, relative to the mice housed at thermoneutrality[48]. Nevertheless, acclimation at 4°C in murine models has shown promising metabolic effects that could be applied to human health and disease prevention[7,69].

BAT activation has also been studied in humans under acute and chronic cold-exposure conditions[72,73]. It was initially considered that BAT-mediated thermogenesis was only observed in newborns without developed thermoregulatory mechanisms, and that BAT activity would gradually dissipate and be negligible in adults[38,74]. However, it is now understood that adults possess BAT and it becomes more active when the individual is subjected to cold stress[72]. Anatomically, BAT depots in humans differ from those of murine models, where human BAT activity is predominantly found in the supraclavicular, chest and abdominal regions[72], including BAT localized to the vertebral column, aorta, axillary and neck regions[74,75] (Figure 6). To study the activity of these thermogenic fat depots in humans, [^{18}F]-fluorodeoxyglucose (^{18}FDG) is injected into the subject and its uptake is monitored using positron emission tomography (PET)[72,73]. Using this method, van Marken et al. were able to demonstrate that an acute 2h bout of cold exposure in male adults was sufficient to activate BAT[72]. These experiments were conducted in a climate chamber set to 16 °C[72]. Alternatively, cold exposure can be achieved through the use

of a suit[73]. In fact, Blondin et al. used a liquid-conditioned-suit to expose their subjects to 10°C, 2h per day for 4 weeks[73]. They observed that this significantly increased the volume of active BAT in subjects and significantly enhanced the oxidative capacity of the brown fat[73]. Together, murine and human studies suggest that cold-acclimation can enhance substrate oxidation[7,73] and potentially serve as a therapeutic tool for the management of obesity and insulin resistance[70]. In addition to cold, diet can also activate BAT in a phenomenon known as diet-induced thermogenesis (DIT)[38].

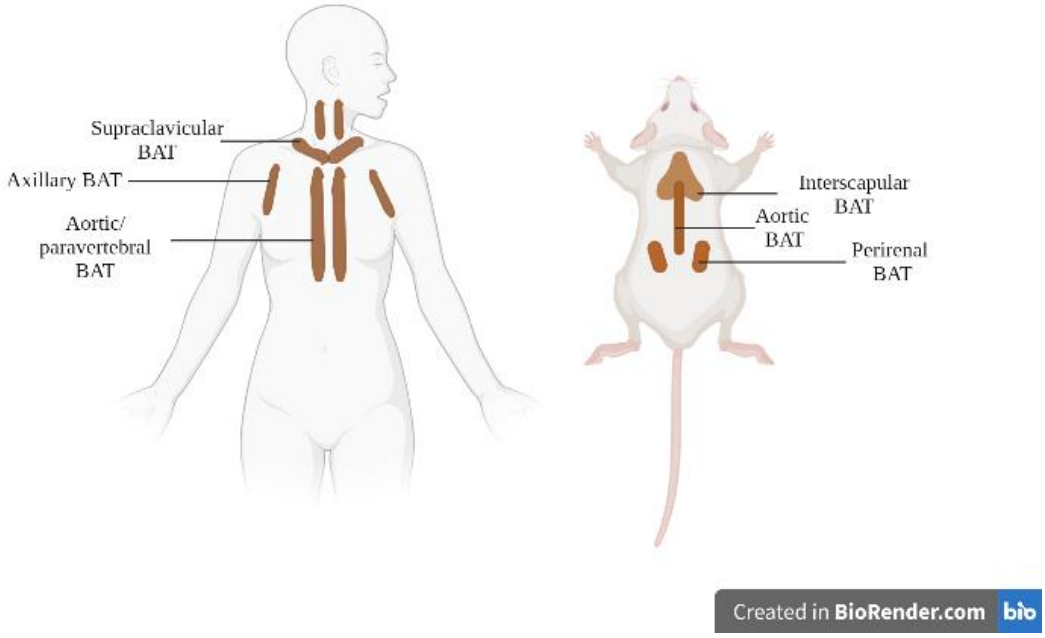

Figure 6: Schematic illustration of anatomical distributions of BAT in human and murine models. Human BAT activity is predominantly viewed in the supraclavicular, chest and abdominal regions, including BAT localized to the vertebral column, aorta, axillary and neck regions, whereas in rodents, BAT is present mainly in the interscapular, aortic, perirenal regions, among others.

2.2.6. Diet-induced thermogenesis (DIT)

Thermogenesis is activated following a single meal[76]. This was demonstrated in humans, where BAT oxygen consumption was significantly elevated post-prandially[46]. Interestingly, the diet-induced increase in BAT oxygen consumption was comparable to oxygen consumption under conditions of cold stress[46]. The macronutrient composition of a diet also appears to influence post-

prandial BAT activity[46,47,76]. In fact, it has been shown that the consumption of a carbohydrate-rich meal significantly increases respiratory exchange ratio and attenuates BAT FA uptake, when compared to cold exposed individuals[46]. The post-prandial preference of the BAT for carbohydrates was also supported by data showing that individuals with relatively higher BAT activity displayed enhanced energy expenditure and DIT following a high-carbohydrate meal, whereas a high-protein meal did not appear to be associated with DIT and did not elicit differences in energy expenditures between individuals with high and low BAT activity levels[76]. Noteworthy, the high-fat meal did enhance DIT in individuals with high BAT activity for the first hour following the meal, suggesting a possible role for fat in the post-prandial activation of BAT thermogenesis[76]. However, this increase was not sustained past this interval of time[76]. Despite the apparent post-prandial preference of the BAT for carbohydrates, respiratory quotient is lower in individuals with high BAT activity, when compared to individuals with low BAT activity after a meal[47]. Moreover, high BAT activity over 24h was correlated with a lower respiratory quotient[47]. Thus, there is evidence to suggest that fat is still used as a substrate for post-prandial thermogenesis, although carbohydrate consumption exhibits a greater capacity to activate BAT[46,76].

The activating mechanism for post-prandial DIT is distinct from that of cold exposure[46]. With cold stress, NE activates BAT thermogenesis[38], which is supported by the acute elevation in the levels of this hormone[46]. Conversely, circulating NE levels are not altered immediately following a meal[46]. The post-prandial activator of BAT is poorly understood[38], however it has been proposed that adrenaline is correlated to BAT activity following a meal (Fig. 5)[46]. With diet-induced obesity (DIO), BAT DIT is also transiently activated, albeit through distinct mechanisms[38,77].

DIT with chronic overfeeding is mediated primarily by leptin[38,77,78]. The expansion in adiposity observed with a surplus of energy intake is accompanied by an enhanced secretion of AT-derived leptin[38,77]. Leptin deficiency, classically demonstrated in the ob/ob mouse model, causes obesity that can be reversed with leptin administration[79]. This suggests leptin treatment may help in the treatment of obesity[80]. However, obesity causes an elevation in circulating leptin levels[77,80], pointing to leptin resistance as the potential physiopathology underlying the development of obesity[77,80]. Leptin has been shown to signal through the hypothalamus to enhance SNS stimulation to the BAT and enhance thermogenesis[78]. This was demonstrated in an Sh2b1 knockout in mice[78]. Sh2b1 is a protein that is implicated in leptin receptor signaling in the hypothalamus[78]. When this protein was knocked-out, mice exhibited a significant increase in body weight and fat mass, and an attenuation in core body temperature during dark cycle hours[78]. This occurred in the absence of an alteration in food intake or activity levels[78]. Sh2b1 ablation also significantly attenuated Ucp1 gene expression and content in BAT, as well as sympathetic nerve activity to this tissue[78]. Interestingly, Sh2b1 overexpression increased BAT UCP1 content in mice and sensitized the neurons to leptin signaling[78]. This was effective in reversing DIO and insulin resistance in these mice[78].

The importance of BAT UCP1 content for DIT was also highlighted by Feldmann et al. in UCP1-ablated mice[81]. UCP1 ablation significantly increased WAT mass in control and HFD-fed mice[81]. Moreover, NE-induced oxygen consumption was significantly attenuated in mice lacking UCP1[81]. In another study using 129S mice, an obesity-resistant strain, UCP1-knockout significantly elevated Sc Ing mass, whether the mice were consuming a chow or HFD[82]. In mice fed a HFD, the knockout of UCP1 also caused a significant increase in total fat mass and an attenuation in energy expenditure[82].These findings suggest BAT-mediated DIT plays an important

role in enhancing energy expenditure and preventing DIO. This then begs the question as to why individuals still become obese. Leitner et al. demonstrated that obese individuals have a higher volume of BAT than lean individuals[75]. Moreover, other studies show that a HFS diet significantly elevates BAT UCP1 content[8] and BAT homogenate FA oxidative capacity[77]. Logically, these metabolic adaptations would enhance DIT and serve to counteract obesity. However, despite having a higher BAT mass, obesity significantly attenuates BAT activity[75]. This was supported by recent findings showing that HFS feeding attenuates the uncoupled oxidative capacity of the brown adipocyte and instead diverts fat for storage (Figure 7)[8]. This attenuation in uncoupled oxidative capacity can be attributed to suppressed SNS activity[8], which may originate from leptin resistance in the brain[78]. These diet-induced metabolic adaptations lead to a shift in the morphology of the BAT from multilocular to unilocular[8]. Collectively, these modifications make the BAT more morphologically and functionally similar to the WAT[8]. This obesity-induced conversion is known as whitening of the BAT[6,8]. Whitening of BAT was also induced in mice deficient in β-adrenergic receptors, leptin receptors and ATGL, which reinforce the importance of SNS and leptin-mediated activation of the BAT[83]. Moreover, this conversion of the BAT to WAT is accompanied by significant inflammation and the formation of crown-like structures (CLS)[83]. CLS are composed of macrophages that surround and remove dead adipocytes[83]. In this context, DIO causes hypertrophy and inflammation in WAT and BAT, whereby both may contribute to the systemic inflammation that is observed in obesity[83]. The interconversion between BAT and WAT may also happen in the opposite direction whereby WAT appears and functions more similarly to BAT[19]. This conversion is known as “browning” of the WAT and yields beige adipocytes[4].

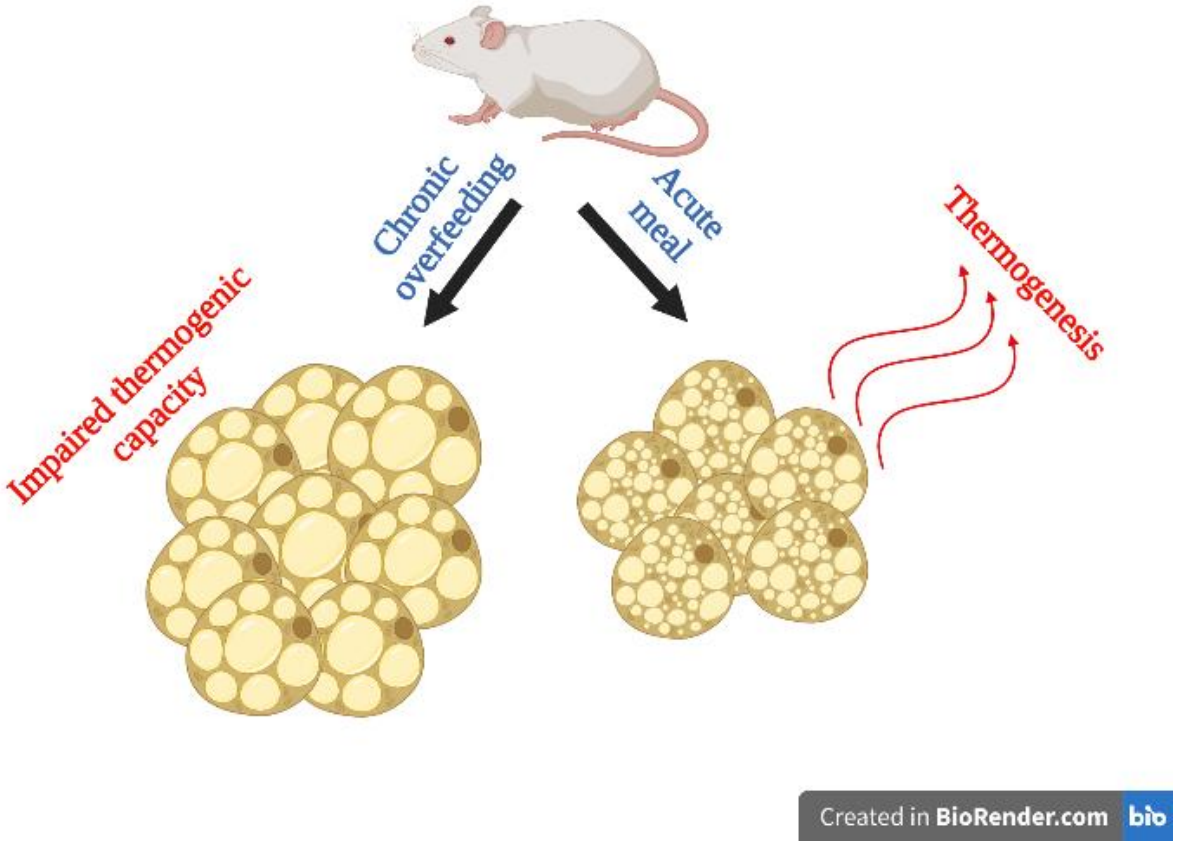

Figure 7: Schematic illustration of dietary effects on BAT DIT. Following an acute meal, thermogenesis is enhanced in BAT. Conversely, under conditions of chronic overfeeding and DIO, thermogenesis becomes impaired in this tissue.

2.2.7. Browning of WAT and Beige Adipocytes

Browning is classically induced with cold exposure[4,7,38] and is characterized by WAT depots that appear darker in colour[19]. It is considered that the appearance of these adipocytes occurs through conversion of existing white adipocytes, rather than the emergence of new adipocytes from fat cell precursors[19]. Depot-specific differences in browning capacity exist, whereby subcutaneous WAT exhibits a greater propensity for browning than visceral WAT[7]. The induction of browning is dependent on SNS stimulation in the WAT[84]. In fact, β3AdR knockout in mice has been shown to significantly suppress UCP1 expression in WAT and maintains a unilocular appearance of the adipocytes under conditions of cold exposure[84]. The importance of the SNS in WAT browning was further reinforced with the administration of Withaferin A, a compound that has been shown

to support leptin signaling through the hypothalamus[85]. In a recent study, Guo et al showed that Withaferin A significantly enhanced tyrosine hydroxylase (TH) content in WAT, an enzyme that is crucial for the synthesis of catecholamines, as well as UCP1 content and the multilocular appearance of the white adipocytes[85]. These effects were ablated with WAT denervation in these mice, suggesting that Withaferin A does indeed induce browning through the SNS[85]. These effects can be attributed to the SNS-induced activation of pr-domain-containing protein 16 (PRDM16), given that the knockdown of this gene significantly reduced markers of browning and uncoupled oxidation in Sc adipocytes, in the absence or presence of catecholaminergic stimulation[86]. Conversely, the overexpression of PRDM16 in WAT upregulated Ucp1 gene expression and browning. PRDM16 enhances peroxisome proliferator-activated receptor gamma co-activator 1a (PGC-1α) transcriptional regulation, which upregulates the browning program in white adipocytes[85,87]. Thus, besides UCP1, PGC1α is also a major indicator of browning and thermogenesis[86]. Despite an elevation in UCP1, browning does not always suggest an enhancement in UCP1-mediated thermogenesis[7] and has prompted investigations into UCP1-independent mechanisms of thermogenesis.

2.2.8. UCP1-Independent Futile Energy Cycles

In WAT, cold exposure increases UCP1 but lowers the uncoupled oxidation of FA in white adipocytes[7]. This suggests that an alternative, UCP1-independent mechanism is mediating thermogenesis in white fat and underlying the conversion from a unilocular to a multilocular appearance[7]. Sepa-Kishi et al. determined that this mechanism was TAG recycling[7]. In cold-acclimated Sc inguinal (Ing) adipocytes, lipolysis and lipogenesis were both significantly enhanced, suggesting that a futile cycle of hydrolysis and re-esterification could contribute to thermogenesis in this tissue under conditions of cold stress[7]. In fact, to support lipogenesis cold-

acclimated adipocytes displayed increased GyK content and the incorporation of glycerol into TAG, both of which are normally low in WAT[33,34]. Together, the increased cycling of fat breakdown and storage could explain the formation of smaller LDs and a multilocular appearance of the AT depot, and proposes a UCP1-independent mechanism of thermogenesis in beige adipocytes[7].

Another thermogenic futile cycle in beige adipocytes that has been described is the creatine (Cr) cycle[88]. This model proposes that mitochondrial creatine kinase regenerates ATP from ADP, driving oxidative phosphorylation[88]. The generated PCr is then hydrolyzed back to Cr, replenishing this substrate for ATP/ADP, PCr/Cr futile cycling[88]. The importance of creatine for thermogenesis was supported by the observation that oxygen consumption in beige adipocytes was significantly reduced with a creatine inhibitor[88]. This futile cycle is amplified in UCP-deficient mice, where its contribution to thermogenesis is enhanced to compensate for the lack of UCP1-mediated heat production[88]. In conclusion, despite acquiring features of BAT, beige adipocytes develop distinct metabolic adaptations to drive thermogenesis[7].

Besides cold stress, browning is also induced by endurance exericse[89]. Similar to cold exposure, exercise elevates UCP1 and PGC-1α contents in Sc Ing fat, increases FA oxidative capacity and makes the adipocytes appear more mulitlocular[89]. Under conditions of exercise, browning has been attributed to the elevation in Sc Ing content of fibronectin domain-containing protein 5, which is believed to exert an autocrine effect to promote thermogenic adaptations in this tissue[89]. Interestingly, exercise has an opposite effect on BAT, whereby it attenuates PGC-1α, UCP1 and FA oxidation, and increases LD size[89]. Because exercise is inherently thermogenic, BAT activity is not required for thermoregulation. Thus, exercise-induced metabolic adaptations shift thermogenic activity away from central regions by attenuating BAT thermogenesis, and likely

increase heat dissipation in peripheral tissues, such as the Sc AT[89]. Regardless of stimulus, browning of WAT and the conversion of this storage-centric depot to a thermogenic, energy-burning tissue poses a promising strategy to reverse obesity[4,90].

In conclusion, WAT and BAT play important physiological roles, including controlled storage and mobilization of energy and energy dissipation in the former and latter, respectively[4]. Importantly, white adipocytes possess metabolic flexibility, whereby they can undergo browning to enhance their energy-dissipating properties[4]. Besides their metabolic functions, ATs are also a prominent endocrine organ that secretes multiple factors (adipokines) that play crucial roles in several tissues and organs[91].

2.3. Endocrine Function of Adipose Tissue

2.3.1 Leptin

Leptin is an AT-derived hormone with a molecular weight of approximately 16 kilo Daltons (kDa)[80]. The level of secretion of this adipokine is directly proportional to the volume of AT[80,92]. In this context, it is considered that leptin functions in a negative feedback mechanism to maintain energy homeostasis through several leptin-mediated circuits[92]. Leptin acts mainly in the hypothalamus, where it binds to its receptor (LepR), of which there are six isoforms: a, b, c, d, e and f[80]. However, isoform e is not membrane bound and binds leptin in the circulation to inhibit its activity[80]. The other leptin isoforms contain a transmembrane domain, however only isoform b possesses all necessary signaling proteins on its intracellular domain, making it the predominant receptor isoform through which leptin acts in the brain[80,92]. In order to access the hypothalamus, circulating leptin must be transported across the blood brain barrier[80,92]. Upon binding to its receptor, it activates a downstream signaling cascade that is initiated by janus kinase 2 (JAK2) binding and activation[80]. Once activated, JAK2 phosphorylates the LepR on three residues, each

of which triggers a distinct physiological circuit[80].The phosphorylation of signal-transducer-and-activator-of-transcription 3 (STAT3) is what modulates hypothalamic energy balance mechanisms that reduce food intake and increase energy expenditure[80]. In fact, the effects of leptin on energy dissipating pathways are mediated largely through BAT[80]. Thus, by attenuating energy intake and promoting thermogenesis, leptin leads to a reduction in adiposity[80,92]. Conversely, under conditions of energy deficiency, AT leptin secretion is significantly reduced, enhancing food intake and suppressing energy expenditure to reverse weight loss[80,92].

With obesity, circulating leptin is characteristically elevated[77]. Under these conditions, however, leptin signaling is abrogated in the hypothalamus, a condition which is known as leptin resistance[80]. The impairment in leptin signaling can be attributed to an increase in suppressor of cytokine signaling 3 (SOCS3), which inhibits JAK-STAT signaling[80,93]. In fact, in SOCS3-deficient mice, leptin-induced STAT3 phosphorylation was significantly enhanced[93]. Moreover, SOCS3-deficient mice fed a HFD did not gain more weight than SOCS3-deficient mice fed a chow diet and did not display hyperleptinemia or hyperinsulinemia[93]. Together, these findings highlight the impact of SOCS3 on leptin sensitivity and its importance for whole-body energy homeostasis. Another major adipokine is adiponectin.

2.3.2. Adiponectin

Adiponectin is another major adipokine expressed exclusively in WAT and BAT[94]. Contrary to leptin, the secretion of this hormone is inversely proportional to WAT mass and has been shown to be reduced under conditions of obesity-related metabolic disorders[94]. Adiponectin naturally exists in several multimeric forms, of which there are three major complexes: a trimer, a hexamer and a 12-18-mer[94]. Adiponectin circulates mainly in its full length form but may also be cleaved into its globular form, both of which act on adiponectin receptor 1 and adiponectin receptor 2

(AdipoR1 and AdipoR2, respectively)[94]. Globular and full-length adiponectin activate AMPK, which increases glucose uptake and FA oxidation[95]. In muscle cells, both globular and full-length adiponectin mediate these effects, whereas in hepatocytes only full-length adiponectin activates AMPK[95]. Regardless of cell-type, AMPK inhibition impaired adiponectin-induced increases in FA oxidation and glucose uptake[95], suggesting a critical role for AMPK in adiponectin action. The beneficial metabolic effects of adiponectin and its potential for management of obesity and insulin resistance have sparked research in the development of mimetics for this adipokine.

The AdipoR agonist, AdipoRon has been used as a reliable agonist for adiponectin-induced responses in several tissues[16]. AdipoRon binds to both AdipoR1 and AdipoR2 and has been shown to significantly improve insulin sensitivity, increase markers of mitochondrial biogenesis in skeletal muscle, attenuate inflammatory gene expression in WAT, exert an anti-steatotic effect in liver, and upregulate the activation of AMPK in muscle and liver[16]. Importantly, the ablation of both AdipoRs reversed the AdipoRon-induced effects[16], reinforcing the effect of adiponectin stimulation on the above metabolic effects[16].

Another adiponectin mimetic that has been studied is ALY688[96], which was shown by Sung et al. to significantly enhance AMPK and ACC phosphorylation, insulin-signaling and insulin-stimulated glucose uptake in L6 muscle cells[96]. In fact, ALY688-induced AMPK phosphorylation was not different from that of globular adiponectin. This compound also enhanced signaling through an alternative AdipoR pathway, p38 mitogen-activated protein kinase (MAPK)[96], which likely mediated the dose-dependent increases in glucose uptake observed in the muscle cells treated with this drug[17,96].

More recently, there has been the development of a novel AdipoR agonist that suppresses inflammation as potently as AdipoRon[97]. This compound is an AdipoRon analogue known as anti-

inflammation adiponectin (AdipoAI)[97]. Qiu et al designed and tested AdipoAI in bone marrow-derived macrophages treated with LPS, where co-treatment with AdipoAI or AdipoRon drastically reduced inflammatory cytokines interleukin-6 (IL-6) and interleukin-1β (IL-1β)[97]. In vivo results exhibited similar anti-inflammatory effects, where oral administration of AdipoAI lowered AT and spleen gene expression levels of IL-6 and IL-1β, as well as serum levels of these cytokines in obese mice[97]. Interestingly, IL6 and IL-1β expression levels were unaffected by AdipoRon administration, suggesting a superior effect of AdipoAI on inflammation under conditions of DIO[97]. In this context, the metabolic and anti-inflammatory effects induced by adiponectin and adiponectin mimetics[16,96,97] under conditions of DIO[94] point to this adipokine as a promising therapeutic agent for the management of obesity and insulin resistance.

With regards to adiponectin and leptin, the relative ratio of these two adipokines is an important determinant of metabolic health[98]. In older adults, the adiponectin:leptin ratio was negatively correlated with adiposity and body mass index (BMI)[98]. Moreover, in female participants this ratio was also positively correlated to high density lipoprotein (HDL) cholesterol and inversely related to insulinemia and inflammatory factors such as C-reactive protein and IL-6[98]. This highlights the integrative nature of adipokines and proposes the ratio of adiponectin:leptin as a biomarker for AT functional status and overall metabolic health[98]. In addition to these adipokines, the AT expresses markers of inflammation[44,99].

2.3.3. Adipose-derived Inflammatory Cytokines

Chronic obesity is accompanied by systemic, low-grade inflammation which is attributable to AT-mediated secretion of inflammatory cytokines[100]. These cytokines are produced by resident immune cells[10,83,100,101] but are also expressed by adipocytes[101]. For instance, tumour necrosis factor alpha (TNFα) expression in white adipocytes is positively associated with obesity and body

fat percentage[101]. In fact, weight loss attenuates the expression of this cytokine in WAT[101]. TNFα stimulates lipolysis, propagates inflammatory cytokine production and downregulates the expression of adipogenic genes such as PPARγ in white adipocytes[102]. TNFα also inhibits lipogenesis in adipocytes by impairing glucose uptake and the insulin signaling pathway[44]. Specifically, incubation of 3T3-F442A adipocytes with TNFα demonstrated a time-dependent inhibition of this cytokine on insulin-stimulated phosphorylation of IRS1[44]. Similarly, BAT TNFα expression was increased under conditions of obesity and significantly impaired the function of this AT depot[103]. In fact, Nisoli et al. demonstrated that the incubation of brown adipocytes with TNFα elicited a dose-dependent suppression of β3AdR expression, and significantly blunted BAT UCP1 gene expression[103]. In line with this, the inhibition of TNFα signaling preserved the expression of these two thermogenic genes and supported thermoregulation under conditions of cold exposure[103]. Together, existing reports indicate that obesity mediates an increase in WAT and BAT TNFα expression, which may exert an autocrine and paracrine effect on the adipocytes that disrupts normal energy metabolism[44,103]. In addition to TNFα, DIO also increases circulating levels of IL-6[12], which can be attributed to AT-mediated expression of inflammatory markers[99].

IL-6 expression in AT is derived from both the adipocytes and resident inflammatory cells[99]. This was demonstrated by Han et al. in IL-6 deficient mice in which reduced expression of adipocyte-derived IL-6 significantly decreased BAT and gonadal WAT IL-6 levels[99]. Interestingly, IL-6 deficiency improved insulin-signaling in the WAT of HFD-fed mice[99], but not in the liver or skeletal muscle[99]. This may be attributed to DIO-induced inflammation in AT temporally preceding inflammation in non-adipose tissues[10]. Moreover, reduced IL-6 expression reversed HFD-induced immune cell infiltration in the AT, which likely promoted the formation of CLS around dysfunctional adipocytes[83,99]. In this context, obesity-related AT inflammation is

crucial in the pathogenesis of adipocyte dysfunction[44], adipocyte removal following cell death[83] and contributes to systemic inflammation[10]. These pro-inflammatory effects in AT could, in part, be attributed to diet-induced alterations in components of the Renin-Angiotensin System (RAS)[104].

2.4. Renin-angiotensin system (RAS)

Recently, the Renin-Angiotensin-Aldosterone System (RAAS) has been identified as an important factor associated with metabolic alterations in AT and obesity-related metabolic disorders[104,105]. Briefly, the RAAS is triggered initially by the synthesis of renin from the kidney and angiotensinogen from the liver. Renin is released into the circulation in a rate-limiting, controlled manner[106], whereas angiotensinogen often circulates in excess relative to renin[106]. Under hypotensive conditions, both renin and angiotensinogen are secreted in larger quantities from their respective tissues[106]. In the circulation, renin converts angiotensinogen into angiotensin-I (Ang-I)[106]. Ang-I is then processed, mainly in the pulmonary circulation[107], by endothelial cell-derived angiotensin converting enzyme (ACE1) into angiotensin-II (Ang-II)[106]. Ang-II exerts its effects by binding to the G-protein coupled receptor[108] angiotensin type 1 receptor (AT_1R)[106]. There are two isoforms of the AT_1R: $AT_{1a}r$ and $AT_{1b}R$[108]. The former is expressed in a variety of tissues, whereas the latter is expressed mostly in the central nervous system; however, they play similar physiological roles[108,109]. Activation of AT_1R exerts the classical effects of the RAAS, including vasoconstriction, water retention, SNS stimulation, and aldosterone release from the adrenal gland[106]. Aldosterone further enhances mineral and water retention in the kidney by stimulating mineralocorticoid receptors[106]. Together, these AT_1R-mediated functions allow for the regulation of systemic blood pressure[106,108]. However, excess Ang-II and aldosterone seen in RAAS hyperactivation and obesity[110] causes several detrimental effects, including fibrosis, oxidative damage, and inflammation in the kidney and heart, as well as vascular dysfunction[106,109]. In this

context, the counterregulatory arm of the RAAS system has drawn great attention as a therapeutic intervention for RAAS dysregulation. These effects are mediated by angiotensin type 2 receptor (AT_2R)[106], which is not abundant in adult tissues, although its expression is increased under conditions of AT_1R hyperactivation[111]. Besides Ang-II, Ang-(1-9) can also directly bind to AT_2R[109]. Ang-(1-9) is derived from Ang-I in a reaction catalyzed by ACE2, a second angiotensin converting enzyme[106]. Ang-(1-9) and Ang-II then act on AT_2R to promote flux through the counterregulatory RAS arm, anti-inflammatory effects and vasodilation[106]. Furthermore, ACE2-mediated conversion of Ang-II to Ang-(1-7) also exerts protective effects via the Mas receptor (MasR)[106] (Figure 8).

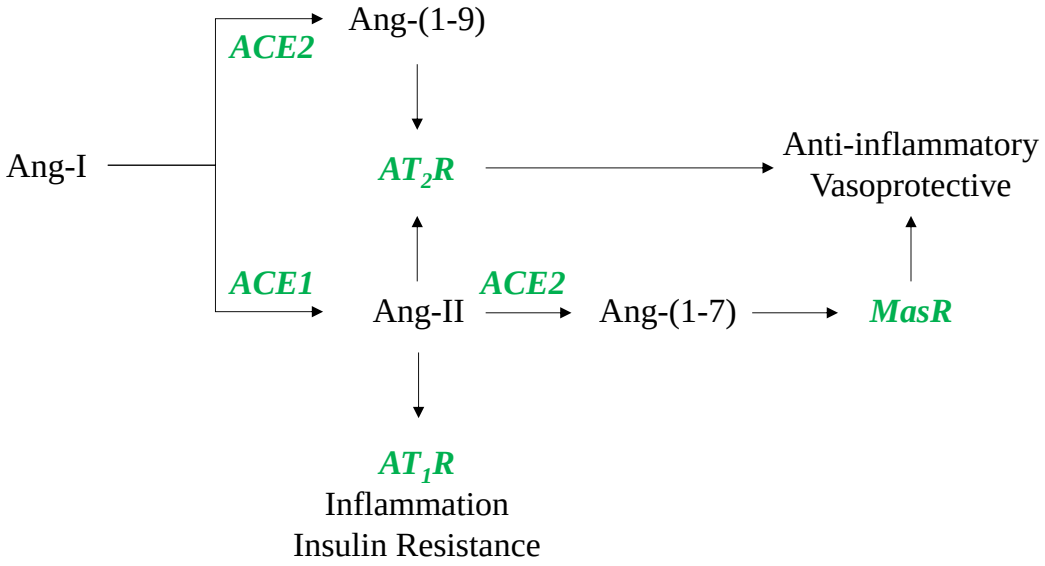

Figure 8: Schematic illustration of RAS. Angiotensin I (Ang-I) is converted to angiotensin II (Ang II) by angiotensin converting enzyme (ACE1). Ang-II binds to angiotensin II, type I receptor (AT_1R) and causes inflammation and insulin resistance in adipocytes, vasculature, etc. Alternatively, Ang-II can bind directly to angiotensin II, type 2 receptor (AT_2R), or it can be converted to Ang-(1-9) or Ang-(1-7), which then bind to AT_2R and the Mas receptor (MasR), respectively. Signaling through these receptors promotes anti-inflammatory effects and vasodilation.

2.4.1. RAS in Adipose Tissue

Despite being predominantly studied in the context of cardiovascular function, adipose tissue also expresses components of the renin-angiotensin system (RAS)[105,107]. The RAS is highly influential in WAT and BAT metabolism by regulating the functions of these two fat compartments. In fact, in high fat (HF)-fed mice, Giori et al. showed an increase in the flux through the ACE1/Ang-II/AT_1R arm of the RAS in WAT[105], which is known to promote inflammation and insulin resistance in fat cells[104]. Interestingly, injecting HF-fed mice with ACE2 increased BAT mass, UCP1 expression and thermogenesis[104]. This significantly improved whole-body glucose homeostasis and insulin sensitivity in animals fed an obesogenic diet[104]. Furthermore, ACE2 injection has been shown to promote lipolysis in subcutaneous WAT and increase UCP1 expression in this tissue[104]. This causes white adipocytes to take on a more "brown" appearance[104], and is commonly observed with increased flux through the ACE2/Ang(1,7)/Mas arm of the RAS[105]. Morimoto et al. also observed an enhancement in BAT thermogenesis with the administration of Ang-(1,7) in HF-fed mice[112]. However, they did not observe increased UCP1 content in the WAT of these animals, despite reducing lipid accumulation in the white adipocytes[112]. This is in contrast to what was found with ACE2 injection; however, they attributed this lack of browning to a low MasR content in WAT[112]. Thus, it is plausible that supplementing Ang-(1,7) did not have the same effect on browning as administering an enzyme that can convert endogenous Ang-II to Ang-(1,7). Regardless, both studies indicated that the activation of the counterregulatory arm of the RAAS system improved whole-body glucose homeostasis and reduced body weight, which is of great importance for the treatment of obesity and insulin resistance[104,112]. Besides manipulating a single arm to produce beneficial effects, the effects of the

RAS on AT appear to be regulated by a balance between the ACE1/Ang-II/AT_1R arm and the ACE2/Ang-(1,7)/AT_2R arm. This has been demonstrated with aerobic exercise[105].

It has been reported that the WAT ACE1:ACE2 ratio, AT_1R expression, and Ang-II:Ang-(1,7) levels increased in mice fed a high-fat (HF) diet[105]. Interestingly, these parameters were completely reversed with aerobic training and could underlie the observed increase in markers of WAT browning[105]. In order to compare exercise to the effects of a pharmacological agent, an additional group of mice fed a HF diet was also treated with enalapril, a widely used ACE1 inhibitor[105]. Similar to the endurance-trained group, HF-fed enalapril mice had reduced ACE1:ACE2 and Ang-II:Ang-(1-7) ratios[105]. Furthermore, in both the trained and the enalapril-treated groups, Sc and visceral adipose tissue masses were reduced[105]. Despite similarities in these phenotypic adaptations, the mechanism by which these alterations took place differed between the two groups. The enalapril group experienced an expected reduction in ACE1 activity[105]. Conversely, ACE2 activity increased significantly in the WAT of these animals[105]. This mechanism attenuated the HF diet-induced elevations in Ang-II and increased Ang-(1-7)[105]. Interestingly, exercise did not significantly alter ACE1 or ACE2 activity, when compared to the HF-fed mice[105]. There was also no change in Ang-II levels, however, Ang-(1,7) was significantly elevated in the trained mice[105]. This indicates that the exercise-induced alteration in ACE1:ACE2 content was sufficient to drive the conversion of the present Ang-II to Ang-(1,7), regardless of the activity of these enzymes[105]. Moreover, despite the sustained Ang-II levels, the reduction in AT_1R levels likely diverted Ang-II to existing AT_2R in exercised mice[105]. In this context, Ang-II may have signalled through AT_2R and contributed to browning in the WAT of the trained animals[105]. This, however, remains speculative as AT_2R was not measured in the study. It is important to note that unlike exercise, enalapril treatment did not induce browning in the WAT[105]. Thus, it is likely

that the reduction in fat mass in the enalapril group may have occurred as a result of the activity of an alternative thermogenic tissue[105]. In this case, the authors hypothesized that this tissue was BAT, and that enalapril was enhancing thermogenesis in this fat pad[105]. Taken together, these studies indicate that the RAS regulates several metabolic mechanisms in adipose tissue and can be greatly influenced by diet. Interestingly, diet-induced alterations in the RAS also has implications for other tissues and body systems, including the cardiovascular and cardiorespiratory systems. In fact, this has emerged as a major field of research in the midst of the COVID-19 pandemic[113].

2.4.2. The RAS in lung, heart and vascular tissue: Implications for COVID-19 disease severity

The novel severe acute respiratory syndrome (SARS) coronavirus, also know as SARS-CoV-2 provokes respiratory disease and can be fatal[114,115]. SARS-CoV-2 enters the system via the respiratory tract[116] and is able to infect the host cells via ACE2, which acts as a cellular receptor for this pathogen[115]. This interaction occurs between ACE2 and a specific protein on the virus known as the spike (S) protein[115]. In brief, the S protein is cleaved into 2 subunits by the cell surface protein transmembrane protease, serine 2 (TMPRSS2), which primes the S1 subunit to bind to ACE2[115]. Subsequently, the virus enters the host cell through endocytosis and can thereafter transcribe its viral ribonucleic acid (RNA) by using the host's ribosomes[117]. This enables the transcription and translation of viral proteins and eventually leads to replication of the virus[117]. As the virus replicates, it is able to spillover into the circulation and thereafter access other ACE2-expressing tissues, including the heart, gastrointestinal tract and vasculature, among others, where it can continue to exert its viral effects (Figure 9)[117].

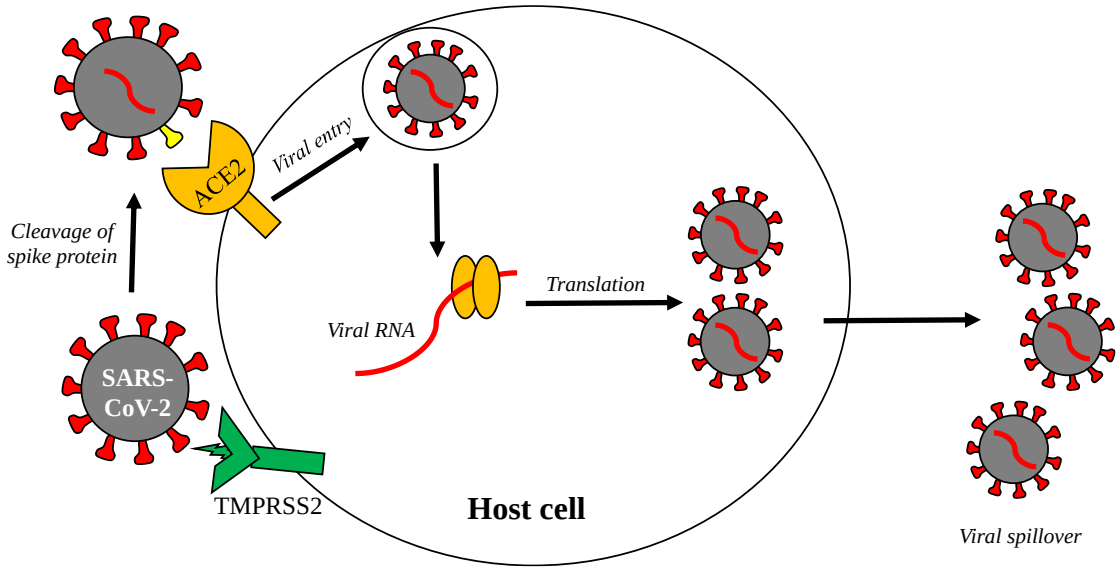

Figure 9: Schematic illustration of cellular infection with COVID-19. SARS-CoV-2 reaches the host cell where its spike (S) protein is cleaved by transmembrane protease serine 2 (TMPRSS2). This primes the S protein (in yellow) for binding with ACE2, which facilitates entry into the host cell. From there, the virus uses the cell's ribosomes to translate its RNA and promote viral replication. Eventually, replication of the novel coronavirus leads to spillover into the circulation, where it can then migrate to other tissues and repeat this cycle.

Consequently, SARS-Cov-2 causes cellular damage and apoptosis which recruits immune cells to the site of injury[118]. In addition to this, the novel coronavirus is able to induce lymphocytic apoptosis, which triggers a robust immune response that activates and recruits more immune cells[118]. These immune cells then release a number of cytokines, including interleukin-6 (IL-6), IL-1β, and TNFα among several others[116,119], which further potentiate the recruitment of other immune cells and promotes a positive feedback cycle of cytokine release and immune cell recruitment[119]. The aberrant activation of the immune system and the corresponding release of pro-inflammatory cytokines is called a "cytokine storm" and leads to oxidative stress and organ damage in COVID patients[119]. In parallel to this, the binding of SARS-CoV-2 to the ACE2 receptor on lung cells reduces ACE2 availability for the conversion of Ang-II to Ang-(1,9)[119]. As a result, there is a shift to the ACE1-Ang-II-AT_1R arm of the RAS system which facilitates inflammation in the lung[119]. In this context, patients with compromised immune function are more susceptible

to the severe outcomes of COVID-19 infection[118]. Another group of patients that are at an elevated risk for severe symptoms are obese individuals[118].

As previously mentioned, obesity is characterized by an elevation in WAT mass caused by the hyperplasia and hypertrophy of white adipocytes[19]. Once adipocytes reach a critical size, they experience hypoxia and become dysfunctional[19,118]. As a result, the adipocytes release cytokines and recruit macrophages to their periphery, which promotes hypercytokinemia and dysfunction of the innate immune system[19,118]. Additionally, cells of the adaptive immunity have been shown to be reduced in obese individuals[118]. This inflammatory profile is characteristic of the low-grade, systemic inflammation seen in obese patients, and has an impact on several aspects of physiology, including respiration[118,120]. In fact, obesity has been linked to asthma and airway inflammation[120]. Umetsu et al. demonstrated this in obese mice[120], which had an increased number of inflammatory macrophages, nucleotide-binding domain, leucine-rich repeat, and pyrin domain-containing protein 3 (NLRP3) inflammasome activation and IL-1β expression in lung tissues[120]. As a result, IL-1β enhanced the recruitment of innate lymphoid cells (ILCs)[120]. ILCs produce interleukin-17 (IL-17), which is implicated in airway hyperreactivity and lung resistance in HF-fed animals[120]. Evidently, obesity creates a dysregulated inflammatory condition in the airway[113,118]. In addition to this, obesity has also been linked to increased susceptibility to viral infection[113].

As previously mentioned, obesity induces changes in RAS components in adipose tissue that leads to detrimental metabolic and inflammatory profiles[105]. However, obesity has also been linked to alterations in ACE2 in the respiratory tract, which is associated with the more severe outcomes observed in this cohort[113]. Sarver and Wong examined the effect of the HF diet on ACE2 and TMPRSS2 in mouse lungs and trachea[113]. These authors found that ACE2 expression was increased by the HF diet in both tissues in male mice[113]. In contrast, HF-feeding did not alter

TMPRSS2 expression in either the lungs or trachea[113]. This indicates that ACE2 plays a more important role in the susceptibility of obese individuals to more severe COVID-related outcomes or that there are other proteins that facilitate the fusion of SARS-CoV-2 that are impacted to a greater extent by the HF diet[113]. For instance, furin is a protease that can also cleave the spike protein to facilitate viral entry into the cell[121]. However, existing work shows that inhibition of proteases cathepsin B and L, and TMPRSS2, significantly attenuates viral entry of SARS-CoV and SARS-CoV-2 into Vero cells[122], Nevertheless, the consistent, diet-induced enhancements in ACE2 expression in the lungs and tracheas of male mice provides a plausible mechanism whereby obesity facilitates a higher viral load and more severe outcomes[113]. It is important to note that female mice on a chow-diet exhibited similar lung ACE2 expression levels as male obese mice, and significantly more ACE2 than chow-fed male mice[113]. However, this is not consistent with human sequencing data that shows there is no difference in ACE2 expression in lungs based on sex[123,124]. Similarly, Batchu et al. observed no change in ACE2 or TMPRSS2 gene expression in the lungs of diabetic, HF-fed mice; however, the content of these two proteins increased significantly in this tissue[125]. In this context, this discrepancy can be consolidated by the fact that ACE2 protein availability is likely enhanced by post-transcriptional modifications, which is not accounted for in gene expression data[125]. Thus, although Sarver and Wong reported higher levels of ACE2 in chow-fed females when compared to chow-fed males, it is still unclear whether this translates to differences in protein content[113]. Nevertheless, an important finding from their study is that HF feeding does not change ACE2 gene expression in females, whereas in males, as previously stated, it causes an upregulation in lung ACE2 levels[113]. This sexual dimorphism in response to a HF diet could explain why males are more susceptible to severe COVID-19 outcomes[124]. Furthermore, the identification of obesity as a major risk factor has generated great

interest in the identification of therapeutic tools that could potentially treat obesity, its related metabolic disorders, and more recently, the risk for COVID-19-related disease.

2.5. The Ketogenic Diet (KD), Ketosis and Ketone Body Metabolism

The KD is rich in fat and drastically limited in carbohydrates[126]. Under these dietary conditions, hepatic ketone body synthesis is enhanced in a process known as ketogenesis[126] that leads to a state of nutritional ketosis. Human ketonemia is normally <0.1mM[127], whereas the KD elevates this to >0.5 mM[15,127]. A restriction in dietary carbohydrate intake leads to reduced blood insulin levels and enhanced WAT lipolysis[126]. Consequently, NEFAs travel to the liver and undergo β-oxidation and conversion into acetyl-CoA molecules[126]. In individuals consuming a KD, FA supply to the liver overwhelms the oxidative capacity of hepatocytes, leading to a buildup of acetyl-CoA molecules, which are eventually diverted to ketone body synthesis (Figure 10)[126].

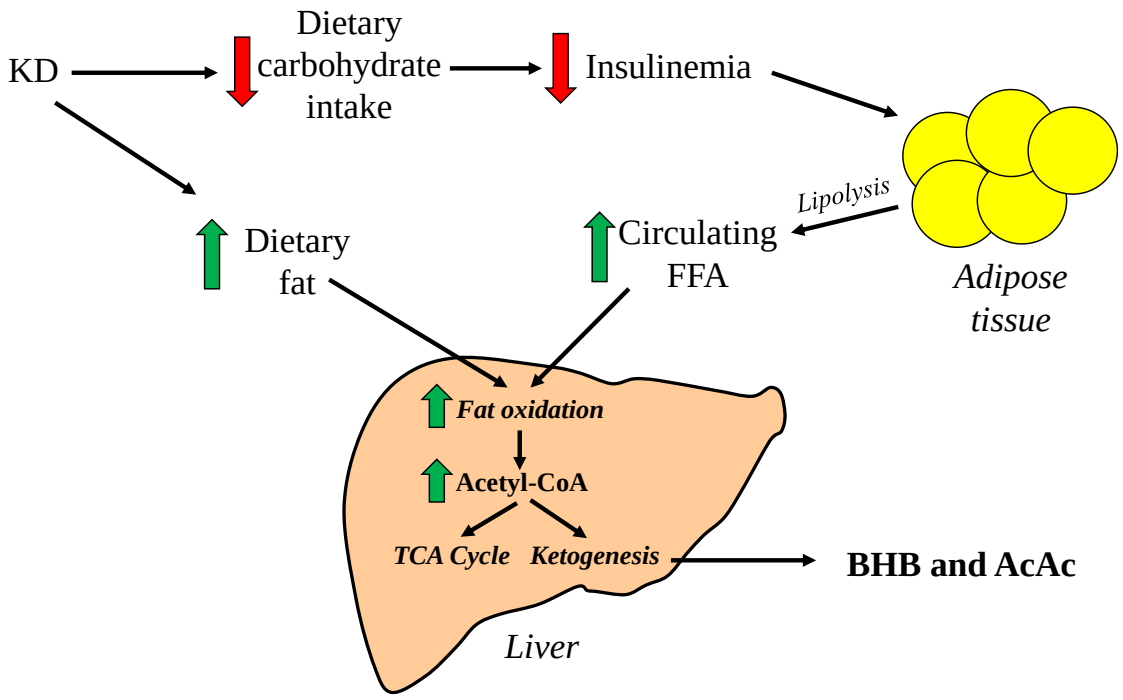

Figure 10: Schematic illustration of dietary-induced activation of ketogenesis.

First, acetyl-CoA is combined with another to form acetoacetyl-CoA, a reaction that is catalyzed by acetyl-CoA acetyltransferase (ACAT1)[127]. Next, acetoacetyl-CoA is processed by 3-hydroxy-3-methylglutaryl-CoA synthase 2 and (HMGCS2) and HMG-CoA lyase (HMGCL), in sequence, to produce HMG-CoA and acetoacetate (AcAc), respectively[127]. AcAc can then exit the mitochondrion, or it can further be processed into β-hydroxybutyrate (βHB) by βHB dehydrogenase 1 (BDH1) before leaving the organelle[127]. AcAc and βHB can then enter the circulation and access extrahepatic tissues where they may be metabolized[126]. Ketogenesis is suppressed by insulin and enhanced by glucagon[128]. Thus, fasting and diabetes also significantly increase ketogenesis[127]. Importantly, ketone bodies themselves trigger a negative feedback mechanism to attenuate further FA release from the AT and ketosis[129,130]. In fact, incubation of adipocytes with ketones significantly enhances the suppressive effect of insulin on lipolysis and increases glucose uptake with submaximal insulin stimulation[130]. Nevertheless, KD-induced ketogenesis has sparked interest in the diet for several beneficial health effects, including as an energy substrate for ketolytic tissues[61,127,128]. Cardiac and cerebral tissues, as well as skeletal muscle, oxidize ketones to produce energy[127,128,131]. To perform ketone oxidation, these tissues must import ketone bodies using monocarboxylic acid transporter (MCT)[127,128]. In the mitochondria, βHB is converted to AcAc by BDH1 and AcAc is then converted to acetoacetyl-CoA by 3-oxoacid-CoA transferase 1 (OXCT1)[127]. OXCT1 is a rate-limiting enzyme for ketone body catabolism and is highly expressed in tissues such as the heart, brain and kidney[132]. In contrast, the liver, which is ketogenic[127], has a low expression of Oxct1 and exhibits low enzymatic activity of this protein[132]. OXCT1-formed acetoacetyl-CoA is modified into acetyl-CoA by ACAT1 (Figure 11)[127], whereby this substrate can enter the Krebs cycle to produce intermediates for the ETC and ATP production[50].

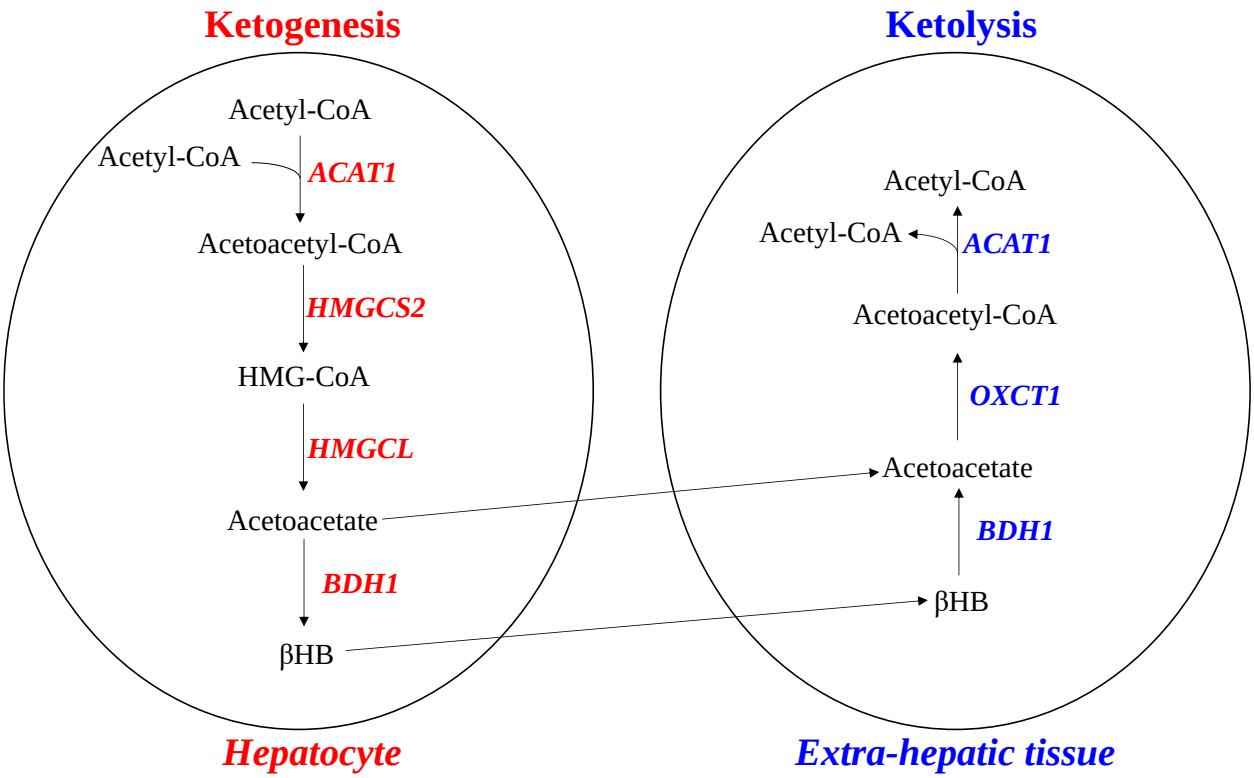

Figure 11: Schematic illustration of ketogenic and ketolytic pathways. Acetyl-CoA is combined with another to form acetoacetyl-CoA, a reaction that is catalyzed by acetyl-CoA acetyltransferase (ACAT1). Next, acetoacetyl-CoA is processed by 3-hydroxy-3-methylglutaryl-CoA synthase 2 and (HMGCS2) and HMG-CoA lyase (HMGCL), in sequence, to produce HMG-CoA and acetoacetate, respectively. Acetoacetate can exit the mitochondrion, or it can further be processed into β-hydroxybutyrate (βHB) by βHB dehydrogenase 1 (BDH1) before leaving the mitochondrion. AcAc and BHB can then enter the circulation and access extrahepatic tissues where they may be metabolized. In extra-hepatic tissues βHB is converted to AcAc by BDH1 and AcAc is then converted to acetoacetyl-CoA by 3-oxoacid-CoA transferase 1 (OXCT1). OXCT1-formed acetoacetyl-CoA is finally modified into acetyl-CoA by ACAT1.

2.5.1. The Origins of the KD and Initial Clinical Applications

Ketones were first identified in diabetic patients and were considered deleterious due to accumulation of circulating ketones under conditions of diabetic ketoacidosis[133]. Interestingly, before insulin was discovered, low-carbohydrate diets were recommended to individuals with T1D [134]. This was one of the few limited options for the management of glycaemia in this population[134]. However, in the 1920's, the clinical understanding of ketones shifted significantly with its application to treat epileptic seizures[133]. This was led by Peterman who devised a ketogenic diet

that was 4 parts fat and 1 part carbohydrate and protein (in grams)[133,135]. This diet is known as the 4:1 KD, or the Peterman KD, and it became the standard intervention for the reduction of epileptic seizures in patients[133,135]. Several decades later, the beneficial neurological effects of the high-fat, low carbohydrate diet was attributed to ketones[133] and the stabilizing effect of this metabolite on brain function[131,133].

2.5.2. The KD in Obesity and Metabolic Disorders

In the last few decades, the KD has re-emerged as an intervention for several conditions. One of the most common applications is obesity and T2D, where the KD has demonstrated success in controlling glycaemia and reversing these conditions[15]. In fact, Walton et al. reported an attenuation in BMI, body weight and blood pressure, and an improvement in glycaemic control in obese women fed a KD for 90 days[15]. In the study by Walton et al., these changes were expressed relative to baseline in obese subjects[15]. However, evidence exists to highlight the superior effect of the KD relative to the more commonly prescribed low-fat diet. This was highlighted in a study by Yancy et al. where healthy subjects on a KD lost significantly more weight, and exhibited a decrease in blood TG, when compared to the low-fat diet group[14] In addition to improving the aforementioned physiological parameters, the KD was more effective than the recommended low-glycemic index diet at reducing the required medications in diabetic subjects. Rodent studies exhibit similar effects of the KD on metabolic health and outcomes. In fact, a recent study from our lab found that the KD exerted an anti-steatotic effect in rat livers by reducing intra-hepatic lipid accumulation and preserving insulin sensitivity, when compared to the HF-sucrose-enriched (HFS) rats[11]. Moreover, Roberts et al. highlighted the longevity-promoting effect of the KD in mice, and show a preservation in whole-body insulin responsiveness with this diet[136]. Interestingly, several studies, including human and rodent studies, report that the KD impairs glucose

tolerance[60,136,137]. In mice, this has been attributed to an apparent reduction in pancreatic β-cell mass[137], which could hinder the insulin-mediated clearance of circulating glucose following the absorption of a bolus of this substrate. These effects, however, are not indicative of disease[60]. Instead, KD-induced glucose intolerance is reflective of a low systemic demand for glucose clearance and a corresponding adaptation that reflects this[60,61]. Another notorious feature of the KD is that, relative to the obesogenic diet, it attenuates the expression of inflammatory markers[11,138].

2.5.3. KD and Inflammation

In a rat model of osteoarthritis, the KD significantly reduced NLRP3 inflammasome content, as well as its activating proteins in the knee-joint[138]. This is significant, given that activation of the NLRP3 inflammasome triggers an inflammatory response and the recruitment of inflammatory cytokines[138]. Indeed the authors of this study also observed a significant attenuation in knee joint levels of the inflammatory cytokines IL-1β and IL-18[138]. This anti-inflammatory effect can be attributed to the ketone body βHB[139]. In fact, in mouse bone marrow-derived macrophages (BMDM), the activation of the NLRP3 inflammasome was attenuated by βHB treatment in a dose-dependent manner[139]. Importantly, inactivation of this inflammasome was not achieved with AcAc treatment, which points to βHB as the specific ketone body underlying inflammatory regulation[139]. KD-mediated anti-inflammatory effects were also reported in the brain and have significant implications for neurodegenerative disorders[140].

The use of the KD for the preservation of cognitive function and brain health originated in its effective treatment of epilepsy[133,140] and has prompted investigations into its application for neurodegenerative disorders, including dementia. Alzheimer's disease (AD) is the most common form of dementia and is characterized by neuronal instability, cognitive impairment and memory

loss[140]. These effects are commonly attributed to plaque accumulation in the brain but are also implicated by neuroinflammation[140]. Recently, the KD has emerged as a potential preventative treatment for this condition due to its anti-inflammatory effect in the brain[140]. This was highlighted in a mouse model of AD fed a KD, where the contents of inflammatory cytokines were significantly attenuated in the cortex and hippocampus of the brain[140]. These mechanistic adaptations were linked to improvements in learning and memory in KD-fed mice with AD[140]. Because these beneficial anti-inflammatory effects have been attributed to βHB[141], this has sparked interest in exogenous ketone ingestion in place of a KD.

2.5.4. Ketone esters

Ketone esters (KE) are compounds that can be injected or ingested orally[142] and provide a rapid increase in ketonemia[142,143]. This method of increasing blood ketone levels provides an alternative solution for individuals struggling to adhere to a KD[143]. Similar to the KD, KE also induce a potent anti-inflammatory effect[143]. In a recent study, Soni et al. tested this using three groups of mice: a control group and two lipopolysaccharide (LPS) injected groups to induce sepsis[143]. In one of the two LPS groups, mice were fed ketone esters for three days prior to the LPS injection[143]. Remarkably, KE treatment significantly attenuated circulating levels of inflammatory cytokines and decreased inflammatory gene expression in cardiac and hepatic tissues[143]. These data suggest that KE effectively suppress systemic inflammation and exert a protective effect in various organs[143]. With respect to glucose homeostasis, KE ingestion has been reported to not cause any adverse effects and was effective in reducing glycaemia and glycated hemoglobin (HbA1C) levels in T2D patients[144].

2.5.5. Effects of the KD in AT

The consumption of a KD has been shown to attenuate visceral AT mass in humans and has produced promising metabolic and anti-inflammatory effects in this tissue[145,146]. This was demonstrated by Asrih et al. who fed mice either a control or KD for 4 weeks and observed that KD-fed rats exhibited significantly lower expressions of IL-6, TNFα and NLRP3[146]. Moreover, the KD attenuated the expressions of Lpl and Cd36, which are involved in lipid storage, and increased the gene expression of Ucp1[146]. In this context, KD-feeding appears to enhance browning and attenuates inflammation in visceral AT. The anti-inflammatory effects of the KD were further investigated by Ryu et al. in the context of SARS-Cov-2 infection severity[145]. In this study, mice were fed either a control diet or a KD for 5 days prior to being inoculated with a mouse-compatible CoV[145]. Remarkably, the KD enhanced the probability of survival in younger mice inoculated with a fatal dose of the virus, although this measure was not significantly different between the two dietary groups in old mice[145]. Moreover, a lower dose of the virus was used to assess CoV-induced inflammation 7 days following inoculation in older mice[145]. Consistent with previous findings, the authors reported an attenuation in inflammation in lung, visceral AT and hypothalamus samples from KD-fed rats[145]. Together, these results support the effectiveness of the KD in suppressing inflammation and enhancing browning in visceral fat depots.

The KD also appears to induce browning in the Sc Ing WAT. Douris et al. performed a comprehensive analysis of markers of browning in this depot and found that Ucp1, Cpt1b and other genes were upregulated with a KD[147]. Interestingly, merely supplementing animals fed a HF, high sugar (HFHS) diet with ketones significantly decreased Ing and epididymal (Epid) WAT masses[148], the latter being a model for visceral AT[43]. Thus, KD-induced browning[146,147] could potentially be enhancing energy-expending pathways in AT, leading to a reduction in its mass.

In BAT, the KD has been demonstrated to enhance UCP1[147] content and proteins of the ETC[149]. These effects are largely attributable to the increased sympathetic nerve output to the BAT under conditions of KD-feeding[147,149]. In fact, βAdR deficiency significantly attenuated BAT UCP1 protein content in KD-fed mice and impaired KD-induced weight loss[147]. Thus, the KD plays a prominent role in SNS-mediated activation of the BAT and may also enhance whole-body energy expenditure through the activation of this tissue. In line with this, KE upregulated contents of UCP1, proteins of the ETC and PPARγ and PGC-1α in BAT[150]. Importantly, PGC-1α is the inducing factor for mitochondrial biogenesis, even commonly being referred to as the master-regulator of mitochondrial biogenesis[151]. PGC-1α enhances the expression of nuclear respiratory factor 1 (NRF1), which, in turn increases the expression of mitochondrial transcription factor A (TFAM)[151]. TFAM then acts on the mitochondrial DNA (mtDNA) to upregulate the expression of mitochondrial proteins and promote mitochondrial biogenesis[151]. This likely underlies the KE-mediated enhancement in mitochondrial biogenesis in BAT[150]. Moreover, these effects were likely driven by SNA to the brown fat[150], and suggest that both KE and KD-feeding promote similar effects in BAT that are mediated by similar mechanisms.

Importantly, AT does not exist in isolation and is one component of a larger integrative system. As mentioned earlier in the review, one physiological role of AT is to function as an energy reservoir, storing energy under conditions of energy surplus and releasing it as FA under conditions of energy demand[4]. One major fate for these FAs is oxidation by skeletal muscle, making it an important focus in the context of whole-body substrate partitioning and energy homeostasis[18].

2.6. Skeletal muscle

Skeletal muscle comprises approximately 40% of body mass in humans and houses the majority of the body's proteins[152]. Muscles differ significantly from one another based on fiber-

type compositions[129]. Several systems of characterization exist, including the colour of the muscle (red or white), speed of twitch, fatigability, oxidative or glycolytic capacity, among others[152]. For the purpose of this dissertation, muscle-fibers will be named based on their staining appearance and their classification type: Type I and Type II fibers[129,153]. Type I fibers are oxidative, slow-twitch fibers that are resistant to fatigue[129,152]. Type II fibers can be further characterized based on subtypes Type IIA and Type IIB, which are fast oxidative and fast glycolytic, respectively[129,152], as well as fiber type IIx, which are fast glycolytic[129] and an intermediate between IIA and IIB[154]. In this context, muscles with a higher oxidative capacity would be composed predominantly of Type I and IIA fibers, whereas more glycolytic muscles would contain more Type IIB and IIX fibers[12,155,156]. In rats, the soleus (Sol), extensor digitorum longus (EDL) and epitrochlearis (Epit) muscles can be used as models of oxidative, mixed-fiber type and glycolytic muscles, respectively[12,157,158]. Regardless of fiber-type composition, skeletal muscles develop insulin resistance under conditions of DIO[12].

2.6.1. Insulin resistance in skeletal muscles

Skeletal muscles account for 85% of insulin-stimulated glucose uptake following a meal[159]. This makes muscle a crucial tissue for whole-body glycaemic control[12]. Insulin-stimulation induces a similar signaling cascade as in adipocytes that culminates with the translocation of the GLUT4 vesicle to facilitate glucose entry into the muscle cell[31]. Glucose taken up by muscles goes through glycolysis and oxidation[18], but the majority of it is diverted to the synthesis of glycogen[160,161]. Glycogen synthesis is enhanced by insulin-stimulation, whereby the activation of AKT leads to the phosphorylation and inhibition of glycogen synthase kinase (GSK)[160]. GSK, when active, inhibits glycogen synthase (GS), which drives glycogen synthesis[160]. Thus, the

inhibition of GSK disinhibits GS and promotes the storage of the incoming glucose as glycogen (Figure 12)[160].

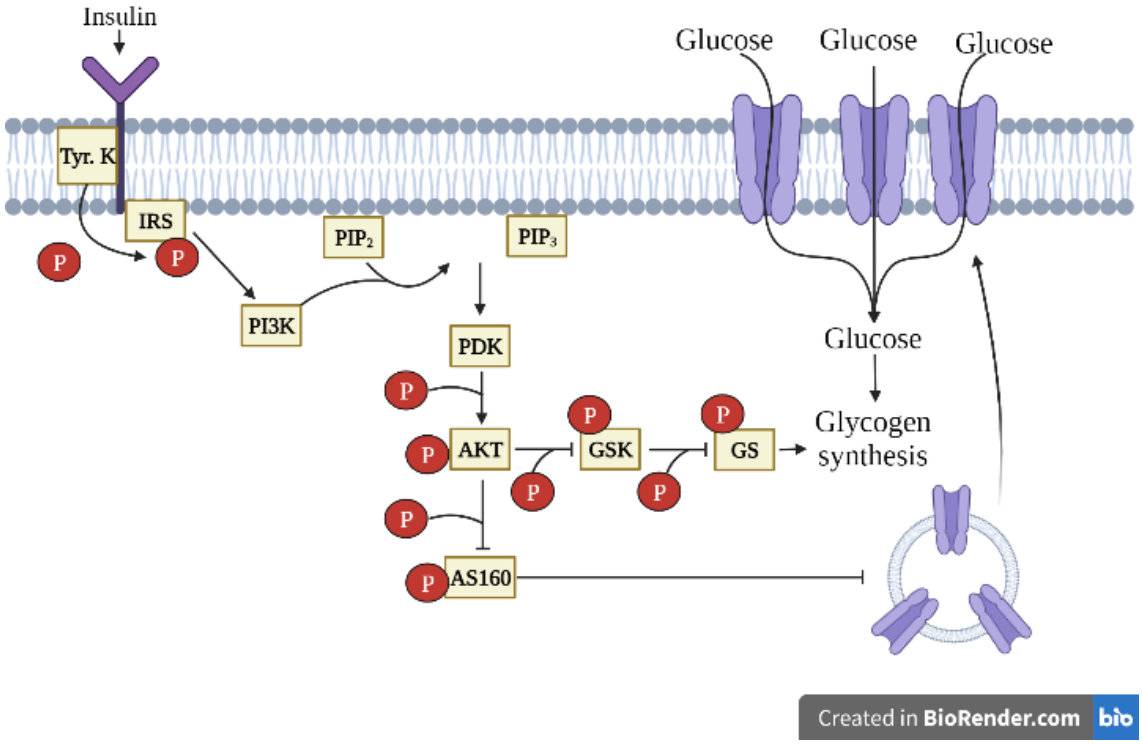

Figure 12: Schematic illustration of insulin signaling pathways in skeletal muscles. Insulin-stimulation induces a similar signaling cascade as in adipocytes that culminates with the translocation of the GLUT4 vesicle to facilitate glucose entry into the muscle cell. The majority of the glucose taken up by the muscle cell is diverted to the synthesis of glycogen[160,161]. Glycogen synthesis is enhanced by insulin-stimulation, whereby the activation of AKT leads to the phosphorylation and inhibition of glycogen synthesis kinase (GSK). GSK, when active, inhibits glycogen synthase (GS), which drives glycogen synthesis. Thus, the inhibition of GSK disinhibits GS and promotes the storage of the imported glucose as glycogen.

Under conditions of obesity, insulin-stimulated glycogen synthesis, glucose oxidation and lactate production are suppressed[12,158]. The underlying mechanisms of DIO-mediated insulin resistance in skeletal muscles have been extensively studied. One proposed mechanism is reactive oxygen species (ROS) production in the skeletal muscles of obesogenic diet-fed rats, which can be generated by NADPH oxidase 2 (Nox2), the major isoform of this protein in muscle[162]. This was supported by evidence showing that Nox2 deficiency rescued insulin-stimulated AKT phosphorylation and GLUT4 translocation in the gastrocnemius muscles of mice fed a HFD[162]. In

line with this, C2C12 myotube treatment with the ROS H_2O_2 or FA significantly attenuated insulin-stimulated glucose uptake and AKT phosphorylation, whereas treatment with the antioxidant catalase[157] preserved these functions[162]. Other mechanisms underlying insulin resistance in muscle include inflammation and the accumulation of lipid intermediates[12]. However, recent studies show that distinct mechanisms mediate these effects in muscles with different fiber-type compositions[12,158].

The accumulation of lipid intermediates, including DAGs, have been linked to protein kinase C (PKC) mediated insulin resistance in skeletal muscle[5,12,163]. DAG, namely the 1,2-DAG isoform[5], accumulates in muscle under conditions of DIO[5,12]. This occurs despite the elevation in FA oxidation in skeletal muscles fed a high-fat, sucrose-enriched diet (HFS), indicating that the elevated lipid content of the diet exceeds the muscles' capacities to oxidize fat[12]. DAG accumulation activates PKC, translocating it to the membrane[12]. Thereafter, PKC interferes with the insulin signaling pathway, causing insulin resistance[5]. In line with this, PKC activation was enhanced in the Sol and EDL muscles of rats fed a HFS diet and was linked to the impairment in insulin-stimulated glycogen synthesis[12]. Conversely, in the Epit muscle, PKC activation was not increased by the HFS diet and insulin resistance was instead associated to the upregulation in inflammatory markers in this tissue[12]. This provides evidence that mechanisms of insulin resistance are not uniformly expressed in all muscles and instead are displayed in a fiber-type specific manner[12]. Nevertheless, limiting ectopic lipid accumulation and inflammation appears to be crucial to prevent insulin resistance in skeletal muscle and carries implications for whole-body glucose homeostasis. These beneficial effects could be achieved through the KD.

2.6.2. KD in skeletal muscles

KD-feeding elevates mitochondrial mass[164], mitochondrial proteins and PGC1α levels, and AMPK activation in gastrocnemius muscle[165]. These adaptations could support the shift from glucose to fat metabolism in this muscle[166]. In addition to mitochondrial biogenesis, the KD also enhances the efficiency of mitochondria to generate ATP from fat[167]. KD-induced metabolic adaptations in skeletal muscle mitochondria are promising in the context of combating insulin resistance[167]. However, more recently, researchers have proposed a beneficial role for these metabolic alterations in the context of exercise[61]. In exercising individuals, substrate utilization for energy production is determined by the intensity of the exercise[168]. At rest and with lower exercise intensities, fat is considered to be the primary source of fuel for skeletal muscles[168]. As intensity increases, the utilization of carbohydrates for energy production is enhanced, decreasing the reliance on fat. At approximately 60-65% maximum intensity, carbohydrates surpass fat in their relative contribution to energy production[168]. This alteration in substrate preference is enhanced progressively with increasing intensity, and at approximately 85-90% maximum exercise intensity energy production is almost exclusively derived from carbohydrates[168].

The crossover point, however, is not fixed and can be altered using a number of interventions, including dietary macronutrient manipulation[168]. As mentioned earlier in this review, metabolic substrate preference in tissues is determined by the relative availability of the specific macronutrients, where glucose or FA oxidation will suppress oxidation of one another[56,58,169]. In individuals consuming a high carbohydrate, low fat diet, energy is derived predominantly from carbohydrates, even at lower intensities, and at no point is fat equal to or above carbohydrates in its contribution to energy production[168]. Conversely, the consumption of a HF, low carbohydrate diet increases peak fat oxidizing capacity and shifts the crossover point to

approximately 85% of maximal exercise intensity[168], delaying the reliance on carbohydrates to higher intensities. This could be attributed to improved mitochondrial function[168] and could serve to spare muscle glycogen[61].

It is important to consider that ketones are also metabolic substrates and substitute glucose in many tissues for energy production, including muscle[61,169]. The shift of metabolism to fat and ketones preserves carbohydrate and muscle glycogen and may potentially enhance endurance exercise performance through sparing this energy reserve[61]. In line with this, Cox et al. demonstrated that ingestion of a KE drink suppressed carbohydrate utilization during exercise and shifted metabolism to ketones[169]. Remarkably, this shift occurred even under anaerobic exercise conditions where glycolytic drive is typically enhanced[169]. This metabolic effect can be at least partially attributed to an oxidative shift in fiber-type composition under KD conditions[170]. Interestingly, to some extent, the KD-induced shift in metabolic substrate preference renders individuals glucose intolerant[60]. This was exhibited in cyclists on a KD who did not clear glucose as efficiently following the ingestion of a bolus of glucose[60], which was attributed to the attenuation in GLUT4 and IRS protein contents in the vastus lateralis muscle[60]. Although this may be suggestive of whole-body metabolic dysregulation and metabolic inflexibility towards carbohydrates, it is likely an adaptation to the low dietary availability of this substrate rather than disease[60].

When assessing the existing literature surrounding KD-induced metabolic adaptations in skeletal muscle, it is important to consider that the observed effects are dependent on the specific muscles being studied. For instance, studies showing that PGC-1α content was unaltered by the KD in Sol[165], EDL[170], or quadriceps[59] muscles, are contrasted by findings of elevated PGC-1α in the gastrocnemius of KD-fed animals[165]. Similarly, Fukazawa et al. reported an increase in OXCT

protein content in Epit with a KD[171], whereas Shimizu et al. demonstrated that the expression of this ketolytic enzyme was attenuated with KD-feeding in the gastrocnemius[166]. Therefore, fiber-type specific differences exist in the metabolic adaptations in skeletal muscles under KD conditions and may mediate different effects in metabolic flexibility accordingly. This warrants an investigation comparing the effects of the KD on muscles with distinct fiber-type compositions and is the focus of one of the chapters in this dissertation.

An additional potential limitation in several existing studies using the KD is the macronutrient composition of the diet. Specifically, protein contents are considerably lower in the KD group than in the control group, including KDs with protein contents ranging from 4.8-10% [137,164,172]. The differences in protein content significantly impact muscle mass and metabolism[172], affecting the interpretation of the effects of the KD in this tissue. In line with this, Huang et al. used a higher protein content for their KD (16.1% kcal), which they posited was a more representative protein content for a rodent diet, and observed that protein matching a KD with a control diet elicited an increase in body weight, fat mass and lean mass in the KD group, relative to control[59]. Conversely, Asrih et al. used a KD that was lower in protein than the control diet and observed a decrease in body weight, an increase in fat mass, and a significant decrease in lean mass[146]. These observed differences with the KD may not necessarily be attributable to the high-fat, low carbohydrate profile that is typical of the diet, but rather likely due to differences in protein content. This highlights the important of macronutrient composition for the interpretation of KD-induced effects.

Reducing protein in the KD, however, is beneficial for inducing a more robust ketogenic response[173]. Bielohuby et al. demonstrated this by feeding rats three KDs with varying amounts of protein, while maintaining carbohydrates constant[173]. Protein content in the diet was inversely

proportional to ketonemia, as well as liver expression of HMGCL and PGC-1α[173]. The attenuated ketogenic response with elevated protein levels can be attributed to the gluconeogenic and insulinotropic effect of amino acids[173,174].

2.6.3. KD and Gluconeogenesis

Under conditions of starvation or limited dietary carbohydrates, ketogenesis is initiated in the liver to produce ketones as an alternative metabolic substrate to glucose[127,133]. However, ketones do not substitute glucose in all cells and tissues, and therefore, the maintenance of glycaemia within a homeostatic physiological range is crucial[174]. This is achieved through a process known as gluconeogenesis, where the liver synthesizes glucose from extrahepatic sources of glycerol, lactate, pyruvate and select amino acids[174]. Carbohydrate restriction enhances the release of these substrates, driving hepatic gluconeogenesis[126,129,174]. Gluconeogenesis begins with the conversion of lactate and amino acids to form oxaloacetate, which is converted to PEP by PCK[174]. Reversal of the glycolytic pathway then yields glucose from these precursors[174]. Glycerol-derived glucose production occurs upstream in the glycolytic pathway, where this substrate is phosphorylated to G3P by GyK, followed by a conversion to DHAP by GAPDH[129]. The DHAP is thereafter subject to 'reverse glycolysis' to produce glucose[174]. This mechanism serves to maintain glycaemia under conditions of KD or starvation[129].

Importantly, a KD with a higher protein content could elevate amino acid-mediated gluconeogenesis, provoking a higher secretion of insulin from the pancreas[31], which could act to inhibit ketosis[129]. Accordingly, animals fed a KD with a lower protein content significantly decreased insulinemia relative to chow-fed rats, whereas higher protein KDs did not reduce this parameter relative to control[173]. Again, this highlights the importance of macronutrient composition in the determination of metabolic outcome.

In consideration of the literature and existing gaps, it is apparent that further research is required into the effects of the KD on substrate partitioning in skeletal muscles with varying fiber-type compositions. This would enhance our understanding of dietary macronutrient manipulation on glucose, fat, and ketone metabolism in oxidative and glycolytic muscles. Moreover, it is warranted that the investigation of these effects be conducted using a normal protein KD to eliminate protein content as a confounding variable and influence on muscle metabolism.

Chapter 3: Objectives and Hypotheses

This dissertation includes five projects that collectively aim to address the research objectives. They include:

Study 1 (Chapter 4): In rodents, BAT mass is significantly elevated with a HFS diet[175]. Despite the diet-induced increase in this thermogenic tissue, HFS-fed animals develop obesity[175]. This can be attributed to the suppressed activity of BAT under conditions of obesity[75]. However, little is known regarding the underlying mechanisms for the diet-induced decrease in thermogenic capacity as well as substrate partitioning in brown adipocytes with HFS feeding. Therefore, the objectives of the first study were:

1) To investigate the effects of HFS-feeding on glucose and fat oxidation in isolated brown adipocytes.
2) To determine alternative metabolic fates for glucose and fat in the BAT of HFS-fed rats.
3) To study underlying mechanisms mediating the suppression in BAT DIT under conditions of obesity.

Hypotheses:

1) The HFS diet will increase the protein contents of proteins involved in oxidative capacity, including CPT1B, PGC-1α and UCP1. Despite this, uncoupled oxidative capacity will be suppressed in the brown adipocytes of HFS-fed rats.
2) Glucose and FA will be diverted to lipogenesis, underlying an increase in adipocyte size. This will be supported by an upregulation in the gene expression of FA uptake machinery *Lpl and Cd36*, as well as an elevation in glycerol and palmitate incorporation into lipids.

3) The suppressed thermogenic activity of the BAT will be linked to an attenuation in lipolytic capacity, including decreased protein contents of TH, β3AdR, ATGL and HSL phosphorylation.

Study 2 (Chapter 5): The KD has previously been reported to enhance browning in visceral[146] and Sc WAT[147] and to increase UCP1 and thermogenic capacity in BAT[147,149]. These effects are promising for the therapeutic intervention of obesity. However, it is unclear whether these KD-induced adaptations translate to functional outcomes in these tissues. This includes BAT thermogenic capacity, as well as UCP1-independent mechanisms of energy expenditure in WAT, such as TAG recycling. Thus, the **objectives** of the first study were:

1) To determine whether the KD would enhance uncoupled FA oxidation and thermogenic machinery in BAT.
2) To examine the effects of the KD on UCP1 content and TAG recycling machinery in WAT.

Hypotheses:

1) Despite both diets inducing an increase in BAT UCP1 content, the HFS and KD will attenuate and enhance uncoupled fat oxidation, respectively in BAT. This will be accompanied by KD-induced elevations in other thermogenic proteins, including PGC-1α, β3AdR, GyK and ATGL.
2) The KD will enhance UCP1 content in Sc Ing WAT, and upregulate TAG recycling machinery, which will contribute to reduce fat mass in KD-fed rats. The upregulation in TAG recycling will be driven by the KD-mediated preservation of lipolysis and lipogenesis in visceral and Sc WAT, as well as the enhanced content of GyK protein, which will support this energy-dissipating pathway.

Study 3 (Chapter 6): The KD is known to promote beneficial metabolic and anti-inflammatory effects in AT[146], however, the effects of the KD on RAS components in WAT and BAT has not been fully elucidated. In this context, the **objective** of the first study was:

1) To compare the abundance of individual RAS proteins in WAT and BAT and to investigate AT depot-specific effects of the HFS and KD on RAS components in these tissues.

Hypothesis:

1) The HFS diet will enhance the classical arm of the RAS in WAT and BAT, whereas the KD will upregulate the counterregulatory arm. In HFS-fed rats, this will include an attenuation in ACE2 protein content and MasR expression, and an upregulation in ACE1 and AT_1R in WAT and BAT, whereas the opposite would be observed with KD-feeding.

Study 4 (Chapter 7): Diet-induced alterations in inflammation, and shifts in the RAS profiles of lung and heart tissues could impact susceptibility to ACE2-mediated SARS-Cov-2 infection. This has not been investigated in the context of the KD. Thus, the **objectives** of this study were:

1) To investigate the effects of the HFS and KD on viral entry proteins ACE2 and TMPRSS2 in lung and heart, as well as other RAS proteins
2) To determine the effects of the HFS and KD on the expression of inflammatory markers in pulmonary and cardiac tissues.

Hypotheses:

1) The HFS diet would increase ACE1, AT_1R as well as ACE2 in the heart and lung tissues, whereas the KD would decrease the contents of these proteins and confer a protective effect against potential viral infection.

2) HFS-induced alterations in lung and heart RAS components would shift the RAS to the classical inflammatory arm in these tissues, causing an upregulation in the expression of inflammatory markers. Conversely, the KD would attenuate the contents of classical RAS components and attenuate inflammation in pulmonary and cardiac tissues.

Study 5 (Chapter 8): The reported effects of the KD on skeletal muscle glucose, fat and ketone metabolism vary from study to study, due primarily to differences in muscles being examined. This points to an apparent fiber-type specific response to the KD. Thus, the **objectives** of this study were:

1) To compare the effect of the HFS and KDs on FA oxidative capacity in oxidative and glycolytic muscles.
2) To determine whether the KD could enhance ketolytic capacity in muscles with distinct fiber-type compositions.
3) To investigate the effects of the HFS and KD on insulin-stimulated glucose metabolism in oxidative and glycolytic muscles.

Hypotheses:

1) The KD would enhance FA oxidation, PGC-1α and TFAM in oxidative and glycolytic muscles, relative to the HFS diet.
2) KD-feeding would also upregulate ketolytic machinery, including OXCT and ACAT1 in muscles with distinct fiber-type compositions.
3) Despite the shift to ketones and FAs, the KD would preserve insulin-stimulated glycogen synthesis, lactate production and glucose oxidation in Sol, EDL and Epit muscles.

Study 6 (Chapter 9): In AT, the effects of adiponectin on metabolic function are poorly studied and warrant further investigation into its potential application for AT-mediated regulation of FA and glucose metabolism. In this context, the **objective** of the final study was:

1) To determine whether treatment with ALY688, an adiponectin mimetic, would increase AMPK signaling by enhancing the phosphorylation of AMPK, ACC and p38 in adipocytes incubated with ALY688.
2) To assess the effects of ALY688 on glucose and FA metabolism in visceral and Sc WAT, including the effects of this compound on glucose uptake, lipogenesis, lipolysis, glucose oxidation and FA oxidation.

Hypotheses:

1) ALY688 would increase AMPK, ACC and p38 phosphorylation in Sc Ing and Epid fat depots through activation of the AdipoRs.
2) ALY688 treatment would enhance insulin-stimulated glucose uptake, lipogenesis and glucose oxidation, as well as FA oxidation in adipocytes from visceral and Sc WATs.

Chapter 4: An obesogenic diet impairs uncoupled substrate oxidation and promotes whitening of the brown adipose tissue in rats

Daniel Da Eira[1], Shailee Jani[1] and Rolando B. Ceddia[1]

[1]Muscle Health Research Centre – School of Kinesiology and Health Science, York University, North York, ON, Canada.

This manuscript was published in ***The Journal of Physiology***. ***The Journal of Physiology's*** copyright policies regarding the reproduction of published manuscripts allows the authors to include the manuscript, without charge, in published academic dissertations.

Da Eira D, Jani S, Ceddia RB. An obesogenic diet impairs uncoupled substrate oxidation and promotes whitening of the brown adipose tissue in rats. *J Physiol*. 2023;601(1):69-82. doi:10.1113/JP283721.

Statement of Labour

The work in this study was performed by DD. DD fed the rats the SC, and HFS diet and weighed the animals over the course of the feeding period. DD also extracted tissues and performed the functional assays, Western blotting and qPCR experiments outlined in this manuscript. Moreover, DD collected and analyzed the data, prepared figures and wrote and revised the manuscript. DD was funded by the Alexander Graham Bell – Canada Graduate Scholarship (Doctoral). Due to the length of the study and the logistics of tissue extraction procedures, SJ assisted in the feeding, measurements of body weight, tissue extraction, adipocyte isolation and the performance of some of the functional assays.

Dr. Rolando Ceddia is the principal investigator and was involved in all stages of this study. The work presented in this manuscript was funded by grants awarded to RBC, including the Discovery Grant from the Natural Science and Engineering Research Council of Canada (NSERC) and by infrastructure grants from the Canada Foundation for Innovation (CFI) and the Ontario Research Fund (ORF).

4.1. Abstract

Brown adipose tissue (BAT) is rich in mitochondria containing uncoupling protein 1 (UCP1) and dissipates energy through thermogenesis. However, even though BAT mass and its UCP1 content increase in rodents chronically fed a high-fat sucrose-enriched diet (HFS), marked expansion of adiposity still occurs in these animals, suggesting insufficient BAT-mediated HFS diet-induced thermogenesis. Thus, the objective of this study was to investigate the metabolic and molecular mechanisms that regulate BAT thermogenesis in HFS-induced obesity. To accomplish this, rats were fed either a standard chow or HFS for 8 weeks. Subsequently, glucose and fatty acid metabolism and the molecular mechanisms underlying these processes were assessed in freshly isolated primary BAT adipocytes. Despite increasing BAT mass and its UCP1 content, HFS diet reduced uncoupled glucose and palmitate oxidation in BAT adipocytes. It also markedly diminished tyrosine hydroxylase content and lipolysis in these cells. Conversely, glucose uptake, lactate production, glycerol incorporation into lipids, palmitate incorporation into triacylglycerol (TAG), phosphoenolpyruvate carboxykinase and glycerol kinase levels, and lipoprotein lipase and cluster of differentiation 36 gene expression were increased. In summary, a HFS diet enhanced glyceroneogenesis and shifted BAT metabolism toward TAG synthesis by impairing UCP1-mediated substrate oxidation and by enhancing fatty acid esterification in intact brown adipocytes. These adaptive metabolic responses to chronic HFS feeding attenuated BAT thermogenic capacity and favored the development of obesity.

4.2. Introduction

Despite variations in the availability of food/energy, body weight can be maintained relatively constant over long periods of time[176]. This is possible because under conditions of food abundance and overeating, the organism activates mechanisms that promote energy dissipation and attenuate weight gain. Conversely, under conditions of food scarcity and reduced intake, energy-sparing mechanisms are activated and oppose weight loss[177,178]. These adaptive metabolic responses are referred to as diet-induced thermogenesis (DIT), and play an important role in regulating body weight and whole-body energy homeostasis[177]. The ability to dissipate energy under conditions of overeating has been, at least partially, attributed to sympathetic nervous system (SNS)-mediated activation of brown adipose tissue (BAT)[177]. This is because UCP1 uncouples oxidative phosphorylation from ATP synthesis, resulting in the production of heat in a process known as non-shivering thermogenesis (NST)[38,177,179]. This process is triggered by the release of norepinephrine (NE) that binds to β-adrenergic receptors on brown adipocytes and promotes lipolysis within the cells. The release of fatty acids (FA) then leads to the activation of UCP1 that ultimately promotes mitochondrial uncoupling and NST in BAT adipocytes[38,180].

A role for BAT in DIT is supported by studies demonstrating that the mass of this tissue expands and its UCP1 content increases under diet-induced obesity (DIO) conditions in rats[89,175], and also by the fact that UCP1 ablation causes obesity in mice living at thermoneutrality[81]. However, despite evidence of tissue enlargement and increased UCP1 content in BAT, great expansion of adiposity still occurs in animals subject to DIO[89,175]. This suggests that NST is either insufficient to offset the energy surplus or that it might even be suppressed under conditions of chronic overeating. In both cases the magnitude of energy dissipation through NST in BAT would be limited, allowing for extensive growth of the white adipose tissue (WAT) to occur. In this

context, we have found that in the first and second weeks of feeding rats *ad libitum* a HFS diet, whole-body energy expenditure increased by ~14 and 11%, respectively, in comparison to standard laboratory chow (SC) diet-fed controls[175]. However, as HFS feeding continued through six additional weeks, whole-body energy expenditure no longer differed from that of SC diet fed rats[175], suggesting that an initial thermogenic response was mounted, but it was not sustained in rats chronically exposed to a HFS diet. Thus, it could be that NST in BAT was suppressed in a time-dependent manner, even though expansion of tissue mass and its UCP1 content persisted with continued overfeeding. This is consistent with recent human studies using ^{18}F-labeled fluorodeoxyglucose positron emission tomography-computed tomography (PET/CT) to measure BAT volume and its activity in lean and obese subjects[75]. In fact, it has been reported that after 5h of tolerable cold exposure (16^{o}C), activated BAT in obese men corresponded to only ~39% of that of lean counterparts, even though the total volume of BAT-containing depots was almost two-fold higher in the former than the latter group of subjects[75]. Thus, it was clear that BAT mass was increased in obese subjects, whereas its recruitment for thermogenesis was not[75]. We have previously reported that the HFS diet-induced increase in BAT UCP1 levels was accompanied by increased rates of fatty acid oxidation in homogenized BAT samples[77,89]. This was consistent with an enhanced machinery that consumes substrate under conditions of activated NST. However, any regulatory mechanisms that could potentially regulate substrate consumption in BAT adipocytes was lost in tissue homogenates. It could be that, in intact BAT adipocytes, cellular regulatory mechanisms shift the flux of substrate toward pathways that promote storage as opposed to energy dissipation. This could help explain why increased BAT tissue mass and UCP1 levels do not prevent adipose tissue expansion in rodents and humans under conditions of DIO. In this context, the objective of this study was to investigate the molecular and metabolic mechanisms that regulate

DIT in BAT under conditions of DIO and identify alterations in substrate flux that could lead to fat accumulation instead of energy dissipation. To this end, rats were fed either a SC or HFS diet for eight weeks. Subsequently, glucose and fat metabolism and the molecular mechanisms underlying these processes were assessed in freshly isolated intact BAT adipocytes. A detailed assessment of the metabolic pathways that regulate energy storage and dissipation in BAT adipocytes was performed. We found that despite increased tissue mass and UCP1 content in BAT, chronic exposure to HFS reduced UCP1-mediated glucose and fat oxidation, attenuated lipolysis, and shifted metabolism towards TAG synthesis/storage in intact brown adipocytes. Altogether, these molecular and metabolic changes induced by chronic exposure to an obesogenic HFS diet contributed to lower uncoupled substrate oxidation in BAT and favored the development of obesity.

4.3. Materials and Methods

Ethical approval – The investigators understand the ethical principles under which the journal operates and that their work complies with this animal ethics checklist. The protocol containing all animal procedures described in this study was specifically approved by the Committee on the Ethics of Animal Experiments of York University (York University Animal Care Committee, YUACC, permit number: 2021-03) and was performed strictly in accordance with the YUACC guidelines. All tissue extraction procedures were performed under ketamine/xylazine anesthesia (90 mg and 10 mg/100 g body weight, respectively), and all efforts were made to minimize suffering. Upon completion of tissue extraction, all animals were decapitated. All experiments in this study were carried out in compliance with the ARRIVE guidelines.

Reagents — Type II collagenase, isoproterenol, FA-free bovine serum albumin (BSA), palmitic acid, and the free glycerol determination kit were purchased from Sigma (St. Louis, MO, USA).

Oligomycin was purchased from Cayman Chemical (Ann Arbor, MI, USA). [1-^{14}C] palmitic acid and [U-^{14}C] glycerol and D-[U-^{14}C] glucose were purchased from American Radiolabeled Chemicals (St. Louis, MO, USA). The lactate assay kit was from BioVision (Milpitas, CA, USA). Protease (cOmplete Ultra Tablets) and phosphatase (PhosSTOP) inhibitors were obtained from Roche Diagnostics GmbH (Mannheim, Germany). β-actin (Cat # 4967), tyrosine hydroxylase (TH; Cat # 2792), adipose triglyceride lipase (ATGL; Cat # 2138), hormone-sensitive lipase (HSL; Cat # 4107), and $pHSL_{Ser660}$ (Cat # 4126) antibodies were purchased from Cell Signaling (Danvers, MA, USA). β_3-adrenergic receptor (β_3-AdR, Cat # sc-50436) and glucose transporter 4 (GLUT4, Cat # sc-7938) antibodies were purchased from Santa Cruz Biotechnology (Dallas, TX, USA). Carnitine palmitoyltransferase 1B (CPT1B, Cat # PB9491) antibody was purchased from BosterBio (Pleasanton, CA, USA). Glucose transporter 1 (GLUT1, Cat # ab115730), glycerol kinase (GYK) (Cat # ab180525), phosphoenolpyruvate carboxykinase cytoplasmic (PEPCK-C, Cat # ab28455), and uncoupling protein 1 (UCP1, Cat # ab23841) were purchased from Abcam (Toronto, ON, Canada). Peroxisome proliferator-activated receptor gamma coactivator-1α (PGC-1α, Cat # AB3242) antibody was purchased from Millipore (Temecula, CA, USA).

Animals and diet – Male albino rats (Wistar strain) at approximately 250g were group-housed at 22°C on a 12/12-h light/dark cycle. These rats were assigned to either a standard laboratory chow (SC) diet (27% protein, 13% fat and 60% carbohydrates from Test Diet Cat #5012, Richmond, IN, USA) group or a high-fat sucrose-enriched (HFS) diet (20% protein, 60% fat (laird/soybean oil), 20% carbohydrates (sucrose) from Research Diets, Cat # D12492, New Brunswick, NJ, USA) group and were fed *ad libitum* for 8 weeks. After 8 weeks of feeding, animals were anesthetized and tissues were harvested for experiments.

Body weight and fat mass – Changes in body weight were measured by comparing weekly weight recordings to a baseline measurement. Interscapular brown adipose tissue (iBAT), aortic BAT (aBAT), subcutaneous inguinal (Sc Ing), and epididymal (Epid) fat pads were extracted, trimmed of any non-fat tissue, and individually weighed.

Brown adipose tissue extraction and brown adipocyte isolation – iBAT and aBAT were extracted and carefully trimmed of any muscle, connective tissue, and white fat and used for adipocyte isolation as previously described[181]. iBAT and aBAT were combined to maximize the yield of brown adipocytes. The tissues were initially incubated in Krebs-Ringer bicarbonate HEPES buffer prepared fresh on the day of each experiment from stock solutions of salts and buffers (stored at 4^{o}C) to give the following final concentrations: 120 mM NaCl, 4.8 mM KCl, 2.5 mM $CaCl_2$, 1.2 mM KH_2PO_4, 1.2 mM $MgSO_4$, 15 mM $NaHCO_3$, and 30 mM HEPES. The solution was gassed for 45 min with carbogen (95% O_2, 5% CO_2) and then bovine serum albumin (4%) and glucose (5.5 mM) were added. The pH of the buffer was adjusted to 7.4 with NaOH before use. Subsequently, the combined tissues were vortexed for 5s and filtered, with the filtrate being discarded. The remaining tissues were finely minced and incubated in fresh KRBH-4% BSA containing collagenase (0.83 mg/ml) at 37°C under orbital agitation (120 orbital strokes/min) for about 20 – 30 min. The digested tissue was then strained using a nylon mesh and isolated cells were transferred to plastic tubes, washed three times, and resuspended in KRBH containing 3.5% FA-free BSA (KRBH-3.5% BSA). In order to distribute an equal number of adipocytes in each treatment condition, cell diameters were measured and total cell counts were determined[182].

Glucose and palmitate oxidation – Glucose and palmitate oxidation as a measure of oxidative capacity were assessed by $^{14}CO_2$ release in isolated BAT adipocytes ($5x10^5$ cells) as previously described[183]. Adipocytes were incubated in KRBH-3.5% BSA containing either 0.2 μCi/ml of [1-

^{14}C] palmitic acid and 200 μM non-labelled palmitate, or 0.2 μCi/ml of D-[U-^{14}C] glucose and 5.5 mM non-labeled D-glucose for 1h. To examine the effect of lipolysis on substrate oxidation, the β-agonist isoproterenol (Iso, 100 nM) was added to the media. To distinguish substrate oxidation for ATP production (coupled respiration) from UCP1-mediated proton leak (uncoupled respiration), the ATP Synthase inhibitor oligomycin (Oligo, 100 μM) was added to cells 15 min prior to the incubation in the absence or presence of Iso. Following the 1h incubation period, the media were acidified using 0.2 ml of H_2SO_4 (5N) and kept sealed for one additional hour for the release and collection of $^{14}CO_2$ from the cells and media. The incubation vials were prepared with a centered well containing a filter paper that was moistened with 0.2 ml of 2-phenylethylamine/methanol (1:1, v:v) for the capture of $^{14}CO_2$. At the end of the incubation, the filter paper was removed from the well and placed in scintillation fluid for radioactive counting[42,184].

Lipolysis – Lipolysis was measured in isolated BAT adipocytes ($7.5x10^5$ cells) either under basal or Iso-stimulated (100 nM) conditions. Each assay was conducted in triplicates and samples were incubated for 75 min at 37°C with gentle shaking (50 orbital strokes/min). Following the incubation, a 200 μl aliquot of the incubation medium was extracted from each vial for the determination of glycerol concentration.

Glycerol incorporation into lipids and palmitate incorporation into TAG – Glycerol incorporation into lipids and palmitate incorporation into TAG were measured using isolated BAT adipocytes ($5x10^5$ cells). Adipocytes were incubated in KRBH-3.5% BSA containing 0.2 μCi/ml of [U-^{14}C] glycerol for 1h. Subsequently, lipid extraction took place according to the method of Dole and Meinertz[185] and counted for radioactivity[184]. Palmitate incorporation into TAG was measured in isolated BAT adipocytes ($5x10^5$ cells) incubated in KRBH-3.5% BSA containing 0.2

μCi/ml of [1-^{14}C] palmitic acid and 200 μM non-labelled palmitate for 1h. Lipids were extracted from these adipocytes using the Folch's method[186], dried under nitrogen, and resuspended in 50 μl of chloroform:methanol (2:1, v:v). Four μl of sample and TG standard (triolein, Nu-chek Prep Inc., Elysian, MN, USA) were spotted 2 cm above the lower edge of silica coated flexible polyester thin layer chromatography plates (20 cm x 20 cm) (Whatman, Maidstone, United Kingdom). Lipids were separated using a hexane–diethyl ether–acetic acid (70:30:1, v:v:v) solvent and then exposed to iodine vapor for visualization. After the evaporation of iodine, the spots adjacent to the standard, corresponding to TG, were scraped off the plate and counted for radioactivity.

Glucose Uptake – Isolated adipocytes were used to determine glucose uptake as described previously[187]. Briefly, adipocytes were resuspended in glucose-free KRB containing HEPES (30 mM; KRB-HEPES) and 1% BSA, pH 7.4. Subsequently, 1x10^6 cells were transferred to plastic tubes and incubated at 37°C for 1h. Insulin (100 nM) was added for the final 20 min of the incubation period. Subsequently, KRB-HEPES containing 0.5 mM 2-deoxy-D-glucose and 0.5 μCi of 2-[1,2-^{3}H]deoxy-D-glucose was added to the cells for 3 min, and the incubations were terminated by the addition of cytochalasin B (1.5 mM stock solution). Aliquots of cell suspension (240 μl) were quickly placed in plastic microtubes containing 100 μl of di-"isononyl" phthalate. The tubes were centrifuged for 30s (6000 × g) to separate cells from the radioactive incubation medium. Subsequently, fat cells were collected by cutting the tubes through the oil phase and transferred to scintillation vials to be counted for radioactivity. Radioactivity of the cells unrelated to glucose transport (nonspecific transport) was determined in the same conditions by adding cytochalasin B (50 μM final concentration) to the medium before the addition of cells[187]. Nonspecific values were subtracted from all conditions.

Measurement of Lactate Production – Lactate production was measured using a commercially-available kit (BioVision, Milpitas, CA, USA) as per the manufacturer's instructions. Briefly, cells were isolated as described above and incubated in KRBH-3.5% BSA for 75 min. Following incubation, an aliquot of media was extracted and stored at -80°C until analysis.

RNA isolation and quantitative PCR – BAT samples were flash frozen in liquid nitrogen and stored at -80°C until RNA isolation. RNA was isolated using TRIzol™ (ThermoFisher Scientific, Waltham, MA, USA) and complimentary DNA (cDNA) was made with 2 μg of RNA using ABM EasyScript™ Reverse Transcriptase cDNA Synthesis kit (Diamed, Mississauga, ON, Canada) as per the manufacturer's instructions. Primers were designed using the software PrimerQuest (IDT) based on probe sequences available at the Affymetrix database (NetAffx™ Analysis Centre, http://www.affymetrix.com/ analysis) for each given gene. Samples were run in duplicates on a 96-well plate. Each 20 μl reaction contained 4 μl of cDNA, 0.4 μl of primer, 10 μl of Brightgreen 2x qPCR Mastermix (Diamed) and 5.6 μl of RNase-free water. qPCR analysis was performed using a Bio-Rad CFX96 Real Time PCR Detection System (Bio-Rad, Mississauga, ON, Canada) using the following amplification conditions: 95°C (10 min); 40 cycles of 95°C (15 s), 60°C (1 min). All genes were normalized to the housekeeping-gene β-actin, and relative differences in gene expression between treatment groups were determined using the ΔΔCt method[188]. Values are presented as fold increases relative to the SC group. The primers used were as follows: Cluster of differentiation (*Cd36*) forward (ACGACTGCAGGTCAACATACTGGT), reverse (TGGTCCCAGTCTCATTTAGCCACA); lipoprotein lipase (*Lpl*) forward (TTGAGAAAGGGCTCTGCCTGAGTT), reverse (TGCTTCTCTTGGCTCTGACCTTGT).

Western blotting – BAT samples were extracted from each rat, snap frozen in liquid nitrogen, and frozen at -80°C for later use. Tissues were homogenized in buffer containing 25 mM Tris-HCl,

25 mM NaCl (pH 7.4), 1 mM $MgCl_2$, 2.7 mM KCl, 1% Triton X-100 and protease and phosphatase inhibitors (Roche Diagnostics). Following centrifugation of the homogenates, the infranatant was collected. An aliquot of each sample was used in a Bradford assay to determine protein concentration. The samples were then diluted 1:1 with 2x Laemmli sample buffer and incubated at 95°C for 5 min. Twenty-five μg of protein from each sample was loaded onto gels and subject to SDS-PAGE, transferred to a PVDF membrane, and probed with the antibody of interest. The antibody dilutions were 1:1000 and the loading control was β-actin. Densitometry analysis was conducted using the Scion Image program.

Adipose tissue morphology – Morphological analysis of iBAT was performed using light microscopy as described previously[89,183]. Briefly, a sample (~50–100 mg) of each fat tissue was collected and fixed in 4% paraformaldehyde, 0.1 M phosphate-buffered saline (PBS), pH 7.4, for 24h at room temperature. Following fixation, adipose tissue samples were washed three times in PBS and stored at 4°C in 70% ethanol. Samples were then embedded in paraffin blocks, sectioned, and stained with hematoxylin and eosin (H & E). Digital images of tissue sections were captured with a Nikon Eclipse Ti (Nikon Canada, Mississauga, ON, Canada) under x20 and x40 magnification.

Statistical Analysis – Statistical analyses were conducted by using either Student's unpaired *t*-test or ANOVA with the Bonferroni post-hoc comparison using the GraphPad Prism statistical analysis program (GraphPad Software Inc., San Diego, CA, USA). Tests for normality distribution were performed using the D'Agostino & Pearson test, Anderson-Darling test, Shapiro-Wilk test, and Kolmogorov-Smirnov test. All statistical analyses were conducted using the GraphPad Prism statistical analysis program. Data are expressed as mean ± SD.

4.4. Results

Effects of HFS-feeding on body weight, fat mass, and BAT adipocyte morphology – To confirm that obesity was induced by a HFS diet, we measured weight gain relative to baseline and adipose tissue mass throughout the feeding period. The weight gained in weeks 1–3 was not statistically significantly different between the two groups, although the average weight gained in the HFS group was higher in each of these weeks. After week 4, the weight gained in the HFS group was significantly higher than in the SC animals (188.6 g ± 25.8 vs. 127.8 ± 44.3) (Table 1). This difference in weight gain persisted until the end of the study, culminating with HFS rats gaining ~50% more weight than SC controls after eight weeks of feeding. Differences in weight gain were essentially due to enhanced growth of the WAT in the HFS animals because the masses of the Sc Ing and Epid fat pads in HFS rats were 2.6- and 3-fold larger, respectively, than those of SC controls (Fig. 13A). Similarly, iBAT and aBAT masses both increased 1.6-fold in the HFS animals (Fig. 13B). Furthermore, H&E staining revealed that iBAT from SC rats contained adipocytes that were essentially multilocular, whereas iBAT from HFS rats contained many cells of unilocular appearance (Fig. 13C).

Table 1: Cumulative weight gain of rats fed either standard chow (SC) or a high-fat sucrose-enriched diet (HFS) for 8 weeks.

	Weeks of feeding							
Groups	1	2	3	4	5	6	7	8
SC	31.2 ± 3.8g	68.5 ± 18.6g	103.1 ± 31.9g	127.8 ± 44.3g	151.0 ± 54.7g	167.8 ± 61.9g	187.6 ± 62.1g	210.0 ± 69.0g
HFS	41.5 ± 14.4g	101.8 ± 17.4g	149.6 ± 19.9g	188.6* ± 25.8g	223.2* ± 33.8g	254.3* ± 38.3g	283.2* ± 41.3g	314.2* ± 44.0g

*$p<0.05$ vs. SC. Repeated measures two-way ANOVA was used to compare groups/weeks. *n* = 10-13 rats.

Effects of HFS-feeding on PGC-1α, CPT1B, and UCP1 contents – After observing an increase in BAT mass, it was important to determine whether this was accompanied by an increase in thermogenic proteins. Indeed, animals in the HFS group exhibited 1.65-, 17-, and 2.2-fold increases in protein contents of PGC-1α (Fig. 13D), CPT1B (Fig. 13E), and UCP1 (Fig. 13F), respectively, relative to the control group. Taken together, these results indicate that the molecular machinery necessary for oxidation and thermogenesis was enhanced in BAT under conditions of DIO.

Effects of isoproterenol and oligomycin on glucose and palmitate oxidation in BAT adipocytes – To test whether the increased content of thermogenic proteins was accompanied by enhanced substrate oxidation in BAT adipocytes, we measured glucose and palmitate oxidation in these cells. Measurements were conducted under basal conditions as well as in the presence of the β-adrenergic stimulator isoproterenol (Iso) and of the ATP synthase inhibitor oligomycin (Oligo). We found that rates of glucose oxidation in BAT adipocytes from SC and HFS rats were not affected by incubation with either Iso or Oligo or by a combination of both agents (Fig. 14A). However, the rates of glucose oxidation in adipocytes from HFS trended to decrease under all conditions investigated, and reached statistical significance under Oligo conditions. In fact, glucose oxidation under basal conditions was 48% lower in BAT adipocytes from HFS- than from SC-fed rats (Fig. 14A). Similarly, rates of glucose oxidation in the presence of either Iso or Oligo or Iso+Oligo were 49%, 62%, and 57% lower in HFS than SC BAT adipocytes, respectively (Fig. 14A). The incubation of BAT adipocytes with Oligo did not reduce glucose oxidation relative to basal conditions, which is consistent with mitochondrial uncoupling accounting for most of the glucose being oxidized in both SC and HFS cells. We then assessed the oxidation rates of fatty acids, which are major thermogenic substrates in brown adipocytes[38]. Under basal conditions,

palmitate oxidation did not differ between the SC and HFS groups (Fig. 14B). However, in the presence of Oligo, palmitate oxidation significantly increased by 2.7-fold in BAT adipocytes from SC-fed animals, whereas in BAT adipocytes from HFS animals, Oligo did not cause any alteration in this parameter (Fig. 14B) in comparison to basal values. Therefore, when comparing rates of palmitate oxidation between SC BAT and HFS BAT adipocytes incubated with Oligo, we found it to be 57% lower in the latter than the former cells (Fig. 14B). Furthermore, when incubated with both Iso and Oligo, palmitate oxidation was reduced by 45% in the brown adipocytes of the HFS group (Fig. 14B), although this was not statistically significant. These findings demonstrated that UCP1-mediated palmitate oxidation was impaired under conditions of chronic HFS-feeding.

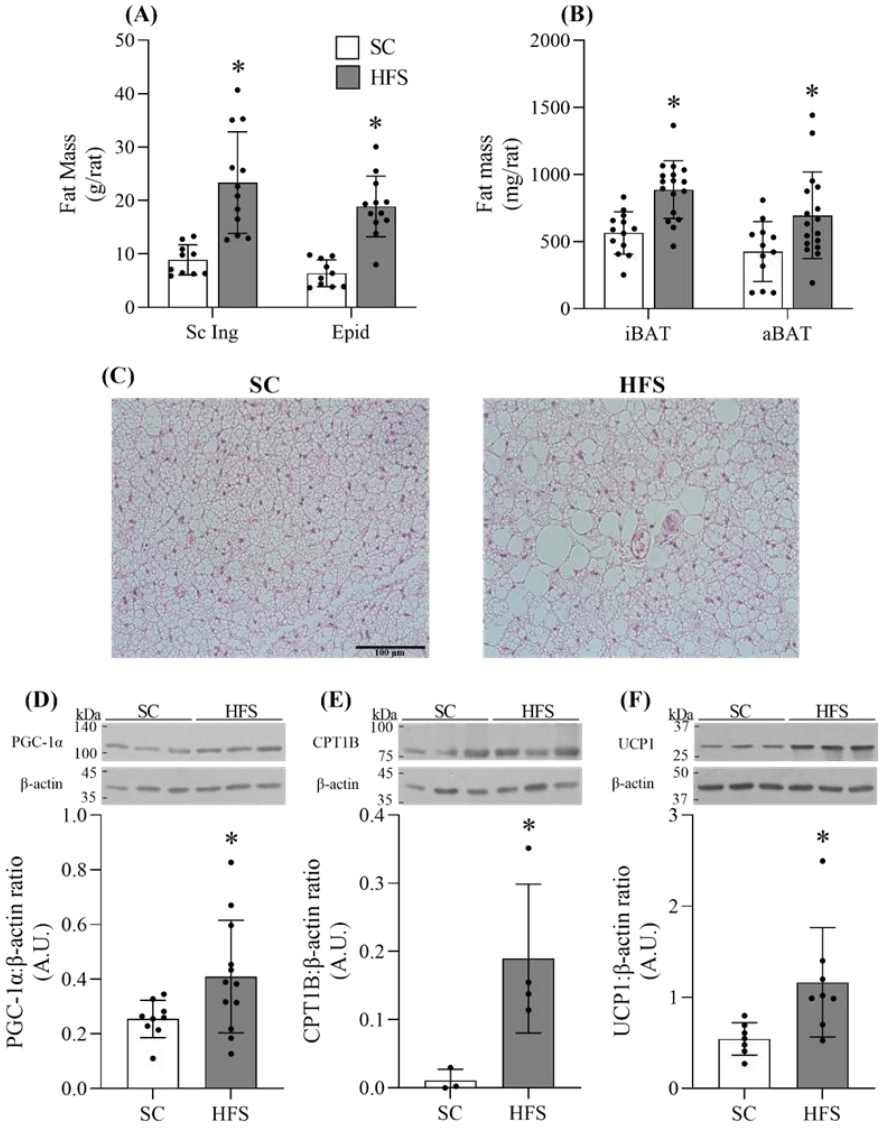

Figure 13: HFS diet increases the masses of white (A) and brown (B) adipose tissues, the unilocular appearance of brown adipocytes (C), and the contents of PGC-1α (D), CPT1B (E), and UCP1 (F) in brown adipose tissue. *$p<0.05$ vs. SC. T-tests were used to compare differences between groups in panels A-B and D-F. Data are means ± SD. n=3-15 rats.

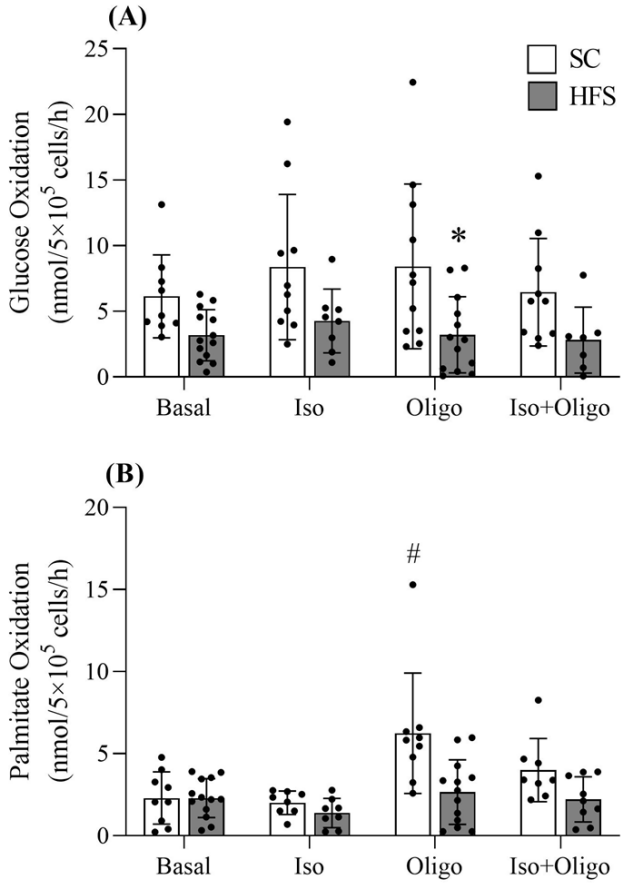

Figure 14: Isolated brown adipocytes from rats fed a HFS diet displayed reduced rates of Oligo-induced glucose (A) and palmitate oxidation (B) in isolated brown adipocytes. Two-way ANOVA was used to compare groups/conditions. *$p<0.05$ vs. SC. $^{\#}p<0.05$ vs. all conditions except SC Iso + Oligo. Data are means ± SD. n=7-13 rats.

Effects of HFS-feeding on glucose uptake, lactate production, and GLUT1 and GLUT4 protein contents in isolated brown adipocytes – Given that rates of glucose oxidation were reduced in HFS BAT adipocytes, we conducted additional experiments to assess whether the uptake of glucose was also affected in these cells. It could be that low rates of glucose oxidation were driven by reduced intake of this substrate. However, we found that basal glucose uptake in HFS BAT adipocytes was 4-fold higher than in SC BAT adipocytes. In the presence of insulin, SC BAT adipocytes displayed a 4-fold increase in glucose uptake, whereas HFS BAT adipocytes increased glucose uptake 1.83-fold when stimulated with insulin (Fig. 15A). Nevertheless, insulin-

stimulated glucose uptake was higher in the brown adipocytes of HFS-fed animals than in the SC animals (Fig. 15A). To further investigate the metabolic fate of glucose, we measured lactate production in isolated BAT adipocytes and found that, under basal conditions, cells from HFS animals produced 2.7-fold more lactate than adipocytes from SC-fed animals (Fig. 15B). These effects of HFS adipocytes were accompanied by a significant increase of ~24-fold in GLUT1 (Fig. 15C) and no alteration in GLUT4 protein contents in iBAT (Fig. 15D). Taken together, these findings provide evidence that a HFS diet enhances glucose uptake and shifts glucose metabolism toward lactate production in BAT adipocytes.

Glycerol incorporation into lipids and palmitate incorporation into TAG in brown adipocytes – Because an increased number of unilocular adipocytes was found within BAT from HFD rats, we then measured pathways involved in TAG synthesis. We found that a HFS diet enhanced *g*lycerol incorporation into lipids (Fig. 16A) and palmitate incorporation into TAG (Fig. 16B) by 1.8- and 1.7-fold, respectively in BAT adipocytes. This indicated that fatty acids and glycerol were indeed diverted by chronic HFS feeding towards esterification in isolated BAT adipocytes.

PEPCK and GyK protein levels and Lpl and CD36 gene expression in BAT – PEPCK (Fig. 16C) and GyK (Fig. 16D) increased 1.8- and 2.1-fold, respectively, which was accompanied by increases of 3.6-fold in *Lpl* and 3.7-fold in *Cd36* (Fig. 16E) mRNA expression in BAT. Therefore, our findings provide evidence that the molecular machinery that supports TAG storage was enhanced in BAT by chronic HFS.

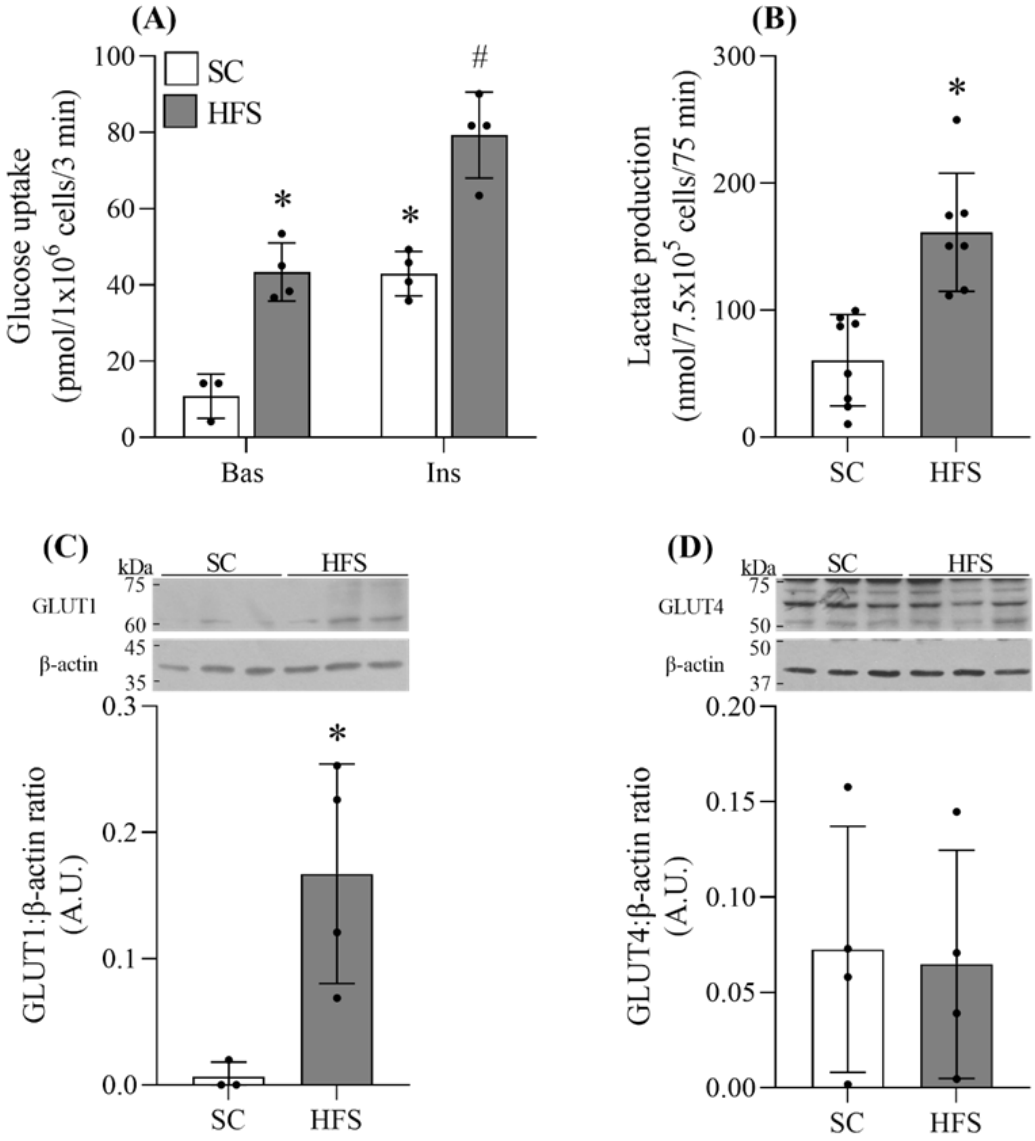

Figure 15: HFS feeding increased basal and insulin-stimulated glucose uptake (A), and lactate production (B) in isolated BAT adipocytes. HFS also had higher GLUT1 content (C) than standard chow (SC) BAT, whereas GLUT4 content (D) did not differ between SC and HFS BAT. $^{\#}p<0.05$ vs. HFS Basal and SC Ins in A. $^{*}p<0.05$ vs. SC Basal in A. $^{*}p<0.05$ vs. SC in B-D. T-test was used to compare groups except for glucose uptake (A) where a Two-way ANOVA was used to compare groups/conditions. Data are means ± SD. n=3-9 rats.

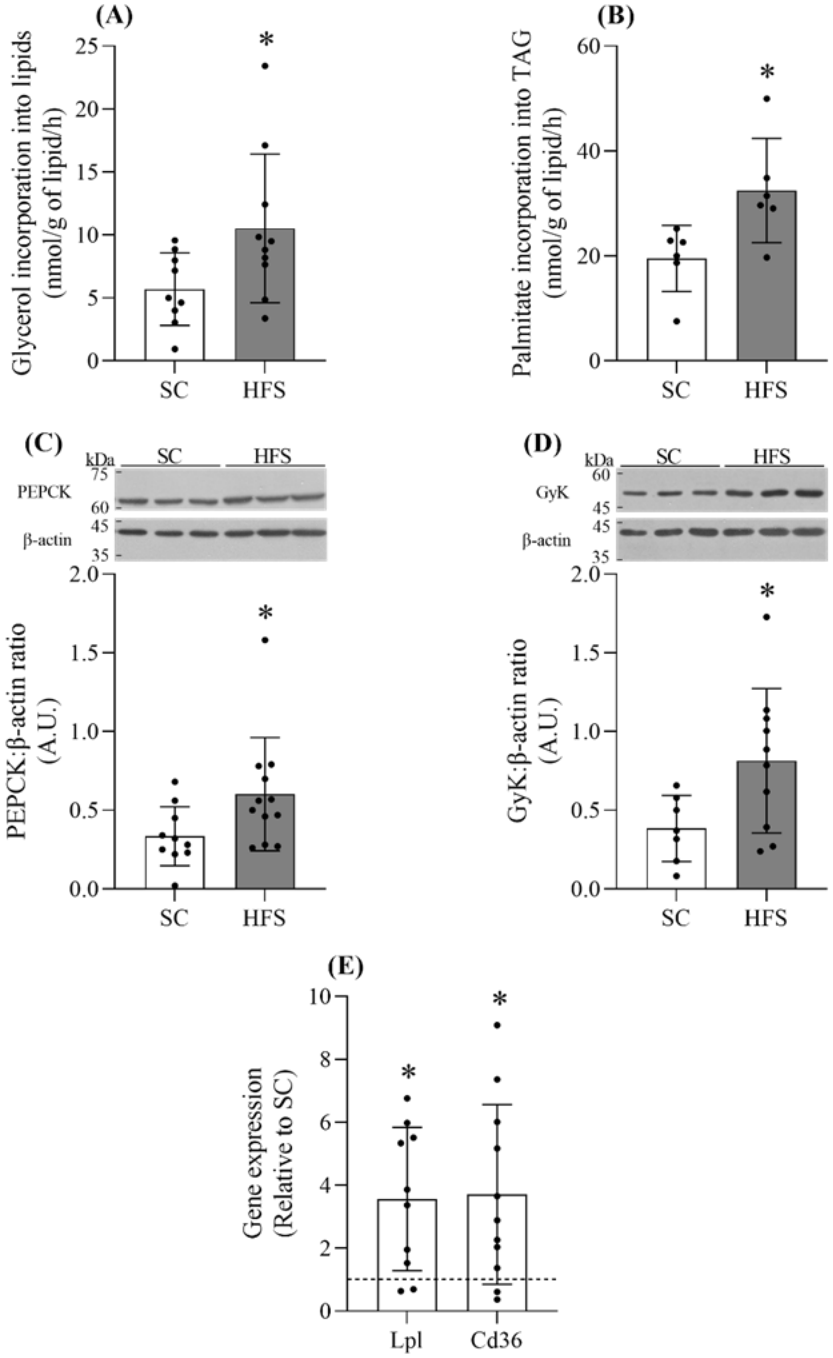

Figure 16: HFS feeding enhanced the incorporation of glycerol into lipids (A) and palmitate into triacylglycerol (TAG) (B) in isolated brown adipocytes, and increased phosphoenolpyruvate-carboxy kinase (PEPCK) (C) and glycerol kinase (Gyk) (D) contents, as well as the gene expression of lipoprotein lipase (Lpl) and cluster of differentiation 36 (Cd36) (E) in BAT. t test was used to compare groups. *$p<0.05$ vs. SC. Data are means ± SD. n=6-12 rats.

Lipolysis, β3-AdR, TH, ATGL, and pHSL contents in BAT – Basal lipolysis was reduced by 65% in BAT adipocytes from HFS rats in comparison to the SC group (Fig. 17A). Western blot analysis of the molecular machinery involved in lipolysis revealed that ATGL content was significantly reduced by 28% (Fig. 17B), whereas HSL_{660} phosphorylation was increased under conditions of HFS-feeding, although not statistically significant (Fig. 17C). Furthermore, the contents of TH (Fig. 17D) and β3AdR (Fig. 17E) were reduced and increased by 84% and 6-fold, respectively, in BAT of HFS rats in comparison to SC controls. Based on these findings, it was evident that the observed downregulation of lipolysis in HFS BAT adipocytes derived from distinct alterations in the lipolytic machinery.

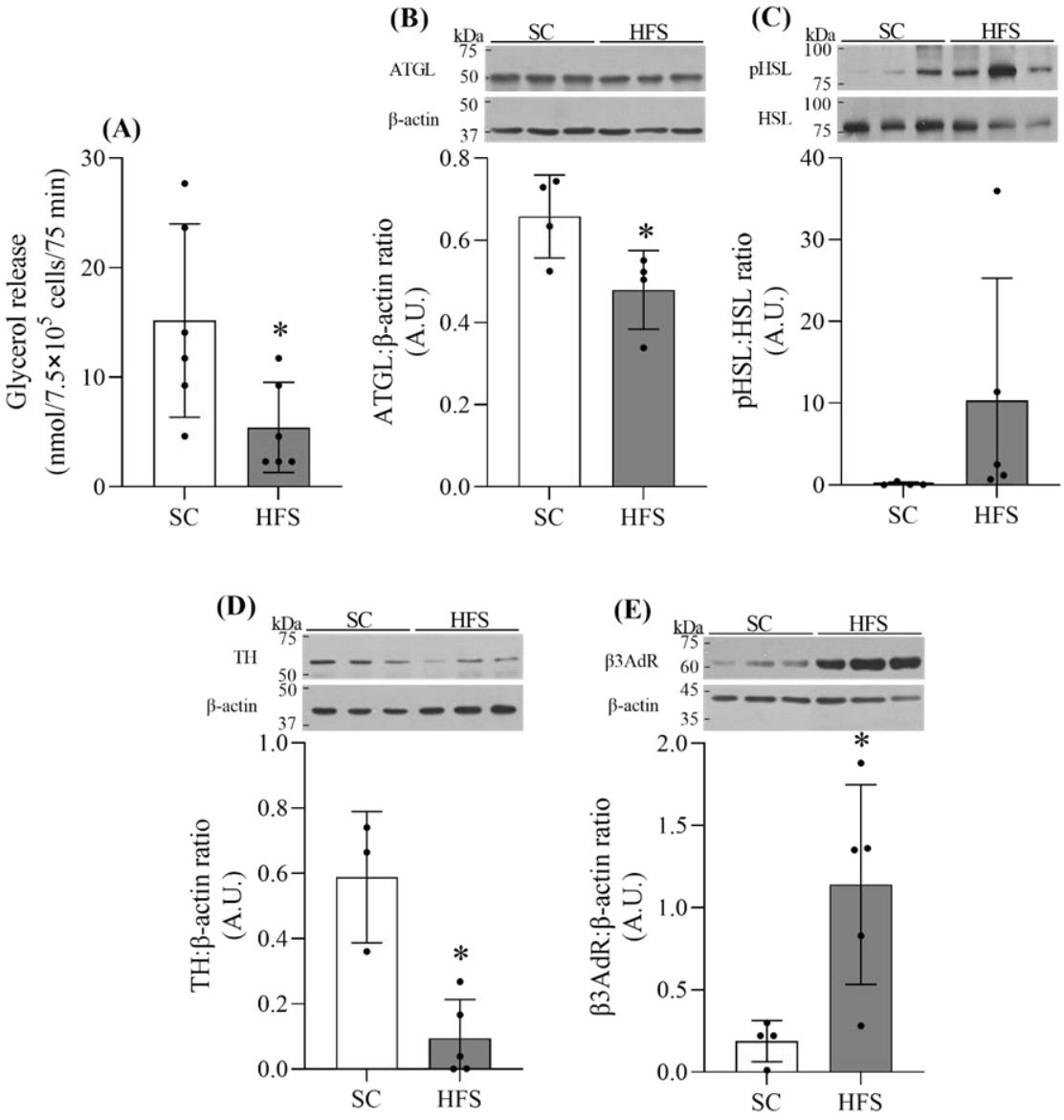

Figure 17: HFS diet reduced basal lipolysis (A) in isolated BAT adipocytes and the content of adipose triglyceride lipase (ATGL) (B), but did not significantly affect hormone sensitive lipase (HSL) phosphorylation (C). HFS diet also reduced tyrosine hydroxylase (TH) (D) and increased β3-adrenergic receptor (β3-AdR) (E) contents in BAT. *$p<0.05$ vs. SC. T-tests were used to compare differences between groups. Data are means ± SD. n=3-6 rats.

4.5. Discussion

Here, we provide evidence that UCP1-mediated glucose and fatty acid oxidation in intact and freshly isolated rat brown adipocytes is reduced under conditions of chronic HFS feeding, even though BAT mass and its UCP1 content increased. These findings are consistent with an adaptive response of the organism to the HFS diet that led to attenuation of DIT and expansion of WAT mass. Moreover, BAT itself developed functional and morphological characteristics that resemble WAT, which was characterized by brown adipocytes enhancing their ability to store TAG and by increasing the number of cells displaying a unilocular appearance within BAT. The mechanisms underlying these adaptive responses of BAT to HFS-induced obesity involved a major shift in brown adipocyte metabolism. Lipolysis was suppressed and glucose and FA were essentially diverted away from oxidation and toward pathways that culminated in TAG synthesis and enlargement of the lipid droplet in HFS BAT adipocytes (Fig. 18). Thus, our data provide evidence that there are regulatory mechanisms in intact brown adipocytes cells that shift substrate partitioning in response to alterations in dietary macronutrient composition. In this context, we demonstrated that UCP1-mediated mitochondrial uncoupling was impaired under conditions of DIO, confirming our original hypothesis.

It is well established that when BAT is in its activated state (*e.g.* cold exposure and β3-adrenergic stimulation), the uptake and utilization of glucose by brown adipocytes is enhanced [38,189,190]. Thus, we expected that DIT in response to the HFS diet would elicit a similar effect in BAT adipocytes. However, given that previous studies had reported reduced *in vivo* glucose utilization in BAT of rodent models of obesity [191–193] and humans [75,194], it was also possible that the uptake and oxidation of glucose would be impaired in these cells. Instead, our measurements of glucose uptake in isolated HFS BAT adipocytes revealed that it was significantly increased

under both basal and insulin-stimulated conditions. This likely supported the elevated lactate production, indicating that glucose was being processed through the glycolytic pathway in these cells. Therefore, the α-glycerophosphate moiety necessary for enhanced FA esterification could be supplied in two ways: 1) by the formation of glycerol 3-phosphate as an intermediary step of glycolysis, and/or 2) through glyceroneogenesis. Because lactate is a major substrate for the latter pathway[195], its abundance also allowed for increased TAG synthesis. This was supported by elevated PEPCK content and confirmed by the enhanced incorporation of palmitate into TAG found in HFS BAT adipocytes. Additionally, because the content of GyK was increased in these cells, TAG synthesis from exogenous FA and glycerol was facilitated, which was also confirmed by significantly higher rates of glycerol incorporation into lipids in HFS than in SC BAT adipocytes. Lastly, with increased expression of *Lpl* and *Cd36*, the TAG content of BAT adipocytes could be enriched through the esterification of the abundant dietary fat carried by lipoproteins. In this context, less UCP1-mediated oxidation of glucose and fatty acids could be explained by a diversion of these substrates towards pathways of TAG synthesis as opposed to uncoupled oxidation. Altogether, these effects led to a reduction in the number of small lipid droplets and conferred a more unilocular appearance to adipocytes within BAT.

Interestingly, some adaptive responses of BAT adipocytes to the HFS diet (*e.g.* increased contents of PGC-1α, β3-AdR, and CPT1B) were compatible with activation of a thermogenic response by these cells to overfeeding. This then begged the question why didn't this translate into increased UCP1-mediated substrate oxidation to support DIT? Importantly, we also found that TH content, the rate-limiting enzyme for catecholamine biosynthesis, was markedly reduced in HFS BAT, indicating lower SNS-mediated recruitment of BAT activity. This is in line with our findings of reduced basal lipolysis in HFS BAT adipocytes, which could consequently lead to less UCP1

activation, even though the content of this protein and of others that support thermogenesis was increased. In this context, the increased content of β3-AdR we found in HFS BAT was likely a compensatory mechanism employed by the cell to maximize adrenergic activation, although, *in vivo*, it is futile given the drastic reduction in TH content and impaired catecholamine production in BAT of HFS rats. Thus, maintaining the ability of the SNS to promote UCP1 activation during prolonged HFS feeding seems to be crucial to sustain DIT and counteract weight gain. This is supported by previous studies reporting that basal sympathetic activation of BAT is reduced in rats chronically maintained on a HF diet[196,197], and that diet-induced recruitment of BAT in mice depends essentially on sustained SNS-mediated activation[66]. Reduced SNS-mediated recruitment of BAT activity in HFS-induced obesity could originate from the development of leptin resistance. Indeed, rodent models of obesity lacking either functional leptin or a functional isoform of the leptin receptor display reduced SNS-mediated activation of BAT and DIT[178,198]. Additionally, altered SNS activity[199] and reduced central leptin sensitivity[200] have been demonstrated in rats with diet-induced obesity. Therefore, it is likely that the molecular adaptations to the HFS diet we found in BAT originated from the diminished sympathetic output from the hypothalamus as a result of diet-induced leptin resistance[175]. In fact, we have previously reported that plasma leptin levels of rats fed a HFS diet for 8 weeks were almost 2-fold higher than SC diet-fed controls[175], indicating that these animals indeed had reduced sensitivity to this adipokine. However, because the production and release of leptin is proportional to WAT mass[178], a gap exists between the beginning of HFS feeding and the time for adipose tissue to expand and leptin resistance to occur. This might be the reason why rats displayed increased whole-body energy expenditure in the first 2 weeks of HF feeding, and then lost this response afterwards[175] as leptin resistance developed. Thus, it could be that the increased UCP1 content in BAT we found after 8 weeks of a HFS diet

was reminiscent of this initial DIT response mounted by the animal. Future studies are necessary to investigate this possibility.

It is important to note that animals were housed at room temperature and not at thermoneutrality, which has been shown to have a significant impact on BAT UCP1 protein content and the contents of other mitochondrial proteins[48]. This poses a potential limitation to our study as both groups of animals may have experienced BAT activation to some extent, which could have masked the effects of the diets. Moreover, the experiments in this study were conducted on male rats. Future studies assessing these parameters are warranted in female rats to identify sex-based differences, if any, in the adaptive responses of BAT to an obesogenic diet.

In summary, our findings provide novel evidence that increased BAT mass and its UCP1 content under chronic HFS feeding does not translate into elevated consumption of glucose or fatty acids through UCP1-mediated mitochondrial uncoupling. In fact, uncoupled glucose and fatty acid oxidation were even lower in HFS BAT adipocytes than in SC-fed controls after coupled respiration was inhibited in these cells by Oligo. Therefore, our findings are contrary to the idea that DIT is induced in brown adipocytes under conditions of diet-induced obesity. Rather, when an obesogenic high fat sucrose-enriched diet was supplied for extended periods of time, brown adipocytes enhanced their ability to uptake and store glucose and FA, and did so by diverting substrate away from oxidation (Fig. 18). Collectively, these effects may impair BAT-induced DIT and likely contribute to the development of obesity and its related metabolic disorders.

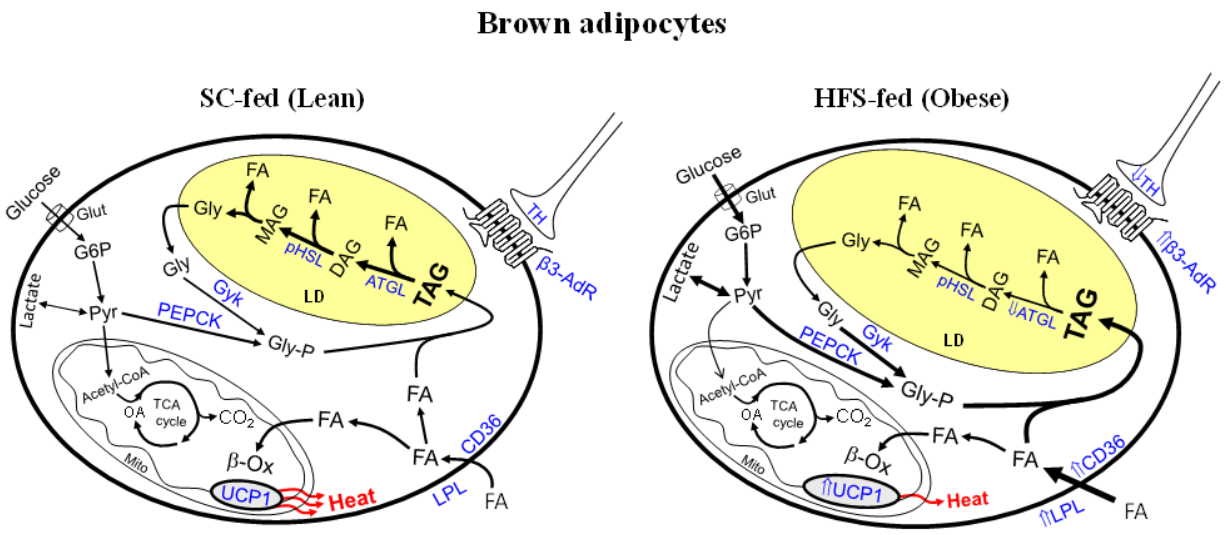

Figure 18: In brown adipocytes from lean rats fed a SC diet, glucose and fatty acids (FA) were diverted essentially toward UCP1-mediated substrate oxidation. These substrates were also used to sustain a high rate of triacylglycerol (TAG) breakdown/resynthesis. This was supported by a highly responsive molecular machinery that involved the activation of β3-adrenergic receptors (β3-AdR) via sympathetic nervous system (SNS)-mediated release of norepinephrine and activation of the major lipolytic enzymes adipose triglyceride lipase (ATGL) and hormone-sensitive lipase (HSL). Conversely, in BAT of rats fed a HFS obesogenic diet, despite increases in UCP1 and β3-AdR contents, substrate metabolism in BAT adipocytes was shifted toward TAG synthesis/storage. This was characterized by reduced UCP1-mediated glucose and fatty acid oxidation, impairment of lipolysis, and reduction in tyrosine hydroxylase content in BAT. These adaptive responses to chronic HFS were supported by increased glucose uptake, contents of phosphoenolpyruvate carboxykinase (PEPCK) and glycerol kinase (GyK), elevated rates of glycerol incorporation into lipids and palmitate incorporation into TAG, and by enhanced gene expression of lipoprotein lipase (Lpl) and cluster of differentiation 36 (Cd36) in BAT. β-ox = β-oxidation; DAG = diacylglycerol; Glut = glucose transporter; G6P = glucose-6-phospate; Gly = glycerol; Gly-P = glycerol phosphate; LD = lipid droplet; MAG = monoacylglycerol; Mito = mitochondria; OA = oxaloacetate; Pyr = pyruvate. ⇑ = increase; ⇓ = reduction. Thicker arrows indicate higher flow through the pathway.

Chapter 5: The ketogenic diet promotes triacylglycerol recycling in white adipose tissue and uncoupled fat oxidation in brown adipose tissue, but does not reduce adiposity in rats

Daniel Da Eira[1], Shailee Jani[1], Mateja Stefanovic[1] and Rolando B. Ceddia[1]

[1]Muscle Health Research Centre – School of Kinesiology and Health Science, York University, North York, ON, Canada.

Key words: Metabolism, UCP1, glycerol kinase, insulin resistance, PGC1α

Statement of Labour

The work in this study was performed by DD. DD fed the rats the SC, HFS and KD, weighed the animals and measured food intake and glycaemia over the course of the feeding period. DD also extracted tissues and performed the functional assays and Western blotting experiments outlined in this manuscript. Moreover, DD collected and analyzed the data, prepared figures and wrote and revised the manuscript. DD was funded by the Alexander Graham Bell – Canada Graduate Scholarship (Doctoral). Due to the length of the study and the logistics of tissue extraction procedures, SJ assisted in the feeding, measurements of body weight and glycaemia, tissue extraction, adipocyte isolation and the performance of some of the functional assays. MS assisted also assisted with tissue extractions, as well as some of the Western blotting experiments.

Dr. Rolando Ceddia is the principal investigator and was involved in all stages of this study. The work presented in this manuscript was funded by grants awarded to RBC, including the Discovery Grant from the Natural Science and Engineering Research Council of Canada (NSERC) and by infrastructure grants from the Canada Foundation for Innovation (CFI) and the Ontario Research Fund (ORF).

5.1. Abstract

The purpose of this study was to determine whether the weight-reducing and fat burning effects of the ketogenic diet (KD) could be attributed to alterations in the energy dissipating pathways of brown adipose tissue (BAT) uncoupled oxidation, and white adipose tissue (WAT) browning and triacylglycerol (TAG) recycling. To investigate this, male Wistar rats were fed one of the following three diets for either 8 or 16 weeks: a standard chow (SC), a high-fat, sucrose-enriched (HFS) obesogenic diet, or a KD. At the end of the intervention, subcutaneous inguinal (Sc Ing) and epididymal (Epid) fat, and interscapular and aortic BAT (iBAT and aBAT, respectively) were extracted. These tissues were used for the analysis of proteins involved in WAT browning and thermogenesis. Isolated adipocytes from WAT were assayed for basal and isoproterenol (Iso)-stimulated lipolysis and basal and insulin-stimulated lipogenesis, and BAT adipocytes were assayed for the determination of coupled and uncoupled glucose and palmitate oxidation. Adiposity similarly increased in HFS- and KD-fed rats at weeks 8 and 16. However, in HFS-fed animals insulin-stimulated lipogenesis and Iso-stimulated lipolysis were impaired in WAT adipocytes, whereas in KD-fed animals these pathways remained intact. The KD also significantly elevated WAT glycerol kinase levels, and favored TAG recycling under conditions of enhanced lipolysis. In BAT, the KD significantly increased uncoupling protein-1 levels and uncoupled fat oxidation. In summary, the KD preserved insulin sensitivity and lipolytic capacity in WAT and also upregulated energy-dissipating pathways in BAT, but it was not sufficient to prevent an increase in adiposity.

5.2. Introduction

Functional adipose tissue (AT) is crucial for the prevention of insulin resistance and Type 2 diabetes[5]. There are generally two main forms of AT with distinct physiological roles: white and brown. White adipose tissue (WAT) stores energy substrate under conditions of energy surplus, and releases fatty acids and glycerol under conditions of energy deficit[7,77,89]. On the other hand, brown adipose tissue (BAT) burns glucose and fatty acids and releases the energy as heat[7,89]. Thermogenesis in BAT mainly occurs through uncoupling protein-1 (UCP1), which uncouples oxidative phosphorylation from ATP production[7]. Under conditions of obesity, WAT and BAT functions are altered differently. Diet-induced obesity enhances the thermogenic capacity by increasing UCP1 content and fatty acid oxidation in BAT[77,89]. This serves to counteract energy storage through a mechanism known as diet-induced thermogenesis[77,89]. However, this is not sufficient to prevent the excess storage of fat in white adipocytes and the development of insulin resistance in the WAT[5,201]. In fact, chronically elevated caloric intake overwhelms the hypertrophic capacity of the adipocyte, leading to cellular hypoxia and immune cell infiltration[5,201]. At the level of the WAT, inflammation inhibits insulin signaling, which ends up enhancing basal lipolysis[5], although catecholamine-stimulated lipolysis becomes severely limited under conditions of obesity[42,202]. The dysregulation in lipid storage and breakdown redirects lipids to ectopic tissues such as liver[5] and muscle[5,12]. This is detrimental to insulin sensitivity and metabolism in these tissues, and negatively impacts whole-body glucose homeostasis[5,12]. In this context, interventions that combat adiposity and restore AT function are of great interest for the prevention and treatment of obesity and insulin resistance.

A dietary intervention that exerts anti-obesity and insulin-sensitizing effects is the ketogenic diet (KD). The KD is typically low in carbohydrates and high in fat[126]. Despite being abundant in

fat, recent evidence shows that 3 months of KD-feeding significantly attenuated body weight (BW) and blood pressure, and improved glycaemia in diabetic women[15]. Furthermore, as little as 6 days of KD significantly reduced intra-hepatic triglycerides in overweight and obese subjects[203]. These promising health effects have prompted investigations into the effects of the KD on cellular metabolism. In BAT and WAT, the KD increases UCP1 content and UCP1 gene expression, respectively[147]. This elevation in WAT UCP1 is characteristic of a process known as browning, whereby WAT acquires structural and functional features that resemble BAT[4,7,89]. Additionally, by lowering circulating insulin levels, the KD favors WAT lipolysis and the release of non-esterified fatty acids (NEFAs) into the bloodstream[204]. NEFAs not undergoing oxidation return to the WAT where they are recycled back to triacylglycerol (TAG). This latter process creates an energy-consuming "futile cycle" that can also contribute to whole-body energy expenditure[7]. Thus, the combined effects of the KD on BAT uncoupled oxidation, WAT browning, and TAG cycling could potentially support the diet-induced shift from energy storage to dissipation in WAT and reduce adiposity. However, the effects of the KD on WAT TAG recycling and BAT uncoupled oxidative capacity, and whether these two mechanisms lead to reduced adiposity, is yet to be confirmed. Therefore, the purpose of our study was to assess KD-induced alterations in these energy-consuming pathways in brown and white adipocytes. We hypothesized that the KD would increase UCP1 content and enhance fat consumption in BAT, whereas in WAT the machinery for TAG recycling would be up-regulated, ultimately contributing to a reduction in adiposity. To test this hypothesis, rats were fed for up to 16 weeks either a high-fat, sucrose enriched (HFS) obesogenic diet or a KD to compare the effects of these diets on WAT and BAT metabolism. To test potential time-dependent effects of the KD on metabolic pathways involved in energy dissipation, we assessed, in BAT and WAT, the thermogenic and TAG recycling machineries at 8

and 16 weeks of the dietary interventions. Here, we show that KD-feeding promoted distinct TAG recycling effects in subcutaneous and visceral WAT and enhanced the capacity of BAT to consume fatty acids. However, the induction of these energy consuming pathways by the KD did not lead to a reduction in adiposity.

5.3. Materials and Methods

Reagents – Type II collagenase, isoproterenol (Iso), fatty acid-free bovine serum albumin (BSA), palmitic acid, and the free glycerol determination kit were obtained from Sigma (St. Louis, MO, USA). Oligomycin (Oligo) was purchased from Cayman Chemical (Ann Arbor, MI, USA). [1-^{14}C] palmitic acid and D-[U-^{14}C] glucose were purchased from American Radiolabeled Chemicals (St. Louis, MO, USA). Protease (cOmplete Ultra Tablets) and phosphatase (PhosSTOP) inhibitors were obtained from Roche Diagnostics GmbH (Mannheim, Germany). The β-hydroxybutyrate (βHB; cat. no. ab83390) assay kit, and the UCP1 (ab23841) and glycerol kinase (GyK; cat. no. ab180525) antibodies were purchased from Abcam (Toronto, ON, Canada). β-actin (cat. no. 4967) and adipose triglyceride lipase (ATGL; cat. no. 2138) antibodies were purchased from Cell Signaling (Danvers, MA, USA). The peroxisome proliferator-activated receptor gamma coactivator 1-alpha (PGC1α; cat. no. ab3242) was purchased from Millipore (Burlington, MA, USA). The β3-adrenergic receptor (β3AdR; sc-50436) antibody was purchased from Santa Cruz Biotechnology, Inc (Dallas, TX, USA).

Animals – Male albino rats from the Wistar strain (Envigo, Indianapolis, IN, USA) weighing 200 – 250 g (initial weight) were maintained in a constant-temperature (23 ^{o}C), with a fixed 12-h light/12-h dark cycle and fed for either 8 or 16 weeks *ad libitum* either a standard chow diet (SC, 27.0 %, 13.0 %, and 60.0 % of calories provided by protein, fat, and carbohydrates, respectively), a HF, sucrose-enriched (HFS) diet (20.0%, 60.0%, and 20.0% of calories provided by protein, fat,

and carbohydrates [sucrose], respectively) or a KD (20%, 80% and 0% of calories provided by protein, fat and carbohydrates, respectively). Caloric densities of the diets were 3.43-, 5.24- and 6.14 kcal/g for the SC, HFS and KD, respectively. The saturated, monounsaturated and polyunsaturated fatty acid % contribution to the total fatty acids in each of the diets was 20.8, 26.7 and 52.5% for the SC, 32.2, 35.9 and 31.9% for the HFS diet and 32.6, 36.2 and 31.1 for the KD (Table 2). The SC (standard rat chow, catalog # 5012) was purchased from LabDiet (Richmond, IN, USA). The HFS and ketogenic diets (catalog # D12492 and D03022101, respectively) were purchased from Research Diets Inc. (New Brunswick, NJ, USA). At the end of the feeding period, animals were anesthetized under ketamine/xylazine anesthesia (90 mg and 10 mg/100 g B.W., respectively) and the subcutaneous inguinal (Sc Ing), Epid, interscapular BAT (iBAT) and aortic BAT (aBAT) fat pads were extracted and weighed. A sample of each fat depot was immediately frozen in liquid nitrogen for subsequent experiments.

Table 2: Fatty acid (FA) profile of the SC, HFS and KD expressed as % of the total fatty acids.

	SC	**HFS**	**KD**
Saturated FA	20.8	32.2	32.6
Monounsaturated FA	26.7	35.9	36.2
Polyunsaturated FA	52.5	31.9	31.1

Ethics approval – The protocol containing all animal procedures described in this study was specifically approved by the Committee on the Ethics of Animal Experiments of York University (York University Animal Care Committee, YUACC, permit number: 2021-03) and performed strictly in accordance with the YUACC guidelines. All tissue extraction procedures were performed under ketamine/xylazine anesthesia, and all efforts were made to minimize suffering[205]. All experiments in this study were carried out in compliance with the ARRIVE guidelines[206].

Measurement of blood glucose levels – Blood from all animals in the fed state was collected between 15:00 and 16:00 h by saphenous vein bleeding and used to determine plasma glucose

using the Contour Next one meter blood glucose monitoring system by Ascensia Diabetes Care US (Parsippany, NJ, USA).

Adipocyte isolation from Epid and Sc Ing fat depots – Adipocyte isolation from the Epid and Sc Ing fat pads was performed as previously described[7]. Briefly, the adipose tissue was minced in Krebs-Ringer bicarbonate HEPES buffer (KRBH) prepared fresh on the day of each experiment from stock solutions of salts and buffers (stored at 4°C) to give the following final concentrations: 120 mM NaCl, 4.8 mM KCl, 2.5 mM $CaCl_2$, 1.2 mM KH_2PO_4, 1.2 mM $MgSO_4$, 15 mM $NaHCO_3$, 30 mM HEPES, and type II collagenase (0.5 mg/ml). Before use, KRBH was gassed for 45 min with carbogen (95% O_2, 5% CO_2) and then BSA (3.5%) and glucose (5.5 mM) were added. pH of the buffer was adjusted to 7.4 with NaOH. Minced tissues were incubated at 37°C with gentle agitation (120 orbital strokes/ min) for ~25–30 min. The digested tissue was then strained using a nylon mesh, and cells were transferred to 50 ml tubes, washed three times, and resuspended in KRBH containing 3.5% fatty acid-free BSA (KRBH-3.5% BSA). To distribute an equal number of adipocytes in each treatment condition, cell diameters were measured and total cell numbers were determined[182].

Isolation of BAT adipocytes – iBAT and aBAT were extracted and carefully trimmed of any muscle, connective tissue, and white fat. The tissues were then used for adipocyte isolation as previously described[181]. To increase the yielding of brown adipocytes, iBAT and aBAT were combined. The tissues were initially incubated in KRBH-4% BSA supplemented with collagenase (0.83 mg/ml) at 37°C under orbital agitation (120 orbital strokes/min) for 5 min. Subsequently, the combined tissues were vortexed for 5 s, the contents of the vial were filtered, and the filtrate was discarded. The remaining tissues were finely minced and incubated in fresh KRBH-4% BSA containing collagenase (0.83 mg/ml) at 37°C under orbital agitation (120 orbital strokes/min) until

complete digestion. The procedure then continued as described above for WAT adipocyte isolation.

Measurement of glucose and palmitate oxidation - Glucose and palmitate oxidation as measures of oxidative capacity were assessed by production of $^{14}CO_2$ in BAT adipocytes (5×10^5 cells), as previously described[7]. Briefly, cells were incubated in KRBH-3.5% BSA containing either 0.2 μCi/ml of [1-^{14}C]palmitic acid and 200 μM nonlabeled palmitate or 0.2 μCi/ml of D-[U-^{14}C]glucose and 5.5 mM nonlabeled D-glucose for 1h. To distinguish substrate utilization used for ATP synthesis (coupled oxidation) from proton leak (uncoupled oxidation), 15 min before incubation, adipocytes were treated with the ATP synthase inhibitor oligomyocin (Oligo)[7]. Following 1h of incubation, either in the absence or continuous presence of Oligo (100 μM), the media were acidified with 0.2 ml of H_2SO_4 (5 N), and the vials were maintained sealed at 37°C for an additional 1h for the collection of $^{14}CO_2$ released from the cells and the media. The vials used for incubation had a centered isolated well containing a loosely folded piece of filter paper that was moistened with 0.2 ml of 2-phenylethylamine/methanol (1:1, vol:vol) for the capture of $^{14}CO_2$. At the end of the incubation, the filter paper was removed and transferred to a scintillation vial for radioactivity counting[7,42,184]. All oxidation values are expressed as fold change of Oligo-induced oxidation over basal oxidation.

Measurement of glucose incorporation into lipids – Glucose incorporation into lipids was measured in isolated adipocytes (5×10^5 cells) from the Epid and Sc Ing fat depots as previously described[184]. Briefly, cells were incubated in KRBH-3.5% BSA containing 0.2 μCi/ml of D-[U-^{14}C] glucose and 5.5 mM non-labelled D-glucose for 1h in the absence or presence of insulin (100 nM). Lipids were then extracted according to the method of Dole and Meinertz[207] and assessed for

radioactivity[184]. Data are expressed as the fold change of insulin-stimulated glucose incorporation into lipids, relative to basal glucose incorporation into lipids.

Measurement of glycerol release – Lipolysis was measured in isolated Epid and Sc Ing adipocytes (6 x 10^5 cells). Adipocytes were incubated in the absence or presence of 100 nM Iso (β-non-specific agonist)[208]. Each condition was assayed in triplicates and the samples were incubated for 75 min at 37°C with gentle agitation (80 orbital strokes/min). After incubation, a 200 µl aliquot of medium was taken from each vial for the determination of glycerol concentration. Data are expressed as Iso-stimulated glycerol release, over basal glycerol release.

Western blotting analysis of UCP1, PGC1α, β3AdR, ATGL and GyK in WAT and BAT – Sc Ing, Epid and iBAT samples were homogenized in a buffer containing 25 mM Tris-HCl, 25 mM NaCl (pH 7.4), 1 mM $MgCl_2$, 2.7 mM KCl, 1% Triton X-100 and protease and phosphatase inhibitors (Roche Diagnostics GmbH, Mannheim, Germany). Homogenates were centrifuged, the infranatant was collected, and an aliquot was used to measure protein by the Bradford method. Samples were diluted 1:1 (vol:vol) with 2x Laemmli sample buffer and heated to 95°C for 5 min. 25 µg of protein were loaded in each well. Samples were then subjected to SDS-PAGE, transferred to PVDF membrane, and probed for the proteins of interest. All primary antibodies were used at a dilution of 1:1,000. All densitometry analyses were performed using the ImageJ program.

Statistical Analyses – Data were expressed as Mean ± SEM. Statistical analyses were performed by using mixed-model analyses and one-way ANOVAs with Bonferroni multiple comparison post-hoc tests, as indicated in the figure legends. The GraphPad Prism software version 9.1.12 was used for all statistical analyses and for the preparation of all graphs. The level of significance was set to $p<0.05$.

5.4. Results

Effect of diet on body weight (BW), plasma BHB levels, and blood glucose concentration – As expected, all groups of animals displayed a progressive increase in BW throughout the 16-week feeding period. At the end of the study, BW was slightly higher in HFS- and KD-fed rats than the SC-fed counterparts, however these differences were not statistically significant (Table 3). When expressed as percent increase in weight gain relative to baseline, the HFS and KD induced 1.2-fold increases in this parameter (Table 3). Plasma BHB was significantly elevated by the KD at weeks 4, 8 and 16 when compared to both the SC and HFS groups (Table 3). At week 8, BHB levels were significantly higher in HFS-fed rats than the SC-fed group; however, at week 16, BHB levels did not differ between these two groups (Table 3). Fed-state blood glucose levels were significantly higher in HFS- than SC-fed animals at weeks 4 and 16, whereas in KD-fed rats glycaemia was not significantly increased (Table 3).

Table 3: The effects of a standard chow (SC), high-fat, sucrose-enriched (HFS) diet or a ketogenic diet (KD) on body weight, % increase in body weight relative to baseline, plasma β-hydroxybutyrate (BHB) levels and blood glucose concentration after 0, 4, 8 and 16 weeks of feeding.

		Duration of study (weeks)			
		0	4	8	16
Body weight (g)	SC	247.2 ± 4.7	403.8 ± 15.9	486.3 ± 17.8	553.9 ± 20.0
	HFS	232.7 ± 4.2	407 ± 14.7	504.7 ± 16.2	590.3 ± 24.3
	KD	245.3 ± 5.1	409.3 ± 9.2	511.4 ± 13.0	607.9 ± 19.1
Body weight increase relative to week 0 (%)	SC	-	64.2 ± 4.9	96.7 ± 5.9	124.1 ± 6.6
	HFS	-	76.3 ± 3.7	116.8 ± 5.4	153.2 ± 8.1*
	KD	-	70.3 ± 4.5	108.9 ± 5.7	148.1 ± 7.5*

Plasma BHB (mM)	SC	0.12 ± 0.01	0.13 ± 0.01	0.14 ± 0.01	0.15 ± 0.01
	HFS	0.16 ± 0.02	0.19 ± 0.03	0.24 ± 0.03*	0.15 ± 0.02
	KD	0.13 ± 0.02	0.30 ± 0.03#	0.38 ± 0.03#	0.29 ± 0.02#
Blood glucose (mM)	SC	7.4 ± 0.2	6.8 ± 0.3	6.8 ± 0.2	5.9 ± 0.3
	HFS	7.3 ± 0.1	7.3 ± 0.2*	7.2± 0.1	6.7 ± 0.3*
	KD	7.3 ± 0.1	7.2 ± 0.1	7.0 ± 0.1	6.6 ± 0.2

*p<0.05 vs. SC in the respective week; #p<0.05 vs. all other groups. Data are expressed as mean ± SEM. Mixed-effects model analysis. n=6-9 for body weight and % increase in weight gain. n=6-7 for BHB. n=6-15 for blood glucose.

Energy intake and energy efficiency in SC, HFS and KD-fed animals – Total energy intake during the 16-week feeding period was similar between the three groups (Table 4). However, energy efficiency at week 16 was significantly elevated in KD-fed animals when compared to the SC group (Table 4).

Table 4: Effect of diet on total energy intake for the 16-week intervention and energy efficiency

	SC	HFS	KD
Total energy intake (kcal)	9554 ± 478.1	8814 ± 318.3	9010 ± 517.7
Energy efficiency (g/kcal)	$0.033 \pm 7.4 \times 10^{-4}$	$0.035 \pm 9.7 \times 10^{-4}$	0.039 ± 0.002*

*p<0.05 vs. SC. Data are expressed as mean ± SEM. One-way ANOVA. n=4.

Effect of diet on WAT and BAT masses – At week 8 of the intervention, Sc Ing fat mass was 2.6- and 2.1-fold higher in HFS and KD-fed animals than SC-fed rats, respectively (Fig. 19). At week 16, Sc Ing mass increased significantly in all three groups in comparison to week 8, but HFS and KD-fed animals continued to display significantly higher Sc Ing fat masses than SC-fed rats (Fig. 19). Similarly, at week 8, Epid fat mass was significantly elevated in HFS- (~2.7-fold) and KD-

fed (~2-fold) rats when compared to SC-fed counterparts (Fig. 19B). At week 16, Epid fat masses of HFS- and KD-fed animals were 2- and 1.9-fold higher than the SC group, respectively (Fig. 19B). With respect to BAT, the HFS diet and the KD increased week 8 iBAT mass by 1.6- and 1.4-fold, respectively, relative to the SC animals (Fig. 19C). At week 16, the HFS diet and KD-induced elevation in iBAT mass was maintained (Fig. 19C). The aBAT was also found to be elevated by the HFS diet at weeks 8 and 16, and by the KD at week 16 (Fig. 19D), relative to the SC group. Therefore, despite possessing different macronutrient compositions, the HFS diet and KD induced similar alterations in WAT and BAT mass (Fig. 19).

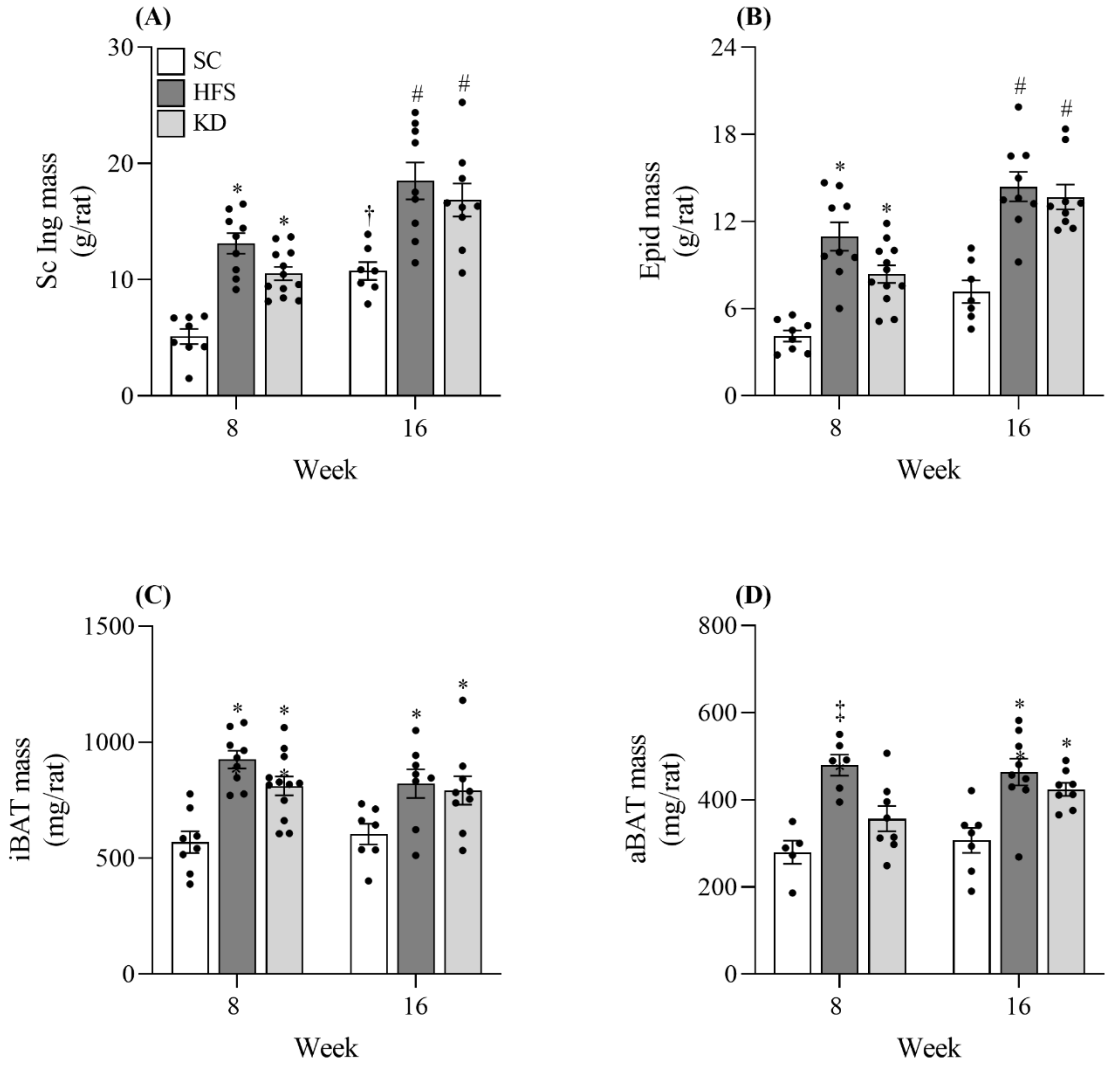

Figure 19: HFS and KD-feeding significantly elevated subcutaneous inguinal (Sc Ing) (A) and epididymal (Epid) (B) fat masses. Sc Ing mass increased from week 8 to week 16 with all diets (A); however, only the HFS and KDs significantly enhanced Epid mass over this time (B). Interscapular BAT (iBAT) (C) and aortic BAT (aBAT) (D) masses were elevated in both the HFS and KD-fed animals at week 16 of the intervention. However, at week 8, only the HFS diet caused aBAT growth (D). *p<0.05 vs. SC, within the respective week; #p<0.05 vs. week 8, within the respective group, and week 16 SC; †p<0.05 vs. week 8, within group; ‡p<0.05 vs. week 8 SC and week 8 KD. Bars represent mean ± SEM. Two-way ANOVA. n=5-12.

Effects of diet on browning, lipolytic proteins, and β-adrenergic-stimulated lipolysis in Sc Ing fat – Given these diet-induced differences in fat mass, it was important to investigate how the interventions were influencing metabolism at the tissue and cellular levels. Firstly, Sc Ing UCP1 levels were measured to determine whether the KD induced browning in this tissue. We found that

Sc Ing UCP1 was undetectable after either 8 or 16 weeks of any of the three dietary interventions (Fig. 20A). At week 8 of the intervention, Sc Ing β3AdR and ATGL levels were elevated 4.5- (Fig. 20B) and 4-fold (Fig. 20C), respectively, in KD-fed animals. Sc Ing ATGL was also increased by the HFS diet at week 8 (Fig. 20C). However, at week 16, no differences were detected in β3AdR levels among the three groups (Fig. 20D), although ATGL was 2.1-fold higher in HFS- than SC-fed rats (Fig. 20E). In line with these findings, β-adrenergic stimulated glycerol release was not significantly different between the three diet groups (Fig. 20F). Thus, the KD did not induce browning and although it promoted a transient increase in lipolytic capacity, these effects were not sustained at week 16.

Effects of diet on browning, lipolytic proteins and β-adrenergic-stimulated lipolysis in Epid fat –Similar to the Sc Ing fat, UCP1 was not detectable in the Epid fat depot with any of the three diets (Fig. 21A). At week 8, Epid β3AdR (Fig. 21B) and ATGL (Fig. 21C) levels were not significantly different between the three groups, although much lower levels of ATGL ($p=0.06$ vs. SC) were found in the Epid fat of HFS-fed rats. At week 16, Epid β3AdR levels were significantly elevated 3.6- and 4.7-fold by the HFS diet and KD, respectively (Fig. 21D), whereas ATGL content was not altered (Fig. 21E). Despite elevations in Epid β3AdR content, the HFS diet attenuated (~49%) Iso-stimulated lipolysis in comparison to the SC group (Fig. 21F). Conversely, in Epid adipocytes from KD-fed rats, Iso-stimulated lipolysis was maintained at the same levels as those of SC-fed counterparts (Fig. 21F).

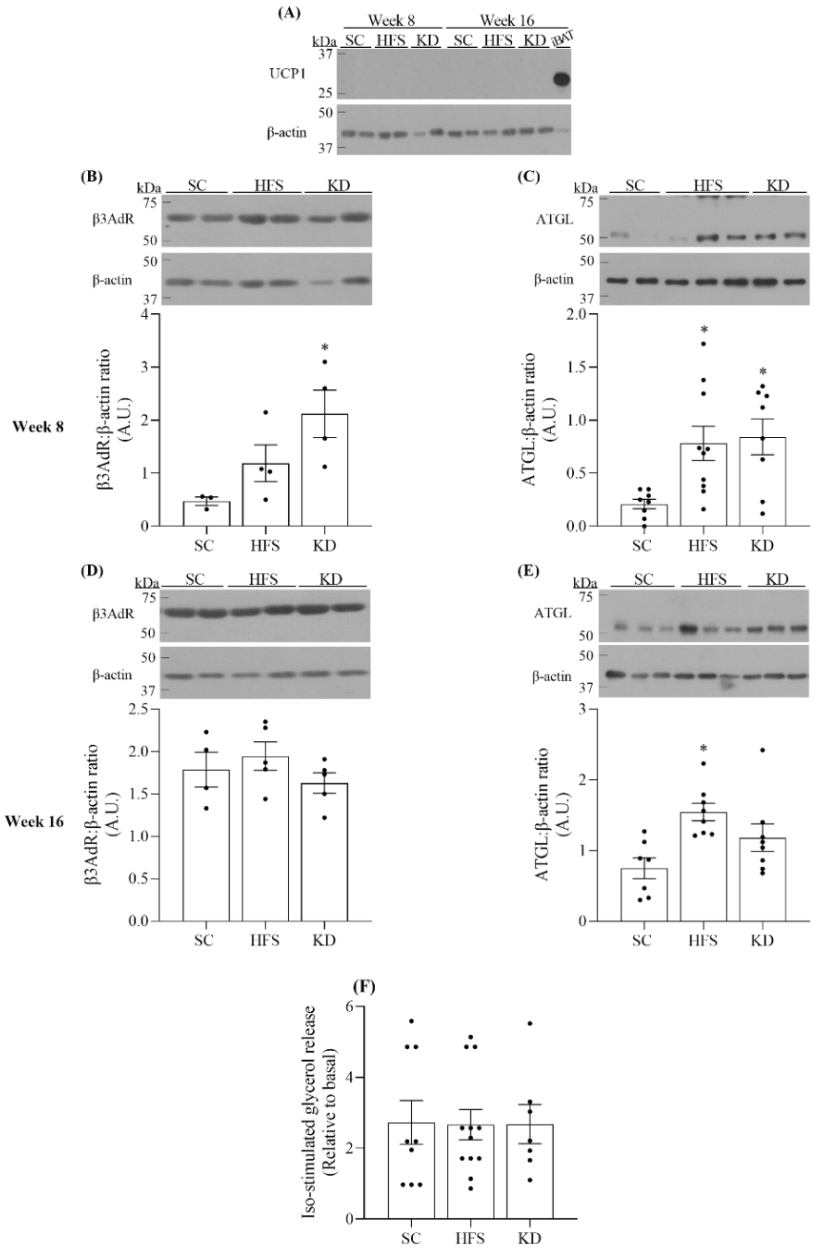

Figure 20: Uncoupling protein-1 (UCP1) levels were undetectable in Sc Ing fat either at week 8 or 16 (A). At week 8 of the intervention, β3-adrenergic receptor (β3AdR) levels were increased by the KD (B), and adipose triglyceride lipase (ATGL) was significantly elevated by HFS and KD (C). At week 16, β3AdR (D) and ATGL (E) protein levels diminished, where β3AdR was not altered by any of the diets and ATGL was only increased by the HFS diet (D and E, respectively). Isoproterenol (Iso)-stimulated lipolysis was not significantly different between the three groups (F). *p<0.05 vs. SC. Bars represent mean ± SEM. One-way ANOVA. n=3-12.

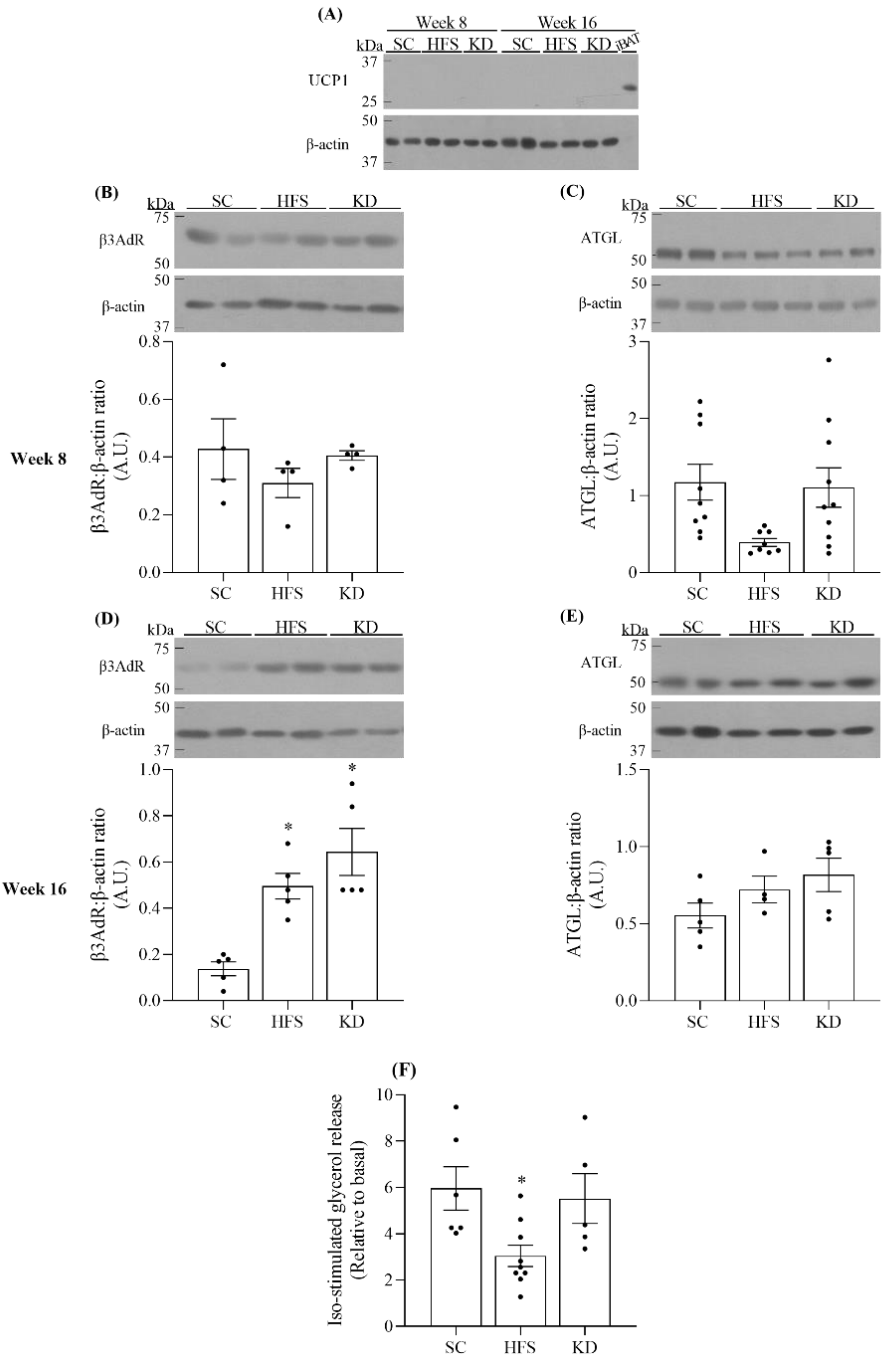

Figure 21: In Epid fat, UCP1 levels (A) were undetectable and β3AdR (B) and ATGL (C) levels were not altered at week 8, although, Epid ATGL did show a trend to decrease with the HFS diet (C). At week 16, β3AdR levels were increased in the Epid fat of HFS and KD-fed animals (D). ATGL did not differ among the groups (E). The HFS diet significantly attenuated isoproterenol (Iso)-stimulated lipolysis in Epid adipocytes (F). *p<0.05 vs. SC. Bars represent mean ± SEM. One-way ANOVA. n=4-10.

Effect of diet on glucose incorporation into lipids and GyK content in Sc Ing and Epid fat – In Sc Ing adipocytes from HFS-fed rats, insulin-stimulated lipogenesis was 82.6% lower than the SC group (Fig. 22A), whereas in adipocytes from KD-fed rats this variable did not differ from the SC group (Fig. 22A). This indicates that the KD preserved insulin sensitivity and lipid deposition in Sc Ing adipocytes. In Epid adipocytes, insulin-stimulated lipogenesis was not altered by diet (Fig. 22B), showing fat-depot specific differences in response to dietary intervention. Furthermore, in Sc Ing and Epid adipocytes, the KD increased GyK levels by 7- and 5.5-fold, respectively (Fig. 22C and D). Thus, the KD preserved the ability of adipocytes to promote lipogenesis in response to insulin and to also recycle TAG by increasing GyK levels.

Effects of diet on BAT uncoupled oxidation – At week 16, uncoupled palmitate oxidation was elevated 1.9-fold in brown adipocytes from KD-fed animals when compared to HFS-fed animals (Fig. 23A), whereas glucose oxidation was not altered by diet (Fig. 23B). UCP1 levels did not significantly increase in BAT of HFS-fed animals (Fig. 23C); however, in BAT adipocytes from KD-fed rats UCP1 levels increased 4.9- and 2.1-fold, when compared to the SC and HFS groups, respectively (Fig. 23C). Other thermogenic proteins such as PGC1α (Fig. 23D), β3AdR (Fig. 23E), and ATGL (Fig. 23F) were not changed by any of the diets, but GyK levels increased 4.2- and 6.5-fold in BAT of HFS and KD-fed animals, respectively (Fig. 23G).

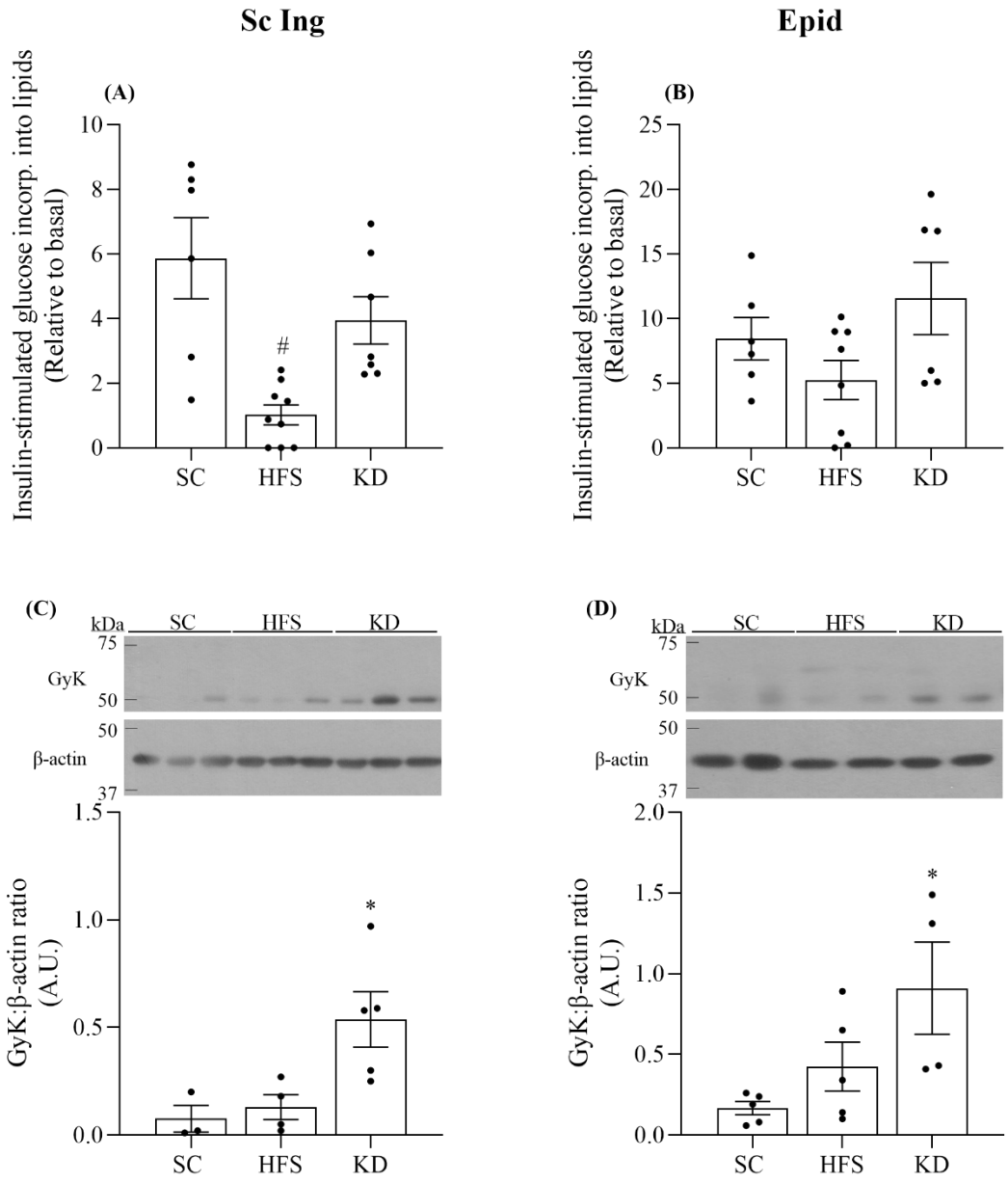

Figure 22: HFS-feeding significantly impaired insulin-stimulated glucose incorporation into lipids (A) in Sc Ing adipocytes, but not in Epid adipocytes (B). The KD significantly elevated glycerol kinase (GyK) levels in Sc Ing (C) and Epid (D) fat pads. *p<0.05 vs. SC; #p<0.05 vs. all other groups. Bars represent mean ± SEM. One-way ANOVA. n=3-9.

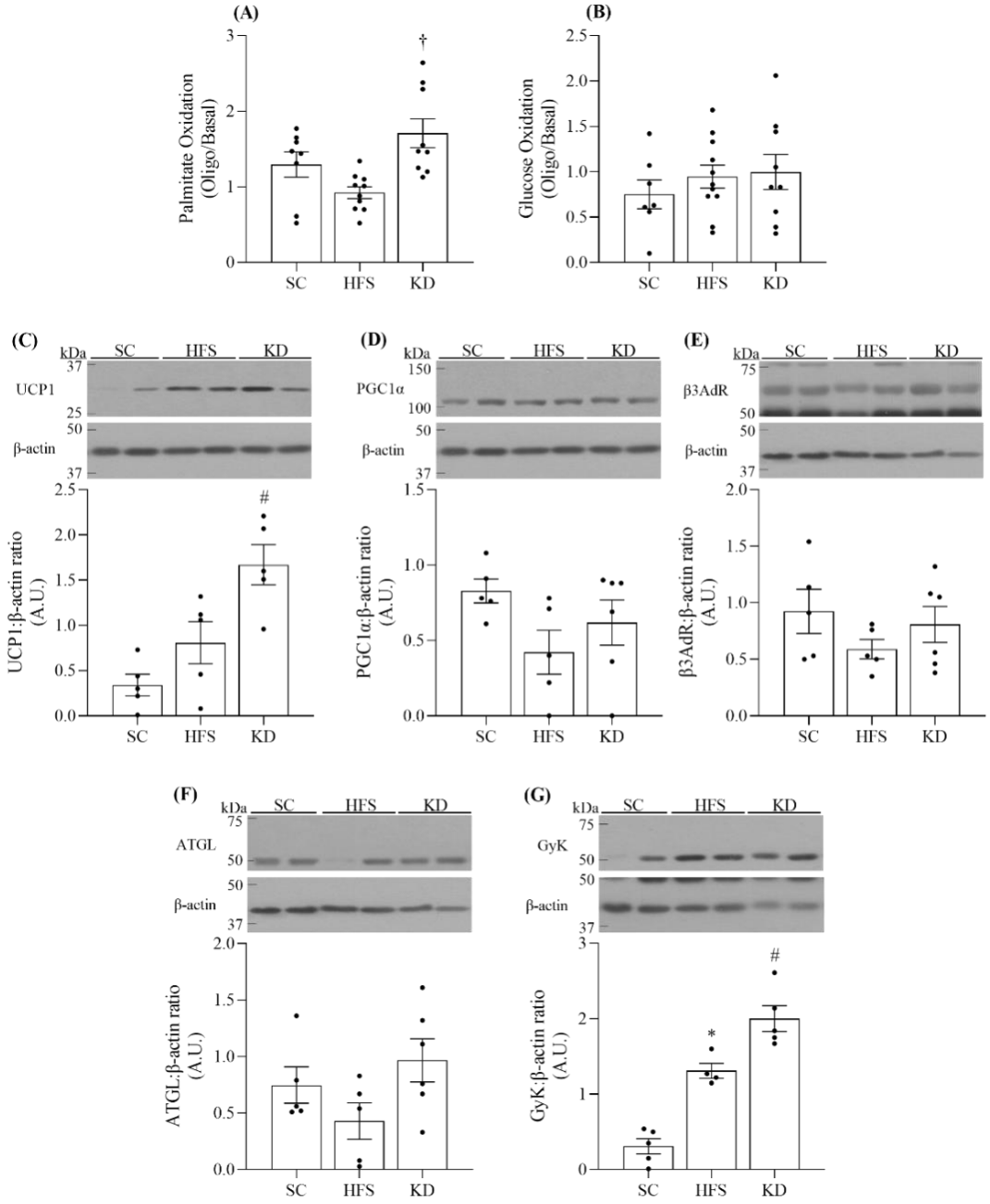

Figure 23: The KD increased uncoupled oxidation of palmitate (A) but not glucose oxidation (B) in brown adipocytes. The KD also increased UCP1 levels in BAT (C), whereas peroxisome proliferator-activated receptor gamma coactivator 1-alpha (PGC1α) (D), β3AdR (E), and ATGL (F) did not change with dietary intervention. However, GyK (G) was significantly elevated by HFS and KD, reaching higher levels in the latter. *p<0.05 vs. SC; #p<0.05 vs. all other groups; †p<0.05 vs. HFS. Bars represent mean ± SEM. One-way ANOVA. n=4-11.

5.5. Discussion

In this study, we show that a high-fat KD, devoid of carbohydrate, increased BAT uncoupled FA oxidative capacity and the machinery involved in lipolysis and TAG recycling in WAT. This was characterized by elevated UCP1 levels and uncoupled fatty acid oxidation in BAT, and increased GyK levels in WAT. Despite these adaptive responses being typically associated with dissipation as opposed to energy storage[204], the WAT mass of KD-fed animals increased to a level similar to the HFS diet. However, a major difference between the KD and the HFS diet was that the former sustained insulin-stimulated lipogenesis, whereas the latter impaired it. Thus, contrary to the obesogenic HFS diet, the KD-induced increase in adiposity did not impair the classical physiological functions of the WAT. Besides maintaining insulin-stimulated lipogenesis and Iso-stimulated lipolysis, the KD also upregulated a pathway by which white adipocytes can recycle TAG via GyK-mediated glycerol phosphorylation. These adaptive responses in WAT are compatible with an enhanced ability of this tissue to handle an abundant supply of food-derived fat and of NEFAs that escape oxidation in peripheral tissues and return to the WAT.

Neither the Sc Ing nor the Epid fat depots had detectable levels of UCP1, which indicates that the KD did not induce browning of the WAT. Previous studies have proposed that the KD causes browning in Sc Ing[147] and Epid[146] WAT. However, these studies measured the gene expression of UCP1[146,147] and other markers of browning[147]. Evidently, this does not necessarily translate to KD-induced alterations in protein levels, indicating that UCP1-mediated thermogenesis was not enhanced by KD in WAT. However, the WAT of KD-fed rats displayed time-dependent and depot-specific responses to different diets with regards to levels of lipolytic proteins and how each fat depot responded to β-adrenergic-induced lipolysis. This was evident for β3-AdR and ATGL levels that increased in the Sc Ing fat depot at week 8 of KD and HFS feeding,

whereas at week 16 only ATGL was elevated in HFS-fed rats. Conversely, the Epid fat of KD- and HFS-fed rats had unchanged levels of β3-AdR and ATGL at week 8, but at week 16 both diets elevated β3-AdR levels in the tissue. Furthermore, rates of Iso-stimulated lipolysis were not affected by the dietary interventions in Sc Ing adipocytes, whereas in Epid fat adipocytes the HFS diet markedly reduced it. This impairment in lipolytic capacity is supported by existing literature reporting that obesity causes catecholamine resistance and blunts β-adrenergic-stimulated lipolysis[202]. Along the same lines, the HFS diet-induced elevation in Epid β3AdR was not sufficient to reverse the attenuation in β-adrenergic signaling. These fat-depot specific patterns of adaptations in WAT indicate that fat accumulation was favoured in visceral over Sc WAT, which is metabolically detrimental[5]. Additionally, because adiposity similarly increased in HFS- and KD-fed rats at weeks 8 and 16, time and fat depot-specific effects of the KD do not seem to dictate accrual of fat mass. However, by preserving the lipolytic and lipogenic responses of the WAT, the KD likely exerted a protective effect against the potentially harmful effects of diet-induced obesity.

In addition to the WAT-specific effects, the KD also altered metabolism in BAT. Similar to previous studies, we found that the KD increased BAT UCP1 content[147,149]. However, to our knowledge, the effects of the KD on palmitate and glucose oxidation in brown adipocytes have not been investigated. We measured Oligo-induced versus basal oxidation as a measure of uncoupled oxidation, where the ratio between Oligo-induced and basal oxidation represents the capacity for proton leak and, thus, uncoupling capacity in brown adipocytes[7]. Here, we show that the KD enhanced the Oligo-induced oxidation of fatty acids in BAT, relative to basal, when compared to the HFS diet group. In line with these findings, the KD also significantly elevated BAT GyK content. In BAT, GyK mediates the replenishment of the TAG supply for thermogenesis[209]. In fact, it has been shown that cold exposure significantly increased BAT GyK

activity and expression in rats[209]. Thus, the observed elevations in UCP1, GyK and palmitate oxidation suggest that KD-feeding could potentially enhance BAT thermogenesis. These effects were consistent with the enhancement in BAT mass in the KD-fed animals. On the other hand, the HFS-induced elevation in iBAT mass could be attributed to the increased GyK content that was not met with an increase in fat consumption, leading to lipid accumulation and BAT growth.

The KD-induced increase in body weight and adiposity was contrary to our original hypothesis and contradicts what has been reported in studies that show that KD attenuates body weight, body mass index[15], and fat mass[203]. However, in these studies, energy intake was either not reported[15] or the KD was hypocaloric[203]. This is relevant because it did not discriminate whether the observed effects were caused by reduced energy intake or due to altered macronutrient composition of the diet. In fact, studies that use a KD that is isocaloric to the control diet generally show that fat mass is not significantly reduced[149,210], and may even be elevated under KD conditions[146]. Similarly, we also observed a KD-induced increase in fat mass under isocaloric conditions, which was likely supported by the enhanced energy efficiency observed in these animals, and a reduction in energy expenditure[204]. In this context, the KD-induced elevation in BAT thermogenic capacity was likely not sufficient to account for the increased dietary fat intake under chronic KD conditions. Furthermore, TAG recycling may not have increased energy expenditure enough to induce fat loss[211]. This limited capacity to oxidize fat could have led to the diversion of fatty acids for storage in the WAT, driving the increase in adiposity. Nevertheless, TAG recycling remains a crucial mechanism under KD conditions because it allowed the WAT to cope with the abundance of dietary fat[7,212], which likely facilitated the preservation of catecholamine and insulin sensitivity in the white adipocytes[5,42]. In turn, it is plausible that the maintenance of insulin-stimulated lipogenesis and β-adrenergic stimulated lipolysis prevented

hyperglycaemia in these animals, despite the robust increase in fat mass[5]. Altogether, our data support the notion that adiposity is not necessarily the cause of disease[5]. Rather, it is the dysfunctional storage and breakdown of fat that triggers the onset of metabolic disorders[5].

It is important to consider that the protein contents of the HFS and KDs differed from that of the SC diet, where the two former diets had 20% kcal from protein and the latter was 27%. Because total energy intake was not different, this means that kcal from protein was lower in the HFS and KDs. Importantly, a low protein diet has been shown to increase sympathetic flux to BAT and induce thermogenesis in this tissue[213]. Therefore, we cannot discard the possibility that lower dietary protein content in KD- and HFS-fed rats could have induced BAT activation and potentially impacted BAT uncoupled oxidation, when compared to the SC group. However, despite equal protein contents in the HFS and KD groups, we observed an elevation in uncoupled oxidative capacity in the BAT of KD-fed animals, relative to HFS. Additionally, GyK was measured as an indication of fat-storing capacity and was proposed to enhance the supply for uncoupled FA oxidation in BAT from KD-fed animals. However, glycerol 3-phosphate may also be used by mitochondrial glycerol 3-phosphate dehydrogenase (mGPDH) to provide reducing equivalents for the electron transport chain[214]. This points to an alternative fate for glycerol 3-phosphate that contributes to thermogenesis in BAT[214]. However, mGPDH activity was not assessed in the present study and warrants future investigations into the potential effects of the KD on the glycerol 3-phosphate shuttle and mGPDH-mediated thermogenesis.

In conclusion, the KD enhanced uncoupled FA oxidation in BAT, increased the machinery for TAG recycling in white adipocytes, and preserved insulin sensitivity and lipolytic capacity in visceral and Sc WAT (Fig. 24). Despite upregulating these energy-dissipating pathways, this was not sufficient to overcome the abundance of dietary fat, leading to increased storage in the white

fat depots. However, the induction of these pathways was crucial to prevent metabolic dysregulation and preserve insulin-stimulated lipogenesis[42] in a condition of increased adiposity in KD-fed rats. Together, these effects maintained WAT function and could prevent ectopic lipid accumulation, which is of great importance to counteract obesity-induced dysfunctional metabolic alterations in WAT[5,12].

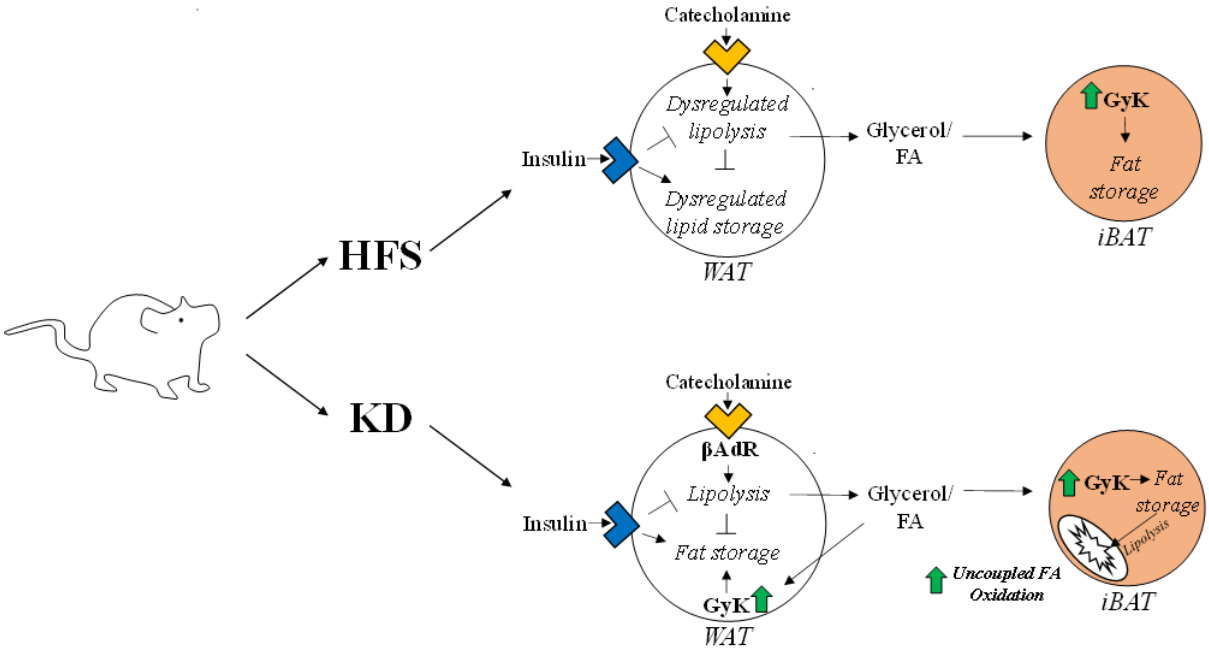

Figure 24: The HFS diet impaired insulin-stimulated glucose incorporation into lipids and Iso-stimulated lipolysis in WAT. The HFS diet also decreased uncoupled FA oxidation and upregulated GyK in BAT. These metabolic adaptations likely enhanced the lipid storage in BAT as lipogenesis in WAT was impaired. In contrast, the KD preserved lipolysis and lipogenesis in the white adipocytes and increased GyK levels. These KD effects enabled the WAT to recycle glycerol and resynthesize lipids under conditions of enhanced lipolysis. Furthermore, the BAT of KD-fed animals had increased levels of UCP1 and enhanced uncoupled fat oxidation. The fat supply for uncoupled oxidation in BAT was maintained by the elevation in GyK. These energy-dissipating mechanisms allowed the WAT and BAT from KD-fed rats to better cope with the abundance of fat in the diet.

Chapter 6: Obesogenic versus ketogenic diets in the regulation of the renin-angiotensin system in rat white and brown adipose tissues

Daniel Da Eira[1], Shailee Jani[1], Mateja Stefanovic[1] and Rolando B. Ceddia[1]

[1]Muscle Health Research Centre – School of Kinesiology and Health Science, York University, North York, ON, Canada.

Da Eira D, Jani S, Stefanovic M, Ceddia RB. Obesogenic versus ketogenic diets in the regulation of the renin–angiotensin system in rat white and brown adipose tissues. *Nutrition*. 2023;105:111862.

Statement of Labour

The work in this study was performed by DD. DD fed the rats the SC, HFS and KD and weighed the animals over the course of the feeding period. DD also extracted tissues and performed all Western blotting and qPCR experiments. Moreover, DD collected and analyzed the data, prepared figures and wrote and revised the manuscript. DD was funded by the Alexander Graham Bell – Canada Graduate Scholarship (Doctoral). Due to the length of the study and the logistics of tissue extraction procedures, SJ and MS assisted with the feeding of the diets and the tissue extractions.

Dr. Rolando Ceddia is the principal investigator and was involved in all stages of this study. The work presented in this manuscript was funded by grants awarded to RBC, including the Discovery Grant from the Natural Science and Engineering Research Council of Canada (NSERC) and by infrastructure grants from the Canada Foundation for Innovation (CFI) and the Ontario Research Fund (ORF).

6.1. Abstract

The ketogenic diet (KD) has been reported to reverse metabolic dysfunction in obesity. However, it remains unknown how the KD affects the balance between the classical and counterregulatory renin-angiotensin system (RAS) arms in adipose tissue, which carries important implications for metabolic function in adipocytes. The aim of this study was to compare the effects of the obesogenic and ketogenic diets on RAS balance in white and brown fat. To investigate this, male Wistar rats were fed a standard chow (SC; n=9), high-fat sucrose-enriched (HFS) obesogenic diet (n=11), or a KD (n=12). At the end of the 8-week feeding period, subcutaneous inguinal (Sc Ing), epididymal (Epid) and interscapular brown adipose tissue (iBAT) fat depots were extracted and subsequently used for the measurement of RAS proteins and MasR gene expression. *Results*: In SC-fed rats, the Sc Ing fat displayed the highest levels of Angiotensin converting enzyme 1 (ACE1), but very low levels of Angiotensin-II type 1 and 2 receptors (AT_1R and AT_2R) and ACE2. Conversely, the highest levels of ACE2, AT_1R, and AT_2R were found in iBAT. The HFS diet increased AT_1R protein in Sc Ing fat and iBAT, while the KD maintained low AT_1R levels in these fat depots. However, in Sc Ing and Epid fat depots, KD elevated AT_2R levels and significantly reduced Epid ACE1 levels. Therefore, despite fat depot-specific differences in RAS components, the obesogenic diet promoted the classical RAS arm, whereas the KD attenuated it and enhanced the counterregulatory arm.

6.2. Introduction

The RAS is well-known for its role in regulating blood pressure and fluid balance[215]. Under conditions of low blood pressure, renin is released in a rate-controlled manner from the kidney. Renin cleaves liver-derived angiotensinogen (Agt) to produce Angiotensin-I (Ang-I)[106]. Ang-I is then converted to angiotensin-II (Ang-II) by angiotensin converting enzyme 1 (ACE1)[106]. Finally, Ang-II interacts with the Ang-II type 1 receptor (AT_1R) to promote, through the classical RAS arm, vasoconstriction and fluid retention, thereby regulating blood pressure and fluid balance to homeostatic conditions[106,215]. However, hyperactivation of this pathway often leads to deleterious effects such as hypertension, fibrosis, and inflammation[106,215]. In opposition to the classical arm of the RAS is the counterregulatory arm. The latter is mediated by angiotensin converting enzyme 2 (ACE2)[105,216], that converts Ang-II to angiotensin-(1,7) (Ang-(1,7)). Through the Mas receptor (MasR), Ang-(1,7) elicits several physiological effects that oppose the ACE1/Ang-II/AT_1R arm of the RAS, including vasodilation, insulin sensitization, and anti-inflammatory effects[105,112,216,217].

One condition that promotes RAS hyperactivation is obesity[105,218], which is characterized by the expansion of adipose tissue[19,219]. Of the two major types of adipose tissue, the white adipose tissue (WAT) is specialized in energy storage, whereas the brown adipose tissue (BAT) burns energy and releases heat in a process known as thermogenesis[4,7,19]. Besides their role in energy storage and thermogenesis, both WAT and BAT act as endocrine organs and express components of the RAS[90,220,221], although RAS regulation has been mostly attributed to alterations in WAT, particularly under conditions of obesity[217,221]. In fact, hyperactivation of the classical ACE1/Ang-II/AT_1R arm of the RAS lead to insulin resistance and WAT inflammation in mice overexpressing Agt[222]. These mice exhibited an elevated expression of the pro-inflammatory cytokine monocyte chemotactic protein-1 (MCP-1) in their epididymal (Epid) fat[222]. Consistent with these findings,

Lee et al. observed an elevation in the expression of MCP-1 in the Epid fat of Otsuka Long-Evans Tokushima Fatty (OLETF) rats that was significantly reduced with the administration of an angiotensin receptor blocker[221]. Furthermore, incubation of 3T3-L1 adipocytes with Ang-II caused a reduction in insulin-stimulated glucose uptake in these cells, an effect that was reversed by angiotensin receptor blockade[221]. At the whole-body level, treatment with an angiotensin receptor blocker also improved glucose tolerance in OLETF rats[221]. These findings suggest that RAS activation in WAT has a major effect on insulin sensitivity and inflammation, and plays a crucial role in the development of obesity-related metabolic disorders[221]. Conversely, the administration of Ang-(1,7) to high-fat (HF)-fed mice increased BAT Akt phosphorylation, and improved homeostatic model assessment-insulin resistance (HOMA-IR)[112]. It has also been reported that an elevation in WAT MasR expression, induced by the ACE-inhibitor enalapril, caused morphological and functional conversion of WAT adipocytes into brown adipocytes (WAT browning), which carries great potential for the management of obesity and its related metabolic disorders[4,105]. In addition to the ACE2/Ang-(1,7)/MasR axis, another angiotensin receptor type, known as Ang-II type 2 receptor (AT_2R), exerts effects that are counterregulatory to the classical arm of the RAS, including improvements to insulin sensitivity[223] and inflammatory profile[217], as well as WAT browning[220]. Therefore, interventions that alter the balance between the classical and counterregulatory arms of the RAS appear to be effective at reversing obesity-related metabolic disorders. One dietary intervention that has been successful at reducing adiposity, improving insulin resistance, and attenuating inflammation has been the ketogenic diet (KD)[14,146]. However, to the best of our knowledge, it remains to be determined whether major differences exist in RAS regulation in WAT and BAT under obesogenic and ketogenic dietary conditions. In this context, we tested the hypothesis that, due to its anti-obesogenic effect[14,146], a KD would enhance the

counterregulatory arm of the RAS in WAT and BAT, whereas under obesogenic dietary conditions, the classical RAS arm would be heightened in both fat depots. Here, we show that the KD shifted the WAT RAS profile to the counterregulatory arm and that the obesogenic diet elevated the ACE1/Ang-II/AT_1R arm in both WAT and BAT.

6.3. Materials and Methods

Reagents – Protease (cOmplete Ultra Tablets) and phosphatase (PhosSTOP) inhibitors were obtained from Roche Diagnostics GmbH (Mannheim, Germany). The ACE1 (ab254222), ACE2 (ab108252), AT_1R (ab124734), and AT_2R (ab92445) antibodies were purchased from Abcam (Toronto, ON, Canada), and the β-actin (cat. no. 4967), p44/42 Mitogen-activated protein kinase (MAPK) (ERK1/2) (cat. no. 4695) and phosphorylated p44/42 $MAPK^{Thr202/Tyr204}$ (pERK1/2) (cat. no. 9101) antibodies were purchased from Cell Signaling (Danvers, MA, USA).

Animals – Male albino rats from the Wistar strain (Envigo, Indianapolis, IN, USA) weighing 200 – 250g (initial weight) were maintained in a constant-temperature (23ºC), with a fixed 12-h light/12-h dark cycle and fed for 8 weeks ad libitum either a standard chow diet (n=9) (SC, 27.0%, 13.0%, and 60.0% of calories provided by protein, fat, and carbohydrates, respectively) a HF, sucrose-enriched (HFS) diet (n=11) (20.0%, 60.0%, and 20.0% of calories provided by protein, fat, and carbohydrates [sucrose], respectively) or a KD (n=12) (20%, 80% and 0% of calories provided by protein, fat and carbohydrates, respectively). The SC (standard rat chow, catalog # 5012) was purchased from TestDiet (Richmond, IN, USA). The HFS and ketogenic diets (catalog # D12492 and D03022101, respectively) were purchased from Research Diets Inc. (New Brunswick, NJ, USA). At the end of the feeding period, animals were anesthetized (0.4 mg ketamine and 8 mg xylazine per 100g of body weight) and the Sc Ing, Epid, and iBAT fat pads

were extracted and weighed. A sample of each fat depot was immediately frozen in liquid nitrogen for subsequent experiments.

Ethics approval – The protocol containing all animal procedures described in this study was specifically approved by the Committee on the Ethics of Animal Experiments of York University (York University Animal Care Committee, YUACC, permit number: 2021-03) and performed strictly in accordance with the YUACC guidelines. All tissue extraction procedures were performed under ketamine/xylazine anesthesia, and all efforts were made to minimize suffering[205]. All experiments in this study were carried out in compliance with the ARRIVE guidelines[206].

Western blotting analysis of ERK phosphorylation and ACE1, ACE2, AT_1R, and AT_2R protein levels in the Sc Ing, Epid and iBAT fat depots – Sc Ing, Epid and iBAT samples were homogenized in a buffer containing 25 mM Tris-HCl, 25 mM NaCl (pH 7.4), 1 mM $MgCl_2$, 2.7 mM KCl, 1% Triton X-100 and protease and phosphatase inhibitors (Roche Diagnostics GmbH, Mannheim, Germany). Homogenates were centrifuged, the infranatant was collected, and an aliquot was used to measure protein by the Bradford method. Samples were diluted 1:1 (vol:vol) with 2x Laemmli sample buffer and heated to 95°C for 5 min. Twenty five μg of protein were loaded in each well. Samples were then subjected to SDS-PAGE, transferred to PVDF membrane, and probed for the proteins of interest. All primary antibodies were used at a dilution of 1:1,000. All densitometry analyses were performed using the ImageJ program. The comparative analysis of Sc Ing, Epid and iBAT RAS components (Fig. 25) was performed using samples from animals fed a SC diet for 8 weeks. The remaining blots contained samples from SC-, HFS- and KD-fed animals.

RNA isolation and quantitative PCR – Primers were designed using the software PrimerQuest (IDT) based on probe sequences available at the Affymetrix database (NetAffx™ Analysis Centre,

http://www.affymetrix.com/analysis) for each given gene. RNA was isolated from Sc Ing, Epid and iBAT tissues using Trizol™ (ThermoFisher Scientific, Waltham, MA, USA). Complimentary DNA (cDNA) was made from 2µg of extracted RNA using the ABM OneScript cDNA Synthesis kit (Diamed, Mississauga, ON, Canada), according to the manufacturer's instructions. Samples were run in duplicates on 96-well plates, and each 20µl reaction contained 4µl of cDNA, 0.4µl of primer, 10µl of Brightgreen 2x qPCR Mastermix (Diamed, Mississauga, ON, Canada) and 5.6µl of RNase-free water. Real-time PCR analysis was performed using a Bio-Rad CFX96 Real Time PCR Detection System (Bio-Rad, Mississauga, ON, Canada) using the following amplification conditions: 95°C (10 min); 40 cycles of 95°C (15s), 60°C (60s). All genes were normalized to the control gene β-actin, and differences in gene expression between groups were determined using the ΔΔCt method[188]. Values are expressed as fold increase relative to the SC group. Primer sequences utilized were as follows: Mas1 forward (CGCCAACCCTTTCATCTACT) and reverse (CCTAGGTTGCATCTCGTCTTT); and β-actin forward (GTGAAAAGATGACCCAGATC) and reverse (CACCGCCTGGATGGCTACGT).

Statistical Analyses – Data were expressed as Mean ± SEM. Statistical analyses were performed by using mixed-model analyses and one-way ANOVAs with Bonferroni multiple comparison post-hoc tests, as indicated in the figure legends. The GraphPad Prism software version 9.1.12 was used for all statistical analyses and for the preparation of all graphs. The level of significance was set to $p<0.05$.

6.4. Results

Body weight (BW) of SC, HFS and KD-fed animals at weeks 0, 4 and, 8 of the feeding period – All three diet groups experienced progressive weight gain from weeks 0 to 8 (Table 5). As expected, BW was significantly higher in the HFS than the SC animals at weeks 4 and 8 (Table

5). However, BW was not significantly different between the HFS and KD-fed animals at any point during the feeding period. Moreover, when compared to the SC animals, the KD elevated BW by 10 and 13.9%, at weeks 4 and 8, respectively (Table 5).

Table 5: Body weights of SC, HFS and KD-fed animals at weeks 0, 4 and 8 of the feeding period.

		Duration (weeks)		
		0	4	8
Body weight (g)	SC	213.5 ± 3.8	344.8 ± 11.2*	416.7 ± 15.3$^{\#}$
	HF	219.2 ± 4.8	385.7 ± 8.7*†	480.0 ± 14.0$^{\#\dagger}$
	KD	225.0 ± 3.9	379.3 ± 5.8*†	474.7 ± 9.1$^{\#\dagger}$

*$p<0.05$ vs. week 0 in respective group. $^{\#}p<0.05$ vs. weeks 0 and 4 in respective group. $^{\dagger}p<0.05$ vs. SC in respective week. Data are expressed as mean ± SEM. Mixed-effects model analysis. n=5 in the SC group, n=7 in the HFS group and n=8 in the KD group.

Tissue comparison of RAS proteins in Sc Ing, Epid, and iBAT fat depots –To assess the potential physiological importance of individual RAS components in the distinct fat depots, we measured RAS protein levels in the WAT and BAT of rats fed a SC diet for 8 weeks. ACE1 was 4.9- and 9.6-fold higher in Sc Ing fat than in Epid fat and iBAT, respectively (Fig. 25A), whereas ACE2 was most abundant in iBAT (Fig. 25B). In fact, ACE2 levels in iBAT were 11.6-fold higher than in Sc Ing fat (Fig. 25B). Although the difference between Sc Ing and Epid ACE2 contents did not reach statistical significance, Epid fat had the lowest ACE2 levels of all three fat depots (Fig 25B). With respect to AT_1R and AT_2R, iBAT displayed significantly higher contents of these two receptors than Sc Ing and Epid fat pads (Fig. 25C and D).

Effects of diet on Sc Ing, Epid and iBAT ACE1 and ACE2 protein contents – HFS-feeding significantly suppressed ACE1 content by ~82% in Sc Ing fat, relative to the SC animals (Fig. 26A), but did not alter Epid ACE1 levels (Fig. 26C). KD-feeding, on the other hand, attenuated both Sc Ing and Epid ACE1 by ~75 and 87%, respectively (Fig. 26A and 26C). ACE2 was also significantly decreased by both the HFS and KDs in Sc Ing fat (Fig. 26B). However, neither diet

altered Epid ACE2 content (Fig. 26D). In this context, the KD did not influence Epid ACE2 and decreased ACE1, indicating a shift toward the counterregulatory arm of the RAS in this tissue. With regards to iBAT, HFS- and KD-feeding attenuated ACE1 content (Fig. 26E) and the HFS diet suppressed ACE2 (Fig. 26F); however, these effects were not statistically significant.

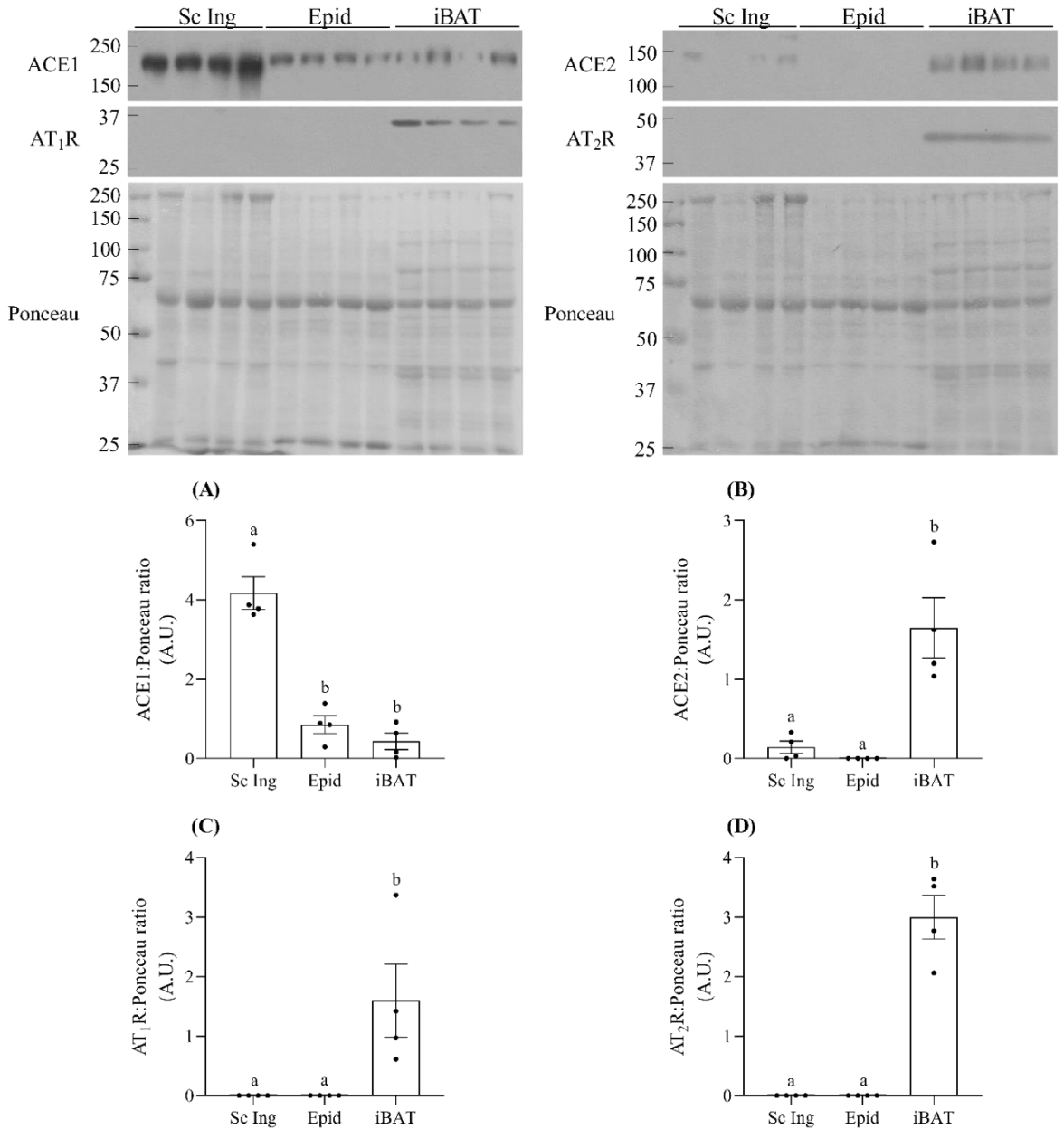

Figure 25: Angiotensin converting enzyme 1 (ACE1) content was highest in the subcutaneous inguinal (Sc Ing) fat (A). However, angiotensin converting enzyme 2 (ACE2), angiotensin II type

1 receptor (AT_1R) and angiotensin II type 2 receptor (AT_2R) (B, C and D, respectively) were more abundant in interscapular brown adipose tissue (iBAT) than in Sc Ing or epididymal (Epid) fat depots. ACE2 levels were elevated in Sc Ing fat, relative to Epid fat, however this difference did not reach statistical significance (B). Statistically significant differences denoted by different letters. $p<0.05$. Bars represent mean ± SEM. One-way ANOVA. n=4 rats.

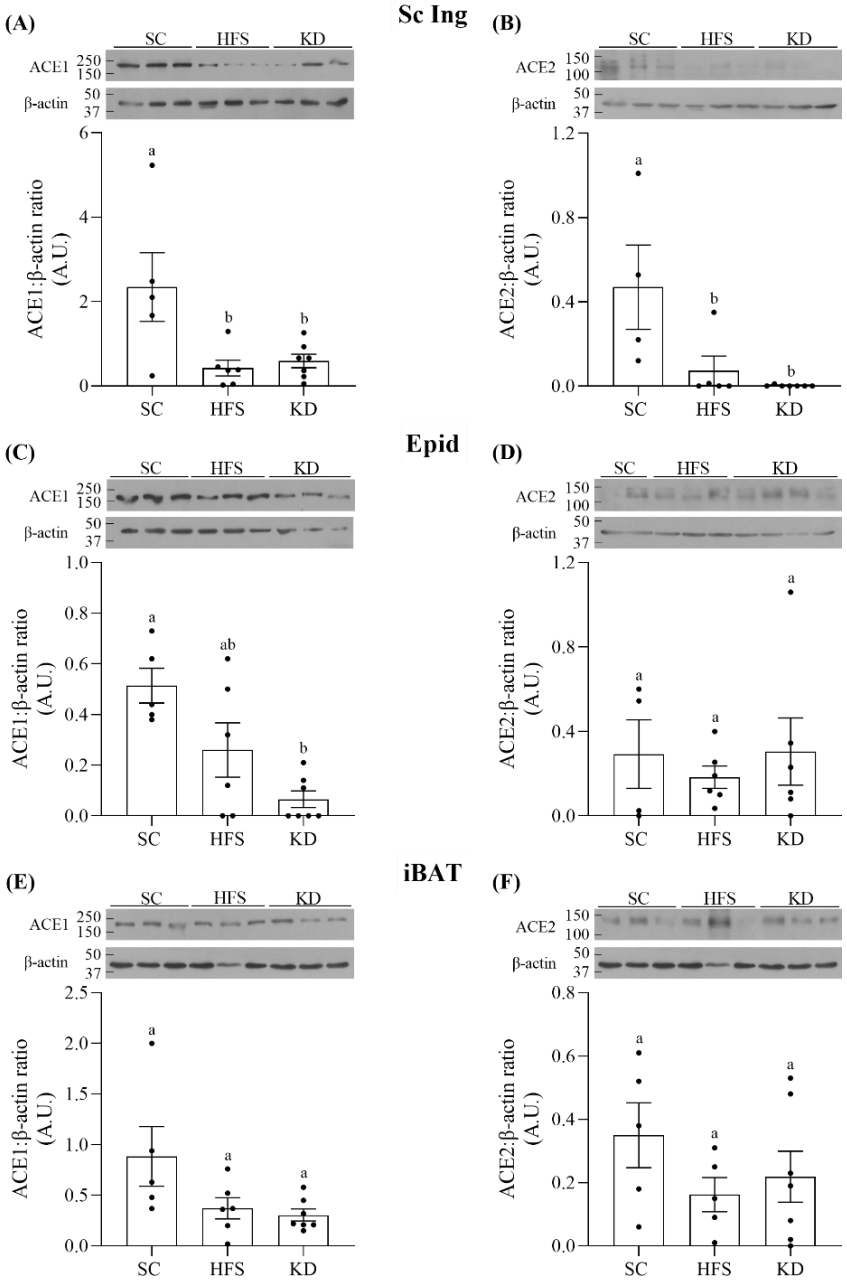

Figure 26: The high-fat sucrose-enriched (HFS) diet and the ketogenic diet (KD) significantly reduced Sc Ing ACE1 and ACE2 protein contents (A and B, respectively). In Epid fat, only the KD significantly attenuated ACE1 levels, relative to the SC group (C). However, diet did not affect ACE2 levels in this tissue (D). Finally, ACE1 and ACE2 levels were not significantly

altered by dietary intervention in iBAT (E and F, respectively). Statistically significant differences denoted by different letters. $p<0.05$. Bars represent mean ± SEM. One-way ANOVA. n=4-7 rats.

Effects of diet on Sc Ing, Epid and iBAT AT_1R and AT_2R protein contents – Sc Ing and iBAT AT_1R levels increased ~4.6- and 3-fold, respectively, in the HFS group, relative to the SC group (Fig. 27A and E, respectively). In the Epid fat, AT_1R levels were neither altered by the HFS diet nor the KD (Fig. 27C). However, the KD increased AT_2R protein levels by 23.4- and 5.2-fold in Sc Ing and Epid fat, respectively (Fig. 27B and D, respectively). In iBAT, no significant alteration in AT_2R protein levels was detected with any of the diets (Fig. 27F). Altogether, these findings demonstrate that the HFS and KD exerted tissue-specific effects with respect to AT_1R and AT_2R levels in Sc Ing, Epid, and iBAT fat depots.

Effect of diet on Sc Ing, Epid, and iBAT MasR gene expression – Sc Ing expression of *Mas1*, the gene that encodes the MasR, was downregulated by ~82 and 80% in HFS- and KD-fed animals, respectively (Fig. 28A), whereas in Epid and iBAT the expression of the MasR was not altered by diet (Fig. 28B and C). These *Mas1*-related findings indicate that both the HFS and KD exerted a potential reduction of the counterregulatory ACE2/Ang-(1,7)/MasR/AT_2R arm of RAS, although this effect was restricted to the Sc Ing WAT.

Phosphorylation of ERK1/2 in WAT and BAT following the dietary interventions – To assess whether diet-induced changes in RAS receptors were influencing Ang signalling in WAT and BAT, we measured phosphorylation of the downstream protein ERK1/2[220,224]. ERK1/2 phosphorylation in Sc Ing, Epid, and iBAT did not differ among diets (Fig. 29A, B and C). However, the pERK1/2/ERK1/2 ratio tended to increase with KD-feeding in all three tissues, relative to the HFS group (Fig. 29).

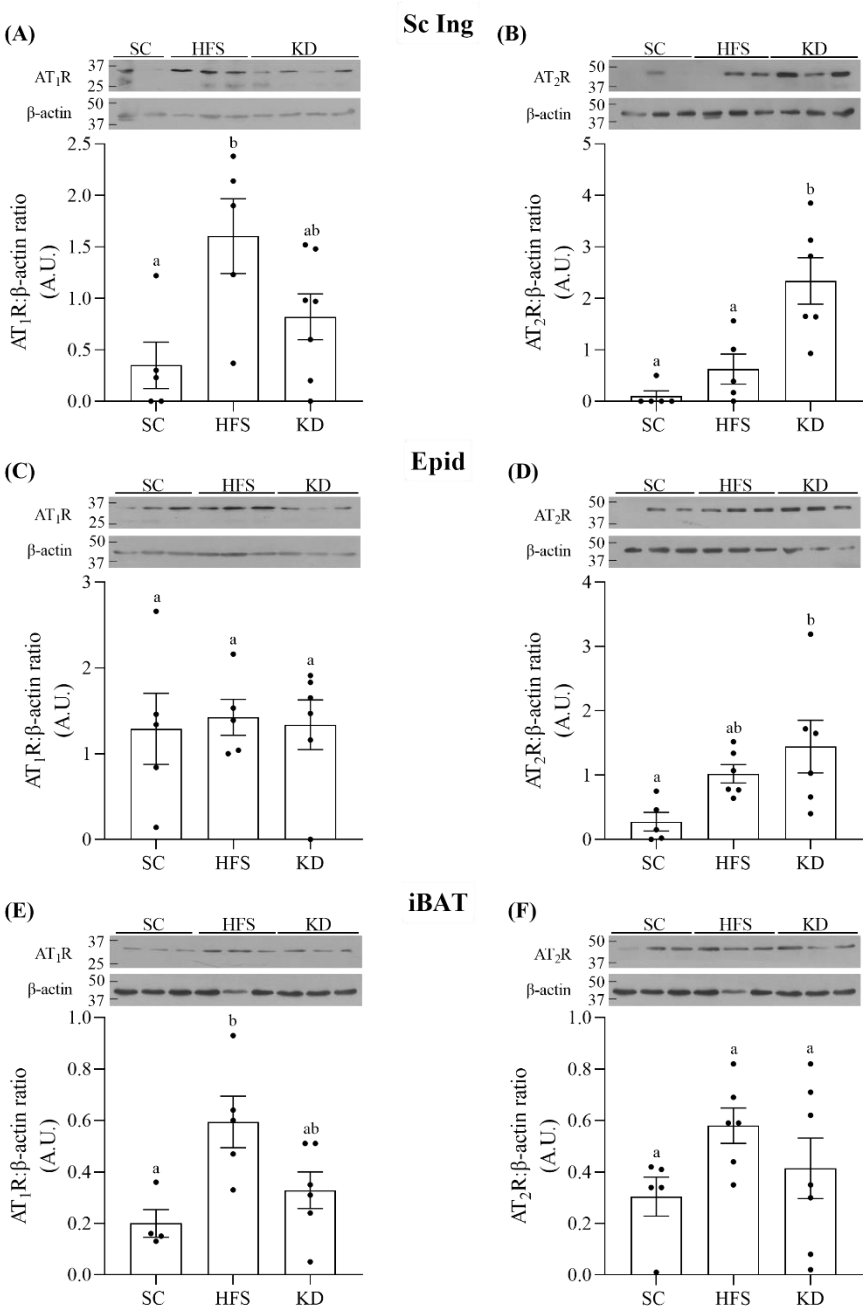

Figure 27: AT_1R content was significantly increased in Sc Ing fat with the HFS, but not KD (A). In contrast, the KD, but not the HFS diet, elevated Sc Ing AT_2R (B). In Epid fat, AT_1R was not altered with diet (C), however AT_2R content was increased in animals fed the KD (D). Similar to the Sc Ing fat, iBAT AT_1R content was elevated in the HFS-fed animals (E). Conversely, AT_2R was not influenced by diet (F). Statistically significant differences denoted by different letters. $p<0.05$. Bars represent mean ± SEM. One-way ANOVA. n=4-7 rats.

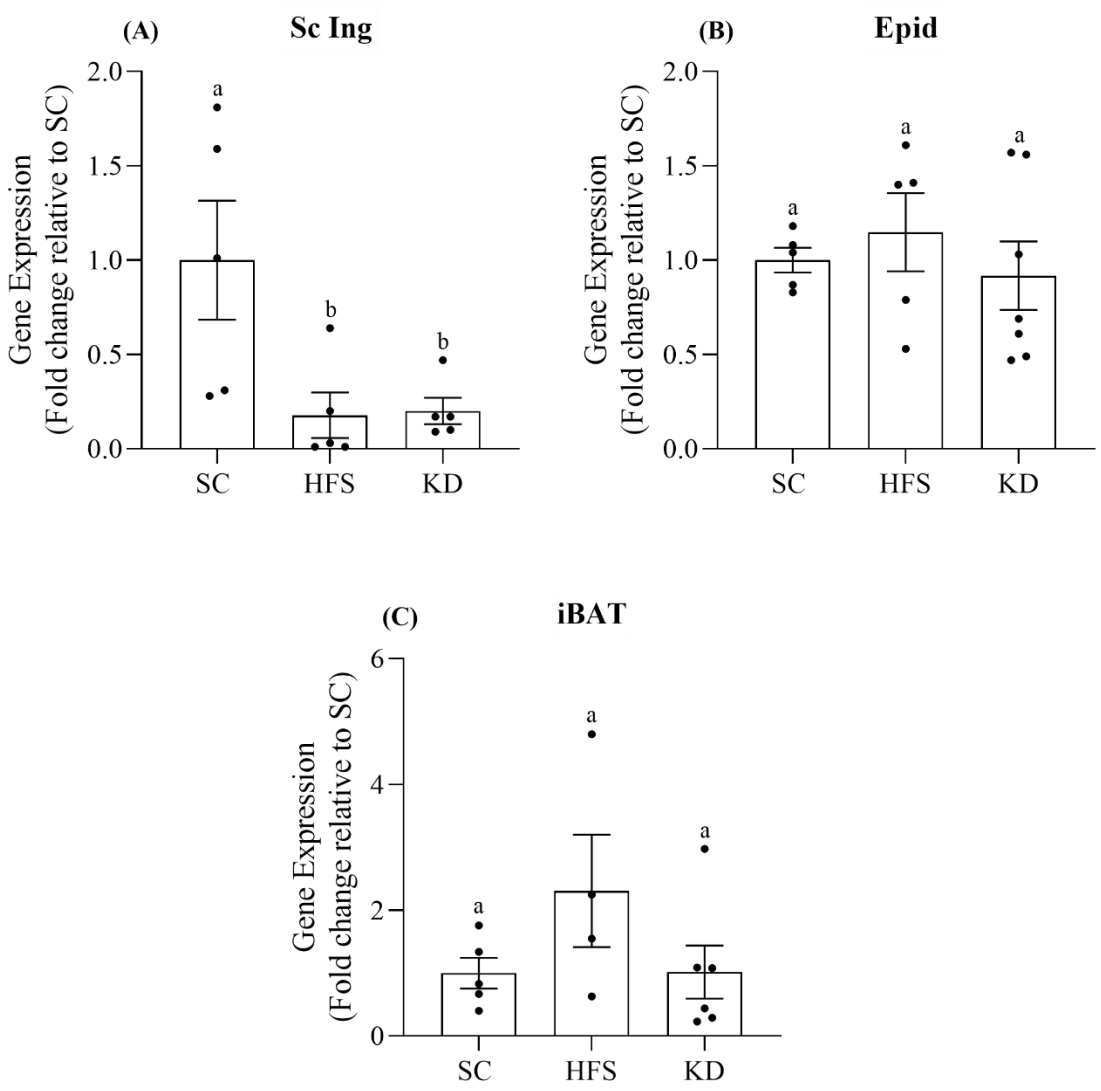

Figure 28: Mas receptor (MasR) expression was significantly attenuated in Sc Ing fat by both the HFS diet and KD (A). However, gene expression of the MasR was not altered by diet in Epid fat or BAT (B and C, respectively). Statistically significant differences denoted by different letters. $p<0.05$. One-way ANOVA. n=4-7 rats.

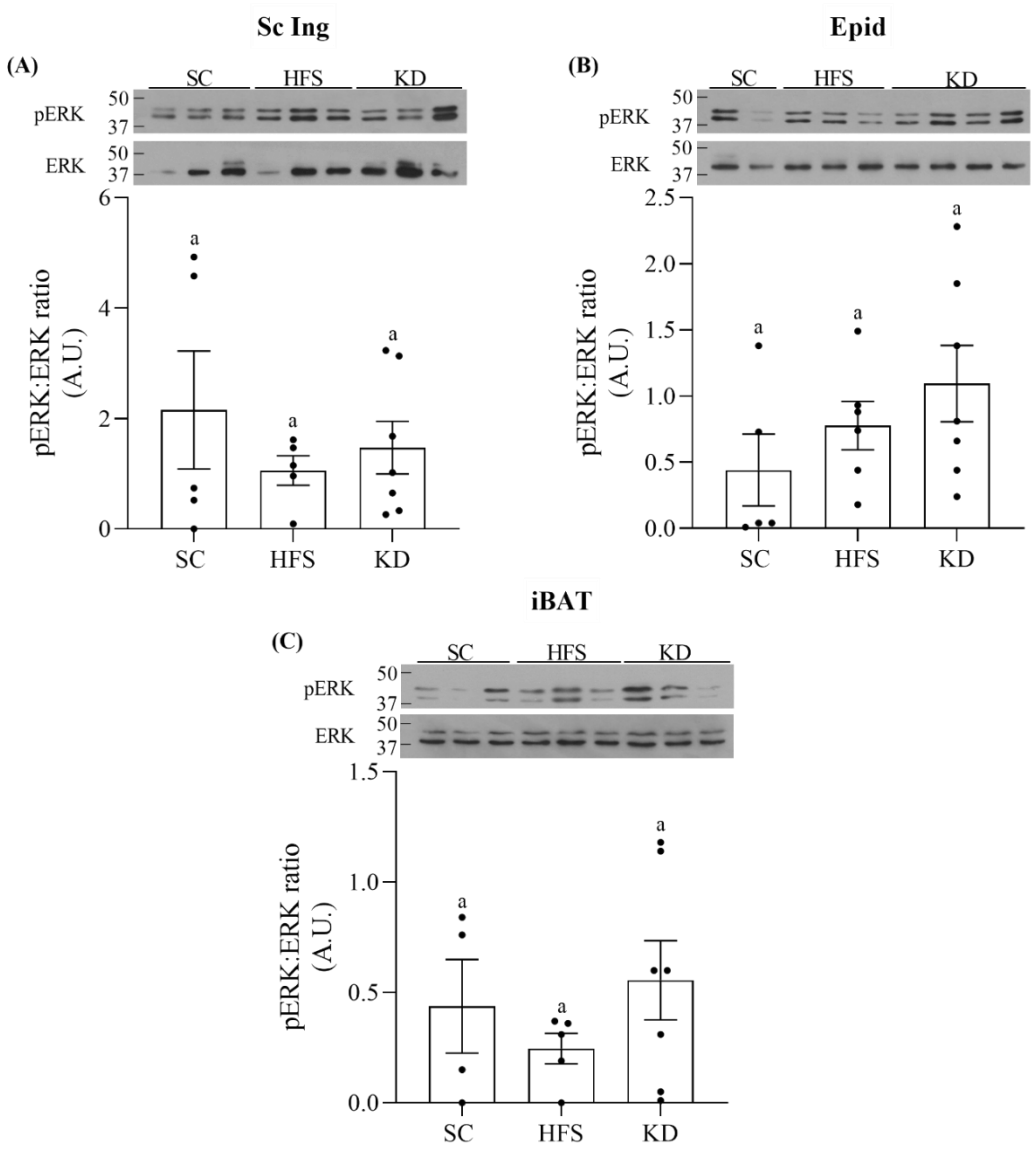

Figure 29: p44/42 mitogen activated protein kinase (ERK1/2) phosphorylation was not influenced by diet in the Sc Ing, Epid or iBAT fat depots (A, B and C, respectively). Statistically significant differences denoted by different letters. $p<0.05$. One-way ANOVA. n=4-7 rats.

6.5. Discussion

Here, we demonstrate that levels of RAS components differ significantly between WAT and BAT, and that the HFS and KD regulated ACE1 and ACE2, as well as AT_1R, AT_2R protein contents and *Mas1* gene expression in a fat depot-specific manner. In line with our original hypothesis, overall, the HFS obesogenic diet enhanced the classical arm of the RAS, whereas the KD enhanced the protective, counterregulatory RAS arm. This was supported by our findings that, despite major fat depot differences with respect to their contents in RAS proteins, the KD significantly increased AT_2R and attenuated ACE1 levels in both WAT depots. Importantly, because the Sc Ing fat exhibited the highest levels of ACE1, the marked reduction of ACE1 by the KD is consistent with attenuated activity of the classical RAS arm in this tissue. This is in line with previous observations that elevations in Sc Ing WAT Ang-II levels under conditions of HF diet-induced obesity are dependent on ACE1 in mice[105].

In Sc Ing fat, ACE1 levels were also reduced by the HFS diet, which is apparently at odds with our initial hypothesis because it suggests that the obesogenic diet attenuated the classical arm of the RAS. However, in both HFS- and KD-fed animals, the decrease in ACE1 content was accompanied by a reduction in ACE2 in the SC Ing fat depot. Thus, although lower ACE1 levels could potentially lead to suppressed Ang-II formation in this tissue, the concomitant reduction of ACE2 favored impairment in the conversion of Ang-II to Ang-(1,7), likely leaving the Ang-II levels unaffected and Ang-(1,7) levels potentially reduced. In line with this, Giori et al. observed unchanged levels of Ang-II, and a trend to decrease Ang-(1,7) in the Sc WAT of HF-fed mice compared to controls[105]. In this context, the diet-induced shift of the Sc Ing RAS does not appear to be influenced by alterations to ACE1 or ACE2 contents and is instead mediated by changes in the expressions of the Ang receptors.

Analysis of AT_1R and AT_2R protein levels revealed that these receptors were not very prominent in the WAT fat depots from SC-fed rats. However, in the Sc Ing fat and iBAT of HFS-fed rats, AT_1R levels were significantly increased, whereas the KD did not affect the levels of this receptor in any of the tissues. In white adipocytes, stimulation of AT_1R has been shown to increase inflammatory markers, such as MCP-1 mRNA expression and NFκβ transcription[221]. Furthermore, in a rat model of metabolic dysfunction, administration of the AT_1R antagonist L158809 improved glucose tolerance[221]. Thus, the HFS diet-induced elevation in the content of this receptor is consistent with activation of the classical RAS arm and induction of detrimental metabolic effects observed in adipose tissue in obesity[104,105,221]. In addition to the enhanced AT_1R content, Sc Ing MasR expression was significantly reduced in HFS-fed animals. Indeed, other studies have reported that an obesogenic diet attenuates MasR expression in subcutaneous fat and reduces the activity of the counterregulatory RAS arm[105]. Importantly, KD-feeding did not alter AT_1R levels in any of the fat depots studied but induced a robust increase in Sc Ing and Epid AT_2R levels, an effect that likely compensated for the KD-induced attenuation in MasR expression in Sc Ing fat. This is compatible with our finding that the KD caused a reduction in Sc Ing ACE2 (Fig. 26B), which potentially decreased Ang-(1,7)/MasR signaling and, consequently, the expression of the MasR[224]. Therefore, the KD-induced elevation of AT_2R could potentially counteract the classical, pro-inflammatory arm of the RAS[105] in WAT. In iBAT, however, neither the HFS nor the KD altered AT_2R levels, despite this tissue displaying the highest relative abundance of this receptor. The lack of an effect of dietary intervention on BAT AT_2R can be explained by the reduced physiological importance of this receptor for thermogenesis in mature adipocytes. This is compatible with reports that the differentiation of brown adipocytes depends on AT_2R signaling[220], whereas fully differentiated cells rely on MasR signaling for BAT activation[90]. As previously

mentioned, the gene expression of MasR was unchanged by any of the dietary interventions, and this likely sufficed to maintain iBAT activity. Nevertheless, the elevated abundance of the Ang receptors and ACE2 in BAT indicates a higher capacity for Ang signaling in this tissue.

A complex network involving several factors determines the downstream signaling of Ang receptors[217,220]. One protein that is particularly relevant for Ang signaling in the adipose tissue is ERK1/2[224]. In adipocytes, ERK1/2 phosphorylation is enhanced by AT_1R stimulation, whereas stimulation of the MasR or AT_2R attenuates ERK1/2 phosphorylation[220,224]. In the present study, ERK1/2 phosphorylation was not significantly altered by diet in any of the three fat depots studied, although tissue-specific trends in ERK1/2 phosphorylation appear to exist. It is noteworthy that studies demonstrating Ang-II-mediated ERK phosphorylation were performed in isolated adipocytes, incubated in the absence or presence of Ang-II, Ang-(1,7)[224] and angiotensin receptor antagonists[220]. Although this experimental model is valuable for the observation of isolated effects induced by individual factors on cellular signaling pathways, it does not account for other circulating hormones that also act on the same downstream targets. For instance, fibroblast growth factor 21 (FGF21), which is known to be altered with KD-feeding[146], promotes ERK1/2 phosphorylation[20]. In this study, freshly isolated whole WAT was used to assess ERK1/2 phosphorylation, and the presence of cells other than adipocytes in the stromal vascular fraction (fibroblasts, blood and blood vessels, immune cells, and nerve tissue) also likely affected the results. Thus, we cannot discard the possibility that the dietary interventions meaningfully affected the ability of the classical and counterregulatory arms of the RAS to signal through ERK1/2 phosphorylation in adipocytes.

The KD has been demonstrated to cause significant reductions in adiposity and body weight (BW) in humans[14,15]. In this study, we found that KD-fed rats displayed lower BW than

HFS-fed rats, although this difference was not statistically significantly, which is inconsistent with the typical effects of KD on adiposity in humans. However, this apparent discrepancy can be explained by species differences with respect to BW responses to feeding. This is also evident when comparing mice vs. rats and even among distinct rat strains utilized in studies reporting the effects of KD on BW[146,218]. In fact, in a previous study conducted in Sprague-Dawley (SD) rats[218], we observed that animals fed for 8 weeks with the same KD reached lower BW than their counterparts fed a HFS diet. In this study, we used Wistar rats, which display a very distinct pattern of food intake and fat and BW gain when compared to SD rats fed similar diets. Nevertheless, the elevation in BW did not prevent the KD-induced shift of WAT RAS components toward the counterregulatory arm.

In conclusion, major depot-specific differences in RAS components were detected between WAT and BAT. This was evidenced by the Sc Ing fat displaying the highest levels of ACE1, but very low levels of AT_1R, AT_2R, and ACE2. Conversely, the highest levels of ACE2, AT_1R, and AT_2R were found in iBAT. Despite these differences, the HFS diet increased the ACE1/Ang-II/AT_1R arm of the RAS, whereas the KD enhanced the ACE2/Ang-(1,7)/MasR/AT_2R counterregulatory arm of the RAS in WAT. These findings provide evidence that the KD can be a valuable dietary intervention for the management of the adipose tissue RAS, and can thereby serve to potentially counteract the dysfunctional metabolism and inflammation[104] that are observed in adipose tissue with obesity.

Chapter 7: Obesogenic and ketogenic diets distinctly regulate the SARS-CoV-2 entry proteins ACE2 and TMPRSS2 and the Renin-Angiotensin System in rat lung and heart tissues

Daniel Da Eira, Shailee Jani and Rolando B. Ceddia

Muscle Health Research Centre—School of Kinesiology and Health Science, York University, North York, ON, M3J1P3, Canada

Da Eira D, Jani S, Ceddia RB. Obesogenic and Ketogenic Diets Distinctly Regulate the SARS-CoV-2 Entry Proteins ACE2 and TMPRSS2 and the Renin-Angiotensin System in Rat Lung and Heart Tissues. *Nutrients*. 2021; 13(10):3357.

Statement of Labour

The work in this study was performed by DD. DD fed the rats the SC, HFS and KD and weighed and measured glycaemia in the animals over the course of the feeding period. DD also extracted tissues and performed all Western blotting and qPCR experiments. Moreover, DD collected and analyzed the data, prepared figures and wrote and revised the manuscript. DD was funded by the Alexander Graham Bell – Canada Graduate Scholarship (Doctoral). Due to the length of the study and the logistics of tissue extraction procedures, SJ assisted with the feeding of the diets, glycaemia measurements and tissue extractions.

Dr. Rolando Ceddia is the principal investigator and was involved in all stages of this study. The work presented in this manuscript was funded by grants awarded to RBC, including the Discovery Grant from the Natural Science and Engineering Research Council of Canada (NSERC) and by infrastructure grants from the Canada Foundation for Innovation (CFI) and the Ontario Research Fund (ORF).

7.1. Abstract

Obesity increases the severity of SARS-CoV-2 outcomes. Thus, this study tested whether obesogenic and ketogenic diets distinctly affect SARS-CoV-2 entry proteins and the renin-angiotensin system (RAS) in rat pulmonary and cardiac tissues. To investigate this, male Sprague-Dawley rats were fed either standard chow (SC), a high-fat sucrose-enriched diet (HFS), or a ketogenic diet (KD) for 16 weeks. Afterwards, levels of angiotensin converting enzyme 2 (ACE2), transmembrane protease serine 2 (TMPRSS2), RAS components, and inflammatory genes were measured in the lungs and hearts of these animals. In the lungs, HFS elevated ACE2 and TMPRSS2 levels relative to SC diet, whereas the KD lowered the levels of these proteins and the gene expressions of toll-like receptor 4 and interleukin-6 receptor relative to HFS. The diets did not alter ACE2 and TMPRSS2 in the heart, although ACE2 was more abundant in heart than lung tissues. Thus, diet-induced obesity increased the levels of viral entry proteins in the lungs, providing a mechanism whereby SARS-CoV-2 infectivity can be enhanced in obese individuals. Conversely, by maintaining low levels of ACE2 and TMPRSS2 and by exerting an anti-inflammatory effect, the KD can potentially attenuate the severity of infection and migration of SARS-CoV-2 to other ACE2-expressing tissues.

7.2. Introduction

Obesity is characterized by an expansion in white adipose tissue (WAT) mass and is linked to a number of comorbidities, including hypertension and diabetes[225]. More recently, obesity has emerged as a major risk factor for severe illness related to COVID-19 infection[226,227]. Infection with the severe acute respiratory syndrome-coronavirus-2 (SARS-CoV-2) occurs mainly through the airway[113]. At the cellular level, the virus binds to its receptor, ACE2[113,122]. The interaction between ACE2 and SARS-CoV-2 occurs via the virus's spike (S) protein; however, an additional crucial step catalyzed by transmembrane protease serine 2 (TMPRSS2) leads to cleavage of the S protein[113,122]. This latter step allows for fusion of the virus and host cell membranes so endocytosis of the virus can occur. Once inside the cell, the virus can utilize the cell's ribosomes to transcribe its own RNA and undergo replication[117]. The enhanced susceptibility of obese individuals to severe COVID-19 outcomes has been linked to elevations in ACE2 and TMPRSS2 in lung tissues[113,125]. In fact, Sarver and Wong showed that ACE2 expression was elevated in the lungs and tracheas of male, obese mice[113]. Similarly, Batchu et al. reported elevations in ACE2 and TMPRSS2 protein contents in the lungs of HF-fed, diabetic mice[125]. In this context, the diet-induced elevations in SARS-CoV-2 entry proteins provide a plausible mechanism that explains the increased susceptibility of obese individuals to severe outcomes. It is important to note that ACE2 is also a component of the renin-angiotensin aldosterone system (RAS) which has emerged as another possible mechanism mediating COVID-19-related illness[228].

The RAS is classically responsible for the regulation of fluid balance and blood pressure[228]. In short, the kidney releases renin, which converts liver-derived angiotensinogen into angiotensin I (Ang-I)[106]. Ang-I is then processed into angiotensin-II (Ang-II), mainly in the pulmonary circulation[107], by angiotensin converting enzyme (ACE1)[106]. Ang-II can then bind to the G-protein

coupled receptor angiotensin-II, type 1 receptor (AT_1R)[106] where it induces vasoconstriction, water retention and sympathetic nervous system activation[106]. Under conditions of hypertension and obesity, hyperactivation of the RAS leads to inflammation, fibrosis and oxidative damage[228]. In this context, therapies aimed at increasing flux through the counterregulatory arm of the RAS have gained attention as a potential treatment for hypertension and obesity[226,228]. These effects are mainly mediated by ACE2, which converts Ang-II into Ang(1,7)[228]. Ang(1,7) binds to the Mas receptor (MasR) which exerts protective, anti-inflammatory effects[106]. Moreover, Ang-II can also bind to angiotensin II, type 2 receptor (AT_2R)[226]. AT_2R exerts similar effects to MasR, however it is mainly expressed under conditions of AT_1R hyperactivation and injury to suppress inflammation and oxidative stress[111,226]. Following COVID infection, ACE2 becomes downregulated[226]. Consequently, the obesity-induced elevation in Ang-II increases signaling through AT_1R, which promotes inflammation and tissue damage[226]. Thus, the role of ACE2 in COVID-19-related illness extends beyond serving as a viral entry protein. Rather, it is also implicated in the inflammatory response that ensues, which carries a profound impact for tissue damage and organ failure[226]. In this context, shifting obese individuals from the ACE1/Ang-II/AT_1R arm to the ACE2/Ang(1,7)/MasR and AT_2R arm is of great importance to reduce the susceptibility of obese individuals to severe COVID-19 outcomes.

Recently, the ketogenic diet (KD) has sparked interest as a potential therapeutic tool for the management of obesity. In fact, it has been shown that the KD improved blood pressure, glycemia and body weight in Type 2 diabetic patients[15] and carries potential as a anti-inflammatory diet[146]. However, to our knowledge, little is known regarding the effect of the KD on the RAS components in lung and heart tissues. Moreover, despite there being evidence that obesity enhances the expression of ACE2 and TMPRSS2 in lung tissue, to the best of our knowledge no

studies have evaluated whether a KD can affect molecular steps involved in SARS-CoV-2 infection. In this context, our study aims to compare the effects of different dietary interventions on the contents of viral entry proteins and RAS components in lung and heart tissues. Here we provide a detailed analysis of how an obesogenic diet regulates ACE2 and TMPRSS2 contents, as well as AT_1R and AT_2R levels in lung and cardiac tissues. Additionally, we test whether a KD can alter the levels of these proteins and reduce the expression of inflammatory genes in the lungs.

7.3. Materials and Methods

Reagents – Protease (cOmplete Ultra Tablets) and phosphatase (PhosSTOP) inhibitors were obtained from Roche Diagnostics GmbH (Mannheim, Germany). The Insulin ELISA kit was be purchased from Millipore-Sigma (Burlington, MA, USA). The ACE1 (ab254222), ACE2 (ab239924), AT_1R (ab124734), AT_2R (ab92445) and TMPRSS2 (ab92323) antibodies were purchased from Abcam (Toronto, ON, Canada) and the β-actin (cat. no. 4967) antibody was purchased from Cell Signaling (MA, USA).

Animals – Male albino rats from the Sprague-Dawley strain (Envigo, IN, USA) weighing 200 – 250 g (initial weight) were maintained in a constant-temperature (23 ^{o}C), with a fixed 12-h light/12-h dark cycle and fed for 16 weeks *ad libitum* either a standard chow diet (SC, 27.0 %, 13.0 %, and 60.0 % of calories provided by protein, fat, and carbohydrates, respectively) a HF, sucrose-enriched (HFS) diet (20.0%, 60.0%, and 20.0% of calories provided by protein, fat, and carbohydrates [sucrose], respectively) or a KD (20%, 80% and 0% of calories provided by protein, fat and carbohydrates, respectively). The energy densities for the SC, HFS and ketogenic diets were 3.43, 5.24 and 6.14 kcal/g, respectively. The SC diet (standard rat chow, catalog # 5012) was purchased from TestDiet (Richmond, IN, USA). The HFS and ketogenic diets (catalog # D12492 and D03022101, respectively) were purchased from Research Diets Inc. (New Jersey, NJ, USA).

Energy intake was not significantly different between the three groups at weeks 0, 4 and 8 (Table 6). At week 16, the KD-fed animals had 17.9 and and 18.1% lower energy intake than the SC and HFS-fed animals, respectively (Table 6).

Table 6: Energy intake at weeks 0, 4, 8, and 16 in the SC-, HFS-, and KD-fed animals.

	Week	SC	HFS	KD
Energy intake (kcal/rat/day)	0	69.23 ± 3.8	66.49 ± 2.3	66.49 ± 2.9
	4	72.60 ± 4.2	68.37 ± 4.0	63.83 ± 0.76
	8	65.83 ± 2.9	66.94 ± 3.2	59.82 ± 1.1
	16	69.65 ± 2.1	69.75 ± 6.0	57.15 ± 5.0 *

* $p < 0.05$ vs. SC and HFS within the respective week. Data are expressed as mean ± SEM. Two-way ANOVA. n = 3–7.

Ethics approval – The protocol containing all animal procedures described in this study was specifically approved by the Committee on the Ethics of Animal Experiments of York University (York University Animal Care Committee, YUACC, permit number: 2021-03) and performed strictly in accordance with the YUACC guidelines. All tissue extraction procedures were performed under ketamine/xylazine anesthesia, and all efforts were made to minimize suffering[205]. All experiments in this study were carried out in compliance with the ARRIVE guidelines[206].

Glucose monitoring and determination of plasma insulin concentrations – Blood from all animals was collected in the fed state between 15:00 and 16:00 h by saphenous vein bleeding and used to determine plasma glucose using the OneTouch UltraMini blood glucose monitoring system from LifeScan Canada Ltd (Vancouver, BC, Canada). Insulin was measured using a commercially available kit listed in the reagents section. All procedures were performed according to instructions provided by the manufacturer of the kit.

Western blotting analysis of ACE1, ACE2, AT_1R, AT_2R, and TMPRSS2 protein levels in lung and cardiac tissues – Lung and heart tissues were homogenized in a buffer containing 25 mM Tris-HCl, 25 mM NaCl (pH 7.4), 1 mM $MgCl_2$, 2.7 mM KCl, 1% Triton X-100 and protease and

phosphatase inhibitors (Roche Diagnostics GmbH, Mannheim, Germany). Homogenates were centrifuged, the supernatant was collected, and an aliquot was used to measure protein by the Bradford method. Samples were diluted 1:1 (vol:vol) with 2x Laemmli sample buffer and heated to 95°C for 5 min. 25 µg of protein were loaded in each well. Samples were then subjected to SDS-PAGE, transferred to PVDF membrane, and probed for the proteins of interest. All primary antibodies were used at a dilution of 1:1,000. All densitometry analyses were performed using the ImageJ program.

RNA isolation and quantitative PCR – Primers were designed using the software PrimerQuest (IDT) based on probe sequences available at the Affymetrix database (NetAffx™ Analysis Centre, http://www.affymetrix.com/analysis) for each given gene. RNA was isolated from lung and heart tissues using Trizol™ (Fisher Scientific, MA, USA). Complimentary DNA (cDNA) was made from 2 µg of extracted RNA using the ABM OneScript cDNA Synthesis kit (Diamed, Mississauga, ON, Canada), according to the manufacturer's instructions. Samples were run in duplicates on 96-well plates, and each 20 µl reaction contained 4 µl of cDNA, 0.4 µl of primer, 10 µl of Brightgreen 2x qPCR Mastermix (Diamed, Mississauga, ON, Canada) and 5.6 µl of RNase-free water. Real-time PCR analysis was performed using a Bio-Rad CFX96 Real Time PCR Detection System (Bio-Rad, Mississauga, ON, Canada) using the following amplification conditions: 95°C (10 min); 40 cycles of 95°C (15 s), 60°C (60 s). All genes were normalized to the control gene β-actin, and values are expressed as fold increases relative to control[188]. Primer sequences utilized are shown in Table 7.

Table 7: Primer sequences for qPCR.

	Forward	Reverse
mas1	5′-CGCCAACCCTTTCATCTACT-3′	5′-CCTAGGTTGCATCTCGTCTTT-3′
tlr4	5′-ACCTAAGGAGAGGAGGCTAAG-3′	5′-GGTAACTGCAGCACACTACA-3′
il6r	5′-TGGAGCAGACAGAGAGACTT-3′	5′-AGCTTACAGGTAACAGAGCATAAA-3′
tnfr1	5′-CCCTGTGAACCTCCTCTTTG-3′	5′-CTATGTACACCAAGTCGGTAGC-3′
β-actin	5′-GTGAAAAGATGACCCAGATC-3′	5′-CACCGCCTGGATGGCTACGT-3′

Statistical Analyses – Data were expressed as Mean ± SE. Statistical analyses were performed by using mixed-model analyses and one-way ANOVAs with Bonferroni multiple comparison post-hoc tests, as indicated in the figure legends. The GraphPad Prism software version 9.1.12 was used for all statistical analyses and for the preparation of all graphs. The level of significance was set to $p<0.05$.

7.4. Results

Body weight (BW), glycemia, and insulinemia – HFS-fed animals gained significantly more weight than the SC and KD-fed animals (Table 8). This difference in BW was statistically significant at weeks 8 (409.77 ± 14.6 grams in the HFS group vs. 370.21 ± 14.3 and 374.24 ± 6.6 g in the SC and KD groups, respectively), 12 (452.3 ± 15.7 g in the HFS group vs. 400.47 ± 15 and 404.69 ± 6.5 g in the SC and KD groups, respectively), and 16 (470.81 ± 17.1 g in the HFS group vs. 421.29 ± 15.7 and 425.54 ± 4.7 g in the SC and KD groups, respectively).

Table 8: Body weight of SC-, HFS-, and KD-fed rats at the beginning of the study (week 0) and after 4, 8, 12, and 16 weeks of dietary intervention.

		Duration of Study (Weeks)				
	Groups	**0**	**4**	**8**	**12**	**16**
Body mass (g)	SC	231.97 ± 7.1	317.21 ± 10.4	370.21 ± 14.3	400.47 ± 15.0	421.29 ± 15.7
	HFS	236.18 ± 5.4	345.97 ± 10.7	409.77 ± 14.6 *	452.3 ± 15.7 *	470.81 ± 17.1 *
	KD	230.12 ± 3.6	321.21 ± 4.5	374.24 ± 6.6	404.69 ± 6.5	425.54 ± 4.7

* $p < 0.05$ vs. SC and KD within the respective weeks. Data are expressed as mean ± SEM. Mixed-effects model analysis. $n = 7–9$.

With respect to blood glucose levels, there was no significant difference among the three groups

at weeks 0 and 16 (Table 9). Insulinemia increased in both the HFS (1.90 ± 0.33 to 7.68 ± 1.54 ng/ml) and KD groups (2.18 ± 0.34 to 5.85 ± 0.66 ng/ml) from week 0 to week 16 (Table 9). However, at week 16, only the HFS had significantly higher blood insulin levels than the SC group (Table 9). In fact, the HFS diet-induced elevation in blood insulin concentration was of 79%, relative to the SC animals (Table 9), which is an indication of insulin-resistance in these animals. In contrast, the SC and KD groups did not have statistically significant blood insulin levels at week 16 (Table 9).

Table 9: Glycemia and insulinemia levels at the beginning (week 0) and at the end of the dietary intervention (week 16) in SC-, HFS-, and KD-fed rats.

		Duration of Study (Weeks)	
Blood Parameters	**Groups**	**0**	**16**
Glucose (mmol/l)	SC	6.85 ± 0.12	5.72 ± 0.18 #
	HFS	6.77 ± 0.21	5.91 ± 0.10 #
	KD	6.59 ± 0.12	5.71 ± 0.07 #
Insulin (ng/mL)	SC	2.16 ± 0.50	4.30 ± 0.43
	HFS	1.90 ± 0.33	7.68 ± 1.54 *#
	KD	2.18 ± 0.34	5.85 ± 0.66 #

* $p < 0.05$ vs. SC within the respective week; # $p < 0.05$ vs. week 0 measurement. Data are expressed as mean ± SEM. Mixed-effects model analysis, $n = 6–7$.

ACE2 and TMPRSS2 levels in lung and heart tissues – We extracted lung and heart tissues from the animals for measurement of SARS-CoV-2 cellular entry proteins ACE2 and TMPRSS2. The HFS diet increased lung ACE2 content 3.8- and 6-fold, when compared to the SC and KD groups, respectively (Fig. 30A). A similar pattern was observed for TMPRSS2 where, for the HFS diet, the levels of this protein increased by 5.1- and 3.4-fold, relative to the SC and KD groups, respectively (Fig. 30B). However, in cardiac tissue, no significant differences were detected for ACE2 or TMPRSS2 levels when comparing the different dietary interventions (Fig. 30C and D, respectively). These data indicate that the HFS diet increased SARS-CoV-2 entry proteins in lung tissue, but not in the heart.

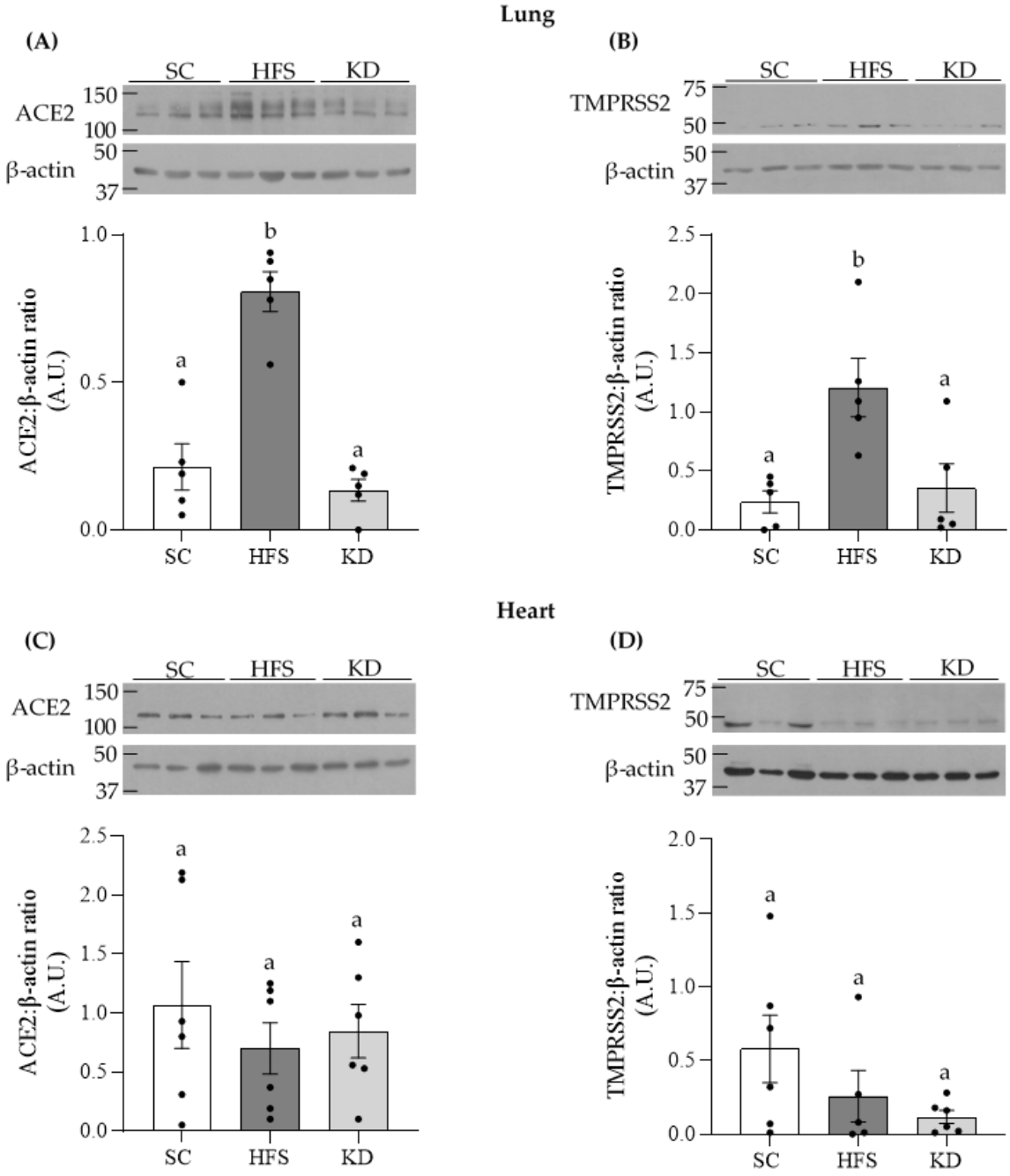

Figure 30: Lung contents of angiotensin converting enzyme 2 (ACE2) (**A**) and transmembrane protease serine 2 (TMPRSS2) (**B**) were significantly elevated by the HFS, but not by the KD. In contrast, diet did not alter the contents of these proteins in heart tissue (**C**,**D**). Statistical significance is denoted by different letters $p < 0.05$. Bars represent mean ± SEM. One-way ANOVA, n = 5–6.

ACE1, AT_1R, and AT_2R levels in lung and heart tissues – In pulmonary tissue, the KD attenuated ACE1 protein content by 56%, relative to the SC group (Fig. 31A). Furthermore, KD also reduced AT_1R protein content in this tissue; however, it was not statistically significant (Fig. 31C). Pulmonary AT_2R levels were not altered by diet either (Fig. 31E). In cardiac tissue, ACE1 was not significantly different among the groups (Fig. 31B). However, the HFS diet induced 2.6 and 4.9-fold increases in AT_1R (Fig. 31D) and AT_2R (Fig. 31F) levels, respectively, when compared to the SC group. The contents of these proteins were not significantly different between the SC- and KD-fed animals.

Comparison of ACE1, ACE2, AT_1R, and AT_2R in lung and heart tissues – Upon observing the diet-induced changes in RAS proteins and the tissue-specific nature of these changes, we then decided to compare the contents of ACE1, ACE2, AT_1R, and AT_2R in the lung and heart. Pulmonary tissue displayed higher levels of ACE1 than cardiac tissue (Fig. 32), whereas more ACE2, AT_1R, and AT_2R was found in the heart than in the lungs (Fig. 32).

Gene expressions of Mas1, tlr4, il6r, and tnfr1 in lung and heart tissues – The gene expression of *mas1* was not significantly different among any of the three dietary interventions in either lung (Fig. 33A) or heart tissue (Fig. 33E). However, the gene expressions of *tlr4* and *il6r* were significantly reduced by 74 and 79%, respectively, in the lungs of KD-fed animals, when compared to the HFS animals (Fig. 33B and 33C, respectively). KD also suppressed *tnfr1* gene expression in this tissue by ~73% (Fig. 33D), although this was not statistically significant ($p=0.059$). In the heart, no significant differences were found for *tlr4, il6r, and tnfr1* gene expressions among the three diet groups (Fig. 33F, 33G and 33H, respectively). Altogether, these results indicate that the KD exerted an anti-inflammatory effect in the lungs, but not in the heart.

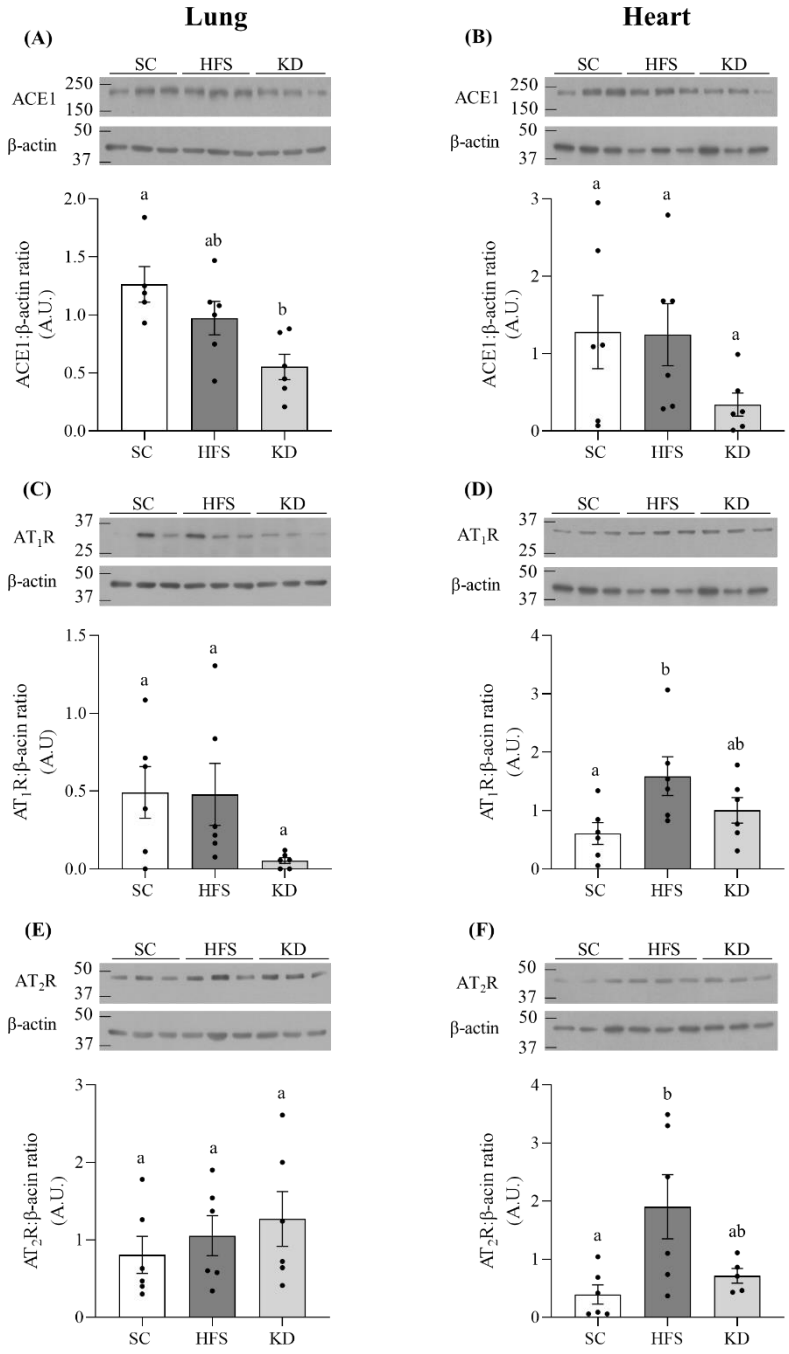

Figure 31: The KD attenuated angiotensin converting enzyme 1 (ACE1) and angiotensin II, type I receptor (AT1R) contents in pulmonary tissue (A,C, respectively), however only the former was found to be statistically significant. Angiotensin II, type 2 receptor (AT2R) was unaltered in the lungs, regardless of diet (E). On the other hand, dietary intervention did not influence heart ACE1 content (B), however AT1R and AT2R were significantly elevated in the cardiac tissues of HFS-fed rats (D,F, respectively). Significant differences are denoted by different letters $p < 0.05$. Bars represent mean ± SEM. One-way ANOVA, n = 5–6.

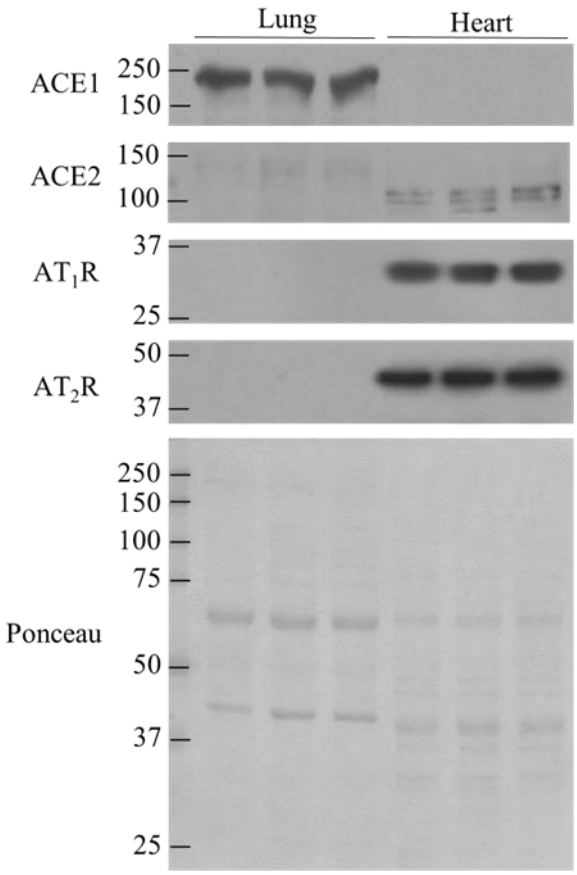

Figure 32: AT1R, AT2R and ACE2 are more abundant in heart tissue than in lung tissue. In contrast, lung tissue contains more ACE1. n = 3.

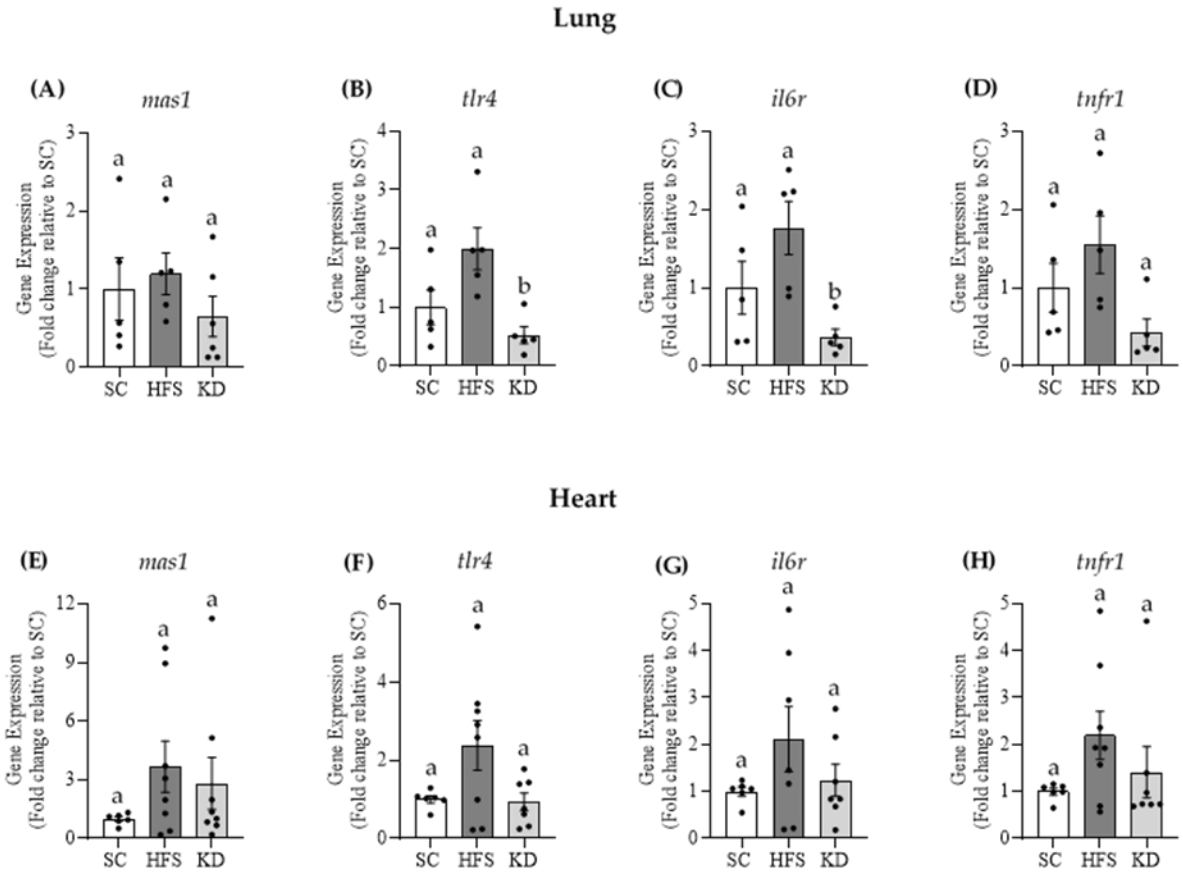

Figure 33: The KD does not affect mas1 gene expression in lung (A) or heart (E) tissues. Interestingly, KD-feeding significantly reduces toll-like receptor 4 (tlr4) and interleukin-6 receptor (il6r) gene expression in pulmonary tissues (B,C, respectively), when compared to the HFS diet. The KD also reduced tumour necrosis factor receptor 1 (tnfr1) gene expression in lungs (D), though this was not statistically significant. Tlr4, il6r and tnfr1 were not significantly altered by diet in cardiac tissues (F–H, respectively). Statistical significance is denoted by different letters $p < 0.05$. Bars represent mean ± SEM. One-way ANOVA, n = 5–8.

7.5. Discussion

Here, we show that obesogenic and ketogenic diets regulate in a distinct and tissue-specific manner proteins of the RAS, as well as major components of the molecular machinery involved in cellular infection by SARS-CoV-2. In fact, rats fed the HFS obesogenic diet displayed elevated insulinemia and much higher levels of ACE2 and TMPRSS2 in the lung than animals fed either SC or a KD. This is consistent with previous findings of increased lung levels of ACE2 and TMPRSS2 in diabetic mice[125], and with reports linking insulin resistance and Type 2 diabetes to severe COVID outcomes[125,226]. However, to our knowledge, this is the first study to show that besides attenuating weight gain and insulinemia, a KD maintained lower ACE2 and TMPRSS2 protein levels in the lungs in comparison to a HFS diet. This is relevant for the prevention of severe COVID-19-related illness, given that ACE2 and TMPRSS2 have been identified as crucial components of the molecular machinery used by SARS-CoV-2 to infects cells[122]. In fact, the use of a specific TMPRSS2 inhibitor, camostat mesylate, has been shown to inhibit SARS-CoV-2 entry in Caco-2 cells and anti-ACE2 antibody incubation with Vero cells blocked SARS-Cov-1 and SARS-CoV-2 entry[122]. Thus, the observed elevation in these two proteins in the lungs of HFS-fed rats provides a plausible mechanism whereby obese individuals are more susceptible to severe infection with SARS-CoV-2. The underlying mechanisms that explain this diet-induced elevation in ACE2 have not been fully elucidated[229]. However, under conditions of obesity, adipose tissue secretes angiotensinogen, which can eventually be converted to Ang-II, leading to hyperactivation of the ACE1/Ang-II/AT_1R arm of the RAS and subsequent tissue damage[226,228]. Hyperinsulinemia may also cause RAS dysregulation[228]. In this context, the observed elevation in ACE2 is likely a counterregulatory mechanism to attenuate the detrimental effects induced by obesity-mediated RAS hyperactivation[229]. Furthermore, non-alcoholic fatty liver disease (NAFLD) is a major

comorbidity of obesity, and it has been linked to increased hepatic expression of ACE2 and TMPRSS2[230], which could contribute to the aggravate morbidity in SARS-CoV-2 patients. Importantly, ketogenic diets have been shown to be very effective in combating NAFLD[231–233] and attenuate the potential deleterious effects of SARS-CoV-2 in the liver. However, we did not assess any variable associated with NAFLD in our studies; therefore, we could not make any inferences about hepatic expression of SARS-CoV-2 critical entry points.

Although there were no significant alterations in ACE2 and TMPRSS2 in the heart with any of the dietary interventions, ACE2 was found to be more abundant in cardiac than in lung tissue. Thus, because the obesogenic diet significantly increased ACE2 in the lung, COVID-19 infection still poses a significant risk for the cardiac health in obese individuals since it is one of the primary points of infection. This could potentially enhance the severity of the infection in pulmonary tissues, leading to viral spillover, whereby the virus can access other tissues, including the heart which is already abundant in ACE2 and, as a result, predisposed to infection and damage[117,226]. The roles of ACE2 in SARS-CoV-2 infection, as well as the RAS are not independent. Thus, the other RAS components are also emerging as therapeutic targets to treat illness related to COVID-19. In fact, the use of angiotensin receptor blockers (ARB) or ACE inhibitors have been proposed as treatments for SARS-CoV-2 patients[226]. This serves to increase flux through the ACE2/Ang(1,7)/MasR and AT_2R arm of the RAS and to promote anti-inflammatory mechanisms that counteract the COVID-induced cytokine storm[117,226,228]. In the present study, we observed no alteration in AT_1R or AT_2R in lung tissues with any of the three dietary interventions. However, the KD did significantly reduce ACE1 levels. This indicates that the RAS system was shifted away from the ACE1/Ang-II/AT_1R arm and towards the counterregulatory, anti-inflammatory RAS arm, given that we also observed reductions in *tlr4*, and

il6r gene expressions as well as a trend to decrease *tnfr1* gene expression. The observed reduction in the expression of these inflammatory genes is relevant, as IL-6 and TNFα are two major cytokines that facilitate the coronavirus-induced cytokine storm[226]. Furthermore, Zhao et al. demonstrated that TLR4 inhibition suppressed interleukin-1β release in cells treated with the SARS-CoV-2 S protein[234].

Our findings are in line with other studies that report the anti-inflammatory nature of the KD[146,235], and suggest that this diet could reduce the risk of severe infection and inflammatory response related to COVID-19. We have not investigated the mechanism by which the KD led to lower levels of expression of inflammatory genes in comparison to the obesogenic diet. However, the KD is characterized by increased liver production of ketones[236]. Thus, the anti-inflammatory effect of the KD could be at least partially attributed to increased levels of circulating ketones, particularly β-hydroxybutyrate (β-HB), upon KD feeding[237]. In fact, β-HB has been demonstrated to block the nucleotide-binding domain leucine-rich-containing family pyrin domain-containing-3 (NLRP3) inflammasome and NLRP3 inflammasome-mediated interleukin (IL)-1β and IL-18 production by monocytes[141]. Additionally, the KD has been shown to exert its anti-inflammatory effects by inhibiting nuclear factor kappa-light-chain-enhancer of activated B cells (NF-kB) activation, suppressing the activity of histone deacetylases (HDACs), reducing the production of reactive oxygen species (ROS), and by improving mitochondrial respiration[236]. Thus, all these KD effects can ameliorate chronic low-grade inflammation and its associated diseases. It is important to mention that the KD used in this study was completely devoid of carbohydrates, which differs from the commonly used KD that recommends low carbohydrate content (less than 50 g/day) and not the complete elimination of this macronutrient from the diet[238]. Thus, caution should be taken when extrapolating our findings to human subjects. However, the absence of carbohydrates in the

diet allowed us to identify that it is the combination of HF with sucrose, as opposed to HF alone, that promotes the deleterious metabolic effects associated with increased levels of SARS-CoV-2 entry proteins and inflammation in lung and heart tissues in obesity.

We did not find any significant difference in the cardiac gene expressions of Mas1 or the aforementioned inflammatory genes, although a trend to increase the latter in the HFS-fed rats was detected. However, the HFS diet did increase AT_1R content, which was also met by a similar increase in AT_2R. This likely served to offset the proinflammatory response mediated by AT_1R. Indeed, it has been reported that AT_2R increases in response to AT_1R hyperactivation and injury [111,226]. Interestingly, AT_1R and AT_2R are more abundant in the heart than in the lung. In this context, it is possible that the elevated expression of these receptors allows for an enhanced flexibility of this tissue to regulate its inflammatory status. It is important to note that AT_1R and AT_2R levels did not change in the hearts of KD-fed animals, relative to the SC animals, suggesting that this diet did not provoke RAS activation. Unlike the lung, heart ACE1 content was not altered by diet. This could be attributed to the lower ACE1 content in the heart, compared to the lung, suggesting that the reliance of the former on ACE1 for RAS regulation is lower than the latter, where there was a diet-induced alteration in the content of this protein. This is consistent with the notion that the ACE1-dependent conversion of Ang-I to Ang-II takes place predominantly in pulmonary circulation[107].

In conclusion, these data indicate that the HFS diet increases body weight, insulinemia RAS hyperactivation and lung ACE2 and TMPRSS2, which could explain the predisposition of obese individuals to severe COVID-19 outcomes. In contrast, the KD did not elicit the same elevations in weight gain and insulinemia as the HFS diet did. Our data also suggest that there is not a hyperactivation of the RAS in KD-fed animals, as indicated by the reductions in pulmonary

ACE1 and the expressions of inflammatory genes as well as unaltered cardiac AT_1R and AT_2R contents. Thus, a counterregulatory elevation in lung ACE2 was not observed in KD animals. Unlike the lung, the heart does not experience a diet-induced alteration in ACE2, however the abundance of this protein, relative to the lung, makes it a susceptible organ to SARS-CoV-2 damage following viral spillover from pulmonary tissues. In this context, despite altering RAS proteins in a tissue-specific manner, it is clear that the KD offers a promising potential therapeutic tool for its reduction in SARS-CoV-2 entry proteins and its induction of an anti-inflammatory profile.

Chapter 8: Sucrose-enriched and carbohydrate-free high-fat diets distinctly affect substrate metabolism in oxidative and glycolytic muscles of rats

Daniel Da Eira, Shailee Jani, Mateja Stefanovic, and Rolando B. Ceddia

Muscle Health Research Centre - School of Kinesiology and Health Science, York University, Toronto, ON, Canada.

Keywords: PGC-1α, TFAM, ketolysis, insulin resistance, anaplerosis, ketogenic diet.

Da Eira D, Jani S, Stefanovic M, Ceddia RB. Sucrose-Enriched and Carbohydrate-Free High-Fat Diets Distinctly Affect Substrate Metabolism in Oxidative and Glycolytic Muscles of Rats. *Nutrients*. 2024; 16(2):286.

Statement of Labour

The work in this study was performed by DD. DD fed the rats the SC, HFS and KD and measured glycaemia in the animals over the course of the feeding period. DD also extracted tissues and performed functional assays and Western blotting experiments. Moreover, DD collected and analyzed the data, prepared figures and wrote and revised the manuscript. DD was funded by the Alexander Graham Bell – Canada Graduate Scholarship (Doctoral). Due to the length of the study and the logistics of functional assays, SJ assisted with the feeding of the diets, glycaemia measurement, tissue extractions and the performance of the functional assays, including the glycogen synthesis and lactate determination assays. MS also assisted with tissue extractions and Western blotting experiments.

Dr. Rolando Ceddia is the principal investigator and was involved in all stages of this study. The work presented in this manuscript was funded by grants awarded to RBC, including the Discovery Grant from the Natural Science and Engineering Research Council of Canada (NSERC) and by infrastructure grants from the Canada Foundation for Innovation (CFI) and the Ontario Research Fund (ORF).

8.1. Abstract

Skeletal muscle substrate preference for fuel is largely influenced by dietary macronutrient availability. The abundance of dietary carbohydrates promotes the utilization of glucose as a substrate for energy production, whereas an abundant dietary fat supply elevates rates of fatty acid (FA) oxidation. The objective of this study was to determine whether an obesogenic, high-fat, sucrose-enriched (HFS) diet or a carbohydrate-free ketogenic diet (KD) exert distinct effects on fat, glucose, and ketone metabolism in oxidative and glycolytic skeletal muscles. Male Wistar rats were fed either a HFS diet or a KD for 16 weeks. Subsequently, the soleus (Sol), extensor digitorum longus (EDL), and epitrochlearis (Epit) muscles were extracted to measure palmitate oxidation, insulin-stimulated glucose metabolism, and markers of mitochondrial biogenesis, ketolytic capacity, and cataplerotic and anaplerotic machinery. Sol, EDL, and Epit muscles from KD-fed rats preserved their ability to elevate glycogen synthesis and lactate production in response to insulin, whereas all muscles from rats fed with the HFS diet displayed blunted responses to insulin. The maintenance of metabolic flexibility with the KD was accompanied by muscle-fiber-type-specific adaptive responses. This was characterized by the Sol muscle in KD-fed rats enhancing mitochondrial biogenesis and ketolytic capacity without elevating its rates of FA oxidation in comparison with that in HFS feeding. Conversely, in the Epit muscle, rates of FA oxidation were increased, whereas the ketolytic capacity was markedly reduced by the KD in comparison with that by HFS feeding. In the EDL muscle, the KD also increased rates of FA oxidation, although it did so without altering its ketolytic capacity when compared to HFS feeding. In conclusion, even though obesogenic and ketogenic diets have elevated contents of fat and alter whole-body substrate partitioning, these two dietary interventions are associated with opposite outcomes with respect to skeletal muscle metabolic flexibility.

8.2. Introduction

The suppression of glucose metabolism under conditions of an abundant dietary fat supply can be partially attributed to changes in cellular substrate partitioning. The metabolic shift that coincides with the elevation of whole-body FA oxidation and glucose intolerance has been of concern in diabetic and insulin-resistant patients[239]. Conversely, from the perspective of endurance performance, a higher rate of skeletal muscle FA oxidation could be advantageous due to its potential glycogen-sparing effect[61]. Thus, the utilization of high-fat low-carbohydrate diets in endurance athletes has recently gained attention, particularly the ketogenic diet (KD)[240] that provides an abundance of fat and ketones as alternative sources of fuel for skeletal muscles[61,241]. In fact, the skeletal muscle gene expression of *Cpt1b*[166], fat oxidation[241], and markers of the mitochondrial biogenesis[165] and fractional areas[164] were elevated, whereas glucose oxidation[241], GLUT4 and IRS1 contents, and glucose tolerance were reduced by the KD in exercise-trained individuals[60]. The KD has also been shown to significantly enhance ketone-mediated ATP production relative to glucose- or fat-mediated ATP production[241]. Thus, the abundance of fat and relatively lower content of dietary carbohydrates shift the metabolic substrate preference away from glucose and toward FAs.

Skeletal muscles display distinct oxidative and glycogenolytic capacities[242] and activities of enzymes involved in ketone oxidation[243]. Thus, the ability of oxidative and glycolytic muscles to adjust substrate partitioning according to fat and glucose dietary abundance may also significantly differ. Indeed, Fukazawa et al. showed that a KD increased the protein content of the ketolytic enzyme 3-oxoacid CoA transferase (OXCT) in the epitrochlearis (Epit) muscle[171], whereas Shimizu et al. reported a significant attenuation of OXCT gene expression in the gastrocnemius muscle[166]. Moreover, there is evidence that the KD increases mitochondrial mass

in the red gastrocnemius muscle[164], which was contrasted by reports that the KD did not alter PGC-1α levels in the extensor digitorum longus (EDL)[170] or soleus (Sol) muscles[165]. Taken together, these data point to an apparent gap in the literature where KD-induced metabolic adaptations in substrate preference in muscles of varying oxidative and glycolytic capacities are yet to be fully elucidated. In this context, this study aimed to investigate whether the obesogenic, high-fat sucrose-enriched (HFS) diet and the KD would differ in their effects on metabolic substrate selection in muscles with varying fiber-type compositions. To achieve this, we compared the metabolic responses of Sol, EDL, and Epit rat muscles to either a KD (80% fat, lard; 0% carbohydrate; 20% protein) or typical obesogenic HFS diet (60% fat, lard; 20% sucrose; 20% protein). Furthermore, previous studies comparing the KD to a control diet had significantly different protein contents[59,164,171]. Importantly, skeletal muscle atrophy has been found in studies that reduce the protein content of a KD[172], whereas studies that use a normal protein diet report the maintenance of lean mass[59]. Varying protein contents also elicit distinct metabolic adaptations. For instance, Nakao et al. used a KD that was 4.8% kcal protein, compared to the control diet that was ~14% kcal protein, and observed a decrease in gastrocnemius pyruvate dehydrogenase (PDH) activity[172]. Huang et al., on the other hand, used a KD with a similar protein level to the control diet (16%) and reported no alteration in PDH activity[59]. Therefore, it is possible that the muscle metabolic adaptations do not derive from the low-carb high-fat content of the KD itself, but rather from its low protein content. To eliminate this as a confounding variable, we equalized the protein contents in both diets. Additionally, despite the high fat content in both the obesogenic HFS diet and the KD, the latter diet has been shown to improve metabolic health[241], whereas the former is detrimental to metabolic health. This suggests that the high fat content may not by itself be the main disruptor of normal metabolic function in skeletal muscles. Finally, because the KD was

devoid of carbohydrates and hepatic ketone production is enhanced by the KD[240], besides rates of FA oxidation, we also assessed markers of mitochondrial biogenesis and the content of specific enzymes involved in the ketolytic, anaplerotic, and cataplerotic machineries in skeletal muscles with distinct fiber-type compositions. Here, we provide evidence that, contrary to the HFS diet, the carbohydrate-free KD enhances rates of FA oxidation and ketolytic capacity without impairing insulin-stimulated glucose metabolism in oxidative and glycolytic skeletal muscles.

8.3. Materials and Methods

Reagents—Fatty-acid (FA)-free bovine serum albumin (BSA), glycogen, and palmitic acid were obtained from Sigma (St. Louis, MO, USA). Human insulin (Humulin R) was purchased from Eli Lilly Inc. (Toronto, ON, Canada). D-[U-^{14}C]glucose and [1-^{14}C]palmitic acid were acquired from GE Healthcare Radiochemicals (Quebec City, QC, Canada). The Lactate Colorimetric/Fluorometric Assay Kit was purchased from BioVision (Milpitas, CA, USA). Protease (cOmplete Ultra Tablets) and phosphatase (PhosSTOP) inhibitors were obtained from Roche Diagnostics GmbH (Mannheim, Germany). The peroxisome proliferator-activated receptor γ coactivator-1α (PGC-1α, cat. no. AB3242) antibody was purchased from Millipore (Temecula, CA, USA). The β-hydroxybutyrate (BHB; cat. No. ab83390) assay kit and the mitochondrial transcription factor A (TFAM; Cat. # ab131607), 3-oxoacid CoA-transferase 1 (OXCT; Cat. # ab224250), and acetoacetyl-CoA acetyltransferase 1 (ACAT1; Cat # ab168342) antibodies were purchased from Abcam (Toronto, ON, Canada). Pyruvate carboxylase (PC; Cat # 49381), phosphoenolpyruvate carboxykinase 1 (PCK1; Cat. # 12940), and phosphoenolpyruvate carboxykinase 2 (PCK2; 6924) antibodies were purchased from Cell Signaling (Danvers, MA, USA).

Animals and diet—Male albino rats (Wistar strain) at approximately 250 g were individually housed at 22 °C on a 12/12-h light–dark cycle. These rats were assigned either a high-fat sucrose-enriched (HFS) diet (20% kcal protein; 60% kcal fat (lard/soybean oil); 20% kcal carbohydrate (sucrose)) or KD (20% kcal protein; 80% kcal fat (lard/soybean oil); 0% kcal carbohydrate) and fed for 16 weeks ad libitum. Both diets were purchased from Research Diets (New Brunswick, NJ, USA).

Ethics approval—The protocol containing all animal procedures described in this study was specifically approved by the Committee on the Ethics of Animal Experiments of York University (York University Animal Care Committee, YUACC, permit number: 2021-03) and performed strictly in accordance with the YUACC guidelines. Date of approval: 18 July 2023. All tissue extraction procedures were performed under ketamine/xylazine anesthesia, and all efforts were made to minimize suffering[12]. All experiments in this study were carried out in compliance with the ARRIVE guidelines[206].

Measurement of blood glucose levels—Blood from all animals in the fed state was collected between 15:00 and 16:00 h with saphenous vein bleeding. Plasma glucose was measured using a Contour Next one meter blood glucose monitoring system by Ascensia Diabetes Care US (Parsippany, NJ, USA).

Muscle isolation and incubation—All animals were anesthetized with a single intraperitoneal injection of ketamine (90 mg/100 g BW) and xylazine (10 mg/100 g BW). Subsequently, Sol, EDL, and Epit muscles were quickly extracted. The percentages of type I, type IIa, and type IIb in Sol, EDL, and Epit muscles are 84/16/0, 3/57/40[155], and 15/20/65[156], respectively. From these muscles, strips were cut (18–22 mg) and pinned onto thin stainless steel wire clips to maintain muscle length. Thereafter, muscle strips were immediately placed in plastic scintillation vials

containing 2 ml of pre-gassed (30 min with O_2:CO_2-95:5% (vol/vol)) Krebs–Ringer bicarbonate (KRB) buffer containing 3.5% FA-free BSA and 5.5 mM glucose. Vials were sealed and subjected to continuous gasification for the entirety of the 1 h pre-incubation period.

Measurement of glucose oxidation, glycogen synthesis, and lactate production—Following the pre-incubation period, one set of muscles was then transferred to vials containing 2 mL of the same KRB buffer plus D-[U-^{14}C]glucose (0.2 μCi/mL) and incubated under continuous gasification for one additional hour, either in the absence (basal) or presence of insulin (100 nM) for the determination of glycogen synthesis and glucose oxidation, as previously described[244]. For lactate production, media aliquots were first deproteinated using 10 kDa filters (centrifuged at 13,000 rpm for 15 min at 4 °C) and then assayed using a colorimetric assay kit, according to the manufacturer's instructions.

Measurement of palmitate oxidation in isolated muscles—Palmitate oxidation was measured by assessing the production of $^{14}CO_2$ from [1-^{14}C]palmitic acid. Muscles were pre-incubated as previously described and then transferred to vials containing 2 mL of KRB buffer plus 0.2 mM of cold palmitic acid, previously complexed with FA-free BSA and [1-^{14}C] palmitic acid (0.2 μCi/mL). The muscles were incubated under continuous gasification for 1 h, and the vials had a centered isolated well containing a loosely folded piece of filter paper moistened with 0.2 mL of 2-phenylethylamine/methanol (1:1, vol/vol). Following the incubation and acidification of the media, the filter papers were carefully removed and transferred to scintillation vials for radioactivity counting[12].

Western blotting analysis of PGC1*α*, TFAM, OXCT, ACAT1, PC, PCK1, and PCK2 contents in Sol, EDL and Epit muscles—Muscle samples that were not subject to incubation were flash frozen in liquid nitrogen and stored at −80 °C until the Western blotting analysis. Muscle tissues

from the Sol, EDL and Epit muscles were homogenized in a buffer containing 25 mM Tris-HCl, 25 mM NaCl (pH 7.4), 1 mM $MgCl_2$, 2.7 mM KCl, 1% Triton X-100, and protease and phosphatase inhibitors (Roche Diagnostics GmbH, Mannheim, Germany). The homogenates were centrifuged, the supernatant was collected, and an aliquot was used for protein determination with the Bradford method. Samples were diluted 1:1 vol:vol with a 2× Laemmli sample buffer and heated to 95 °C for 5 min. Subsequently, 25 µg of protein was loaded into each well. Samples were thereafter subjected to SDS-PAGE, transferred to a PVDF membrane, and probed for the proteins of interest. All primary antibodies were used at a dilution of 1:1000. Ponceau staining was used as a loading control. All densitometry analyses were performed using the ImageJ program, version 1.46r.

Statistical Analyses—Data were expressed as mean ± SD. Statistical analyses were performed using two-way ANOVAs with Bonferroni post hoc and Student's *t*-tests, as indicated in the figure legends. If data were not normally distributed, or if data had an inequality of variance, Mann–Whitney and Welch's tests were used, respectively. GraphPad Prism software version 9.1.12 was used for all statistical analyses. The level of significance was set to $p < 0.05$.

8.4. Results

Effects of diet on glycaemia and plasma βHB levels—Blood glucose levels did not differ between the HFS and KD groups at weeks 8 and 16 (Table 10). However, the KD significantly elevated plasma βHB levels 1.6- and 1.9-fold at weeks 8 and 16, respectively, relative to the HFS diet (Table 10). The concentration of βHB in the circulation changed in a time-dependent manner in KD-fed animals, being highest at week 8 (Table 10). Despite a 24% reduction in plasma βHB from weeks 8 to 16 in the KD group, week 16 levels were elevated 2.2-fold, relative to week 0 (Table 10).

Table 10: Blood glucose and plasma beta-hydroxybutyrate (βHB) levels at weeks 0, 8, and 16 of dietary intervention. Blood glucose levels were not different between the two dietary groups; however, βHB was elevated in the KD group at weeks 8 and 16, relative to that in the HFS group.

		Week		
		0	8	16
Glycaemia	HFS	7.31 ± 0.54	7.19 ± 0.47	6.77 ± 0.72‡
(mM)	KD	7.29 ± 0.35	6.99 ± 0.34	6.57 ± 0.43‡
βHB	HFS	0.16 ± 0.06	0.24 ± 0.08	0.15 ± 0.04
(mM)	KD	0.13 ± 0.04	0.38 ± 0.08#	0.29 ± 0.05†

#$p < 0.05$ vs. week 0 KD and week 8 HFS; †$p < 0.05$ vs. week 0 KD, week 8 KD, and week 16 HFS. ‡$p < 0.05$ vs. week 0. Data are expressed as mean ± SD. Mixed-effect model analysis. N = 7–15 for glycaemia. N = 6–7 for βHB.

Effects of diet on palmitate and glucose oxidation in skeletal muscle—Sol palmitate oxidation did not significantly differ between the HFS- and KD-fed rats (Figure 34A); however, in both the EDL and Epit muscles, the KD increased palmitate oxidation ~1.7-fold in comparison with the HFS diet (Figure 34B and C, respectively). These muscle-specific adaptive responses were also observed with respect to glucose oxidation. In the Sol, EDL, and Epit muscles in HFS-fed animals, insulin-stimulated glucose oxidation was blunted (Figure 34D–F). In the KD-fed rats, the rates of insulin-stimulated glucose oxidation in the Sol, EDL, and Epit muscles were higher than the basal values, but did not reach statistical significance (Figure 34D–F). Only the EDL muscles in the KD-fed rats displayed rates of insulin-stimulated glucose oxidation that were significantly higher than those in the HFS-fed rats (Figure 34E). Thus, whereas the KD enhanced FA oxidation in a muscle-specific manner, insulin-stimulated glucose oxidation was similarly impaired in all muscles.

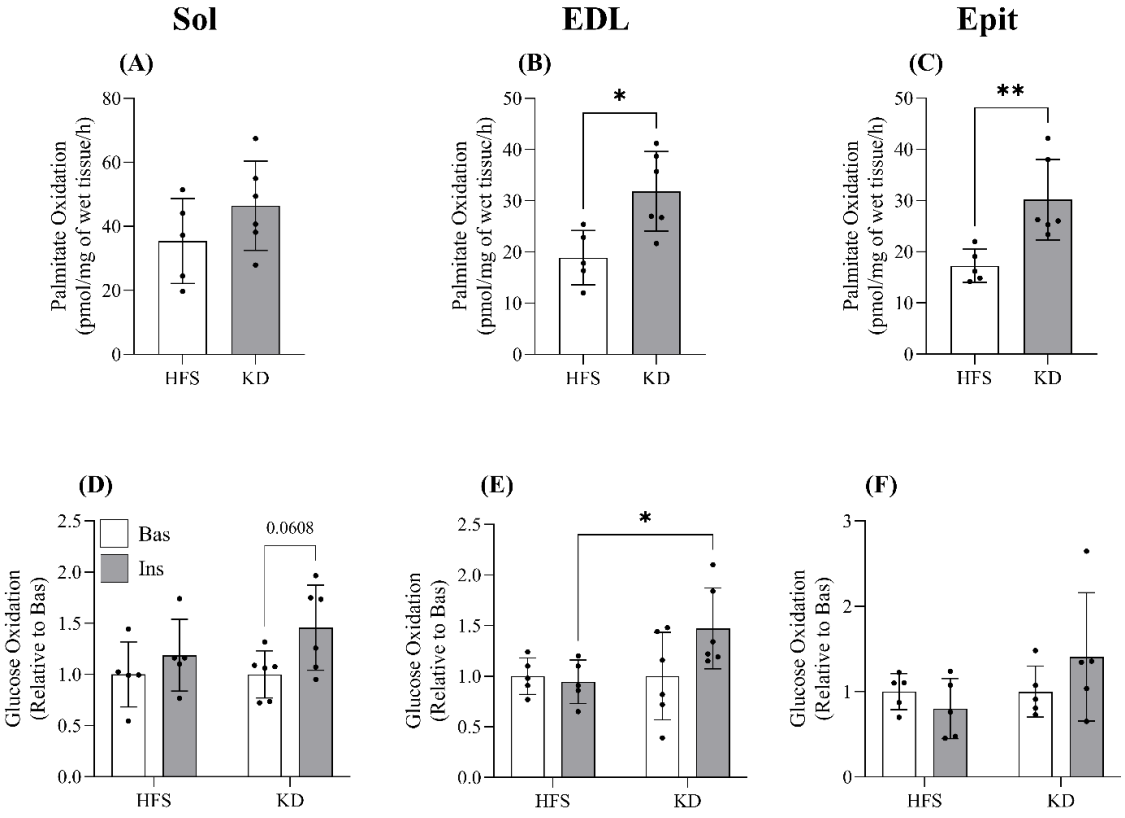

Figure 34: Palmitate oxidation was not significantly altered by diet in the soleus muscle (Sol, (**A**)); however, it was significantly elevated by the ketogenic diet (KD) in the extensor digitorum longus (EDL, (**B**)) and epitrochlearis (Epit, (**C**)) muscles. Conversely, glucose oxidation was not significantly enhanced in either of the two groups in any of the muscles with insulin (Ins) stimulation (**D**–**F**). Despite this, the fold increase in insulin-stimulated glucose oxidation in the EDL muscle, relative to basal (Bas) values, was enhanced by the KD (**E**). Data are expressed as mean ± SD. n = 5–6 rats. Student's t-test was used to compare groups for (**A**–**C**), whereas a two-way ANOVA with Bonferroni post hoc comparisons was used for (**D**–**F**). *$p < 0.05$, **$p < 0.01$.

Effects of diet on insulin-stimulated glycogen synthesis and lactate production—Insulin-stimulated rates of glycogen synthesis were blunted in the Sol, EDL, and Epit muscles in rats fed with the HFS diet (Figure 35A, C and E, respectively), whereas in the Sol and EDL muscles of KD-fed rats, insulin increased this variable 1.8-fold (Figure 35A) and 1.5-fold (Figure 35C), respectively, in comparison with basal values. In Epit muscles from KD-fed rats, insulin stimulation did not significantly elevate glycogen synthesis in comparison to basal values; however, the glycogen synthesis response to insulin was significantly higher than that of the HFS-

fed rats (Figure 35E). Insulin-stimulated lactate production, an indication of glycolytic capacity[245], was also blunted in the Sol, EDL, and Epit muscles from HFS-fed rats; whereas in the KD-fed rats, the Sol, EDL, and Epit muscles incubated with insulin displayed 2.1-, 2.1-, and 1.9-fold increases in lactate production in comparison to basal values (Figure 35B, D and F, respectively). Therefore, the KD preserved the capacity of oxidative and glycolytic muscles to store glycogen and perform glycolysis when stimulated with insulin.

Effects of the KD on the contents of ketolytic enzymes OXCT and ACAT1 in Sol, EDL, and Epit muscles—Because the circulating βHB levels were elevated in KD-fed rats compared with those of the HFS-fed rats, it was possible that the effects of ketones on substrate partitioning in skeletal muscles would also be different between the dietary interventions and fiber-type compositions. To assess that possibility, we measured the ketolytic enzymes OXCT and ACAT1 in Sol, EDL, and Epit muscles from rats fed either with the HFS diet or KD. We found that the OXCT content increased 1.6-fold in the Sol muscles of KD-fed animals (Figure 36A), whereas ACAT1 levels were unaltered by either of the two diets in this highly oxidative muscle (Figure 36B). In the EDL, OXCT and ACAT1 contents did not differ between the HFS- and KD-fed rats (Figure 36C and D, respectively). In contrast, the Epit OXCT and ACAT1 contents were 63% and 77% lower, respectively, in KD-fed animals when compared to those in the HFS group (Figure 36E and F, respectively). Therefore, in comparison to the HFS diet, the KD enhanced and suppressed the ketolytic capacity of the Sol and Epit muscles, respectively, whereas in the EDL muscle, the ketolytic capacity was unaffected by either the HFS diet or KD.

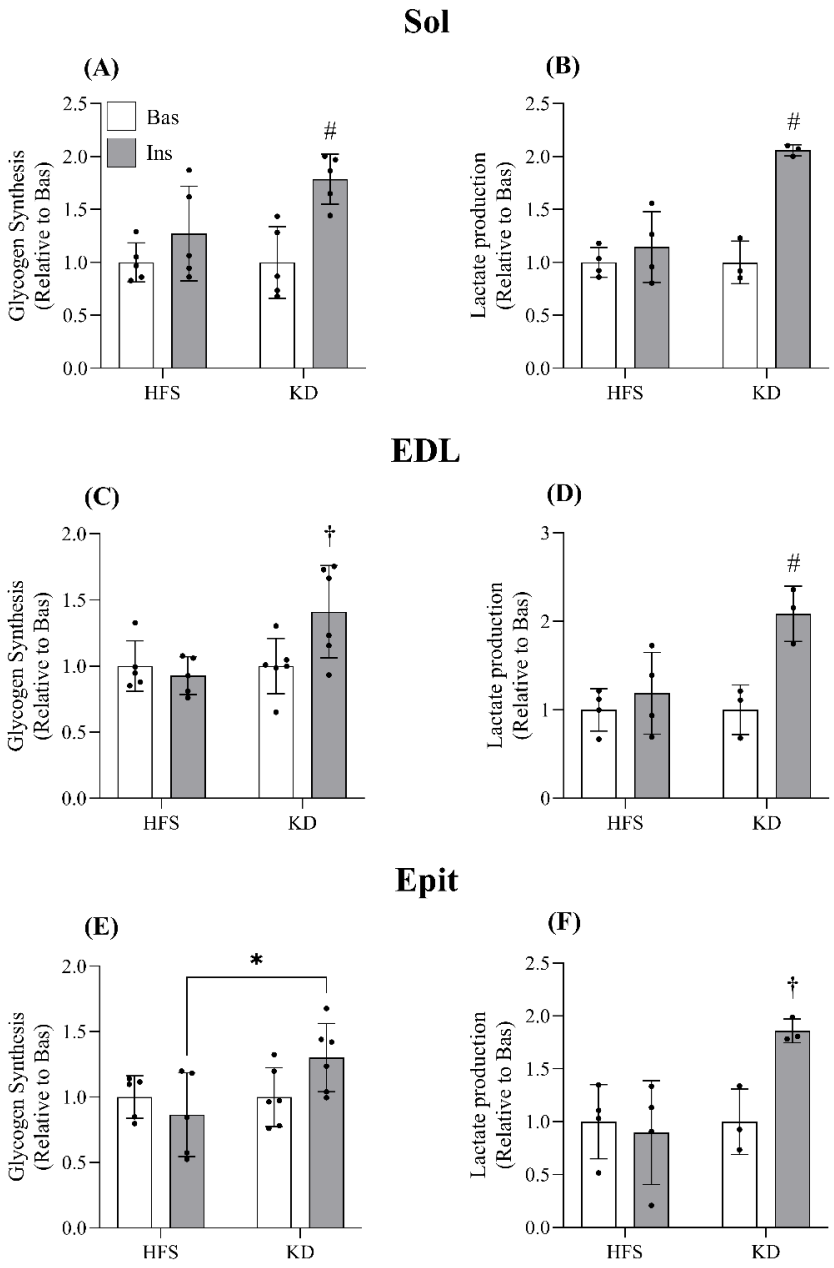

Figure 35: Ins stimulation increased glycogen synthesis in the Sol and EDL muscles of KD-fed rats (**A** and **C**, respectively). Epit glycogen synthesis did not increase relative to Bas values in either of the two groups; however, the fold increase in Ins-stimulated glycogen synthesis was greater with KD (**E**). Similarly, Ins significantly enhanced lactate production in all three muscles of KD-fed rats (**B**, **D** and **F**). Data are expressed as mean ± SD. n = 3–6. A two-way ANOVA with Bonferroni post hoc tests was used to compare the groups. $^{*}p < 0.05$; $^{\#}p < 0.05$ vs. all other groups; $^{\dagger}p < 0.05$ vs. HFS Ins and KD Bas.

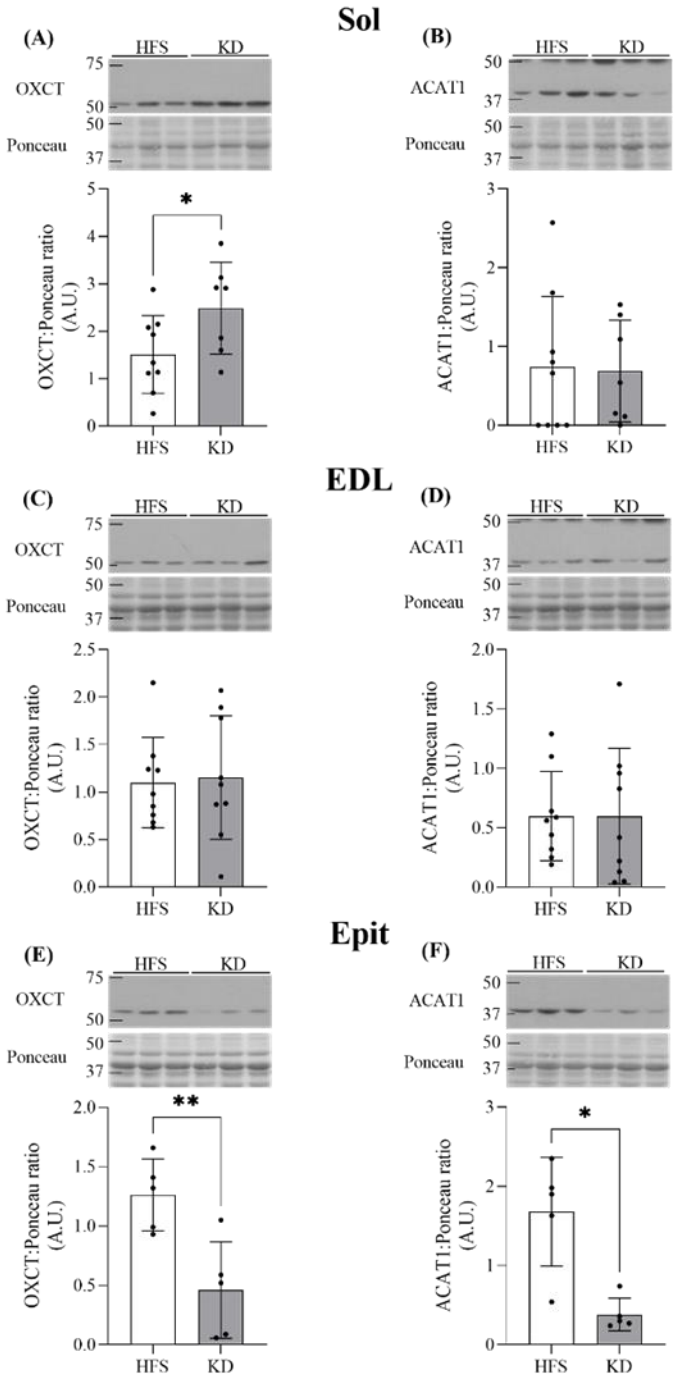

Figure 36: Sol OXCT content was significantly elevated by the KD (**A**), whereas Sol ACAT1 was unaffected by diet (**B**). Neither diet altered EDL muscle contents of OXCT or ACAT1 (**C** and **D**, respectively). Conversely, OXCT and ACAT1 contents were attenuated in the Epit muscle of KD-fed animals (E and F, respectively). Data are expressed as mean ± SD. n = 5–9. Student's *t*-test was used to compare groups, except for (**B**) and (**F**), where the Mann–Whitney test was used. *$p < 0.05$, **$p < 0.01$.

Effects of diet on PGC-1α and TFAM protein levels in Sol, EDL, and Epit muscles – The muscle-specific differences in substrate preference could be attributed to distinct dietary effects on mitochondrial biogenesis. Thus, we measured the contents of PGC-1α and TFAM, which are markers of mitochondrial biogenesis and content[246]. In Sol muscles, despite not increasing palmitate oxidation, the KD significantly elevated PGC-1α and TFAM contents 1.9- and 6-fold, respectively (Figure 37A and B, respectively). However, in the EDL (Figure 37C and D) and Epit (Figure 37E and F) muscles, PGC-1α or TFAM levels did not differ between the HFS diet and KD.

Effects of the KD on PC, PCK1, and PCK2 levels in Sol, EDL, and Epit muscles – Substrate oxidation is dependent on the availability of tricarboxylic acid (TCA) cycle intermediates, which is largely controlled by cataplerotic and anaplerotic enzymes[51]. To investigate whether the shift toward FA oxidation induced by both diets, and particularly the carbohydrate-free KD, could be attributed to this, we assessed the contents of the anaplerotic protein PC, and the cataplerotic PCK1 and PCK2[51,247]. Despite differences in oxidative and glycolytic capacities among the three muscles, no differences were found in the protein levels of PC, PCK1, and PCK2 in the Sol (Figure 38A–C), EDL (Figure 38D–F), or Epit (Figure 38G–I) muscles when comparing the HFS diet and KD. Thus, the contents of anaplerotic and cataplerotic enzymes in oxidative and glycolytic muscles did not contribute to the muscle-specific diet effects on substrate oxidation.

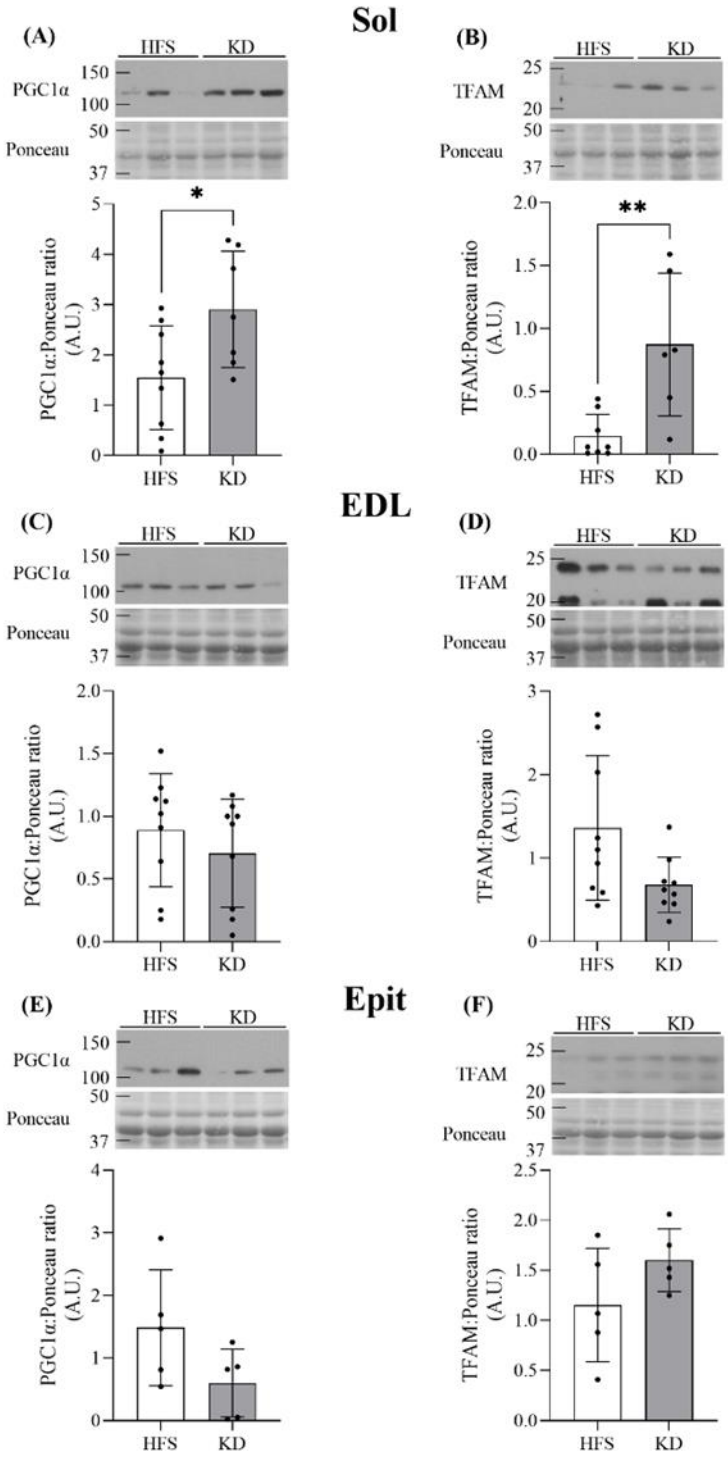

Figure 37: The Sol muscle demonstrated KD-induced elevations in PGC1α and TFAM (**A** and **B**, respectively), whereas diet did not alter the contents of either of these proteins in either the EDL (**C** and **D**) or Epit (**E** and **F**) muscles. Data are expressed as mean ± SD. n = 5–9. Student's t-test was used to compare groups, except for (**B**) and (**D**), where the Mann–Whitney test and Welch's t-test were used, respectively. *$p < 0.05$, **$p < 0.01$.

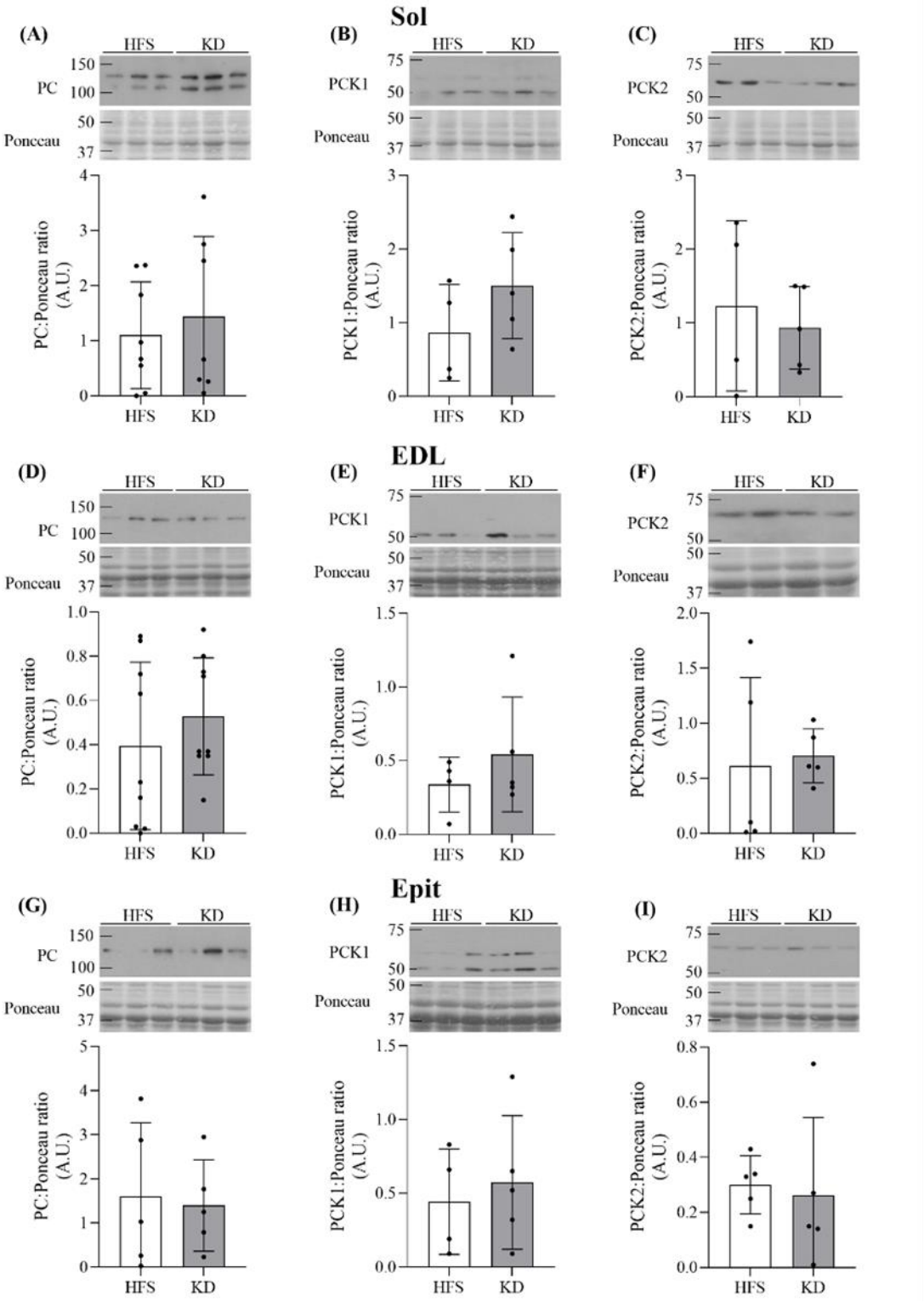

Figure 38: PC, PCK1, and PCK2 were not altered by diet in the Sol (**A**–**C**, respectively), EDL (**D**–**F**, respectively) or Epit (**G**–**I**, respectively) muscles. Data are expressed as mean ± SD. n = 4–9. Student's t-test was used to compare groups, except for (**E**), where the Mann–Whitney test was used.

8.5. Discussion

The main finding of this study was that despite inducing a higher rate of FA oxidation than the HFS diet, the KD preserved the ability of oxidative and glycolytic muscles to elevate glucose metabolism in response to insulin. Thus, our data provided compelling evidence that it is the chronic exposure to a combination of high fat and sugar, rather than solely to the elevated fat content of the diet, that disrupts the ability of skeletal muscles to process glucose in response to insulin. This was supported by elevated rates of insulin-stimulated glycogen synthesis and lactate production in the Sol, EDL, and Epit muscles in the KD-fed rats, which contrasted with the blunted responses displayed by these muscles in rats fed with the HFS diet. The analysis of insulin-stimulated glucose oxidation also revealed a similar trend when comparing both diets, although with KD eliciting a much less pronounced and fiber-type-specific effect on this variable than on rates of insulin-stimulated glycogen synthesis and lactate production. Because Sol muscles are rich in Type I fibers[155] and normally display higher capacities for FA oxidation when exposed to an HFS diet[12,59,248], the ability of these muscles to further elevate glucose oxidation when exposed to the KD may have been limited. Also, KD-fed Sol muscles were the only ones eliciting higher levels of the ketolytic enzyme OXCT than the HFS-fed counterparts, which likely enhanced the capacity of the Sol muscles to oxidize ketones. Thus, in Sol muscles, more glucose was diverted towards other pathways of glucose metabolism when stimulated with insulin as compared to the EDL and Epit muscles. Indeed, the rates of insulin-stimulated glycogen synthesis and lactate production in the Sol muscle were the highest among the muscles studied.

In well-trained cyclists habituated to a KD, GLUT4 and IRS1 protein contents were decreased in vastus lateralis muscles, which is consistent with the whole-body glucose intolerance found in these athletes[60]. KD-induced glucose intolerance has previously been attributed to

attenuated β-cell mass in the pancreas[137]. In the present study, we found that both glycogen synthesis and lactate production were preserved in the EDL of KD-fed rats, as indicated by the sensitivity of this muscle to insulin. Moreover, the elevation of glucose oxidation in the EDL muscle in response to insulin was significantly higher in the KD-fed rats than that in the HFS-fed rats. Together, these findings indicated that the KD leads to a disuse-mediated adaptation in pancreatic cell function that renders the organism less tolerant to a bolus of glucose. However, in line with the preserved response to insulin in the EDL, this mechanism is not indicative of disease and does not impact the capacity of skeletal muscles to metabolize glucose. In fact, despite the muscle-specific shift in substrate partitioning toward fatty acid oxidation and enhanced ketolytic capacity, all three skeletal muscles in the KD group demonstrated an enhanced ability to store glycogen and use glucose when exposed to insulin. Conversely, muscles from the HFS group displayed the classical impairment in insulin-stimulated glucose handling.

As expected, the KD significantly enhanced blood ketone levels, albeit not to the same extent as reported in other rodent KD studies[137,170,172]. This could be explained by the difference in the macronutrient composition of the KD used. In the present study, the protein content of the diet was 20% calories, whereas in studies showing a higher induction of ketosis, the protein contents ranged from 4.8–10% calories[137,170,172]. This is an important distinction, given that decreasing the protein content of a KD has been shown to significantly increase βHB levels in rats[173]. Furthermore, the apparent attenuation in βHB from weeks 8 to 16 points to a KD-induced adaptation, whereby ketolytic tissues, including those in the Sol muscle, enhanced their metabolic capacities for ketones, which likely led to an attenuation in the circulating levels of this substrate[61].

It was surprising to find that despite increasing PGC-1α and TFAM, the KD did not increase palmitate oxidation in Sol muscles, when compared to the HFS diet. Conversely, in EDL

and Epit muscles, PGC-1α and TFAM protein levels did not differ between the KD- and HFS-fed rats, yet the rates of FA oxidation in the former diet were significantly higher than those in the latter. In this context, despite increasing the proteins involved in mitochondrial biogenesis, the 20% additional fat content of the KD in comparison to that of the HFS diet did not further elevate the FA oxidative capacity of Sol muscles. Instead, the induction of mitochondrial biogenesis in the Sol muscle could also have served to increase the utilization of circulating ketone bodies as a fuel source, which is consistent with the KD-induced elevation in Sol muscles of OXCT protein levels, a major rate-limiting ketolytic enzyme[127]. In line with this, the administration of a ketone ester drink prior to exercise to endurance-trained athletes suppressed glycolysis and increased reliance on ketones for energy in the vastus lateralis muscle[169]. Thus, it is plausible that in the current study, ketones displaced glucose as an oxidative substrate in the Sol muscles of KD-fed rats, which could further attenuate the reliance on glucose and explain the modest insulin-stimulated glucose oxidation response in all three muscles from KD-fed rats. Conversely, the KD-induced enhancement in glycolytic capacity likely served to replenish oxaloacetate to support fat and ketone oxidation in the absence of dietary carbohydrate intake[51]. However, oxaloacetate availability for complete oxidation of acetyl-CoA produced from ketone bodies may also have been provided by acetoacetate activation via the conversion of succinyl-CoA to succinate in the TCA cycle, with the latter being converted to oxaloacetate through the subsequent reactions of the TCA cycle[129]. This likely facilitated the entry of more acetyl-CoA into the cycle without causing alterations to the levels of anaplerotic or cataplerotic enzymes.

Even though the Epit is a highly glycolytic muscle[156], its rates of FA oxidation were significantly higher in the KD rats than in the HFS-fed animals. This was surprising given that both diets were high in fat. In fact, the HFS diet had already been show to enhance Epit FA

oxidation in comparison to standard chow[12,248]. Thus, this study provided evidence that the absence of carbohydrates in the KD potentiated the reliance of the Epit muscle on fat as an oxidative substrate. Interestingly, this occurred independently of alterations in mitochondrial biogenesis proteins and, also, by marked reductions in the levels of the ketolytic enzymes OXCT and ACAT1, suggesting that Epit muscles enhanced their capacities to oxidize fat at the expense of ketones.

The EDL muscle displayed an intermediate effect relative to the Sol and Epit muscles. Like in the Epit muscle, palmitate oxidation was enhanced, whereas markers of mitochondrial biogenesis were unaltered. In line with this, KD feeding enhanced the aerobic capacity of the EDL muscle, despite not altering PGC1α content[170]. Moreover, other muscles with mixed-fiber-type compositions[155], including the gastrocnemius[59,166] and vastus lateralis[241] muscles, showed a KD-induced upregulation of fat oxidative capacity. However, unlike the Epit muscle, ketolytic capacity in the EDL muscle did not differ between the two dietary interventions. The preserved ketolytic capacity in the EDL versus Epit muscles, despite the similar enhancement in fat oxidation, could be attributed to the relatively higher oxidative capacity of the former[155], and therefore, the ability to perform FA oxidation without altering ketolytic capacity. Nevertheless, in the present study, we observed that only fat oxidation was increased in the EDL muscle, suggesting that the upregulation of mitochondrial biogenesis may be required to enhance the ketone-oxidizing capacity of the EDL muscle when under conditions of abundant dietary FA availability.

In conclusion, despite eliciting a higher rate of FA oxidation than the obesogenic HFS diet, the carbohydrate-free KD preserved the ability of oxidative and glycolytic muscles to elevate glucose metabolism in response to insulin. Thus, it is the chronic exposure to a combination of high fat and sugar, rather than solely to the elevated fat content of the diet, that disrupts the ability of skeletal muscles to process glucose in response to insulin. This was characterized by the KD-

induced elevation in mitochondrial biogenesis and ketolytic capacity in the Sol muscle, despite the lack of alteration in FA oxidation relative to that in the HFS group. In contrast, Epit FA oxidation was significantly elevated with KD feeding, whereas proteins involved in ketolysis were markedly reduced. Similarly, FA oxidation was increased in the EDL muscle of KD-fed rats, although the ketolytic capacity was unaltered in this muscle with the KD, relative to that in the HFS-fed rats. Lastly, the levels of anaplerotic and cataplerotic enzymes in all muscles studied did not differ, even though the KD was devoid of carbohydrates. Collectively, these findings indicated that, contrary to the obesogenic HFS diet, the carbohydrate-free KD maintained skeletal muscle metabolic flexibility while also enhancing, in a muscle-specific manner, rates of FA oxidation and ketolytic capacity.

Chapter 9: Effects of the adiponectin mimetic compound ALY688 on glucose and fat metabolism in visceral and subcutaneous rat adipocytes

Daniel Da Eira[1], Shailee Jani[1], Hyekyoung Sung[2], Gary Sweeney[2], Rolando B. Ceddia[1]

[1]School of Kinesiology and Health Science and [2]Department of Biology, York University, North York, Ontario, Canada, M3J 1P3.

This manuscript was published in the journal ***Adipocyte***. ***Adipocyte's*** copyright policies are based in the Creative Commons Open Access License whereby the full article can be reproduced without charge.

Da Eira D, Jani S, Sung H, Sweeney G, Ceddia RB. Effects of the adiponectin mimetic compound ALY688 on glucose and fat metabolism in visceral and subcutaneous rat adipocytes. *Adipocyte*. 2020 Dec;9(1):550-562.

Statement of Labour

The work in this study was performed by DD. DD performed functional assays and Western blotting and qPCR experiments. Moreover, DD collected and analyzed the data, prepared figures and wrote and revised the manuscript. DD was funded by the Alexander Graham Bell – Canada Graduate Scholarship (Doctoral). Due to the logistics of functional assays, SJ assisted with tissue extractions, adipocyte isolation and the performance of the functional assays. HS and GS were our collaborators on this project and provided the compound ALY688 from Allysta Pharmaceuticals.

Dr. Rolando Ceddia is the principal investigator and was involved in all stages of this study. The work presented in this manuscript was funded by grants awarded to RBC, including the Discovery Grant from the Natural Science and Engineering Research Council of Canada (NSERC) and by infrastructure grants from the Canada Foundation for Innovation (CFI) and the Ontario Research Fund (ORF).

9.1. Abstract

Adiponectin regulates white adipose tissue (WAT) metabolism and promotes insulin-sensitizing and anti-atherosclerotic effects *in vivo*. In this context, small molecule adiponectin receptor agonists have become of great therapeutic value for the treatment of metabolic diseases. Here, we investigated the effects of the adiponectin mimetic compound ALY688 on WAT metabolism. To accomplish this, rat epididymal (Epid) and subcutaneous inguinal (Sc Ing) adipocytes were isolated and incubated with ALY688. Subsequently, several parameters of glucose and fat metabolism were assessed. ALY688 promoted AMP-activated protein kinase (AMPK) and acetyl-CoA carboxylase (ACC) phosphorylation, enhanced glucose oxidation, and suppressed fat oxidation in adipocytes from both fat depots. ALY688 did not affect basal and insulin-stimulated rates of glucose uptake, glucose incorporation into lipids and AKT_{Ser473} and p38 mitogen-activated protein kinase (MAPK) phosphorylations in Epid or Sc Ing adipocytes. ALY688 did not alter basal lipolysis in Epid or Sc Ing adipocytes, but it enhanced isoproterenol-induced lipolysis in Epid adipocytes. Adiponectin receptor 2 (AdipoR2) mRNA was the prevalent isoform expressed in all adipocytes, and Epid adipocytes displayed significantly higher AdipoR2 mRNA expression than Sc Ing adipocytes. In conclusion, ALY688 can regulate adiposity and affect glycemic control by altering substrate portioning in the WAT in a fat depot-specific manner.

9.2. Introduction

Maintenance of whole-body glucose homeostasis depends on the coordinated action of multiple hormones that allow the organism to respond to daily oscillations in the availability of dietary carbohydrate and other macronutrients[5]. In this context, the adipose tissue plays an important role in maintaining whole-body glucose homeostasis. It does so by serving as a compartment where energy can be stored or mobilized and also by secreting hormones that regulate glucose and fat metabolism in multiple organs and tissues[249]. To date, many bioactive adipose-derived factors (adipokines) have been identified[249]. Among them is adiponectin, a secreted protein abundantly present in plasma, that has been demonstrated to exert potent insulin sensitizing, glucose lowering, and lipid catabolizing functions in peripheral tissues[250]. Two adiponectin receptors (AdipoRs) have been cloned (AdipoR1 and AdipoR2), which are expressed in various tissues including liver, skeletal muscle, white adipose tissue (WAT), hypothalamus, and vasculature[251]. The metabolic effects of adiponectin vary in a tissue-specific manner, depending in part on tissue-specific expression of AdipoR1 and AdipoR2, as well as cell-specific, intracellular signaling pathways[251]. For instance, AdipoR1 is abundant in skeletal muscles and macrophages, whereas WAT and the vasculature are rich in AdipoR2. The liver abundantly expresses both AdipoRs[251].

Once bound to its receptors, adiponectin has been shown to promote the activation of AMP-activated protein kinase (AMPK) and peroxisome proliferator-activated receptor α (PPARα)[251,252]. In liver and skeletal muscles, activated AMPK phosphorylates acetyl-CoA carboxylase (ACC) and leads to enhanced mitochondrial import and oxidation of long-chain fatty acids[253,254]. Adiponectin has also been shown to exert anti-lipotoxic effects through the induction of the transcriptional effects of PPARα[255], culminating in the downregulation of lipid synthesis enzymes, the elevation in carnitine palmitoyltransferase 1 (CPT1) levels, and the enhanced production and secretion of

HDL by the liver[256]. In the WAT, adiponectin has been demonstrated to elevate the fat-storing capacity of adipocytes by promoting glucose uptake[257] and lipogenesis[258] and by decreasing lipolysis[259], although the enhancement of fat oxidation has also been cited as an effect of adiponectin in fat cells[250]. The opposing lipogenic and fatty acid oxidative effects of adiponectin on adipocytes have been proposed to confer metabolic flexibility to the WAT, which contributes to minimizing ectopic lipid deposition in non-adipose tissues, preventing adipose inflammation and fibrosis, and maintaining healthy WAT expansion[250,260]. However, the findings that support an elevation in fatty acid oxidation induced by adiponectin originate from studies conducted in C_2C_{12} muscle cells[254,255,261], isolated mouse skeletal muscles[253,255,261,262], mouse hepatocytes[253], and hepa-1-6 hepatocytes in culture[261]. To the best of our knowledge, no direct evidence exists that adiponectin indeed promotes fatty acid oxidation in adipocytes. Disruption of both AdipoR1 and AdipoR2 has been reported to significantly decrease the expression of genes encoding for *Cat* and *Sod* and increase oxidative stress in WAT, but there were no reports of alterations in the capacity of the WAT to oxidize fat in mice lacking AdipoR1 and AdipoR2[263]. Thus, it is likely that the metabolic responses of WAT to adiponectin differ from those of skeletal muscles and liver with respect to fatty acid oxidation.

Reduced circulating levels of adiponectin and impaired AdipoR action are found in obesity, insulin resistance, type 2 diabetes, and atherosclerosis[252]. Therefore, increasing adiponectin production and/or adiponectin signaling are attractive targets for therapeutic interventions for the prevention or treatment of obesity-related derangements in metabolism. In fact, a small-molecule, AdipoR-activating compound named AdipoRon (AR) has been reported to improve insulin resistance and lifespan in mice consuming a high-fat diet[16]. These findings in rodents have provided support for the development of other adiponectin mimetic compounds to target substrate

metabolism in organs that play major roles in regulating whole-body glucose and lipid homeostasis in humans. In this context, a peptide-based adiponectin mimetic named ALY688 (also referred to as ADP355) has been developed[264]. The compound has been shown to bind to both AdipoR1 and AdipoR2 and induce adiponectin-specific signaling in several cell types[265]. A potential advantage of peptide mimetics is that they can provide great potency and specificity compared with small molecule mimetics.

Because the WAT plays an important role in the regulation of glucose and lipid homeostasis[5] and only a few studies have focused on the effects of adiponectin on this tissue, we assessed the effects of ALY688 as an adiponectin mimetic on glucose uptake and fatty acid oxidation in isolated white adipocytes. Also, due to metabolic differences between visceral (Vc) and subcutaneous (Sc) fat depots and their implications to obesity-related metabolic diseases[266], adipocytes isolated from epididymal (Epid) and Sc inguinal (Sc Ing) fat depots were used. We assessed the potential direct effects of ALY688 on glucose uptake, incorporation of glucose into lipids, fatty acid oxidation, and lipolysis, which are major pathways by which adipocytes handle glucose and fatty acids. We also measured the phosphorylation of AMPK, ACC, AKT, and p38 mitogen-activated protein kinase (p38MAPK), which are signaling pathways by which this adiponectin mimetic compound could potentially regulate metabolism in the WAT. Here, we provide evidence that despite enhancing AMPK phosphorylation in Epid and Sc Ing adipocytes, ALY688 reduced fat oxidation and did not affect basal or insulin-stimulated glucose uptake. However, it shifted glucose metabolism towards oxidation and enhanced adrenergic-stimulated lipolysis in a depot-specific manner.

9.3. Material and Methods

Reagents – Type II collagenase, isoproterenol, fatty acid (FA)-free bovine serum albumin (BSA), palmitic acid, and the free glycerol determination kit were purchased from Sigma (St. Louis, MO, USA). [1-^{14}C] palmitic acid and D-[U-^{14}C] glucose were purchased from American Radiolabeled Chemicals (St. Louis, MO, USA). Protease (cOmplete Ultra Tablets) and phosphatase (PhosSTOP) inhibitors were obtained from Roche Diagnostics GmbH (Mannheim, Germany). The β-actin (Cat # 4067), AMPK (Cat # 2532), $pAMPK_{Thr172}$ (Cat # 2535), AKT (Cat # 9272), $pAKT_{Ser473}$ (Cat # 9271), p38 (Cat # 9212), pp38 (Cat # 9211), hormone-sensitive lipase (HSL; Cat # 4107), and $pHSL_{Ser660}$ (Cat # 4126) antibodies were purchased from Cell Signaling (Danvers, MA, USA). The ACC (Cat # ab45174) and $pACC_{Ser79}$ (Cat # ab68191) antibodies were purchased from Abcam (Toronto, ON, Canada). ALY688 was provided by Allysta Pharmaceuticals, Belmont, CA, USA.

Animals – Adipose tissue from the subcutaneous inguinal (Sc Ing) and epididymal (Epid) fat pads were extracted from male albino rats (Wistar strain weighing ~250 g, 50-60 days old), under anaesthesia, and subsequently processed for cell isolation (Fig. 39). All experiments were approved by the Animal Care Committee at York University (York University Animal Care Committee, YUACC, permit number 2016-5) and performed strictly in accordance with the YUACC guidelines. All surgery was performed under ketamine/xylazine anaesthesia, and all efforts were made to minimize suffering.

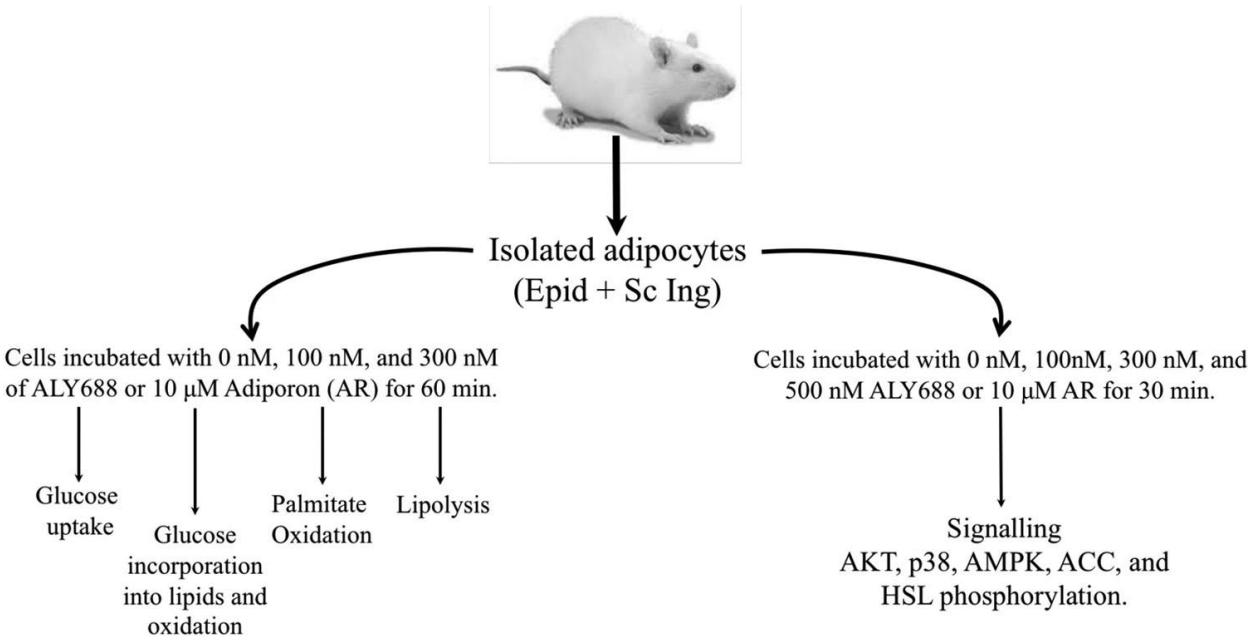

Figure 39: Schematic representation of experimental design.

Adipocyte isolation – Adipocyte isolation from the Epid and Sc Ing fat pads was performed as previously described[7]. Briefly, the adipose tissue was minced in Krebs-Ringer bicarbonate HEPES buffer (KRBH), containing type II collagenase (0.5 mg/ml), prepared fresh on the day of each experiment from stock solutions of salts and buffers (stored at 4°C) to give the following final concentrations: 120 mM NaCl, 4.8 mM KCl, 2.5 mM $CaCl_2$, 1.2 mM KH_2PO_4, 1.2 mM $MgSO_4$, 15 mM $NaHCO_3$, and 30 mM HEPES. Before use, KRBH was gassed for 45 min with carbogen (95% O_2, 5% CO_2) and then bovine serum albumin (3.5%) and glucose (5.5 mM) were added. Following this, the pH of the buffer was adjusted to 7.4 with NaOH. Minced tissues were incubated at 37°C with gentle agitation (120 orbital strokes/min) for approximately 25-30 min. The digested tissue was then strained using a nylon mesh (500 μm pore size) and cells were transferred to 50 ml plastic tubes, where the stromal vascular fraction (SVF) and mature adipocytes separated into two distinct phases. The SVF sitting at the bottom of the tube was discarded by aspiration and the floating adipocytes were washed 3 times prior to being resuspended in KRBH containing 3.5% fatty acid-free BSA (KRBH-3.5% BSA). In order to distribute an equal number of adipocytes in

each treatment condition, cell diameters were measured and total cell numbers determined as previously described[182].

Measurement of glucose uptake – Glucose uptake was measured either under basal or insulin-stimulated (10 and 100 nM) conditions following the treatment of adipocytes either without (control) or with ALY688. Our initial choice of doses was based on experiments conducted with ALY688 in other cell types (renal fibroblasts, breast cancer cells, etc.) in which concentrations around 100 nM of the compound caused significant effects. Therefore, we decided to start with a similar dose of 100 nM and increase the concentrations to 300 and 500 nM to assess whether higher doses would be required for broader metabolic responses from Epid and Sc Ing adipocytes. We also used AR (10 μM) to test whether another AdipoR agonist would elicit similar effects. Isolated adipocytes ($4x10^5$ cells) were transferred to plastic tubes either with or without ALY688 and incubated at 37°C for 1h. Insulin was added to the medium for the final 20 min of the incubation period. Subsequently, KRB-HEPES containing 0.5 mM 2-deoxy-D-glucose and 0.5 μCi of 2-[1,2-^{3}H]deoxy-D-glucose was added to the cells for 3 min, and the incubations were terminated by the addition of cytochalasin B (1.5 mM stock solution). Aliquots of cell suspension (240 μl) were quickly placed in plastic microtubes containing 100 μl of di-"isononyl" phthalate. The tubes were centrifuged for 30s (6000 × g) to separate cells from the radioactive incubation medium. Subsequently, fat cells were collected by cutting the tubes through the oil phase and transferring the portion containing the cells to scintillation vials to be counted for radioactivity. Radioactivity of the cells unrelated to glucose transport (nonspecific transport) was determined in the same conditions by adding cytochalasin B (50 μM final concentration) to the medium before the addition of 2-[1,2-^{3}H]deoxy-D-glucose[187]. Nonspecific values were subtracted from all conditions.

Measurement of glucose incorporation into lipids – Glucose incorporation into lipids was measured in isolated adipocytes (5 x 10^5 cells) from the Epid and Sc Ing fat depots as previously described[184]. Briefly, cells were incubated in KRBH-3.5% BSA containing 0.2 μCi/ml of D-[U-^{14}C] glucose and 5.5 mM non-labeled D-glucose for 1h either in the absence or presence of ALY688 (100 and 300 nM) and in the absence or presence of insulin (100 nM). Lipids were then extracted according to the method of Dole and Meinertz[207] and assessed for radioactivity[184].

Measurement of glucose and palmitate oxidation – Glucose and palmitate oxidation as measures of oxidative capacity were assessed by production of $^{14}CO_2$ in Epid and Sc Ing isolated adipocytes (5 x 10^5 cells) as previously described[42]. In order to measure palmitate oxidation, cells were incubated in KRBH-3.5% BSA containing 0.2 μCi/ml of [1-^{14}C] palmitic acid and 200 μM non-labelled palmitate. For glucose oxidation, cells were incubated with 0.2 μCi/ml of D-[U-^{14}C] glucose and 5.5 mM non-labeled D-glucose. Glucose and palmitate oxidation were measured during 1h either in the absence or presence of ALY688 (100 nM and 300 nM). For glucose oxidation only, cells were also incubated in the absence or presence of insulin (100 nM). Following 1 h of incubation, the media were acidified with 0.2 ml of H_2SO_4 (5 N), and the vials were maintained sealed at 37°C for an additional 1h for the collection of $^{14}CO_2$ released from the cells and the media. Each vial used for incubation had a centered isolated well containing a loosely folded piece of filter paper that was moistened with 0.2 ml of 2-phenyl- ethylamine/methanol (1:1, *vol:vol*) to capture $^{14}CO_2$. At the end of the incubation, the filter paper was removed and transferred to a scintillation vial for radioactivity counting[42].

Determination of lipolysis – Lipolysis was measured in isolated Epid and Sc Ing adipocytes (6 x 10^5 cells). Adipocytes were incubated in the absence or presence of ALY688 and with or without 100 nM isoproterenol (β-non-specific agonist)[267]. Each condition was assayed in triplicates and

the samples were incubated for 75 min at 37°C with gentle agitation (80 orbital strokes/min). After incubation, a 200 µl aliquot of medium was taken from each vial for the determination of glycerol concentration.

RNA isolation and quantitative PCR – Primers were designed using the software PrimerQuest (IDT) based on probe sequences available at the Affymetrix database (NetAffx™ Analysis Centre, http://www.affymetrix.com/ analysis) for each given gene. RNA was isolated from adipose tissue and isolated adipocytes using the RNeasy Lipid Tissue Kit (Germantown, MD, USA) and complimentary DNA (cDNA) was made from 2 µg of extracted RNA using the ABM EasyScript™ cDNA Synthesis kit (Diamed, Mississauga, ON, Canada), according to the manufacturer's instructions. Samples were run in duplicate on 96-well plates, and each 20 µl reaction contained 4 µl of cDNA, 0.4 µl of primer, 10 µl of Brightgreen 2x qPCR Mastermix (Diamed, Mississauga, ON, Canada) and 5.6 µl of RNA-free water. Real-time PCR analysis was performed using a Bio-Rad CFX96 Real Time PCR Detection System (Bio-Rad, Mississauga, ON, Canada) using the following amplification conditions: 95°C (10 min); 40 cycles of 95°C (15 s), 60°C (60 s). Values are presented as fold increases relative to GAPDH gene expression[188]. The primers used to probe for rat AdipoR1 and AdipoR2 mRNA levels using qPCR were as follows:

AdipoR1: Forward: 5'-ACTTTGTAACCTGGCGGATGACAG-3'
Reverse: 5'-ATCAAGGCGTGGCTTTGTTTGTCC-3'

AdipoR2: Forward: 5'-AATGATGGCGTTTCTCTCTGGTGC-3'
Reverse: 5'-CACACTTCTTGCGAACGGCATTCA-3'

GAPDH: Forward: 5'-TGACTCTACCCACGGCAAGTTCAA-3'
Reverse: 5'-ACGACATACTCAGCACCAGCATCA-3'

Western blotting analysis of content and phosphorylation of proteins – Isolated adipocytes from the Epid and Sc Ing fat depots were incubated in the absence or presence of ALY688 for 30 min

and then immediately homogenized in a buffer containing 25 mM Tris-HCl, 25 mM NaCl (pH 7.4), 1 mM $MgCl_2$, 2.7 mM KCl, 1% Triton X-100 and protease and phosphatase inhibitors (Roche Diagnostics GmbH, Mannheim, Germany). Homogenates were centrifuged, the infranatant collected, and an aliquot was used to measure protein by the Bradford method. Samples were diluted 1:1 (vol:vol) with 2x Laemmli sample buffer and heated to 95°C for 5 min. 25 μg of protein were loaded in each well. Samples were then subjected to SDS-PAGE, transferred to PVDF membrane, and probed for the proteins of interest. All primary antibodies were used at a dilution of 1:1,000 and β-actin was used as a loading control. All densitometry analyses were performed using the Scion Image program.

Statistical analyses – Statistical analyses were performed by either unpaired two-tailed t-tests or one and two-way analysis of variance (ANOVA) with Bonferroni post-hoc tests using the GraphPad Prism statistical software program. Bars represent mean ± SEM. Statistical significance was set at $p<0.05$.

9.4. Results

AMPK and ACC phosphorylation – We detected an increase in AMPK phosphorylation when adipocytes were incubated with 100, 300, and 500 nM of ALY688. In Epid adipocytes, 100 and 300 nM of ALY688 significantly increased AMPK phosphorylation by 2.37- and 2.7-fold, relative to 0 nM, respectively, whereas AR (10μM) increased this variable by 1.57-fold (Fig. 40A). In Sc Ing adipocytes, 300 nM of ALY688 increased AMPK phosphorylation by 3.81-fold relative to 0 nM, which was of similar magnitude to the AR effect in these cells (Fig. 40B). However, an increase in AMPK phosphorylation was not observed in this depot with 100 nM of the drug (Fig. 40B). To confirm that phosphorylation of AMPK was accompanied by an increase in its activity, we also assessed the phosphorylation of ACC, a downstream target of AMPK. In the presence of

500 nM of ALY688, AMPK phosphorylation increased 6.2-fold (Fig. 40C), and this was accompanied by a 2.13-fold increase in ACC phosphorylation (Fig. 40D). The generation of cell lysates from primary adipocytes requires a large amount of adipose tissue; thus, in order to optimize the preparation, we used the Sc Ing fat depot where the amount of tissue available and the yield of cells were the highest. Also, in order to have three replicates for control and the compound, we used only one dose of ALY688 (500 nM) as shown in Fig. 40C and D.

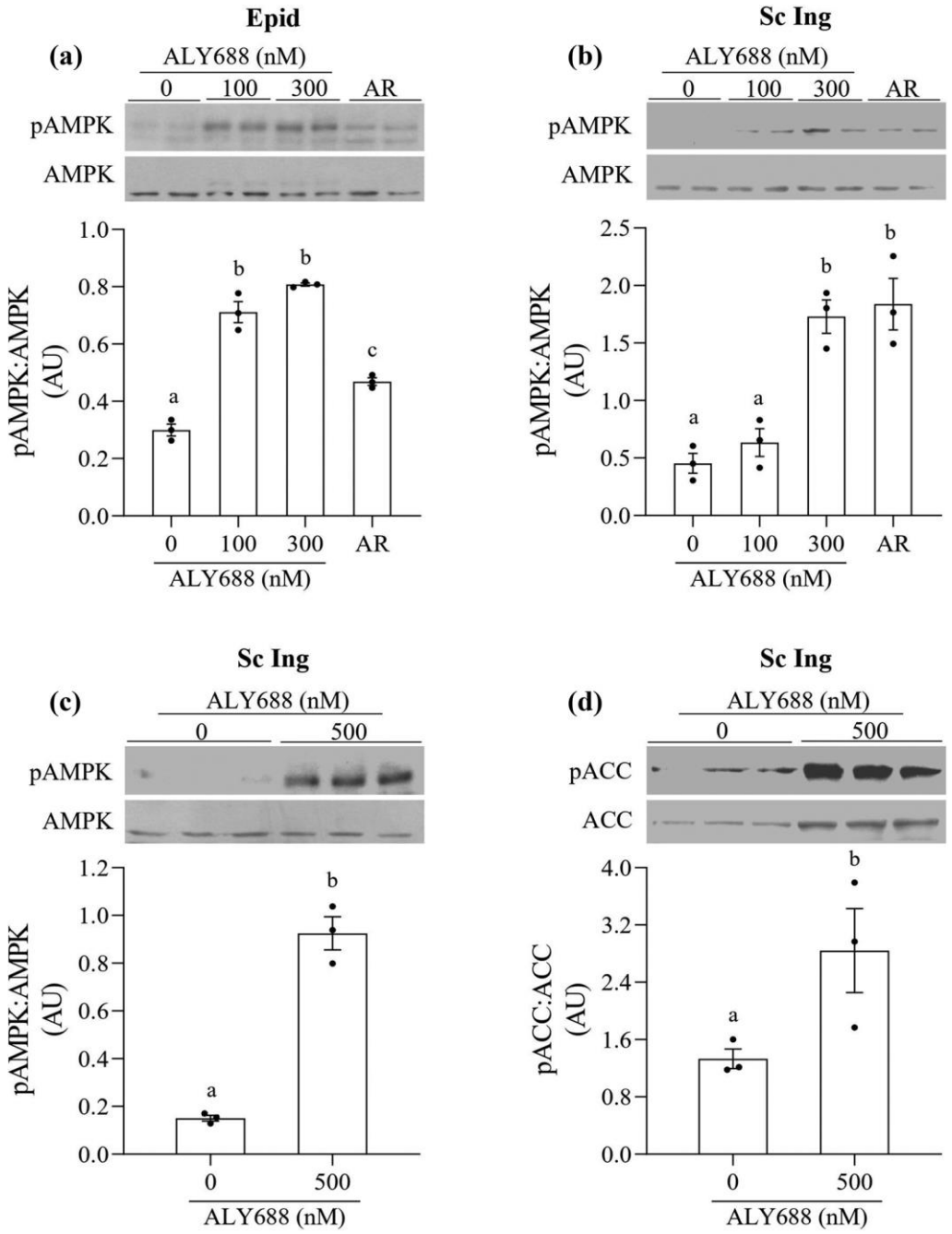

Figure 40: ALY688 (100 and 300 nM) induced AMPK phosphorylation in epididymal (Epid, A) and subcutaneous inguinal (Sc Ing, B) adipocytes. AdipoRon (AR) was used as a positive control. In Sc Ing adipocytes, a higher dose of ALY688 also increased the phosphorylation of AMPK (C) and ACC (D). Different letters denote statistical significance ($p<0.05$). One-way ANOVA for AB and t-test for C-D, n=3.

Glucose uptake – As expected, glucose uptake was increased upon insulin stimulation in both Sc Ing and Epid adipocytes. However, no significant effects of any concentration of either ALY688

or AR (10 μM) on basal and insulin-stimulated glucose uptake were detected (Fig. 41A and B). Because supraphysiological insulin concentrations (100 nM) were used in the initial experiments, it could be that glucose uptake was maximized, masking a potential effect of ALY688 on this variable. To explore this, we conducted additional experiments using a lower (more within the physiological range, 10 nM) insulin concentration. Also, we used a higher concentration of the compound (500 nM) to test whether this would be more effective in adipocytes than the previous doses used (Fig. 41C). Despite this, we found that even under lower doses of insulin, glucose uptake was not significantly affected by 500 nM of ALY688 in Epid adipocytes (Fig. 41C), and similar results were also found for Sc Ing adipocytes.

AKT and p38 MAPK phosphorylation – To test whether major steps of the insulin signaling pathway were affected by ALY688, we measured AKT_{Ser473} phosphorylation in both Epid and Sc Ing adipocytes exposed to 0, 100, 300, and 500 nM of the compound. No effect of ALY688 was detected on AKT_{Ser473} phosphorylation in Epid (Fig. 42A) and Sc Ing (Fig. 42B) adipocytes, which is consistent with the lack of effect on glucose uptake in these cells. As a positive control, cells isolated from both fat depots were also treated with insulin (100 nM), and it caused a robust AKT_{Ser473} phosphorylation response to the hormone (Fig. 42A and B). Additionally, because adiponectin initiates a series of tissue-dependent signal transduction events through distinct signaling pathways, including p38 MAPK[254], we also tested whether this would be the case in Epid and Sc Ing adipocytes. As shown in Fig. 42C and D, p38 phosphorylation was not affected by 100 and 300 nM of ALY688 in Epid and Sc Ing adipocytes. However, a robust induction of p38 MAPK phosphorylation was detected when adipocytes from both fat depots were incubated with 10 μM of AR (Fig. 42C and D).

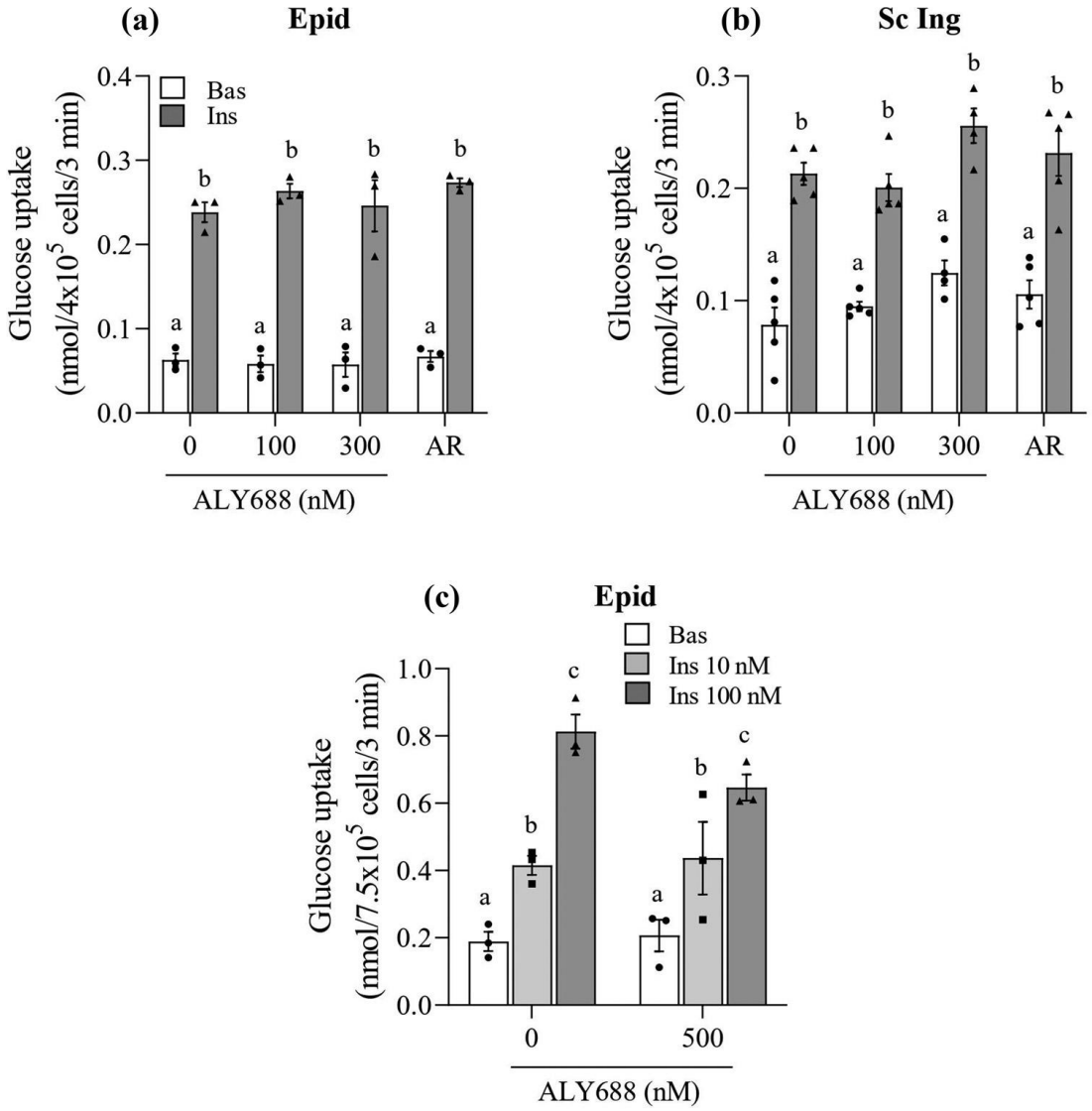

Figure 41: No effect of ALY688 (100, 300, and 500 nM) on basal (Bas) and insulin (Ins, 100 nM)-stimulated glucose uptake in epididymal (Epid, A) and subcutaneous inguinal (Sc Ing, B) adipocytes. Glucose uptake was also assessed in Epid adipocytes exposed to 500 nM of ALY688 for 60 min (C) and then stimulated with 10 and 100 nM of insulin. Different letters denote statistical significance ($p<0.05$). Two-way ANOVA, n=3-5.

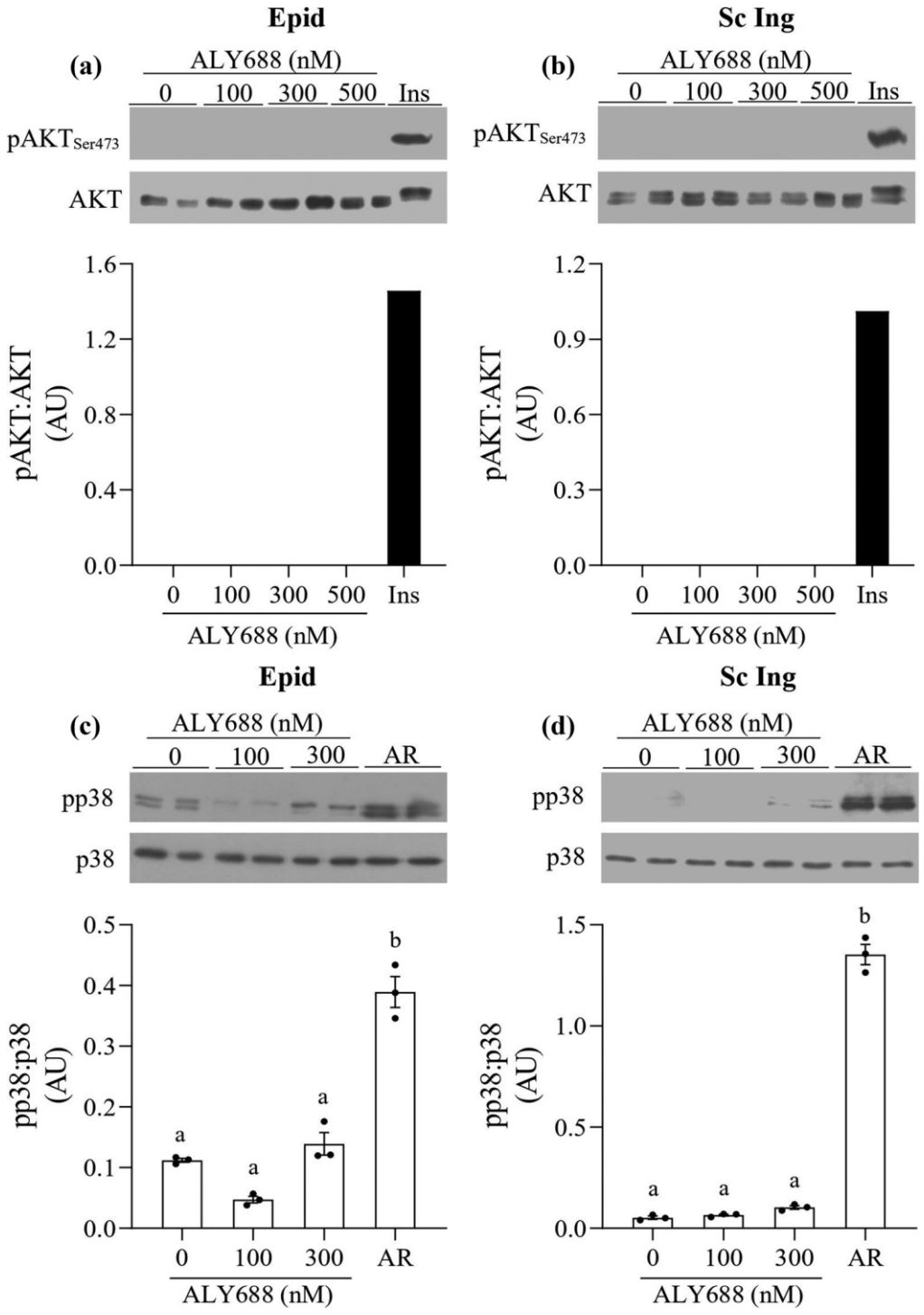

Figure 42: ALY688 did not affect AKT$_{Ser473}$ and p38 MAPK phosphorylation in Epid (A and C) and Sc Ing adipocytes (B and D), whereas AdipoRon (AR) and insulin induced robust increases in AKTSer473 and p38 MAPK phosphorylations in adipocytes from both fat depots. Different letters denote statistical significance ($p<0.05$). One-way ANOVA, n=3.

Glucose incorporation into lipids and glucose oxidation – ALY688 did not affect glucose uptake in Epid and Sc Ing adipocytes; however, it could still affect metabolism of this substrate inside the cells. To evaluate this, we measured the incorporation of glucose into lipids and also glucose oxidation in Epid and Sc Ing adipocytes under basal and insulin-stimulated conditions. We found that neither Epid nor Sc Ing rates of glucose incorporation into lipids (lipogenesis) were affected by the compound (Fig. 43A and B). However, ALY688 caused dose and tissue-specific effects on glucose oxidation in Epid and Sc Ing adipocytes. This was characterized by significantly enhanced basal glucose oxidation by 49% and 39% in Epid adipocytes in the presence of 100 and 300 nM of ALY688, respectively, when compared to cells incubated in the absence of insulin and ALY688 (Fig. 43C). In Sc Ing adipocytes, 100 and 300 nM of ALY688 increased basal glucose oxidation by 37% and 64%, respectively, with only the latter concentration reaching statistical significance when compared to 0 nM ALY688 (Fig. 43D). Insulin-stimulated glucose oxidation was also enhanced by the compound, although only in Epid adipocytes treated with 300 nM of ALY688 or AR (Fig. 43C).

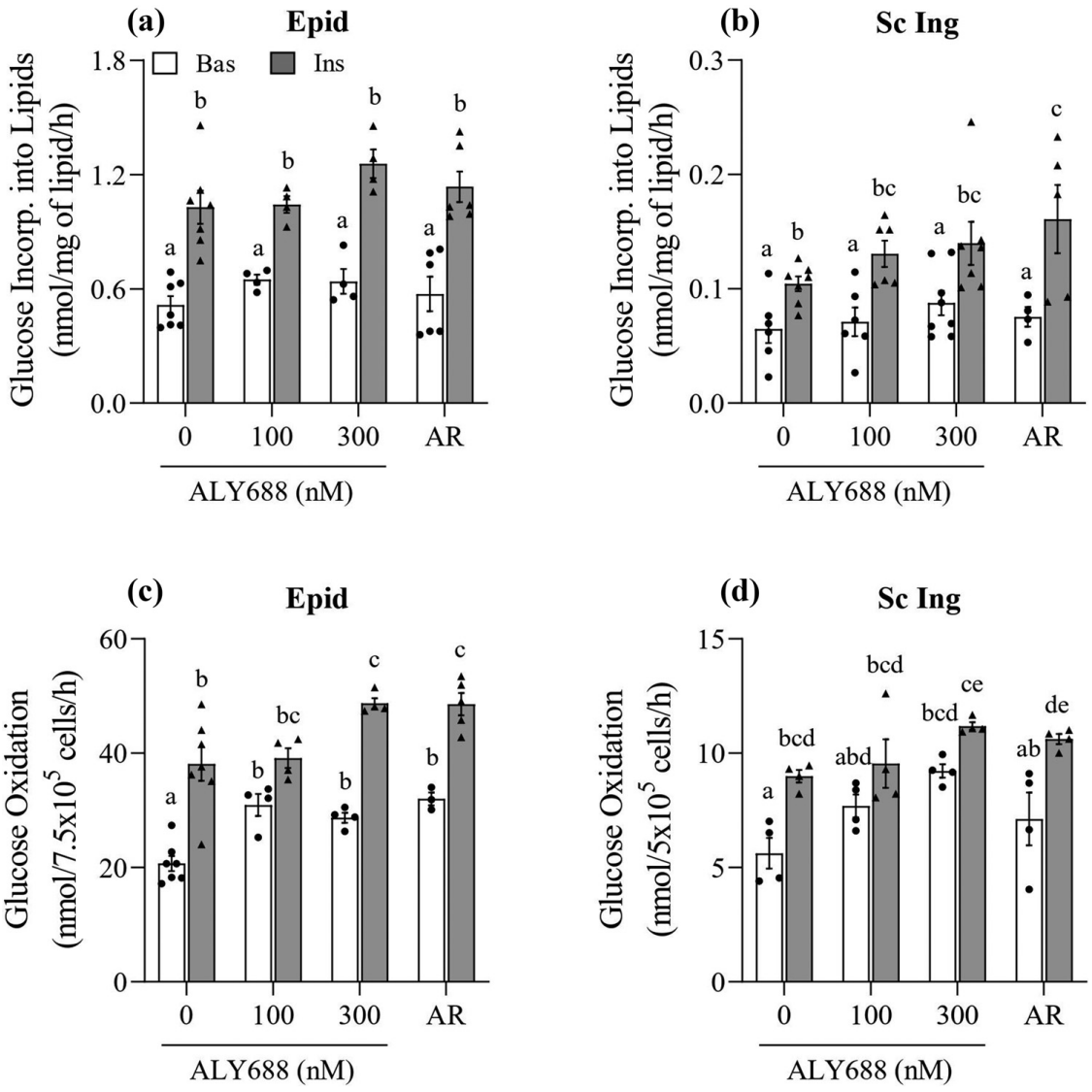

Figure 43: ALY688 (100 and 300 nM) did not affect glucose incorporation into lipids (A and B), but it enhanced in a dose-dependent and tissue-specific manner basal (Bas) and insulin (Ins)-stimulated rates of glucose oxidation in Epid (C) and Sc Ing (D) adipocytes. Different letters denote statistical significance ($p < 0.05$). Two-way ANOVA, n = 3–7.

Palmitate oxidation – Because ALY688 induced a consistent increase in AMPK and ACC phosphorylation in isolated adipocytes from both fat depots, we tested whether such effect was also accompanied by a functional metabolic alteration in these cells. The initial expectation was that increased AMPK phosphorylation would increase rates of fatty acid oxidation, as it is frequently reported in skeletal muscle cells[255,261]. However, to our surprise, 300 and 500 nM of ALY688 suppressed basal palmitate oxidation by ~55% and ~35% in both the Epid and Sc Ing

adipocytes, respectively, relative to the 0 nM group (Fig. 44A and B). No effect on palmitate oxidation was observed in either depot with 100 nM of ALY688 (Fig. 44A and B).

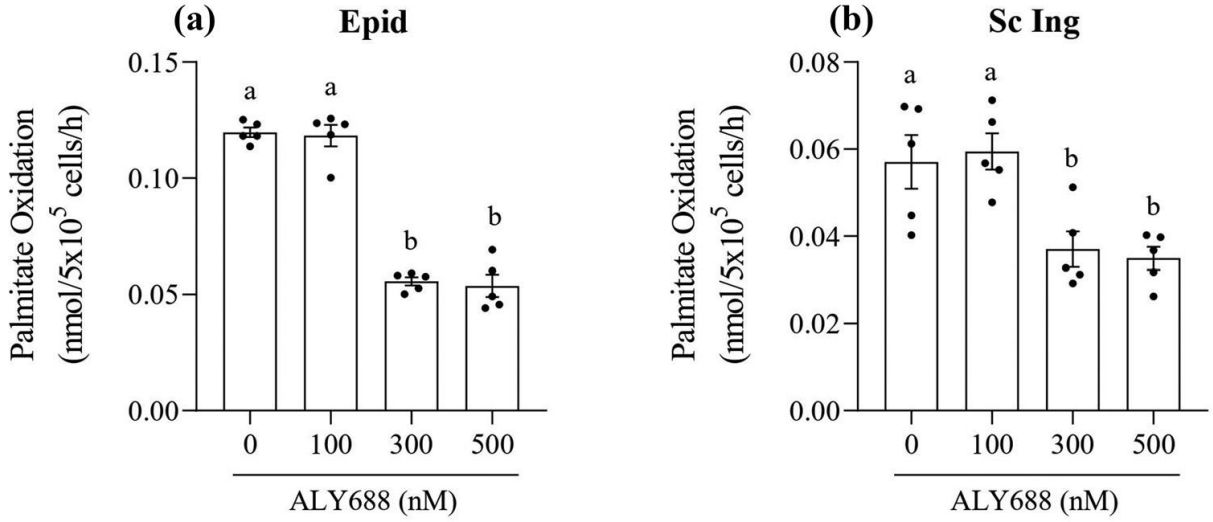

Figure 44: As the concentration of ALY688 increased beyond 100 nM, rates of palmitate oxidation were reduced in both epididymal (Epid, A) and subcutaneous inguinal (Sc Ing, B) adipocytes. Different letters denote statistical significance ($p < 0.05$). One-way ANOVA, $n = 5$.

Lipolysis – In order to assess whether ALY688 could affect the ability of adipocytes to export fatty acids, we also measured lipolysis in these cells. We found that basal lipolysis was not affected by treating cells with ALY688; however, when Epid adipocytes were stimulated with 100 and 300 nM of ALY688 and 100 nM of isoproterenol, glycerol release increased by 45% and 70%, respectively, when compared to cells incubated with isoproterenol only (Fig. 45A). In Sc Ing adipocytes, ALY688 had no significant effect on rates of glycerol release either under basal or isoproterenol (Iso)-stimulated conditions (Fig. 45B). In order to assess potential mechanisms by which ALY688 enhanced Iso-stimulated glycerol release in Epid adipocytes, we measured phosphorylation of hormone sensitive lipase (HSL_{Ser660}) in both Epid and Sc Ing adipocytes. As depicted in Fig. 45C and D, ALY688 increased phosphorylation of HSL_{Ser660} in Epid, but not in Sc Ing adipocytes. This suggests that ALY688-induced HSL phosphorylation could be linked to the increase in glycerol release seen in Epid adipocytes. However, we could not perform a

statistical analysis because we had only 2 samples probed for HSL phosphorylation. Furthermore, even though HSL plays a very important role in adipose tissue lipolysis, adipose triglyceride lipase (ATGL) activity could also be affected by ALY688. However, the activity of this latter lipase was not measured in this study.

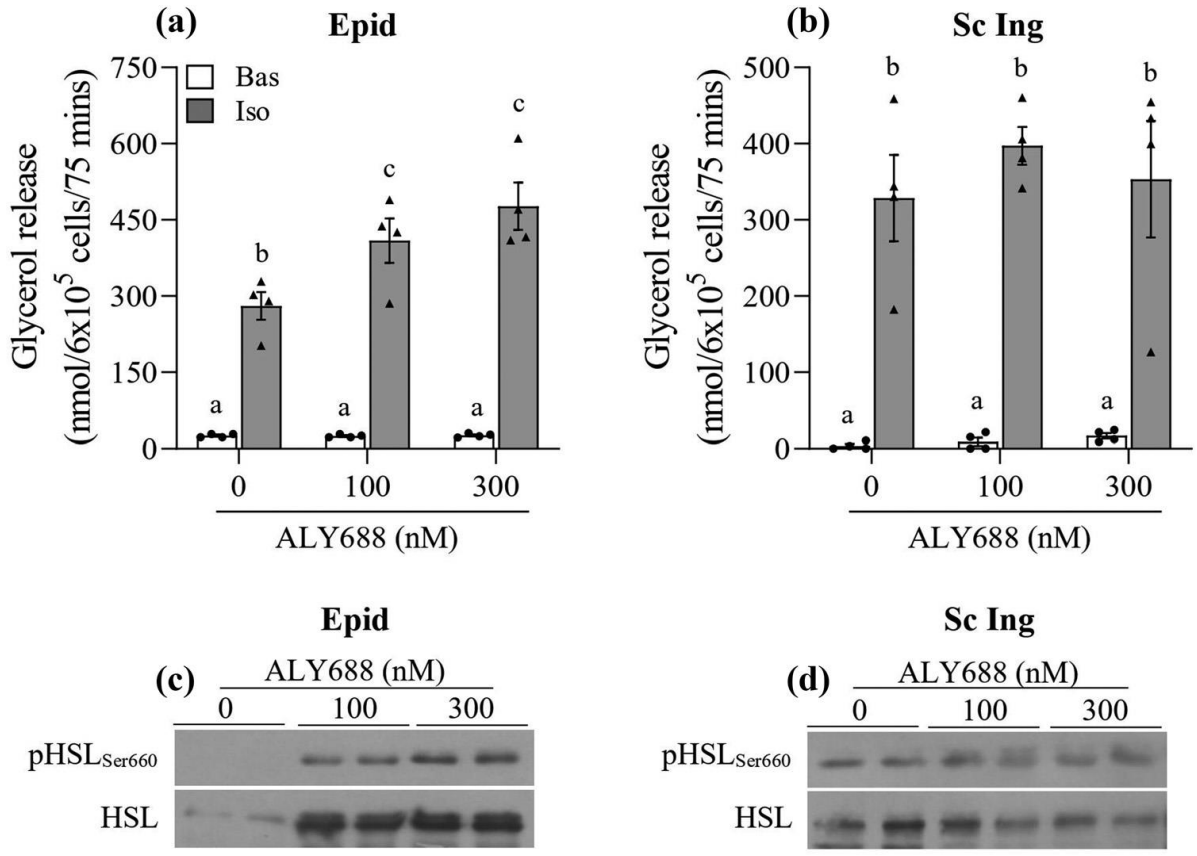

Figure 45: Lipolysis was affected in tissue-specific manner by ALY688. In Epididymal (Epid) adipocytes, isoproterenol (Iso)-stimulated lipolysis increased (A), whereas no effect of ALY688 (100 and 300 nM) was detected in Sc Ing (B) adipocytes either under basal (Bas) or Iso-stimulated conditions. Similarly, HSL phosphorylation was elevated in Epid (C), but not in Sc Ing (D) adipocytes. Different letters denote statistical significance ($p < 0.05$). Two-way ANOVA, n = 4 for glycerol release and n = 2 for HSL content and phosphorylation.

Adiponectin receptor gene expression in isolated adipocytes and whole WAT – In isolated adipocytes, we found that the mRNA expression of AdipoR2 was 1.85-fold and 1.75-fold higher than AdipoR1 in Epid and Sc Ing cells, respectively (Fig. 46A). Furthermore, the mRNA expression of both receptors was significantly lower in Sc Ing than Epid cells. In fact, AdipoR1

and AdipoR2 mRNA expressions were ~45% lower in Sc Ing than in Epid adipocytes (Fig. 46A). In whole Epid fat tissue, AdipoR2 mRNA expression was 2.5-fold higher than AdipoR1, which was similar to what we found in isolated cells. However, in the Sc Ing fat pad the reverse was found, with AdipoR1 mRNA expression being 1.3-fold higher than AdipoR2 (Fig. 46B). All our experiments were conducted in isolated cells; therefore, it is possible that the higher expression of AdipoR2 in Epid adipocytes dictated the distinct metabolic responses that ALY688 treatment elicited in isolated cells from visceral and subcutaneous fat depots.

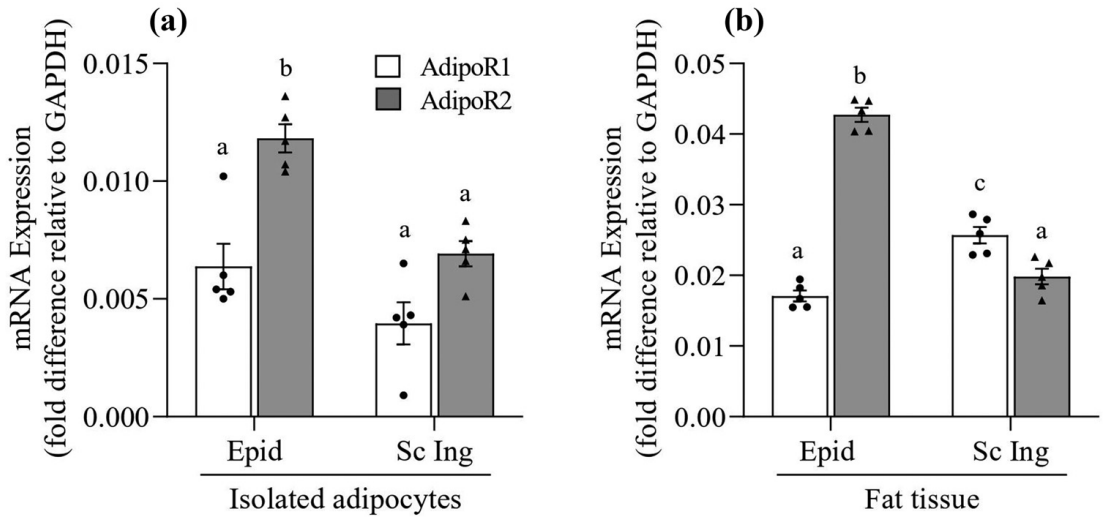

Figure 46: Distinct profile of AdipoR1 and AdipoR2 mRNA expression between epididymal (Epid) and subcutaneous inguinal (Sc Ing) adipocytes (A) and fat depots (B). Different letters denote statistical significance ($p < 0.05$). Two-way ANOVA, n = 5.

9.5. Discussion

Our findings provide evidence that acute exposure of isolated Epid and Sc Ing rat adipocytes to ALY688 did not alter AKT and p38 MAPK phosphorylation, basal and insulin-stimulated glucose uptake, and glucose incorporation into lipids (lipogenesis) in these cells. However, ALY688 treatment increased AMPK and ACC phosphorylation, although this was accompanied by suppression instead of stimulation of palmitate oxidation in Epid and Sc Ing adipocytes. This latter finding is contrary to what has been demonstrated in skeletal muscle cells under adiponectin-

stimulated AMPK activation[255,261], suggesting a distinct regulatory role for adiponectin-mediated AMPK activation in WAT glucose and fat metabolism in comparison to liver and skeletal muscle. In fact, ALY688 enhanced rates of glucose oxidation in a concentration-dependent and tissue-specific manner in Epid and Sc Ing adipocytes. Basal rates of glucose oxidation consistently increased in cells from both fat depots, whereas under insulin-stimulated conditions only higher concentrations (300 nM) of the compound elicited an effect in Epid adipocytes. The data indicate that acute ALY688 treatment diverts glucose towards oxidation in adipocytes, which could positively contribute to whole-body glycemic control. We have also found that both AR and ALY688 enhanced AMPK phosphorylation in Epid and Sc Ing adipocytes, whereas only AR increased p38 MAPK phosphorylation in these cells. However, because neither ALY688 nor AR affected either basal or insulin-stimulated uptake of glucose and its incorporation into lipids, the ability of AR to induce p38 MAPK phosphorylation did not seem to have any direct impact on glucose metabolism in adipocytes from both fat depots.

There are at least three potential explanations for the reduction in fatty acid oxidation despite ALY688 inducing AMPK phosphorylation in isolated adipocytes: 1) it could be that enhanced glucose oxidation provided energy for the cells and caused a shift in fatty acid metabolism away from oxidation, even though AMPK phosphorylation was increased by ALY688. This could be possible because there is a relatively small number of mitochondria in white adipocytes, which normally limits the ability of these cells to elicit an elevated rate of fat oxidation[7,268]. However, because ALY688 consistently increased basal glucose oxidation in Epid and Sc Ing adipocytes, this must have led to a condition in which even fewer fatty acids were required and used for β-oxidation and energy production in these cells. Therefore, a shift in substrate utilization seems a plausible mechanism by which ALY688 led to the suppression of palmitate oxidation, despite

increased AMPK phosphorylation in adipocytes; 2) enhancement of fatty acid oxidation by adiponectin in skeletal muscle cells has been shown to depend on the sequential activation of AMPK and p38 MAPK, leading to induction of PPARα transcriptional activity and of its target oxidative genes (*e.g.* ACO and CPT1)[254]. In our studies, even though ALY688 caused AMPK activation in Epid and Sc Ing adipocytes, p38 MAPK phosphorylation was not affected by the compound. Thus, it could be that ALY688 promoted only partial activation of signaling events required for the enhancement of fatty acid oxidation in adipocytes. Under these conditions, glucose was clearly the preferred substrate for oxidation in these cells, which, as previously described, likely led to fewer fatty acids being diverted for oxidation; and finally, 3) it is also possible that fatty acid uptake was impaired under concentrations of ALY688 above 100 nM. This could be an AMPK-independent dose-dependent effect of the compound that suppressed specific adipocyte functions.

ALY688 did not affect basal rates of lipolysis either in Epid or Sc Ing adipocytes; however, isoproterenol-stimulated lipolysis increased in Epid adipocytes treated with ALY688. The mechanism underlying this depot-specific enhancement of beta-adrenergic-stimulated lipolysis by ALY688 seems to involve an increase in HSL phosphorylation. These findings differ from previous reports in which adiponectin suppressed lipolysis via inhibition of HSL phosphorylation in mouse adipocytes[259], and that a collagen domain-derived short adiponectin peptide promoted adipogenesis in 3T3L1 adipocytes[258]. These discrepancies could be attributed to methodological differences between studies. For instance, a lower lipolytic response was previously reported in Epid adipocytes from Adipoq$^{-/-}$ mice exposed to BRL37344 (a selective β3-adrenergic agonist), as well as in 3T3L1 adipocytes maintained in co-culture with FAO cells overexpressing full-length mouse adiponectin[259]. In this study, we performed acute (1h) incubations of primary rat adipocytes

in the presence of a peptide-based adiponectin mimetic and then stimulated the cells with isoproterenol, a non-specific β-adrenergic agent.

From our metabolic studies, it was clear that ALY688 caused tissue-specific and dose-dependent effects on glucose and fat metabolism in adipocytes. In general, Epid adipocytes elicited more pronounced responses to ALY688 than Sc Ing cells, particularly with respect to enhancing glucose oxidation and lipolysis while suppressing palmitate oxidation. Under these conditions, ALY688 could confer metabolic flexibility to the WAT and control WAT expansion, an effect that has been previously attributed to adiponectin[250,260]. This would allow for depot-specific exportation of fatty acids for utilization in peripheral tissues under adrenergic-stimulated conditions, while also enhancing glucose oxidation within the WAT. It could be that the tissue-specific responses resulted from distinct expressions of adiponectin receptors (AdipoR1 and AdipoR2) between Epid and Sc Ing cells. Therefore, we determined the expression profile of AdpoR1 and AdipoR2 in Epid and Sc Ing adipocytes, as well as in intact adipose tissue. It has been reported that it is AdipoR2 that carries out the effects of adiponectin in WAT[251]. Indeed, we found that in isolated Epid and Sc Ing adipocytes, AdipoR2 mRNA expression was approximately two-fold higher than AdipoR1. Also, Epid adipocytes displayed significantly higher AdipoR2 mRNA expression than Sc Ing adipocytes. Similarly, when analyzing whole fat tissue, we also detected much higher AdipoR2 mRNA expression in the Epid than in the Sc Ing fat depot. However, in the Sc Ing fat depot AdipoR1 mRNA expression was slightly higher than AdipoR2 mRNA expression, which could be attributed to the presence of a higher population of non-adipocyte cells in the Sc Ing than in the Epid fat depot. Because our experiments were conducted in isolated adipocytes, it is plausible that the more pronounced responses of Epid than Sc Inc

adipocytes to ALY688 resulted from a much lower expression of AdipoR2 in the latter than the former adipocytes.

In summary, we found that acute treatment with ALY688 increased AMPK phosphorylation in Epid and Sc Ing rat adipocytes; however, this was accompanied by suppression of fat oxidation and no alteration in basal and insulin-stimulated glucose uptake in these cells. Furthermore, ALY688 increased rates of glucose oxidation in Epid and Sc Ing adipocytes and enhanced adrenergic-stimulated lipolysis, although the latter effect was only detected in Epid adipocytes. These findings provide evidence that the AdipoR agonist ALY688 can regulate adiposity and affect glycemic control by altering substrate portioning in adipocytes in a fat depot-specific manner.

Chapter 10: Integrative Summary

The focus of this dissertation was to examine the effects of dietary macronutrient manipulation on WAT and BAT function, including its metabolic and endocrine roles. Importantly, AT does not act in isolation and induces metabolic and inflammatory effects in other tissues, including skeletal muscle and cardiac and pulmonary tissues, which was the focus of the second part of the thesis. To conclude, an alternative approach to modifying AT function was taken using an adiponectin mimetic. Together, these 5 studies provide insight into the effect of dietary and drug-mediated metabolic and RAS-related adaptations in AT, and potential effects in non-adipose tissues.

The objective of the second study was to assess the effect of dietary intervention on substrate metabolism and energy-expending mechanisms in WAT and BAT. Previous studies have shown the KD elevates whole-body energy expenditure[147], which has been linked to WAT browning[146,147] and elevated BAT sympathetic stimulation and UCP1 content[147]. However, to my knowledge, Project 1 is the first to investigate distinct functional mechanisms of energy expenditure in WAT and BAT. It was surprising to find that the KD elevated Sc Ing and Epid fat mass similar to the HFS diet. Earlier studies show that under isocaloric conditions, fat mass is unaltered or even increased in animals fed a KD, but this is typically compared to a chow-fed group[59,146]. Here, I show that the growth in fat mass is comparable to that of the obesogenic diet. Importantly, the HFS and KD diverged with respect to functional physiological mechanisms. Specifically, HFS-feeding impaired Iso-stimulated lipolysis and lipogenesis in the Epid and Sc Ing adipocytes, respectively. Conversely, KD-feeding preserved these functions and upregulated GyK content in both visceral and Sc WAT depots, providing the necessary machinery for TAG recycling. It is important to note that the KD did not promote browning of the WAT, which has

been proposed to be upregulated under these dietary conditions in previous studies[146,147]. However, the elevation in TAG recycling likely enhanced the ability of the WAT to handle the excess dietary FAs from the KD and preserved the ability of the visceral and Sc fat depots to respond to Iso and insulin-stimulation. Nevertheless, it is clear from our findings that WAT mass may not necessarily be the determinant for health. Rather, preservation of WAT function may be crucial for the prevention of disease[5].

Excess FAs may have travelled through the circulation and been oxidized by the BAT, which would have been supported by the KD-induced increase in uncoupled FA oxidative capacity, relative to the HFS diet. In line with this, GyK and BAT were significantly elevated in the BAT from KD-fed animals. Alternatively, EDL and Epit muscles from KD-fed animals displayed an elevation in palmitate oxidizing capacity, which may have been an alternative fate for AT or diet-derived FA.

The KD-mediated preservation of WAT and BAT function, as well as the activation of TAG recycling, could potentially be explained by the upregulation of the classical RAS arm in these tissue depots. It is understood that inflammation may exacerbate adipocyte dysfunction under conditions of obesity[5,44], and that the pro-inflammatory state of the AT could be mediated by an upregulation in the classical arm of the RAS[107]. In this context, a shift towards the counterregulatory ACE2/Ang(1,7)/MasR may suppress inflammation and support energy metabolism in brown and white fat[90]. As shown in study 3, KD-feeding significantly attenuated ACE1 protein content in Sc Ing and Epid fat depots, shifting the RAS profile away from the classical arm. Interestingly, the HFS diet also suppressed ACE1 content and both the HFS and KD lowered ACE2 protein levels in the Sc Ing fat, suggesting that RAS effects in this depot may be more attributable to the Ang receptors. Indeed, in the Sc Ing fat depot, the HFS diet elevated AT_1R

content and did not alter the counterregulatory Ang receptors AT_2R and MasR, whereas AT_1R did not increase and AT_2R was robustly upregulated with a KD in this fat pad. Similarly, KD-feeding also elevated AT_2R in the Epid fat. In BAT, only AT_1R levels were altered with dietary intervention, where the HFS, but not the KD, significantly increased the content of this protein. The importance of AT_1R in the brown fat is relatively higher, given its elevated abundance in this tissue compared to the subcutaneous and visceral fat. Similar to Sc Ing and Epid fat, the KD also did not increase AT_1R levels in BAT. Thus, the HFS diet promoted a shift to the ACE1/Ang-II/AT_1R arm of the RAS, whereas the KD did not influence RAS profile in the BAT. Regardless of depot-specific differences in the alterations of RAS proteins with diet, the HFS diet consistently shifts the RAS profile of WAT and BAT towards the classical arm of the RAS and the KD upregulates the counterregulatory arm of the RAS. The KD-mediated alteration in AT RAS could have driven the upregulation of the energy-dissipating machinery in WAT and BAT assessed in Study 2. Existing work has shown that exercise and pharmacological agents effect RAS protein expression in WAT[105]. However, to my knowledge, this is the first study to show KD-mediated alterations in RAS protein profile in visceral and subcutaneous WAT and BAT, highlighting the importance and novelty of this work in the context of AT metabolism and endocrine functions.

AT dysfunction underlies systemic, low-grade inflammation, which could induce a compensatory RAS shift in non-adipose tissues to mitigate these effects. In the lungs, this is characterized by an elevation in ACE2[113]. However, this protein acts as the receptor for SARS-CoV-2, which could enhance the susceptibility of obese individuals to infection. Moreover, the existing inflammatory environment could prime the organism for an exacerbated inflammatory response that could induce severe organ damage[116]. Thus, the application of an intervention that suppresses the activation of the classical RAS arm poses a potential protective effect against

infectivity and severity of infection. I conducted this research at the height of the pandemic where not much was known regarding COVID-19. However, what was well established was that obesity and diabetes increase pulmonary ACE2 levels and may underlie the increased risk of infection in these clinical populations[125,229]. Given the distinct impacts of the HFS and KD in AT RAS, we asked a question that had not been previously investigated: how does the KD influence RAS proteins in the lungs and heart? The findings from this study could provide novel information into how manipulation of dietary macronutrient composition could potentially influence disease susceptibility and severity. In our study, we observed that the KD significantly reduced ACE1 content in the lung, which is a major contributor to systemic Ang-II levels[107]. This likely led to an attenuation in ACE2, where the demand for a counterregulatory mechanism to ACE1 was decreased. As expected, the obesogenic diet increased ACE2 and TMPRSS2 contents in the lungs, which could potentially increase the susceptibility to infection with SARS-CoV-2. ACE1 is far more abundant in the lung than the heart. Thus, the KD-induced attenuation in protein likely had a major impact on the RAS profile of this tissue, supporting the decrease in inflammatory markers *tlr4* and *il6r*. Conversely, although the HFS diet did not increase ACE2 levels in the heart, this organ is abundant in this RAS protein. In this context, the increase in viral entry potential in the lung could support viral load and spillover into the circulation, eventually leading to SARS-CoV-2 reaching the heart and entering through the highly available ACE2. Instead of altering ACEs, the HFS diet, but not the KD, upregulated protein levels of AT_1R and AT_2R. The upregulation of AT_2R may have served as a compensatory mechanism for the enhanced levels of AT_1R and could explain the lack of inflammation in cardiac tissue.

In addition to the lungs and heart, the AT is also crucial for skeletal muscle function due to its role in energy mobilization. As previously mentioned, the FA released from the AT could

potentially be oxidized by EDL and Epit muscles, particularly under conditions of KD-feeding where the capacities of these muscles to burn fat were enhanced. Additionally, the FFA released from the WAT supported ketone body production in the liver, which provided energy substrate for the Sol muscle that demonstrated an enhanced capacity to oxidize ketones. Regardless of these fiber-type specific differences in metabolic adaptations to the KD, all muscles displayed an ability to metabolize glucose in response to insulin. This was supported by the increased in glycogen synthesis and lactate production, indicating two major pathways whereby glucose could be diverted in skeletal muscle. This was strongly contrasted by the lack of response to insulin in the muscles of HFS rats. Glucose oxidation was not different between the HFS and KD, which can be explained in the KD group by the shift toward fat and ketones as metabolic substrates. Previous studies have assessed the effects of the KD on mitochondrial mass[164] and markers of mitochondrial biogenesis[165] in muscle. Moreover, recent works have investigated KD-induced alterations in the gene expression of proteins involved in fat and ketone metabolism[166], or substrate partitioning in individual skeletal muscles[167]. To my knowledge, this was the first study to conduct a comprehensive analysis of substrate metabolism in muscles with distinct fiber-type compositions under conditions of KD-feeding, including functional measurements of glucose and fat metabolism. The findings from my study contribute to our current understanding of skeletal muscle metabolism and show that the KD shifts substrate preference to FA and ketones in a fiber-type specific manner but preserved the abilities of all muscles to metabolize glucose. Importantly, the study highlights the distinct responses induced by alterations in dietary macronutrient composition, where two diets that are high in fat, but differ in carbohydrate content differently impact metabolic flexibility and their potential regulation of whole-body glycemic control.

In addition to dietary intervention, we applied a pharmacological approach to enhance AT function. Specifically, we used ALY688, an adiponectin mimetic and observed its effects on glucose and fat metabolism in visceral and Sc WAT. This was the first study to assess the effects of this compound on fat and glucose metabolism in adipocytes, and even the effect of an adiponectin mimetic, in general, on fat oxidation in adipocytes. In this context, the findings from this study could contribute to the existing body of knowledge on the potential effects of adiponectin in AT. As expected, treatment with ALY688 activated AMPK and increased ACC phosphorylation in adipocytes. However, ALY688 did not significantly alter basal or Ins-stimulated glucose uptake or glucose incorporation into lipids. Instead, it increased glucose oxidation in Epid and Sc Ing adipocytes and enhanced lipolytic capacity in the former. The shift to glucose oxidation likely attenuated the reliance on fat for energy production in these cells, driving the decrease in palmitate oxidation with ALY688 in cells from both fat depots. Nevertheless, this adaptation could enhance the capacity for glucose disposal in the WAT, supporting whole-body glycemic control in the organism.

Together, these works demonstrate the potential of the KD in the regulation of AT function and implications this has for non-adipose tissues, including skeletal muscle, lung and cardiac tissues. Moreover, treatment with an adiponectin mimetic can also have potential for the regulation of AT function. These interventions carry great potential for the management of obesity and its related metabolic disorders and suggest that KD could potentially be protective against infection and/or the ensuing inflammatory response.

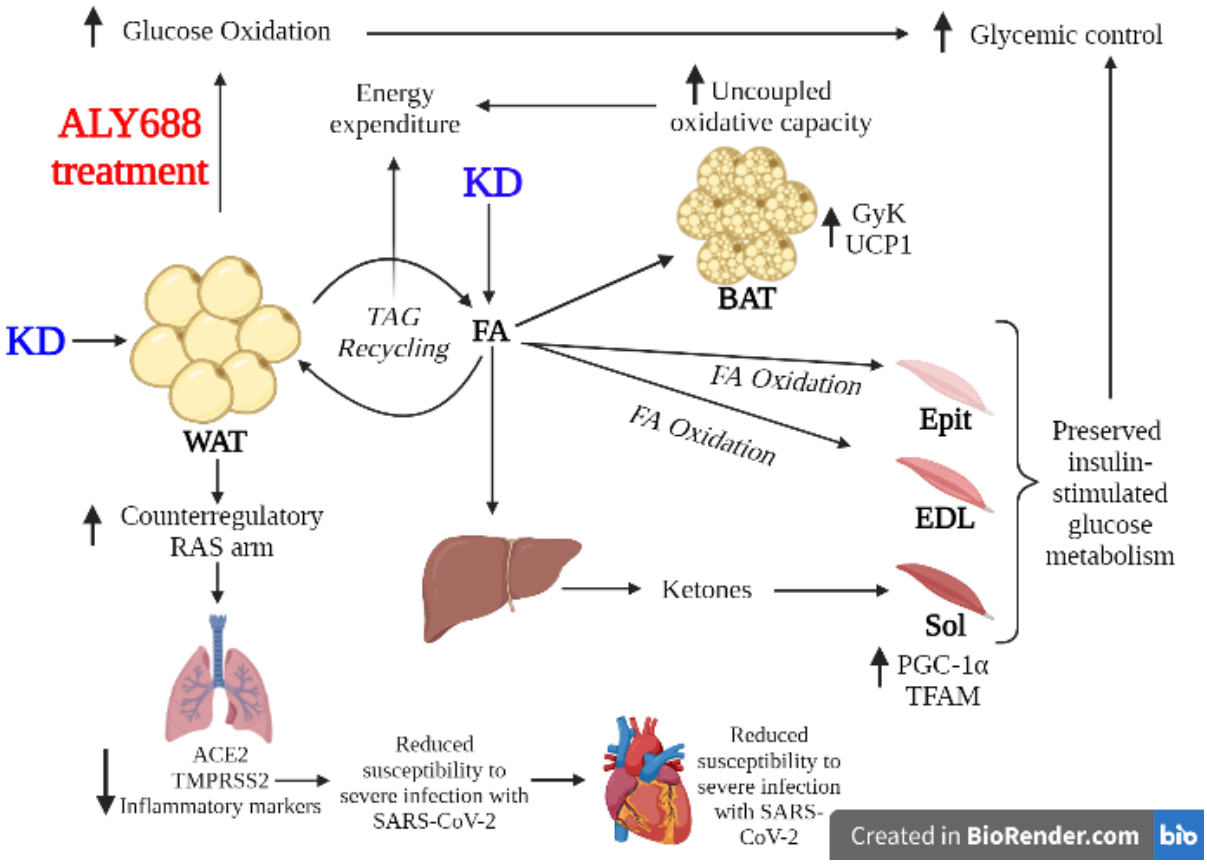

Figure 47: Schematic illustration of integrated summary. The consumption of a KD significantly enhances the TAG recycling capacity of the WAT. Excess FA from the diet, or FA that escape recycling, are oxidized in the BAT via the KD-induced elevation in uncoupled oxidative capacity, driven by the increase in UCP1 and GyK contents in this tissue. Together, the elevation in TAG recycling and uncoupled oxidation potentially contribute to energy expenditure in KD-fed rats. Alternatively, FA are oxidized in the liver, where they are diverted to ketone body synthesis, or they are oxidized in the skeletal muscles. Interestingly, EDL and Epit muscles demonstrated an elevation in palmitate oxidation, relative to the HFS animals, whereas the Sol muscle did not, despite PGC-1α and TFAM being elevated in this muscle, exclusively. Instead, KD-feeding elevated the ketolytic capacity of this tissue, suggesting this substrate was preferred in the Sol for energy production. Regardless of fiber-type composition, all muscles displayed an ability to metabolize glucose in response to insulin, which could potentially promote whole-body glycemic control. KD-feeding also caused a shift to the counterregulatory RAS arm in the WAT, which likely underlies the suppression in AT-derived systemic inflammation, potentially leading to an attenuation in pulmonary ACE2, a counterregulatory RAS protein that is also the receptor for SARS-CoV-2. In line with this, an attenuation in inflammatory gene expression was observed in this tissue. Moreover, TMPRSS2 content was decreased. Together, these effects could lower the severity of infection in this tissue and, given that the lungs are the primary entry point of SARS-CoV-2 in the body, may also contribute to lower viral infectivity in the heart. Finally, treating white adipocytes with the adiponectin mimetic ALY688 promoted glucose oxidation, which also has potential for the regulation of whole-body glucose homeostasis.

Chapter 11: Limitations

It is important to acknowledge that some limitations do exist in our studies. In Studies 1 and 2, the housing temperature was approximately 23 °C, which is below thermoneutrality for rats. This could have inherently activated thermogenic mechanisms in the animals and masked the effects of the diets. This is supported by Weber et al., who demonstrated that KD-feeding at thermoneutrality yielded a reduction in energy expenditure relative to KD mice at room temperature[269]. Although the relative difference in energy expenditure and weight reduction between the HFS and KD-fed mice was maintained regardless of housing temperature, it is apparent that energy expenditure decreased significantly with temperature within diet groups[269]. This indicates housing temperature could be impacting energy dissipating mechanisms in AT and is a potential limitation in our first two studies.

In study 3, RAS proteins were measured in AT depots under different dietary conditions. As mentioned in the manuscript, one potential limitation is that we were not able to observe alterations in ERK phosphorylation, an indicator of Ang signaling. This limitation could be attributed to the model we used, where *in vivo* assessments of the effect of a single factor are complicated by the complex hormonal milieu that exists in an organism. Moreover, we are assuming that the KD-induced shift in RAS proteins may contribute to the anti-inflammatory effects of the diet in AT. However, under the present study conditions, this is merely an association, and a causal link cannot be established without the performance of additional experiments.

Study 4 highlights the effects of dietary intervention on SARS-CoV-2 entry proteins in lung and cardiac tissue. Importantly, despite suggesting the KD as a potential intervention for the prevention against severe infection with COVID-19, this was never directly measured.

Additionally, it is proposed that the elevation in cardiac AT_2R levels exerted a protective effect against inflammation in the cardiac tissue. This is speculative and warrants further investigation.

Study 5 demonstrates fiber-type specific differences in the effects of the KD on glucose, fat and ketone metabolism in skeletal muscles. This study, however, was conducted in male rats. In this context, extending the findings to females is limited, especially since it is known sexual dimorphisms exist in muscle physiology[270]. An additional limitation was that fiber-type compositions were not assessed following the feeding of the diets. A previous study demonstrated that KD feeding caused a shift in EDL muscle fibers to make the muscle more oxidative[170]. This could potentially underlie the enhanced FA oxidative capacity in EDL, as well as the Epit muscle in our study.

Finally, study 6 was one of the first investigations into the effects of ALY688. To our knowledge, we were the first group to study ALY688 treatment in primary adipocytes. The results of our paper are promising, but limitations exist. First, the observed effects were under acute treatment with the compound. It is plausible that chronic exposure to ALY688 could impact gene expression and alter glucose and fat metabolism, accordingly. Secondly, the adipocytes used in our experiments were isolated from the fat pads of younger animals, which could mask the beneficial effects of this drug. In this context, it is important to test the effects of this drug on the AT from diabetic or obese animals to determine whether ALY688 treatment could enhance glucose and fat metabolism in an organism with metabolic dysfunction.

In conclusion, these limitations give rise to several future directions that will serve to strengthen our understanding of AT metabolism and RAS function, as well as muscle and lung physiology under conditions of KD.

Chapter 12: Future Directions

In consideration of the outlined limitations, as well as existing gaps in the literature, future directions in each of the studies exist. In our first study, we observed a diet-induced suppression in uncoupled oxidative capacity in the brown adipocytes of HFS-fed rats. However, given the importance of the localization of mitochondria in brown adipocytes for the determination of functional outcome[71] (see Chapter 2), it would be of interest to analyze subfractions of brown adipocyte mitochondria to determine the effect of diet on the relative distributions of lipid-droplet bound and cytoplasmic mitochondria.

In Study 2 (Chapter 5), the demonstrated elevation in TAG recycling in WAT is a thermogenic mechanism that is also induced by cold exposure[7]. To our knowledge, however, the combined effects of the KD with cold exposure have not been studied. In this context, a future area of research could be to house animals at 4 °C and feed them a KD, to determine whether this combined approach would additively enhance energy expenditure in this tissue, and potentially support a loss in fat mass. Moreover, recent work shows that KE supplementation in animals fed an obesogenic diet attenuates WAT mass[148]. This begs the question whether KE activates energy expending mechanisms in WAT and BAT, similar to the KD. To investigate this, animals could receive KE in drinking water or the KE could be administered by gavage over a time course, to account for potential time-dependent effects of this treatment. Following the KE supplementation period, AT would be extracted for adipocyte isolation, and thermogenic mechanisms within WAT and BAT could be assessed.

In study 3, the effects of dietary intervention on WAT and BAT RAS components provides novel evidence of a KD-induced shift towards the counterregulatory arm in these tissues. However, whether this shift underlies the anti-inflammatory effects of the diet in WAT[146], as well as the

enhanced uncoupled oxidative capacity of BAT remains to be elucidated. Future work can assess these effects be isolating adipocytes from the same HFS and KD fed animals, treating the adipocytes with Ang-II and measuring the expression of inflammatory cytokines. Moreover, insulin-stimulated lipogenesis as well as BAT activation can be assessed by treating WAT and BAT adipocytes from HFS and KD-fed animals with Ang-II to assess whether the diet-induced shifts in RAS profiles could underlie alterations in metabolic function. These approaches will assist in the isolation of the RAS-mediated effects on the observed outcomes with the KD.

When study 4 was submitted for publication, the application of a KD for the assessment of its effects on COVID-19 infection severity had not yet been investigated. In the same year this study was published, Ryu et al. published their article detailing the anti-inflammatory and preventative effects of the KD in mice inoculated with CoV[145]. To follow up on these studies, it is of interest to confirm whether these effects could be attributed to the alteration in RAS proteins in the lung. In this context, extracting and isolating the pulmonary cells and incubating them with CoV, in the absence or presence of an ACE2 antibody could help identify whether the reduced severity of infection is due to the anti-inflammatory effect of the diet or whether it can also limit viral entry through altering the contents of this protein. In this context, the findings from this study could establish a stronger link between KD-feeding and prevention against severe COVID-19 infection.

As mentioned in Chapter 11 (Limitations) the analysis of the effects of dietary intervention on glucose, fat and ketone metabolism in oxidative and glycolytic muscles was performed only in males. Our lab has previously published studies on skeletal muscle insulin resistance in both males and females. In this context, the effects of the KD on substrate metabolism in muscles with distinct fiber-type compositions is something that is yet to be studied in female rats and is a future direction

to follow up our existing work. To study this, we could similarly feed female rats a KD for 16 weeks, extract Sol, EDL and Epit muscles and assess fat, ketone and glucose metabolism in these tissues. Furthermore, it would strengthen our study to simultaneously feed male rats and have four groups: HFS-male, HFS-female, KD-male, KD-female. This approach would allow for a direct comparison of diet and sex effects on muscle metabolism. Also, our KD studies use a relatively strict diet in terms of carbohydrate restriction. In future studies, we plan on titrating increasing amount of carbohydrate into the KD, bringing down the protein content, albeit still within a normal range for protein intake in rodents. For instance, having a KD with 5, 15 and 80% kcal from carbohydrate, protein, and fat, respectively. This will further our understanding of the effects of macronutrient composition on metabolic outcomes in AT.

Finally, future directions for the ALY688 studies include treating rodents with the drug, extracting the adipocytes and assessing glucose uptake, lipogenic capacity, fat oxidation and AMPK signaling. This would provide information of the *in vivo* effects of this diet on AT metabolism and would also assess the effects of this compound with longer term treatment. Moreover, it would be valuable to perform *in vivo* tests of whole-body glycemic control and insulin resistance, including glucose and insulin tolerance tests. This will help link the effects of the drug on AT to its potential applications in the regulation of systemic glucose homeostasis. In addition, the effectiveness of ALY688 as an adiponectin mimetic could be assessed by treating HFS-fed animals with this drug and assessing adipocyte responsiveness to insulin, inflammation, as well as other measures of metabolic function.

References

1. Apovian CM. Obesity: definition, comorbidities, causes, and burden. *Am J Manag Care*. 2016;22(7):s176-s185.

2. Hales CM, Carroll MD, Fryar CD, Ogden CL. Prevalence of Obesity and Severe Obesity Among Adults : United States, 2017-2018. *NCHS Data Brief*. 2020;(360):2017-2018.

3. Lytvyak E, Straube S, Modi R, Lee KK. Trends in obesity across Canada from 2005 to 2018: a consecutive cross-sectional population-based study. *C open*. 2022;10(2):E439-E449. doi:10.9778/cmajo.20210205

4. Sepa-Kishi DM, Ceddia RB. Exercise-Mediated Effects on White and Brown Adipose Tissue Plasticity and Metabolism. *Exerc Sport Sci Rev*. 2016;44(1):37-44. doi:10.1249/JES.0000000000000068

5. Roden M, Shulman GI. The integrative biology of type 2 diabetes. *Nature*. 2019;576:51-60. doi:10.1038/s41586-019-1797-8

6. Cinti S. Adipose Organ Development and Remodeling. *Compr Physiol*. 2018;8(4):1357-1431. doi:10.1002/cphy.c170042

7. Sepa-Kishi DM, Jani S, Da Eira D, Ceddia RB. Cold acclimation enhances UCP1 content, lipolysis, and triacylglycerol resynthesis, but not mitochondrial uncoupling and fat oxidation, in rat white adipocytes. *Am J Physiol - Cell Physiol*. 2019;316(3):C365-C376. doi:10.1152/ajpcell.00122.2018

8. Da Eira D, Jani S, Ceddia RB. An obesogenic diet impairs uncoupled substrate oxidation and promotes whitening of the brown adipose tissue in rats. *J Physiol*. 2023;601(1):69-82. doi:10.1113/JP283721

9. Da Eira D, Jani S, Stefanovic M, Ceddia RB. Obesogenic versus ketogenic diets in the regulation of the renin–angiotensin system in rat white and brown adipose tissues. *Nutrition*. 2023;105:111862. doi:10.1016/j.nut.2022.111862

10. van der Heijden RA, Sheedfar F, Morrison MC, et al. High-fat diet induced obesity primes inflammation in adipose tissue prior to liver in C57BL/6j mice. *Aging (Albany NY)*. 2015;7(4):256-268. doi:10.18632/aging.100738

11. Jani S, Da Eira D, Stefanovic M, Ceddia RB. The ketogenic diet prevents steatosis and insulin resistance by reducing lipogenesis, diacylglycerol accumulation and protein kinase C activity in male rat liver. *J Physiol*. 2022;600(18):4137-4151. doi:10.1113/JP283552

12. Jani S, Da Eira D, Hadday I, et al. Distinct mechanisms involving diacylglycerol, ceramides, and inflammation underlie insulin resistance in oxidative and glycolytic muscles from high fat-fed rats. *Sci Rep*. 2021;11(1). doi:10.1038/s41598-021-98819-7

13. Johnstone AM, Horgan GW, Murison SD, Bremner DM, Lobley GE. Effects of a high-protein ketogenic diet on hunger, appetite, and weight loss in obese men feeding ad libitum. *Am J Clin Nutr*. 2008;87(1):44-55. doi:10.1093/ajcn/87.1.44

14. Yancy WS, Olsen MK, Guyton JR, Bakst RP, Westman EC. A low-carbohydrate, ketogenic diet versus a low-fat diet to treat obesity and hyperlipidemia. *Ann Intern Med*.

2004;13(8):18-19. doi:10.1016/j.accreview.2004.07.104

15. Walton CM, Perry K, Hart RH, Berry SL, Bikman BT. Improvement in Glycemic and Lipid Profiles in Type 2 Diabetics with a 90-Day Ketogenic Diet. *J Diabetes Res*. Published online 2019. doi:10.1155/2019/8681959

16. Okada-Iwabu M, Yamauchi T, Iwabu M, et al. A small-molecule AdipoR agonist for type 2 diabetes and short life in obesity. *Nature*. 2013;503(7477):493-499. doi:10.1038/nature12656

17. Kadowaki T, Yamauchi T. Adiponectin and Adiponectin Receptors. *Endocr Rev*. 2005;26(3):439-451. doi:10.1210/er.2005-0005

18. Dimitriadis G, Mitron P, Lambadiari V, Maratou E, Raptis SA. Insulin effects in muscle and adipose tissue. *Diabetes Res Clin Pract*. 2011;93S:52-59. doi:10.1016/S0168-8227(11)70014-6

19. Cinti S. Transdifferentiation properties of adipocytes in the adipose organ. *Am J Physiol - Endocrinol Metab*. 2009;297(5). doi:10.1152/ajpendo.00183.2009

20. Sepa-Kishi DM, Ceddia RB. Circulating fibroblast growth factor 21 is reduced, whereas its production is increased in a fat depot-specific manner in cold-acclimated rats. *Adipocyte*. 2018;7(4):238-247. doi:10.1080/21623945.2018.1504591

21. Shen W, Wang Z, Punyanita M, et al. Adipose Tissue Quantification by Imaging Methods: A Proposed Classification. *Obes Res*. 2003;11(1):5-16.

22. Sakers A, De Siqueira MK, Seale P, Villanueva CJ. Adipose-tissue plasticity in health and disease. *Cell*. 2022;185(3):419-446. doi:10.1016/j.cell.2021.12.016

23. Cohen P, Spiegelman BM, Drubin DG. Cell biology of fat storage. *Mol Biol Cell*. 2016;27(16):2523-2527. doi:10.1091/mbc.E15-10-0749

24. Seale P, Bryan Bjork, Yang W, et al. PRDM16 Controls a Brown Fat/Skeletal Muscle Switch. *Nature*. 2008;454(7207):961-967. doi:10.1038/nature07182.PRDM16

25. Tontonoz P, Hu E, Spiegelman BM. Stimulation of adipogenesis in fibroblasts by PPARγ2, a lipid-activated transcription factor. *Cell*. 1994;79(7):1147-1156. doi:10.1016/0092-8674(94)90006-X

26. Lefterova MI, Zhang Y, Steger DJ, et al. PPARγ and C/EBP factors orchestrate adipocyte biology via adjacent binding on a genome-wide scale. *Genes Dev*. 2008;22(21):2941-2952. doi:10.1101/gad.1709008

27. Ghaben AL, Scherer PE. Adipogenesis and metabolic health. *Nat Rev Mol Cell Biol*. 2019;20(4):242-258. doi:10.1038/s41580-018-0093-z

28. Czech MP, Tencerova M, Pedersen DJ, Aouadi M. Insulin signalling mechanisms for triacylglycerol storage. *Diabetologia*. 2013;56(5):949-964. doi:10.1007/s00125-013-2869-1

29. Morigny P, Boucher J, Arner P, Langin D. Lipid and glucose metabolism in white adipocytes: pathways, dysfunction and therapeutics. *Nat Rev Endocrinol*. 2021;17(5):276-

295. doi:10.1038/s41574-021-00471-8

30. Santoro A, McGraw T, Kahn B. Insulin action in adipocytes, adipose remodeling, and systemic effects. *Cell Metab*. 2019;33(80):678-687. doi:10.1016/j.cmet.2021.03.019.Insulin

31. Tokarz VL, MacDonald PE, Klip A. The cell biology of systemic insulin function. *J Cell Biol*. 2018;217(7):2273-2289. doi:10.1083/jcb.201802095

32. Bhattacharya S, Dey D, Roy S. Molecular mechanism of insulin resistance. *J Biosci*. 2007;32(2):405-413.

33. Buzelle SL, Przygodda F, Rossi-Valentim R, et al. Activation of adipose tissue glycerokinase contributes to increased white adipose tissue mass in mice fed a high-fat diet. *Endocrine*. 2020;69(1):79-91. doi:10.1007/s12020-020-02288-3

34. Bertin R, Andriamihaja M, Portet R. Glycerokinase activity in brown and white adipose tissues of cold-adapted obese Zucker rats. *Biochimie*. 1984;66(7-8):569-572. doi:10.1016/0300-9084(84)90152-4

35. Rahib L, MacLennan NK, Horvath S, Liao JC, Dipple KM. Glycerol kinase deficiency alters expression of genes involved in lipid metabolism, carbohydrate metabolism, and insulin signaling. *Eur J Hum Genet*. 2007;15(6):646-657. doi:10.1038/sj.ejhg.5201801

36. Czech MP, Tencerova M, Pedersen DJ, Aouadi M. Insulin signalling mechanisms for triacylglycerol storage. *Diabetologia*. 2013;56(5):949-964. doi:10.1007/s00125-013-2869-1.Insulin

37. Tansey JT, Sztalryd C, Hlavin EM, Kimmel AR, Londos C. The central role of perilipin A in lipid metabolism and adipocyte lipolysis. *IUBMB Life*. 2004;56(7):379-385. doi:10.1080/15216540400009968

38. Cannon B, Nedergaard J. Brown Adipose Tissue: Function and Physiological Significance. *Physiol Rev*. 2004;84(1):277-359. doi:10.1152/physrev.00015.2003

39. Valentine JM, Ahmadian M, Keinan O, et al. β3-Adrenergic receptor downregulation leads to adipocyte catecholamine resistance in obesity. *J Clin Invest*. 2022;132(2):1-16. doi:10.1172/JCI153357

40. Carmen GY, Víctor SM. Signalling mechanisms regulating lipolysis. *Cell Signal*. 2006;18(4):401-408. doi:10.1016/j.cellsig.2005.08.009

41. Sztalryd C, Xu G, Dorward H, et al. Perilipin A is essential for the translocation of hormone-sensitive lipase during lipolytic activation. *J Cell Biol*. 2003;161(6):1093-1103. doi:10.1083/jcb.200210169

42. Gaidhu MP, Anthony NM, Patel P, Hawke TJ, Ceddia RB. Dysregulation of lipolysis and lipid metabolism in visceral and subcutaneous adipocytes by high-fat diet: Role of ATGL, HSL, and AMPK. *Am J Physiol - Cell Physiol*. 2010;298(4):961-971. doi:10.1152/ajpcell.00547.2009

43. Gaidhu MP, Anthony NM, Patel P, Hawke TJ, Ceddia RB. Dysregulation of lipolysis and

lipid metabolism in visceral and subcutaneous adipocytes by high-fat diet : role of ATGL , HSL , and AMPK. *Am J Physiol Cell Physiol*. 2010;298(4):961-971. doi:10.1152/ajpcell.00547.2009.

44. Hotamisligil GS, Murray DL, Choy LN, Spiegelman BM. Tumor necrosis factor a inhibits signaling from the insulin receptor. *Proc Nadl Acad Sci USA*. 1994;91(May):4854-4858. https://www.ncbi.nlm.nih.gov/pmc/articles/PMC43887/pdf/pnas01133-0254.pdf

45. Guo F, Xu S, Zhu Y, et al. PPARgamma Transcription Deficiency Exacerbates High-Fat Diet-Induced Adipocyte Hypertrophy and Insulin Resistance in Mice. *Front Pharmacol*. 2020;11:1-12. doi:10.3389/fphar.2020.01285

46. U Din M, Saari T, Raiko J, et al. Postprandial Oxidative Metabolism of Human Brown Fat Indicates Thermogenesis. *Cell Metab*. 2018;28(2):207-216.e3. doi:10.1016/j.cmet.2018.05.020

47. Hibi M, Oishi S, Matsushita M, et al. Brown adipose tissue is involved in diet-induced thermogenesis and whole-body fat utilization in healthy humans. *Int J Obes*. 2016;40(11):1655-1661. doi:10.1038/ijo.2016.124

48. McKie GL, Medak KD, Knuth CM, et al. Housing temperature affects the acute and chronic metabolic adaptations to exercise in mice. *J Physiol*. 2019;597(17):4581-4600. doi:10.1113/JP278221

49. Adeva-Andany MM, Carneiro-Freire N, Seco-Filgueira M, Fernández-Fernández C, Mouriño-Bayolo D. Mitochondrial β-oxidation of saturated fatty acids in humans. *Mitochondrion*. 2019;46:73-90. doi:10.1016/j.mito.2018.02.009

50. Akram M. Citric Acid Cycle and Role of its Intermediates in Metabolism. *Cell Biochem Biophys*. 2014;68(3):475-478. doi:10.1007/s12013-013-9750-1

51. Owen OE, Kalhan SC, Hanson RW. The key role of anaplerosis and cataplerosis for citric acid cycle function. *J Biol Chem*. 2002;277(34):30409-30412. doi:10.1074/jbc.R200006200

52. Nolfi-Donegan D, Braganza A, Shiva S. Mitochondrial electron transport chain: Oxidative phosphorylation, oxidant production, and methods of measurement. *Redox Biol*. 2020;37:101674. doi:10.1016/j.redox.2020.101674

53. Fuller GG, Kim JK. Compartmentalization and metabolic regulation of glycolysis. *J Cell Sci*. 2021;134(20). doi:10.1242/jcs.258469

54. Akram M. Mini-review on glycolysis and cancer. *J Cancer Educ*. 2013;28(3):454-457. doi:10.1007/s13187-013-0486-9

55. Gray LR, Tompkins SC, Taylor EB. Regulation of pyruvate metabolism and human disease. *Cell Mol Life Sci*. 2014;71(14):2577-2604. doi:10.1007/s00018-013-1539-2

56. Hue L, Taegtmeyer H. The Randle cycle revisited: A new head for an old hat. *Am J Physiol - Endocrinol Metab*. 2009;297(3):578-591. doi:10.1152/ajpendo.00093.2009

57. Kelley DE, Mokan M, Simoneau JA, Mandarino LJ. Interaction between glucose and free

fatty acid metabolism in human skeletal muscle. *J Clin Invest*. 1993;92(1):91-98. doi:10.1172/JCI116603

58. Randle PJ, Garland PB, Hales CN, Newsholme EA. The Glucose Fatty-Acid Cycle Its Role in Insulin Sensitivity and the Metabolic Disturbances of Diabetes Mellitus. *Lancet*. 1963;281(7285):785-789. doi:10.1016/S0140-6736(63)91500-9

59. Huang TY, Linden MA, Fuller SE, et al. Combined effects of a ketogenic diet and exercise training alter mitochondrial and peroxisomal substrate oxidative capacity in skeletal muscle. *Am J Physiol - Endocrinol Metab*. 2021;320(6):E1053-E1067. doi:10.1152/AJPENDO.00410.2020

60. Webster CC, Van Boom KM, Armino N, et al. Reduced glucose tolerance and skeletal muscle GLUT4 and IRS1 content in cyclists habituated to a long-term low-carbohydrate, high-fat diet. *Int J Sport Nutr Exerc Metab*. 2020;30(3):210-217. doi:10.1123/ijsnem.2019-0359

61. Sherrier M, Li H. The impact of keto-adaptation on exercise performance and the role of metabolic-regulating cytokines. *Am J Clin Nutr*. 2019;110(3):562-573. doi:10.1093/ajcn/nqz145

62. McGarry JD, Mannaerts GP, Foster DW. A possible role for malonyl CoA in the regulation of hepatic fatty acid oxidation and ketogenesis. *J Clin Invest*. 1977;60(1):265-270. doi:10.1172/JCI108764

63. Ronnett G V., Kleman AM, Kim EK, Landree LE, Tu Y. Fatty acid metabolism, the central nervous system, and feeding. *Obesity (Silver Spring)*. 2006;14 Suppl 5. doi:10.1038/oby.2006.309

64. Fediuc S, Gaidhu MP, Ceddia RB. Regulation of AMP-activated protein kinase and acetyl-CoA carboxylase phosphorylation by palmitate in skeletal muscle cells. *J Lipid Res*. 2006;47(2):412-420. doi:10.1194/jlr.M500438-JLR200

65. Fang K, Wu F, Chen G, et al. Diosgenin ameliorates palmitic acid-induced lipid accumulation via AMPK/ACC/CPT-1A and SREBP-1c/FAS signaling pathways in LO2 cells. *BMC Complement Altern Med*. 2019;19(1):255. doi:10.1186/s12906-019-2671-9

66. Fischer AW, Schlein C, Cannon B, Heeren J, Nedergaard J. Intact innervation is essential for diet-induced recruitment of brown adipose tissue. *Am J Physiol Metab*. 2019;316(3):E487-E503.

67. Klingenberg M. UCP1 - A sophisticated energy valve. *Biochimie*. 2017;134:19-27. doi:10.1016/j.biochi.2016.10.012

68. Chaudhry A, Granneman JG. Differential regulation of functional responses by β-adrenergic receptor subtypes in brown adipocytes. *Am J Physiol - Regul Integr Comp Physiol*. 1999;277(1 46-1):147-153. doi:10.1152/ajpregu.1999.277.1.r147

69. Wang Z, Ning T, Song A, Rutter J, Wang QA, Jiang L. Chronic cold exposure enhances glucose oxidation in brown adipose tissue. *EMBO Rep*. 2020;21(11):1-13. doi:10.15252/embr.202050085

70. Vallerand AL, Lupien J, Bukowiecki LJ. Cold exposure reverses the diabetogenic effects of high-fat feeding. *Diabetes*. 1986;35(3):329-334. doi:10.2337/diab.35.3.329

71. Benador IY, Veliova M, Mahdaviani K, et al. Mitochondria Bound to Lipid Droplets Have Unique Bioenergetics, Composition, and Dynamics that Support Lipid Droplet Expansion. *Cell Metab*. 2018;27(4):869-885.e6. doi:10.1016/j.cmet.2018.03.003

72. van Marken Lichtenbelt WD, Vanhommerig JW, Smulders NM, et al. Cold-Activated Brown Adipose Tissue in Healthy Men. *N Engl J Med*. 2009;360(15):1500-1508. doi:10.1056/nejmoa0808718

73. Blondin DP, Labbé SM, Tingelstad HC, et al. Increased brown adipose tissue oxidative capacity in cold-acclimated humans. *J Clin Endocrinol Metab*. 2014;99(3):438-446. doi:10.1210/jc.2013-3901

74. Nedergaard J, Bengtsson T, Cannon B. Unexpected evidence for active brown adipose tissue in adult humans. *Am J Physiol - Endocrinol Metab*. 2007;293(2):444-452. doi:10.1152/ajpendo.00691.2006

75. Leitner BP, Huang S, Brychta RJ, et al. Mapping of human brown adipose tissue in lean and obese young men. *Proc Natl Acad Sci*. 2017;114(32):8649-8654.

76. Aita S, Matsushita M, Yoneshiro T, et al. Brown fat-associated postprandial thermogenesis in humans: Different effects of isocaloric meals rich in carbohydrate, fat, and protein. *Front Nutr*. 2022;9(October):1-9. doi:10.3389/fnut.2022.1040444

77. So M, Gaidhu MP, Maghdoori B, Ceddia RB. Analysis of time-dependent adaptations in whole-body energy balance in obesity induced by high-fat diet in rats. *Lipids Health Dis*. 2011;10(99). doi:10.1186/1476-511X-10-99

78. Jiang L, Su H, Wu X, et al. Leptin receptor-expressing neuron Sh2b1 supports sympathetic nervous system and protects against obesity and metabolic disease. *Nat Commun*. 2020;11(1):1-13. doi:10.1038/s41467-020-15328-3

79. Holmström MH, Zachariah R, Björnholm M, Garcia-roves PM, Zierath JR. Effect of leptin treatment on mitochondrial function in obese leptin-deficient ob/ob mice. *Metabolism*. 2013;62(9):1258-1267. doi:10.1016/j.metabol.2013.04.001

80. Munzberg H, Morrison C. Structure, production and signaling of leptin. *Metabolism*. 2015;64(1):13-23. doi:10.1016/j.metabol.2014.09.010.Structure

81. Feldmann HM, Golozoubova V, Cannon B, Nedergaard J. UCP1 Ablation Induces Obesity and Abolishes Diet-Induced Thermogenesis in Mice Exempt from Thermal Stress by Living at Thermoneutrality. *Cell Metab*. 2009;9(2):203-209. doi:10.1016/j.cmet.2008.12.014

82. Luijten IHN, Feldmann HM, Essen G Von, Cannon B, Nedergaard J. In the absence of UCP1-mediated diet-induced thermogenesis , obesity is augmented even in the obesity-resistant 129S mouse strain. *Am J Physiol - Endocrinol Metab*. 2019;316:729-740. doi:10.1152/ajpendo.00020.2019

83. Kotzbeck P, Giordano A, Mondini E, et al. Brown adipose tissue whitening leads to brown

adipocyte death and adipose tissue inflammation. *J Lipid Res*. 2018;59.

84. Jimenez M, Barbatelli G, Allevi R, Cinti S, Seydoux J. B3 -Adrenoceptor knockout in C57BL / 6J mice depresses the occurrence of brown adipocytes in white fat. *Eur J Biochem*. 2003;270:699-705. doi:10.1046/j.1432-1033.2003.03422.x

85. Guo B, Liu J, Wang B, et al. Withaferin A Promotes White Adipose Browning and Prevents Obesity Through Sympathetic Nerve – Activated Prdm16-FATP1 Axis. *Diabetes*. 2022;71(February):249-263.

86. Seale P, Conroe HM, Estall J, et al. Prdm16 determines the thermogenic program of subcutaneous white adipose tissue in mice. *J Clin Invest*. 2011;121(1):53-56. doi:10.1172/JCI44271.96

87. Inagaki T, Sakai J, Kajimura S. Transcriptional and epigenetic control of brown and beige adipose cell fate and function. *Nat Rev Mol Cell Biol*. 2016;17:480-495. doi:10.1038/nrm.2016.62

88. Kazak L, Chouchani ET, Jedrychowski MP, et al. A Creatine-Driven Substrate Cycle Enhances Energy Expenditure and Thermogenesis in Beige Fat. *Cell*. 2015;162(3):643-655. doi:10.1016/j.jconrel.2012.07.004.Enhanced

89. Wu M V., Bikopoulos G, Hung S, Ceddia RB. Thermogenic capacity is antagonistically regulated in classical brown and white subcutaneous fat depots by high fat diet and endurance training in rats: Impact on whole-body energy expenditure. *J Biol Chem*. 2014;289(49):34129-34140. doi:10.1074/jbc.M114.591008

90. Cao X, Shi TT, Zhang CH, et al. ACE2 pathway regulates thermogenesis and energy metabolism. *Elife*. 2022;11:1-21.

91. Kershaw EE, Flier JS. Adipose tissue as an endocrine organ. *J Clin Endocrinol Metab*. 2004;89(6):2548-2556. doi:10.1210/jc.2004-0395

92. Friedman JM, Halaas JL. Leptin and the regulation of body weight in mammals. *Nature*. 1998;395:763-770.

93. Howard JK, Cave BJ, Oksanen LJ, Tzameli I, Bjørbæk C, Flier JS. Enhanced leptin sensitivity and attenuation of diet- induced obesity in mice with haploinsufficiency of Socs3. *Nat Med*. 2004;10(7):734-738. doi:10.1038/nm1072

94. Kadowaki T, Yamauchi T, Kubota N, Hara K, Ueki K, Tobe K. Adiponectin and adiponectin receptors in insulin resistance, diabetes, and the metabolic syndrome. *J Clin Invest*. 2006;116(7):1784-1792. doi:10.1172/JCI29126.1784

95. Amauchi TY, Amon JK, Inokoshi YM, et al. Adiponectin stimulates glucose utilization and fatty-acid oxidation by activating AMP-activated protein kinase. *Nat Med*. 2002;8(11). doi:10.1038/nm788

96. Sung HK, Mitchell PL, Gross S, Marette A, Sweeney G. ALY688 elicits adiponectin-mimetic signaling and improves insulin action in skeletal muscle cells. *Am J Physiol - Cell Physiol*. 2022;322:C151-C163. doi:10.1152/ajpcell.00603.2020

97. Qiu W, Wu H, Hu Z, et al. Identification and characterization of a novel adiponectin receptor agonist adipo anti-inflammation agonist and its anti-inflammatory effects in vitro and in vivo. *Br J Pharmacol*. 2021;178(2):280-297. doi:10.1111/bph.15277.Identification

98. Senkus KE, Crowe-White KM, Bolland AC, Locher JL, Ard JD. Changes in adiponectin:leptin ratio among older adults with obesity following a 12-month exercise and diet intervention. *Nutr Diabetes*. 2022;12(1):1-7. doi:10.1038/s41387-022-00207-1

99. Han MS, White A, Perry RJ, et al. Regulation of adipose tissue inflammation by interleukin 6. *Proc Natl Acad Sci U S A*. 2020;117(6):2751-2760. doi:10.1073/pnas.1920004117

100. Ouchi N, Parker J, Lugus J, Walsh K. Adipokines in inflammation and metabolic disease. *Nat Rev Immunol*. 2011;11(2):85-97. doi:10.1038/nri2921.Adipokines

101. Kern P, Saghizadeh M, Ong J, Bosch R, Deem R, Simsolo R. The Expression of Tumor Necrosis Factor in Human Adipose Tissue. *J Clin Invest*. 1995;95(5):2111-2119.

102. Jack BU, Mamushi M, Viraragavan A, Dias S, Pheiffer C. Comparing the effects of tumor necrosis factor alpha, lipopolysaccharide and palmitic acid on lipid metabolism and inflammation in murine 3T3-L1 adipocytes. *Life Sci*. 2022;297(February):120422. doi:10.1016/j.lfs.2022.120422

103. Nisoli E, Briscini L, Giordano A, et al. Tumor necrosis factor α mediates apoptosis of brown adipocytes and defective brown adipocyte function in obesity. *Proc Natl Acad Sci U S A*. 2000;97(14):8033-8038. doi:10.1073/pnas.97.14.8033

104. Kawabe Y, Mori J, Morimoto H, et al. ACE2 exerts anti-obesity effect via stimulating brown adipose tissue and induction of browning in white adipose tissue. *Am J Physiol - Endocrinol Metab*. 2019;317(6):E1140-E1149. doi:10.1152/AJPENDO.00311.2019

105. Giori IG, Magliano DC, Alexandre-Santos B, et al. Enalapril and treadmill running reduce adiposity, but only the latter causes adipose tissue browning in mice. *J Cell Physiol*. 2021;236(2):900-910. doi:10.1002/jcp.29900

106. Ames MK, Atkins CE, Pitt B. The renin-angiotensin-aldosterone system and its suppression. *J Vet Intern Med*. 2019;33(2):363-382. doi:10.1111/jvim.15454

107. Marcus Y, Shefer G, Stern N. Adipose tissue renin-angiotensin-aldosterone system (RAAS) and progression of insulin resistance. *Mol Cell Endocrinol*. 2013;378(1-2):1-14. doi:10.1016/j.mce.2012.06.021

108. Mehta PK, Griendling KK. Angiotensin II cell signaling: Physiological and pathological effects in the cardiovascular system. *Am J Physiol - Cell Physiol*. 2007;292(1):82-97. doi:10.1152/ajpcell.00287.2006

109. Benigni A, Cassis P, Remuzzi G. Angiotensin II revisited: New roles in inflammation, immunology and aging. *EMBO Mol Med*. 2010;2(7):247-257. doi:10.1002/emmm.201000080

110. Schütten MTJ, Houben AJHM, De Leeuw PW, Stehouwer CDA. The link between adipose tissue renin-angiotensin-aldosterone system signaling and obesity-associated

hypertension. *Physiology*. 2017;32(3):197-209. doi:10.1152/physiol.00037.2016

111. Schulman IH, Raij L. The angiotensin II type 2 receptor: What is its clinical significance? *Curr Hypertens Rep*. 2008;10(3):188-193. doi:10.1007/s11906-008-0036-8

112. Morimoto H, Mori J, Nakajima H, et al. Angiotensin 1–7 stimulates brown adipose tissue and reduces diet-induced obesity. *Am J Physiol - Endocrinol Metab*. 2018;314(2):E131-E138. doi:10.1152/ajpendo.00192.2017

113. Sarver DC, Wong GW. Obesity alters Ace2 and Tmprss2 expression in lung, trachea, and esophagus in a sex-dependent manner: Implications for COVID-19. *Biochem Biophys Res Commun*. 2021;538:92-96.

114. Chaolin H, Wang Y, Li X, et al. Clinical features of patients infected with 2019 novel coronavirus in Wuhan, China. *Lancet*. 2020;395:497-506.

115. Ragia G, Manolopoulos VG. Inhibition of SARS-CoV-2 entry through the ACE2/TMPRSS2 pathway: a promising approach for uncovering early COVID-19 drug therapies. *Eur J Clin Pharmacol*. 2020;76(12):1623-1630. doi:10.1007/s00228-020-02963-4

116. Ioganathan S, Kuppusamy M, Wankhar W, et al. Angiotensin-converting enzyme 2 (ACE2): COVID 19 gate way to multiple organ failure syndromes. *Respir Physiol Neurobiol*. 2021;283:1035-1048.

117. Machhi J, Herskovitz J, Senan AM, et al. The Natural History, Pathobiology, and Clinical Manifestations of SARS-CoV-2 Infections. *J Neuroimmune Pharmacol*. 2020;15(3):359-386. doi:10.1007/s11481-020-09944-5

118. Korakas E, Ikonomidis I, Kousathana F, et al. Obesity and COVID-19: Immune and metabolic derangement as a possible link to adverse clinical outcomes. *Am J Physiol - Endocrinol Metab*. 2020;319(1):E105-E109. doi:10.1152/ajpendo.00198.2020

119. Song P, Li W, Xie J, Hou Y, You C. Cytokine storm induced by SARS-CoV-2. *Clin Chim Acta*. 2020;509:280-287.

120. Kim H, Lee H, Chang Y, et al. IL-17 producing innate lymphoid cells and the NLRP3 inflammasome facilitate obesity-associated airway hyperreactivity. *Nat Med*. 2014;20(1):54-61. doi:10.1038/nm.3423.IL-17

121. Wu C, Zheng M, Yang Y, et al. Furin: A Potential Therapeutic Target for COVID-19. *iScience*. 2020;23(10):101642. doi:10.1016/j.isci.2020.101642

122. Hoffmann M, Kleine-Weber H, Schroeder S, et al. SARS-CoV-2 Cell Entry Depends on ACE2 and TMPRSS2 and Is Blocked by a Clinically Proven Protease Inhibitor. *Cell*. 2020;181(2):271-280.e8. doi:10.1016/j.cell.2020.02.052

123. Li M, Li L, Zhang Y, Wang X. Expression of the SARS-CoV-2 cell receptor gene ACE2 in a wide variety of human tissues. *Infect Dis Poverty*. 2020;9(45):1-7. doi:10.21203/rs.2.24751/v1

124. Bienvenu LA, Noonan J, Wang X, Peter K. Higher mortality of COVID-19 in males: Sex

differences in immune response and cardiovascular comorbidities. *Cardiovasc Res*. 2020;116(14):2197-2206. doi:10.1093/cvr/cvaa284

125. Batchu SN, Kaur H, Yerra VG, et al. Lung and Kidney ACE2 and TMPRSS2 in Renin-Angiotensin System Blocker–Treated Comorbid Diabetic Mice Mimicking Host Factors That Have Been Linked to Severe COVID-19. *Diabetes*. 2021;70(3):759-771. doi:10.2337/db20-0765

126. Longo R, Peri C, Cricr D, et al. Ketogenic Diet : A New Light Shining on Old but Gold Biochemistry. *Nutrients*. 2019;11(10):1-22.

127. Hwang CY, Choe W, Yoon KS, et al. Molecular Mechanisms for Ketone Body Metabolism, Signaling Functions, and Therapeutic Potential in Cancer. *Nutrients*. 2022;14(22).

128. Cotter DG, Schugar RC, Crawford PA. Ketone body metabolism and cardiovascular disease. *Am J Physiol - Hear Circ Physiol*. 2013;304(8):1060-1076. doi:10.1152/ajpheart.00646.2012

129. Newsholme E, Leech A. *Functional Biochemistry in Health and Disease*. 2nd ed. John Wiley & Sons, Ltd; 2010.

130. Green BA, Newsholme EA. Sensitivity of Glucose Uptake and Lipolysis of White Adipocytes of the Rat to Insulin and Effects of some Metabolites. *Biochem J*. 1979;180:365-370.

131. Mujica-Parodi LR, Amgalan A, Sultan SF, et al. Diet modulates brain network stability, a biomarker for brain aging, in young adults. *Proc Natl Acad Sci U S A*. 2020;117(11):6170-6177. doi:10.1073/pnas.1913042117

132. Tanaka H, Iguchi N, Miyagawa Y, Koga M, Kohroki J, Nishimune Y. Differential expression of succinyl CoA transferase (SCOT) genes in somatic and germline cells of the mouse testis. *Int J Androl*. 2003;26(1):52-56. doi:10.1046/j.1365-2605.2003.00389.x

133. Vanitallie TB, Nufert TH. Ketones : Metabolism ' s Ugly Duckling. *Nutr Rev*. 1967;61(10). doi:10.131/nr.2003.oct.327

134. Bolla AM, Caretto A, Laurenzi A, Scavini M, Piemonti L. Low-Carb and Ketogenic Diets in Type 1 and Type 2 Diabetes. *Nutrients*. 2019;11(5):1-14.

135. Peterman M. The ketogenic diet in epilepsy. *JAMA*. 1925;84(26).

136. Roberts MN, Wallace MA, Tomilov AA, et al. A ketogenic diet extends longevity and healthspan in adult mice. *Cell Metab*. 2018;26(3):539-546. doi:10.1016/j.cmet.2017.08.005.A

137. Ellenbroek JH, van Dijck L, Töns HA, et al. Long-term ketogenic diet causes glucose intolerance and reduced β- and α-cell mass but no weight loss in mice. *Am J Physiol - Endocrinol Metab*. 2014;306(5):552-558. doi:10.1152/ajpendo.00453.2013

138. Kong G, Wang J, Li R, Huang Z, Wang L. Ketogenic diet ameliorates inflammation by inhibiting the NLRP3 inflammasome in osteoarthritis. *Arthritis Res Ther*. 2022;24(1):1-

11. doi:10.1186/s13075-022-02802-0

139. Youm YH, Nguyen KY, Grant RW, et al. Ketone body β-hydroxybutyrate blocks the NLRP3 inflammasome-mediated inflammatory disease. *Nat Med*. 2015;21(3):263-269. doi:10.1038/nm.3804.Ketone

140. Xu Y, Jiang C, Wu J, et al. Ketogenic diet ameliorates cognitive impairment and neuroinflammation in a mouse model of Alzheimer ' s disease. *CNS Neurosci Ther*. 2022;28:580-592. doi:10.1111/cns.13779

141. Youm YH, Nguyen KY, Grant RW, et al. The ketone metabolite β-hydroxybutyrate blocks NLRP3 inflammasome–mediated inflammatory disease. *Nat Med*. 2015;21(3):263-269. doi:10.1038/nm.3804

142. Evans E, Walhin J philippe, Hengist A, Betts JA, Dearlove DJ, Gonzalez JT. Ketone monoester ingestion increases postexercise serum erythropoietin concentrations in healthy men. *Am J Physiol Endocrinol Metab*. 2023;324:56-61. doi:10.1152/ajpendo.00264.2022

143. Soni S, Martens MD, Takahara S, et al. Exogenous ketone ester administration attenuates systemic inflammation and reduces organ damage in a lipopolysaccharide model of sepsis. *BBA - Mol Basis Dis*. 2022;1868(11):166507. doi:10.1016/j.bbadis.2022.166507

144. Mota AS, Norwitz NG, Evans R, Clarke K, Barber TM. Exogenous ketosis in patients with type 2 diabetes : Safety , tolerability and effect on glycaemic control. *Endocrinol Diabetes Metab*. 2021;4(3):1-7. doi:10.1002/edm2.264

145. Ryu S, Shchukina I, Youm YH, et al. Ketogenic diet restrains aging-induced exacerbation of coronavirus infection in mice. *Elife*. 2021;10:1-25. doi:10.7554/eLife.66522

146. Asrih M, Altirriba J, Rohner-Jeanrenaud F, Jornayvaz FR. Ketogenic diet impairs FGF21 signaling and promotes differential inflammatory responses in the liver and white adipose tissue. *PLoS One*. 2015;10(5):1-14. doi:10.1371/journal.pone.0126364

147. Douris N, Desai BN, Fisher M, et al. Beta-adrenergic receptors are critical for weight loss but not for other metabolic adaptations to the consumption of a ketogenic diet in male mice. *Mol Metab*. 2017;6(8):854-862. doi:10.1016/j.molmet.2017.05.017

148. Rushing KA, Bolyard ML, Kelty T, et al. Dietary ketone ester attenuates the accretion of adiposity and liver steatosis in mice fed a high-fat, high-sugar diet. *Front Physiol*. 2023;14(April):1-11. doi:10.3389/fphys.2023.1165224

149. Srivastava S, Baxa U, Niu G, Chen X, Veech RL. A Ketogenic Diet Increases Brown Adipose Tissue Mitochondrial Proteins and UCP1 Levels in Mice. *IUBMB Life*. 2013;65(1).

150. Srivastava S, Kashiwaya Y, King MT, et al. Mitochondrial biogenesis and increased uncoupling protein 1 in brown adipose tissue of mice fed a ketone ester diet. *FASEB J*. 2012;26(6):2351-2362. doi:10.1096/fj.11-200410

151. Popov LD. Mitochondrial biogenesis: An update. *J Cell Mol Med*. 2020;24(9):4892-4899. doi:10.1111/jcmm.15194

152. Frontera WR, Ochala J. Skeletal Muscle: A Brief Review of Structure and Function. *Calc Tissue Int*. 2015;96:183-195. doi:10.1007/s00223-014-9915-y

153. Saltin B, Henriksson J, Nygaard E, Andersen P, Jansson E. Fiber Types and Metabolic Potentials of Skeletal. *Ann N Y Acad Sci*. 1977;301:3-29.

154. Schiaffino S, Reggiani C. Fiber types in Mammalian skeletal muscles. *Physiol Rev*. 2011;91(4):1447-1531. doi:10.1152/physrev.00031.2010

155. Ariano MA, Armstrong RB, Edgerton VR. Hindlimb muscle fiber populations of five mammals. *J Histochem Cytochem*. 1973;21(1):51-55.

156. Nesher R, Karl IE, Kaiser KE, Kipnis DM. Epitrochlearis muscle. I. Mechanical performance, energetics, and fiber composition. *Am J Physiol*. 1980;239(6):E454-60. doi:10.1152/ajpendo.1980.239.6.E454

157. Pinho RA, Sepa-Kishi DM, Bikopoulos G, et al. High-fat diet induces skeletal muscle oxidative stress in a fiber type-dependent manner in rats. *Free Radic Biol Med*. 2017;110:381-389. doi:10.1016/j.freeradbiomed.2017.07.005

158. Jani S, Da Eira D, Ceddia RB. Insulin-resistant female rat skeletal muscles display diacylglycerol-mediated PKC activation and inflammation without ceramides accumulation. *J Physiol*. Published online 2023. doi:10.1113/JP284324

159. Honka MJ, Latva-Rasku A, Bucci M, et al. Insulin-stimulated glucose uptake in skeletal muscle, adipose tissue and liver: A positron emission tomography study. *Eur J Endocrinol*. 2018;178(5):523-531. doi:10.1530/EJE-17-0882

160. Sylow L, Tokarz VL, Richter EA, Klip A. The many actions of insulin in skeletal muscle, the paramount tissue determining glycemia. *Cell Metab*. 2021;33(4):758-780. doi:10.1016/j.cmet.2021.03.020

161. Shulman G, Rothman DL, Jue T, Stein P, Defronzo RA, Shulman R. Quantitation of Muscle Glycogen Synthesis in Normal Subjects and Subjects with Non-Insulin-Dependent Diabetes by 13C Nuclear Magnetic Resonance Spectroscopy. *New English J Med*. 1990;323(4):223-228.

162. De Figueiredo ASP, Salmon AB, Bruno F, et al. Nox2 mediates skeletal muscle insulin resistance induced by a high fat diet. *J Biol Chem*. 2015;290(21):13427-13439. doi:10.1074/jbc.M114.626077

163. Petersen MC, Shulman GI. Mechanisms of insulin action and insulin resistance. *Physiol Rev*. 2018;98(4):2133-2223. doi:10.1152/physrev.00063.2017

164. Zhou Z, Vidales J, González-Reyes JA, et al. A 1-month ketogenic diet increased mitochondrial mass in red gastrocnemius muscle, but not in the brain or liver of middle-aged mice. *Nutrients*. 2021;13(8):1-9. doi:10.3390/nu13082533

165. Pathak SJ, Zhou Z, Steffen D, et al. 2-Month Ketogenic Diet Preferentially Alters Skeletal Muscle and Augments Cognitive Function in Middle Aged Female Mice. *Aging Cell*. 2022;21(10):1-15. doi:10.1111/acel.13706

166. Shimizu K, Saito H, Sumi K, Sakamoto Y, Tachi Y, Iida K. Short-term and long-term ketogenic diet therapy and the addition of exercise have differential impacts on metabolic gene expression in the mouse energy-consuming organs heart and skeletal muscle. *Nutr Res*. 2018;60:77-86. doi:10.1016/j.nutres.2018.09.004

167. Miller VJ, LaFountain RA, Barnhart E, et al. A ketogenic diet combined with exercise alters mitochondrial function in human skeletal muscle while improving metabolic health. *Am J Physiol - Endocrinol Metab*. 2020;319(6):E995-E1007. doi:10.1152/AJPENDO.00305.2020

168. Noakes TD, Prins PJ, Volek JS, D'Agostino DP, Koutnik AP. Low carbohydrate high fat ketogenic diets on the exercise crossover point and glucose homeostasis. *Front Physiol*. 2023;14(March):1-14. doi:10.3389/fphys.2023.1150265

169. Cox PJ, Kirk T, Ashmore T, et al. Nutritional Ketosis Alters Fuel Preference and Thereby Endurance Performance in Athletes. *Cell Metab*. 2016;24(2):256-268. doi:10.1016/j.cmet.2016.07.010

170. Ogura Y, Kakehashi C, Yoshihara T, et al. Ketogenic diet feeding improves aerobic metabolism property in extensor digitorum longus muscle of sedentary male rats. *PLoS One*. 2020;15(10):1-16. doi:10.1371/journal.pone.0241382

171. Fukazawa A, Koike A, Karasawa T, Tsutsui M, Kondo S, Terada S. Effects of a ketogenic diet containing medium-chain triglycerides and endurance training on metabolic enzyme adaptations in rat skeletal muscle. *Nutrients*. 2020;12(5). doi:10.3390/nu12051269

172. Nakao R, Abe T, Yamamoto S, Oishi K. Ketogenic diet induces skeletal muscle atrophy via reducing muscle protein synthesis and possibly activating proteolysis in mice. *Sci Rep*. 2019;9(1):1-14. doi:10.1038/s41598-019-56166-8

173. Bielohuby M, Menhofer D, Kirchner H, et al. Induction of ketosis in rats fed low-carbohydrate, high-fat diets depends on the relative abundance of dietary fat and protein. *Am J Physiol - Endocrinol Metab*. 2011;300(1). doi:10.1152/ajpendo.00478.2010

174. Jitrapakdee S. Transcription factors and coactivators controlling nutrient and hormonal regulation of hepatic gluconeogenesis. *Int J Biochem Cell Biol*. 2012;44(1):33-45. doi:10.1016/j.biocel.2011.10.001

175. So M, Gaidhu MP, Maghdoori B, Ceddia RB. Analysis of time-dependent adaptations in whole- body energy balance in obesity induced by high- fat diet in rats. *Lipids Health Dis*. 2011;10(1):99. doi:10.1186/1476-511X-10-99

176. Rosenbaum M, Leibel RL. The physiology of body weight regulation: relevance to the etiology of obesity in children. *Pediatrics*. 1998;101(3 Pt 2):525-539.

177. Trayhurn P. Origins and early development of the concept that brown adipose tissue thermogenesis is linked to energy balance and obesity. *Biochimie*. 2017;134:62-70. doi:10.1016/j.biochi.2016.09.007

178. Leibel RL. Molecular physiology of weight regulation in mice and humans. *Int J Obes (Lond)*. 2008;32 Suppl 7:S98-108.

179. Kozak LP. Brown Fat and the Myth of Diet-Induced Thermogenesis. *Cell Metab*. 2010;11(4):263-267. doi:10.1016/j.cmet.2010.03.009

180. Fedorenko A, Lishko P V., Kirichok Y. Mechanism of Fatty-Acid-Dependent UCP1 Uncoupling in Brown Fat Mitochondria. *Cell*. 2013;151(2):400-413. doi:10.1016/j.cell.2012.09.010.Mechanism

181. Cannon B, Nedergaard J. Respiratory and Thermogenic Capacities of Cells and Mitochondria from Brown and White Adipose Tissue. In: Ailhaud G, ed. *Adipose Tissue Protocols*. Humana Press Inc.; 2001:295-304.

182. Fine JB, DiGirolamo M. A simple method to predict cellular density in adipocyte metabolic incubations. *Int J Obes Relat Metab Disord*. 1997;21(9):764-768.

183. Gaidhu MP, Frontini A, Hung S, Pistor K, Cinti S, Ceddia RB. Chronic AMP-kinase activation with AICAR reduces adiposity by remodeling adipocyte metabolism and increasing leptin sensitivity. *J Lipid Res*. 2011;52(9):1702-1711. doi:10.1194/jlr.M015354

184. Gaidhu MP, Fediuc S, Anthony NM, et al. Prolonged AICAR-induced AMP-kinase activation promotes energy dissipation in white adipocytes: novel mechanisms integrating HSL and ATGL. *J Lipid Res*. 2009;50(4):704-715. doi:10.1194/jlr.M800480-JLR200

185. Dole P. Microdetermination of Long-chain Fatty Acids in Plasma and Tissues *. *J Biol Chem*. 1980;235:2595-2599.

186. Folch J, Lees M, Sloane Stanley GH. A simple method for the isolation and purification of total lipides from animal tissues. *J Biol Chem*. 1957;226(1):497-509.

187. Gaidhu MP, Fediuc S, Ceddia RB. 5-Aminoimidazole-4-carboxamide-1-beta-D-ribofuranoside-induced AMP-activated protein kinase phosphorylation inhibits basal and insulin-stimulated glucose uptake, lipid synthesis, and fatty acid oxidation in isolated rat adipocytes. *J Biol Chem*. 2006;281(36):25956-25964. doi:10.1074/jbc.M602992200

188. Livak KJ, Schmittgen TD. Analysis of Relative Gene Expression Data Using Real-Time Quantitative PCR and the 2−ΔΔCT Method. *Methods*. 2001;25(4):402-408.

189. Labbe SM, Caron A, Bakan I, et al. In vivo measurement of energy substrate contribution to cold-induced brown adipose tissue thermogenesis. *FASEB J*. Published online 2015.

190. Olsen JM, Csikasz RI, Dehvari N, et al. β 3 -Adrenergically induced glucose uptake in brown adipose tissue is independent of UCP1 presence or activity: Mediation through the mTOR pathway. *Mol Metab*. 2017;6(6):611-619.

191. Ferré P, Burnol AF, Leturque A, et al. Glucose utilization *in vivo* and insulin-sensitivity of rat brown adipose tissue in various physiological and pathological conditions. *Biochem J*. 1986;233(1):249-252.

192. Lapa C, Arias-loza P, Hayakawa N, et al. Whitening and Impaired Glucose Utilization of Brown Adipose Tissue in a Rat Model of Type 2 Diabetes Mellitus. *Sci Rep*. 2017;7(1). doi:10.1038/s41598-017-17148-w

193. Ishino S, Sugita T, Kondo Y, et al. Glucose uptake of the muscle and adipose tissues in

diabetes and obesity disease models: evaluation of insulin and β3-adrenergic receptor agonist effects by 18F-FDG. *Ann Nucl Med*. 2017;31(5):413-423.

194. Orava J, Nuutila P, Noponen T, et al. Blunted metabolic responses to cold and insulin stimulation in brown adipose tissue of obese humans. *Obesity*. 2013;21(11):2279-2287.

195. Nye CK, Hanson RW, Kalhan SC. Glyceroneogenesis Is the Dominant Pathway for Triglyceride Glycerol Synthesis *in Vivo* in the Rat. *J Biol Chem*. 2008;283(41):27565-27574.

196. Levin BE, Finnegan M, Triscari J, Sullivan AC. Brown adipose and metabolic features of chronic diet-induced obesity. *Am J Physiol Integr Comp Physiol*. 1985;248(6):R717-R723.

197. Madden CJ, Morrison SF. A high-fat diet impairs cooling-evoked brown adipose tissue activation via a vagal afferent mechanism. *Am J Physiol Metab*. 2016;311(2):E287-E292.

198. Leibel RL, Chung WK, Chua SC. The Molecular Genetics of Rodent Single Gene Obesities. *J Biol Chem*. 1997;272(51):31937-31940.

199. Levin BE, Triscari J, Sullivan AC. Altered sympathetic activity during development of diet-induced obesity in rat. *Am J Physiol Integr Comp Physiol*. 1983;244(3):R347-R355.

200. Levin BE, Dunn-Meynell AA. Reduced central leptin sensitivity in rats with diet-induced obesity. *Am J Physiol Integr Comp Physiol*. 2002;283(4):R941-R948.

201. Guilherme A, Virbasius J V., Puri V, Czech MP. Adipocyte dysfunctions linking obesity to insulin resistance and type 2 diabetes. *Nat Rev Mol Cell Biol*. 2008;9(5):367-377. doi:10.1038/nrm2391.Adipocyte

202. Mowers J, Uhm M, Reilly SM, et al. Inflammation produces catecholamine resistance in obesity via activation of PDE3B by the protein kinases IKKε and TBK1. *Elife*. 2013;132(2):1-18. doi:10.7554/eLife.01119

203. Luukkonen PK, Dufour S, Lyu K, et al. Effect of a ketogenic diet on hepatic steatosis and hepatic mitochondrial metabolism in nonalcoholic fatty liver disease. *Proc Natl Acad Sci U S A*. 2020;117(13):7347-7354. doi:10.1073/pnas.1922344117

204. Basolo A, Magno S, Santini F, Ceccarini G. Ketogenic Diet and Weight Loss: Is There an Effect on Energy Expenditure? *Nutrients*. 2022;14(9). doi:10.3390/NU14091814

205. Pinho RA, Sepa-Kishi DM, Bikopoulos G, et al. High-fat diet induces skeletal muscle oxidative stress in a fiber type-dependent manner in rats. *Free Radic Biol Med*. 2017;110(July):381-389. doi:10.1016/j.freeradbiomed.2017.07.005

206. du Sert NP, Ahluwalia A, Alam S, et al. Reporting animal research: Explanation and elaboration for the arrive guidelines 2.0. *PLoS Biol*. 2020;18(7):e3000411. doi:10.1371/journal.pbio.3000411

207. Dole VP, Meinertz H. Microdetermination of long-chain fatty acids in plasma and tissues. *J Biol Chem*. 1960;235(9):2595-2599. doi:10.1016/s0021-9258(19)76920-8

208. Ahlquist R.P. Present state of alpha- and beta-adrenergic drugs I. The adrenergic receptor.

Am Heart J. 1976;92(5):661-664.

209. Festuccia WTL, Guerra-Sá R, Kawashita NH, et al. Expression of glycerokinase in brown adipose tissue is stimulated by the sympathetic nervous system. *Am J Physiol - Regul Integr Comp Physiol*. 2003;284(6):1536-1541. doi:10.1152/ajpregu.00764.2002

210. Hall KD, Chen KY, Guo J, et al. Energy expenditure and body composition changes after an isocaloric ketogenic diet in overweight and obese men. *Am J Clin Nutr*. 2016;104(2):324-333. doi:10.1371/journal.pone.0222971

211. Elia M, Zed C, Neale G, Livesey G. The energy cost of triglyceride-fatty acid recycling in nonobese subjects after an overnight fast and four days of starvation. *Metabolism*. 1987;36(3):251-255. doi:10.1016/0026-0495(87)90184-3

212. Guan HP, Li Y, Jensen MV, Newgard CB, Steppan CM, Lazar MA. A futile metabolic cycle activated in adipocytes by antidiabetic agents. *Nat Med*. 2002;8(10):1122-1128. doi:10.1038/nm780

213. Pezeshki A, Chelikani PK. Low Protein Diets and Energy Balance: Mechanisms of Action on Energy Intake and Expenditure. *Front Nutr*. 2021;8:1-8. doi:10.3389/fnut.2021.655833

214. Mráček T, Drahota Z, Houštěk J. The function and the role of the mitochondrial glycerol-3-phosphate dehydrogenase in mammalian tissues. *Biochim Biophys Acta - Bioenerg*. 2013;1827(3):401-410. doi:10.1016/j.bbabio.2012.11.014

215. Sparks MA, Crowley SD, Gurley SB, Mirotsou M, Coffman TM. Classical renin-angiotensin system in kidney physiology. *Compr Physiol*. 2014;4(3):1201-1228. doi:10.1002/cphy.c130040

216. Paz Ocaranza M, Riquelme JA, García L, et al. Counter-regulatory renin–angiotensin system in cardiovascular disease. *Nat Rev Cardiol*. 2020;17(2):116-129. doi:10.1038/s41569-019-0244-8

217. Frigolet ME, Torres N, Tovar AR. The renin-angiotensin system in adipose tissue and its metabolic consequences during obesity. *J Nutr Biochem*. 2013;24(12):2003-2015. doi:10.1016/j.jnutbio.2013.07.002

218. Da Eira D, Jani S, Ceddia RB. Obesogenic and ketogenic diets distinctly regulate the SARS-CoV-2 entry proteins ACE2 and TMPRSS2 and the renin-angiotensin system in rat lung and heart tissues. *Nutrients*. 2021;13(10):3357. doi:10.3390/nu13103357

219. Klein S, Gastaldelli A, Yki-Järvinen H, Scherer PE. Why does obesity cause diabetes? *Cell Metab*. 2022;34(1):11-20. doi:10.1016/j.cmet.2021.12.012

220. Than A, Xu S, Li R, Leow MS, Sun L, Chen P. Angiotensin type 2 receptor activation promotes browning of white adipose tissue and brown adipogenesis. *Signal Transduct Target Ther*. 2017;2:1-12. doi:10.1038/sigtrans.2017.22

221. Lee MH, Song HK, Ko GJ, et al. Angiotensin receptor blockers improve insulin resistance in type 2 diabetic rats by modulating adipose tissue. *Kidney Int*. 2008;74(7):890-900. doi:10.1038/ki.2008.313

222. Kalupahana NS, Massiera F, Quignard-Boulange A, et al. Overproduction of angiotensinogen from adipose tissue induces adipose inflammation, glucose intolerance, and insulin resistance. *Obesity*. 2012;20(1):48-56. doi:10.1038/oby.2011.299

223. Shum M, Pinard S, Guimond MO, et al. Angiotensin II type 2 receptor promotes adipocyte differentiation and restores adipocyte size in high-fat/high-fructose diet-induced insulin resistance in rats. *Am J Physiol - Endocrinol Metab*. 2013;304(2). doi:10.1152/ajpendo.00149.2012

224. Than A, Leow MKS, Chen P. Control of adipogenesis by the autocrine interplays between angiotensin 1-7/Mas receptor and angiotensin II/AT1 receptor signaling pathways. *J Biol Chem*. 2013;288(24):15520-15531. doi:10.1074/jbc.M113.459792

225. Longo M, Zatterale F, Naderi J, et al. Adipose tissue dysfunction as determinant of obesity-associated metabolic complications. *Int J Mol Sci*. 2019;20(9):2358. doi:10.3390/ijms20092358

226. Luzi L, Bucciarelli L, Ferrulli A, Terruzzi I, Massarini S. Obesity and COVID-19: the Ominous duet affecting the Renin-Angiotensin System Livio. *Minerva Endocrinol*. 2021;46(2):193-201.

227. Palaiodimos L, Kokkinidis DG, Li W, et al. Severe obesity is associated with higher in-hospital mortality in a cohort of patients with COVID-19 in the Bronx, New York. *Metabolism*. 2020;108:154262. doi:10.1016/j.metabol.2020.154262

228. Akoumianakis I, Filippatos T. The renin–angiotensin–aldosterone system as a link between obesity and coronavirus disease 2019 severity. *Obes Rev*. 2020;21(9):1-8. doi:10.1111/obr.13077

229. Wijnant SRA, Jacobs M, Van Eeckhoutte H, et al. Expression of ACE2, the SARS-CoV-2 Receptor, in Lung Tissue of Patients with Type 2 Diabetes. *Diabetes*. 2020;69(12):2691-2699. doi:10.2337/db20-0669

230. Fondevila M, Mercado-Gómez M, Rodríguez A, et al. Obese patients with NASH have increased hepatic expression of SARS-CoV-2 critical entry points. *J Hepatol*. 2021;74(2):469-471. doi:10.1016/J.JHEP.2020.09.027

231. D'Abbondanza M, Ministrini S, Pucci G, et al. Very Low-Carbohydrate Ketogenic Diet for the Treatment of Severe Obesity and Associated Non-Alcoholic Fatty Liver Disease: The Role of Sex Differences. *Nutrients*. 2020;12(9):1-14. doi:10.3390/NU12092748

232. Watanabe M, Tozzi R, Risi R, et al. Beneficial effects of the ketogenic diet on nonalcoholic fatty liver disease: A comprehensive review of the literature. *Obes Rev*. 2020;21(8). doi:10.1111/OBR.13024

233. Luukkonen P, Dufour S, Lyu K, et al. Effect of a ketogenic diet on hepatic steatosis and hepatic mitochondrial metabolism in nonalcoholic fatty liver disease. *Proc Natl Acad Sci U S A*. 2020;117(13):7347-7354. doi:10.1073/PNAS.1922344117

234. Zhao Y, Kuang M, Li J, et al. SARS-CoV-2 spike protein interacts with and activates TLR41. *Cell Res*. Published online 2021:1-3. doi:10.1038/s41422-021-00495-9

235. Forsythe CE, Phinney SD, Fernandez ML, et al. Comparison of low fat and low carbohydrate diets on circulating fatty acid composition and markers of inflammation. *Lipids*. 2008;43(1):65-77. doi:10.1007/s11745-007-3132-7

236. Pinto A, Bonucci A, Maggi E, Corsi M, Businaro R. Anti-oxidant and anti-inflammatory activity of ketogenic diet: New perspectives for neuroprotection in alzheimer's disease. *Antioxidants*. 2018;7(5). doi:10.3390/antiox7050063

237. Streijger F, Plunet WT, Lee JHT, et al. Ketogenic diet improves forelimb motor function after spinal cord injury in rodents. *PLoS One*. 2013;8(11). doi:10.1371/journal.pone.0078765

238. Batch JT, Lamsal SP, Adkins M, Sultan S, Ramirez MN. Advantages and Disadvantages of the Ketogenic Diet: A Review Article. *Cureus*. 2020;12(8). doi:10.7759/cureus.9639

239. Goodpaster B, Sparks LM. Metabolic flexibility in health and disease. *Physiol Behav*. 2017;25(5):1027-1036. doi:10.1016/j.cmet.2017.04.015.Metabolic

240. Luong TV, Abild CB, Bangshaab M, Gormsen LC, Søndergaard E. Ketogenic Diet and Cardiac Substrate Metabolism. *Nutrients*. 2022;14(7):1-9. doi:10.3390/nu14071322

241. Miller VJ, LaFountain RA, Barnhart E, et al. A ketogenic diet combined with exercise alters mitochondrial function in human skeletal muscle while improving metabolic health. *Am J Physiol Metab*. Published online September 2020:ajpendo.00305.2020. doi:10.1152/ajpendo.00305.2020

242. McLane JA, Holloszy JO. Glycogen synthesis from lactate in the three types of skeletal muscle. *J Biol Chem*. 1979;254(14):6548-6553. doi:10.1016/s0021-9258(18)50402-6

243. Winder WW, Holloszy JO, Baldwin KM. Enzymes involved in ketone utilization in different types of muscle: adaptation to exercise. *Eur J Biochem*. 1974;47(3):461-467. doi:10.1111/J.1432-1033.1974.TB03713.X

244. Fediuc S, Gaidhu MP, Ceddia RB. Inhibition of insulin-stimulated glycogen synthesis by 5-aminoimidasole-4- carboxamide-1-β-D-ribofuranoside-induced adenosine 5′-monophosphate- activated protein kinase activation: Interactions with Akt, glycogen synthase kinase 3-3α/β, and glycogen synth. *Endocrinology*. 2006;147(11):5170-5177. doi:10.1210/en.2006-0480

245. Rabinowitz JD, Enerbäck S. Lactate: the ugly duckling of energy metabolism. *Nat Metab*. 2020;2(7):566-571. doi:10.1038/s42255-020-0243-4

246. Jornayvaz FR, Shulman GI. Regulation of mitochondrial biogenesis. *Essays Biochem*. 2010;47:69-84. doi:10.1042/BSE0470069

247. Brown DM, Williams H, Ryan KJP, et al. Mitochondrial phosphoenolpyruvate carboxykinase (PEPCK-M) and serine biosynthetic pathway genes are co-ordinately increased during anabolic agent-induced skeletal muscle growth. *Sci Rep*. 2016;6:1-14. doi:10.1038/srep28693

248. Pinho RA, Sepa-Kishi DM, Bikopoulos G, et al. High-fat diet induces skeletal muscle oxidative stress in a fiber type-dependent manner in rats. *Free Radic Biol Med*. 2017;110.

doi:10.1016/j.freeradbiomed.2017.07.005

249. Scheja L, Heeren J. The endocrine function of adipose tissues in health and cardiometabolic disease. *Nat Rev Endocrinol*. 2019;15(9):507-524. doi:10.1038/s41574-019-0230-6

250. Tao C, Sifuentes A, Holland WL. Regulation of glucose and lipid homeostasis by adiponectin: effects on hepatocytes, pancreatic β cells and adipocytes. *Best Pract Res Clin Endocrinol Metab*. 2014;28(1):43-58. doi:10.1016/j.beem.2013.11.003

251. Yamauchi T, Iwabu M, Okada-Iwabu M, Kadowaki T. Adiponectin receptors: a review of their structure, function and how they work. *Best Pract Res Clin Endocrinol Metab*. 2014;28(1):15-23. doi:10.1016/j.beem.2013.09.003

252. Yamauchi T, Kamon J, Ito Y, et al. Cloning of adiponectin receptors that mediate antidiabetic metabolic effects. *Nature*. 2003;423(6941):762-769. doi:10.1038/nature01705

253. Yamauchi T, Kamon J, Minokoshi Y, et al. Adiponectin stimulates glucose utilization and fatty-acid oxidation by activating AMP-activated protein kinase. *Nat Med*. 2002;8(11):1288-1295. doi:10.1038/nm788

254. Myeong JY, Gha YL, Chung JJ, Young HA, Seung HH, Jae BK. Adiponectin increases fatty acid oxidation in skeletal muscle cells by sequential activation of AMP-activated protein kinase, p38 mitogen-activated protein kinase, and peroxisome proliferator-activated receptor{alpha}. *Diabetes*. 2006;55(9):2562-2570. doi:10.2337/db05-1322

255. Iwabu M, Yamauchi T, Okada-Iwabu M, et al. Adiponectin and AdipoR1 regulate PGC-1α and mitochondria by Ca 2+ and AMPK/SIRT1. *Nature*. 2010;464(7293):1313-1319. doi:10.1038/nature08991

256. Yoon M. The role of PPARα in lipid metabolism and obesity: Focusing on the effects of estrogen on PPARα actions. *Pharmacol Res*. 2009;60(3):151-159. doi:10.1016/j.phrs.2009.02.004

257. Wu X, Motoshima H, Mahadev K, Stalker TJ, Scalia R, Goldstein BJ. Involvement of AMP-activated protein kinase in glucose uptake stimulated by the globular domain of adiponectin in primary rat adipocytes. *Diabetes*. 2003;52(6):1355-1363. doi:10.2337/diabetes.52.6.1355

258. Sayeed M, Gautam S, Verma DP, et al. A collagen domain-derived short adiponectin peptide activates APPL1 and AMPK signaling pathways and improves glucose and fatty acid metabolisms. *J Biol Chem*. 2018;293(35):13509-13523. doi:10.1074/jbc.RA118.001801

259. Qiao L, Kinney B, Schaack J, Shao J. Adiponectin inhibits lipolysis in mouse adipocytes. *Diabetes*. 2011;60(5):1519-1527. doi:10.2337/db10-1017

260. Sun K, Kusminski CM, Scherer PE. Adipose tissue remodeling and obesity. *J Clin Invest*. 2011;121(6):2094-2101. doi:10.1172/JCI45887

261. Fruebis J. Proteolytic cleavage product of 30-kDa adipocyte complement-related protein increases fatty acid oxidation in muscle and causes weight loss in mice. *Proc Natl Acad*

Sci. 2001;98(4):2005-2010. doi:10.1073/pnas.041591798

262. Tomas E, Tsao TS, Saha AK, et al. Enhanced muscle fat oxidation and glucose transport by ACRP30 globular domain: Acetyl-CoA carboxylase inhibition and AMP-activated protein kinase activation. *Proc Natl Acad Sci U S A*. 2002;99(25):16309-16313. doi:10.1073/pnas.222657499

263. Yamauchi T, Nio Y, Maki T, et al. Targeted disruption of AdipoR1 and AdipoR2 causes abrogation of adiponectin binding and metabolic actions. *Nat Med*. 2007;13(3):332-339. doi:10.1038/nm1557

264. Otvos L, Haspinger E, La Russa F, et al. Design and development of a peptide-based adiponectin receptor agonist for cancer treatment. *BMC Biotechnol*. 2011;11:90. doi:10.1186/1472-6750-11-90

265. Otvos L. Potential Adiponectin Receptor Response Modifier Therapeutics. *Front Endocrinol (Lausanne)*. 2019;10. doi:10.3389/fendo.2019.00539

266. Bódis K, Roden M. Energy metabolism of white adipose tissue and insulin resistance in humans. *Eur J Clin Invest*. 2018;48(11). doi:10.1111/eci.13017

267. Ahlquist RP. Present state of alpha- and beta-adrenergic drugs I. The adrenergic receptor. *Am Heart J*. 1976;92(5):661-664.

268. Sepa-Kishi DM, Ceddia RB. *White and Beige Adipocytes: Are They Metabolically Distinct?*; 2018. doi:10.1515/hmbci-2018-0003

269. Weber A, Medak KD, Townsend LK, Wright DC. Ketogenic diet-induced weight loss occurs independent of housing temperature and is followed by hyperphagia and weight regain after cessation in mice. *J Physiol*. 2022;600(21):4677-4693. doi:10.1113/JP283469

270. Beaudry KM, Devries MC. Sex-based differences in hepatic and skeletal muscle triglyceride storage and metabolism. *Appl Physiol Nutr Metab*. 2019;44(8):805-813. doi:10.1139/apnm-2018-0635

Appendix A – Methods

A. Adipocytes Isolation

White Adipose Tissue

1. Surgically excise the Sc Ing or Epid fat depots and trim away all connective tissue.

1. Finely mince AT depot using a pair of sharp, surgical scissors until AT reaches a uniform consistency.

2. Add minced AT into urine vial containing Krebs Ringer bicarbonate HEPES (KRBH) buffer (120 mM NaCl, 4.8 mM KCl, 2.5 mM $CaCl_2$, 1.2 mM KH_2PO_4, 1.2 mM $MgSO_4$, 15 mM $NaHCO_3$, 30 mM HEPES, 5.5 mM glucose) supplemented with Type II collagenase (0.5 mg/ml).

3. Incubate the AT at 37 °C with orbital shaking. Swirl gently by hand at approximately 5 min intervals. Isolation will be complete within approximately 30 minutes.

4. Strain cells through nylon mesh with a pore size of 500 µm. Transfer liquid into a falcon tube and spin the falcon tube at 1000 rpm for 30 seconds. The cells will have settled at the top of the liquid.

5. Slowly aspirate liquid beneath the cells. Once the aspiration is complete, replace the liquid with fresh KRBH. Pipette KRBH down the side of the tube and wait for cells to settle back at the top before proceeding.

6. Repeat step 6 two more times, replacing the liquid with KRBH or KRBH-3.5% BSA the final time.

8. Count the adipocytes in the preparation.

   a) Lipocrit height is determined by swirling the falcon tube to mix the cells in the buffer and extracting a 300 µl aliquot. Transfer this aliquot into a centrifuge tube and centrifuge at 1000 rpm for 30 seconds. The adipocytes will settle at the top; measure the height of the adipocytes with a ruler.

   b) Average cell diameter is determined by extracting a 20-50 ul aliquot of cell-buffer preparation, pipetting onto a slide and measuring the diameters under a microscope.

   c) Using the above measurements, calculate the number of cells in the preparation tube using the cell volume, lipocrit height and total volume of preparation.

9. Proceed to add pre-determined number of cells into reaction tubes.

Brown adipose tissue

1. Surgically excise interscapular and aortic BAT.

2. Trim any WAT, muscle or connective tissue from the BAT.

3. Add whole BAT into 50 mL falcon tube containing KRBH-4% BSA, supplemented with Type II collagenase (0.83 mg/ml). Combine both BAT depots to enhance cell yield.

4. Incubate BAT-media mixture at 37 °C, with orbital shaking, for 5 minutes.

5. Remove falcon tube from incubation and vortex for 5 secs.

6. Strain tissues through a filter and discard the filtrate.

7. Finely mince tissues with surgical scissors. Avoid crushing the tissue.

7. Add minced BAT to urine vial containing KRBH-4% BSA, supplemented with Type II collagenase.

8. Proceed with steps 4-9 in Appendix A-A.

B. Glycerol Release as an Indication of Lipolysis – Protocol for Sigma Free Glycerol Determination Kit (Cat. # FG0100-1KT).

1. Adipocytes are incubated in the absence or presence of isoproterenol.
2. Add 6 x 10^5 cells to plastic vials. Allow adipocytes to settle at the surface of the media and slowly extract an aliquot of the media for time 0 glycerol determination.
3. Add 100 nM isoproterenol to Iso-stimulated vials.
4. Incubate vials at 37 °C for 75 minutes with gentle orbital shaking.
5. At the end of the incubation period, remove vials from incubation and allow the adipocytes to settle at the surface of the media.
6. Extract a second aliquot from all vials for time 75 measurements.
7. Immediately freeze or proceed to experimental determination of glycerol in the media using the Free Glycerol Determination Kit (FG0100-1KT).
8. Dissolve glycerol reagent in one vial in 40 mL of water.
9. Add 10 µL of water, glycerol standard (Sigma, Cat. # G7793) and sample to labelled cuvettes.
10. Add 800 µL of free glycerol reagent to each of the cuvettes.
11. Mix contents of each reaction cuvette.
12. Incubate cuvettes for 5 minutes at 37 °C.
13. Read absorbance (A) at 540 nm
14. Calculate concentrations of the samples using the following equation:

    $(A_{Sample}-A_{Blank})/(A_{Standard}-A_{Blank})$ x concentration of Standard

C. Glucose/Glycerol Incorporation into Lipids

1. Add desired number of cells to buffer containing KRBH-3.5% BSA with:
    a. 0.2 µCi/mL D-[U-^{14}C] glucose for glucose incorporation into lipids assay or
    b. 0.2 µCi/mL [U-^{14}C] glycerol for glycerol incorporation into lipids assay

2. Incubate for 1 h at 37 °C with orbital shaking (80 rotations/min).

3. Following the 1 h incubation period, extract lipids according to the method of Dole and Meinertz[207].

4. Add 5 mL of Dole's reagent (isopropanol:heptane:H_2SO_4 (0.5 M), 40:10:1 vol:vol:vol) to the vials, cap and vortex vigorously for 1 min.

5. Remove cap and add 3 mL of ddH_2O and 3 mL of heptane.

6. Seal and vortex for another minute.

7. Allow vials to sit for a minimum of 20 minutes.
    a. Solution in vials will separate into an upper and lower phase.

8. Carefully extract 1 mL of the upper phase and transfer to an empty, pre-weighed vial.

9. Leave vial open in fume hood overnight to dry.

10. The following day, weigh vials again.

11. Add 5 mL of scintillation fluid to each vial, cap the vial and vortex for 15 seconds.

12. Count for radioactivity.

D. Palmitate Incorporation into Lipids

Incorporation of [1-^{14}C] palmitate in isolated adipocytes

1. In a scintillation vial, add desired number of adipocytes to KRBH-3.5% BSA containing 0.2 µCi/mL [1-^{14}C] palmitate and 200 µM non-labelled palmitate.

2. Seal vial and incubate for 1 h at 37 °C with orbital shaking (80 rotations/min).

3. Carefully transfer the adipocyte and incubation media to 2 mL Eppendorf tubes and centrifuge at 3000 x g for 1 min.
4. Discard the media, wash adipocytes with PBS (1 mL) and centrifuge again at 3000 x g for 1 min.

5. Repeat step 4 two more times.

6. Discard the PBS and freeze the adipocytes at -80 °C.

Folch's Method of Lipid Extraction

1. Remove samples from freezer.

2. Add 600 µL of chloroform:methanol (2:1, vol:vol) to the adipocytes and vortex for 30s.

3. Centrifuge the samples at 3000 x g for 5 min at 4 °C.

4. Extract the upper chloroform phase into an empty tube and dry with nitrogen gas overnight.

5. The next morning, resuspend in 50 µL of chloroform:methanol (2:1, vol:vol).

Thin Layer Chromatography (TLC)

1. Draw a line on a Whatman TLC plate 2 cm from the bottom of the plate.

2. On the reference line, load 4 µL of TAG standard (triolein) and samples.

3. To a TLC experiment unit add 200 mL of mobile phase (hexane:diethyl ether:acetic acid, 70:30:1, vol:vol:vol).

4. Place TLC plate in experiment unit.

5. Once the mobile phase runs up 80% of the plate, remove the plate from the experiment unit and allow both to air dry for 10 min.

6. Put TLC plate back into the experiment unit and add iodine for the visualization of TAG.

7. Once spots become visible, scrape spots that are in line with the TAG standard.

8. Transfer the scraping-derived debris into scintillation vials pre-filled with 5 mL of scintillation fluid.

9. Count for radioactivity.

E. Glucose and Palmitate Oxidation

For adipocytes:

1. Add desired number of adipocytes to buffer containing 1.5 mL of
    a. Glucose oxidation buffer: KRBH-3.5% BSA with 0.2 µCi/mL D-[U-^{14}C] glucose
    b. Palmitate oxidation buffer: KRBH-3.5% BSA with 0.2 µCi/mL 1-[^{14}C] palmitate and 200 µM non-labelled palmitate
        - To assess the effect of β-adrenergic stimulation on oxidation, 100 nM of isoproterenol (Iso) was added to the appropriate vials.
        - To measure uncoupled oxidation, 100 µM oligomycin (Oligo) was added to the appropriate vials 15 minutes prior to incubation with or without Iso.

2. Insert tube containing loosely folded piece of filter paper into reaction vial and seal with a rubber stopper.

3. Incubate for 1 h at 37 °C with orbital shaking (80 rotations/min).

4. Following the incubation period, use a syringe to wet the filter paper inside the reaction vial with 0.2 mL of 2-phenylethylamine/methanol (1:1, vol/vol) for the collection of $^{14}CO_2$.

5. With a separate syringe, acidify the media with 0.2 mL of H_2SO_4 (5N) for the release of $^{14}CO_2$..

6. Incubate vials for another hour at 37 °C with orbital shaking.

7. Subsequently, remove the rubber stopper from the vials, carefully extract filter paper and add to a separate set of scintillation vial containing scintillation fluid.

8. Proceed to count for radioactivity.

For muscle:

1. Extract muscle and attach each end of a carefully sliced muscle strip to a stainless-steel pin.

2. Add pinned muscle to vial containing KRBH-3.5% BSA. Seal vial and incubate at 37 °C, for one hour, with gentle shaking and continuous gasification.

3. Remove muscle from pre-incubation vial and add to 2 mL of glucose or palmitate oxidation buffers described in D-1a and 1b.

4. Add Eppendorf tube with loosely folded piece of filter paper pre-moistened with 0.2 mL of 2-phenylethylamine/methanol (1:1, vol/vol) for the collection of $^{14}CO_2$.

5. Incubate for 1 h at 37 °C with orbital shaking (80 rotations/min). Maintain continuous gasification.

6. Following the 1 h reaction incubation, remove muscle, wash in PBS and detach from pin. Immediately freeze the muscle strip in liquid nitrogen and use this muscle strip to proceed with the Glycogen Synthesis Assay (Appendix A-F).

7. Re-seal vial with rubber stopper, acidify media with 0.2 mL of H_2SO_4 (5N) for release of $^{14}CO_2$ and incubate again for 1 h at 37 °C with orbital shaking.

8. Subsequently, remove the rubber stopper from the vials, carefully extract filter paper and add to a separate set of scintillation vial containing scintillation fluid.

9. Proceed to count for radioactivity.

F. Glucose Uptake in Adipocytes

1. Add desired number of cells to flat bottom tubes.

2. Add varying concentrations of ALY688 to vials.

3. Incubate for 1 h at 37 °C with orbital shaking (80 rotations/min).

4. In the final 20 mins of the incubation period, add insulin (10 or 100 nM) to the appropriate tubes.

5. At the end of the hour, add KRBH-1% BSA containing 0.5 mM 2-deoxy-D-glucose and 0.5 µCi/mL of 2-[1,2-^{3}H]deoxy-D-glucose to all vials and incubate for 3 min at 37 °C with orbital shaking.

6. Add 1.5 mM cytochalasin B to stop glucose uptake in the cells.
    a. For the measurement of non-specific transport, have two tubes with adipocytes and add cytochalasin B prior to the radioactive medium.

7. Extract 240 µL aliquots of adipocyte suspension and transfer to centrifuge tubes containing 125 µL of di-'isononyl' phthalate.

8. Centrifuge the tubes for 30 seconds at 6000 x g to separate the cells from the radioactive media.

9. Cut through the oil phase using a sharp box-cutter.

10. Transfer the part of the tube containing the adipocytes into a scintillation vial containing 5 ml of scintillation fluid.

11. Seal and shake the scintillation vials, and count for radioactivity.

G. Glycogen Synthesis

1. Take the muscle strip used in the Glucose Oxidation Assay (Appendix A-D), wash in ice cold PBS, blot dry and freeze immediately in liquid nitrogen.

2. Place the muscle strip in 500 µL of 1N KOH at 65° C for 30 min or until completed digested. Vortex samples following digestion.

3. Remove a 100 µL aliquot for other experiments and use the remaining 400 µL for the determination of glycogen synthesis.

4. To the 400 µL sample add:

- 100 µL of glycogen carrier (25 mg/mL)
- 80 µL of saturated Na_2SO_4
- 1.2 mL of 100%, ice cold ethanol

5. Gently vortex each sample (30 s) and incubate overnight at -20° C. A precipitate will form.

6. The next day, remove the samples from the freezer and centrifuge at 3000 rpm for 20 min.

7. Decant the supernatant by dabbing on Kimwipes and resuspend the remaining precipitate in 500 µL ddH_2O.

8. From this solution, transfer a 400 µL aliquot into a scintillation vial containing 5 mL of scintillation fluid.

9. Count for radioactivity.

H. Lactate determination by the Colorimetric/Fluorimetric Lactate Assay Kit (Biovision, Cat. #: K607)

1. Using 10-kDa molecular weight spin columns, filter samples prior to running the assay.

2. Prepare lactate standards using the kit. Mix 990 µL of Assay Buffer with 10 µL of the included standard.

3. Load 0, 2, 4, 6, 8 and 10 µL of the prepared standard into a 96-well plate. This will correspond to 0, 2, 4, 6, 8 and 10 nmol/well for the standards. Bring volume to 50 µL with Assay Buffer.

4. Load up to 50 µL of sample per well. If sample is less than 50 µL, adjust volume to 50 µL with Assay Buffer.

5. To each well, add 46 µL of Assay buffer, 2 µL of Lactate Enzyme (resuspended in Assay Buffer) and 2 µL of Lactate Probe. Mix well.

6. Incubate plate for 30 mins at room temperature. Protect the plate from light.

7. Using a plate reader, read absorbance at 570 nm.

I. Western Blotting

Protein extraction

1. Add 50 mg of lung, heart and skeletal muscle tissue to 200 µL of lysis buffer (25 mM Tris-HCl, 25 mM NaCl (pH 7.4), 1 mM $MgCl_2$, 2.7 mM KCl, 10% glycerol and 1% Triton X-100). For adipose tissue samples, add 200 mg of tissue to the same volume of lysis buffer.

2. Homogenize tissues using a homogenizer.

3. Sonicate lysates for 9 seconds and then centrifuge at 13, 200 RPM for 10 mins at 4 °C.

4. For the lung, heart, and skeletal muscle samples, extract the supernatant and transfer to an empty tube. Adipose tissue samples will yield a layer of fat at the top. Extract the infranatant and transfer to a new tube.

5. Determine the protein concentration of the lysates using the Bradford method.

6. Aliquot lysates and store at -80 °C until electrophoresis.

Western blotting

1. Buffers

    1.1. 2x Laemmli sample buffer (Bio-Rad Laboratories, Cat. #:161-0737)
        1. Prepare sample buffer by adding 50 µL of β-mercaptoethanol to 950 µL of Laemmli buffer.
        2. Dilute samples 1:1 with prepared sample buffer, boil for 5 mins at 95 °C and allow samples to cool. Quickly centrifuge prior to loading.

    1.2. 1.5 M Tris-HCl (pH 8.8)
        1. Add 27.3 g of Tris base to 80 mL of ddH_2O and mix.
        2. Use 6N HCl to adjust pH to 8.8.
        3. Bring volume to 150 mL with ddH_2O.

    1.3. 0.5 M Tris-HCl (pH 6.8)
        1. Add 6 g of Tris base to 60 mL of ddH_2O and mix.
        2. Adjust pH to 6.8 with 6 N HCl.
        3. Bring volume to 100 mL with ddH_2O.

    1.4.10x Electrode (Running) Buffer
        Dissolve 30.3 g of Tris base, 144 g of glycine and 10 g of SDS in ddH_2O. Bring total volume to 1 L.

2. Gel formulation

2.1.Prepare resolving layer of gel using the following recipe:

% Gel	ddH$_2$O (mL)		30% Acrylamide/Bis (mL)		1.5 M Tris-HCl (pH 8.8) (mL)		10% SDS (mL)	
	2 Gels	4 Gels	2 Gels	4 Gels	2 Gels	4 Gels	2 Gels	4 Gels
8	8.05	16.1	4.53	9.06	4.25	8.5	0.17	0.34
10	6.91	13.82	5.67	11.34	4.25	8.5	0.17	0.34
12	5.78	11.56	6.8	13.6	4.25	8.5	0.17	0.34

2.2. Add 10% APS (100 µL for 2 gels and 200 µL for 4 gels) and TEMED (20 µL for 2 gels and 40 µL for 4 gels) to polymerize gels and add to glass gel casting plates immediately.

2.3.Once the resolving gel has polymerized, make a stacking layer using the following formulation:

ddH$_2$O (mL)		30% Acrylamide/Bis (mL)		0.5 M Tris-HCl (pH 6.8) (mL)		10% SDS (mL)	
2 Gels	4 Gels	2 Gels	4 Gels	2 Gels	4 Gels	2 Gels	4 Gels
3.94	7.88	0.87	1.73	1.63	3.25	0.065	0.13

2.4.Add 10% APS (50 µL and 100 µL for 2 and 4 gels, respectively) and TEMED (10 µL and 20 µL for 2 and 4 gels, respectively). Mix and immediately add on top of resolving layer. Insert combs to form wells.

2.4.1. Following approximately 20 minutes, insert gels into running apparatus and fill with 1x running buffer.

3. Loading and running the gels

Load samples in wells and run the gels for approximately 2 h at 110 V. Prepare transfer buffer in the meanwhile.

3.1. 10x Transfer buffer

Dissolve 30.3 g of Tris base and 144 g of glycine in ddH$_2$O and bring total volume to 1 L.

3.2. 1x Transfer buffer

7 parts ddH$_2$O: 2 parts methanol: 1 part 10x transfer buffer. Leave in -20 °C freezer to cool

4. Wet transfer

4.1. Activate PVDF membranes by soaking in methanol for 30 sec. Rinse membranes with ddH_2O and soak again in 1x Transfer buffer.

4.2. Add enough 1x transfer buffer to a casserole dish to cover the bottom. Assemble a transfer "*sandwich*".

4.3. Assemble the transfer "sandwich" starting with a transfer cassette, black side down, on the casserole dish.

4.4. Add a foam pad and two sheets of pre-cut filter paper that had been pre-soaked in the 1x transfer buffer.

4.5. Remove one of the gels from the running apparatus. Using a pick, open the glass plates carefully and soak the gel in the transfer buffer in the casserole dish to prevent drying.

4.6. Gentle remove the gel from the large glass casting plate and place it on the filter paper in the sandwich.

4.7. Add a membrane onto the gel and roll out any bubbles that exist between the membrane and gel using a roller.

4.8. Add two pieces of pre-soaked filter paper on top of the membrane, rolling out bubbles between each.

4.9. Add a foam pad and seal the transfer cassette.

4.10. Place in transfer apparatus. Fill with 1x transfer buffer and add ice pack to the transfer apparatus.

4.11. Place lid on the apparatus and transfer under the following conditions: 120V for 2 h.

4.12. Following the transfer, prepare for blocking and probing the membrane.

5. Washing and blocking buffers

5.1.10x Wash buffer (1 L)

To make 1 L of 10x wash buffer dissolve 60.57 g of Tris base and 87.66 g of NaCl in ddH_2O.

5.2.1x Wash buffer (1 L)

1. Dilute 10x wash buffer to 1x using ddH_2O.
2. While the magnetic stirrer is spinning, add 0.5 mL of Tween and 0.5 mL of Nonidet P40.

5.3. Blocking buffer (3%)

Add 1.5 g of BSA to 50 mL of 1x wash buffer.

6. Blocking the membrane

6.1. Move membranes into containers.

6.2. Add 5 mL of blocking buffer to each membrane and incubate, with gentle shaking, for 1 h at room temperature.

7. Probing with antibodies

7.1. Discard the blocking buffer and add primary antibody of interest in blocking buffer.

7.2. Incubate membrane with primary antibody overnight at 4°C or for 2 h at room temperature.

7.3. Following the incubation period, discard the antibody from the membrane container and wash with 1x wash buffer 3 times, 15 minutes each wash.

7.4. Dilute secondary antibody in blocking buffer and add to membrane. Incubate for 1 h at room temperature.

7.5. Discard secondary antibody and wash membrane again using 1x wash buffer. Wash 3 times, 15 minutes each wash.

8. Developing the membrane

8.1. Discard the wash buffer after the final wash.

8.2. Add 2.5 mL of Immobilon Forte Western HRP Substrate (Millipore, Cat. #: WBLUF0500) and shake by hand for 2 minutes.

8.3. Discard the Immobilon and place the membrane in the developing cassette.

8.4. In the dark room, Cut a piece of x-ray film and carefully place over the membrane on the plastic cover.

8.5. Following the desired exposure time, extract the film using a pair of tongs and dip in developer solution until signal begins to appear.

8.6. Rinse film in water and place film in fixer solution.

8.7. Once the film has been adequately fixed, rinse excess fixer solution under running water.

J. qPCR

RNA extraction using Trizol reagent (Invitrogen)

1. Add 50-100 mg of tissue to 1 mL of Trizol reagent.
2. Homogenize tissues rapidly and incubate at room temperature for 5 mins.
3. Add 0.2 mL of chloroform to each sample, shake vigorously for 15 seconds and incubate at room temperature for 2-3 mins.
4. Centrifuge samples at 13, 200 RPM for 15 mins at 4 °C. The sample will separate into three phases.
5. Remove the upper aqueous phase into a separate empty tube.
6. Add 0.5 mL of isopropanol and invert the tube several times to mix.
7. Incubate again at room temperature for 10 mins.
8. Centrifuge at 13, 200 RPM for 10 mins at 4 °C.
9. The RNA pellet will become visible following centrifugation. Discard isopropanol surrounding the pellet and resuspend the pellet in 1 mL of 75% ethanol.
10. Centrifuge the sample at 13, 200 RPM for 10 min at 4° C.
11. Discard the existing ethanol and re-suspend the pellet once more in 75% ethanol.
12. Centrifuge again, this time for 5 mins.
13. Discard the ethanol and allow the pellet to air dry for 5-10 minutes.
14. Re-suspend the pellet in 20-50 µL of RNase-free water.

RNA extraction using the RNeasy Lipid Tissue Mini Kit (Qiagen, cat. #:74804)

1. Homogenize tissues or cells in 1 mL of QIAzol Lysis Reagent.

2. Incubate for 5 mins at room temperature.

3. Add 0.2 mL of chloroform and shake for 15 s.

4. Allow the samples to sit at room temperature for 2-3 minutes.

5. Centrifuge the samples at 12, 000 x g for 15 mins at 4 °C.

6. Transfer the upper phase of the centrifuged homogenate to a new tube.

7. Add 70% ethanol (one volume) to each sample and vortex.

8. The kit includes spin columns inserted into 2 mL collection tubes. Transfer 700 µL of sample to a spin column.

9. Centrifuge at room temperature for 15s at minimum 8000 x g. Discard flow through liquid.

10. Repeat steps 8 and 9 for the remaining sample.

11. Add 700 µL of Buffer RW1 to the column and centrifuge at room temperature for 15 s at a minimum speed of 8000 x g. Discard the flow through liquid.

12. Prepare Buffer RPE by adding 4 parts of 100% ethanol. Add 500 µL of Buffer RPE to the column and spin at a minimum of 8000 x g for 15 s at room temperature. Discard flow through liquid.

13. Add 500 µL of Buffer RPE to each column and spin for 2 mins at a minimum of 8000 x g.

14. Transfer the spin column to a new tube, add 30-50 µL of RNase-free water and spin for 1 min at a minimum of 8000 x g.

cDNA Synthesis

1. Synthesize cDNA from 2 µg of RNA using the ABM OneScript cDNA Synthesis kit (Diamed).

2. Into microtubes, add volume of RNA corresponding to 2 µg.

3. Bring total volume to 12.5 µL with RNase-free water.

4. Add 1 µL of random primers and 1 µL of dNTP to each sample.

5. Gently mix, centrifuge briefly and incubate for 5 mins at 65 °C.

6. Leave samples on ice for 1 min and centrifuge briefly, thereafter.

7. To each sample, add 4 µL of 5x RT buffer, 1 µL of OneScript and 0.5 µL of RNase OFF Ribonuclease inhibitor.

8. Mix gently, centrifuge briefly and heat samples to 25 °C for 10 mins.

9. For cDNA synthesis, heat samples to 42 °C for 50 mins.

10. To terminate the reaction, heat samples to 85 °C for 5 mins.

11. Allow samples to cool on ice. They are ready for downstream applications or can be stored at -20 °C until use.

qPCR

1. In a 96-well PCR plate, load 10 ng of sample per well.

2. Add master mix of primer of interest to each well. Master mix will consist of 5.6 µL of RNase-free water, 0.4 µL of forward and reverse primers and 10 µL of ABM Brightgreen 2x qPCR Master mix.

3. Seal plate and centrifuge for 5 mins at 2500 RPM (4 °C).

4. Using a BioRad Thermal Cycler, set amplification conditions to 40 cycles of 95 °C (15s), 60 °C (1 min).

5. Results are normalized to the housekeeping gene and values are calculated using the ΔΔCt method[188].

K. Insulin ELISA (Millipore, Cat. #: EZRMI-13K)

1. Dilute 10x wash buffer in ddH_2O.

2. Wash the wells of the Assay plate with 300 µL of 1x wash buffer 3 times. Discard wash buffer between washes by tapping the plate against clean filter paper.

3. Load 10 µL of Assay buffer in Blank and Sample wells.

4. Load 10 µL of Matrix solution to Blank, Standard and Control wells.

5. Load 10 µL of Standards, Samples and Controls to the appropriate wells.

6. Add 80 µL of Detection Antibody to all wells, seal plate and incubate with orbital shaking for 2 h at room temperature.

7. Remove plate sealer and decant liquid from wells.

8. Wash plate 3 times with 300 µL of wash buffer. Decant liquid between washes.

9. Add 100 µL of Enzyme Solution to all wells. Seal the plate and incubate for 30 mins at room temperature with orbital shaking.

10. Remove plate sealer, decant liquid from wells and wash plate 6 times with 300 µL of wash buffer.

11. Add 100 µL of Substrate Solution to all wells. Seal and incubate for 5-20 minutes at room temperature with orbital shaking. Blue colour should form in Standard wells with intensities corresponding to concentrations.

12. Add 100 µL of Stop Solution. Shake by hand and read absorbance at 450 nm and 590 nm. Be sure there are no air bubbles in the wells.

13. Determine sample concentrations from standard curve.

L. β-hydroxybutyrate determination using the Abcam βHB Colorimetric Assay Kit (Abcam, cat. #: ab83390)

1. Reconstitute βHB standard in 100 µL of ddH_2O and dilute this standard preparation by adding 10 µL to 90 µL of ddH_2O. The concentration of the prepared standard is 1 mM. Prepare standard curve by making the following dilutions and loading 50 µL of each standard per well in a 96-well plate.

Volume of standard (µL)	Volume of assay buffer (µL)	nmol/well
0	150	0
6	144	2
12	138	4
18	132	6
24	126	8
30	120	10

2. Load 1-50 µL of sample per well.

3. Bring total volume of sample wells to 50 µL with Assay Buffer.

4. Add 46 µL of Assay Buffer, 2 µL of Enzyme Mix and 2 µL of Substrate Mix to each standard and sample.

    - Substrate and Enzyme mixes must be reconstituted in 220 µL of Assay Buffer prior to use.

5. Incubate plate at room temperature for 30 mins in the dark.

6. Read OD at 450 nm.

Appendix B – Published Manuscripts

The Journal of Physiology

J Physiol 601.1 (2023) pp 69–82

An obesogenic diet impairs uncoupled substrate oxidation and promotes whitening of the brown adipose tissue in rats

Daniel Da Eira, Shailee Jani and Rolando B. Ceddia

Muscle Health Research Centre, School of Kinesiology and Health Science, York University, Toronto, Ontario, Canada

Handling Editors: Michael Hogan & Bettina Mittendorfer

The peer review history is available in the Supporting information section of this article (https://doi.org/10.1113/JP283721#support-information-section).

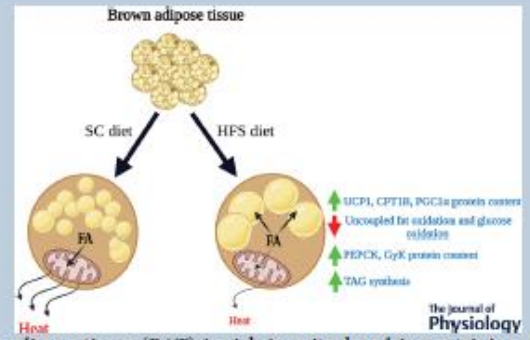

Abstract Brown adipose tissue (BAT) is rich in mitochondria containing uncoupling protein 1 (UCP1), and dissipates energy through thermogenesis. However, even though BAT mass and its UCP1 content increase in rodents chronically fed a high-fat sucrose-enriched (HFS) diet, marked expansion of adiposity still occurs in these animals, suggesting insufficient BAT-mediated HFS diet-induced thermogenesis. Thus, the objective of this study was to investigate the metabolic and molecular mechanisms that regulate BAT thermogenesis in HFS-induced obesity. To accomplish this, rats were fed either a standard chow or HFS diet for 8 weeks. Subsequently, glucose and fatty acid metabolism and the molecular mechanisms underlying these processes were assessed in freshly isolated primary BAT adipocytes. Despite increasing BAT mass and its UCP1 content, the HFS diet reduced uncoupled glucose and palmitate oxidation in BAT adipocytes. It also markedly diminished tyrosine hydroxylase content and lipolysis in these cells. Conversely, glucose uptake, lactate production, glycerol incorporation into lipids, palmitate incorporation into triacylglycerol (TAG), phosphoenolpyruvate carboxykinase and glycerol kinase levels, and lipoprotein lipase and cluster of differentiation 36 gene expression were increased. In summary, a HFS diet enhanced

Daniel Da Eira is a PhD candidate in the School of Kinesiology and Health Science at York University, where he also completed his undergraduate and master's degrees. His Master's research focused on the effects of diet-induced obesity on the thermogenic capacity of brown adipose tissue. As such, he has investigated the mechanisms that regulate fat and glucose metabolism leading to either energy storage or dissipation in brown and beige adipocytes. At present he is completing his doctoral work investigating the impact of a ketogenic diet on the thermogenic machinery in brown and white adipose tissues, as well as the influence of this diet on components of the renin–angiotensin system in brown and white fat.

DOI: 10.1113/JP283721

glyceroneogenesis and shifted BAT metabolism toward TAG synthesis by impairing UCP1-mediated substrate oxidation and by enhancing fatty acid esterification in intact brown adipocytes. These adaptive metabolic responses to chronic HFS feeding attenuated BAT thermogenic capacity and favoured the development of obesity.

(Received 10 August 2022; accepted after revision 9 November 2022; first published online 23 November 2022)
Corresponding author R. B. Ceddia: Muscle Health Research Center, School of Kinesiology and Health Science, York University, 4700 Keele St, North York, ON M3J 1P3, Canada. Email: roceddia@yorku.ca

Abstract figure legend In brown adipocytes from lean rats fed a standard laboratory chow (SC) diet, glucose and fatty acids (FA) were diverted essentially toward uncoupling protein 1 (UCP1)-mediated substrate oxidation and thermogenesis. Conversely, in brown adipose tissue (BAT) of rats fed a high-fat sucrose-enriched (HFS) obesogenic diet, despite increases in UCP1, carnitine palmitoyltransferase 1B (CPT1B), and peroxisome proliferator-activated receptor γ coactivator 1α (PGC-1α) contents, substrate metabolism was shifted toward triacylglycerol (TAG) synthesis/storage. This was characterized by reduced UCP1-mediated glucose and fatty acid oxidation. These adaptive responses to a chronic HFS diet were supported by increased contents of phosphoenolpyruvate carboxykinase (PEPCK) and glycerol kinase (GyK).

Key points

- Despite increasing brown adipose tissue (BAT) mass and levels of thermogenic proteins such as peroxisome proliferator-activated receptor γ coactivator 1α, carnitine palmitoyltransferase 1B and uncoupling protein 1 (UCP1), an obesogenic high-fat sucrose-enriched (HFS) diet attenuated uncoupled glucose and fatty acid oxidation in brown adipocytes.
- Brown adipocytes diverted glycerol and fatty acids toward triacylglycerol (TAG) synthesis by elevating the cellular machinery that promotes fatty acid uptake along with phosphoenolpyruvate carboxykinase and glycerol kinase levels.
- The HFS diet increased glucose uptake that supported lactate production and provided substrate for glyceroneogenesis and TAG synthesis in brown adipocytes.
- Impaired UCP-1-mediated thermogenic capacity and enhanced TAG storage in BAT adipocytes were consistent with reduced adipose triglyceride lipase and tyrosine hydroxylase levels in HFS diet-fed animals.

Introduction

Despite variations in the availability of food/energy, body weight can be maintained relatively constant over long periods of time (Rosenbaum & Leibel, 1998). This is possible because under conditions of food abundance and overeating, the organism activates mechanisms that promote energy dissipation and attenuate weight gain. Conversely, under conditions of food scarcity and reduced intake, energy-sparing mechanisms are activated and oppose weight loss (Leibel, 2008; Trayhurn, 2017). These adaptive metabolic responses are referred to as diet-induced thermogenesis (DIT), and play an important role in regulating body weight and whole-body energy homeostasis (Trayhurn, 2017). The ability to dissipate energy under conditions of overeating has been, at least partially, attributed to sympathetic nervous system (SNS)-mediated activation of brown adipose tissue (BAT) (Trayhurn, 2017). This is because uncoupling protein 1 (UCP1) uncouples oxidative phosphorylation from ATP synthesis, resulting in the production of heat in a process known as non-shivering thermogenesis (NST) (Barbara & Nedergaard, 2004; Kozak, 2010; Trayhurn, 2017). This process is triggered by the release of noradrenaline that binds to β-adrenergic receptors on brown adipocytes and promotes lipolysis within the cells. The release of fatty acids (FA) then leads to the activation of UCP1 that ultimately promotes mitochondrial uncoupling and NST in BAT adipocytes (Barbara & Nedergaard, 2004; Fedorenko et al., 2013).

A role for BAT in DIT is supported by studies demonstrating that the mass of this tissue expands and its UCP1 content increases under diet-induced obesity (DIO) conditions in rats (So et al., 2011; Wu et al., 2014), and also by the fact that UCP1 ablation causes obesity in mice living at thermoneutrality (Feldmann et al., 2009). However, despite evidence of tissue enlargement and increased UCP1 content in BAT, great expansion of adiposity still occurs in animals subject to DIO (So et al., 2011; Wu et al.,

2014). This suggests that NST is either insufficient to offset the energy surplus or that it might even be suppressed under conditions of chronic overeating. In both cases the magnitude of energy dissipation through NST in BAT would be limited, allowing for extensive growth of the white adipose tissue (WAT) to occur. In this context, we have found that in the first and second weeks of feeding rats *ad libitum* a high-fat sucrose-enriched (HFS) diet, whole-body energy expenditure increased by ∼14 and 11%, respectively, in comparison to standard laboratory chow (SC) diet-fed controls (So et al., 2011). However, as HFS feeding continued through six additional weeks, whole-body energy expenditure no longer differed from that of SC diet fed rats (So et al., 2011), suggesting that an initial thermogenic response was mounted, but it was not sustained in rats chronically exposed to a HFS diet. Thus, it could be that NST in BAT was suppressed in a time-dependent manner, even though expansion of tissue mass and its UCP1 content persisted with continued overfeeding. This is consistent with recent human studies using ^{18}F-labelled fluorodeoxyglucose positron emission tomography–computed tomography to measure BAT volume and its activity in lean and obese subjects (Leitner et al., 2017). In fact, it has been reported that after 5 h of tolerable cold exposure (16°C), activated BAT in obese men corresponded to only ∼39% of that of lean counterparts, even though the total volume of BAT-containing depots was almost two-fold higher in the former than the latter group of subjects (Leitner et al., 2017). Thus, it was clear that BAT mass was increased in obese subjects, whereas its recruitment for thermogenesis was not (Leitner et al., 2017). We have previously reported that the HFS diet-induced increase in BAT UCP1 levels was accompanied by increased rates of fatty acid oxidation in homogenized BAT samples (So et al., 2011; Wu et al., 2014). This was consistent with an enhanced machinery that consumes substrate under conditions of activated NST. However, any regulatory mechanisms that could potentially regulate substrate consumption in BAT adipocytes was lost in tissue homogenates. It could be that, in intact BAT adipocytes, cellular regulatory mechanisms shift the flux of substrate toward pathways that promote storage as opposed to energy dissipation. This could help explain why increased BAT tissue mass and UCP1 levels do not prevent adipose tissue expansion in rodents and humans under conditions of DIO. In this context, the objective of this study was to investigate the molecular and metabolic mechanisms that regulate DIT in BAT under conditions of DIO and identify alterations in substrate flux that could lead to fat accumulation instead of energy dissipation. To this end, rats were fed either a SC or a HFS diet for 8 weeks. Subsequently, glucose and fat metabolism and the molecular mechanisms underlying these processes were assessed in freshly isolated intact BAT adipocytes. A detailed assessment of the metabolic pathways that regulate energy storage and dissipation in BAT adipocytes was performed. We found that despite increased tissue mass and UCP1 content in BAT, chronic exposure to a HFS diet reduced UCP1-mediated glucose and fat oxidation, attenuated lipolysis and shifted metabolism towards TAG synthesis/storage in intact brown adipocytes. Altogether, these molecular and metabolic changes induced by chronic exposure to an obesogenic HFS diet contributed to lower uncoupled substrate oxidation in BAT and favoured the development of obesity.

Methods

Ethical approval

The investigators understand the ethical principles under which *The Journal* operates and their work complies with *The Journal*'s animal ethics checklist. The protocol containing all animal procedures described in this study was specifically approved by the Committee on the Ethics of Animal Experiments of York University (York University Animal Care Committee, YUACC, permit number: 2021-03) and was performed strictly in accordance with the YUACC guidelines. All tissue extraction procedures were performed under ketamine/xylazine anaesthesia (90 mg and 10 mg/100 g body weight, respectively), and all efforts were made to minimize suffering. Upon completion of tissue extraction, all animals were decapitated. All experiments in this study were carried out in compliance with the ARRIVE guidelines.

Reagents

Type II collagenase, isoproterenol, FA-free bovine serum albumin (BSA), palmitic acid, and the free glycerol determination kit were purchased from Sigma (St Louis, MO, USA). Oligomycin was purchased from Cayman Chemical (Ann Arbor, MI, USA). [1-^{14}C]Palmitic acid, [U-^{14}C]glycerol and D-[U-^{14}C]glucose were purchased from American Radiolabelled Chemicals (St Louis, MO, USA). The lactate assay kit was from BioVision (Milpitas, CA, USA). Protease (cOmplete Ultra Tablets) and phosphatase (PhosSTOP) inhibitors were obtained from Roche Diagnostics GmbH (Mannheim, Germany). β-Actin (cat. no. 4967), tyrosine hydroxylase (TH; cat. no. 2792), adipose triglyceride lipase (ATGL; cat. no. 2138), hormone-sensitive lipase (HSL; cat. no. 4107), and pHSL$_{Ser660}$ (cat. no. 4126) antibodies were purchased from Cell Signaling Technology (Danvers, MA, USA). β_3-adrenergic receptor (β_3-AdR, cat. no. sc-50 436) and glucose transporter 4 (GLUT4, cat. no. sc-7938) antibodies were purchased from Santa Cruz Biotechnology (Dallas, TX, USA). Carnitine palmitoyltransferase 1B

(CPT1B, cat. no. PB9491) antibody was purchased from BosterBio (Pleasanton, CA, USA). Glucose transporter 1 (GLUT1, cat. no. ab115730), glycerol kinase (GYK) (cat. no. ab180525), phosphoenolpyruvate carboxykinase cytoplasmic (PEPCK-C, cat. no. ab28455), and uncoupling protein 1 (UCP1, cat. no. ab23841) were purchased from Abcam (Toronto, ON, Canada). Peroxisome proliferator-activated receptor γ coactivator-1α (PGC-1α, cat. no. AB3242) antibody was purchased from Millipore (Temecula, CA, USA).

Animals and diet

Male albino rats (Wistar strain) at approximately 250 g were group-housed at 22°C on a 12/12-h light–dark cycle. These rats were assigned to either a standard laboratory chow (SC) diet (27% protein, 13% fat and 60% carbohydrates from Test Diet cat. no.5012, Richmond, IN, USA) group or a high-fat sucrose-enriched (HFS) diet (20% protein, 60% fat (laird/soybean oil), 20% carbohydrates (sucrose); from Research Diets, cat. no. D12492, New Brunswick, NJ, USA) group and were fed *ad libitum* for 8 weeks. After 8 weeks of feeding, animals were anaesthetized and tissues were harvested for experiments.

Body weight and fat mass

Changes in body weight were measured by comparing weekly weight recordings to a baseline measurement. Interscapular brown adipose tissue (iBAT), aortic BAT (aBAT), subcutaneous inguinal (Sc Ing), and epididymal (Epid) fat pads were extracted, trimmed of any non-fat tissue and individually weighed.

Brown adipose tissue extraction and brown adipocyte isolation

iBAT and aBAT were extracted and carefully trimmed of any muscle, connective tissue and white fat and used for adipocyte isolation as previously described (Cannon & Nedergaard, 2001). iBAT and aBAT were combined to maximize the yield of brown adipocytes. The tissues were initially incubated in Krebs–Ringer bicarbonate HEPES (KRBH) buffer prepared fresh on the day of each experiment from stock solutions of salts and buffers (stored at 4°C) to give the following final concentrations: 120 mM NaCl, 4.8 mM KCl, 2.5 mM $CaCl_2$, 1.2 mM KH_2PO_4, 1.2 mM $MgSO_4$, 15 mM $NaHCO_3$ and 30 mM HEPES. The solution was gassed for 45 min with carbogen (95% O_2, 5% CO_2) and then bovine serum albumin (4%) and glucose (5.5 mM) were added. The pH of the buffer was adjusted to 7.4 with NaOH before use. Subsequently, the combined tissues were vortexed for 5 s and filtered, with the filtrate being discarded. The remaining tissues were finely minced and incubated in fresh KRBH–4% BSA containing collagenase (0.83 mg ml^{-1}) at 37°C under orbital agitation (120 orbital strokes/min) for about 20–30 min. The digested tissue was then strained using a nylon mesh and isolated cells were transferred to plastic tubes, washed three times, and resuspended in KRBH containing 3.5% FA-free BSA (KRBH–3.5% BSA). In order to distribute an equal number of adipocytes in each treatment condition, cell diameters were measured and total cell counts were determined (Fine & DiGirolamo, 1997).

Glucose and palmitate oxidation

Glucose and palmitate oxidation as a measure of oxidative capacity were assessed by $^{14}CO_2$ release in isolated BAT adipocytes (5×10^5 cells) as previously described (Gaidhu et al., 2011). Adipocytes were incubated in KRBH–3.5% BSA containing either 0.2 μCi ml^{-1} of [1-^{14}C]palmitic acid and 200 μM non-labelled palmitate, or 0.2 μCi ml^{-1} of D-[U-^{14}C]glucose and 5.5 mM non-labelled D-glucose for 1 h. To examine the effect of lipolysis on substrate oxidation, the β-agonist isoproterenol (Iso, 100 nM) was added to the medium. To distinguish substrate oxidation for ATP production (coupled respiration) from UCP1-mediated proton leak (uncoupled respiration), the ATP synthase inhibitor oligomycin (Oligo, 100 μM) was added to cells 15 min prior to the incubation in the absence or presence of Iso. Following the 1 h incubation period, the media were acidified using 0.2 ml of H_2SO_4 (5 M) and kept sealed for one additional hour for the release and collection of $^{14}CO_2$ from the cells and media. The incubation vials were prepared with a centred well containing a filter paper that was moistened with 0.2 ml of 2-phenylethylamine–methanol (1:1, v:v) for the capture of $^{14}CO_2$. At the end of the incubation, the filter paper was removed from the well and placed in scintillation fluid for radioactive counting (Gaidhu et al., 2009, 2010).

Lipolysis

Lipolysis was measured in isolated BAT adipocytes (7.5×10^5 cells). Each assay was conducted in triplicate and samples were incubated for 75 min at 37°C with gentle shaking (50 orbital strokes/min). Following the incubation, a 200 μl aliquot of the incubation medium was extracted from each vial for the determination of glycerol concentration.

Glycerol incorporation into lipids and palmitate incorporation into TAG

Glycerol incorporation into lipids and palmitate incorporation into TAG were measured using isolated BAT adipocytes (5×10^5 cells). Adipocytes were

incubated in KRBH–3.5% BSA containing 0.2 μCi ml^{-1} of [U-^{14}C]glycerol for 1 h. Subsequently, lipid extraction took place according to the method of Dole & & Meinertz (1960) and counted for radioactivity (Gaidhu et al., 2009). Palmitate incorporation into TAG was measured in isolated BAT adipocytes (5×10^5 cells) incubated in KRBH–3.5% BSA containing 0.2 μCi ml^{-1} of [1-^{14}C]palmitic acid and 200 μM non-labelled palmitate for 1 h. Lipids were extracted from these adipocytes using Folch's method (Folch et al., 1957), dried under nitrogen, and resuspended in 50 μl of chloroform:methanol (2:1, v:v). Four microlitres of sample and TG standard (triolein, Nu-Chek Prep Inc., Elysian, MN, USA) were spotted 2 cm above the lower edge of silica coated flexible polyester thin layer chromatography plates (20 cm × 20 cm) (Whatman, Maidstone, UK). Lipids were separated using a hexane–diethyl ether–acetic acid (70:30:1, v:v:v) solvent and then exposed to iodine vapour for visualization. After the evaporation of iodine, the spots adjacent to the standard, corresponding to TG, were scraped off the plate and counted for radioactivity.

Glucose uptake

Isolated adipocytes were used to determine glucose uptake as described previously (Gaidhu et al., 2006). Briefly, adipocytes were resuspended in glucose-free KRB containing HEPES (30 mM; KRB-HEPES) and 1% BSA, pH 7.4. Subsequently, 1×10^6 cells were transferred to plastic tubes and incubated at 37°C for 1 h. Insulin (100 nM) was added for the final 20 min of the incubation period. Subsequently, KRB-HEPES containing 0.5 mM 2-deoxy-D-glucose and 0.5 μCi of 2-[1,2-^{3}H]deoxy-D-glucose was added to the cells for 3 min, and the incubations were terminated by the addition of cytochalasin B (1.5 mM stock solution). Aliquots of cell suspension (240 μl) were quickly placed in plastic microtubes containing 100 μl of di-'isononyl' phthalate. The tubes were centrifuged for 30 s (6000 *g*) to separate cells from the radioactive incubation medium. Subsequently, fat cells were collected by cutting the tubes through the oil phase and transferred to scintillation vials to be counted for radioactivity. Radioactivity of the cells unrelated to glucose transport (nonspecific transport) was determined in the same conditions by adding cytochalasin B (50 μM final concentration) to the medium before the addition of cells (Gaidhu et al., 2006). Non-specific values were subtracted from all conditions.

Measurement of lactate production

Lactate production was measured using a commercially available kit (BioVision; Milpitas, CA, USA) as per the manufacturer's instructions. Briefly, cells were isolated as described above and incubated in KRBH–3.5% BSA for 75 min. Following incubation, an aliquot of medium was extracted and stored at −80°C until analysis.

RNA isolation and quantitative PCR

BAT samples were flash-frozen in liquid nitrogen and stored at −80°C until RNA isolation. RNA was isolated using TRIzol™ (Thermo Fisher Scientific, Waltham, MA, USA) and complimentary DNA (cDNA) was made with 2 μg of RNA using ABM EasyScript™ Reverse Transcriptase cDNA Synthesis kit (Diamed, Mississauga, ON, Canada) as per the manufacturer's instructions. Primers were designed using the software PrimerQuest (IDT) based on probe sequences available at the Affymetrix database (NetAffx™ Analysis Center, http://www.affymetrix.com/ analysis) for each given gene. Samples were run in duplicate on a 96-well plate. Each 20 μl reaction contained 4 μl of cDNA, 0.4 μl of primer, 10 μl of Brightgreen 2× qPCR Mastermix (Diamed) and 5.6 μl of RNase-free water. qPCR analysis was performed using a Bio-Rad CFX96 Real Time PCR Detection System (Bio-Rad, Mississauga, ON, Canada) using the following amplification conditions: 95°C (10 min); 40 cycles of 95°C (15 s), 60°C (1 min). All genes were normalized to the housekeeping-gene β-actin, and relative differences in gene expression between treatment groups were determined using the $\Delta\Delta C_t$ method (Livak & Schmittgen, 2001). Values are presented as fold increases relative to the SC group. The primers used were as follows: cluster of differentiation 36 (*Cd36*) forward (ACGACTGCAGGTCAACATACTGGT), reverse (TGGTCCCAGTCTCATTTAGCCACA); lipoprotein lipase (*Lpl*) forward (TTGAGAAAGGG CTCTGCCTGAGTT), reverse (TGCTTCTCTTGGCTC TGACCTTGT).

Western blotting

BAT samples were extracted from each rat, snap-frozen in liquid nitrogen and frozen at −80°C for later use. Tissues were homogenized in buffer containing 25 mM Tris–HCl, 25 mM NaCl (pH 7.4), 1 mM $MgCl_2$, 2.7 mM KCl, 1% Triton X-100 and protease and phosphatase inhibitors (Roche Diagnostics). Following centrifugation of the homogenates, the infranatant was collected. An aliquot of each sample was used in a Bradford assay to determine protein concentration. The samples were then diluted 1:1 with 2× Laemmli sample buffer and incubated at 95°C for 5 min. Twenty-five micrograms of protein from each sample was loaded onto gels and subject to SDS-PAGE, transferred to a polyvinylidene difluoride membrane and probed with the antibody of interest. The antibody dilutions were 1:1000 and the loading control

Table 1. Cumulative weight gain of rats fed either standard chow (SC) or a high-fat sucrose-enriched (HFS) diet for 8 weeks

	Cumulative weight gain (g)							
Group	1 week	2 weeks	3 weeks	4 weeks	5 weeks	6 weeks	7 weeks	8 weeks
SC	31.2 ± 3.8	68.5 ± 18.6	103.1 ± 31.9	127.8 ± 44.3	151.0 ± 54.7	167.8 ± 61.9	187.6 ± 62.1	210.0 ± 69.0
HFS	41.5 ± 14.4	101.8 ± 17.4	149.6 ± 19.9	188.6* ± 25.8	223.2* ± 33.8	254.3* ± 38.3	283.2* ± 41.3	314.2* ± 44.0

*$P < 0.05$ *vs.* SC. Repeated measures two-way ANOVA was used to compare groups/weeks. $n = 10–13$ rats.

was β-actin. Densitometry analysis was conducted using the Scion Image program.

Adipose tissue morphology

Morphological analysis of iBAT was performed using light microscopy as described previously (Gaidhu et al., 2011; Wu et al., 2014). Briefly, a sample (~50–100 mg) of each fat tissue was collected and fixed in 4% paraformaldehyde, 0.1 M phosphate-buffered saline (PBS), pH 7.4, for 24 h at room temperature. Following fixation, adipose tissue samples were washed three times in PBS and stored at 4°C in 70% ethanol. Samples were then embedded in paraffin blocks, sectioned, and stained with haematoxylin and eosin (H & E). Digital images of tissue sections were captured with a Nikon Eclipse Ti (Nikon Canada, Mississauga, ON, Canada) under ×20 and ×40 magnification.

Statistical analysis

Statistical analyses were conducted by using either Student's unpaired *t* test or ANOVA with the Bonferroni *post hoc* comparison using the GraphPad Prism statistical analysis program (GraphPad Software Inc., San Diego, CA, USA). Tests for normality of the distribution were performed using the D'Agostino–Pearson test, Anderson–Darling test, Shapiro–Wilk test and Kolmogorov–Smirnov test. All statistical analyses were conducted using GraphPad Prism. Data are expressed as mean ± SD.

Results

Effects of HFS feeding on body weight, fat mass and BAT adipocyte morphology

To confirm that obesity was induced by a HFS diet, we measured weight gain relative to baseline and adipose tissue mass throughout the feeding period. The weight gained in weeks 1–3 was not statistically significantly different from the SC groups, although the average weight gained in the HFS group was higher in each of these weeks. After week 4, the weight gained in the HFS group was significantly higher than in the SC animals (188.6 ± 25.8 *vs.* 127.8 ± 44.3 g) (Table 1). This difference in weight gain persisted until the end of the study, culminating with HFS rats gaining ~50% more weight than SC controls after 8 weeks of feeding. Differences in weight gain were essentially due to enhanced growth of the WAT in the HFS animals because the masses of the Sc Ing and Epid fat pads in HFS rats were 2.6- and 3-fold larger, respectively, than those of SC controls (Fig. 1*A*). Similarly, iBAT and aBAT masses both increased 1.6-fold in the HFS animals (Fig. 1*B*). Furthermore, H&E staining revealed that iBAT from SC rats contained adipocytes that were essentially multilocular, whereas iBAT from HFS rats contained many cells of unilocular appearance (Fig. 1*C*).

Effects of HFS feeding on PGC-1α, CPT1B and UCP1 contents

After observing an increase in BAT mass, it was important to determine whether this was accompanied by an increase in thermogenic proteins. Indeed, animals in the HFS group exhibited 1.65-, 17- and 2.2-fold increases in protein content of PGC-1α (Fig. 1*D*), CPT1B (Fig. 1*E*), and UCP1 (Fig. 1*F*), respectively, relative to the control group. Taken together, these results indicate that the molecular machinery necessary for oxidation and thermogenesis was enhanced in BAT under conditions of DIO.

Effects of isoproterenol and oligomycin on glucose and palmitate oxidation in BAT adipocytes

To test whether the increased content of thermogenic proteins was accompanied by enhanced substrate oxidation in BAT adipocytes, we measured glucose and palmitate oxidation in these cells. Measurements were conducted under basal conditions as well as in the presence of the β-adrenergic stimulator isoproterenol (Iso) and of the ATP synthase inhibitor oligomycin (Oligo). We found that rates of glucose oxidation in BAT adipocytes from SC and HFS rats were not affected by incubation with either Iso or Oligo or by a combination of both agents (Fig. 2*A*). However, the rates of glucose oxidation in adipocytes from HFS rats

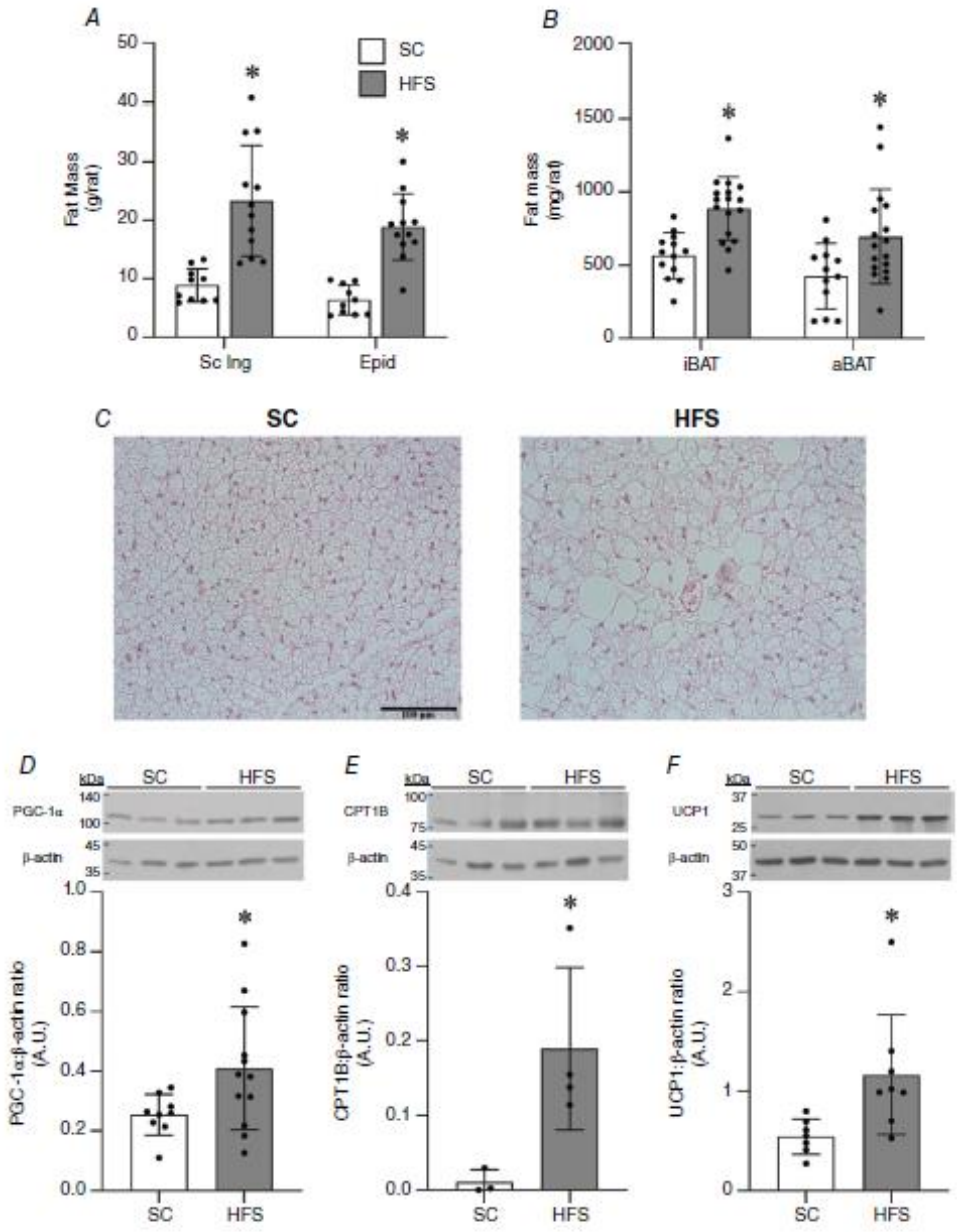

Figure 1. HFS diet increases the masses of white (*A*) and brown (*B*) adipose tissues, the unilocular appearance of brown adipocytes (*C*), and the contents of PGC-1α (*D*), CPT1B (*E*) and UCP1 (*F*) in brown adipose tissue

Data are means ± SD; n = 3–15 rats.*P < 0.05 *vs.* SC. Student's t test was used to compare differences between groups in *A*, *B* and *D*–*F*. [Colour figure can be viewed at wileyonlinelibrary.com]

trended to decrease under all conditions investigated, and reached statistical significance under Oligo conditions. In fact, glucose oxidation under basal conditions was 48% lower in BAT adipocytes from HFS- than from SC-fed rats (Fig. 2*A*). Similarly, rates of glucose oxidation in the presence of either Iso or Oligo or Iso+Oligo were 49%, 62% and 57% lower in HFS than SC BAT adipocytes, respectively (Fig. 2*A*). The incubation of BAT adipocytes with Oligo did not reduce glucose oxidation relative to basal conditions, which is consistent with mitochondrial uncoupling accounting for most of the glucose being oxidized in both SC and HFS cells. We then assessed the oxidation rates of fatty acids, which are major thermogenic substrates in brown adipocytes (Barbara & Nedergaard, 2004). Under basal conditions, palmitate oxidation did not differ between the SC and HFS groups (Fig. 2*B*). However, in the presence of Oligo, palmitate oxidation significantly increased by 2.7-fold in BAT adipocytes compared with SC-fed animals, whereas in BAT adipocytes from HFS animals, Oligo did not cause any alteration in this parameter (Fig. 2*B*) in comparison to basal values. Therefore, when comparing rates of palmitate oxidation between SC BAT and HFS BAT adipocytes incubated with Oligo, we found it to be 57% lower in the latter than the former cells (Fig. 2*B*). Furthermore, when incubated with both Iso and Oligo, palmitate oxidation was reduced by 45% in the brown adipocytes of the HFS group (Fig. 2*B*), although this was not statistically significant. These findings demonstrated that UCP1-mediated palmitate oxidation was impaired under conditions of chronic HFS feeding.

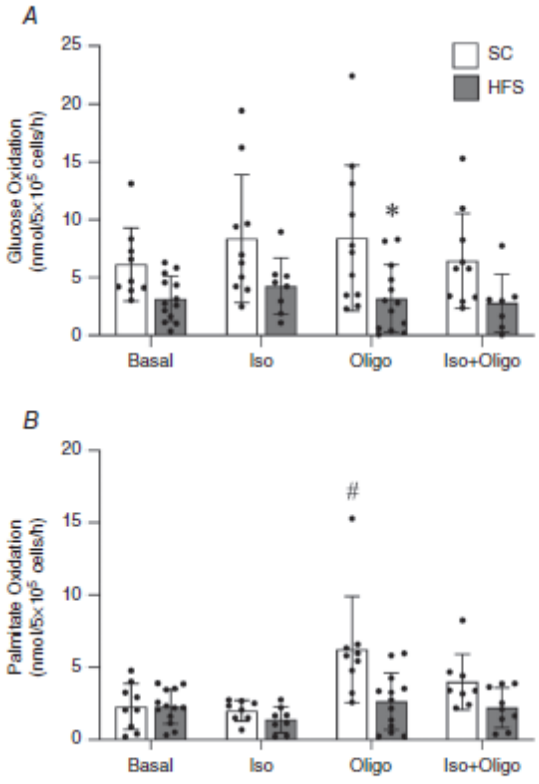

Figure 2. Isolated brown adipocytes from rats fed a HFS diet displayed reduced rates of Oligo-induced glucose (*A*) and palmitate oxidation (*B*) in isolated brown adipocytes
Data are means ± SD; $n = 7$–13 rats. Two-way ANOVA was used to compare groups/conditions. $^{*}P < 0.05$ *vs.* SC; $^{\#}P < 0.05$ *vs.* all conditions except SC Iso+Oligo.

Effects of HFS feeding on glucose uptake, lactate production, and GLUT1 and GLUT4 protein contents in isolated brown adipocytes

Given that rates of glucose oxidation were reduced in HFS BAT adipocytes, we conducted additional experiments to assess whether the uptake of glucose was also affected in these cells. It could be that low rates of glucose oxidation were driven by reduced intake of this substrate. However, we found that basal glucose uptake in HFS BAT adipocytes was 4-fold higher than in SC BAT adipocytes. In the presence of insulin, SC BAT adipocytes displayed a 4-fold increase in glucose uptake, whereas HFS BAT adipocytes increased glucose uptake 1.83-fold when stimulated with insulin (Fig. 3*A*). Nevertheless, insulin-stimulated glucose uptake was higher in the brown adipocytes of HFS-fed animals than in the SC animals (Fig. 3*A*). To further investigate the metabolic fate of glucose, we measured lactate production in isolated BAT adipocytes and found that, under basal conditions, cells from HFS animals produced 2.7-fold more lactate than adipocytes from SC-fed animals (Fig. 3*B*). These effects of HFS adipocytes were accompanied by a significant increase of ∼24-fold in GLUT1 (Fig. 3*C*) and no alteration in GLUT4 protein contents in iBAT (Fig. 3*D*). Taken together, these findings provide evidence that a HFS diet enhances glucose uptake and shifts glucose metabolism toward lactate production in BAT adipocytes.

Glycerol incorporation into lipids and palmitate incorporation into TAG in brown adipocytes

Because an increased number of unilocular adipocytes was found within BAT from HFS rats, we then measured pathways involved in TAG synthesis. We found that a HFS diet enhanced glycerol incorporation into lipids (Fig. 4*A*) and palmitate incorporation into TAG (Fig. 4*B*) by 1.8- and 1.7-fold, respectively, in BAT adipocytes. This indicated that fatty acids and glycerol were indeed diverted

by chronic HFS feeding towards esterification in isolated BAT adipocytes.

PEPCK and GyK protein levels and *Lpl* and *Cd36* gene expression in BAT

PEPCK (Fig. 4*C*) and GyK (Fig. 4*D*) increased 1.8- and 2.1-fold, respectively, which was accompanied by increases of 3.6-fold in *Lpl* and 3.7-fold in *Cd36* mRNA expression in BAT (Fig. 4*E*). Therefore, our findings provide evidence that the molecular machinery that supports TAG storage was enhanced in BAT by a chronic HFS diet.

Lipolysis, β3-AdR, TH, ATGL and pHSL contents in BAT

Basal lipolysis was reduced by 65% in BAT adipocytes from HFS rats in comparison to the SC group (Fig. 5*A*). Western blot analysis of the molecular machinery involved in lipolysis revealed that ATGL content was significantly reduced by 28% (Fig. 5*B*), whereas HSL_{660} phosphorylation was increased under conditions of HFS feeding, although not statistically significant (Fig. 5*C*). Furthermore, the contents of TH (Fig. 5*D*) and β3AdR (Fig. 5*E*) were reduced and increased by 84% and 6-fold, respectively, in BAT of HFS rats in comparison to SC controls. Based on these findings, it was evident that the observed downregulation of lipolysis in HFS BAT adipocytes derived from distinct alterations in the lipolytic machinery.

Discussion

Here, we provide evidence that UCP1-mediated glucose and fatty acid oxidation in intact and freshly isolated rat brown adipocytes is reduced under conditions of chronic HFS feeding, even though BAT mass and its UCP1 content increased. These findings are consistent with an adaptive response of the organism to the HFS diet that led to attenuation of DIT and expansion of WAT mass. Moreover, BAT itself developed functional and morphological characteristics that resemble WAT, which was characterized by brown adipocytes enhancing their ability to store TAG and by increasing the number

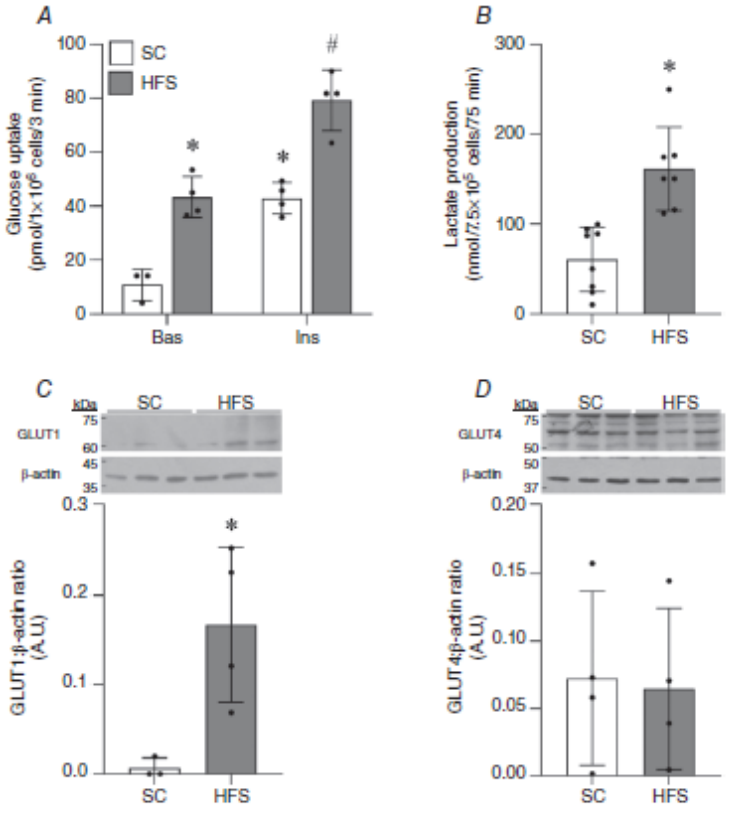

Figure 3. HFS feeding increased basal and insulin-stimulated glucose uptake (*A*), and lactate production (*B*) in isolated BAT adipocytes. HFS also had higher GLUT1 content (C) than standard chow (SC) BAT, whereas GLUT4 content (*D*) did not differ between SC and HFS BAT
Data are means ± SD; n = 3–9 rats. $^{\#}P < 0.05$ *vs.* HFS Basal and SC Ins in A. $^{*}P < 0.05$ *vs.* SC Basal in *A*. $^{*}P < 0.05$ *vs.* SC in *B–D*. Student's t test was used to compare groups except for glucose uptake (*A*) where a two-way ANOVA was used to compare groups/conditions.

of cells displaying a unilocular appearance within BAT. The mechanisms underlying these adaptive responses of BAT to HFS-induced obesity involved a major shift in brown adipocyte metabolism. Lipolysis was suppressed and glucose and FA were essentially diverted away from oxidation and toward pathways that culminated in TAG synthesis and enlargement of the lipid droplet in HFS BAT adipocytes (Fig. 6). Thus, our data provide evidence that there are regulatory mechanisms in intact brown adipocytes cells that shift substrate partitioning in response to alterations in dietary macronutrient composition. In this context, we demonstrated that UCP1-mediated mitochondrial uncoupling was impaired under conditions of DIO, confirming our original hypothesis.

It is well established that when BAT is in its activated state (e.g. cold exposure and β3-adrenergic stimulation), the uptake and utilization of glucose by brown adipocytes are enhanced (Barbara & Nedergaard, 2004; Labbe et al., 2015; Olsen et al., 2017). Thus, we expected that DIT in response to the HFS diet would elicit a similar effect in BAT adipocytes. However, given that previous studies

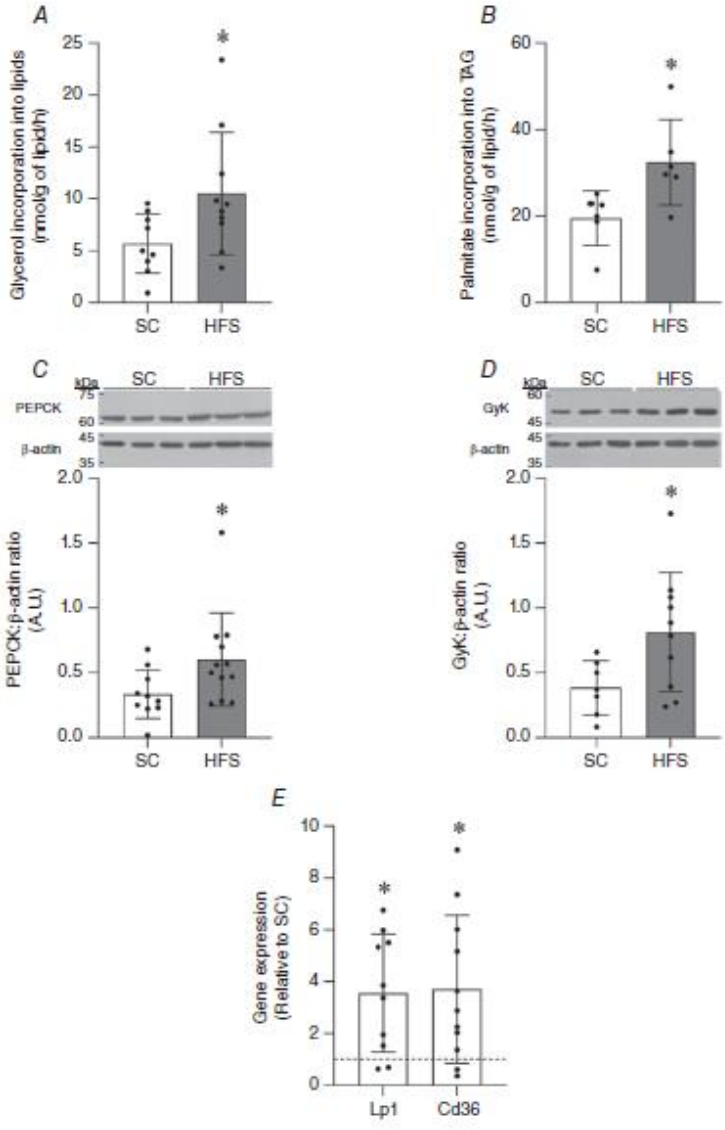

Figure 4. HFS feeding enhanced the incorporation of glycerol into lipids (*A*) and palmitate into triacylglycerol (TAG) (*B*) in isolated brown adipocytes, and increased phosphoenolpyruvate carboxykinase (PEPCK) (*C*) and glycerol kinase (Gyk) (*D*) contents, as well as the gene expression of lipoprotein lipase (*Lpl*) and cluster of differentiation 36 (*Cd36*) (*E*) in BAT
Data are means ± SD; n = 6–12 rats. Student's t test was used to compare groups. *P < 0.05 *vs.* SC.

had reported reduced *in vivo* glucose utilization in BAT of rodent models of obesity (Ferré et al., 1986; Ishino et al., 2017; Lapa et al., 2017) and humans (Leitner et al., 2017; Orava et al., 2013), it was also possible that the uptake and oxidation of glucose would be impaired in these cells. Instead, our measurements of glucose uptake in isolated HFS BAT adipocytes revealed that it was significantly increased under both basal and insulin-stimulated conditions. This likely supported the elevated lactate production, indicating that glucose was being processed through the glycolytic pathway in these cells. Therefore, the α-glycerophosphate moiety necessary for enhanced FA esterification could be supplied in two ways: (1) by the formation of glycerol 3-phosphate as an intermediary step of glycolysis, and/or (2) through glyceroneogenesis. Because lactate is a major substrate for the latter pathway (Nye et al., 2008), its abundance also allowed for increased TAG synthesis. This was supported by elevated PEPCK content and confirmed by the enhanced incorporation of palmitate into TAG found in HFS BAT adipocytes. Additionally, because the content of GyK was increased in these cells, TAG synthesis from exogenous FA and glycerol was facilitated, which was also confirmed by significantly higher rates of glycerol incorporation into lipids in HFS than in SC BAT adipocytes. Lastly, with increased expression of *Lpl* and *Cd36*, the TAG content of BAT adipocytes could be enriched through the esterification of the abundant dietary fat carried by lipoproteins. In this context, less UCP1-mediated oxidation of glucose and fatty acids could be explained by a diversion of these substrates towards pathways of TAG synthesis as opposed to uncoupled oxidation. Altogether, these effects led to a reduction in the number of small lipid droplets and conferred a more unilocular appearance to adipocytes within BAT.

Interestingly, some adaptive responses of BAT adipocytes to the HFS diet (e.g. increased contents of PGC-1α, β3-AdR and CPT1B) were compatible with activation of a thermogenic response by these cells to overfeeding. This then begged the question why didn't this translate into increased UCP1-mediated substrate oxidation to support DIT? Importantly, we also found that content of TH, the rate-limiting enzyme for catecholamine biosynthesis, was markedly reduced in HFS BAT, indicating lower SNS-mediated recruitment of BAT activity. This is in line with our findings of reduced basal lipolysis in HFS BAT adipocytes, which could consequently lead to less UCP1 activation, even

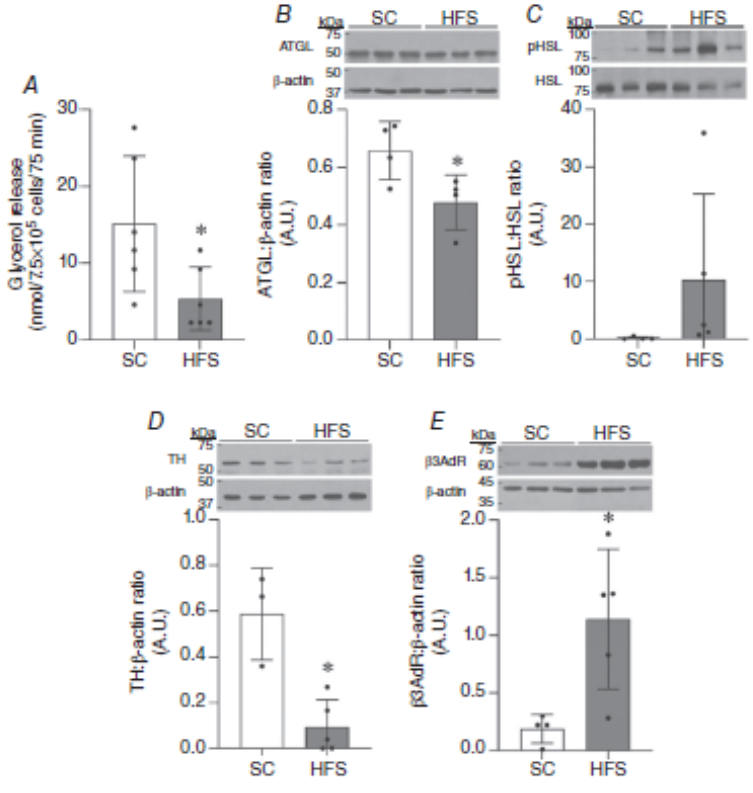

Figure 5. HFS diet reduced basal lipolysis (*A*) in isolated BAT adipocytes and the content of adipose triglyceride lipase (ATGL) (*B*), but did not signifiantly affect hormone sensitive lipase (HSL) phosphorylation (C). HFS diet also reduced tyrosine hydroxylase (TH) (*D*) and increased β3-adrenergic receptor (β3-Adr) (*E*) contents in BAT
Data are means ± SD; n = 3–6 rats.
*P < 0.05 *vs.* SC. Student's t test was used to compare differences between groups.

though the content of this protein and of others that support thermogenesis was increased. In this context, the increased content of β3-AdR we found in HFS BAT was likely a compensatory mechanism employed by the cell to maximize adrenergic activation, although, *in vivo*, it is futile given the drastic reduction in TH content and impaired catecholamine production in BAT of HFS rats. Thus, maintaining the ability of the SNS to promote UCP1 activation during prolonged HFS feeding seems to be crucial to sustain DIT and counteract weight gain. This is supported by previous studies reporting that basal sympathetic activation of BAT is reduced in rats chronically maintained on a high-fat diet (Levin et al., 1985; Madden & Morrison, 2016), and that diet-induced recruitment of BAT in mice depends essentially on sustained SNS-mediated activation (Fischer et al., 2019). Reduced SNS-mediated recruitment of BAT activity in HFS-induced obesity could originate from the development of leptin resistance. Indeed, rodent models of obesity lacking either functional leptin or a functional isoform of the leptin receptor display reduced SNS-mediated activation of BAT and DIT (Leibel et al., 1997; Leibel, 2008). Additionally, altered SNS activity (Levin et al., 1983) and reduced central leptin sensitivity (Levin & Dunn-Meynell, 2002) have been demonstrated in rats with diet-induced obesity. Therefore, it is likely that the molecular adaptations to the HFS diet we found in BAT originated from the diminished sympathetic output from the hypothalamus as a result of diet-induced leptin resistance (So et al., 2011). In fact, we have previously reported that plasma leptin levels of rats fed a HFS diet for 8 weeks were almost 2-fold higher than in SC diet-fed controls (So et al., 2011), indicating that these animals indeed had reduced sensitivity to this adipokine. However, because the production and release of leptin is proportional to WAT mass (Leibel, 2008), a gap exists between the beginning of HFS feeding and the time for adipose tissue to expand and leptin resistance to occur. This might be the reason why rats displayed increased whole-body energy expenditure in the first 2 weeks of high-fat feeding, and then lost this response afterwards (So et al., 2011) as leptin resistance developed. Thus, it could be that the increased UCP1 content in BAT we found after 8 weeks of a HFS diet was reminiscent of this initial DIT response mounted by the animal. Future studies are necessary to investigate this possibility.

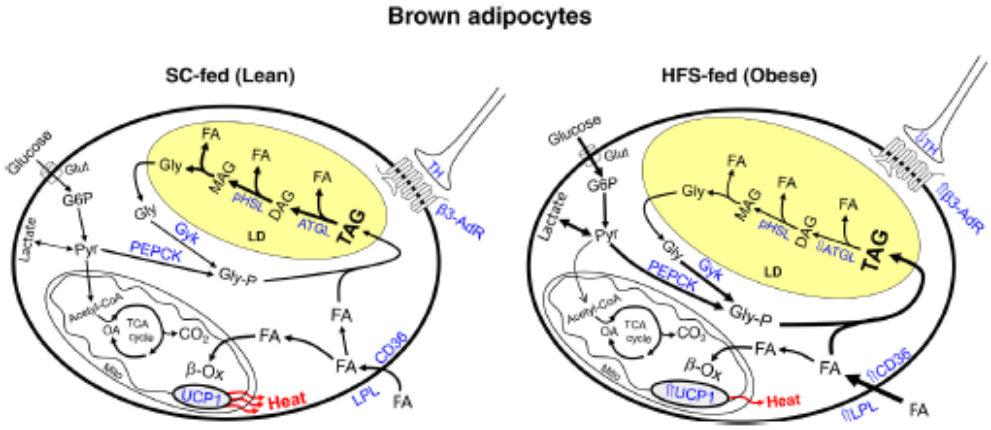

Figure 6. In brown adipocytes from lean rats fed a SC diet, glucose and fatty acids (FA) were diverted essentially toward UCP1-mediated substrate oxidation. These substrates were also used to sustain a high rate of triacylglycerol (TAG) breakdown/resynthesis. This was supported by a highly responsive molecular machinery that involved the activation of β3-adrenergic receptors (β3-AdR) via sympathetic nervous system-mediated release of noradrenaline and activation of the major lipolytic enzymes adipose triglyceride lipase (ATGL) and hormone sensitive lipase (HSL). Conversely, in BAT of rats fed a HFS obesogenic diet, despite increases in UCP1 and β3-AdR contents, substrate metabolism in BAT adipocytes was shifted toward TAG synthesis/storage. This was characterized by reduced UCP1-mediated glucose and fatty acid oxidation, impairment of lipolysis and reduction in tyrosine hydroxylase content in BAT. These adaptive responses to chronic HFS were supported by increased glucose uptake, contents of phosphoenolpyruvate carboxykinase (PEPCK) and glycerol kinase (GyK), elevated rates of glycerol incorporation into lipids and palmitate incorporation into TAG, and by enhanced gene expression of lipoprotein lipase (LPL) and cluster of differentiation 36 (CD36) in BAT
β-ox, β-oxidation; DAG, diacylglycerol; G6P, glucose-6-phospate; Glut, glucose transporter; Gly, glycerol; Gly-P, glycerol phosphate; LD, lipid droplet; MAG, monoacylglycerol; Mito, mitochondria; OA, oxaloacetate; Pyr, pyruvate. ⇑, increase; ⇓, reduction; thicker arrows indicate higher flow through the pathway. [Colour figure can be viewed at wileyonlinelibrary.com]

It is important to note that animals were housed at room temperature and not at thermoneutrality, which has been shown to have a significant impact on BAT UCP1 protein content and the contents of other mitochondrial proteins (McKie et al., 2019). This poses a potential limitation to our study as both groups of animals may have experienced BAT activation to some extent, which could have masked the effects of the diets. Moreover, the experiments in this study were conducted on male rats. Future studies assessing these parameters are warranted in female rats to identify sex-based differences, if any, in the adaptive responses of BAT to an obesogenic diet.

In summary, our findings provide novel evidence that increased BAT mass and its UCP1 content under chronic HFS feeding does not translate into elevated consumption of glucose or fatty acids through UCP1-mediated mitochondrial uncoupling. In fact, uncoupled glucose and fatty acid oxidation were even lower in HFS BAT adipocytes than in SC-fed controls after coupled respiration was inhibited in these cells by Oligo. Therefore, our findings are contrary to the idea that DIT is induced in brown adipocytes under conditions of diet-induced obesity. Rather, when an obesogenic high fat–sucrose-enriched diet was supplied for extended periods of time, brown adipocytes enhanced their ability to uptake and store glucose and FA, and did so by diverting substrate away from oxidation (Fig. 6). Collectively, these effects may impair BAT-induced DIT and likely contribute to the development of obesity and its related metabolic disorders.

References

Barbara, C., & Nedergaard, J. (2004). Brown adipose tissue: Function and physiological significance. *Physiological Reviews*, **84**, 277–359.

Cannon, B., & Nedergaard, J. (2001). Respiratory and thermogenic capacities of cells and mitochondria from brown and white adipose tissue. In G. Ailhaud (Ed.), *Adipose tissue protocols* (pp. 295–304). Humana Press Inc.

Dole, P. & Meinertz, H. (1960). Microdetermination of long-chain fatty acids in plasma and tissues. *Journal of Biological Chemistry*, **235**(9), 2595–2599.

Fedorenko, A., Lishko, P. V., & Kirichok, Y. (2013). Mechanism of fatty-acid-dependent UCP1 uncoupling in brown fat mitochondria. *Cell*, **151**(2), 400–413.

Feldmann, H. M., Golozoubova, V., Cannon, B., & Nedergaard, J. (2009). UCP1 ablation induces obesity and abolishes diet-induced thermogenesis in mice exempt from thermal stress by living at thermoneutrality. *Cell Metabolism*, **9**(2), 203–209.

Ferré, P., Burnol, A. F., Leturque, A., Terretaz, J., Penicaud, L., Jeanrenaud, B., & Girard, J. (1986). Glucose utilization *in vivo* and insulin-sensitivity of rat brown adipose tissue in various physiological and pathological conditions. *Biochemical Journal*, **233**(1), 249–252.

Fine, J. B., & DiGirolamo, M. (1997). A simple method to predict cellular density in adipocyte metabolic incubations. *International Journal of Obesity and Related Metabolic Disorders*, **21**(9), 764–768.

Fischer, A. W., Schlein, C., Cannon, B., Heeren, J., & Nedergaard, J. (2019). Intact innervation is essential for diet-induced recruitment of brown adipose tissue. *American Journal of Physiology. Endocrinology and Metabolism*, **316**(3), E487–E503.

Folch, J., Lees, M., & Sloane Stanley, G. H. (1957). A simple method for the isolation and purification of total lipides from animal tissues. *Journal of Biological Chemistry*, **226**(1), 497–509.

Gaidhu, M. P., Anthony, N. M., Patel, P., Hawke, T. J., & Ceddia, R. B. (2010). Dysregulation of lipolysis and lipid metabolism in visceral and subcutaneous adipocytes by high-fat diet: Role of ATGL, HSL, and AMPK. *American Journal of Physiology. Cell Physiology*, **298**(4), C961–C971.

Gaidhu, M. P., Fediuc, S., Anthony, N. M., So, M., Mirpourian, M., Perry, R. L. S., & Ceddia, R. B. (2009). Prolonged AICAR-induced AMP-kinase activation promotes energy dissipation in white adipocytes: novel mechanisms integrating HSL and ATGL. *Journal of Lipid Research*, **50**(4), 704–715.

Gaidhu, M. P., Fediuc, S., & Ceddia, R. B. (2006). 5-Aminoimidazole-4-carboxamide-1-beta-D-ribofuranoside-induced AMP-activated protein kinase phosphorylation inhibits basal and insulin-stimulated glucose uptake, lipid synthesis, and fatty acid oxidation in isolated rat adipocytes. *Journal of Biological Chemistry*, **281**(36), 25956–25964.

Gaidhu, M. P., Frontini, A., Hung, S., Pistor, K., Cinti, S., & Ceddia, R. B. (2011). Chronic AMP-kinase activation with AICAR reduces adiposity by remodeling adipocyte metabolism and increasing leptin sensitivity. *Journal of Lipid Research*, **52**(9), 1702–1711.

Ishino, S., Sugita, T., Kondo, Y., Okai, M., Tsuchimori, K., Watanabe, M., Mori, I., Hosoya, M., Horiguchi, T., & Kamiguchi, H. (2017). Glucose uptake of the muscle and adipose tissues in diabetes and obesity disease models: Evaluation of insulin and β3-adrenergic receptor agonist effects by 18F-FDG. *Annals of Nuclear Medicine*, **31**(5), 413–423.

Kozak, L. P. (2010). Brown fat and the myth of diet-induced thermogenesis. *Cell Metabolism*, **11**(4), 263–267.

Labbe, S. M., Caron, A., Bakan, I., Laplante, M., Carpentier, A. C., Lecomte, R., & Richard, D. (2015). In vivo measurement of energy substrate contribution to cold-induced brown adipose tissue thermogenesis. *FASEB Journal*, **29**(5), 2046–2058.

Lapa, C., Arias-loza, P., Hayakawa, N., Wakaba, H., Werner, A., Chen, X., Shinaji, T., Herrmann, K., & Pelzer, T. (2017). Whitening and impaired glucose utilization of brown adipose tissue in a rat model of type 2 diabetes mellitus. *Scientific Reports*, **7**(1), 16795.

Leibel, R. L. (2008). Molecular physiology of weight regulation in mice and humans. *International Journal of Obesity*, **32**(S7), S98-S108.

Leibel, R. L., Chung, W. K., & Chua, S. C. (1997). The molecular genetics of rodent single gene obesities. *Journal of Biological Chemistry*, **272**(51), 31937–31940.

Leitner, B. P., Huang, S., Brychta, R. J., Duckworth, C. J., Baskin, A. S., McGehee, S., Tal, I., Dieckmann, W., Gupta, G., Kolodny, G. M., Pacak, K., Herscovitch, P., Cypess, A. M., & Chen, K. Y. (2017). Mapping of human brown adipose tissue in lean and obese young men. *Proceedings of the National Academy of Sciences, USA*, **114**(32), 8649–8654.

Levin, B. E., & Dunn-Meynell, A. A. (2002). Reduced central leptin sensitivity in rats with diet-induced obesity. *American Journal of Physiology. Regulatory, Integrative and Comparative Physiology*, **283**(4), R941–R948.

Levin, B. E., Finnegan, M., Triscari, J., & Sullivan, A. C. (1985). Brown adipose and metabolic features of chronic diet-induced obesity. *American Journal of Physiology. Regulatory, Integrative and Comparative Physiology*, **248**(6), R717–R723.

Levin, B. E., Triscari, J., & Sullivan, A. C. (1983). Altered sympathetic activity during development of diet-induced obesity in rat. *American Journal of Physiology. Regulatory, Integrative and Comparative Physiology*, **244**(3), R347–R355.

Livak, K. J., & Schmittgen, T. D. (2001). Analysis of relative gene expression data using real-time quantitative PCR and the $2-\Delta\Delta CT$ method. *Methods*, **25**(4), 402–408.

Madden, C. J., & Morrison, S. F. (2016). A high-fat diet impairs cooling-evoked brown adipose tissue activation via a vagal afferent mechanism. *American Journal of Physiology. Endocrinology and Metabolism*, **311**(2), E287–E292.

McKie, G. L., Medak, K. D., Knuth, C. M., Shamshoum, H., Townsend, L. K., Peppler, W. T., & Wright, D. C. (2019). Housing temperature affects the acute and chronic metabolic adaptations to exercise in mice. *Journal of Physiology*, **597**(17), 4581–4600.

Nye, C. K., Hanson, R. W., & Kalhan, S. C. (2008). Glyceroneogenesis is the dominant pathway for triglyceride glycerol synthesis *in vivo* in the rat. *Journal of Biological Chemistry*, **283**(41), 27565–27574.

Olsen, J. M., Csikasz, R. I., Dehvari, N., Lu, L., Sandström, A., Öberg, A. I., Nedergaard, J., Stone-Elander, S., & Bengtsson, T. (2017). β 3-Adrenergically induced glucose uptake in brown adipose tissue is independent of UCP1 presence or activity: Mediation through the mTOR pathway. *Molecular Metabolism*, **6**(6), 611–619.

Orava, J., Nuutila, P., Noponen, T., Parkkola, R., Viljanen, T., Enerbäck, S., Rissanen, A., Pietiläinen, K. H., & Virtanen, K. A. (2013). Blunted metabolic responses to cold and insulin stimulation in brown adipose tissue of obese humans. *Obesity*, **21**(11), 2279–2287.

Rosenbaum, M., & Leibel, R. L. (1998). The physiology of body weight regulation: Relevance to the etiology of obesity in children. *Pediatrics*, **101**(Supplement_2), 525–539.

So, M., Gaidhu, M. P., Maghdoori, B., & Ceddia, R. B. (2011). Analysis of time-dependent adaptations in whole-body energy balance in obesity induced by high-fat diet in rats. *Lipids in Health and Disease*, **10**(1), 99.

Trayhurn, P. (2017). Origins and early development of the concept that brown adipose tissue thermogenesis is linked to energy balance and obesity. *Biochimie*, **134**, 62–70.

Wu, M. V., Bikopoulos, G., Hung, S., & Ceddia, R. B. (2014). Thermogenic capacity is antagonistically regulated in classical brown and white subcutaneous fat depots by high fat diet and endurance training in rats: Impact on whole-body energy expenditure. *Journal of Biological Chemistry*, **289**(49), 34129–34140.

Additional information

Data availability statement

All data supporting the results are included within the figures revealing their range and distribution.

Competing interests

The authors state no conflict or duality of interest with regards to this work.

Author contributions

Conception or design of the work: R.B.C. Acquisition, analysis or interpretation of data for the work: D.D.E. and S.J. Drafting the work or revising it critically for important intellectual content: D.D.E., S.J. and R.B.C. All authors have read and approved the final version of the manuscript and agree to be accountable for all aspects of the work in ensuring that questions related to the accuracy or integrity of any part of the work are appropriately investigated and resolved. All persons designated as authors qualify for authorship, and all those who qualify for authorship are listed.

Funding

This research was funded by a Discovery Grant from the Natural Science and Engineering Research Council of Canada (NSERC) and by infrastructure grants from the Canada Foundation for Innovation (CFI) and the Ontario Research Fund (ORF) awarded to R.B.C. D.D.E. was funded by NSERC Alexander Graham Bell Canada graduate scholarship-Doctoral.

Keywords

diet-induced thermogenesis, glyceroneogenesis, GyK, obesity, PEPCK, PGC-1α

Supporting information

Additional supporting information can be found online in the Supporting Information section at the end of the HTML view of the article. Supporting information files available:

Statistical Summary Document
Peer Review History

Available online at www.sciencedirect.com

ScienceDirect

Journal of Nutritional Biochemistry 120 (2023) 109412

Journal of Nutritional Biochemistry

RESEARCH PAPER

The ketogenic diet promotes triacylglycerol recycling in white adipose tissue and uncoupled fat oxidation in brown adipose tissue, but does not reduce adiposity in rats

Daniel Da Eira, Shailee Jani, Mateja Stefanovic, Rolando B. Ceddia*

Muscle Health Research Centre – School of Kinesiology and Health Science, York University, North York, ON, Canada

Received 12 December 2022; received in revised form 6 June 2023; accepted 3 July 2023

Abstract

The purpose of this study was to determine whether the weight-reducing and fat burning effects of the ketogenic diet (KD) could be attributed to alterations in the energy dissipating pathways of brown adipose tissue (BAT) uncoupled oxidation, and white adipose tissue (WAT) browning and triacylglycerol (TAG) recycling. To investigate this, male Wistar rats were fed one of the following three diets for either 8 or 16 weeks: a standard chow (SC), a high-fat, sucrose-enriched (HFS) obesogenic diet, or a KD. At the end of the intervention, subcutaneous inguinal (Sc Ing) and epididymal (Epid) fat, and interscapular and aortic BAT (iBAT and aBAT, respectively) were extracted. These tissues were used for the analysis of proteins involved in WAT browning and thermogenesis. Isolated adipocytes from WAT were assayed for basal and isoproterenol (Iso)-stimulated lipolysis and basal and insulin-stimulated lipogenesis, and BAT adipocytes were assayed for the determination of coupled and uncoupled glucose and palmitate oxidation. Adiposity similarly increased in HFS- and KD-fed rats at weeks 8 and 16. However, in HFS-fed animals insulin-stimulated lipogenesis and Iso-stimulated lipolysis were impaired in WAT adipocytes, whereas in KD-fed animals these pathways remained intact. The KD also significantly elevated WAT glycerol kinase levels, and favored TAG recycling under conditions of enhanced lipolysis. In BAT, the KD significantly increased uncoupling protein-1 levels and uncoupled fat oxidation. In summary, the KD preserved insulin sensitivity and lipolytic capacity in WAT and also upregulated energy-dissipating pathways in BAT, but it was not sufficient to prevent an increase in adiposity.

Keywords: Lipolysis; UCP1; Glycerol kinase; Insulin-stimulated lipogenesis; PGC-1α.

1. Introduction

Functional adipose tissue (AT) is crucial for the prevention of insulin resistance and Type 2 diabetes [1]. There are generally two main forms of AT with distinct physiological roles: white and brown. White adipose tissue (WAT) stores energy substrate under conditions of energy surplus, and releases fatty acids and glycerol under conditions of energy deficit [2–4]. On the other hand, brown adipose tissue (BAT) burns glucose and fatty acids and releases the energy as heat [2,4]. Thermogenesis in BAT mainly occurs through uncoupling protein-1 (UCP1), which uncouples oxidative phosphorylation from ATP production [2]. Under conditions of obesity, WAT and BAT functions are altered differently. Diet-induced obesity enhances the thermogenic capacity by increasing UCP1 content and fatty acid oxidation in BAT [3,4]. This serves to counteract energy storage through a mechanism known as diet-induced thermogenesis [3,4]. However, this is not sufficient to prevent the excess storage of fat in white adipocytes and the development of insulin resistance in the WAT [1,5]. In fact, chronically elevated caloric intake overwhelms the hypertrophic capacity of the adipocyte, leading to cellular hypoxia and immune cell infiltration [1,5]. At the level of the WAT, inflammation inhibits insulin signaling, which ends up enhancing basal lipolysis [1], although catecholamine-stimulated lipolysis becomes severely limited under conditions of obesity [6,7]. The dysregulation in lipid storage and breakdown redirects lipids to ectopic tissues such as liver [1] and muscle [1,8]. This is detrimental to insulin sensitivity and metabolism in these tissues, and negatively impacts whole-body glucose homeostasis [1,8]. In this context, interventions that combat adiposity and restore AT function are of great interest for the prevention and treatment of obesity and insulin resistance.

A dietary intervention that exerts anti-obesity and insulin-sensitizing effects is the ketogenic diet (KD). The KD is typically low in carbohydrates and high in fat [9]. Despite being abundant

* Corresponding author at: Rolando B. Ceddia, York University, 4700 Keele St., North York, ON, Canada, M3J 1P3, Tel.: (416) 736 2100 ext 77204, fax (416) 736 5774.
E-mail address: roceddia@yorku.ca (R.B. Ceddia).

https://doi.org/10.1016/j.jnutbio.2023.109412
0955-2863/

in fat, recent evidence shows that 3 months of KD-feeding significantly attenuated body weight (BW) and blood pressure, and improved glycaemia in diabetic women [10]. Furthermore, as little as 6 days of KD significantly reduced intra-hepatic triglycerides in overweight and obese subjects [11]. These promising health effects have prompted investigations into the effects of the KD on cellular metabolism. In BAT and WAT, the KD increases UCP1 content and UCP1 gene expression, respectively [12]. This elevation in WAT UCP1 is characteristic of a process known as browning, whereby WAT acquires structural and functional features that resemble BAT [2,4,13]. Additionally, by lowering circulating insulin levels, the KD favors WAT lipolysis and the release of non-esterified fatty acids (NEFAs) into the bloodstream [14]. NEFAs not undergoing oxidation return to the WAT where they are recycled back to triacylglycerol (TAG). This latter process creates an energy-consuming "futile cycle" that can also contribute to whole-body energy expenditure [2]. Thus, the combined effects of the KD on BAT uncoupled oxidation, WAT browning, and TAG cycling could potentially support the diet-induced shift from energy storage to dissipation in WAT and reduce adiposity. However, the effects of the KD on WAT TAG recycling and BAT uncoupled oxidative capacity, and whether these two mechanisms lead to reduced adiposity, is yet to be confirmed. Therefore, the purpose of our study was to assess KD-induced alterations in these energy-consuming pathways in brown and white adipocytes. We hypothesized that the KD would increase UCP1 content and enhance fat consumption in BAT, whereas in WAT the machinery for TAG recycling would be up-regulated, ultimately contributing to a reduction in adiposity. To test this hypothesis, rats were fed for up to 16 weeks either a high-fat, sucrose enriched (HFS) obesogenic diet or a KD to compare the effects of these diets on WAT and BAT metabolism. To test potential time-dependent effects of the KD on metabolic pathways involved in energy dissipation, we assessed, in BAT and WAT, the thermogenic and TAG recycling machineries at 8 and 16 weeks of the dietary interventions. Here, we show that KD-feeding promoted distinct TAG recycling effects in subcutaneous and visceral WAT and enhanced the capacity of BAT to consume fatty acids. However, the induction of these energy consuming pathways by the KD did not lead to a reduction in adiposity.

2. Materials and methods

2.1. Reagents

Type II collagenase, isoproterenol (Iso), fatty acid-free bovine serum albumin (BSA), palmitic acid, and the free glycerol determination kit were obtained from Sigma (St. Louis, MO, USA). Oligomycin (Oligo) was purchased from Cayman Chemical (Ann Arbor, MI, USA). [1-^{14}C] palmitic acid and D-[U-^{14}C] glucose were purchased from American Radiolabeled Chemicals (St. Louis, MO, USA). Protease (cOmplete Ultra Tablets) and phosphatase (PhosSTOP) inhibitors were obtained from Roche Diagnostics GmbH (Mannheim, Germany). The β-hydroxybutyrate (BHB; cat. no. ab83390) assay kit, and the UCP1 (ab23841) and glycerol kinase (GyK; cat. no. ab180525) antibodies were purchased from Abcam (Toronto, ON, Canada). β-actin (cat. no. 4967) and adipose triglyceride lipase (ATGL; cat. no. 2138) antibodies were purchased from Cell Signaling (Danvers, MA, USA). The peroxisome proliferator-activated receptor gamma coactivator 1-alpha (PGC1α; cat. no. ab3242) was purchased from Millipore (Burlington, MA, USA). The β3-adrenergic receptor (β3AdR; sc-50436) antibody was purchased from Santa Cruz Biotechnology, Inc (Dallas, TX, USA).

Table 1
Fatty acid (FA) profile of the SC, HFS and KD expressed as % of the total fatty acids.

	SC	HFS	KD
Saturated FA	20.8	32.2	32.6
Monounsaturated FA	26.7	35.9	36.2
Polyunsaturated FA	52.5	31.9	31.1

2.2. Animals

Male albino rats from the Wistar strain (Envigo, Indianapolis, IN, USA) weighing 200–250 g (initial weight) were maintained in a constant-temperature (23 °C), with a fixed 12-h light/12-h dark cycle and fed for either 8 or 16 weeks *ad libitum* either a standard chow diet (SC, 27.0 %, 13.0 %, and 60.0 % of calories provided by protein, fat, and carbohydrates, respectively), a HF, sucrose-enriched (HFS) diet (20.0%, 60.0%, and 20.0% of calories provided by protein, fat, and carbohydrates [sucrose], respectively) or a KD (20%, 80%, and 0% of calories provided by protein, fat and carbohydrates, respectively). Caloric densities of the diets were 3.43-, 5.24- and 6.14 kcal/g for the SC, HFS and KD, respectively. The saturated, monounsaturated and polyunsatured fatty acid % contribution to the total fatty acids in each of the diets was 20.8, 26.7, and 52.5% for the SC, 32.2, 35.9, and 31.9% for the HFS diet and 32.6, 36.2, and 31.1 for the KD (Table 1). The SC (standard rat chow, catalog # 5012) was purchased from LabDiet (Richmond, IN, USA). The HFS and ketogenic diets (catalog # D12492 and D03022101, respectively) were purchased from Research Diets Inc. (New Brunswick, NJ, USA). At the end of the feeding period, animals were anesthetized under ketamine/xylazine anesthesia (90 mg and 10 mg/100 g BW, respectively) and the subcutaneous inguinal (Sc Ing), Epid, interscapular BAT (iBAT) and aortic BAT (aBAT) fat pads were extracted and weighed. A sample of each fat depot was immediately frozen in liquid nitrogen for subsequent experiments.

2.3. Ethics approval

The protocol containing all animal procedures described in this study was specifically approved by the Committee on the Ethics of Animal Experiments of York University (York University Animal Care Committee, YUACC, permit number: 2021-03) and performed strictly in accordance with the YUACC guidelines. All tissue extraction procedures were performed under ketamine/xylazine anesthesia, and all efforts were made to minimize suffering [15]. All experiments in this study were carried out in compliance with the ARRIVE guidelines [16].

2.4. Measurement of blood glucose levels

Blood from all animals in the fed state was collected between 15:00 and 16:00 h by saphenous vein bleeding and used to determine plasma glucose using the Contour Next one meter blood glucose monitoring system by Ascensia Diabetes Care US (Parsippany, NJ, USA).

2.5. Adipocyte isolation from Epid and Sc Ing fat depots

Adipocyte isolation from the Epid and Sc Ing fat pads was performed as previously described [2]. Briefly, the adipose tissue was minced in Krebs-Ringer bicarbonate HEPES buffer (KRBH) prepared fresh on the day of each experiment from stock solutions of salts

and buffers (stored at 4°C) to give the following final concentrations: 120 mM NaCl, 4.8 mM KCl, 2.5 mM $CaCl_2$, 1.2 mM KH_2PO_4, 1.2 mM $MgSO_4$, 15 mM $NaHCO_3$, 30 mM HEPES, and type II collagenase (0.5 mg/mL). Before use, KRBH was gassed for 45 min with carbogen (95% O_2, 5% CO_2) and then BSA (3.5%) and glucose (5.5 mM) were added. pH of the buffer was adjusted to 7.4 with NaOH. Minced tissues were incubated at 37°C with gentle agitation (120 orbital strokes/ min) for ~25–30 min. The digested tissue was then strained using a nylon mesh, and cells were transferred to 50 mL tubes, washed three times, and resuspended in KRBH containing 3.5% fatty acid-free BSA (KRBH-3.5% BSA). To distribute an equal number of adipocytes in each treatment condition, cell diameters were measured and total cell numbers were determined [17].

2.6. Isolation of BAT adipocytes

iBAT and aBAT were extracted and carefully trimmed of any muscle, connective tissue, and white fat. The tissues were then used for adipocyte isolation as previously described [18]. To increase the yielding of brown adipocytes, iBAT and aBAT were combined. The tissues were initially incubated in KRBH-4% BSA supplemented with collagenase (0.83 mg/mL) at 37°C under orbital agitation (120 orbital strokes/min) for 5 min. Subsequently, the combined tissues were vortexed for 5 s, the contents of the vial were filtered, and the filtrate was discarded. The remaining tissues were finely minced and incubated in fresh KRBH-4% BSA containing collagenase (0.83 mg/mL) at 37°C under orbital agitation (120 orbital strokes/min) until complete digestion. The procedure then continued as described above for WAT adipocyte isolation.

2.7. Measurement of glucose and palmitate oxidation

Glucose and palmitate oxidation as measures of oxidative capacity were assessed by production of $^{14}CO_2$ in BAT adipocytes (5×10^5 cells), as previously described [2]. Briefly, cells were incubated in KRBH-3.5% BSA containing either 0.2 μCi/mL of [1-^{14}C]palmitic acid and 200 μM nonlabeled palmitate or 0.2 μCi/mL of D-[U-^{14}C]glucose and 5.5 mM nonlabelled D-glucose for 1h. To distinguish substrate utilization used for ATP synthesis (coupled oxidation) from proton leak (uncoupled oxidation), 15 min before incubation, adipocytes were treated with the ATP synthase inhibitor oligomycin (Oligo) [2]. Following 1 h of incubation, either in the absence or continuous presence of Oligo (100 μM), the media were acidified with 0.2 mL of H_2SO_4 (5 N), and the vials were maintained sealed at 37°C for an additional 1 h for the collection of $^{14}CO_2$ released from the cells and the media. The vials used for incubation had a centered isolated well containing a loosely folded piece of filter paper that was moistened with 0.2 mL of 2-phenylethylamine/methanol (1:1, vol:vol) for the capture of $^{14}CO_2$. At the end of the incubation, the filter paper was removed and transferred to a scintillation vial for radioactivity counting [2,6,19]. All oxidation values are expressed as fold change of Oligo-induced oxidation over basal oxidation.

2.8. Measurement of glucose incorporation into lipids

Glucose incorporation into lipids was measured in isolated adipocytes (5×10^5 cells) from the Epid and Sc Ing fat depots as previously described [19]. Briefly, cells were incubated in KRBH-3.5% BSA containing 0.2 μCi/mL of D-[U-^{14}C] glucose and 5.5 mM nonlabelled D-glucose for 1 h in the absence or presence of insulin (100 nM). Lipids were then extracted according to the method of Dole and Meinertz [20] and assessed for radioactivity [19]. Data are expressed as the fold change of insulin-stimulated glucose incorporation into lipids, relative to basal glucose incorporation into lipids.

2.9. Measurement of glycerol release

Lipolysis was measured in isolated Epid and Sc Ing adipocytes (6×10^5 cells). Adipocytes were incubated in the absence or presence of 100 nM Iso (β-nonspecific agonist) [21]. Each condition was assayed in triplicates and the samples were incubated for 75 min at 37°C with gentle agitation (80 orbital strokes/min). After incubation, a 200 μL aliquot of medium was taken from each vial for the determination of glycerol concentration. Data are expressed as Iso-stimulated glycerol release, over basal glycerol release.

2.10. Western blotting analysis of UCP1, PGC1α, β3AdR, ATGL and GyK in WAT and BAT

Sc Ing, Epid and iBAT samples were homogenized in a buffer containing 25 mM Tris-HCl, 25 mM NaCl (pH 7.4), 1 mM $MgCl_2$, 2.7 mM KCl, 1% Triton X-100 and protease and phosphatase inhibitors (Roche Diagnostics GmbH, Mannheim, Germany). Homogenates were centrifuged, the infranatant was collected, and an aliquot was used to measure protein by the Bradford method. Samples were diluted 1:1 (vol:vol) with 2x Laemmli sample buffer and heated to 95°C for 5 min. 25 μg of protein were loaded in each well. Samples were then subjected to SDS-PAGE, transferred to PVDF membrane, and probed for the proteins of interest. All primary antibodies were used at a dilution of 1:1,000. All densitometry analyses were performed using the ImageJ program.

2.11. Statistical analyses

Data were expressed as Mean ± SEM. Statistical analyses were performed by using mixed-model analyses and one-way ANOVAs with Bonferroni multiple comparison *post hoc* tests, as indicated in the figure legends. The GraphPad Prism software version 9.1.12 was used for all statistical analyses and for the preparation of all graphs. The level of significance was set to $P<.05$.

3. Results

3.1. Effect of diet on body weight (BW), plasma BHB levels, and blood glucose concentration

As expected, all groups of animals displayed a progressive increase in BW throughout the 16-week feeding period. At the end of the study, BW was slightly higher in HFS- and KD-fed rats than the SC-fed counterparts, however these differences were not statistically significant (Table 2). When expressed as percent increase in weight gain relative to baseline, the HFS and KD induced 1.2-fold increases in this parameter (Table 2). Plasma BHB was significantly elevated by the KD at weeks 4, 8, and 16 when compared to both the SC and HFS groups (Table 2). At week 8, BHB levels were significantly higher in HFS-fed rats than the SC-fed group; however, at week 16, BHB levels did not differ between these two groups (Table 2). Fed-state blood glucose levels were significantly higher in HFS- than SC-fed animals at weeks 4 and 16, whereas in KD-fed rats glycaemia was not significantly increased (Table 2).

3.2. Energy intake and energy efficiency in SC, HFS and KD-fed animals

Total energy intake during the 16-week feeding period was similar between the three groups (Table 3). However, energy efficiency at week 16 was significantly elevated in KD-fed animals when compared to the SC group (Table 3).

Table 2
The effects of a standard chow (SC), high-fat, sucrose-enriched (HFS) diet or a ketogenic diet (KD) on body weight, % increase in body weight relative to baseline, plasma β-hydroxybutyrate (BHB) levels and blood glucose concentration after 0, 4, 8, and 16 weeks of feeding.

		Duration of study (weeks)			
		0	4	8	16
Body weight (g)	SC	247.2 ± 4.7	403.8 ± 15.9	486.3 ± 17.8	553.9 ± 20.0
	HFS	232.7 ± 4.2	407 ± 14.7	504.7 ± 16.2	590.3 ± 24.3
	KD	245.3 ± 5.1	409.3 ± 9.2	511.4 ± 13.0	607.9 ± 19.1
Body weight increase relative to week 0 (%)	SC	-	64.2 ± 4.9	96.7 ± 5.9	124.1 ± 6.6
	HFS	-	76.3 ± 3.7	116.8 ± 5.4	153.2 ± 8.1*
	KD	-	70.3 ± 4.5	108.9 ± 5.7	148.1 ± 7.5*
Plasma BHB (mM)	SC	0.12 ± 0.01	0.13 ± 0.01	0.14 ± 0.01	0.15 ± 0.01
	HFS	0.16 ± 0.02	0.19 ± 0.03	0.24 ± 0.03*	0.15 ± 0.02
	KD	0.13 ± 0.02	0.30 ± 0.03†	0.38 ± 0.03†	0.29 ± 0.02†
Blood glucose (mM)	SC	7.4 ± 0.2	6.8 ± 0.3	6.8 ± 0.2	5.9 ± 0.3
	HFS	7.3 ± 0.1	7.3 ± 0.2*	7.2 ± 0.1	6.7 ± 0.3*
	KD	7.3 ± 0.1	7.2 ± 0.1	7.0 ± 0.1	6.6 ± 0.2

* $P<.05$ vs SC in the respective week;
† $P<.05$ vs all other groups. Data are expressed as mean ± SEM. Mixed-effects model analysis. $n=6–9$ for body weight and % increase in weight gain. $n=6–7$ for BHB. $n=6–15$ for blood glucose.

Table 3
Effect of diet on total energy intake for the 16-week intervention and energy efficiency.

	SC	HFS	KD
Total energy intake (kcal)	9554 ± 478.1	8814 ± 318.3	9010 ± 517.7
Energy efficiency (g/kcal)	$0.033 \pm 7.4 \times 10^{-4}$	$0.035 \pm 9.7 \times 10^{-4}$	0.039 ± 0.002*

* $P<.05$ vs SC. Data are expressed as mean ± SEM. One-way ANOVA. $n=4$.

3.3. Effect of diet on WAT and BAT masses

At week 8 of the intervention, Sc Ing fat mass was 2.6- and 2.1-fold higher in HFS and KD-fed animals than SC-fed rats, respectively (Fig. 1A). At week 16, Sc Ing mass increased significantly in all three groups in comparison to week 8, but HFS and KD-fed animals continued to display significantly higher Sc Ing fat masses than SC-fed rats (Fig. 1A). Similarly, at week 8, Epid fat mass was significantly elevated in HFS- (~2.7-fold) and KD-fed (~2-fold) rats when compared to SC-fed counterparts (Fig. 1B). At week 16, Epid fat masses of HFS- and KD-fed animals were 2- and 1.9-fold higher than the SC group, respectively (Fig. 1B). With respect to BAT, the HFS diet and the KD increased week 8 iBAT mass by 1.6- and 1.4-fold, respectively, relative to the SC animals (Fig. 1C). At week 16, the HFS diet and KD-induced elevation in iBAT mass was maintained (Fig. 1C). The aBAT was also found to be elevated by the HFS diet at weeks 8 and 16, and by the KD at week 16 (Fig. 1D), relative to the SC group. Therefore, despite possessing different macronutrient compositions, the HFS diet and KD induced similar alterations in WAT and BAT mass (Fig. 1).

3.4. Effects of diet on browning, lipolytic proteins, and β-adrenergic-stimulated lipolysis in Sc Ing fat

Given these diet-induced differences in fat mass, it was important to investigate how the interventions were influencing metabolism at the tissue and cellular levels. Firstly, Sc Ing UCP1 levels were measured to determine whether the KD induced browning in this tissue. We found that Sc Ing UCP1 was undetectable after either 8 or 16 weeks of any of the three dietary interventions (Fig. 2A). At week 8 of the intervention, Sc Ing β3AdR and ATGL levels were elevated 4.5- (Fig. 2B) and 4-fold (Fig. 2C), respectively, in KD-fed animals. Sc Ing ATGL was also increased by the HFS diet at week 8 (Fig. 2C). However, at week 16, no differences were detected in β3AdR levels among the three groups (Fig. 2D), although ATGL was 2.1-fold higher in HFS- than SC-fed rats (Fig. 2E). In line with these findings, β-adrenergic stimulated glycerol release was not significantly different between the three diet groups (Fig. 2F). Thus, the KD did not induce browning and although it promoted a transient increase in lipolytic capacity, these effects were not sustained at week 16.

3.5. Effects of diet on browning, lipolytic proteins and β-adrenergic-stimulated lipolysis in Epid fat

Similar to the Sc Ing fat, UCP1 was not detectable in the Epid fat depot with any of the three diets (Fig. 3A). At week 8, Epid β3AdR (Fig. 3B) and ATGL (Fig. 3C) levels were not significantly different between the three groups, although much lower levels of ATGL ($P=.06$ vs SC) were found in the Epid fat of HFS-fed rats. At week 16, Epid β3AdR levels were significantly elevated 3.6- and 4.7-fold by the HFS diet and KD, respectively (Fig. 3D), whereas ATGL content was not altered (Fig. 3E). Despite elevations in Epid β3AdR content, the HFS diet attenuated (~49%) Iso-stimulated lipolysis in comparison to the SC group (Fig. 3F). Conversely, in Epid adipocytes from KD-fed rats, Iso-stimulated lipolysis was maintained at the same levels as those of SC-fed counterparts (Fig. 3F).

3.6. Effect of diet on glucose incorporation into lipids and GyK content in Sc Ing and Epid fat

In Sc Ing adipocytes from HFS-fed rats, insulin-stimulated lipogenesis was 82.6% lower than the SC group (Fig. 4A), whereas in adipocytes from KD-fed rats this variable did not differ from the SC group (Fig. 4A). This indicates that the KD preserved insulin sensitivity and lipid deposition in Sc Ing adipocytes. In Epid adipocytes, insulin-stimulated lipogenesis was not altered by diet

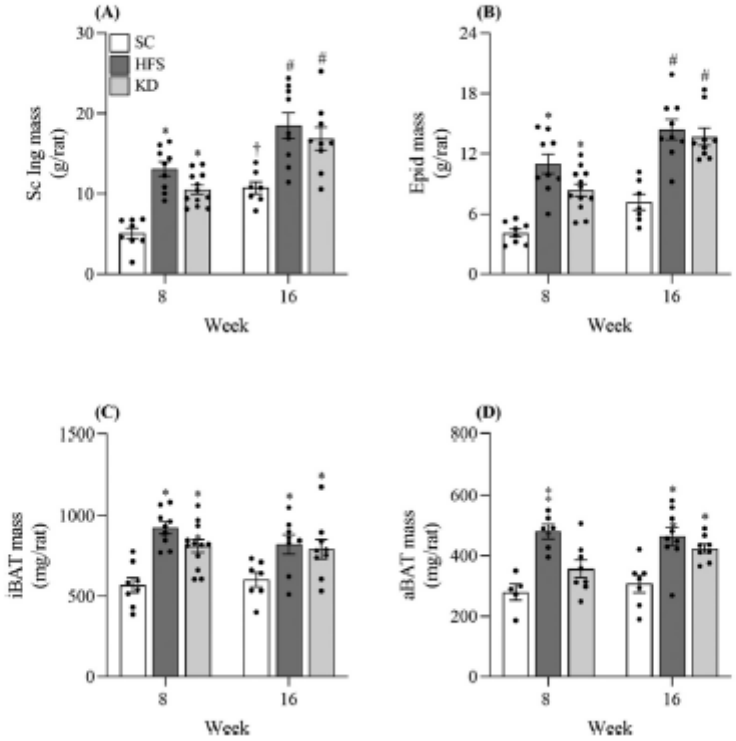

Fig. 1. HFS and KD-feeding significantly elevated subcutaneous inguinal (Sc Ing) (A) and epididymal (Epid) (B) fat masses. Sc Ing mass increased from week 8 to week 16 with all diets (A); however, only the HFS and KDs significantly enhanced Epid mass over this time (B). Interscapular BAT (iBAT) (C) and aortic BAT (aBAT) (D) masses were elevated in both the HFS and KD-fed animals at week 16 of the intervention. However, at week 8, only the HFS diet caused aBAT growth (D). *$P<.05$ vs SC, within the respective week; #$P<.05$ vs week 8, within the respective group, and week 16 SC; †$P<.05$ vs week 8, within group; ‡$P<.05$ vs week 8 SC and week 8 KD. Bars represent mean ± SEM. Two-way ANOVA. $n=5$–12.

(Fig. 4B), showing fat-depot specific differences in response to dietary intervention. Furthermore, in Sc Ing and Epid adipocytes, the KD increased GyK levels by 7- and 5.5-fold, respectively (Fig. 4C and D). Thus, the KD preserved the ability of adipocytes to promote lipogenesis in response to insulin and to also recycle TAG by increasing GyK levels.

3.7. Effects of diet on BAT uncoupled oxidation

At week 16, uncoupled palmitate oxidation was elevated 1.9-fold in brown adipocytes from KD-fed animals when compared to HFS-fed animals (Fig. 5A), whereas glucose oxidation was not altered by diet (Fig. 5B). UCP1 levels did not significantly increase in BAT of HFS-fed animals (Fig. 5C); however, in BAT adipocytes from KD-fed rats UCP1 levels increased 4.9- and 2.1-fold, when compared to the SC and HFS groups, respectively (Fig. 5C). Other thermogenic proteins such as PGC1α (Fig. 5D), β3AdR (Fig. 5E), and ATGL (Fig. 5F) were not changed by any of the diets, but GyK levels increased 4.2- and 6.5-fold in BAT of HFS and KD-fed animals, respectively (Fig. 5G).

4. Discussion

In this study, we show that a high-fat KD, devoid of carbohydrate, increased BAT uncoupled FA oxidative capacity and the machinery involved in lipolysis and TAG recycling in WAT. This was characterized by elevated UCP1 levels and uncoupled fatty acid oxidation in BAT, and increased GyK levels in WAT. Despite these adaptive responses being typically associated with dissipation as opposed to energy storage [14], the WAT mass of KD-fed animals increased to a level similar to the HFS diet. However, a major difference between the KD and the HFS diet was that the former sustained insulin-stimulated lipogenesis, whereas the latter impaired it. Thus, contrary to the obesogenic HFS diet, the KD-induced increase in adiposity did not impair the classical physiological functions of the WAT. Besides maintaining insulin-stimulated lipogenesis and Iso-stimulated lipolysis, the KD also upregulated a pathway by which white adipocytes can recycle TAG via GyK-mediated glycerol phosphorylation. These adaptive responses in WAT are compatible with an enhanced ability of this tissue to handle an abundant supply of food-derived fat and of NEFAs that escape oxidation in peripheral tissues and return to the WAT.

Neither the Sc Ing nor the Epid fat depots had detectable levels of UCP1, which indicates that the KD did not induce browning of the WAT. Previous studies have proposed that the KD causes browning in Sc Ing [12] and Epid [22] WAT. However, these studies measured the gene expression of UCP1 [12,22] and other markers of browning [12]. Evidently, this does not necessarily translate to KD-induced alterations in protein levels, indicating that

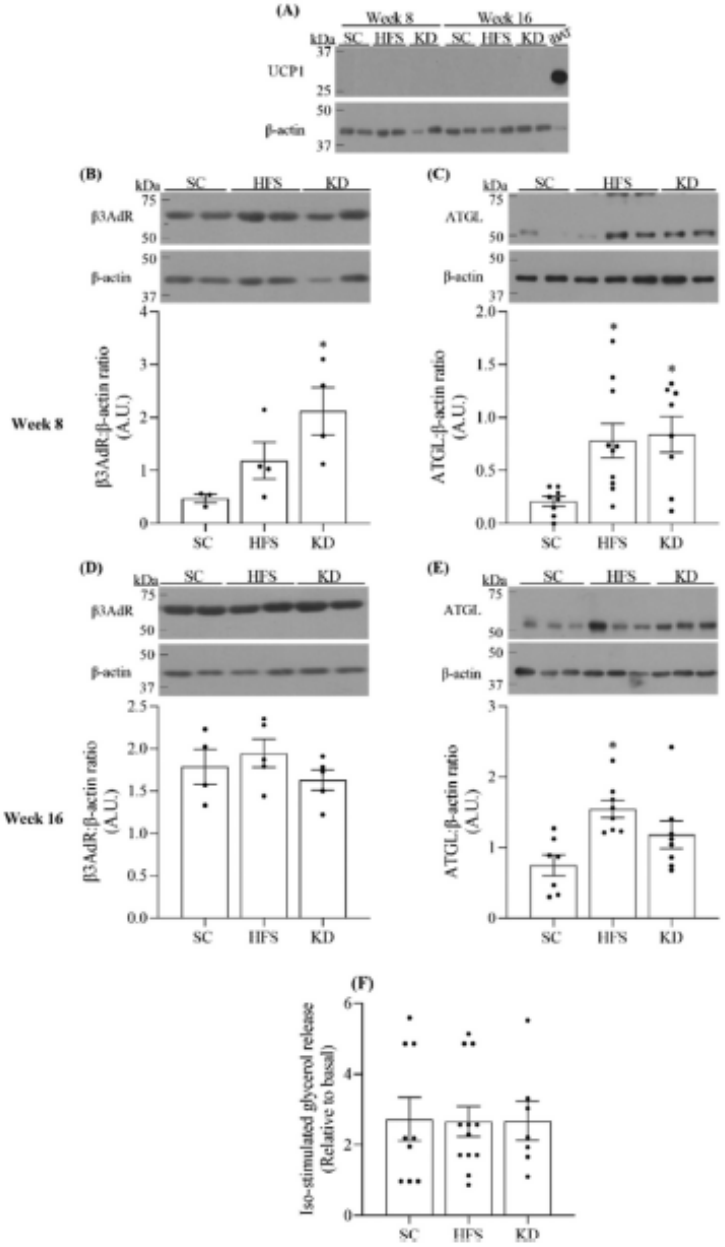

Fig. 2. Uncoupling protein-1 (UCP1) levels were undetectable in Sc Ing fat either at week 8 or 16 (A). At week 8 of the intervention, β3-adrenergic receptor (β3AdR) levels were increased by the KD (B), and adipose triglyceride lipase (ATGL) was significantly elevated by HFS and KD (C). At week 16, β3AdR (D) and ATGL (E) protein levels diminished, where β3AdR was not altered by any of the diets and ATGL was only increased by the HFS diet (D and E, respectively). Isoproterenol (Iso)-stimulated lipolysis was not significantly different between the three groups (F). *$P<.05$ vs SC. Bars represent mean ± SEM. One-way ANOVA. $n=3–12$.

UCP1-mediated thermogenesis was not enhanced by KD in WAT. However, the WAT of KD-fed rats displayed time-dependent and depot-specific responses to different diets with regards to levels of lipolytic proteins and how each fat depot responded to β-adrenergic-induced lipolysis. This was evident for β3-AdR and ATGL levels that increased in the Sc Ing fat depot at week 8 of KD and HFS feeding, whereas at week 16 only ATGL was elevated in HFS-fed rats. Conversely, the Epid fat of KD- and HFS-fed rats had unchanged levels of β3-AdR and ATGL at week 8, but at week 16 both diets elevated β3-AdR levels in the tissue. Furthermore, rates of Iso-stimulated lipolysis were not affected by the dietary interventions in Sc Ing adipocytes, whereas in Epid fat adipocytes the

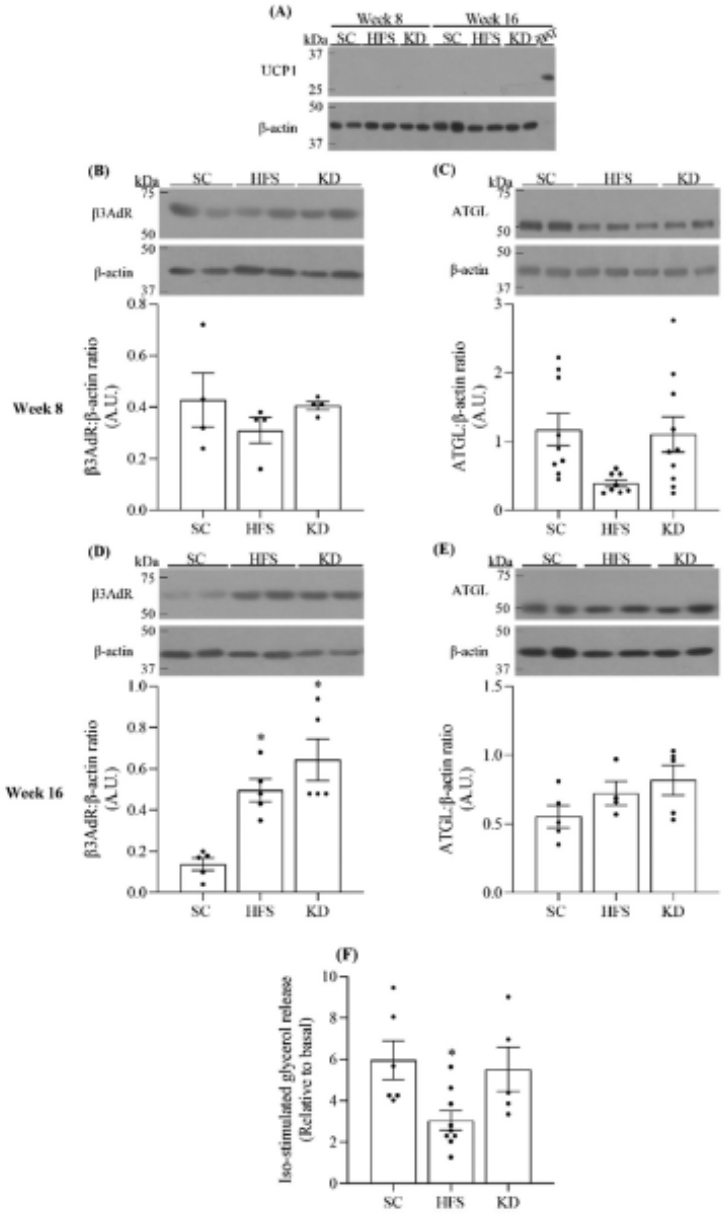

Fig. 3. In Epid fat, UCP1 levels (A) were undetectable and β3AdR (B) and ATGL (C) levels were not altered at week 8, although, Epid ATGL did show a trend to decrease with the HFS diet (C). At week 16, β3AdR levels were increased in the Epid fat of HFS and KD-fed animals (D). ATGL did not differ among the groups (E). The HFS diet significantly attenuated isoproterenol (Iso)-stimulated lipolysis in Epid adipocytes (F). *$P<.05$ vs SC. Bars represent mean ± SEM. One-way ANOVA. $n=4–10$.

HFS diet markedly reduced it. This impairment in lipolytic capacity is supported by existing literature reporting that obesity causes catecholamine resistance and blunts β-adrenergic-stimulated lipolysis [7]. Along the same lines, the HFS diet-induced elevation in Epid β3AdR was not sufficient to reverse the attenuation in β-adrenergic signaling. These fat-depot specific patterns of adaptations in WAT indicate that fat accumulation was favored in visceral over Sc WAT, which is metabolically detrimental [1]. Additionally, because adiposity similarly increased in HFS- and KD-fed rats at weeks 8 and 16, time and fat depot-specific effects of the KD do not seem to dictate accrual of fat mass. However, by preserving the lipolytic and lipogenic responses of the WAT, the KD likely exerted a protective effect against the potentially harmful effects of diet-induced obesity.

In addition to the WAT-specific effects, the KD also altered metabolism in BAT. Similar to previous studies, we found that the

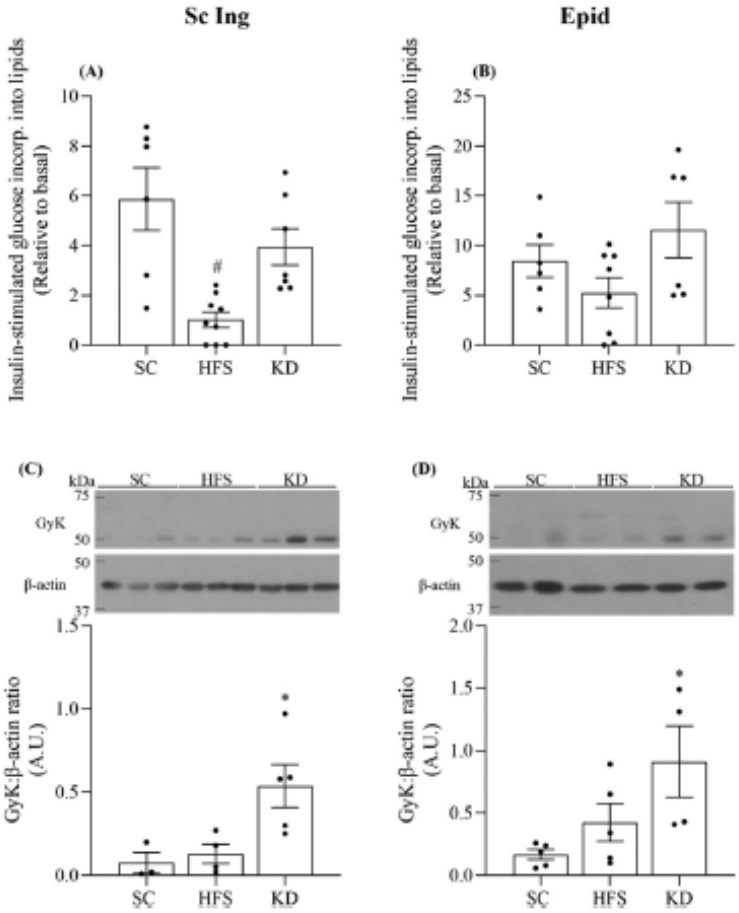

Fig. 4. HFS-feeding significantly impaired insulin-stimulated glucose incorporation into lipids (A) in Sc Ing adipocytes, but not in Epid adipocytes (B). The KD significantly elevated glycerol kinase (GyK) levels in Sc Ing (C) and Epid (D) fat pads. *$P<.05$ vs SC; #$P<.05$ vs all other groups. Bars represent mean ± SEM. One-way ANOVA. $n=3$–9.

KD increased BAT UCP1 content [12,23]. However, to our knowledge, the effects of the KD on palmitate and glucose oxidation in brown adipocytes have not been investigated. We measured Oligo-induced vs basal oxidation as a measure of uncoupled oxidation, where the ratio between Oligo-induced and basal oxidation represents the capacity for proton leak and, thus, uncoupling capacity in brown adipocytes [2]. Here, we show that the KD enhanced the Oligo-induced oxidation of fatty acids in BAT, relative to basal, when compared to the HFS diet group. In line with these findings, the KD also significantly elevated BAT GyK content. In BAT, GyK mediates the replenishment of the TAG supply for thermogenesis [24]. In fact, it has been shown that cold exposure significantly increased BAT GyK activity and expression in rats [24]. Thus, the observed elevations in UCP1, GyK and palmitate oxidation suggest that KD-feeding could potentially enhance BAT thermogenesis. These effects were consistent with the enhancement in BAT mass in the KD-fed animals. On the other hand, the HFS-induced elevation in iBAT mass could be attributed to the increased GyK content that was not met with an increase in fat consumption, leading to lipid accumulation and BAT growth.

The KD-induced increase in body weight and adiposity was contrary to our original hypothesis and contradicts what has been reported in studies that show that KD attenuates body weight, body mass index [10], and fat mass [11]. However, in these studies, energy intake was either not reported [10] or the KD was hypocaloric [11]. This is relevant because it did not discriminate whether the observed effects were caused by reduced energy intake or due to altered macronutrient composition of the diet. In fact, studies that use a KD that is isocaloric to the control diet generally show that fat mass is not significantly reduced [23,25], and may even be elevated under KD conditions [22]. Similarly, we also observed a KD-induced increase in fat mass under isocaloric conditions, which was likely supported by the enhanced energy efficiency observed in these animals, and a reduction in energy expenditure [14]. In this context, the KD-induced elevation in BAT thermogenic capacity was likely not sufficient to account for the increased dietary fat intake under chronic KD conditions. Furthermore, TAG recycling may not have increased energy expenditure enough to induce fat loss [26]. This limited capacity to oxidize fat could have led to the diversion of fatty acids for storage in the WAT, driving the increase in adiposity. Nevertheless, TAG recycling remains a crucial mechanism under KD conditions because it allowed the WAT to cope with the abundance of dietary fat [2,27], which likely facilitated the preservation of catecholamine and

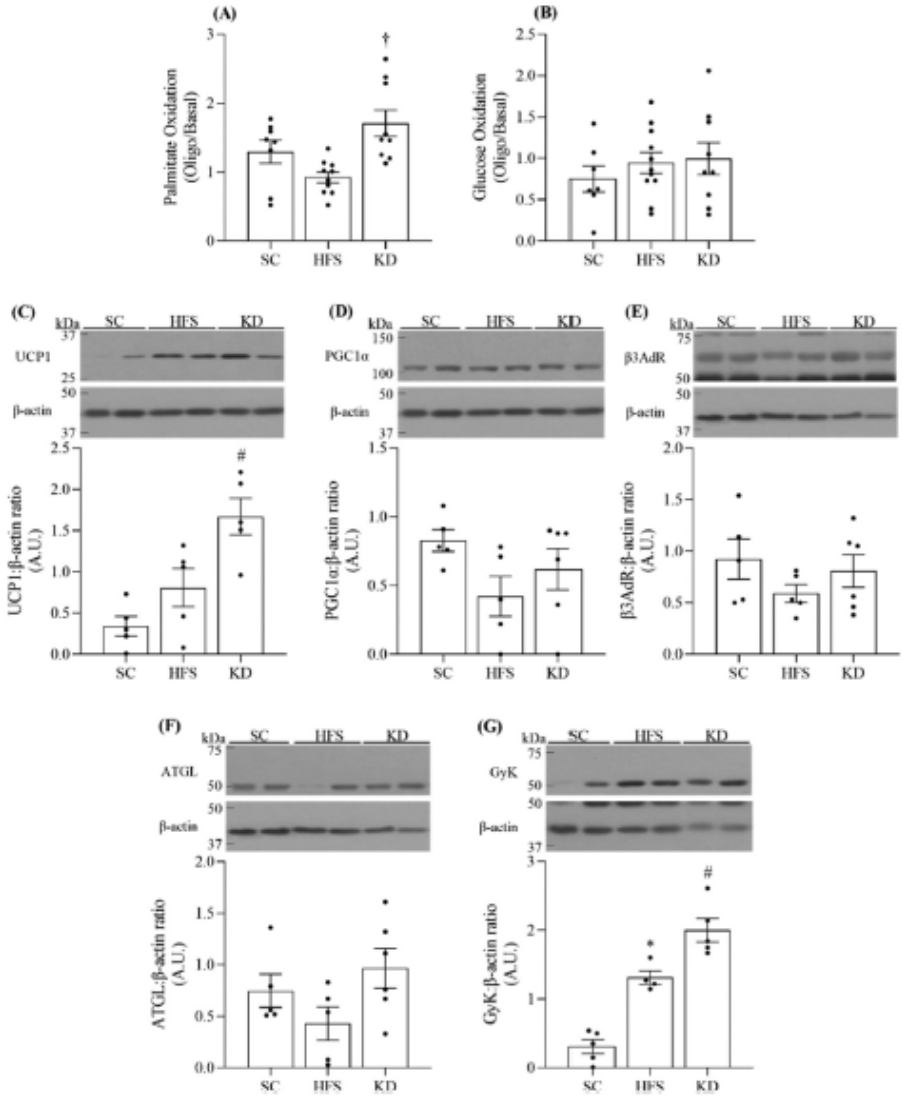

Fig. 5. The KD increased uncoupled oxidation of palmitate (A) but not glucose oxidation (B) in brown adipocytes. The KD also increased UCP1 levels in BAT (C), whereas peroxisome proliferator-activated receptor gamma coactivator 1-alpha (PGC1α) (D), β3AdR (E), and ATGL (F) did not change with dietary intervention. However, GyK (G) was significantly elevated by HFS and KD, reaching higher levels in the latter . *$P<.05$ vs SC; #$P<.05$ vs all other groups; †$P<.05$ vs HFS. Bars represent mean ± SEM. One-way ANOVA. $n=4$–11.

insulin sensitivity in the white adipocytes [1,6]. In turn, it is plausible that the maintenance of insulin-stimulated lipogenesis and β-adrenergic stimulated lipolysis prevented hyperglycemia in these animals, despite the robust increase in fat mass [1]. Altogether, our data support the notion that adiposity is not necessarily the cause of disease [1]. Rather, it is the dysfunctional storage and breakdown of fat that triggers the onset of metabolic disorders [1].

It is important to consider that the protein contents of the HFS and KDs differed from that of the SC diet, where the two former diets had 20% kcal from protein and the latter was 27%. Because total energy intake was not different, this means that kcal from protein was lower in the HFS and KDs. Importantly, a low protein diet has been shown to increase sympathetic flux to BAT and induce thermogenesis in this tissue [28]. Therefore, we cannot discard the possibility that lower dietary protein content in KD- and HFS-fed rats could have induced BAT activation and potentially impacted BAT uncoupled oxidation, when compared to the SC group. However, despite equal protein contents in the HFS and

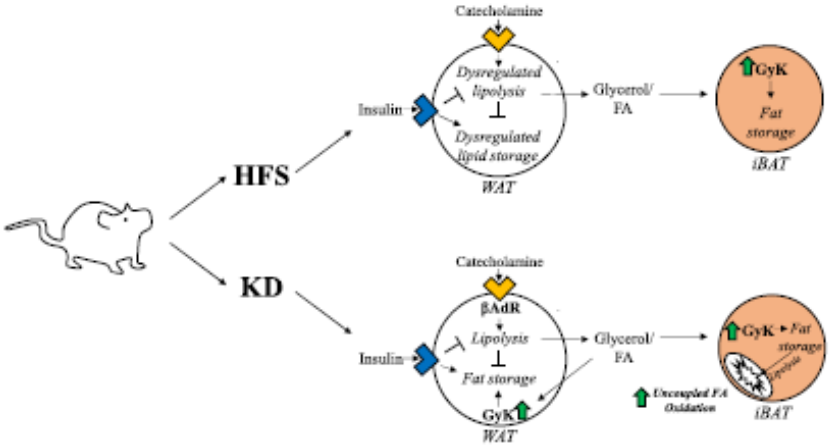

Fig. 6. The HFS diet impaired insulin-stimulated glucose incorporation into lipids and Iso-stimulated lipolysis in WAT. The HFS diet also decreased uncoupled FA oxidation and upregulated GyK in BAT. These metabolic adaptations likely enhanced the lipid storage in BAT as lipogenesis in WAT was impaired. In contrast, the KD preserved lipolysis and lipogenesis in the white adipocytes and increased GyK levels. These KD effects enabled the WAT to recycle glycerol and resynthesize lipids under conditions of enhanced lipolysis. Furthermore, the BAT of KD-fed animals had increased levels of UCP1 and enhanced uncoupled fat oxidation. The fat supply for uncoupled oxidation in BAT was maintained by the elevation in GyK. These energy-dissipating mechanisms allowed the WAT and BAT from KD-fed rats to better cope with the abundance of fat in the diet. Abbreviation: BAT, brown adipose tissue; KD, ketogenic diet; WAT, white adipose tissue; UCP1, Uncoupling protein-1.

KD groups, we observed an elevation in uncoupled oxidative capacity in the BAT of KD-fed animals, relative to HFS. Additionally, GyK was measured as an indication of fat-storing capacity and was proposed to enhance the supply for uncoupled FA oxidation in BAT from KD-fed animals. However, glycerol 3-phosphate may also be used by mitochondrial glycerol 3-phosphate dehydrogenase (mGPDH) to provide reducing equivalents for the electron transport chain [29]. This points to an alternative fate for glycerol 3-phosphate that contributes to thermogenesis in BAT [29]. However, mGPDH activity was not assessed in the present study and warrants future investigations into the potential effects of the KD on the glycerol 3-phosphate shuttle and mGPDH-mediated thermogenesis.

In conclusion, the KD enhanced uncoupled FA oxidation in BAT, increased the machinery for TAG recycling in white adipocytes, and preserved insulin sensitivity and lipolytic capacity in visceral and Sc WAT (Fig. 6). Despite upregulating these energy-dissipating pathways, this was not sufficient to overcome the abundance of dietary fat, leading to increased storage in the white fat depots. However, the induction of these pathways was crucial to prevent metabolic dysregulation and preserve insulin-stimulated lipogenesis [6] in a condition of increased adiposity in KD-fed rats. Together, these effects-maintained WAT function and could prevent ectopic lipid accumulation, which is of great importance to counteract obesity-induced dysfunctional metabolic alterations in WAT [1,8].

Authors Contributions

DD was involved in the conception and design of the study, conducted experiments, analyzed the results, prepared figures, drafted the article, and revised the manuscript. SJ conducted experiments, analyzed the results, and revised the manuscript. MS conducted experiments, analyzed the results, and revised the manuscript. RBC was involved in the conception and design of the study, conducted experiments, drafted the article, and revised the manuscript. All authors gave final approval of the revised version submitted and agreed to be accountable for all aspects of the work in ensuring that questions that may arise related to the accuracy or integrity of any part of the work are appropriately investigated and resolved.

Declarations of Competing Interest

The authors declare that there are no conflicts of interest.

Funding

This research was funded by a Natural Science and Engineering Research Council of Canada Discovery Grant (RBC, #311818-2011) and infrastructure grants from the Canada Foundation for Innovation and the Ontario Research Fund awarded to RBC. DD was supported by the Natural Sciences and Engineering Research Council of Canada Alexander Graham Bell Canada Graduate Scholarship-Doctoral.

References

[1] Roden M, Shulman GI. The integrative biology of type 2 diabetes. Nature 2019;576:51–60. doi:10.1038/s41586-019-1797-8.
[2] Sepa-Kishi DM, Jani S, Da Eira D, Ceddia RB. Cold acclimation enhances UCP1 content, lipolysis, and triacylglycerol resynthesis, but not mitochondrial uncoupling and fat oxidation, in rat white adipocytes. Am J Physiol - Cell Physiol 2019;316:C365–76. doi:10.1152/ajpcell.00122.2018.
[3] So M, Gaidhu MP, Maghdoori B, Ceddia RB. Analysis of time-dependent adaptations in whole-body energy balance in obesity induced by high-fat diet in rats. Lipids Health Dis 2011;10:1–12. doi:10.1186/1476-511X-10-99.
[4] Wu MV, Bikopoulos G, Hung S, Ceddia RB. Thermogenic capacity is antagonistically regulated in classical brown and white subcutaneous fat depots by high fat diet and endurance training in rats: Impact on whole-body energy expenditure. J Biol Chem 2014;289:34129–40. doi:10.1074/jbc.M114.591008.
[5] Guilherme A, Virbasius JV, Puri V, Czech MP. Adipocyte dysfunctions linking obesity to insulin resistance and type 2 diabetes. Nat Rev Mol Cell Biol 2008;9:367–77. doi:10.1038/nrm2391.Adipocyte.
[6] Gaidhu MP, Anthony NM, Patel P, Hawke TJ, Ceddia RB. Dysregulation of lipolysis and lipid metabolism in visceral and subcutaneous adipocytes by high-fat diet: Role of ATGL, HSL, and AMPK. Am J Physiol - Cell Physiol 2010;298:961–71. doi:10.1152/ajpcell.00547.2009.
[7] Mowers J, Uhm M, Reilly SM, Simon J, Leto D, Chiang SH, et al. Inflammation produces catecholamine resistance in obesity via activation of PDE3B by the protein kinases IKKε and TBK1. Elife 2013;132:1–18. doi:10.7554/eLife.01119.
[8] Jani S, Da Eira D, Hadday I, Bikopoulos G, Mohasses A, de Pinho RA, et al. Distinct mechanisms involving diacylglycerol, ceramides, and inflammation un-

derlie insulin resistance in oxidative and glycolytic muscles from high fat-fed rats. Sci Rep 2021;11:19160. doi:10.1038/s41598-021-98819-7.
[9] Longo R, Peri C, Cricr D, Coppi L, Caruso D, Mitro N, et al. Ketogenic diet : a new light shining on old but gold biochemistry. Nutrients 2019;11:1–22.
[10] Walton CM, Perry K, Hart RH, Berry SL, Bikman BT. Improvement in glycemic and lipid profiles in type 2 diabetics with a 90-day ketogenic diet. J Diabetes Res 2019;2019:1–6. doi:10.1155/2019/8681959.
[11] Luukkonen PK, Dufour S, Lyu K, Zhang XM, Hakkarainen A, Lehtimäki TE, et al. Effect of a ketogenic diet on hepatic steatosis and hepatic mitochondrial metabolism in nonalcoholic fatty liver disease. Proc Natl Acad Sci U S A 2020;117:7347–54. doi:10.1073/pnas.1922344117.
[12] Douris N, Desai BN, Fisher M, Cisu T, Fowler AJ, Zarebidaki E, et al. Beta-adrenergic receptors are critical for weight loss but not for other metabolic adaptations to the consumption of a ketogenic diet in male mice. Mol Metab 2017;6:854–62. doi:10.1016/j.molmet.2017.05.017.
[13] Sepa-Kishi DM, Ceddia RB. Exercise-mediated effects on white and brown adipose tissue plasticity and metabolism. Exerc Sport Sci Rev 2016;44:37–44. doi:10.1249/JES.0000000000000068.
[14] Basolo A, Magno S, Santini F, Ceccarini G. Ketogenic diet and weight loss: is there an effect on energy expenditure? Nutrients 2022;14. doi:10.3390/NU14091814.
[15] Pinho RA, Sepa-Kishi DM, Bikopoulos G, Wu MV, Uthayakumar A, Mohasses A, et al. High-fat diet induces skeletal muscle oxidative stress in a fiber type-dependent manner in rats. Free Radic Biol Med 2017;110:381–9. doi:10.1016/j.freeradbiomed.2017.07.005.
[16] du Sert NP, Ahluwalia A, Alam S, Avey MT, Baker M, Browne WJ, et al. Reporting animal research: Explanation and elaboration for the arrive guidelines 2.0. PLoS Biol 2020;18:e3000411. doi:10.1371/journal.pbio.3000411.
[17] Fine JB, DiGirolamo M. A simple method to predict cellular density in adipocyte metabolic incubations. Int J Obes Relat Metab Disord 1997;21:764–768.
[18] Cannon B, Nedergaard J. Respiratory and thermogenic capacities of cells and mitochondria from brown and white adipose tissue. In: Ailhaud G, editor. Adipose Tissue Protoc. New Jersey: Humana Press Inc.; 2001. p. 295–304.
[19] Gaidhu MP, Fediuc S, Anthony NM, So M, Mirpourian M, Perry RLS, et al. Prolonged AICAR-induced AMP-kinase activation promotes energy dissipation in white adipocytes: novel mechanisms integrating HSL and ATGL. J Lipid Res 2009;50:704–15. doi:10.1194/jlr.M800480-JLR200.
[20] Dole VP, Meinertz H. Microdetermination of long-chain fatty acids in plasma and tissues. J Biol Chem 1960;235:2595–9. doi:10.1016/s0021-9258(19)76920-8.
[21] Ahlquist RP. Present state of alpha- and beta-adrenergic drugs I. The adrenergic receptor. Am Heart J 1976;92:661–4.
[22] Asrih M, Altirriba J, Rohner-Jeanrenaud F, Jornayvaz FR. Ketogenic diet impairs FGF21 signaling and promotes differential inflammatory responses in the liver and white adipose tissue. PLoS One 2015;10:1–14. doi:10.1371/journal.pone.0126364.
[23] Srivastava S, Baxa U, Niu G, Chen X, Veech RL. A Ketogenic diet increases brown adipose tissue mitochondrial proteins and UCP1 levels in Mice. IUBMB Life 2013;65:58–66.
[24] Festuccia WTL, Guerra-Sá R, Kawashita NH, Garófalo MAR, Evangelista EA, Rodrigues V, et al. Expression of glycerokinase in brown adipose tissue is stimulated by the sympathetic nervous system. Am J Physiol - Regul Integr Comp Physiol 2003;284:1536–41. doi:10.1152/ajpregu.00764.2002.
[25] Hall KD, Chen KY, Guo J, Lam YY, Leibel RL, Mayer LES, et al. Energy expenditure and body composition changes after an isocaloric ketogenic diet in overweight and obese men. Am J Clin Nutr 2016;104:324–33. doi:10.1371/journal.pone.0222971.
[26] Elia M, Zed C, Neale G, Livesey G. The energy cost of triglyceride-fatty acid recycling in nonobese subjects after an overnight fast and four days of starvation. Metabolism 1987;36:251–5. doi:10.1016/0026-0495(87)90184-3.
[27] Guan HP, Li Y, Jensen MV, Newgard CB, Steppan CM, Lazar MA. A futile metabolic cycle activated in adipocytes by antidiabetic agents. Nat Med 2002;8:1122–8. doi:10.1038/nm780.
[28] Pezeshki A, Chelikani PK. Low protein diets and energy balance: mechanisms of action on energy intake and expenditure. Front Nutr 2021;8:1–8. doi:10.3389/fnut.2021.655833.
[29] Mráček T, Drahota Z, Houštěk J. The function and the role of the mitochondrial glycerol-3-phosphate dehydrogenase in mammalian tissues. Biochim Biophys Acta - Bioenerg 2013;1827:401–10. doi:10.1016/j.bbabio.2012.11.014.

Nutrition 105 (2023) 111862

Contents lists available at ScienceDirect

Nutrition

journal homepage: www.nutritionjrnl.com

Basic nutritional investigation

Obesogenic versus ketogenic diets in the regulation of the renin–angiotensin system in rat white and brown adipose tissues

Daniel Da Eira MSc, Shailee Jani MSc, Mateja Stefanovic, Rolando B. Ceddia PhD *

Muscle Health Research Centre, School of Kinesiology and Health Science, York University, North York, Ontario, Canada

ARTICLE INFO

Article History:
Received 23 March 2022
Received in revised form 13 June 2022
Accepted 26 September 2022

Keywords:
Obesity
ACE2
ERK
AT_1R
MasR
Subcutaneous fat
Visceral fat

ABSTRACT

Objective: The ketogenic diet (KD) has been reported to reverse metabolic dysfunction in obesity. However, it remains unknown how the KD affects the balance between the classical and counterregulatory renin-angiotensin system (RAS) arms in adipose tissue, which carries important implications for metabolic function in adipocytes. The aim of this study was to compare the effects of the obesogenic diet and the KD on RAS balance in white and brown fat.

Methods: Nine male Wistar rats were fed a standard chow (SC), 11 fed a high-fat sucrose-enriched (HFS) obesogenic diet, and 12 a KD. At the end of the 8-wk feeding period, subcutaneous inguinal (Sc Ing), epididymal (Epid), and interscapular brown adipose tissue (iBAT) fat depots were extracted and subsequently used for the measurement of RAS proteins and *MasR* gene expression.

Results: In SC-fed rats, the Sc Ing fat displayed the highest levels of angiotensin-converting enzyme (ACE)1, but very low levels of angiotensin II types 1 and 2 receptors (AT_1R and AT_2R) and ACE2. Conversely, the highest levels of ACE2, AT_1R, and AT_2R were found in iBAT. The HFS diet increased AT_1R protein in Sc Ing fat and iBAT, whereas the KD maintained low AT_1R levels in these fat depots. However, in Sc Ing and Epid fat depots, the KD elevated AT_2R levels and significantly reduced Epid ACE1 levels.

Conclusion: Despite fat depot-specific differences in RAS components, the obesogenic diet promoted the classical RAS arm, whereas the KD attenuated it and enhanced the counterregulatory arm.

Introduction

The renin-angiotensin system (RAS) is well known for its role in regulating blood pressure (BP) and fluid balance [1]. Under conditions of low BP, renin is released in a rate-controlled manner from the kidney. Renin cleaves liver-derived angiotensinogen to produce angiotensin I (Ang-I) [2]. Ang-I is then converted to angiotensin II (Ang-II) by angiotensin-converting enzyme (ACE)1 [2]. Finally, Ang-II interacts with the Ang II type 1 receptor (AT_1R) to promote, through the classical RAS arm, vasoconstriction and fluid retention, thereby regulating BP and fluid balance to homeostatic conditions [1,2]. However, hyperactivation of this pathway often leads to deleterious effects such as hypertension, fibrosis, and inflammation [1,2]. In opposition to the classical arm of the RAS is the counterregulatory arm. The latter is mediated by ACE2 [3,4], which converts Ang-II to angiotensin-[1,7] (Ang-[1,7]). Through the Mas receptor (MasR), Ang-[1,7] elicits several physiologic effects that oppose the ACE1/Ang-II/AT_1R arm of the RAS, including vasodilation, insulin sensitization, and anti-inflammatory effects [3–6].

One condition that promotes RAS hyperactivation is obesity [4,7], which is characterized by the expansion of adipose tissue [8,9]. Of the two major types of adipose tissue, white adipose tissue (WAT) is specialized in energy storage, whereas brown adipose tissue (BAT) burns energy and releases heat in a process known as thermogenesis [9–11]. In addition to their role in energy storage and thermogenesis, both WAT and BAT act as endocrine organs and express components of the RAS [12–14], although RAS regulation has been mostly attributed to alterations in WAT, particularly under conditions of obesity [6,13]. In fact, hyperactivation of the classical ACE1/Ang-II/AT_1R arm of the RAS lead to insulin resistance and WAT inflammation in mice overexpressing *Agt* [15]. These

This research was funded by a Natural Science and Engineering Research Council of Canada Discovery Grant awarded to RBC (RGPIN-2022–04517) and infrastructure grants from the Canada Foundation for Innovation and the Ontario Research Fund awarded to RBC. DD was supported by the Natural Sciences and Engineering Research Council of Canada – Alexander Graham Bell Canada Graduate Scholarship-Doctoral. DD conducted experiments, analyzed the results, prepared figures, and revised the manuscript. SJ and MS conducted experiments and revised the manuscript. RBC designed the experimental approach, conducted experiments, and revised the manuscript.

*Corresponding author: Tel.: +1 416 736 2100; Fax: +1 4167365774
E-mail address: roceddia@yorku.ca (R.B. Ceddia).

https://doi.org/10.1016/j.nut.2022.111862
0899-9007/

mice exhibited an elevated expression of the proinflammatory cytokine monocyte chemotactic protein (MCP)-1 in their epididymal (Epid) fat [15]. Consistent with these findings, Lee et al. observed an elevation in the expression of *MCP-1* in the Epid fat of Otsuka Long-Evans Tokushima Fatty (OLETF) rats that was significantly reduced with the administration of an angiotensin receptor blocker (ARB) [13]. Furthermore, incubation of 3T3-L1 adipocytes with Ang-II caused a reduction in insulin-stimulated glucose uptake in these cells, an effect that was reversed by angiotensin receptor blockade [13]. At the whole-body level, treatment with an ARB also improved glucose tolerance in OLETF rats [13]. These findings suggest that RAS activation in WAT has a major effect on insulin sensitivity and inflammation and plays a crucial role in the development of obesity-related metabolic disorders [13]. Conversely, the administration of Ang-[1,7] to mice fed a high-fat (HF) diet increased BAT Akt phosphorylation and improved homeostatic model assessment-insulin resistance [5]. It has also been reported that an elevation in WAT *MasR* expression, induced by the ACE-inhibitor enalapril, caused morphologic and functional conversion of WAT adipocytes into brown adipocytes (WAT browning), which carries great potential for the management of obesity and its related metabolic disorders [4,10]. In addition to the ACE2/Ang-[1,7]/MasR axis, another angiotensin receptor type, known as Ang-II type 2 receptor (AT_2R), exerts effects that are counterregulatory to the classical arm of the RAS, including improvements to insulin sensitivity [16] and inflammatory profile [6], as well as WAT browning [12]. Therefore, interventions that alter the balance between the classical and counterregulatory arms of the RAS appear to be effective at reversing obesity-related metabolic disorders. One dietary intervention that has been successful at reducing adiposity, improving insulin resistance, and attenuating inflammation has been the ketogenic diet (KD) [17,18]. However, to the best of our knowledge, it remains to be determined whether major differences exist in RAS regulation in WAT and BAT under obesogenic and ketogenic dietary conditions. In this context, we tested the hypothesis that, because of its anti-obesogenic effect [17,18], a KD would enhance the counterregulatory arm of the RAS in WAT and BAT, whereas under obesogenic dietary conditions, the classical RAS arm would be heightened in both fat depots. Here, we show that the KD shifted the WAT RAS profile to the counterregulatory arm and that the obesogenic diet elevated the ACE1/Ang-II/AT_1R arm in both WAT and BAT.

Materials and methods

Reagents

Protease (cOmplete Ultra Tablets) and phosphatase (PhosSTOP) inhibitors were obtained from Roche Diagnostics GmbH (Mannheim, Germany). The ACE1 (ab254222), ACE2 (ab108252), AT_1R (ab124734), and AT_2R (ab92445) antibodies were purchased from Abcam (Toronto, ON, Canada), and the β-actin, p44/42 mitogen-activated protein kinase (ERK1/2) and phosphorylated p44/42 $MAPK^{Thr202/Tyr204}$ (pERK1/2) antibodies were purchased from Cell Signaling (Danvers, MA, USA).

Animals

Male albino rats from the Wistar strain (Envigo, Indianapolis, IN, USA) weighing 200 to 250 g (initial weight) were maintained in a constant temperature (23°C), with a fixed 12-h light/12-h dark cycle and fed for 8 wk ad libitum either a standard chow (SC; n = 9) diet (27, 13, and 60% of calories provided by protein, fat, and carbohydrates, respectively) a HF, sucrose-enriched (HFS; n = 11) diet (20, 60, and 20% of calories provided by protein, fat, and carbohydrates [sucrose], respectively), or a KD (n = 12; 20, 80, and 0% of calories provided by protein, fat, and carbohydrates, respectively). The SC was purchased from TestDiet (Richmond, IN, USA). The HFS and KD were purchased from Research Diets Inc. (New Brunswick, NJ, USA). At the end of the feeding period, animals were anesthetized (0.4 mg ketamine and 8 mg xylazine per 100 g of body weight) and the subcutaneous inguinal (Sc Ing), Epid, and interscapular brown adipose tissue (iBAT) fat pads were extracted and weighed. A sample of each fat depot was immediately frozen in liquid nitrogen for subsequent experiments.

Ethical approval

The protocol containing all animal procedures described in this study was specifically approved by the Committee on the Ethics of Animal Experiments of York University (York University Animal Care Committee [YUACC]) and performed strictly in accordance with the YUACC guidelines. All tissue extraction procedures were performed under ketamine/xylazine anesthesia, and all efforts were made to minimize suffering [19]. All experiments in this study were carried out in compliance with the ARRIVE guidelines [20].

Western blotting analysis of ERK phosphorylation and ACE1, ACE2, AT_1R, and AT_2R protein levels in the Sc Ing, Epid, and iBAT fat depots

Sc Ing, Epid, and iBAT samples were homogenized in a buffer containing 25 mM Tris-HCl, 25 mM NaCl (pH 7.4), 1 mM $MgCl_2$, 2.7 mM KCl, 1% Triton X-100, and protease and phosphatase inhibitors (Roche Diagnostics GmbH, Mannheim, Germany). Homogenates were centrifuged, the infranatant was collected, and an aliquot was used to measure protein by the Bradford method. Samples were diluted 1:1 (vol:vol) with 2 × Laemmli sample buffer and heated to 95°C for 5 min. Twenty-five μg of protein were loaded in each well. Samples were then subjected to sodium dodecyl-sulfate polyacrylamide gel electrophoresis, transferred to polyvinylidene fluoride membrane, and probed for the proteins of interest. All primary antibodies were used at a dilution of 1:1,000. All densitometry analyses were performed using the ImageJ program. The comparative analysis of Sc Ing, Epid, and iBAT RAS components (Fig. 1) was performed using samples from animals fed the SC diet for 8 wk. The remaining blots contained samples from SC-, HFS-, and KD-fed animals.

RNA isolation and quantitative PCR

Primers were designed using the software PrimerQuest (IDT) based on probe sequences available at the Affymetrix database (NetAffx Analysis Centre, http://www.affymetrix.com/analysis) for each given gene. RNA was isolated from Sc Ing, Epid, and iBAT tissues using Trizol (ThermoFisher Scientific, Waltham, MA, USA). Complimentary DNA (cDNA) was made from 2 μg of extracted RNA using the ABM OneScript cDNA Synthesis kit (Diamed, Mississauga, ON, Canada), according to the manufacturer's instructions. Samples were run in duplicates on 96-well plates, and each 20 μL reaction contained 4 μL of cDNA, 0.4 μL of primer, 10 μL of Brightgreen 2 × quantitative polymerase chain reaction (qPCR) Mastermix (Diamed, Mississauga, ON, Canada) and 5.6 μL of RNase-free water. Real-time PCR analysis was performed using a Bio-Rad CFX96 Real Time PCR Detection System (Bio-Rad, Mississauga, ON, Canada) using the following amplification conditions: 95°C (10 min); 40 cycles of 95°C (15s), and 60°C (60s). All genes were normalized to the control gene β-actin, and differences in gene expression between groups were determined using the ΔΔCt method [21]. Values are expressed as fold increase relative to the SC group. Primer sequences used were as follows: Mas1 forward (CGCCAACCCTTTCATCTACT) and reverse (CCTAGGTTGCATCTCGTCTTT); and β-actin forward (GTGAAAAGATGACCCAGATC) and reverse (CACCGCCTGGATGGCTACGT).

Statistical analyses

Data were expressed as mean ± SEM. Statistical analyses were performed by using mixed-model analyses and one-way analysis of variance with Bonferroni multiple comparison post hoc tests, as indicated in the figure legends. The GraphPad Prism software version 9.1.12 was used for all statistical analyses and for the preparation of all graphs. The level of significance was set to $P < 0.05$.

Results

Body weight of SC, HFS and KD-fed animals at weeks 0, 4, and 8 of the feeding period.

All three diet groups experienced progressive weight gain from weeks 0 to 8 (Table 1). As expected, body weight (BW) was significantly higher in the HFS than the SC animals at weeks 4 and 8 (Table 1). However, BW did not differ significantly between the HFS- and KD-fed animals at any point during the feeding period. Moreover, when compared with the SC animals, the KD elevated BW by 10% and 13.9%, at weeks 4 and 8, respectively (Table 1).

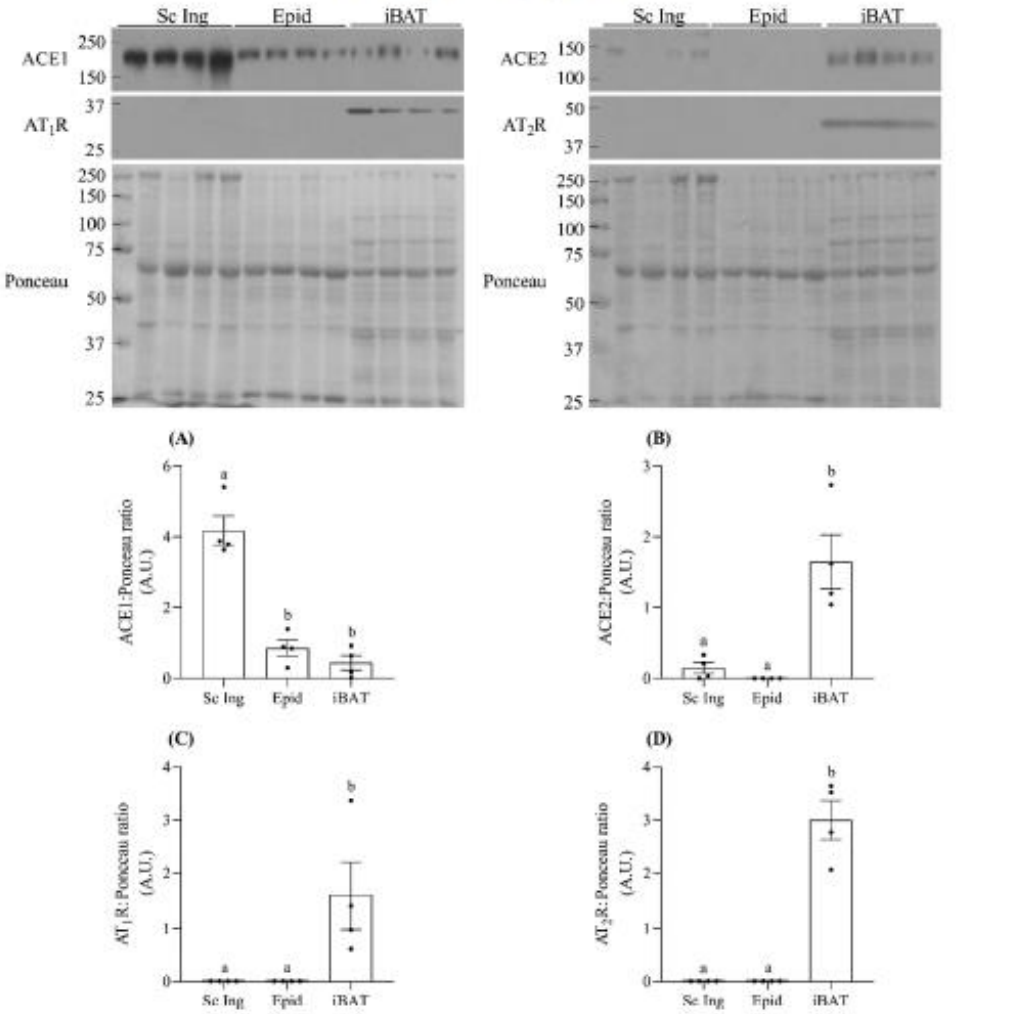

Fig. 1. ACE1 content was highest in the Sc Ing fat (A). However, ACE2, AT_1R, and AT_2R (B, C, and D, respectively) were more abundant in iBAT than in Sc Ing or Epid fat depots. ACE2 levels were elevated in Sc Ing fat, relative to Epid fat; however, this difference did not reach statistical significance (B). Statistically significant differences denoted by different letters. $P < 0.05$. Bars represent mean ± SEM. One-way analysis of variance. n = 4 per group in panels A–D. ACE, angiotensin-converting enzyme; AT_1R, angiotensin II type 1 receptor; AT_2R, angiotensin II type 1 receptor; Epid, epididymal; iBAT, interscapular brown adipose tissue; SC Ing, subcutaneous inguinal.

Table 1
Body weights of SC-, HFS-, and KD-fed animals at weeks 0, 4, and 8 of the feeding periods

Body weight (g)		Duration (wk)		
		0	4	8
	SC (n = 5)	213.5 ± 3.8	344.8 ± 11.2*	416.7 ± 15.3†
	HFS (n = 7)	219.2 ± 4.8	385.7 ± 8.7*,†	480 ± 14*,†
	KD (n = 8)	225 ± 3.9	379.3 ± 5.8*,†	474.7 ± 9.1†,‡

HFS, high-fat sucrose; KD, ketogenic diet; SC, standard chow.
Data expressed as mean ± SEM.
Mixed-effects model analysis.
*$P < 0.05$ vs week 0 in respective group.
†$P < 0.05$ vs weeks 0 and 4 in respective group.
‡$P < 0.05$ vs SC in respective week.

Tissue comparison of RAS proteins in Sc Ing, Epid, and iBAT fat depots

To assess the potential physiologic importance of individual RAS components in the distinct fat depots, we measured RAS protein levels in the WAT and BAT of rats fed a SC diet for 8 wk. ACE1 was 4.9- and 9.6-fold higher in Sc Ing fat than in Epid fat and iBAT, respectively (Fig. 1A), whereas ACE2 was most abundant in iBAT (Fig. 1B). In fact, ACE2 levels in iBAT were 11.6-fold higher than in Sc Ing fat (Fig. 1B). Although the difference between Sc Ing and Epid ACE2 contents did not reach statistical significance, Epid fat had the lowest ACE2 levels of all three fat depots (Fig 1B). With respect to AT_1R and AT_2R, iBAT displayed significantly higher contents of these two receptors than Sc Ing and Epid fat pads (Fig. 1C and D).

Effects of diet on Sc Ing, Epid, and iBAT ACE1 and ACE2 protein contents

HFS feeding significantly suppressed ACE1 content by ~82% in Sc Ing fat, relative to the SC animals (Fig. 2A), but did not alter Epid ACE1 levels (Fig. 2C). KD feeding, on the other hand, attenuated both Sc Ing and Epid ACE1 by ~75% and 87%, respectively (Fig. 2A and C). ACE2 was also significantly decreased by both the HFS and KDs in Sc Ing fat (Fig. 2B). However, neither diet altered Epid ACE2 content (Fig. 2D). In this context, the KD did not influence Epid ACE2 and decreased ACE1, indicating a shift toward the counterregulatory arm of the RAS in this tissue. Regarding iBAT, HFS- and KD feeding attenuated ACE1 content (Fig. 2E) and the HFS diet suppressed ACE2 (Fig. 2F); however, these effects were not statistically significant.

Effects of diet on Sc Ing, Epid, and iBAT AT_1R and AT_2R protein contents

Sc Ing and iBAT AT_1R levels increased ~4.6- and 3-fold, respectively, in the HFS group, compared with the SC group (Fig. 3A and E, respectively). In the Epid fat, AT_1R levels were neither altered by the HFS diet nor the KD (Fig. 3C). However, the KD increased AT_2R protein levels by 23.4- and 5.2-fold in Sc Ing and Epid fat, respectively (Fig. 3B and D, respectively). In iBAT, no significant alteration in AT_2R protein levels was detected with any of the diets (Fig. 3F). Altogether, these findings demonstrate that the HFS and KD exerted tissue-specific effects with respect to AT_1R and AT_2R levels in Sc Ing, Epid, and iBAT fat depots.

Effects of diet on Sc Ing, Epid, and iBAT MasR gene expression

Sc Ing expression of *Mas1*, the gene that encodes the MasR, was downregulated by ~82% and 80% in HFS- and KD-fed animals, respectively (Fig. 4A), whereas in Epid and iBAT the expression of the *MasR* was not altered by diet (Fig. 4B and C). These *Mas1*-related findings indicate that both the HFS and KD exerted a potential reduction of the counterregulatory ACE2/Ang-[1,7]/MasR/AT_2R arm of RAS, although this effect was restricted to the Sc Ing WAT.

Phosphorylation of ERK1/2 in WAT and BAT following the dietary interventions

To assess whether diet-induced changes in RAS receptors were influencing Ang signaling in WAT and BAT, we measured phosphorylation of the downstream protein ERK1/2 [12,22]. ERK1/2 phosphorylation in Sc Ing, Epid, and iBAT did not differ among diets (Fig. 5A–C). However, the pERK1/2/ERK1/2 ratio tended to increase with KD feeding in all three tissues, relative to the HFS group (Fig. 5).

Discussion

Here, we demonstrate that levels of RAS components differ significantly between WAT and BAT, and that the HFS and KD regulated ACE1 and ACE2, as well as AT_1R, AT_2R protein contents, and *Mas1* gene expression in a fat depot-specific manner. In line with our original hypothesis, overall, the HFS obesogenic diet enhanced the classical arm of the RAS, whereas the KD enhanced the protective, counterregulatory RAS arm. This was supported by our findings that, despite major fat depot differences with respect to their contents in RAS proteins, the KD significantly increased AT_2R and attenuated ACE1 levels in both WAT depots. Importantly, because the Sc Ing fat exhibited the highest levels of ACE1, the marked reduction of ACE1 by the KD is consistent with attenuated activity of the classical RAS arm in this tissue. This is in line with previous observations that elevations in Sc Ing WAT Ang-II levels under conditions of HF diet-induced obesity are dependent on ACE1 in mice [4].

In Sc Ing fat, ACE1 levels were also reduced by the HFS diet, which is apparently at odds with our initial hypothesis because it suggests that the obesogenic diet attenuated the classical arm of the RAS. However, in both HFS- and KD-fed animals, the decrease in ACE1 content was accompanied by a reduction in ACE2 in the SC Ing fat depot. Thus, although lower ACE1 levels could potentially lead to suppressed Ang-II formation in this tissue, the concomitant reduction of ACE2 favored impairment in the conversion of Ang-II to Ang-[1,7], likely leaving the Ang-II levels unaffected and Ang-[1,7] levels potentially reduced. In line with this, Giori et al. observed unchanged levels of Ang-II, and a trend to decrease Ang-[1,7] in the Sc WAT of HF-fed mice compared with controls [4]. In this context, the diet-induced shift of the Sc Ing RAS does not appear to be influenced by alterations to ACE1 or ACE2 contents and is instead mediated by changes in the expressions of the Ang receptors.

Analysis of AT_1R and AT_2R protein levels revealed that these receptors were not very prominent in the WAT fat depots from SC-fed rats. However, in the Sc Ing fat and iBAT of HFS-fed rats, AT_1R levels were significantly increased, whereas the KD did not affect the levels of this receptor in any of the tissues. In white adipocytes, stimulation of AT_1R has been shown to increase inflammatory markers, such as MCP-1 mRNA expression and nuclear factor-κβ transcription [13]. Furthermore, in a rat model of metabolic dysfunction, administration of the AT_1R antagonist L158809 improved glucose tolerance [13]. Thus, the HFS diet-induced elevation in the content of this receptor is consistent with activation of the classical RAS arm and induction of detrimental metabolic effects observed in adipose tissue in obesity [4,13,23]. In addition to the enhanced AT_1R content, Sc Ing *MasR* expression was significantly reduced in HFS-fed animals. Indeed, other studies have reported that an obesogenic diet attenuates *MasR* expression in subcutaneous fat and reduces the activity of the counterregulatory RAS arm [4]. Importantly, KD feeding did not alter AT_1R levels in any of the fat depots studied but induced a robust increase in Sc Ing and Epid AT_2R levels, an effect that likely compensated for the KD-induced attenuation in *MasR* expression in Sc Ing fat. This is compatible with our finding that the KD caused a reduction in Sc Ing ACE2 (Fig. 2B), which potentially decreased Ang-[1,7]/MasR signaling and, consequently, the expression of the *MasR* [22]. Therefore, the KD-induced elevation of AT_2R could potentially counteract the classical, proinflammatory arm of the RAS [4] in WAT. In iBAT, however, neither the HFS nor the KD altered AT_2R levels, despite this tissue displaying the highest relative abundance of this receptor. The lack of an effect of dietary intervention on BAT AT_2R can be explained by the reduced physiologic importance of this receptor for thermogenesis in mature adipocytes. This is compatible with reports that the differentiation of brown adipocytes depends on AT_2R signaling [12], whereas fully differentiated cells rely on MasR signaling for BAT activation [14]. As previously mentioned, the gene expression of *MasR* was unchanged by any of the dietary interventions, and this likely sufficed to maintain iBAT activity. Nevertheless, the elevated abundance of the Ang receptors and ACE2 in BAT indicates a higher capacity for Ang signaling in this tissue.

A complex network involving several factors determines the downstream signaling of Ang receptors [6,12]. One protein that is particularly relevant for Ang signaling in the adipose tissue is ERK1/2 [22]. In adipocytes, ERK1/2 phosphorylation is enhanced by AT_1R stimulation, whereas stimulation of the MasR or AT_2R attenuates ERK1/2 phosphorylation [12,22]. In the present study,

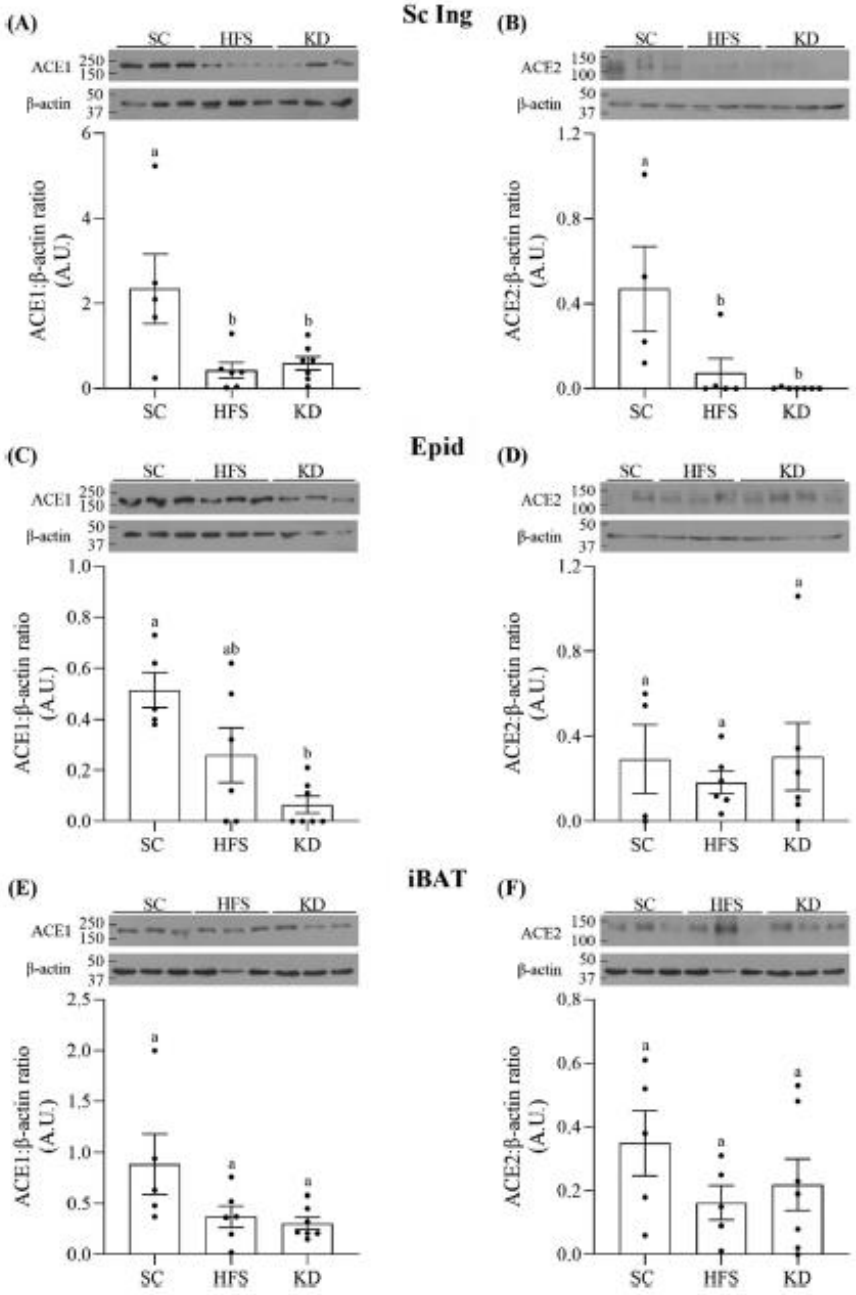

Fig. 2. The HFS-enriched diet and the KD significantly reduced Sc Ing ACE1 and ACE2 protein contents (A and B, respectively). In Epid fat, only the KD significantly attenuated ACE1 levels, relative to the SC group (C). However, diet did not affect ACE2 levels in this tissue (D). Finally, ACE1 and ACE2 levels were not significantly altered by dietary intervention in iBAT (E and F, respectively). Statistically significant differences denoted by different letters. $P < 0.05$. Bars represent mean ± SEM. One-way analysis of variance. n = 5 in the SC group in panels A, C, E and F, and n = 4 in panels B and D. n = 6 in the HFS group in panels A, C, D, and E, and n = 5 in panels B and F. n = 7 in the KD group in all panels, except for panel D where n = 6. ACE, angiotensin-converting enzyme; Epid, epididymal; HFS, high-fat sucrose; iBAT, interscapular brown adipose tissue; KD, ketogenic diet; SC, standard chow; SCIng, subcutaneous inguinal.

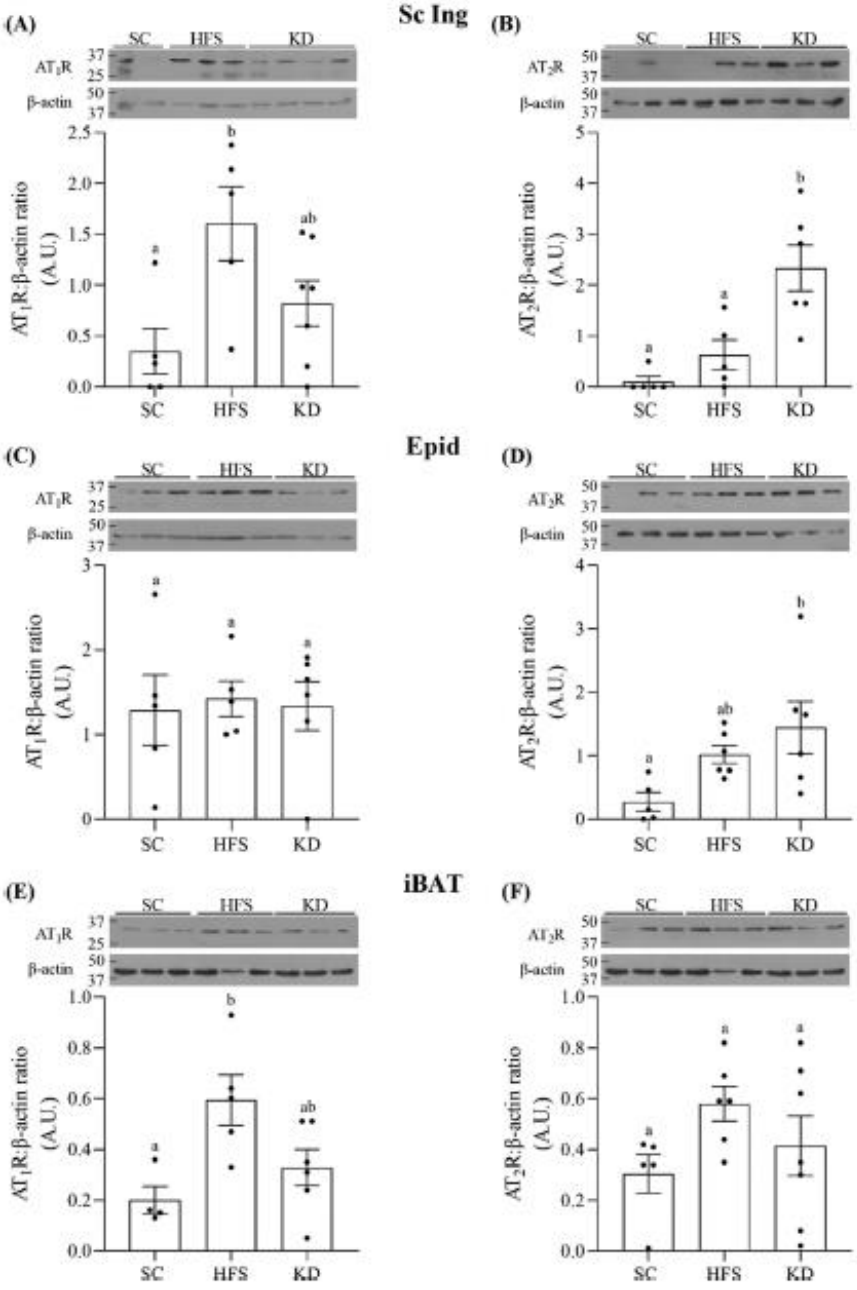

Fig. 3. AT_1R content was significantly increased in Sc Ing fat with the HFS, but not KD (A). In contrast, the KD, but not the HFS diet, elevated Sc Ing AT_2R (B). In Epid fat, AT_1R was not altered with diet (C), however AT_2R content was increased in animals fed the KD (D). Like the Sc Ing fat, iBAT AT_1R content was elevated in the HFS-fed animals (E). Conversely, AT_2R was not influenced by diet (F). Statistically significant differences denoted by different letters. $P < 0.05$. Bars represent mean ± SEM. One-way analysis of variance. n = 5 in the SC group in all panels, except for E where n = 4. n = 5 in the HFS group in panels A, B, C, and E, and n = 6 in panels D and F. n = 7 in the KD group in panels A and F, and n = 6 in panels B, C, D, and E. AT_1R, angiotensin II type 1 receptor; AT_2R, angiotensin II type 1 receptor; Epid, epididymal; HFS, high-fat sucrose; iBAT, interscapular brown adipose tissue; KD, ketogenic diet; SC Ing, subcutaneous inguinal.

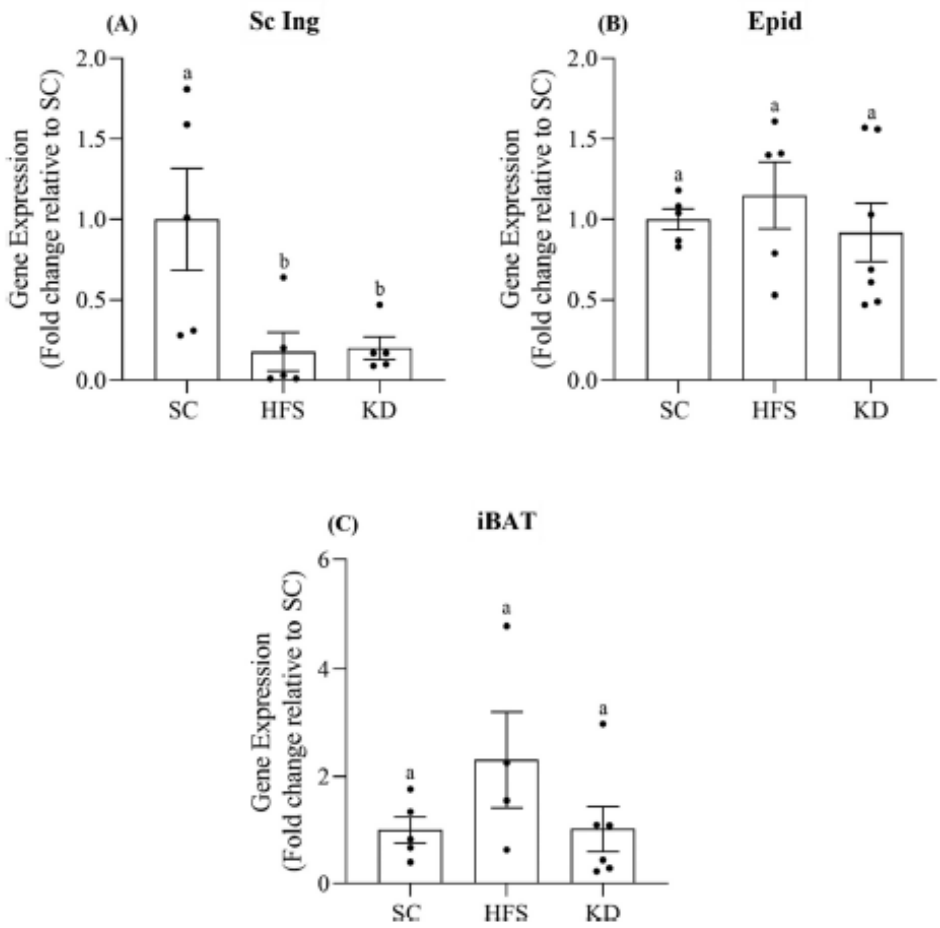

Fig. 4. Mas receptor (*MasR*) expression was significantly attenuated in Sc Ing fat by both the HFS diet and KD (A). However, gene expression of the MasR was not altered by diet in Epid fat or BAT (B and C, respectively). Statistically significant differences denoted by different letters. $P < 0.05$. One-way analysis of variance. n = 5 in the SC group. n = 5 in the HFS group in panels A and B, and n = 4 in panel C. n = 5, 7 and 6 in the KD group in panels A, B, and C, respectively. BAT, brown adipose tissue; Epid, epididymal; HFS, high-fat sucrose; KD, ketogenic diet; SC Ing, subcutaneous inguinal.

ERK1/2 phosphorylation was not significantly altered by diet in any of the three fat depots studied, although tissue-specific trends in ERK1/2 phosphorylation appear to exist. It is noteworthy that studies demonstrating Ang-II–mediated ERK phosphorylation were performed in isolated adipocytes, incubated in the absence or presence of Ang-II, Ang-[1,7] [22] and angiotensin receptor antagonists [12]. Although this experimental model is valuable for the observation of isolated effects induced by individual factors on cellular signaling pathways, it does not account for other circulating hormones that also act on the same downstream targets. For instance, fibroblast growth factor 21, which is known to be altered with KD feeding [17], promotes ERK1/2 phosphorylation [24]. In this study, freshly isolated whole WAT was used to assess ERK1/2 phosphorylation, and the presence of cells other than adipocytes in the stromal vascular fraction (fibroblasts, blood and blood vessels, immune cells, and nerve tissue) also likely affected the results. Thus, we cannot discard the possibility that the dietary interventions meaningfully affected the ability of the classical and counterregulatory arms of the RAS to signal through ERK1/2 phosphorylation in adipocytes.

The KD has been demonstrated to cause significant reductions in adiposity and BW in humans [18,25]. In this study, we found that KD-fed rats displayed lower BW than HFS-fed rats, although this difference was not statistically significantly, which is inconsistent with the typical effects of KD on adiposity in humans. However, this apparent discrepancy can be explained by species differences with respect to BW responses to feeding. This is also evident when comparing mice and rats and even among distinct rat strains utilized in studies reporting the effects of KD on BW [7,17]. In fact, in a previous study conducted in Sprague-Dawley (SD) rats [7], we observed that animals fed for 8 wk with the same KD reached lower BW than their counterparts fed a HFS diet. In this study, we used Wistar rats, which display a very distinct pattern of food intake and fat and BW gain when compared with SD

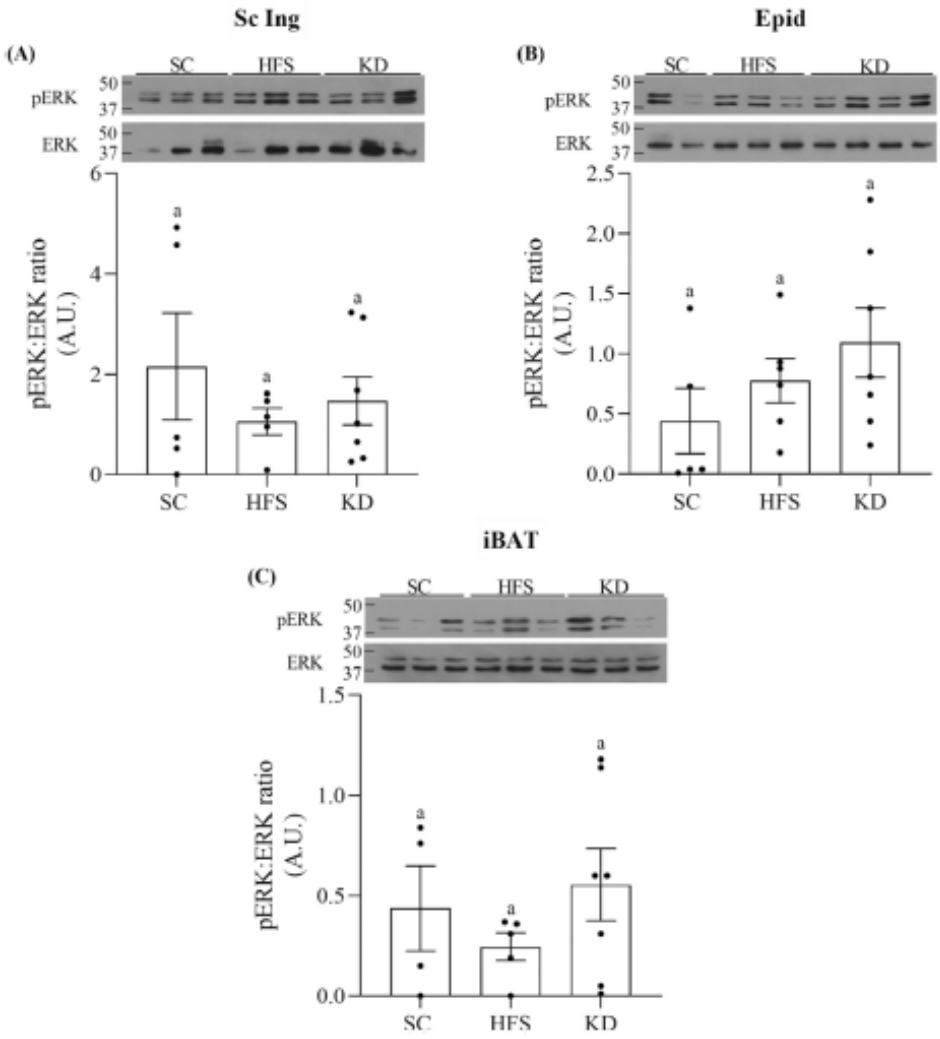

Fig. 5. p44/42 mitogen activated protein kinase (ERK1/2) phosphorylation was not influenced by diet in the Sc Ing, Epid, or iBAT fat depots (A, B, and C, respectively). Statistically significant differences denoted by different letters. $P < 0.05$. One-way analysis of variance. n = 5 in the SC group in panels A and B, and n = 4 in panel C. n = 5 in the HFS group in panels A and C, and n = 6 in panel B. n = 7 in the KD group in all panels. Epid, epididymal; HFS, high-fat sucrose; iBAT, interscapular brown adipose tissue; KD, ketogenic diet; SC, standard chow; SC Ing, subcutaneous inguinal.

rats fed similar diets. Nevertheless, the elevation in BW did not prevent the KD-induced shift of WAT RAS components toward the counterregulatory arm.

Conclusion

Major depot-specific differences in RAS components were detected between WAT and BAT. This was evidenced by the Sc Ing fat displaying the highest levels of ACE1, but very low levels of AT_1R, AT_2R, and ACE2. Conversely, the highest levels of ACE2, AT_1R, and AT_2R were found in iBAT. Despite these differences, the HFS diet increased the ACE1/Ang-II/AT_1R arm of the RAS, whereas the KD enhanced the ACE2/Ang-[1,7]/MasR/AT_2R counterregulatory arm of the RAS in WAT. These findings provide evidence that the KD can be a valuable dietary intervention for the management of the adipose tissue RAS and can thereby serve to potentially counteract the dysfunctional metabolism and inflammation [23] that are observed in adipose tissue with obesity.

References

[1] Sparks MA, Crowley SD, Gurley SB, Mirotsou M, Coffman TM. Classical renin-angiotensin system in kidney physiology. Compr Physiol 2014;4:1201–28.
[2] Ames MK, Atkins CE, Pitt B. The renin-angiotensin-aldosterone system and its suppression. J Vet Intern Med 2019;33:363–82.

[3] Paz Ocaranza M, Riquelme JA, García L, Jalil JE, Chiong M, Santos RAS, et al. Counter-regulatory renin–angiotensin system in cardiovascular disease. Nat Rev Cardiol 2020;17:116–29.
[4] Giori IG, Magliano DC, Alexandre-Santos B, Fernandes T, Oliveira EM, Vieira CP, et al. Enalapril and treadmill running reduce adiposity, but only the latter causes adipose tissue browning in mice. J Cell Physiol 2021;236:900–10.
[5] Morimoto H, Mori J, Nakajima H, Kawabe Y, Tsuma Y, Fukuhara S, et al. Angiotensin 1–7 stimulates brown adipose tissue and reduces diet-induced obesity. Am J Physiol Endocrinol Metab 2018;314:E131–8.
[6] Frigolet ME, Torres N, Tovar AR. The renin-angiotensin system in adipose tissue and its metabolic consequences during obesity. J Nutr Biochem 2013;24:2003–15.
[7] Da Eira D, Jani S, Ceddia RB. Obesogenic and ketogenic diets distinctly regulate the SARS-CoV-2 entry proteins ACE2 and TMPRSS2 and the renin-angiotensin system in rat lung and heart tissues. Nutrients 2021;13:3357.
[8] Klein S, Gastaldelli A, Yki-Järvinen H, Scherer PE. Why does obesity cause diabetes? Cell Metab 2022;34:11–20.
[9] Cinti S. Transdifferentiation properties of adipocytes in the adipose organ. AJP Endocrinol Metab 2009;297:E977–86.
[10] Sepa-Kishi DM, Ceddia RB. Exercise-mediated effects on white and brown adipose tissue plasticity and metabolism. Exerc Sport Sci Rev 2016;44:37–44.
[11] Sepa-Kishi DM, Jani S, Da Eira D, Ceddia RB. Cold acclimation enhances UCP1 content, lipolysis, and triacylglycerol resynthesis, but not mitochondrial uncoupling and fat oxidation, in rat white adipocytes. Am J Physiol Cell Physiol 2019;316:C365–76.
[12] Than A, Xu S, Li R, Leow MS, Sun L, Chen P. Angiotensin type 2 receptor activation promotes browning of white adipose tissue and brown adipogenesis. Signal Transduct Target 2017;2:17022.
[13] Lee MH, Song HK, Ko GJ, Kang YS, Han SY, Han KH, et al. Angiotensin receptor blockers improve insulin resistance in type 2 diabetic rats by modulating adipose tissue. Kidney Int 2008;74:890–900.
[14] Cao X, Shi T-T, Zhang C-H, Jin W-Z, Song L-N, Zhang Y-C, et al. ACE2 pathway regulates thermogenesis and energy metabolism. Elife 2022;11:1–21.
[15] Kalupahana NS, Massiera F, Quignard-Boulange A, Ailhaud G, Voy BH, Wasserman DH, et al. Overproduction of angiotensinogen from adipose tissue induces adipose inflammation, glucose intolerance, and insulin resistance. Obesity 2012;20:48–56.
[16] Shum M, Pinard S, Guimond MO, Labbé SM, Roberge C, Baillargeon JP, et al. Angiotensin II type 2 receptor promotes adipocyte differentiation and restores adipocyte size in high-fat/high-fructose diet-induced insulin resistance in rats. Am J Physiol Endocrinol Metab 2013;304:E197–210.
[17] Asrih M, Altirriba J, Rohner-Jeanrenaud F, Jornayvaz FR. Ketogenic diet impairs FGF21 signaling and promotes differential inflammatory responses in the liver and white adipose tissue. PLoS One 2015;10:1–14.
[18] Yancy WS Jr., MK Olsen, JR Guyton, RP Bakst, EC Westman. A low-carbohydrate, ketogenic diet versus a low-fat diet to treat obesity and hyperlipidemia: a randomized, controlled trial. Ann Intern Med 2004;140:769–79.
[19] Pinho RA, Sepa-Kishi DM, Bikopoulos G, Wu MV, Uthayakumar A, Mohasses A, et al. High-fat diet induces skeletal muscle oxidative stress in a fiber type-dependent manner in rats. Free Radic Biol Med 2017;110.
[20] du Sert NP, Ahluwalia A, Alam S, Avey MT, Baker M, Browne WJ, et al. Reporting animal research: explanation and elaboration for the arrive guidelines 2.0. PLoS Biol 2020;18:e3000411.
[21] Livak KJ, Schmittgen TD. Analysis of relative gene expression data using real-time quantitative PCR and the 2−ΔΔCT method. Methods 2001;25:402–8.
[22] Than A, Leow MKS, Chen P. Control of adipogenesis by the autocrine interplays between angiotensin 1–7/Mas receptor and angiotensin II/AT1 receptor signaling pathways. J Biol Chem 2013;288:15520–31.
[23] Kawabe Y, Mori J, Morimoto H, Yamaguchi M, Miyagaki S, Ota T, et al. ACE2 exerts anti-obesity effect via stimulating brown adipose tissue and induction of browning in white adipose tissue. Am J Physiol Endocrinol Metab 2019;317:E1140–9.
[24] Sepa-Kishi DM, Ceddia RB. Circulating fibroblast growth factor 21 is reduced, whereas its production is increased in a fat depot-specific manner in cold-acclimated rats. Adipocyte 2018;7:238–47.
[25] Walton CM, Perry K, Hart RH, Berry SL, Bliman BT. Improvement in glycemic and lipid profiles in type 2 diabetics with a 90-day ketogenic diet. J Diabetes Res 2019;2019:8681959.

nutrients

MDPI

Article

Obesogenic and Ketogenic Diets Distinctly Regulate the SARS-CoV-2 Entry Proteins ACE2 and TMPRSS2 and the Renin-Angiotensin System in Rat Lung and Heart Tissues

Daniel Da Eira, Shailee Jani and Rolando B. Ceddia *

Muscle Health Research Center, School of Kinesiology and Health Science, York University, Toronto, ON M3J1P3, Canada; DanielDaEira@hotmail.com (D.D.E.); janishailee@gmail.com (S.J.)
* Correspondence: roceddia@yorku.ca; Tel.: +1-(416)-736-2100 (ext. 77204); Fax: +1-(416)-736-5774

Abstract: Background: Obesity increases the severity of SARS-CoV-2 outcomes. Thus, this study tested whether obesogenic and ketogenic diets distinctly affect SARS-CoV-2 entry proteins and the renin-angiotensin system (RAS) in rat pulmonary and cardiac tissues. Methods: Male Sprague-Dawley rats were fed either standard chow (SC), a high-fat sucrose-enriched diet (HFS), or a ketogenic diet (KD) for 16 weeks. Afterwards, levels of angiotensin converting enzyme 2 (ACE2), transmembrane protease serine 2 (TMPRSS2), RAS components, and inflammatory genes were measured in the lungs and hearts of these animals. Results: In the lungs, HFS elevated ACE2 and TMPRSS2 levels relative to SC diet, whereas the KD lowered the levels of these proteins and the gene expressions of toll-like receptor 4 and interleukin-6 receptor relative to HFS. The diets did not alter ACE2 and TMPRSS2 in the heart, although ACE2 was more abundant in heart than lung tissues. Conclusion: Diet-induced obesity increased the levels of viral entry proteins in the lungs, providing a mechanism whereby SARS-CoV-2 infectivity can be enhanced in obese individuals. Conversely, by maintaining low levels of ACE2 and TMPRSS2 and by exerting an anti-inflammatory effect, the KD can potentially attenuate the severity of infection and migration of SARS-CoV-2 to other ACE2-expressing tissues.

Keywords: obesity; ketones; inflammation; TLR4; IL6; TNF-alpha; MasR

Citation: Da Eira, D.; Jani, S.; Ceddia, R.B. Obesogenic and Ketogenic Diets Distinctly Regulate the SARS-CoV-2 Entry Proteins ACE2 and TMPRSS2 and the Renin-Angiotensin System in Rat Lung and Heart Tissues. *Nutrients* **2021**, *13*, 3357. https://doi.org/10.3390/nu13103357

Academic Editors: Anna M. Giudetti and Anna Tagliabue

Received: 7 July 2021
Accepted: 23 September 2021
Published: 25 September 2021

1. Introduction

Obesity is characterized by an expansion in white adipose tissue (WAT) mass and is linked to a number of comorbidities, including hypertension and diabetes [1]. More recently, obesity has emerged as a major risk factor for severe illness related to COVID-19 infection [2,3]. Infection with the severe acute respiratory syndrome-coronavirus-2 (SARS-CoV-2) occurs mainly through the airway [4]. At the cellular level, the virus binds to its receptor, ACE2 [4,5]. The interaction between ACE2 and SARS-CoV-2 occurs via the virus's spike (S) protein; however, an additional crucial step, catalysed by transmembrane protease serine 2 (TMPRSS2), leads to cleavage of the S protein [4,5]. This latter step allows for the fusion of the virus and host cell membranes, so endocytosis of the virus can occur. Once inside the cell, the virus can utilize the cell's ribosomes to transcribe its own RNA and undergo replication [6]. The enhanced susceptibility of obese individuals to severe COVID-19 outcomes has been linked to elevations in ACE2 and TMPRSS2 in lung tissues [4,7]. In fact, Sarver and Wong showed that ACE2 expression was elevated in the lungs and tracheas of male, obese mice [4]. Similarly, Batchu et al. reported elevations in ACE2 and TMPRSS2 protein contents in the lungs of HF-fed, diabetic mice [7]. In this context, the diet-induced elevations in SARS-CoV-2 entry proteins provide a plausible mechanism that explains the increased susceptibility of obese individuals to severe outcomes. It is important to note that ACE2 is also a component of the renin-angiotensin aldosterone system (RAS), which has emerged as another possible mechanism mediating COVID-19-related illness [8].

The RAS is classically responsible for the regulation of fluid balance and blood pressure [8]. In short, the kidney releases renin, which converts liver-derived angiotensinogen

into angiotensin I (Ang-I) [9]. Ang-I is then processed into angiotensin-II (Ang-II), mainly in the pulmonary circulation [10], by the angiotensin converting enzyme (ACE1) [9]. Ang-II can then bind to the G-protein coupled receptor angiotensin-II, type 1 receptor (AT_1R) [9] where it induces vasoconstriction, water retention and sympathetic nervous system activation [9]. Under conditions of hypertension and obesity, hyperactivation of the RAS leads to inflammation, fibrosis and oxidative damage [8]. In this context, therapies aimed at increasing flux through the counterregulatory arm of the RAS have gained attention as a potential treatment for hypertension and obesity [2,8]. These effects are mainly mediated by ACE2, which converts Ang-II into Ang(1,7) [8]. Ang(1,7) binds to the Mas receptor (MasR), which exerts protective, anti-inflammatory effects [9]. Moreover, Ang-II can also bind to angiotensin II, type 2 receptor (AT_2R) [2]. AT_2R exerts similar effects to MasR, however it is mainly expressed under conditions of AT_1R hyperactivation and injury to suppress inflammation and oxidative stress [2,11]. Following COVID infection, ACE2 becomes downregulated [2]. Consequently, the obesity-induced elevation in Ang-II increases signalling through AT_1R, which promotes inflammation and tissue damage [2]. Thus, the role of ACE2 in COVID-19-related illness extends beyond serving as a viral entry protein. Rather, it is also implicated in the inflammatory response that ensues, which carries a profound impact for tissue damage and organ failure [2]. In this context, shifting obese individuals from the ACE1/Ang-II/AT_1R arm to the ACE2/Ang(1,7)/MasR and AT_2R arm is of great importance to reduce the susceptibility of obese individuals to severe COVID-19 outcomes.

Recently, the ketogenic diet (KD) has sparked interest as a potential therapeutic tool for the management of obesity. In fact, it has been shown that the KD improved blood pressure, glycemia and body weight in Type 2 diabetic patients [12] and carries potential as an anti-inflammatory diet [13]. However, to our knowledge, little is known regarding the effect of the KD on the RAS components in lung and heart tissues. Moreover, despite there being evidence that obesity enhances the expression of ACE2 and TMPRSS2 in lung tissue, to the best of our knowledge, no studies have evaluated whether a KD can affect molecular steps involved in SARS-CoV-2 infection. In this context, our study aims to compare the effects of different dietary interventions on the contents of viral entry proteins and RAS components in lung and heart tissues. Here, we provide a detailed analysis of how an obesogenic diet regulates ACE2 and TMPRSS2 contents, as well as AT_1R and AT_2R levels in lung and cardiac tissues. Additionally, we test whether a KD can alter the levels of these proteins and reduce the expression of inflammatory genes in the lungs.

2. Materials and Methods

2.1. Reagents

Protease (cOmplete Ultra Tablets) and phosphatase (PhosSTOP) inhibitors—were obtained from Roche Diagnostics GmbH (Mannheim, Germany). The Insulin ELISA kit was purchased from Millipore-Sigma (Burlington, MA, USA). The ACE1 (ab254222), ACE2 (ab239924), AT_1R (ab124734), AT_2R (ab92445) and TMPRSS2 (ab92323) antibodies were purchased from Abcam (Toronto, ON, Canada) and the β-actin (cat. no. 4967) antibody was purchased from Cell Signaling (Danvers, MA, USA).

2.2. Animals

Male albino rats from the Sprague-Dawley strain (Envigo, Indianapolis, IN, USA) weighing 200–250 g (initial weight)—were maintained in a constant-temperature (23 °C), with a fixed 12-h light/12-h dark cycle and fed for 16 weeks ad libitum either a standard chow diet (SC, 27.0%, 13.0%, and 60.0% of calories provided by protein, fat, and carbohydrates, respectively) a HF, sucrose-enriched (HFS) diet (20.0%, 60.0%, and 20.0% of calories provided by protein, fat, and carbohydrates [sucrose], respectively) or a KD (20%, 80% and 0% of calories provided by protein, fat and carbohydrates, respectively). The energy densities for the SC, HFS and ketogenic diets were 3.43, 5.24 and 6.14 kcal/g, respectively. The SC diet (standard rat chow, catalog # 5012) was purchased from TestDiet (Richmond,

IN, USA). The HFS and ketogenic diets (catalog # D12492 and D03022101, respectively) were purchased from Research Diets Inc. (New Brunswick, NJ, USA). Energy intake was not significantly different between the three groups at weeks 0, 4 and 8 (Table 1). At week 16, the KD-fed animals had 17.9% and 18.1% lower energy intake than the SC and HFS-fed animals, respectively (Table 1).

Table 1. Energy intake at weeks 0, 4, 8, and 16 in the SC-, HFS-, and KD-fed animals.

	Week	SC	HFS	KD
Energy intake (kcal/rat/day)	0	69.23 ± 3.8	66.49 ± 2.3	66.49 ± 2.9
	4	72.60 ± 4.2	68.37 ± 4.0	63.83 ± 0.76
	8	65.83 ± 2.9	66.94 ± 3.2	59.82 ± 1.1
	16	69.65 ± 2.1	69.75 ± 6.0	57.15 ± 5.0 *

* $p < 0.05$ vs. SC and HFS within the respective week. Data are expressed as mean ± SEM. Two-way ANOVA. $n = 3$–7. SC, standard chow; HFS, high-fat sucrose-enriched diet; KD, ketogenic diet.

2.3. Ethics Approval

The protocol containing all animal procedures described in this study was specifically approved by the Committee on the Ethics of Animal Experiments of York University (York University Animal Care Committee, YUACC, permit number: 2021-03) and performed strictly in accordance with the YUACC guidelines. All tissue extraction procedures were performed under ketamine/xylazine anaesthesia, and all efforts were made to minimize suffering [14]. All experiments in this study were carried out in compliance with the ARRIVE guidelines [15].

2.4. Glucose Monitoring and Determination of Plasma Insulin Concentrations

Blood from all animals in a fed state was collected between 15:00 and 16:00 h by saphenous vein bleeding and used to determine plasma glucose, using the OneTouch UltraMini blood glucose monitoring system from LifeScan Canada Ltd. (Vancouver, BC, Canada). Insulin was measured using a commercially available kit listed in the reagents section. All procedures were performed according to instructions provided by the manufacturer of the kit.

2.5. Western Blotting Analysis of ACE1, ACE2, AT_1R, AT_2R, and TMPRSS2 Protein Levels in Lung and Cardiac Tissues

Lung and heart tissues were homogenized in a buffer containing 25 mM Tris-HCl, 25 mM NaCl (pH 7.4), 1 mM $MgCl_2$, 2.7 mM KCl, 1% Triton X-100 and protease and phosphatase inhibitors (Roche Diagnostics GmbH, Mannheim, Germany). Homogenates were centrifuged, the supernatant was collected, and an aliquot was used to measure protein by the Bradford method. Samples were diluted 1:1 (vol:vol) with 2× Laemmli sample buffer and heated to 95 °C for 5 min. Then, 25 µg of protein were loaded in each well. Samples were then subjected to SDS-PAGE, transferred to PVDF membrane, and probed for the proteins of interest. All primary antibodies were used at a dilution of 1:1000. All densitometry analyses were performed using the ImageJ program.

2.6. RNA Isolation and Quantitative PCR

Primers were designed using the software PrimerQuest (IDT) based on probe sequences available at the Affymetrix database (NetAffx™ Analysis Centre, http://www.affymetrix.com/analysis, accessed on 3 May 2020) for each given gene. RNA was isolated from lung and heart tissues using Trizol™ (ThermoFisher Scientific, Waltham, MA, USA). Complimentary DNA (cDNA) was made from 2 µg of extracted RNA using the ABM OneScript cDNA Synthesis kit (Diamed, Mississauga, ON, Canada), according to the manufacturer's instructions. Samples were run in duplicates on 96-well plates, and each 20 µL reaction contained 4 µL of cDNA, 0.4 µL of primer, 10 µL of Brightgreen 2× qPCR Mastermix (Diamed, Mississauga, ON, Canada) and 5.6 µL of RNase-free water. Real-time

PCR analysis was performed using a Bio-Rad CFX96 Real Time PCR Detection System (Bio-Rad, Mississauga, ON, Canada) using the following amplification conditions: 95 °C (10 min); 40 cycles of 95 °C (15 s), 60 °C (60 s). All genes were normalized to the control gene β-actin, and values are expressed as fold increases relative to control [16]. Primer sequences utilized are shown in Table 2.

Table 2. Primer sequences for qPCR.

	Forward	Reverse
mas1	5′-CGCCAACCCTTTCATCTACT-3′	5′-CCTAGGTTGCATCTCGTCTTT-3′
tlr4	5′-ACCTAAGGAGAGGAGGCTAAG-3′	5′-GGTAACTGCAGCACACTACA-3′
il6r	5′-TGGAGCAGACAGAGAGACTT-3′	5′-AGCTTACAGGTAACAGAGCATAAA-3′
tnfr1	5′-CCCTGTGAACCTCCTCTTTG-3′	5′-CTATGTACACCAAGTCGGTAGC-3′
β-actin	5′-GTGAAAAGATGACCCAGATC-3′	5′-CACCGCCTGGATGGCTACGT-3′

2.7. Statistical Analyses

Data were expressed as Mean ± SE. Statistical analyses were performed by using mixed-model analyses, and one-way ANOVAs and two way ANOVAs with Bonferroni multiple comparison post-hoc tests, as indicated in the figure legends. The GraphPad Prism software version 9.1.12 was used for all statistical analyses and for the preparation of all graphs. The level of significance was set to $p < 0.05$.

3. Results

Body weight (BW), glycemia, and insulinemia—HFS-fed animals gained significantly more weight than the SC and KD-fed animals (Table 3). This difference in BW was statistically significant at weeks 8 (409.77 ± 14.6 g in the HFS group vs. 370.21 ± 14.3 and 374.24 ± 6.6 g in the SC and KD groups, respectively), 12 (452.3 ± 15.7 g in the HFS group vs. 400.47 ± 15 and 404.69 ± 6.5 g in the SC and KD groups, respectively), and 16 (470.81 ± 17.1 g in the HFS group vs. 421.29 ± 15.7 and 425.54 ± 4.7 g in the SC and KD groups, respectively). With respect to blood glucose levels, there was no significant difference among the three groups at weeks 0 and 16 (Table 4). Insulinemia increased in both the HFS (1.90 ± 0.33 to 7.68 ± 1.54 ng/mL) and KD groups (2.18 ± 0.34 to 5.85 ± 0.66 ng/mL) from week 0 to week 16 (Table 4). However, at week 16, only the HFS had significantly higher blood insulin levels than the SC group (Table 4). In fact, the HFS diet-induced elevation in blood insulin concentration was 79%, relative to the SC animals (Table 4), which is an indication of insulin-resistance in these animals. In contrast, the SC and KD groups did not have statistically significantly different blood insulin levels at week 16 (Table 4).

Table 3. Body weight of SC-, HFS-, and KD-fed rats at the beginning of the study (week 0) and after 4, 8, 12, and 16 weeks of dietary intervention.

		Duration of Study (Weeks)				
	Groups	0	4	8	12	16
Body mass (g)	SC	231.97 ± 7.1	317.21 ± 10.4	370.21 ± 14.3	400.47 ± 15.0	421.29 ± 15.7
	HFS	236.18 ± 5.4	345.97 ± 10.7	409.77 ± 14.6 *	452.3 ± 15.7 *	470.81 ± 17.1 *
	KD	230.12 ± 3.6	321.21 ± 4.5	374.24 ± 6.6	404.69 ± 6.5	425.54 ± 4.7

* $p < 0.05$ vs. SC and KD within the respective weeks. Data are expressed as mean ± SEM. Mixed-effects model analysis. $n = 7$–9.

Table 4. Glycemia and insulinemia levels at the beginning (week 0) and at the end of the dietary intervention (week 16) in SC-, HFS-, and KD-fed rats.

		Duration of Study (Weeks)	
Blood Parameters	**Groups**	**0**	**16**
Glucose (mmol/L)	SC	6.85 ± 0.12	5.72 ± 0.18 #
	HFS	6.77 ± 0.21	5.91 ± 0.10 #
	KD	6.59 ± 0.12	5.71 ± 0.07 #
Insulin (ng/mL)	SC	2.16 ± 0.50	4.30 ± 0.43
	HFS	1.90 ± 0.33	7.68 ± 1.54 *#
	KD	2.18 ± 0.34	5.85 ± 0.66 #

* $p < 0.05$ vs. SC within the respective week; # $p < 0.05$ vs. week 0 measurement. Data are expressed as mean ± SEM. Mixed-effects model analysis, $n = 6$–7.

3.1. *ACE2 and TMPRSS2 Levels in Lung and Heart Tissues*

We extracted lung and heart tissues from the animals for measurement of SARS-CoV-2 cellular entry proteins ACE2 and TMPRSS2. The HFS diet increased lung ACE2 content 3.8- and 6-fold, when compared to the SC and KD groups, respectively (Figure 1A). A similar pattern was observed for TMPRSS2 where, for the HFS diet, the levels of this protein increased by 5.1- and 3.4-fold, relative to the SC and KD groups, respectively (Figure 1B). However, in cardiac tissue, no significant differences were detected for ACE2 or TMPRSS2 levels when comparing the different dietary interventions (Figure 1C,D, respectively). These data indicate that the HFS diet increased SARS-CoV-2 entry proteins in lung tissue, but not in the heart.

3.2. *ACE1, AT_1R, and AT_2R Levels in Lung and Heart Tissues*

In pulmonary tissue, the KD attenuated ACE1 protein content by 56%, relative to the SC group (Figure 2A). Furthermore, KD also reduced AT_1R protein content in this tissue; however, it was not statistically significant (Figure 2C). Pulmonary AT_2R levels were not altered by diet either (Figure 2E). In cardiac tissue, ACE1 was not significantly different among the groups (Figure 2B). However, the HFS diet induced 2.6 and 4.9-fold increases in AT_1R (Figure 2D) and AT_2R (Figure 2F) levels, respectively, when compared to the SC group. The contents of these proteins were not significantly different between the SC- and KD-fed animals.

3.3. *Comparison of ACE1, ACE2, AT_1R, and AT_2R in lung and Heart Tissues*

Upon observing the diet-induced changes in RAS proteins and the tissue-specific nature of these changes, we then decided to compare the contents of ACE1, ACE2, AT_1R, and AT_2R in the lungs and heart. Pulmonary tissue displayed higher levels of ACE1 than cardiac tissue (Figure 3), whereas more ACE2, AT_1R, and AT_2R was found in the heart than in the lungs. (Figure 3).

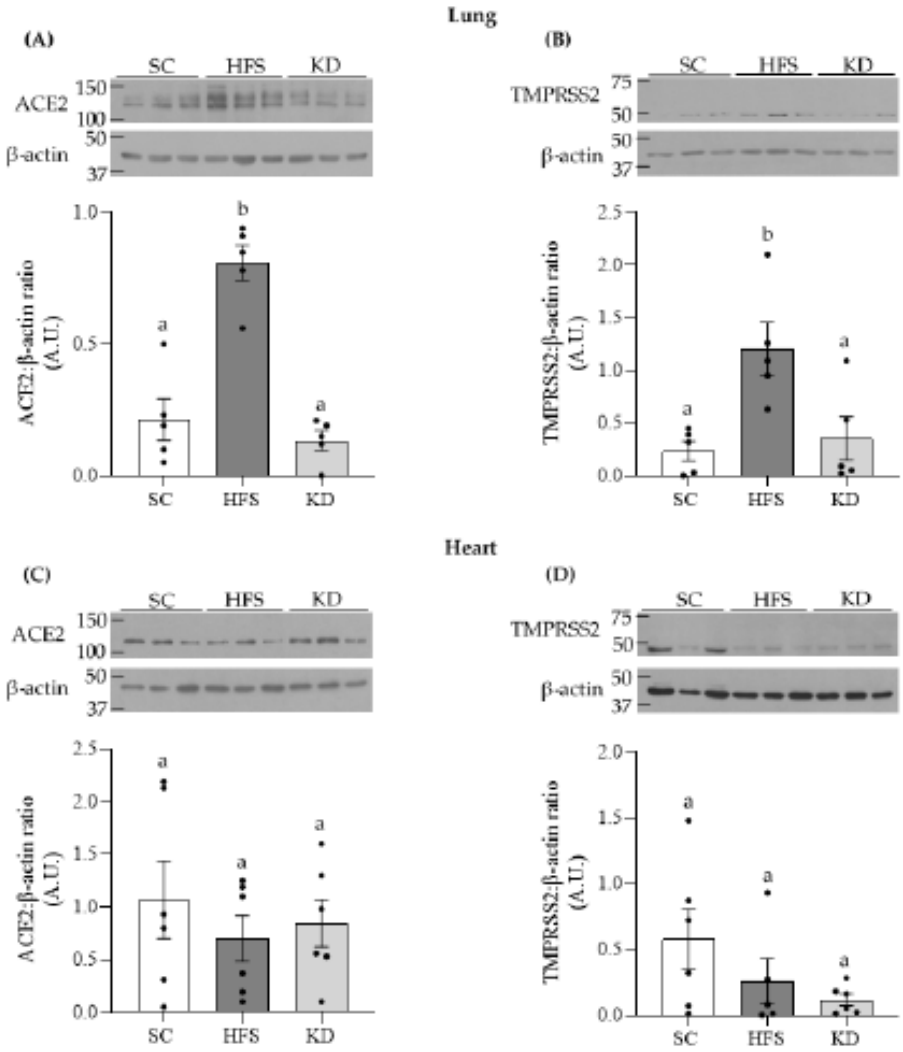

Figure 1. Lung contents of angiotensin converting enzyme 2 (ACE2) (**A**) and transmembrane protease serine 2 (TMPRSS2) (**B**) were significantly elevated by the HFS, but not by the KD. In contrast, diet did not alter the contents of these proteins in heart tissue (**C**,**D**). Statistical significance is denoted by different letters $p < 0.05$. Bars represent mean ± SEM. One-way ANOVA, $n = 5$–6. SC, standard chow; HFS, high-fat sucrose-enriched diet; KD, ketogenic diet.

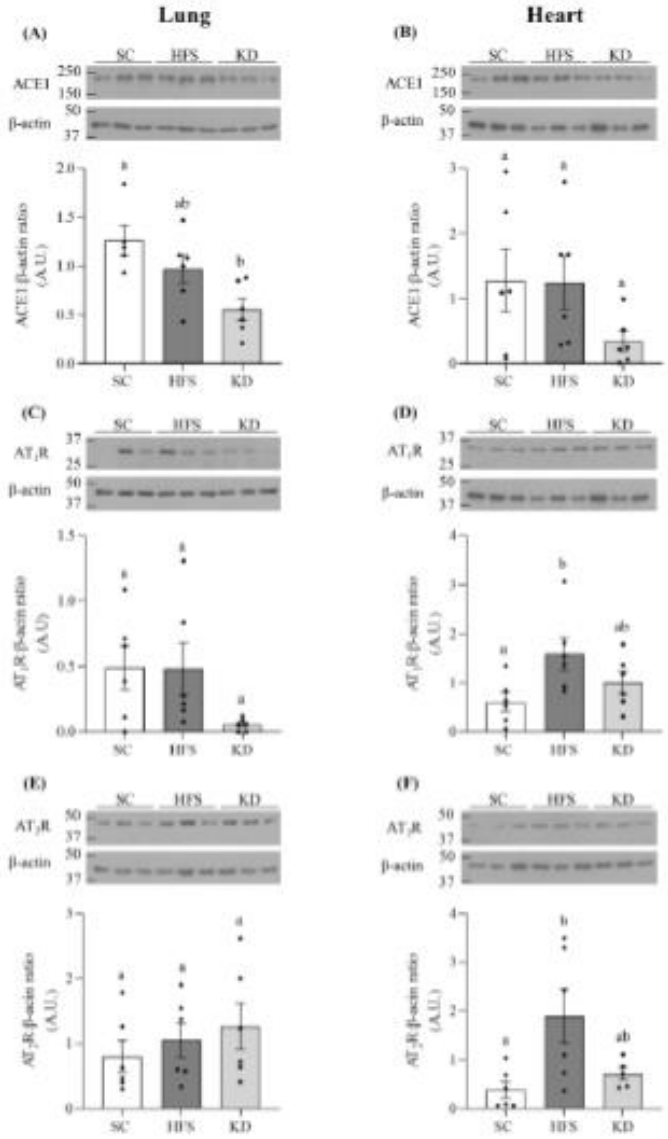

Figure 2. The KD attenuated angiotensin converting enzyme 1 (ACE1) and angiotensin II, type I receptor (AT_1R) contents in pulmonary tissue (**A**,**C**, respectively), however only the former was found to be statistically significant. Angiotensin II, type 2 receptor (AT_2R) was unaltered in the lungs, regardless of diet (**E**). On the other hand, dietary intervention did not influence heart ACE1 content (**B**), however AT_1R and AT_2R were significantly elevated in the cardiac tissues of HFS-fed rats (**D**,**F**, respectively). Significant differences are denoted by different letters $p < 0.05$. Bars represent mean ± SEM. One-way ANOVA, $n = 5–6$.

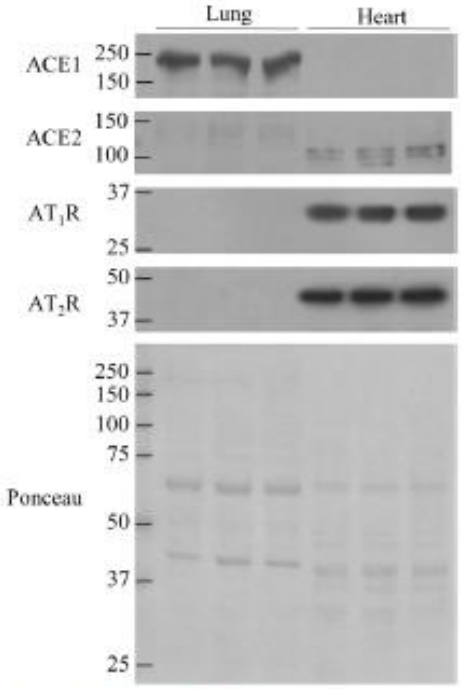

Figure 3. AT_1R, AT_2R and ACE2 are more abundant in heart tissue than in lung tissue. In contrast, lung tissue contains more ACE1. $n = 3$.

3.4. Gene Expressions of *Mas1*, *tlr4*, *il6r*, and *tnfr1* in Lung and Heart Tissues

The gene expression of *mas1* was not significantly different among any of the three dietary interventions in either lung (Figure 4A) or heart tissue (Figure 4E). However, the gene expressions of *tlr4* and *il6r* were significantly reduced by 74% and 79%, respectively, in the lungs of KD-fed animals, when compared to the HFS animals (Figure 4B,C, respectively). KD also suppressed *tnfr1* gene expression in this tissue by −73% (Figure 4D), although this was not statistically significant ($p = 0.059$). In the heart, no significant differences were found for *tlr4*, *il6r*, and *tnfr1* gene expressions among the three diet groups (Figure 4F–H, respectively). Altogether, these results indicate that the KD exerted an anti-inflammatory effect in the lungs, but not in the heart.

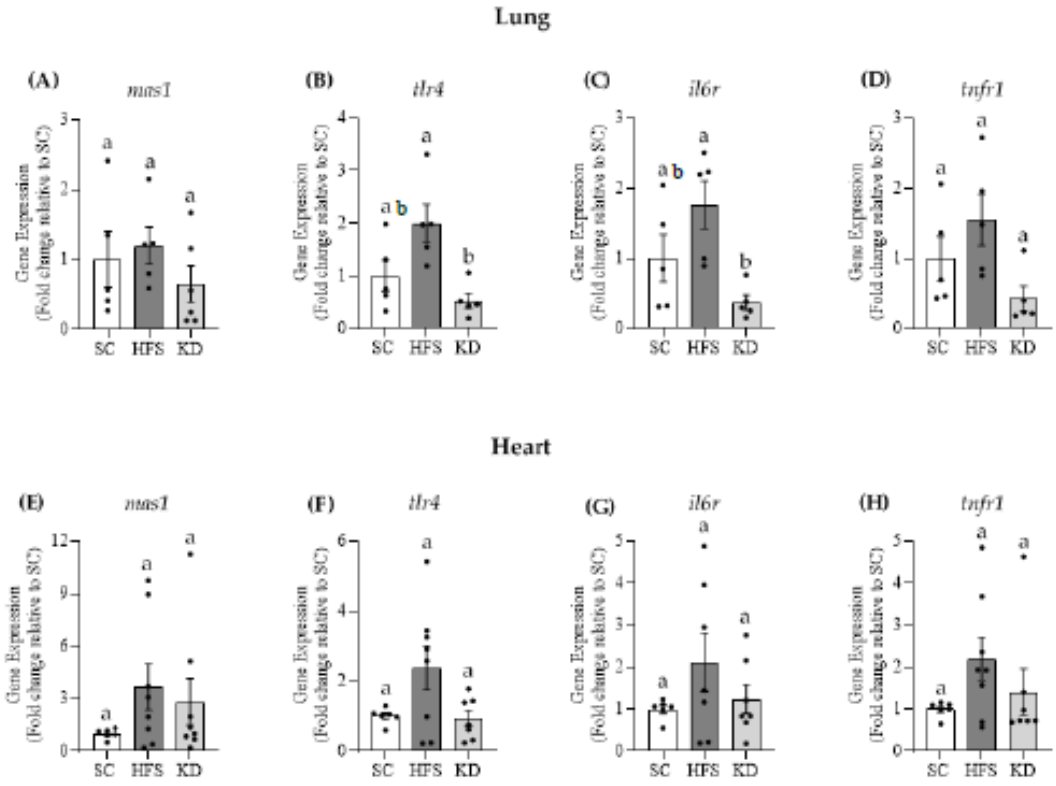

Figure 4. The KD does not affect *mas1* gene expression in lung (**A**) or heart (**E**) tissues. Interestingly, KD-feeding significantly reduces toll-like receptor 4 (*tlr4*) and interleukin-6 receptor (*il6r*) gene expression in pulmonary tissues (**B**,**C**, respectively), when compared to the HFS diet. The KD also reduced tumour necrosis factor receptor 1 (*tnfr1*) gene expression in lungs (**D**), though this was not statistically significant. *Tlr4, il6r and tnfr1* were not significantly altered by diet in cardiac tissues (**F**–**H**, respectively). Statistical significance is denoted by different letters $p < 0.05$. Bars represent mean ± SEM. One-way ANOVA, $n = 5$–8.

4. Discussion

Here, we show that obesogenic and ketogenic diets regulate in a distinct and tissue-specific manner proteins of the RAS, as well as major components of the molecular machinery involved in cellular infection by SARS-CoV-2. In fact, rats fed the HFS obesogenic diet displayed elevated insulinemia and much higher levels of ACE2 and TMPRSS2 in the lungs than animals fed either SC or a KD. This is consistent with previous findings of increased lung levels of ACE2 and TMPRSS2 in diabetic mice [7], and with reports linking insulin resistance and Type 2 diabetes to severe COVID outcomes [2,7]. However, to our knowledge, this is the first study to show that besides attenuating weight gain and insulinemia, a KD maintained lower ACE2 and TMPRSS2 protein levels in the lungs in comparison to a HFS diet. This is relevant for the prevention of severe COVID-19-related illness, given that ACE2 and TMPRSS2 have been identified as crucial components of the molecular machinery used by SARS-CoV-2 to infects cells [5]. In fact, use of the specific TMPRSS2 inhibitor, camostat mesylate, has been shown to inhibit SARS-CoV-2 entry in Caco-2 cells, and anti-ACE2 antibody incubation with Vero cells blocked SARS-CoV-1 and SARS-CoV-2 entry [5]. Thus, the observed elevation in these two proteins in the lungs of HFS-fed rats provides a plausible mechanism whereby obese individuals are more susceptible to severe

infection with SARS-CoV-2. The underlying mechanisms that explain this diet-induced elevation in ACE2 have not been fully elucidated [17]. However, under conditions of obesity, adipose tissue secretes angiotensinogen, which can eventually be converted to Ang-II, leading to hyperactivation of the ACE1/Ang-II/AT_1R arm of the RAS and subsequent tissue damage [2,8]. Hyperinsulinemia may also cause RAS dysregulation [8]. In this context, the observed elevation in ACE2 is likely a counterregulatory mechanism to attenuate the detrimental effects induced by obesity-mediated RAS hyperactivation [17]. Furthermore, non-alcoholic fatty liver disease (NAFLD) is a major comorbidity of obesity, and it has been linked to increased hepatic expression of ACE2 and TMPRSS2 [18], which could contribute to the aggravate morbidity in SARS-CoV-2 patients. Importantly, ketogenic diets have been shown to be very effective in combating NAFLD [19–21] and attenuate the potential deleterious effects of SARS-CoV-2 in the liver. However, we did not assess any variable associated with NAFLD in our studies; therefore, we could not make any inferences about hepatic expression of SARS-CoV-2 critical entry points.

Although there were no significant alterations in ACE2 and TMPRSS2 in the heart with any of the dietary interventions, ACE2 was found to be more abundant in cardiac than in lung tissue. Thus, because the obesogenic diet significantly increased ACE2 in the lungs, COVID-19 infection still poses a significant risk for cardiac health in obese individuals, since it is one of the primary points of infection. This could potentially enhance the severity of the infection in pulmonary tissues, leading to viral spill over, whereby the virus can access other tissues, including the heart, which is already abundant in ACE2 and, as a result, predisposed to infection and damage [2,6]. The roles of ACE2 in SARS-CoV-2 infection, as well as the RAS, are not independent. Thus, the other RAS components are also emerging as therapeutic targets to treat illness related to COVID-19. In fact, the use of angiotensin receptor blockers (ARB) or ACE inhibitors have been proposed as treatments for SARS-CoV-2 patients [2]. This serves to increase flux through the ACE2/Ang(1,7)/MasR and AT_2R arm of the RAS and to promote anti-inflammatory mechanisms that counteract the COVID-induced cytokine storm [2,6,8]. In the present study, we observed no alteration in AT_1R or AT_2R in lung tissues with any of the three dietary interventions. However, the KD did significantly reduce ACE1 levels. This indicates that the RAS system was shifted away from the ACE1/Ang-II/AT_1R arm and towards the counterregulatory, anti-inflammatory RAS arm, given that we also observed reductions in *tlr4*, and *il6r* gene expressions, as well as a trend to decrease *tnfr1* gene expression. The observed reduction in the expression of these inflammatory genes is relevant, as IL-6 and TNFα are two major cytokines that facilitate the coronavirus-induced cytokine storm [2]. Furthermore, Zhao et al. demonstrated that TLR4 inhibition suppressed interleukin-1β release in cells treated with the SARS-CoV-2 S protein [22].

Our findings are in line with other studies that report the anti-inflammatory nature of the KD [13,23], and suggest that this diet could reduce the risk of severe infection and inflammatory response related to COVID-19. We have not investigated the mechanism by which the KD led to lower levels of expression of inflammatory genes in comparison to the obesogenic diet. However, the KD is characterized by increased liver production of ketones [24]. Thus, the anti-inflammatory effect of the KD could be at least partially attributed to increased levels of circulating ketones, particularly β-hydroxybutyrate (β-HB), upon KD feeding [25]. In fact, β-HB has been demonstrated to block the nucleotide-binding domain leucine-rich-containing family pyrin domain-containing-3 (NLRP3) inflammasome and NLRP3 inflammasome-mediated interleukin (IL)-1β and IL-18 production by monocytes [26]. Additionally, the KD has been shown to exert its anti-inflammatory effects by inhibiting nuclear factor kappa-light-chain-enhancer of activated B cells (NF-kB) activation, suppressing the activity of histone deacetylases (HDACs), reducing the production of reactive oxygen species (ROS), and by improving mitochondrial respiration [24]. Thus, all these KD effects can ameliorate chronic low-grade inflammation and its associated diseases. It is important to mention that the KD used in this study was completely devoid of carbohydrates, which differs from the commonly used KD that recommends low carbohydrate

content (less than 50 g/day) and not the complete elimination of this macronutrient from the diet [27]. Thus, caution should be taken when extrapolating our findings to human subjects. However, the absence of carbohydrates in the diet allowed us to identify that it is the combination of HF with sucrose, as opposed to HF alone, that promotes the deleterious metabolic effects associated with increased levels of SARS-CoV-2 entry proteins and inflammation in lung and heart tissues in obesity.

We did not find any significant difference in the cardiac gene expressions of Mas1 or the aforementioned inflammatory genes, although a trend to increase the latter in the HFS-fed rats was detected. However, the HFS diet did increase AT_1R content, which was also met by a similar increase in AT_2R. This likely served to offset the proinflammatory response mediated by AT_1R. Indeed, it has been reported that AT_2R increases in response to AT_1R hyperactivation and injury [2,11]. Interestingly, AT_1R and AT_2R are more abundant in the heart than in the lungs. In this context, it is possible that the elevated expression of these receptors allows for an enhanced flexibility of this tissue to regulate its inflammatory status. It is important to note that AT_1R and AT_2R levels did not change in the hearts of KD-fed animals, relative to the SC animals, suggesting that this diet did not provoke RAS activation. Unlike the lungs, heart ACE1 content was not altered by diet. This could be attributed to the lower ACE1 content in the heart, compared to the lungs, suggesting that the reliance of the former on ACE1 for RAS regulation is lower than the latter, where there was a diet-induced alteration in the content of this protein. This is consistent with the notion that the ACE1-dependent conversion of Ang-I to Ang-II takes place predominantly in pulmonary circulation [10].

In conclusion, these data indicate that the HFS diet increases body weight, insulinemia RAS hyperactivation and lung ACE2 and TMPRSS2, which could explain the predisposition of obese individuals to severe COVID-19 outcomes. In contrast, the KD did not elicit the same elevations in weight gain and insulinemia as the HFS diet did. Our data also suggests that there is not a hyperactivation of the RAS in KD-fed animals, as indicated by the reductions in pulmonary ACE1 and the expressions of inflammatory genes, as well as unaltered cardiac AT_1R and AT_2R contents. Thus, a counterregulatory elevation in lung ACE2 was not observed in KD animals. Unlike the lungs, the heart does not experience a diet-induced alteration in ACE2, however the abundance of this protein, relative to the lungs, makes it a susceptible organ to SARS-CoV-2 damage, following viral spill over from pulmonary tissues. In this context, despite altering RAS proteins in a tissue-specific manner, it is clear that the KD offers a promising potential therapeutic tool for its reduction in SARS-CoV-2 entry proteins and its induction of an anti-inflammatory profile.

Author Contributions: D.D.E. conducted experiments, analyzed the results, and prepared figures, and wrote the manuscript. S.J. conducted experiments and revised the manuscript. R.B.C. designed the experimental approach, conducted experiments, and revised the manuscript. All authors have read and agreed to the published version of the manuscript.

Funding: This research was funded by a Natural Science and Engineering Research Council of Canada Discovery Grant (RBC, #311818-2011) and infrastructure grants from the Canada Foundation for Innovation and the Ontario Research Fund awarded to RBC. DE was supported by the Natural Sciences and Engineering Research Council of Canada Alexander Graham Bell Canada Graduate Scholarship-Doctoral.

Institutional Review Board Statement: The study was conducted according to the guidelines of the Declaration of Helsinki. The protocol containing all animal procedures described in this study was specifically approved by the Committee on the Ethics of Animal Experiments of York University (York University Animal Care Committee, YUACC, permit number: 2021-03, approved 16 March 2021) and performed strictly in accordance with the YUACC guidelines. All tissue extraction procedures were performed under ketamine/xylazine anesthesia, and all efforts were made to minimize suffering [14]. All experiments in this study were carried out in compliance with the ARRIVE guidelines [15].

Informed Consent Statement: Not applicable.

Data Availability Statement: All data are reported in the manuscript.

Conflicts of Interest: No conflict of interest are declared by the authors.

References

1. Longo, M.; Zatterale, F.; Naderi, J.; Parrillo, L.; Formisano, P.; Raciti, G.A.; Beguinot, F.; Miele, C. Adipose tissue dysfunction as determinant of obesity-associated metabolic complications. *Int. J. Mol. Sci.* **2019**, *20*, 2358. [CrossRef]
2. Luzi, L.; Bucciarelli, L.; Ferrulli, A.; Terruzzi, I.; Massarini, S. Obesity and COVID-19: The Ominous duet affecting the Renin-Angiotensin System Livio. *Minerva Endocrinol.* **2021**, *46*, 193–201. [CrossRef]
3. Palaiodimos, L.; Kokkinidis, D.G.; Li, W.; Karamanis, D.; Ognibene, J.; Arora, S.; Southern, W.N.; Mantzoros, C.S. Severe obesity is associated with higher in-hospital mortality in a cohort of patients with COVID-19 in the Bronx, New York. *Metabolism* **2020**, *108*, 154262. [CrossRef] [PubMed]
4. Sarver, D.C.; Wong, G.W. Obesity alters Ace2 and Tmprss2 expression in lung, trachea, and esophagus in a sex-dependent manner: Implications for COVID-19. *Biochem. Biophys. Res. Commun.* **2021**, *538*, 92–96. [CrossRef] [PubMed]
5. Hoffmann, M.; Kleine-Weber, H.; Schroeder, S.; Krüger, N.; Herrler, T.; Erichsen, S.; Schiergens, T.S.; Herrler, G.; Wu, N.H.; Nitsche, A.; et al. SARS-CoV-2 Cell Entry Depends on ACE2 and TMPRSS2 and Is Blocked by a Clinically Proven Protease Inhibitor. *Cell* **2020**, *181*, 271–280.e8. [CrossRef] [PubMed]
6. Machhi, J.; Herskovitz, J.; Senan, A.M.; Dutta, D.; Nath, B.; Oleynikov, M.D.; Blomberg, W.R.; Meigs, D.D.; Hasan, M.; Patel, M.; et al. The Natural History, Pathobiology, and Clinical Manifestations of SARS-CoV-2 Infections. *J. Neuroimmune Pharmacol.* **2020**, *15*, 359–386. [CrossRef] [PubMed]
7. Batchu, S.N.; Kaur, H.; Yerra, V.G.; Advani, S.L.; Golam Kabir, M.; Liu, Y.; Klein, T.; Advani, A. Lung and Kidney ACE2 and TMPRSS2 in Renin-Angiotensin System Blocker–Treated Comorbid Diabetic Mice Mimicking Host Factors That Have Been Linked to Severe COVID-19. *Diabetes* **2021**, *70*, 759–771. [CrossRef]
8. Akoumianakis, I.; Filippatos, T. The renin-angiotensin-aldosterone system as a link between obesity and coronavirus disease 2019 severity. *Obes. Rev.* **2020**, *21*, 1–8. [CrossRef]
9. Ames, M.K.; Atkins, C.E.; Pitt, B. The renin-angiotensin-aldosterone system and its suppression. *J. Vet. Intern. Med.* **2019**, *33*, 363–382. [CrossRef]
10. Marcus, Y.; Shefer, G.; Stern, N. Adipose tissue renin-angiotensin-aldosterone system (RAAS) and progression of insulin resistance. *Mol. Cell. Endocrinol.* **2013**, *378*, 1–14. [CrossRef]
11. Schulman, I.H.; Raij, L. The angiotensin II type 2 receptor: What is its clinical significance? *Curr. Hypertens. Rep.* **2008**, *10*, 188–193. [CrossRef]
12. Walton, C.M.; Perry, K.; Hart, R.H.; Berry, S.L.; Bikman, B.T. Improvement in Glycemic and Lipid Profiles in Type 2 Diabetics with a 90-Day Ketogenic Diet. *J. Diabetes Res.* **2019**. [CrossRef]
13. Asrih, M.; Altirriba, J.; Rohner-Jeanrenaud, F.; Jornayvaz, F.R. Ketogenic diet impairs FGF21 signaling and promotes differential inflammatory responses in the liver and white adipose tissue. *PLoS ONE* **2015**, *10*, e0126364. [CrossRef]
14. Pinho, R.A.; Sepa-Kishi, D.M.; Bikopoulos, G.; Wu, M.V.; Uthayakumar, A.; Mohasses, A.; Hughes, M.C.; Perry, C.G.R.; Ceddia, R.B. High-fat diet induces skeletal muscle oxidative stress in a fiber type-dependent manner in rats. *Free Radic. Biol. Med.* **2017**, *110*. [CrossRef]
15. du Sert, N.P.; Ahluwalia, A.; Alam, S.; Avey, M.T.; Baker, M.; Browne, W.J.; Clark, A.; Cuthill, I.C.; Dirnagl, U.; Emerson, M.; et al. Reporting animal research: Explanation and elaboration for the arrive guidelines 2.0. *PLoS Biol.* **2020**, *18*, e3000411.
16. Livak, K.J.; Schmittgen, T.D. Analysis of Relative Gene Expression Data Using Real-Time Quantitative PCR and the $2^{-\Delta\Delta CT}$ Method. *Methods* **2001**, *25*, 402–408. [CrossRef] [PubMed]
17. Wijnant, S.R.A.; Jacobs, M.; Van Eeckhoutte, H.; Lapauw, B.; Joos, G.F.; Bracke, K.R.; Brusselle, G.G. Expression of ACE2, the SARS-CoV-2 Receptor, in Lung Tissue of Patients with Type 2 Diabetes. *Diabetes* **2020**, *69*, 2691–2699. [CrossRef]
18. Fondevila, M.F.; Mercado-Gómez, M.; Rodríguez, A.; Gonzalez-Rellan, M.J.; Iruzubieta, P.; Valenti, V.; Escalada, J.; Schwaninger, M.; Prevot, V.; Dieguez, C.; et al. Obese patients with NASH have increased hepatic expression of SARS-CoV-2 critical entry points. *J. Hepatol.* **2021**, *74*, 469–471. [CrossRef]
19. D'Abbondanza, M.; Ministrini, S.; Pucci, G.; Nulli Migliola, E.; Martorelli, E.E.; Gandolfo, V.; Siepi, D.; Lupattelli, G.; Vaudo, G. Very Low-Carbohydrate Ketogenic Diet for the Treatment of Severe Obesity and Associated Non-Alcoholic Fatty Liver Disease: The Role of Sex Differences. *Nutrients* **2020**, *12*, 2748. [CrossRef]
20. Watanabe, M.; Tozzi, R.; Risi, R.; Tuccinardi, D.; Mariani, S.; Basciani, S.; Spera, G.; Lubrano, C.; Gnessi, L. Beneficial effects of the ketogenic diet on nonalcoholic fatty liver disease: A comprehensive review of the literature. *Obes. Rev.* **2020**, *21*. [CrossRef] [PubMed]
21. Luukkonen, P.K.; Dufour, S.; Lyu, K.; Zhang, X.M.; Hakkarainen, A.; Lehtimäki, T.E.; Cline, G.W.; Petersen, K.F.; Shulman, G.I.; Yki-Järvinen, H. Effect of a ketogenic diet on hepatic steatosis and hepatic mitochondrial metabolism in nonalcoholic fatty liver disease. *Proc. Natl. Acad. Sci. USA* **2020**, *117*, 7347–7354. [CrossRef] [PubMed]
22. Zhao, Y.; Kuang, M.; Li, J.; Zhu, L.; Jia, Z.; Guo, X.; Hu, Y.; Kong, J.; Yin, H.; Wang, X.; et al. SARS-CoV-2 spike protein interacts with and activates TLR41. *Cell Res.* **2021**, 1–3. [CrossRef]
23. Forsythe, C.E.; Phinney, S.D.; Fernandez, M.L.; Quann, E.E.; Wood, R.J.; Bibus, D.M.; Kraemer, W.J.; Feinman, R.D.; Volek, J.S. Comparison of low fat and low carbohydrate diets on circulating fatty acid composition and markers of inflammation. *Lipids* **2008**, *43*, 65–77. [CrossRef]

24. Pinto, A.; Bonucci, A.; Maggi, E.; Corsi, M.; Businaro, R. Anti-oxidant and anti-inflammatory activity of ketogenic diet: New perspectives for neuroprotection in alzheimer's disease. *Antioxidants* **2018**, *7*, 63. [CrossRef] [PubMed]
25. Streijger, F.; Plunet, W.Y.; Lee, J.H.Y.; Liu, J.; Lam, C.K.; Park, S.; Hilton, B.J.; Fransen, B.L.; Matheson, K.A.J.; Assinck, P.; et al. Ketogenic diet improves forelimb motor function after spinal cord injury in rodents. *PLoS ONE* **2013**, *8*, e78765. [CrossRef]
26. Youm, Y.-H.; Nguyen, K.Y.; Grant, R.W.; Goldberg, E.L.; Bodogai, M.; Kim, D.; D'Agostino, D.; Planavsky, N.; Lupfer, C.; Kanneganti, T.D.; et al. The ketone metabolite β-hydroxybutyrate blocks NLRP3 inflammasome–mediated inflammatory disease. *Nat. Med.* **2015**, *21*, 263–269. [CrossRef]
27. Batch, J.Y.; Lamsal, S.P.; Adkins, M.; Sultan, S.; Ramirez, M.N. Advantages and Disadvantages of the Ketogenic Diet: A Review Article. *Cureus* **2020**, *12*. [CrossRef]

nutrients

MDPI

Article

Sucrose-Enriched and Carbohydrate-Free High-Fat Diets Distinctly Affect Substrate Metabolism in Oxidative and Glycolytic Muscles of Rats

Daniel Da Eira, Shailee Jani, Mateja Stefanovic and Rolando B. Ceddia *

Muscle Health Research Centre, School of Kinesiology and Health Science, York University, Toronto, ON M3J 1P3, Canada
* Correspondence: roceddia@yorku.ca; Tel.: +1-(416)-736-2100 (ext. 77204); Fax: +1-(416)-736-5774

Abstract: Skeletal muscle substrate preference for fuel is largely influenced by dietary macronutrient availability. The abundance of dietary carbohydrates promotes the utilization of glucose as a substrate for energy production, whereas an abundant dietary fat supply elevates rates of fatty acid (FA) oxidation. The objective of this study was to determine whether an obesogenic, high-fat, sucrose-enriched (HFS) diet or a carbohydrate-free ketogenic diet (KD) exert distinct effects on fat, glucose, and ketone metabolism in oxidative and glycolytic skeletal muscles. Male Wistar rats were fed either a HFS diet or a KD for 16 weeks. Subsequently, the soleus (Sol), extensor digitorum longus (EDL), and epitrochlearis (Epit) muscles were extracted to measure palmitate oxidation, insulin-stimulated glucose metabolism, and markers of mitochondrial biogenesis, ketolytic capacity, and cataplerotic and anaplerotic machinery. Sol, EDL, and Epit muscles from KD-fed rats preserved their ability to elevate glycogen synthesis and lactate production in response to insulin, whereas all muscles from rats fed with the HFS diet displayed blunted responses to insulin. The maintenance of metabolic flexibility with the KD was accompanied by muscle-fiber-type-specific adaptive responses. This was characterized by the Sol muscle in KD-fed rats enhancing mitochondrial biogenesis and ketolytic capacity without elevating its rates of FA oxidation in comparison with that in HFS feeding. Conversely, in the Epit muscle, rates of FA oxidation were increased, whereas the ketolytic capacity was markedly reduced by the KD in comparison with that by HFS feeding. In the EDL muscle, the KD also increased rates of FA oxidation, although it did so without altering its ketolytic capacity when compared to HFS feeding. In conclusion, even though obesogenic and ketogenic diets have elevated contents of fat and alter whole-body substrate partitioning, these two dietary interventions are associated with opposite outcomes with respect to skeletal muscle metabolic flexibility.

Keywords: PGC-1α; TFAM; ketolysis; insulin resistance; anaplerosis; ketogenic diet; OXCT; ACAT1

Citation: Da Eira, D.; Jani, S.; Stefanovic, M.; Ceddia, R.B. Sucrose-Enriched and Carbohydrate-Free High-Fat Diets Distinctly Affect Substrate Metabolism in Oxidative and Glycolytic Muscles of Rats. *Nutrients* **2024**, *16*, 286. https://doi.org/10.3390/nu16020286

Academic Editors: Riccardo Calvani, Domenico Azzolino and Gianfranco Vincenzo

Received: 24 December 2023
Revised: 12 January 2024
Accepted: 15 January 2024
Published: 18 January 2024

1. Introduction

The suppression of glucose metabolism under conditions of an abundant dietary fat supply can be partially attributed to changes in cellular substrate partitioning. The metabolic shift that coincides with the elevation of whole-body FA oxidation and glucose intolerance has been of concern in diabetic and insulin-resistant patients [1]. Conversely, from the perspective of endurance performance, a higher rate of skeletal muscle FA oxidation could be advantageous due to its potential glycogen-sparing effect [2]. Thus, the utilization of high-fat low-carbohydrate diets in endurance athletes has recently gained attention, particularly the ketogenic diet (KD) [3] that provides an abundance of fat and ketones as alternative sources of fuel for skeletal muscles [2,4]. In fact, the skeletal muscle gene expression of *Cpt1b* [5], fat oxidation [4], and markers of the mitochondrial biogenesis [6] and fractional areas [7] were elevated, whereas glucose oxidation [4], GLUT4 and IRS1 contents, and glucose tolerance were reduced by the KD in exercise-trained individuals [8]. The KD has also been shown to significantly enhance ketone-mediated ATP production

relative to glucose- or fat-mediated ATP production [4]. Thus, the abundance of fat and relatively lower content of dietary carbohydrates shift the metabolic substrate preference away from glucose and toward FAs.

Skeletal muscles display distinct oxidative and glycogenolytic capacities [9] and activities of enzymes involved in ketone oxidation [10]. Thus, the ability of oxidative and glycolytic muscles to adjust substrate partitioning according to fat and glucose dietary abundance may also significantly differ. Indeed, Fukazawa et al. showed that a KD increased the protein content of the ketolytic enzyme 3-oxoacid CoA transferase (OXCT) in the epitrochlearis (Epit) muscle [11], whereas Shimizu et al. reported a significant attenuation of OXCT gene expression in the gastrocnemius muscle [5]. Moreover, there is evidence that the KD increases mitochondrial mass in the red gastrocnemius muscle [7], which was contrasted by reports that the KD did not alter PGC-1α levels in the extensor digitorum longus (EDL) [12] or soleus (Sol) muscles [6]. Taken together, these data point to an apparent gap in the literature where KD-induced metabolic adaptations in substrate preference in muscles of varying oxidative and glycolytic capacities are yet to be fully elucidated. In this context, this study aimed to investigate whether the obesogenic, high-fat sucrose-enriched (HFS) diet and the KD would differ in their effects on metabolic substrate selection in muscles with varying fiber-type compositions. To achieve this, we compared the metabolic responses of Sol, EDL, and Epit rat muscles to either a KD (80% fat, lard; 0% carbohydrate; 20% protein) or typical obesogenic HFS diet (60% fat, lard; 20% sucrose; 20% protein). Furthermore, previous studies comparing the KD to a control diet had significantly different protein contents [7,11,13]. Importantly, skeletal muscle atrophy has been found in studies that reduce the protein content of a KD [14], whereas studies that use a normal protein diet report the maintenance of lean mass [13]. Varying protein contents also elicit distinct metabolic adaptations. For instance, Nakao et al. used a KD that was 4.8% kcal protein, compared to the control diet that was ~14% kcal protein, and observed a decrease in gastrocnemius pyruvate dehydrogenase (PDH) activity [14]. Huang et al., on the other hand, used a KD with a similar protein level to the control diet (16%) and reported no alteration in PDH activity [13]. Therefore, it is possible that the muscle metabolic adaptations do not derive from the low-carb high-fat content of the KD itself, but rather from its low protein content. To eliminate this as a confounding variable, we equalized the protein contents in both diets. Additionally, despite the high fat content in both the obesogenic HFS diet and the KD, the latter diet has been shown to improve metabolic health [4], whereas the former is detrimental to metabolic health. This suggests that the high fat content may not by itself be the main disruptor of normal metabolic function in skeletal muscles. Finally, because the KD was devoid of carbohydrates and hepatic ketone production is enhanced by the KD [3], besides rates of FA oxidation, we also assessed markers of mitochondrial biogenesis and the content of specific enzymes involved in the ketolytic, anaplerotic, and cataplerotic machineries in skeletal muscles with distinct fiber-type compositions. Here, we provide evidence that, contrary to the HFS diet, the carbohydrate-free KD enhances rates of FA oxidation and ketolytic capacity without impairing insulin-stimulated glucose metabolism in oxidative and glycolytic skeletal muscles.

2. Materials and Methods

Reagents—Fatty-acid (FA)-free bovine serum albumin (BSA), glycogen, and palmitic acid were obtained from Sigma (St. Louis, MO, USA). Human insulin (Humulin R) was purchased from Eli Lilly Inc. (Toronto, ON, Canada). D-[U-^{14}C]glucose and [1-^{14}C]palmitic acid were acquired from GE Healthcare Radiochemicals (Quebec City, QC, Canada). The Lactate Colorimetric/Fluorometric Assay Kit was purchased from BioVision (Milpitas, CA, USA). Protease (cOmplete Ultra Tablets) and phosphatase (PhosSTOP) inhibitors were obtained from Roche Diagnostics GmbH (Mannheim, Germany). The peroxisome proliferator-activated receptor γ coactivator-1α (PGC-1α, cat. no. AB3242) antibody was purchased from Millipore (Temecula, CA, USA). The β-hydroxybutyrate (BHB; cat. No. ab83390) assay kit and the mitochondrial transcription factor A (TFAM; Cat. # ab131607), 3-

oxoacid CoA-transferase 1 (OXCT; Cat. # ab224250), and acetoacetyl-CoA acetyltransferase 1 (ACAT1; Cat # ab168342) antibodies were purchased from Abcam (Toronto, ON, Canada). Pyruvate carboxylase (PC; Cat # 49381), phosphoenolpyruvate carboxykinase 1 (PCK1; Cat. # 12940), and phosphoenolpyruvate carboxykinase 2 (PCK2; 6924) antibodies were purchased from Cell Signaling (Danvers, MA, USA).

Animals and diet—Male albino rats (Wistar strain) at approximately 250 g were individually housed at 22 °C on a 12/12-h light–dark cycle. These rats were assigned either a high-fat sucrose-enriched (HFS) diet (20% kcal protein; 60% kcal fat (lard/soybean oil); 20% kcal carbohydrate (sucrose)) or KD (20% kcal protein; 80% kcal fat (lard/soybean oil); 0% kcal carbohydrate) and fed for 16 weeks ad libitum. Both diets were purchased from Research Diets (New Brunswick, NJ, USA).

Ethics approval—The protocol containing all animal procedures described in this study was specifically approved by the Committee on the Ethics of Animal Experiments of York University (York University Animal Care Committee, YUACC, permit number: 2021-03) and performed strictly in accordance with the YUACC guidelines. Date of approval: 18 July 2023. All tissue extraction procedures were performed under ketamine/xylazine anesthesia, and all efforts were made to minimize suffering [15]. All experiments in this study were carried out in compliance with the ARRIVE guidelines [16].

Measurement of blood glucose levels—Blood from all animals in the fed state was collected between 15:00 and 16:00 h with saphenous vein bleeding. Plasma glucose was measured using a Contour Next one meter blood glucose monitoring system by Ascensia Diabetes Care US (Parsippany, NJ, USA).

Muscle isolation and incubation—All animals were anesthetized with a single intraperitoneal injection of ketamine (90 mg/100 g BW) and xylazine (10 mg/100 g BW). Subsequently, Sol, EDL, and Epit muscles were quickly extracted. The percentages of type I, type IIa, and type IIb in Sol, EDL, and Epit muscles are 84/16/0, 3/57/40 [17], and 15/20/65 [18], respectively. From these muscles, strips were cut (18–22 mg) and pinned onto thin stainless steel wire clips to maintain muscle length. Thereafter, muscle strips were immediately placed in plastic scintillation vials containing 2 mL of pre-gassed (30 min with O_2:CO_2-95:5% (vol/vol)) Krebs–Ringer bicarbonate (KRB) buffer containing 3.5% FA-free BSA and 5.5 mM glucose. Vials were sealed and subjected to continuous gasification for the entirety of the 1 h pre-incubation period.

Measurement of glucose oxidation, glycogen synthesis, and lactate production—Following the pre-incubation period, one set of muscles was then transferred to vials containing 2 mL of the same KRB buffer plus D-[U-^{14}C]glucose (0.2 µCi/mL) and incubated under continuous gasification for one additional hour, either in the absence (basal) or presence of insulin (100 nM) for the determination of glycogen synthesis and glucose oxidation, as previously described [19]. For lactate production, media aliquots were first deproteinated using 10 kDa filters (centrifuged at 13,000 rpm for 15 min at 4 °C) and then assayed using a colorimetric assay kit, according to the manufacturer's instructions.

Measurement of palmitate oxidation in isolated muscles—Palmitate oxidation was measured by assessing the production of $^{14}CO_2$ from [1-^{14}C]palmitic acid. Muscles were pre-incubated as previously described and then transferred to vials containing 2 mL of KRB buffer plus 0.2 mM of cold palmitic acid, previously complexed with FA-free BSA and [1-^{14}C] palmitic acid (0.2 µCi/mL). The muscles were incubated under continuous gasification for 1 h, and the vials had a centered isolated well containing a loosely folded piece of filter paper moistened with 0.2 mL of 2-phenylethylamine/methanol (1:1, vol/vol). Following the incubation and acidification of the media, the filter papers were carefully removed and transferred to scintillation vials for radioactivity counting [15].

Western blotting analysis of PGC1α, TFAM, OXCT, ACAT1, PC, PCK1, and PCK2 contents in Sol, EDL and Epit muscles—Muscle samples that were not subject to incubation were flash frozen in liquid nitrogen and stored at −80 °C until the Western blotting analysis. Muscle tissues from the Sol, EDL and Epit muscles were homogenized in a buffer containing 25 mM Tris-HCl, 25 mM NaCl (pH 7.4), 1 mM $MgCl_2$, 2.7 mM KCl, 1% Triton X-100, and

protease and phosphatase inhibitors (Roche Diagnostics GmbH, Mannheim, Germany). The homogenates were centrifuged, the supernatant was collected, and an aliquot was used for protein determination with the Bradford method. Samples were diluted 1:1 vol:vol with a 2× Laemmli sample buffer and heated to 95 °C for 5 min. Subsequently, 25 µg of protein was loaded into each well. Samples were thereafter subjected to SDS-PAGE, transferred to a PVDF membrane, and probed for the proteins of interest. All primary antibodies were used at a dilution of 1:1000. Ponceau staining was used as a loading control. All densitometry analyses were performed using the ImageJ program, version 1.46r.

Statistical Analyses—Data were expressed as mean ± SD. Statistical analyses were performed using two-way ANOVAs with Bonferroni post hoc and Student's *t*-tests, as indicated in the figure legends. If data were not normally distributed, or if data had an inequality of variance, Mann–Whitney and Welch's tests were used, respectively. GraphPad Prism software version 9.1.12 was used for all statistical analyses. The level of significance was set to $p < 0.05$.

3. Results

Effects of diet on glycaemia and plasma βHB levels—Blood glucose levels did not differ between the HFS and KD groups at weeks 8 and 16 (Table 1). However, the KD significantly elevated plasma βHB levels 1.6- and 1.9-fold at weeks 8 and 16, respectively, relative to the HFS diet (Table 1). The concentration of βHB in the circulation changed in a time-dependent manner in KD-fed animals, being highest at week 8 (Table 1). Despite a 24% reduction in plasma βHB from weeks 8 to 16 in the KD group, week 16 levels were elevated 2.2-fold, relative to week 0 (Table 1).

Table 1. Blood glucose and plasma beta-hydroxybutyrate (βHB) levels at weeks 0, 8, and 16 of dietary intervention. Blood glucose levels were not different between the two dietary groups; however, βHB was elevated in the KD group at weeks 8 and 16, relative to that in the HFS group.

		Week		
		0	**8**	**16**
Glycaemia (mM)	HFS	7.31 ± 0.54	7.19 ± 0.47	6.77 ± 0.72 ‡
	KD	7.29 ± 0.35	6.99 ± 0.34	6.57 ± 0.43 ‡
βHB (mM)	HFS	0.16 ± 0.06	0.24 ± 0.08	0.15 ± 0.04
	KD	0.13 ± 0.04	0.38 ± 0.08 #	0.29 ± 0.05 †

# $p < 0.05$ vs. week 0 KD and week 8 HFS; † $p < 0.05$ vs. week 0 KD, week 8 KD, and week 16 HFS. ‡ $p < 0.05$ vs. week 0. Data are expressed as mean ± SD. Mixed-effect model analysis. N = 7–15 for glycaemia. N = 6–7 for βHB.

Effects of diet on palmitate and glucose oxidation in skeletal muscle—Sol palmitate oxidation did not significantly differ between the HFS- and KD-fed rats (Figure 1A); however, in both the EDL and Epit muscles, the KD increased palmitate oxidation ~1.7-fold in comparison with the HFS diet (Figure 1B and C, respectively). These muscle-specific adaptive responses were also observed with respect to glucose oxidation. In the Sol, EDL, and Epit muscles in HFS-fed animals, insulin-stimulated glucose oxidation was blunted (Figure 1D–F). In the KD-fed rats, the rates of insulin-stimulated glucose oxidation in the Sol, EDL, and Epit muscles were higher than the basal values, but did not reach statistical significance (Figure 1D–F). Only the EDL muscles in the KD-fed rats displayed rates of insulin-stimulated glucose oxidation that were significantly higher than those in the HFS-fed rats (Figure 1E). Thus, whereas the KD enhanced FA oxidation in a muscle-specific manner, insulin-stimulated glucose oxidation was similarly impaired in all muscles.

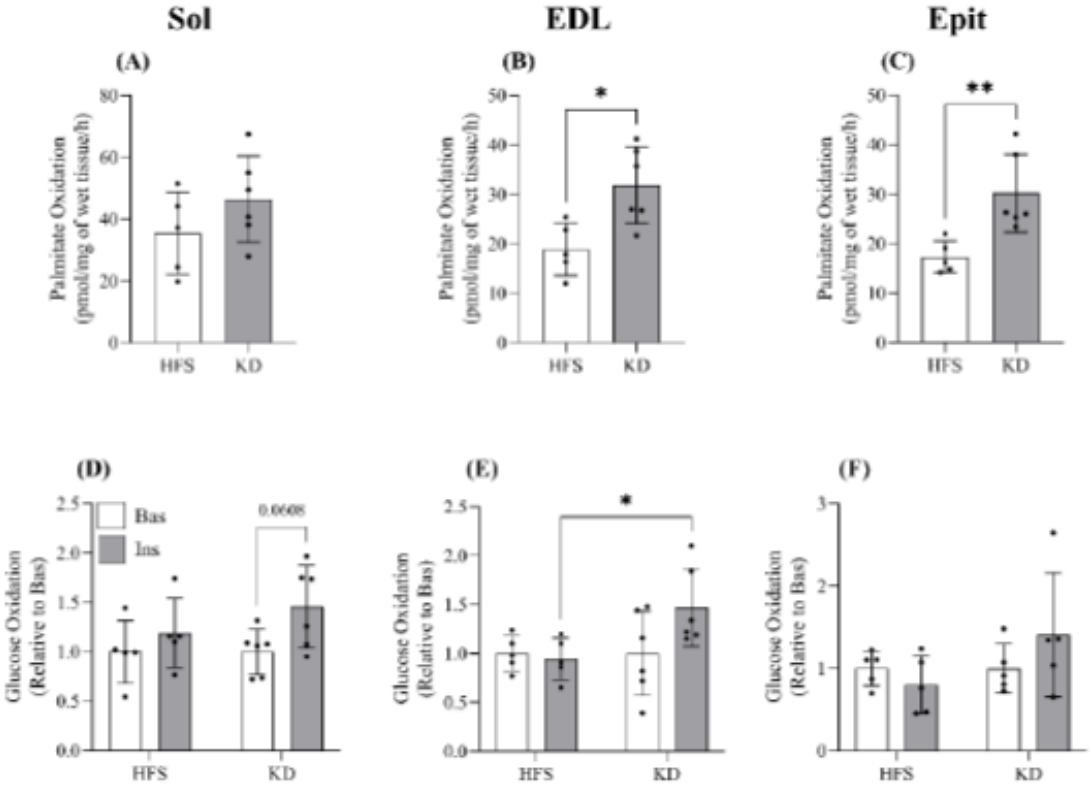

Figure 1. Palmitate oxidation was not significantly altered by diet in the soleus muscle (Sol, (**A**)); however, it was significantly elevated by the ketogenic diet (KD) in the extensor digitorum longus (EDL, (**B**)) and epitrochlearis (Epit, (**C**)) muscles. Conversely, glucose oxidation was not significantly enhanced in either of the two groups in any of the muscles with insulin (Ins) stimulation (**D**–**F**). Despite this, the fold increase in insulin-stimulated glucose oxidation in the EDL muscle, relative to basal (Bas) values, was enhanced by the KD (**E**). Data are expressed as mean ± SD. n = 5–6 rats. Student's *t*-test was used to compare groups for (**A**–**C**), whereas a two-way ANOVA with Bonferroni post hoc comparisons was used for (**D**–**F**). * $p < 0.05$, ** $p < 0.01$.

Effects of diet on insulin-stimulated glycogen synthesis and lactate production—Insulin-stimulated rates of glycogen synthesis were blunted in the Sol, EDL, and Epit muscles in rats fed with the HFS diet (Figure 2A, C and E, respectively), whereas in the Sol and EDL muscles of KD-fed rats, insulin increased this variable 1.8-fold (Figure 2A) and 1.5-fold (Figure 2C), respectively, in comparison with basal values. In Epit muscles from KD-fed rats, insulin stimulation did not significantly elevate glycogen synthesis in comparison to basal values; however, the glycogen synthesis response to insulin was significantly higher than that of the HFS-fed rats (Figure 2E). Insulin-stimulated lactate production, an indication of glycolytic capacity [20], was also blunted in the Sol, EDL, and Epit muscles from HFS-fed rats; whereas in the KD-fed rats, the Sol, EDL, and Epit muscles incubated with insulin displayed 2.1-, 2.1-, and 1.9-fold increases in lactate production in comparison to basal values (Figure 2B, D and F, respectively). Therefore, the KD preserved the capacity of oxidative and glycolytic muscles to store glycogen and perform glycolysis when stimulated with insulin.

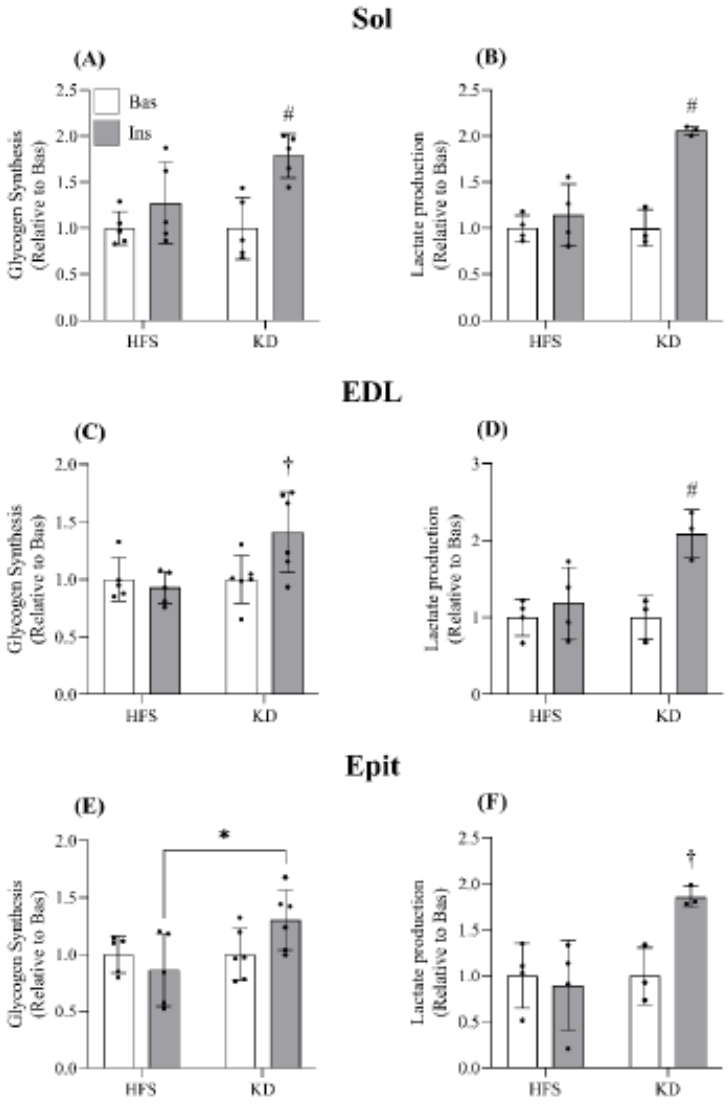

Figure 2. Ins stimulation increased glycogen synthesis in the Sol and EDL muscles of KD-fed rats (**A** and **C**, respectively). Epit glycogen synthesis did not increase relative to Bas values in either of the two groups; however, the fold increase in Ins-stimulated glycogen synthesis was greater with KD (**E**). Similarly, Ins significantly enhanced lactate production in all three muscles of KD-fed rats (**B**,**D**,**F**). Data are expressed as mean ± SD. n = 3–6. A two-way ANOVA with Bonferroni post hoc tests was used to compare the groups. * $p < 0.05$; # $p < 0.05$ vs. all other groups; † $p < 0.05$ vs. HFS Ins and KD Bas.

Effects of the KD on the contents of ketolytic enzymes OXCT and ACAT1 in Sol, EDL, and Epit muscles—Because the circulating βHB levels were elevated in KD-fed rats compared with those of the HFS-fed rats, it was possible that the effects of ketones on substrate partitioning in skeletal muscles would also be different between the dietary interventions and fiber-type compositions. To assess that possibility, we measured the ketolytic enzymes OXCT and ACAT1 in Sol, EDL, and Epit muscles from rats fed either

with the HFS diet or KD. We found that the OXCT content increased 1.6-fold in the Sol muscles of KD-fed animals (Figure 3A), whereas ACAT1 levels were unaltered by either of the two diets in this highly oxidative muscle (Figure 3B). In the EDL, OXCT and ACAT1 contents did not differ between the HFS- and KD-fed rats (Figure 3C and D, respectively). In contrast, the Epit OXCT and ACAT1 contents were 63% and 77% lower, respectively, in KD-fed animals when compared to those in the HFS group (Figure 3E and F, respectively). Therefore, in comparison to the HFS diet, the KD enhanced and suppressed the ketolytic capacity of the Sol and Epit muscles, respectively, whereas in the EDL muscle, the ketolytic capacity was unaffected by either the HFS diet or KD.

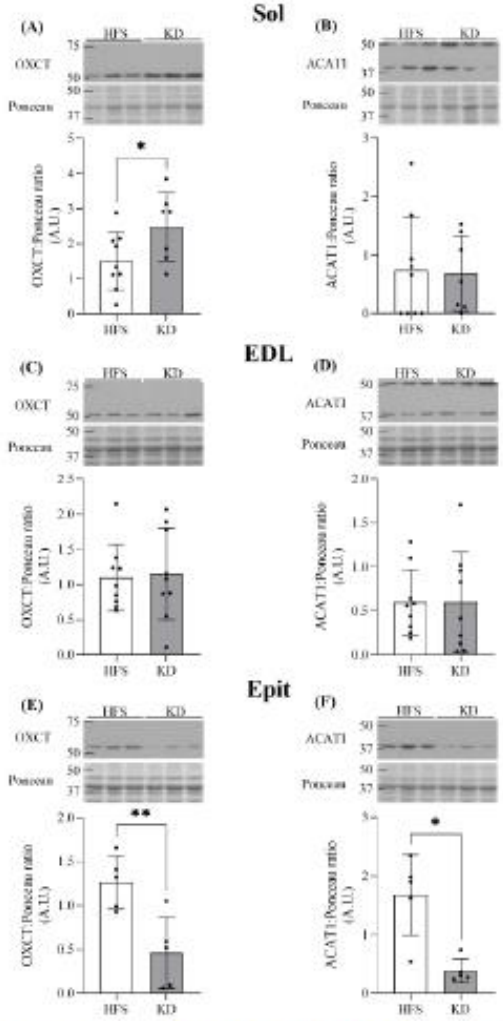

Figure 3. Sol OXCT content was significantly elevated by the KD (**A**), whereas Sol ACAT1 was unaffected by diet (**B**). Neither diet altered EDL muscle contents of OXCT or ACAT1 (**C** and **D**, respectively). Conversely, OXCT and ACAT1 contents were attenuated in the Epit muscle of KD-fed animals (**E** and **F**, respectively). Data are expressed as mean ± SD. n = 5–9. Student's *t*-test was used to compare groups, except for (**B**) and (**F**), where the Mann–Whitney test was used. * $p < 0.05$, ** $p < 0.01$.

Effects of diet on PGC-1α and TFAM protein levels in Sol, EDL, and Epit muscles—The muscle-specific differences in substrate preference could be attributed to distinct dietary effects on mitochondrial biogenesis. Thus, we measured the contents of PGC-1α and TFAM, which are markers of mitochondrial biogenesis and content [21]. In Sol muscles, despite not increasing palmitate oxidation, the KD significantly elevated PGC-1α and TFAM contents 1.9- and 6-fold, respectively (Figure 4A and B, respectively). However, in the EDL (Figure 4C and D) and Epit (Figure 4E and F) muscles, PGC-1α or TFAM levels did not differ between the HFS diet and KD.

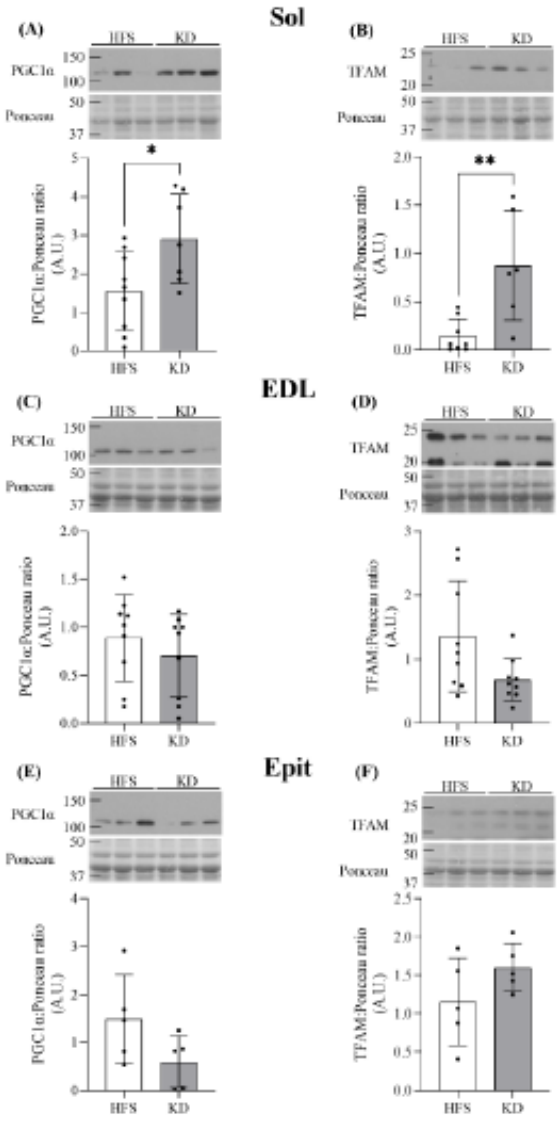

Figure 4. The Sol muscle demonstrated KD-induced elevations in PGC1α and TFAM (**A** and **B**, respectively), whereas diet did not alter the contents of either of these proteins in either the EDL (**C** and **D**) or Epit (**E** and **F**) muscles. Data are expressed as mean ± SD. n = 5–9. Student's *t*-test was used to compare groups, except for (**B**) and (**D**), where the Mann–Whitney test and Welch's *t*-test were used, respectively. * $p < 0.05$, ** $p < 0.01$.

Effects of the KD on PC, PCK1, and PCK2 levels in Sol, EDL, and Epit muscles—Substrate oxidation is dependent on the availability of tricarboxylic acid (TCA) cycle intermediates, which is largely controlled by cataplerotic and anaplerotic enzymes [22]. To investigate whether the shift toward FA oxidation induced by both diets, and particularly the carbohydrate-free KD, could be attributed to this, we assessed the contents of the anaplerotic protein PC, and the cataplerotic PCK1 and PCK2 [22,23]. Despite differences in oxidative and glycolytic capacities among the three muscles, no differences were found in the protein levels of PC, PCK1, and PCK2 in the Sol (Figure 5A–C), EDL (Figure 5D–F), or Epit (Figure 5G–I) muscles when comparing the HFS diet and KD. Thus, the contents of anaplerotic and cataplerotic enzymes in oxidative and glycolytic muscles did not contribute to the muscle-specific diet effects on substrate oxidation.

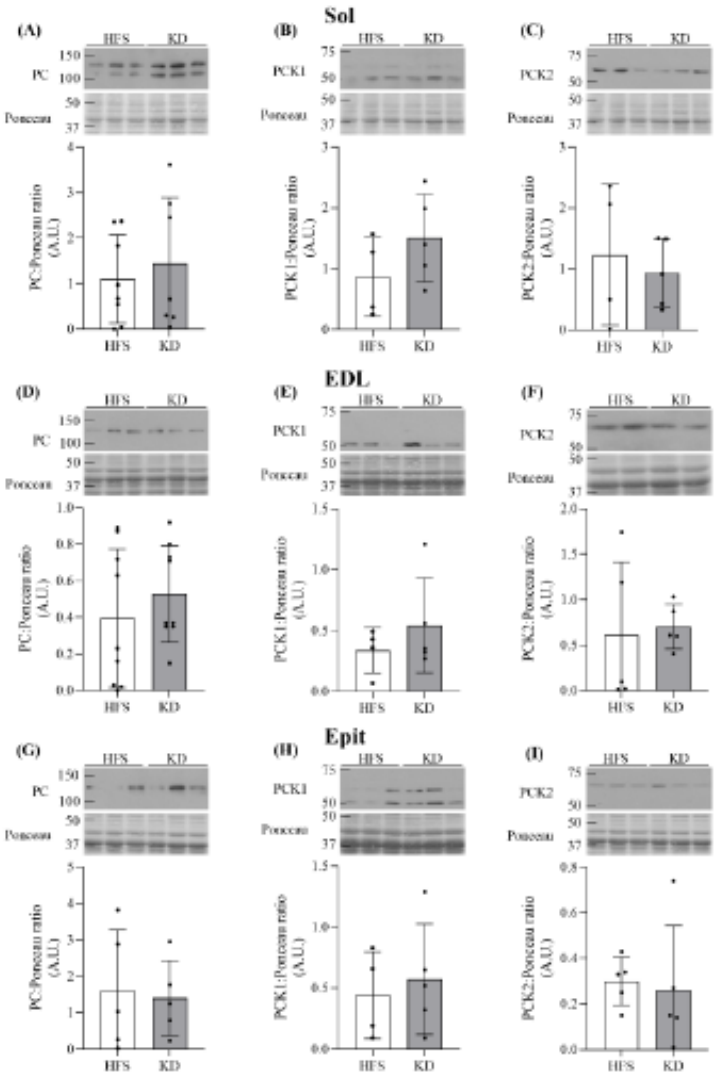

Figure 5. PC, PCK1, and PCK2 were not altered by diet in the Sol (**A–C**, respectively), EDL (**D–F**, respectively) or Epit (**G–I**, respectively) muscles. Data are expressed as mean ± SD. n = 4–9. Student's *t*-test was used to compare groups, except for (**E**), where the Mann–Whitney test was used.

4. Discussion

The main finding of this study was that despite inducing a higher rate of FA oxidation than the HFS diet, the KD preserved the ability of oxidative and glycolytic muscles to elevate glucose metabolism in response to insulin. Thus, our data provided compelling evidence that it is the chronic exposure to a combination of high fat and sugar, rather than solely to the elevated fat content of the diet, that disrupts the ability of skeletal muscles to process glucose in response to insulin. This was supported by elevated rates of insulin-stimulated glycogen synthesis and lactate production in the Sol, EDL, and Epit muscles in the KD-fed rats, which contrasted with the blunted responses displayed by these muscles in rats fed with the HFS diet. The analysis of insulin-stimulated glucose oxidation also revealed a similar trend when comparing both diets, although with KD eliciting a much less pronounced and fiber-type-specific effect on this variable than on rates of insulin-stimulated glycogen synthesis and lactate production. Because Sol muscles are rich in Type I fibers [17] and normally display higher capacities for FA oxidation when exposed to an HFS diet [13,15,24], the ability of these muscles to further elevate glucose oxidation when exposed to the KD may have been limited. Also, KD-fed Sol muscles were the only ones eliciting higher levels of the ketolytic enzyme OXCT than the HFS-fed counterparts, which likely enhanced the capacity of the Sol muscles to oxidize ketones. Thus, in Sol muscles, more glucose was diverted towards other pathways of glucose metabolism when stimulated with insulin as compared to the EDL and Epit muscles. Indeed, the rates of insulin-stimulated glycogen synthesis and lactate production in the Sol muscle were the highest among the muscles studied.

In well-trained cyclists habituated to a KD, GLUT4 and IRS1 protein contents were decreased in vastus lateralis muscles, which is consistent with the whole-body glucose intolerance found in these athletes [8]. KD-induced glucose intolerance has previously been attributed to attenuated β-cell mass in the pancreas [25]. In the present study, we found that both glycogen synthesis and lactate production were preserved in the EDL of KD-fed rats, as indicated by the sensitivity of this muscle to insulin. Moreover, the elevation of glucose oxidation in the EDL muscle in response to insulin was significantly higher in the KD-fed rats than that in the HFS-fed rats. Together, these findings indicated that the KD leads to a disuse-mediated adaptation in pancreatic cell function that renders the organism less tolerant to a bolus of glucose. However, in line with the preserved response to insulin in the EDL, this mechanism is not indicative of disease and does not impact the capacity of skeletal muscles to metabolize glucose. In fact, despite the muscle-specific shift in substrate partitioning toward fatty acid oxidation and enhanced ketolytic capacity, all three skeletal muscles in the KD group demonstrated an enhanced ability to store glycogen and use glucose when exposed to insulin. Conversely, muscles from the HFS group displayed the classical impairment in insulin-stimulated glucose handling.

As expected, the KD significantly enhanced blood ketone levels, albeit not to the same extent as reported in other rodent KD studies [12,14,25]. This could be explained by the difference in the macronutrient composition of the KD used. In the present study, the protein content of the diet was 20% calories, whereas in studies showing a higher induction of ketosis, the protein contents ranged from 4.8–10% calories [12,14,25]. This is an important distinction, given that decreasing the protein content of a KD has been shown to significantly increase βHB levels in rats [26]. Furthermore, the apparent attenuation in βHB from weeks 8 to 16 points to a KD-induced adaptation, whereby ketolytic tissues, including those in the Sol muscle, enhanced their metabolic capacities for ketones, which likely led to an attenuation in the circulating levels of this substrate [2].

It was surprising to find that despite increasing PGC-1α and TFAM, the KD did not increase palmitate oxidation in Sol muscles, when compared to the HFS diet. Conversely, in EDL and Epit muscles, PGC-1α and TFAM protein levels did not differ between the KD- and HFS-fed rats, yet the rates of FA oxidation in the former diet were significantly higher than those in the latter. In this context, despite increasing the proteins involved in mitochondrial biogenesis, the 20% additional fat content of the KD in comparison to that

of the HFS diet did not further elevate the FA oxidative capacity of Sol muscles. Instead, the induction of mitochondrial biogenesis in the Sol muscle could also have served to increase the utilization of circulating ketone bodies as a fuel source, which is consistent with the KD-induced elevation in Sol muscles of OXCT protein levels, a major rate-limiting ketolytic enzyme [27]. In line with this, the administration of a ketone ester drink prior to exercise to endurance-trained athletes suppressed glycolysis and increased reliance on ketones for energy in the vastus lateralis muscle [28]. Thus, it is plausible that in the current study, ketones displaced glucose as an oxidative substrate in the Sol muscles of KD-fed rats, which could further attenuate the reliance on glucose and explain the modest insulin-stimulated glucose oxidation response in all three muscles from KD-fed rats. Conversely, the KD-induced enhancement in glycolytic capacity likely served to replenish oxaloacetate to support fat and ketone oxidation in the absence of dietary carbohydrate intake [22]. However, oxaloacetate availability for complete oxidation of acetyl-CoA produced from ketone bodies may also have been provided by acetoacetate activation via the conversion of succinyl-CoA to succinate in the TCA cycle, with the latter being converted to oxaloacetate through the subsequent reactions of the TCA cycle [29]. This likely facilitated the entry of more acetyl-CoA into the cycle without causing alterations to the levels of anaplerotic or cataplerotic enzymes.

Even though the Epit is a highly glycolytic muscle [18], its rates of FA oxidation were significantly higher in the KD rats than in the HFS-fed animals. This was surprising given that both diets were high in fat. In fact, the HFS diet had already been show to enhance Epit FA oxidation in comparison to standard chow [15,24]. Thus, this study provided evidence that the absence of carbohydrates in the KD potentiated the reliance of the Epit muscle on fat as an oxidative substrate. Interestingly, this occurred independently of alterations in mitochondrial biogenesis proteins and, also, by marked reductions in the levels of the ketolytic enzymes OXCT and ACAT1, suggesting that Epit muscles enhanced their capacities to oxidize fat at the expense of ketones.

The EDL muscle displayed an intermediate effect relative to the Sol and Epit muscles. Like in the Epit muscle, palmitate oxidation was enhanced, whereas markers of mitochondrial biogenesis were unaltered. In line with this, KD feeding enhanced the aerobic capacity of the EDL muscle, despite not altering PGC1α content [12]. Moreover, other muscles with mixed-fiber-type compositions [17], including the gastrocnemius [5,13] and vastus lateralis [4] muscles, showed a KD-induced upregulation of fat oxidative capacity. However, unlike the Epit muscle, ketolytic capacity in the EDL muscle did not differ between the two dietary interventions. The preserved ketolytic capacity in the EDL versus Epit muscles, despite the similar enhancement in fat oxidation, could be attributed to the relatively higher oxidative capacity of the former [17], and therefore, the ability to perform FA oxidation without altering ketolytic capacity. Nevertheless, in the present study, we observed that only fat oxidation was increased in the EDL muscle, suggesting that the upregulation of mitochondrial biogenesis may be required to enhance the ketone-oxidizing capacity of the EDL muscle when under conditions of abundant dietary FA availability.

5. Conclusions

In conclusion, despite eliciting a higher rate of FA oxidation than the obesogenic HFS diet, the carbohydrate-free KD preserved the ability of oxidative and glycolytic muscles to elevate glucose metabolism in response to insulin. Thus, it is the chronic exposure to a combination of high fat and sugar, rather than solely to the elevated fat content of the diet, that disrupts the ability of skeletal muscles to process glucose in response to insulin. This was characterized by the KD-induced elevation in mitochondrial biogenesis and ketolytic capacity in the Sol muscle, despite the lack of alteration in FA oxidation relative to that in the HFS group. In contrast, Epit FA oxidation was significantly elevated with KD feeding, whereas proteins involved in ketolysis were markedly reduced. Similarly, FA oxidation was increased in the EDL muscle of KD-fed rats, although the ketolytic capacity was unaltered in this muscle with the KD, relative to that in the HFS-fed rats. Lastly, the levels

of anaplerotic and cataplerotic enzymes in all muscles studied did not differ, even though the KD was devoid of carbohydrates. Collectively, these findings indicated that, contrary to the obesogenic HFS diet, the carbohydrate-free KD maintained skeletal muscle metabolic flexibility while also enhancing, in a muscle-specific manner, rates of FA oxidation and ketolytic capacity.

Author Contributions: D.D.E. was responsible for data acquisition, analysis, and interpretation, and for preparing and reviewing the manuscript. S.J. was responsible for data acquisition, analysis, and interpretation, and for preparing and reviewing the manuscript. M.S. was involved in data acquisition and analysis. R.B.C. was responsible for the conceptualization of the work, data acquisition, analysis, and interpretation, and for preparing and reviewing the manuscript. All authors have read and agreed to the published version of the manuscript.

Funding: This research was funded by a Discovery Grant from the Natural Science and Engineering Research Council of Canada (NSERC) and by infrastructure grants from the Canada Foundation for Innovation (CFI) and the Ontario Research Fund (ORF) awarded to RBC. DDE was funded by the NSERC Alexander Graham Bell Canada Graduate Scholarship.

Institutional Review Board Statement: The animal study protocol was approved by by the Committee on the Ethics of Animal Experiments of York University (York University Animal Care Committee, YUACC, permit number: 2021-03, approved 18 July 2023).

Data Availability Statement: All data supporting the results are included within the figures revealing their range and distribution.

Conflicts of Interest: The authors declare no conflict of interest.

References

1. Goodpaster, B.; Sparks, L.M. Metabolic Flexibility in Health and Disease. *Physiol. Behav.* **2017**, *25*, 1027–1036. [CrossRef]
2. Sherrier, M.; Li, H. The Impact of Keto-Adaptation on Exercise Performance and the Role of Metabolic-Regulating Cytokines. *Am. J. Clin. Nutr.* **2019**, *110*, 562–573. [CrossRef] [PubMed]
3. Luong, T.V.; Abild, C.B.; Bangshaab, M.; Gormsen, L.C.; Søndergaard, E. Ketogenic Diet and Cardiac Substrate Metabolism. *Nutrients* **2022**, *14*, 1322. [CrossRef]
4. Miller, V.J.; LaFountain, R.A.; Barnhart, E.; Sapper, T.S.; Short, J.; Arnold, W.D.; Hyde, P.N.; Crabtree, C.D.; Kackley, M.L.; Kraemer, W.J.; et al. A ketogenic diet combined with exercise alters mitochondrial function in human skeletal muscle while improving metabolic health. *Am. J. Physiol.-Endocrinol. Metab.* **2020**, *319*, E995–E1007. [CrossRef] [PubMed]
5. Shimizu, K.; Saito, H.; Sumi, K.; Sakamoto, Y.; Tachi, Y.; Iida, K. Short-Term and Long-Term Ketogenic Diet Therapy and the Addition of Exercise Have Differential Impacts on Metabolic Gene Expression in the Mouse Energy-Consuming Organs Heart and Skeletal Muscle. *Nutr. Res.* **2018**, *60*, 77–86. [CrossRef] [PubMed]
6. Pathak, S.J.; Zhou, Z.; Steffen, D.; Tran, T.; Ad, Y.; Ramsey, J.J.; Rutkowsky, J.M.; Baar, K. 2-Month Ketogenic Diet Preferentially Alters Skeletal Muscle and Augments Cognitive Function in Middle Aged Female Mice. *Aging Cell* **2022**, *21*, e13706. [CrossRef] [PubMed]
7. Zhou, Z.; Vidales, J.; González-Reyes, J.A.; Shibata, B.; Baar, K.; Rutkowsky, J.M.; Ramsey, J.J. A 1-Month Ketogenic Diet Increased Mitochondrial Mass in Red Gastrocnemius Muscle, but Not in the Brain or Liver of Middle-Aged Mice. *Nutrients* **2021**, *13*, 2533. [CrossRef]
8. Webster, C.C.; Van Boom, K.M.; Armino, N.; Larmuth, K.; Noakes, T.D.; Smith, J.A.; Kohn, T.A. Reduced Glucose Tolerance and Skeletal Muscle GLUT4 and IRS1 Content in Cyclists Habituated to a Long-Term Low-Carbohydrate, High-Fat Diet. *Int. J. Sport Nutr. Exerc. Metab.* **2020**, *30*, 210–217. [CrossRef]
9. McLane, J.A.; Holloszy, J.O. Glycogen Synthesis from Lactate in the Three Types of Skeletal Muscle. *J. Biol. Chem.* **1979**, *254*, 6548–6553. [CrossRef]
10. Winder, W.W.; Holloszy, J.O.; Baldwin, K.M. Enzymes Involved in Ketone Utilization in Different Types of Muscle: Adaptation to Exercise. *Eur. J. Biochem.* **1974**, *47*, 461–467. [CrossRef]
11. Fukazawa, A.; Koike, A.; Karasawa, T.; Tsutsui, M.; Kondo, S.; Terada, S. Effects of a Ketogenic Diet Containing Medium-Chain Triglycerides and Endurance Training on Metabolic Enzyme Adaptations in Rat Skeletal Muscle. *Nutrients* **2020**, *12*, 1269. [CrossRef]
12. Ogura, Y.; Kakehashi, C.; Yoshihara, T.; Kurosaka, M.; Kakigi, R.; Higashida, K.; Fujiwara, S.E.; Akema, T.; Funabashi, T. Ketogenic Diet Feeding Improves Aerobic Metabolism Property in Extensor Digitorum Longus Muscle of Sedentary Male Rats. *PLoS ONE* **2020**, *15*, e0241382. [CrossRef] [PubMed]

13. Huang, T.Y.; Linden, M.A.; Fuller, S.E.; Goldsmith, F.R.; Simon, J.; Batdorf, H.M.; Scott, M.C.; Essajee, N.M.; Brown, J.M.; Noland, R.C. Combined Effects of a Ketogenic Diet and Exercise Training Alter Mitochondrial and Peroxisomal Substrate Oxidative Capacity in Skeletal Muscle. *Am. J. Physiol.-Endocrinol. Metab.* **2021**, *320*, E1053–E1067. [CrossRef] [PubMed]
14. Nakao, R.; Abe, T.; Yamamoto, S.; Oishi, K. Ketogenic Diet Induces Skeletal Muscle Atrophy via Reducing Muscle Protein Synthesis and Possibly Activating Proteolysis in Mice. *Sci. Rep.* **2019**, *9*, 19652. [CrossRef] [PubMed]
15. Jani, S.; Da Eira, D.; Hadday, I.; Bikopoulos, G.; Mohasses, A.; de Pinho, R.A.; Ceddia, R.B. Distinct Mechanisms Involving Diacylglycerol, Ceramides, and Inflammation Underlie Insulin Resistance in Oxidative and Glycolytic Muscles from High Fat-Fed Rats. *Sci. Rep.* **2021**, *11*, 19160. [CrossRef]
16. du Sert, N.P.; Ahluwalia, A.; Alam, S.; Avey, M.T.; Baker, M.; Browne, W.J.; Clark, A.; Cuthill, I.C.; Dirnagl, U.; Emerson, M.; et al. Reporting Animal Research: Explanation and Elaboration for the Arrive Guidelines 2.0. *PLoS Biol.* **2020**, *18*, e3000411.
17. Ariano, M.A.; Armstrong, R.B.; Edgerton, V.R. Hindlimb Muscle Fiber Populations of Five Mammals. *J. Histochem. Cytochem.* **1973**, *21*, 51–55. [CrossRef] [PubMed]
18. Nesher, R.; Karl, I.E.; Kaiser, K.E.; Kipnis, D.M. Epitrochlearis Muscle. I. Mechanical Performance, Energetics, and Fiber Composition. *Am. J. Physiol.* **1980**, *239*, E454–E460. [CrossRef]
19. Fediuc, S.; Gaidhu, M.P.; Ceddia, R.B. Inhibition of Insulin-Stimulated Glycogen Synthesis by 5-Aminoimidasole-4- Carboxamide-1-β-D-Ribofuranoside-Induced Adenosine 5′-Monophosphate- Activated Protein Kinase Activation: Interactions with Akt, Glycogen Synthase Kinase 3-3α/β, and Glycogen Synth. *Endocrinology* **2006**, *147*, 5170–5177. [CrossRef]
20. Rabinowitz, J.D.; Enerbäck, S. Lactate: The Ugly Duckling of Energy Metabolism. *Nat. Metab.* **2020**, *2*, 566–571. [CrossRef]
21. Jornayvaz, F.R.; Shulman, G.I. Regulation of Mitochondrial Biogenesis. *Essays Biochem.* **2010**, *47*, 69–84. [CrossRef] [PubMed]
22. Owen, O.E.; Kalhan, S.C.; Hanson, R.W. The Key Role of Anaplerosis and Cataplerosis for Citric Acid Cycle Function. *J. Biol. Chem.* **2002**, *277*, 30409–30412. [CrossRef]
23. Brown, D.M.; Williams, H.; Ryan, K.J.P.; Wilson, T.L.; Daniel, Z.C.T.R.; Mareko, M.H.D.; Emes, R.D.; Harris, D.W.; Jones, S.; Wattis, J.A.D.; et al. Mitochondrial Phosphoenolpyruvate Carboxykinase (PEPCK-M) and Serine Biosynthetic Pathway Genes Are Co-Ordinately Increased during Anabolic Agent-Induced Skeletal Muscle Growth. *Sci. Rep.* **2016**, *6*, 28693. [CrossRef] [PubMed]
24. Pinho, R.A.; Sepa-Kishi, D.M.; Bikopoulos, G.; Wu, M.V.; Uthayakumar, A.; Mohasses, A.; Hughes, M.C.; Perry, C.G.R.; Ceddia, R.B. High-Fat Diet Induces Skeletal Muscle Oxidative Stress in a Fiber Type-Dependent Manner in Rats. *Free Radic. Biol. Med.* **2017**, *110*, 381–389. [CrossRef] [PubMed]
25. Ellenbroek, J.H.; van Dijck, L.; Töns, H.A.; Rabelink, T.J.; Carlotti, F.; Ballieux, B.E.P.B.; de Koning, E.J.P. Long-Term Ketogenic Diet Causes Glucose Intolerance and Reduced β- and α-Cell Mass but No Weight Loss in Mice. *Am. J. Physiol.-Endocrinol. Metab.* **2014**, *306*, 552–558. [CrossRef]
26. Bielohuby, M.; Menhofer, D.; Kirchner, H.; Stoehr, B.J.M.; Müller, T.D.; Stock, P.; Hempel, M.; Stemmer, K.; Pfluger, P.T.; Kienzle, E.; et al. Induction of Ketosis in Rats Fed Low-Carbohydrate, High-Fat Diets Depends on the Relative Abundance of Dietary Fat and Protein. *Am. J. Physiol.-Endocrinol. Metab.* **2011**, *300*, E65–E76. [CrossRef]
27. Hwang, C.Y.; Choe, W.; Yoon, K.-S.; Ha, J.; Kim, S.S.; Yeo, E.-J.; Kang, I. Molecular Mechanisms for Ketone Body Metabolism, Signaling Functions, and Therapeutic Potential in Cancer. *Nutrients* **2022**, *14*, 4932. [CrossRef]
28. Cox, P.J.; Kirk, T.; Ashmore, T.; Willerton, K.; Evans, R.; Smith, A.; Murray, A.J.; Stubbs, B.; West, J.; McLure, S.W.; et al. Nutritional Ketosis Alters Fuel Preference and Thereby Endurance Performance in Athletes. *Cell Metab.* **2016**, *24*, 256–268. [CrossRef]
29. Newsholme, E.; Leech, A. *Functional Biochemistry in Health and Disease*, 2nd ed.; John Wiley & Sons, Ltd.: Chichester, UK, 2010; ISBN 978-0-471-98820-5.

ADIPOCYTE
2020, VOL. 9, NO. 1, 550–562
https://doi.org/10.1080/21623945.2020.1817230

RESEARCH PAPER

OPEN ACCESS

Effects of the adiponectin mimetic compound ALY688 on glucose and fat metabolism in visceral and subcutaneous rat adipocytes

Daniel Da Eira[a], Shailee Jani[a], Hyekyoung Sung[b], Gary Sweeney[b], and Rolando B. Ceddia[a]

[a]School of Kinesiology and Health Science, York University, North York, Canada; [b]Department of Biology, York University, North York, Canada

ABSTRACT

Adiponectin regulates white adipose tissue (WAT) metabolism and promotes insulin-sensitizing and anti-atherosclerotic effects *in vivo*. In this context, small molecule adiponectin receptor agonists have become of great therapeutic value for the treatment of metabolic diseases. Here, we investigated the effects of the adiponectin mimetic compound ALY688 on WAT metabolism. To accomplish this, rat epididymal (Epid) and subcutaneous inguinal (Sc Ing) adipocytes were isolated and incubated with ALY688. Subsequently, several parameters of glucose and fat metabolism were assessed. ALY688 promoted AMP-activated protein kinase (AMPK) and acetyl-CoA carboxylase (ACC) phosphorylation, enhanced glucose oxidation, and suppressed fat oxidation in adipocytes from both fat depots. ALY688 did not affect basal and insulin-stimulated rates of glucose uptake, glucose incorporation into lipids, and AKT_{Ser473} and p38 mitogen-activated protein kinase (MAPK) phosphorylations in either Epid or Sc Ing adipocytes. ALY688 did not alter basal lipolysis in Epid and Sc Ing adipocytes, but it enhanced isoproterenol-induced lipolysis in Epid adipocytes. Adiponectin receptor 2 (AdipoR2) mRNA was the prevalent isoform expressed in all adipocytes, and Epid adipocytes displayed significantly higher AdipoR2 mRNA expression than Sc Ing adipocytes. In conclusion, ALY688 can regulate adiposity and affect glycaemic control by altering substrate portioning in the WAT in a fat depot-specific manner.

ARTICLE HISTORY
Received 18 June 2020
Revised 25 August 2020
Accepted 27 August 2020

KEYWORDS
Adipokines; AMPK; adipocyte metabolism; glucose uptake; lipogenesis; lipolysis; insulin; AdipoR1; AdipoR2

Introduction

Maintenance of whole-body glucose homoeostasis depends on the coordinated action of multiple hormones that allow the organism to respond to daily oscillations in the availability of dietary carbohydrate and other macronutrients [1]. In this context, the adipose tissue plays an important role in maintaining whole-body glucose homoeostasis. It does so by serving as a compartment where energy can be stored or mobilized and also by secreting hormones that regulate glucose and fat metabolism in multiple organs and tissues [2]. To date, many bioactive adipose-derived factors (adipokines) have been identified [2]. Among them is adiponectin, a secreted protein abundantly present in plasma, that has been demonstrated to exert potent insulin sensitizing, glucose lowering, and lipid catabolizing functions in peripheral tissues [3]. Two adiponectin receptors (AdipoRs) have been cloned (AdipoR1 and AdipoR2), which are expressed in various tissues including liver, skeletal muscle, white adipose tissue (WAT), hypothalamus, and vasculature [4]. The metabolic effects of adiponectin vary in a tissue-specific manner, depending in part on tissue-specific expression of AdipoR1 and AdipoR2 as well as on cell-specific, intracellular signalling pathways [4]. For instance, AdipoR1 is abundant in skeletal muscles and macrophages, whereas WAT and the vasculature are rich in AdipoR2. The liver abundantly expresses both AdipoRs [4].

Once bound to its receptors, adiponectin has been shown to promote the activation of AMP-activated protein kinase (AMPK) and peroxisome proliferator-activated receptor α (PPARα) [4,5]. In liver and skeletal muscles, activated AMPK phosphorylates acetyl-CoA carboxylase (ACC) and leads to enhanced mitochondrial import and oxidation of long-chain fatty acids [6,7]. Adiponectin has also been shown to exert anti-lipotoxic effects through the induction of the transcriptional effects of PPARα[8], culminating in the down-regulation of lipid synthesis enzymes, the elevation in carnitine palmitoyltransferase 1 (CPT1) levels, and the enhanced production and secretion of HDL by the liver [9]. In the WAT, adiponectin has been demonstrated to elevate the fat-storing capacity of adipocytes by promoting glucose uptake [10] and lipogenesis [11] and by decreasing lipolysis [12], although the enhancement of fat oxidation has also been cited as an effect of

CONTACT Rolando B. Ceddia roceddia@yorku.ca School of Kinesiology and Health Science, York University., North York, Ontario M3J 1P3, Canada

adiponectin in fat cells [3]. The opposing lipogenic and fatty acid oxidative effects of adiponectin on adipocytes have been proposed to confer metabolic flexibility to the WAT, which contributes to minimizing ectopic lipid deposition in non-adipose tissues, preventing adipose inflammation and fibrosis, and maintaining healthy WAT expansion [3,13]. However, the findings that support an elevation in fatty acid oxidation induced by adiponectin originated from studies conducted in C_2C_{12} muscle cells [7,8,14], isolated mouse skeletal muscles [6,8,14,15], mouse hepatocytes [6], and hepa-1-6 hepatocytes in culture [14]. To the best of our knowledge, no direct evidence exists that adiponectin indeed promotes fatty acid oxidation in adipocytes. Disruption of both AdipoR1 and AdipoR2 has been reported to significantly decrease the expression of genes encoding for *Cat* and *Sod* and increase oxidative stress in WAT, but there were no reports of alterations in the capacity of the WAT to oxidize fat in mice lacking AdipoR1 and AdipoR2 [16]. Thus, it is likely that the metabolic responses of WAT to adiponectin differ from those of skeletal muscles and liver with respect to fatty acid oxidation.

Reduced circulating levels of adiponectin and impaired AdipoR action are found in obesity, insulin resistance, type 2 diabetes, and atherosclerosis [5]. Therefore, increasing adiponectin production and/or adiponectin signalling are attractive targets for therapeutic interventions for the prevention or treatment of obesity-related derangements in metabolism. In fact, a small-molecule, AdipoR-activating compound named AdipoRon (AR), has been reported to improve insulin resistance and prolong lifespan in mice consuming a high-fat diet [17]. These findings in rodents have provided support for the development of other adiponectin mimetic compounds to target substrate metabolism in organs that play major roles in regulating whole-body glucose and lipid homoeostasis in humans. In this context, a peptide-based adiponectin mimetic named ALY688 (also referred to as ADP355) has been developed [18]. The compound has been shown to bind to both AdipoR1 and AdipoR2 and induce adiponectin-specific signalling in several cell types [19]. A potential advantage of peptide mimetics is that they can provide great potency and specificity compared with small molecule mimetics.

Because the WAT plays an important role in the regulation of glucose and lipid homoeostasis[1] and only a few studies have focused on the effects of adiponectin on this tissue, we assessed the effects of ALY688 as an adiponectin mimetic on glucose uptake and fatty acid oxidation in isolated white adipocytes. Also, due to metabolic differences between visceral (Vc) and subcutaneous (Sc) fat depots and their implications to obesity-related metabolic diseases [20], adipocytes isolated from epididymal (Epid) and Sc inguinal (Sc Ing) fat depots were used. We assessed the potential direct effects of ALY688 on glucose uptake, incorporation of glucose into lipids, fatty acid oxidation, and lipolysis, which are major pathways by which adipocytes handle glucose and fatty acids. We also measured the phosphorylation of AMPK, ACC, AKT, and p38 mitogen-activated protein kinase (p38MAPK), which are signalling pathways by which this adiponectin mimetic compound could potentially regulate metabolism in the WAT. Here, we provide evidence that despite enhancing AMPK phosphorylation in Epid and Sc Ing adipocytes, ALY688 reduced fat oxidation and did not affect basal or insulin-stimulated glucose uptake. However, it shifted glucose metabolism towards oxidation and enhanced adrenergic-stimulated lipolysis in a depot-specific manner.

Material and methods

Reagents

Type II collagenase, isoproterenol, fatty acid (FA)-free bovine serum albumin (BSA), palmitic acid, and the free glycerol determination kit were purchased from Sigma (St. Louis, MO, USA). [1-^{14}C] palmitic acid and D-[U-^{14}C] glucose were purchased from American Radiolabeled Chemicals (St. Louis, MO, USA). Protease (cOmplete Ultra Tablets) and phosphatase (PhosSTOP) inhibitors were obtained from Roche Diagnostics GmbH (Mannheim, Germany). The β-actin (Cat # 4067), AMPK (Cat # 2532), $pAMPK_{Thr172}$ (Cat # 2535), AKT (Cat # 9272), $pAKT_{Ser473}$ (Cat # 9271), p38 (Cat # 9212), pp38 (Cat # 9211), hormone-sensitive lipase (HSL; Cat # 4107), and $pHSL_{Ser660}$ (Cat # 4126) antibodies were purchased from Cell Signalling (Danvers, MA, USA). The ACC (Cat # ab45174) and $pACC_{Ser79}$ (Cat # ab68191) antibodies were purchased from Abcam (Toronto, ON, Canada). ALY688 was provided by Allysta Pharmaceuticals, Belmont, CA, USA.

Animals

Adipose tissue from the subcutaneous inguinal (Sc Ing) and epidydimal (Epid) fat pads were extracted from male albino rats (Wistar strain weighing ~250 g, 50–60 days old) under anaesthesia, and subsequently processed for cell isolation (Figure 1). All experiments were approved by the Animal Care Committee at York University. (York University Animal Care Committee, YUACC, permit number 2016–5) and performed

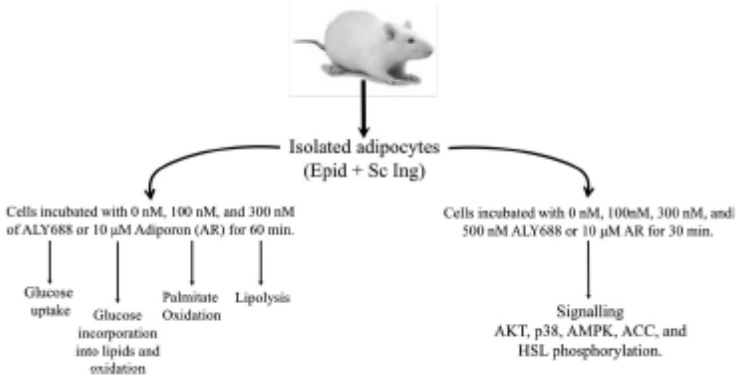

Figure 1. Schematic representation of the experimental design.

strictly in accordance with the YUACC guidelines. All surgery was performed under ketamine/xylazine anaesthesia, and all efforts were made to minimize suffering.

Adipocyte isolation

Adipocyte isolation from the Epid and Sc Ing fat pads (Figure 1) was performed as previously described [21]. Briefly, the adipose tissue was minced in Krebs-Ringer bicarbonate HEPES buffer (KRBH), containing type II collagenase (0.5 mg/ml), prepared fresh on the day of each experiment from stock solutions of salts and buffers (stored at 4°C) to give the following final concentrations: 120 mM NaCl, 4.8 mM KCl, 2.5 mM $CaCl_2$, 1.2 mM KH_2PO_4, 1.2 mM $MgSO_4$, 15 mM $NaHCO_3$, and 30 mM HEPES. Before use, KRBH was gassed for 45 min with carbogen (95% O_2, 5% CO_2) and then bovine serum albumin (3.5%) and glucose (5.5 mM) were added. Following this, the pH of the buffer was adjusted to 7.4 with NaOH. Minced tissues were incubated at 37°C with gentle agitation (120 orbital strokes/min) for approximately 25–30 min. The digested tissue was then strained using a nylon mesh (500 µm pore size) and cells were transferred to 50 ml plastic tubes, where the stromal vascular fraction (SVF) and mature adipocytes separated into two distinct phases. The SVF sitting at the bottom of the tube was discarded by aspiration and the floating adipocytes were washed 3 times prior to being resuspended in KRBH containing 3.5% fatty acid-free BSA (KRBH-3.5% BSA). In order to distribute an equal number of adipocytes in each treatment condition, cell diameters were measured and total cell numbers determined as previously described [22].

Measurement of glucose uptake

Glucose uptake was measured either under basal or insulin-stimulated (10 and 100 nM) conditions following the treatment of adipocytes either without (control) or with ALY688. Our initial choice of doses was based on experiments conducted with ALY688 in other cell types (renal fibroblasts, breast cancer cells, etc.) in which concentrations around 100 nM of the compound caused significant effects. Therefore, we decided to start with a similar dose of 100 nM and increase the concentrations to 300 and 500 nM to assess whether higher doses would be required for broader metabolic responses from Epid and Sc Ing adipocytes. We also used AR (10 µM) to test whether another AdipoR agonist would elicit similar effects. Isolated adipocytes ($4x10^5$ cells) were transferred to plastic tubes either with or without ALY688 and incubated at 37°C for 1 h. Insulin was added to the medium for the final 20 min of the incubation period. Subsequently, KRB-HEPES containing 0.5 mM 2-deoxy-D-glucose and 0.5 µCi of 2-[1,2-[3]H]deoxy-D-glucose was added to the cells for 3 min, and the incubations were terminated by the addition of cytochalasin B (1.5 mM stock solution). Aliquots of cell suspension (240 µl) were quickly placed in plastic microtubes containing 100 µl of di-'isononyl' phthalate. The tubes were centrifuged for 30s (6000 × g) to separate cells from the radioactive incubation medium. Subsequently, fat cells were collected by cutting the tubes through the oil phase and transferring the portion containing the cells to scintillation vials to be counted for radioactivity. Radioactivity of the cells unrelated to glucose transport (non-specific transport) was determined in the same conditions by adding cytochalasin B (50 µM final concentration) to the medium

before the addition of 2-[1,2-[3]H]deoxy-D-glucose [23]. Non-Specific values were subtracted from all conditions.

Measurement of glucose incorporation into lipids

Glucose incorporation into lipids was measured in isolated adipocytes (5 x 10^5 cells) from the Epid and Sc Ing fat depots as previously described [24]. Briefly, cells were incubated in KRBH-3.5% BSA containing 0.2 µCi/ml of D-[1-^{14}C] glucose and 5.5 mM non-labelled D-glucose for 1 h either in the absence or presence of ALY688 (100 and 300 nM) and in the absence or presence of insulin (100 nM). Lipids were then extracted according to the method of Dole and Meinertz [25] and assessed for radioactivity [24].

Measurement of glucose and palmitate oxidation

Glucose and palmitate oxidation as measures of oxidative capacity were assessed by production of [14]CO_2 in Epid and Sc Ing isolated adipocytes (5 x 10^5 cells) as previously described [26]. In order to measure palmitate oxidation, cells were incubated in KRBH-3.5% BSA containing 0.2 µCi/ml of [1–^{14}C] palmitic acid and 200 µM non-labelled palmitate. For glucose oxidation, cells were incubated with 0.2 µCi/ml of D-[U-^{14}C] glucose and 5.5 mM non-labelled D-glucose. Glucose and palmitate oxidation were measured during 1 h either in the absence or presence of ALY688 (100 nM and 300 nM). For glucose oxidation only, cells were also incubated in the absence or presence of insulin (100 nM). Following 1 h of incubation, the media were acidified with 0.2 ml of H_2SO_4 (5 N), and the vials were maintained sealed at 37°C for an additional 1 h for the collection of [14]CO_2 released from the cells and the media. Each vial used for incubation had a centred isolated well containing a loosely folded piece of filter paper that was moistened with 0.2 ml of 2-phenyl- ethylamine/methanol (1:1, *vol*:*vol*) to capture [14]CO_2. At the end of the incubation, the filter paper was removed and transferred to a scintillation vial for radioactivity counting [26].

Determination of lipolysis

Lipolysis was measured in isolated Epid and Sc Ing adipocytes (6 x 10^5 cells). Adipocytes were incubated in the absence or presence of ALY688 and with or without 100 nM isoproterenol (β-non-specific agonist) [27]. Each condition was assayed in triplicates and the samples were incubated for 75 min at 37°C with gentle agitation (80 orbital strokes/min). After incubation, a 200 µl aliquot of medium was taken from each vial for the determination of glycerol concentration.

RNA isolation and quantitative PCR

Primers were designed using the software PrimerQuest (IDT) based on probe sequences available at the Affymetrix database (NetAffx™ Analysis Centre, http://www.affymetrix.com/analysis) for each given gene. RNA was isolated from adipose tissue and isolated adipocytes using the RNeasy Lipid Tissue Kit (Germantown, MD, USA) and complimentary DNA (cDNA) was made from 2 µg of extracted RNA using the ABM EasyScript™ cDNA Synthesis kit (Diamed, Mississauga, ON, Canada), according to the manufacturer's instructions. Samples were run in duplicate on 96-well plates, and each 20 µl reaction contained 4 µl of cDNA, 0.4 µl of primer, 10 µl of Brightgreen 2x qPCR Mastermix (Diamed, Mississauga, ON, Canada) and 5.6 µl of RNA-free water. Real-time PCR analysis was performed using a Bio-Rad CFX96 Real Time PCR Detection System (Bio-Rad, Mississauga, ON, Canada) using the following amplification conditions: 95°C (10 min); 40 cycles of 95°C (15 s), 60°C (60 s). Values are presented as fold increases relative to GAPDH gene expression [28]. The primers used to probe for rat AdipoR1 and AdipoR2 mRNA levels using qPCR were as follows:

AdipoR1: Forward: 5′-ACTTTGTAACCTGGCGGATGACAG-3′

Reverse: 5′-ATCAAGGCGTGGCTTTGTTTGTCC-3′

AdipoR2: Forward: 5′-AATGATGGCGTTTCTCTCTGGTGC-3′

Reverse: 5′-CACACTTCTTGCGAACGGCATTCA-3′

GAPDH: Forward: 5′-TGACTCTACCCACGGCAAGTTCAA-3′

Reverse: 5′-ACGACATACTCAGCACCAGCATCA-3′

Western blotting analysis of content and phosphorylation of proteins

– Isolated adipocytes from the Epid and Sc Ing fat depots were incubated in the absence or presence of ALY688 for 30 min and then immediately homogenized in a buffer containing 25 mM Tris-HCl, 25 mM NaCl (pH 7.4), 1 mM $MgCl_2$, 2.7 mM KCl, 1% Triton X-100 and protease and phosphatase inhibitors (Roche Diagnostics GmbH, Mannheim, Germany). Homogenates were centrifuged, the infranatant collected, and an aliquot was used to measure protein by the Bradford method. Samples were diluted 1:1 (vol:vol) with 2x Laemmli sample buffer and heated to 95°C for 5 min. 25 µg of protein were loaded in each well. Samples were then subjected to SDS-PAGE, transferred to PVDF

membrane, and probed for the proteins of interest. All primary antibodies were used at a dilution of 1:1,000. All densitometry analyses were performed using the Scion Image program.

Statistical analyses

– Statistical analyses were performed by either unpaired two-tailed t-tests or one and two-way analysis of variance (ANOVA) with Bonferroni post-hoc tests using the GraphPad Prism statistical software program. Bars represent mean ± SEM. Statistical significance was set at $p < 0.05$.

Results

AMPK and ACC phosphorylation

– We detected an increase in AMPK phosphorylation when adipocytes were incubated with 100, 300, and 500 nM of ALY688. In Epid adipocytes, 100 and 300 nM of ALY688 significantly increased AMPK phosphorylation by 2.37 and 2.7-fold, relative to 0 nM, respectively, whereas AR (10 μM) increased this variable by 1.57-fold (Figure 2(a)). In Sc Ing adipocytes, 300 nM of ALY688 increased AMPK phosphorylation by 3.81-fold relative to 0 nM, which was of similar magnitude to the AR effect in these cells (Figure 2(b)). However, an increase in AMPK phosphorylation was not observed in this depot with 100 nM of the drug (Figure 2(b)). To confirm that phosphorylation of AMPK was accompanied by an increase in its activity, we also assessed the phosphorylation of ACC, a downstream target of AMPK. In the presence of 500 nM of ALY688, AMPK phosphorylation increased 6.2-fold (Figure 2(c)), and this was accompanied by a 2.13-fold increase in ACC phosphorylation (Figure 2(d)). The generation of cell lysates from primary adipocytes requires a large amount of adipose tissue; thus, in order to optimize the preparation, we used the Sc Ing fat depot where the amount of tissue available and the yield of cells were the highest. Also, in order to have three replicates for control and the compound, we used only one dose of ALY688 (500 nM) as shown in Figure 2(c and d).

Glucose uptake

As expected, glucose uptake was increased upon insulin stimulation in both Sc Ing and Epid adipocytes. However, no significant effects of any concentration of either ALY688 or AR (10 μM) on basal and insulin-stimulated glucose uptake were detected (Figure 3(a and b)). Because supraphysiological insulin concentrations (100 nM) were used in the initial experiments, it could be that glucose uptake was maximized, masking a potential effect of ALY688 on this variable. To explore this, we conducted additional experiments using a lower (more within the physiological range, 10 nM) insulin concentration. Also, we used a higher concentration of the compound (500 nM) to test whether this would be more effective in adipocytes than the previous doses used (Figure 3(c)). Despite this, we found that even under lower doses of insulin, glucose uptake was not significantly affected by 500 nM of ALY688 in Epid adipocytes (Figure 3(c)), and similar results were also found for Sc Ing adipocytes.

AKT and p38 MAPK phosphorylation

To test whether major steps of the insulin signalling pathway were affected by ALY688, we measured AKT_{Ser473} phosphorylation in both Epid and Sc Ing adipocytes exposed to 0, 100, 300, and 500 nM of the compound. No effect of ALY688 was detected on AKT_{Ser473} phosphorylation in Epid (Figures 4(a) and Sc Ing (Figure 4(b)) adipocytes, which is consistent with the lack of effect on glucose uptake in these cells. As a positive control, cells isolated from both fat depots were also treated with insulin (100 nM), and it caused a robust AKT_{Ser473} phosphorylation response to the hormone (Figure 4(a and b)). Additionally, because adiponectin initiates a series of tissue-dependent signal transduction events through distinct signalling pathways, including p38 MAPK [7], we also tested whether this would be the case in Epid and Sc Ing adipocytes. As shown in Figure 4(c and d), p38 phosphorylation was not affected by 100 and 300 nM of ALY688 in Epid and Sc Ing adipocytes. However, a robust induction of p38 MAPK phosphorylation was detected when adipocytes from both fat depots were incubated with 10 μM of AR (Figure 4(c and d)).

Glucose incorporation into lipids and glucose oxidation

ALY688 did not affect glucose uptake in Epid and Sc Ing adipocytes; however, it could still affect metabolism of this substrate inside the cells. To evaluate this, we measured the incorporation of glucose into lipids and also glucose oxidation in Epid and Sc Ing adipocytes under basal and insulin-stimulated conditions. We found that neither Epid nor Sc Ing rates of glucose incorporation into lipids (lipogenesis) were affected by the compound (Figure 5(a and b)). However, ALY688 caused dose and tissue-specific effects on glucose oxidation in Epid and Sc Ing adipocytes. This was characterized by significantly enhanced basal glucose oxidation by 49% and 39% in Epid adipocytes in the presence of 100 and

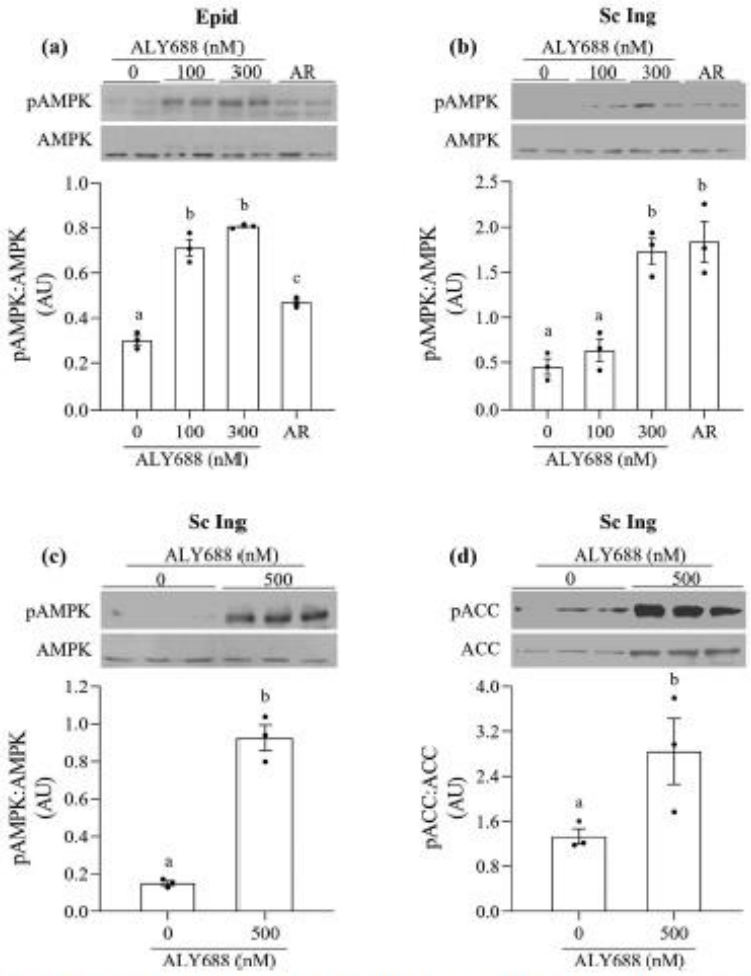

Figure 2. ALY688 (100 and 300 nM) induced AMPK phosphorylation in epididymal (Epid, **A**) and subcutaneous inguinal (Sc Ing, **B**) adipocytes. AdipoRon (AR) was used as a positive control. In Sc Ing adipocytes, a higher dose of ALY688 also increased the phosphorylation of AMPK (c) and ACC (d). Different letters denote statistical significance ($p < 0.05$). One-way ANOVA for A-B and t-test for C-D, n = 3.

300 nM of ALY688, respectively, when compared to cells incubated in the absence of insulin and ALY688 (Figure 5(c)). In Sc Ing adipocytes, 100 and 300 nM of ALY688 increased basal glucose oxidation by 37% and 64%, respectively, with only the latter concentration reaching statistical significance when compared to 0 nM ALY688 (Figure 5(d)).Insulin-stimulated glucose oxidation was also enhanced by the compound, although only in Epid adipocytes treated with 300 nM of ALY688 or AR (Figure 5(c)).

Palmitate oxidation

Because ALY688 induced a consistent increase in AMPK and ACC phosphorylation in isolated adipocytes from both fat depots, we tested whether such effect was also accompanied by a functional metabolic alteration in these cells. The initial expectation was that increased AMPK phosphorylation would increase rates of fatty acid oxidation, as it is frequently reported in skeletal muscle cells [8,14]. However, to our surprise, 300 and 500 nM of ALY688 suppressed basal palmitate oxidation by ~55%

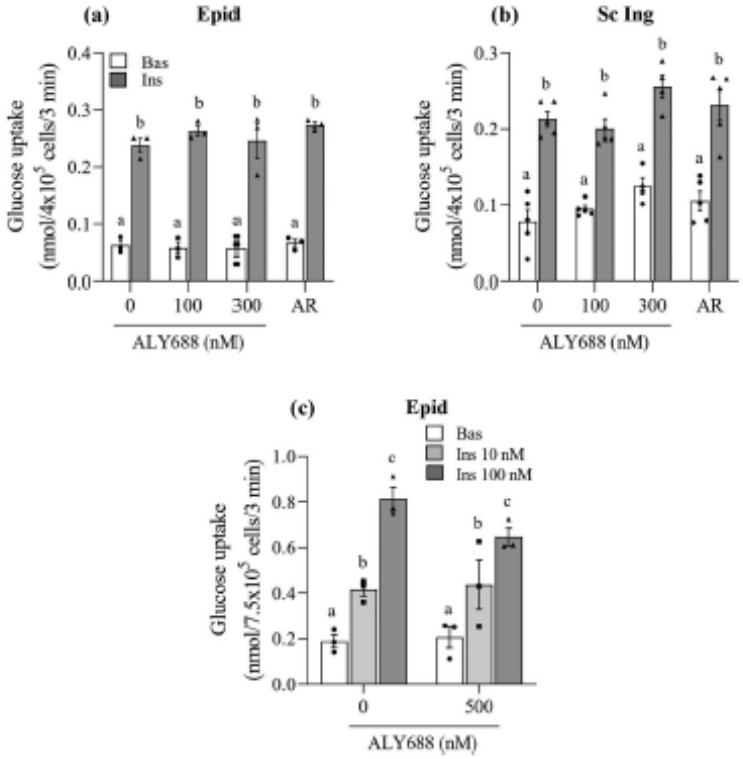

Figure 3. No effect of ALY688 (100, 300, and 500 nM) on basal (Bas) and insulin (Ins, 100 nM)-stimulated glucose uptake in epididymal (Epid, **A**) and subcutaneous inguinal (Sc Ing, **B**) adipocytes. Glucose uptake was also assessed in Epid adipocytes exposed to 500 nM of ALY688 for 60 min (c) and then stimulated with 10 and 100 nM of insulin. Different letters denote statistical significance ($p < 0.05$). Two-way ANOVA, n = 3–5.

and ~35% in both the Epid and Sc Ing adipocytes, respectively, relative to the 0 nM group (Figure 6(a and 6b)). No effect on palmitate oxidation was observed in either depot with 100 nM of ALY688 (Figure 6(a and b)).

Lipolysis

In order to assess whether ALY688 could affect the ability of adipocytes to export fatty acids, we also measured lipolysis in these cells. We found that basal lipolysis was not affected by treating cells with ALY688; however, when Epid adipocytes were stimulated with 100 and 300 nM of ALY688 and 100 nM of isoproterenol, glycerol release increased by 45% and 70%, respectively, when compared to cells incubated with isoproterenol only (Figure 7(a)). In Sc Ing adipocytes, ALY688 had no significant effect on rates of glycerol release either under basal or isoproterenol (Iso)-stimulated conditions (Figure 7(b)). In order to assess potential mechanisms by which ALY688 enhanced Iso-stimulated glycerol release in Epid adipocytes, we measured phosphorylation of hormone sensitive lipase (HSL_{Ser660}) in both Epid and Sc Ing adipocytes. As depicted in Figure 7(c and d), ALY688 increased phosphorylation of HSL_{Ser660} in Epid, but not in Sc Ing adipocytes. This suggests that ALY688-induced HSL phosphorylation could be linked to the increase in glycerol release seen in Epid adipocytes. However, we could not perform a statistical analysis because we had only 2 samples probed for HSL phosphorylation. Furthermore, even though HSL plays a very important role in adipose tissue lipolysis, adipose triglyceride lipase (ATGL) activity could also be affected by ALY688. However, the activity of this latter lipase was not measured in this study.

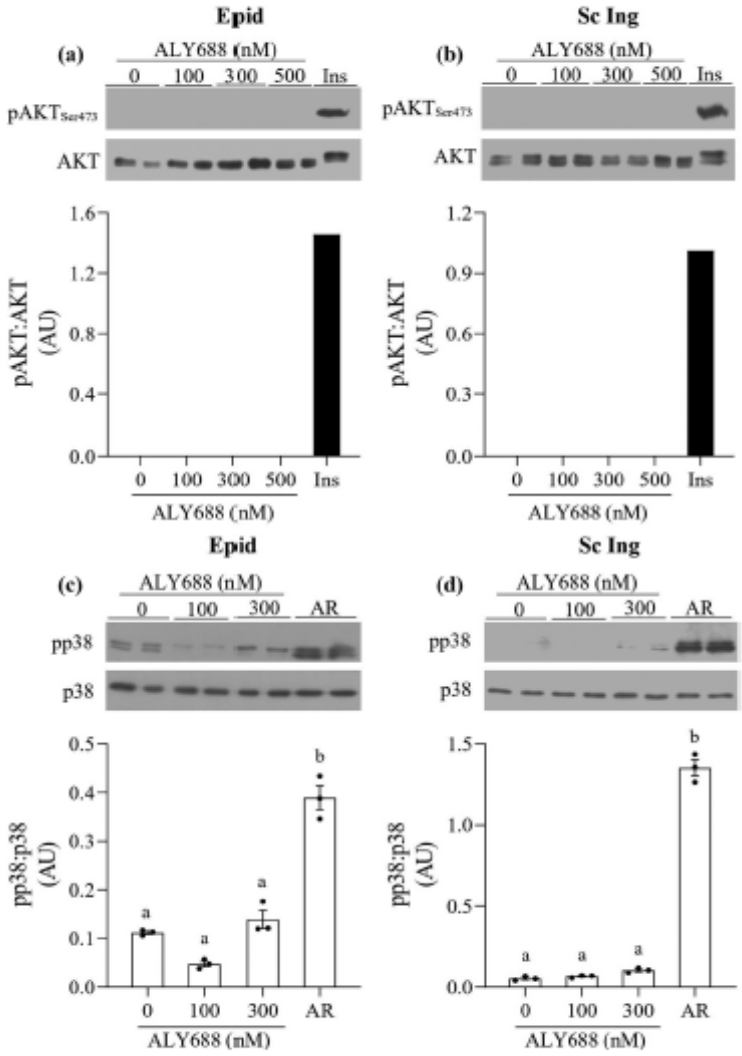

Figure 4. ALY688 did not affect AKT$_{Ser473}$ and p38 MAPK phosphorylation in Epid (a and c) and Sc Ing adipocytes (b and d), whereas AdipoRon (AR) and insulin induced robust increases in AKT$_{Ser473}$ and p38 MAPK phosphorylations in adipocytes from both fat depots. Different letters denote statistical significance ($p < 0.05$). One-way ANOVA, $n = 3$.

Adiponectin receptor gene expression in isolated adipocytes and whole WAT

In isolated adipocytes, we found that the mRNA expression of AdipoR2 was 1.85-fold and 1.75-fold higher than AdipoR1 in Epid and Sc Ing cells, respectively (Figure 8 (a)). Furthermore, the mRNA expression of both receptors was significantly lower in Sc Ing than Epid cells. In fact, AdipoR1 and AdipoR2 mRNA expressions were ~45% lower in Sc Ing than in Epid adipocytes (Figure 8(a)). In whole Epid fat tissue, AdipoR2 mRNA expression was 2.5-fold higher than AdipoR1, which was similar to what we found in isolated cells. However, in the Sc Ing fat pad the reverse was found, with AdipoR1 mRNA expression being 1.3-fold higher than AdipoR2 (Figure 8(b)). All our experiments were conducted in isolated cells; therefore, it is possible that the higher expression of AdipoR2 in Epid

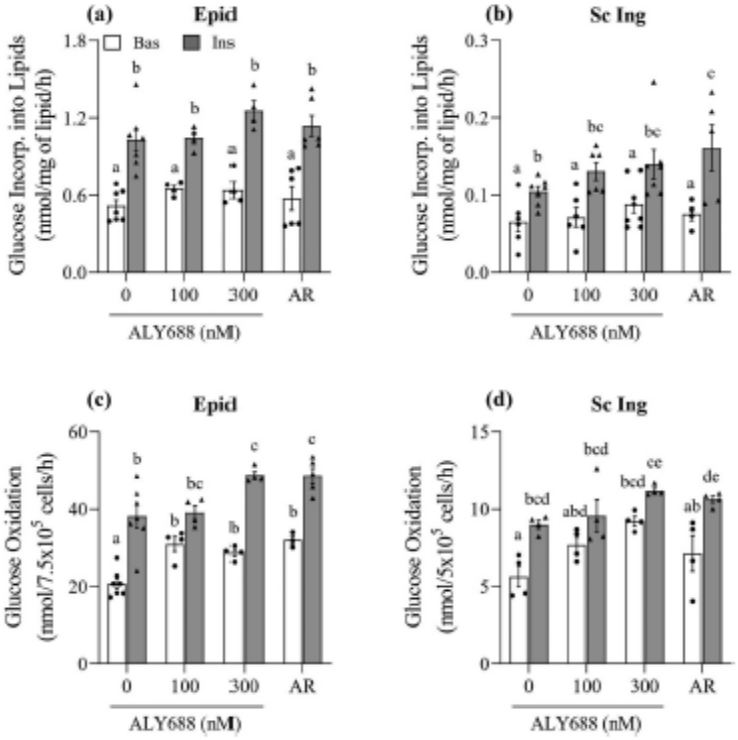

Figure 5. ALY688 (100 and 300 nM) did not affect glucose incorporation into lipids (a and b), but it enhanced in a dose-dependent and tissue-specific manner basal (Bas) and insulin (Ins)-stimulated rates of glucose oxidation in Epid (c) and Sc Ing (d) adipocytes. Different letters denote statistical significance ($p < 0.05$). Two-way ANOVA, n = 3–7.

adipocytes dictated the distinct metabolic responses that ALY688 treatment elicited in isolated cells from visceral and subcutaneous fat depots.

Discussion

Our findings provide evidence that acute exposure of isolated Epid and Sc Ing rat adipocytes to ALY688 did not alter AKT and p38 MAPK phosphorylation, basal and insulin-stimulated glucose uptake, and glucose incorporation into lipids (lipogenesis) in these cells. However, ALY688 treatment increased AMPK and ACC phosphorylation, although this was accompanied by suppression instead of stimulation of palmitate oxidation in Epid and Sc Ing adipocytes. This latter finding is contrary to what has been demonstrated in skeletal muscle cells under adiponectin-stimulated AMPK activation [8,14], suggesting a distinct regulatory role for adiponectin-mediated AMPK activation in WAT glucose and fat metabolism in comparison to liver and skeletal muscle. In fact, ALY688 enhanced rates of glucose oxidation in a concentration-dependent and tissue-specific manner in Epid and Sc Ing adipocytes. Basal rates of glucose oxidation consistently increased in cells from both fat depots, whereas under insulin-stimulated conditions only higher concentrations (300 nM) of the compound elicited an effect in Epid adipocytes. The data indicate that acute ALY688 treatment diverts glucose towards oxidation in adipocytes, which could positively contribute to whole-body glycaemic control. We have also found that both AR and ALY688 enhanced AMPK phosphorylation in Epid and Sc Ing adipocytes, whereas only AR increased p38 MAPK phosphorylation in these cells. However, because neither ALY688 nor AR affected either basal or insulin-stimulated uptake of glucose and its incorporation into lipids, the ability of AR to induce p38 MAPK phosphorylation did not seem to have any direct impact on glucose metabolism in adipocytes from both fat depots.

There are at least three potential explanations for the reduction in fatty acid oxidation despite ALY688

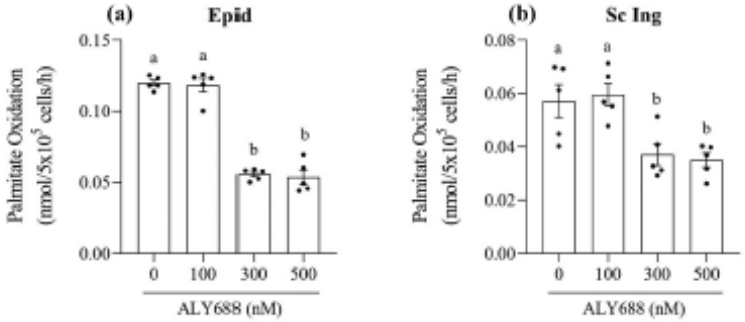

Figure 6. As the concentration of ALY688 increased beyond 100 nM, rates of palmitate oxidation were reduced in both epididymal (Epid, **A**) and subcutaneous inguinal (Sc Ing, **B**) adipocytes. Different letters denote statistical significance ($p < 0.05$). One-way ANOVA, n = 5.

inducing AMPK phosphorylation in isolated adipocytes: 1) it could be that enhanced glucose oxidation provided energy for the cells and caused a shift in fatty acid metabolism away from oxidation, even though AMPK phosphorylation was increased by ALY688. This could be possible because there is a relatively small number of mitochondria in white adipocytes, which normally limits the ability of these cells to elicit an elevated rate of fat oxidation [21,29]. However, because ALY688 consistently increased basal glucose oxidation in Epid and Sc Ing adipocytes, this must have led to a condition in which even fewer fatty acids were required and used for β-oxidation and energy production in these cells. Therefore, a shift in substrate utilization seems a plausible mechanism by which ALY688 led to the suppression of palmitate oxidation, despite increased AMPK phosphorylation in adipocytes; 2) enhancement of fatty acid oxidation by adiponectin in skeletal muscle cells has been shown to depend on the sequential activation of AMPK and

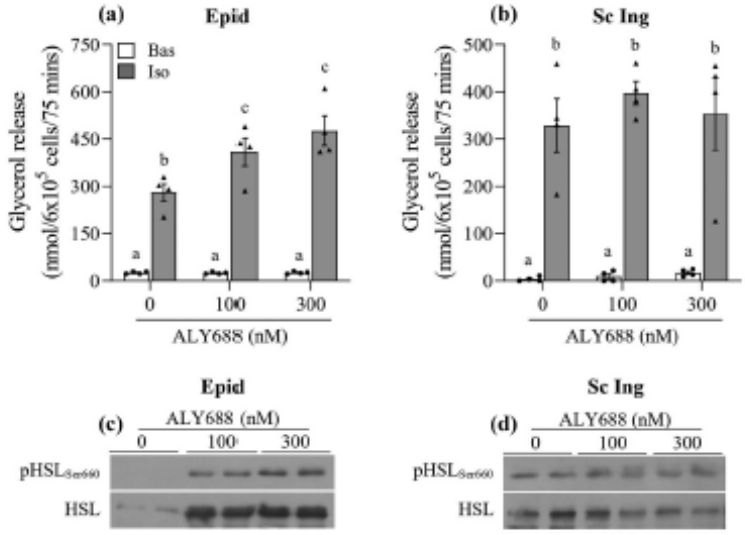

Figure 7. Lipolysis was affected in tissue-specific manner by ALY688. In Epididymal (Epid) adipocytes, isoproterenol (Iso)-stimulated lipolysis increased (a), whereas no effect of ALY688 (100 and 300 nM) was detected in Sc Ing (b) adipocytes either under basal (Bas) or Iso-stimulated conditions. Similarly, HSL phosphorylation was elevated in Epid (c), but not in Sc Ing (d) adipocytes. Different letters denote statistical significance ($p < 0.05$). Two-way ANOVA, n = 4 for glycerol release and n = 2 for HSL content and phosphorylation.

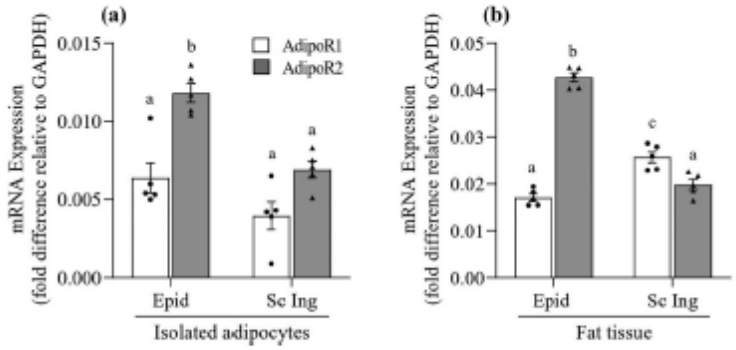

Figure 8. Distinct profile of AdipoR1 and AdipoR2 mRNA expression between epididymal (Epid) and subcutaneous inguinal (Sc Ing) adipocytes (a) and fat depots (b). Different letters denote statistical significance ($p < 0.05$). Two-way ANOVA, n = 5.

p38 MAPK, leading to induction of PPARα transcriptional activity and of its target oxidative genes (*e.g.* ACO and CPT1) [7]. In our studies, even though ALY688 caused AMPK activation in Epid and Sc Ing adipocytes, p38 MAPK phosphorylation was not affected by the compound. Thus, it could be that ALY688 promoted only partial activation of signalling events required for the enhancement of fatty acid oxidation in adipocytes. Under these conditions, glucose was clearly the preferred substrate for oxidation in these cells, which, as previously described, likely led to fewer fatty acids being diverted for oxidation; and finally, 3) it is also possible that fatty acid uptake was impaired under concentrations of ALY688 above 100 nM. This could be an AMPK-independent dose-dependent effect of the compound that suppressed specific adipocyte functions.

ALY688 did not affect basal rates of lipolysis either in Epid or Sc Ing adipocytes; however, isoproterenol-stimulated lipolysis increased in Epid adipocytes treated with ALY688. The mechanism underlying this depot-specific enhancement of beta-adrenergic-stimulated lipolysis by ALY688 seems to involve an increase in HSL phosphorylation. These findings differ from previous reports in which adiponectin suppressed lipolysis via inhibition of HSL phosphorylation in mouse adipocytes [12], and that a collagen domain-derived short adiponectin peptide promoted adipogenesis in 3T3L1 adipocytes [11]. These discrepancies could be attributed to methodological differences between studies. For instance, a lower lipolytic response was previously reported in Epid adipocytes from Adipoq$^{-/-}$ mice exposed to BRL37344 (a selective β3-adrenergic agonist), as well as in 3T3L1 adipocytes maintained in co-culture with FAO cells overexpressing full-length mouse adiponectin [12]. In this study, we performed acute (1 h) incubations of primary rat adipocytes in the presence of a peptide-based adiponectin mimetic and then stimulated the cells with isoproterenol, a non-specific β-adrenergic agent.

From our metabolic studies, it was clear that ALY688 caused tissue-specific and dose-dependent effects on glucose and fat metabolism in adipocytes. In general, Epid adipocytes elicited more pronounced responses to ALY688 than Sc Ing cells, particularly with respect to enhancing glucose oxidation and lipolysis while suppressing palmitate oxidation. Under these conditions, ALY688 could confer metabolic flexibility to the WAT and control WAT expansion, an effect that has been previously attributed to adiponectin [3,13]. This would allow for depot-specific exportation of fatty acids for utilization in peripheral tissues under adrenergic-stimulated conditions, while also enhancing glucose oxidation within the WAT. It could be that the tissue-specific responses resulted from distinct expressions of adiponectin receptors (AdipoR1 and AdipoR2) between Epid and Sc Ing cells. Therefore, we determined the expression profile of AdpoR1 and AdipoR2 in Epid and Sc Ing adipocytes, as well as in intact adipose tissue. It has been reported that it is AdipoR2 that carries out the effects of adiponectin in WAT [4]. Indeed, we found that in isolated Epid and Sc Ing adipocytes, AdipoR2 mRNA expression was approximately two-fold higher than AdipoR1. Also, Epid adipocytes displayed significantly higher AdipoR2 mRNA expression than Sc Ing adipocytes. Similarly, when analysing whole fat tissue, we also detected much higher AdipoR2 mRNA expression in the Epid than in the Sc Ing fat depot. However, in the Sc Ing fat depot AdipoR1 mRNA expression was slightly higher

than AdipoR2 mRNA expression, which could be attributed to the presence of a higher population of non-adipocyte cells in the Sc Ing than in the Epid fat depot. Because our experiments were conducted in isolated adipocytes, it is plausible that the more pronounced responses of Epid than Sc Inc adipocytes to ALY688 resulted from a much lower expression of AdipoR2 in the latter than the former adipocytes.

In summary, we found that acute treatment with ALY688 increased AMPK phosphorylation in Epid and Sc Ing rat adipocytes; however, this was accompanied by suppression of fat oxidation and no alteration in basal and insulin-stimulated glucose uptake in these cells. Furthermore, ALY688 increased rates of glucose oxidation in Epid and Sc Ing adipocytes and enhanced adrenergic-stimulated lipolysis, although the latter effect was only detected in Epid adipocytes. These findings provide evidence that the AdipoR agonist ALY688 can regulate adiposity and affect glycaemic control by altering substrate portioning in adipocytes in a fat depot-specific manner.

Disclosure statement

The authors report no potential conflict of interest.

Funding

This study was funded by a research contract agreement with Allysta Pharmaceuticals Inc.

Ethical statement

All experiments were approved by the Animal Care Committee at York University. (York University Animal Care Committee, YUACC, permit number 2016-5) and performed strictly in accordance with the YUACC guidelines.

References

[1] Roden M, Shulman GI. The integrative biology of type 2 diabetes. Nature. 2019;576(7785):51–60.
[2] Scheja L, Heeren J. The endocrine function of adipose tissues in health and cardiometabolic disease. Nat Rev Endocrinol. 2019;15:507–524.
[3] Tao C, Sifuentes A, Holland WL. Regulation of glucose and lipid homeostasis by adiponectin: effects on hepatocytes, pancreatic β cells and adipocytes. Best Pract Res Clin Endocrinol Metab. 2014;28(1):43–58.
[4] Yamauchi T, Iwabu M, Okada-Iwabu M, et al. Adiponectin receptors: A review of their structure, function and how they work. Best Pract Res Clin Endocrinol Metab. 2014;28(1):15–23.
[5] Yamauchi T, Kamon J, Ito Y, et al. Cloning of adiponectin receptors that mediate antidiabetic metabolic effects. Nature. 2003;423(6941):762–769. .
[6] Yamauchi T, Kamon J, Minokoshi Y, et al. Adiponectin stimulates glucose utilization and fatty-acid oxidation by activating AMP-activated protein kinase. Nat Med. 2002;8(11):1288–1295. .
[7] Myeong JY, Gha YL, Chung JJ, et al. Adiponectin increases fatty acid oxidation in skeletal muscle cells by sequential activation of AMP-activated protein kinase, p38 mitogen-activated protein kinase, and peroxisome proliferator-activated receptor{alpha}. Diabetes. 2006;55(9):2562–2570.
[8] Iwabu M, Yamauchi T, Okada-Iwabu M, et al. Adiponectin and AdipoR1 regulate PGC-1α and mitochondria by Ca 2+ and AMPK/SIRT1. Nature. 2010;464(7293):1313–1319. .
[9] Yoon M. The role of PPARα in lipid metabolism and obesity: focusing on the effects of estrogen on PPARα actions. Pharmacol Res. 2009;60(3):151–159.
[10] Wu X, Motoshima H, Mahadev K, et al. Involvement of AMP-activated protein kinase in glucose uptake stimulated by the globular domain of adiponectin in primary rat adipocytes. Diabetes. 2003;52(6):1355–1363.
[11] Sayeed M, Gautam S, Verma DP, et al. A collagen domain-derived short adiponectin peptide activates APPL1 and AMPK signaling pathways and improves glucose and fatty acid metabolisms. J Biol Chem. 2018;293(35):13509–13523.
[12] Qiao L, Kinney B, Schaack J, et al. Adiponectin inhibits lipolysis in mouse adipocytes. Diabetes. 2011;60(5):1519–1527.
[13] Sun K, Kusminski CM, Scherer PE. Adipose tissue remodeling and obesity. J Clin Invest. 2011;121(6):2094–2101.
[14] Fruebis J. Proteolytic cleavage product of 30-kDa adipocyte complement-related protein increases fatty acid oxidation in muscle and causes weight loss in mice. Proc Natl Acad Sci. 2001;98(4):2005–2010.
[15] Tomas E, Tsao TS, Saha AK, et al. Enhanced muscle fat oxidation and glucose transport by ACRP30 globular domain: acetyl-CoA carboxylase inhibition and AMP-activated protein kinase activation. Proc Natl Acad Sci U S A. 2002;99(25):16309–16313.
[16] Yamauchi T, Nio Y, Maki T, et al. Targeted disruption of AdipoR1 and AdipoR2 causes abrogation of adiponectin binding and metabolic actions. Nat Med. 2007;13(3):332–339. .
[17] Okada-Iwabu M, Yamauchi T, Iwabu M, et al. A small-molecule AdipoR agonist for type 2 diabetes and short life in obesity. Nature. 2013;503(7477):493–499. .
[18] Otvos L, Haspinger E, La Russa F, et al. Design and development of a peptide-based adiponectin receptor agonist for cancer treatment. BMC Biotechnol. 2011;11(1):90. .
[19] Otvos L. Potential Adiponectin Receptor Response Modifier Therapeutics. Front Endocrinol (Lausanne). 2019;10:539.
[20] Bódis K, Roden M. Energy metabolism of white adipose tissue and insulin resistance in humans. Eur J Clin Invest. 2018;48(11):1-14.
[21] Sepa-kishi DM, Jani S, Da Eira D, et al. Cold acclimation enhances UCP1 content, lipolysis, and

triacylglycerol resynthesis, but not mitochondrial uncoupling and fat oxidation, in rat white adipocytes. Am J Physiol Cell Physiol. 2019;316(3):365–376.
[22] Fine JB, DiGirolamo M. A simple method to predict cellular density in adipocyte metabolic incubations. Int J Obes Relat Metab Disord. 1997;21(9):764–768.
[23] Gaidhu MP, Fediuc S, Ceddia RB. 5-Aminoimidazole-4-carboxamide-1-beta-D-ribofuranoside-induced AMP-activated protein kinase phosphorylation inhibits basal and insulin-stimulated glucose uptake, lipid synthesis, and fatty acid oxidation in isolated rat adipocytes. J Biol Chem. 2006;281(36):25956–25964.
[24] Gaidhu MP, Fediuc S, Anthony NM, et al. R-induced AMP-kinase activation promotes energy dissipation in white adipocytes: novel mechanisms integrating HSL and ATGL. J Lipid Res. 2009;50(4):704–715.
[25] Dole VP, Meinertz H. Microdetermination of long-chain fatty acids in plasma and tissues. J Biol Chem. 1960;235:2595–2599.
[26] Gaidhu MP, Anthony NM, Patel P, et al. Dysregulation of lipolysis and lipid metabolism in visceral and subcutaneous adipocytes by high-fat diet: role of ATGL, HSL, and AMPK. Am J Physiol Cell Physiol. 2010;298(4):C961–71.
[27] Ahlquist RP. Present state of alpha- and beta-adrenergic drugs I. The adrenergic receptor. Am Heart J. 1976;92(5):661–664.
[28] Livak KJ, Schmittgen TD. Analysis of relative gene expression data using real-time quantitative PCR and the 2−ΔΔCT method. Methods. 2001;25(4):402–408.
[29] Sepa-Kishi DM, Ceddia RB. White and beige adipocytes: are they metabolically distinct?. Horm Mol Biol Clin Investig. 2018;33(2).

Appendix C: Additional Contributions to Research

Jani S, **Da Eira D**, Ceddia RB. Insulin-resistant female rat skeletal muscles display diacylglycerol-mediated protein kinase C activation and inflammation without ceramide accumulation. *J Physiol*. 2023 May;601(10):1745-1759.

Jani S, **Da Eira D**, Stefanovic M, Ceddia RB. The ketogenic diet prevents steatosis and insulin resistance by reducing lipogenesis, diacylglycerol accumulation and protein kinase C activity in male rat liver. *J Physiol*. 2022 Sep;600(18):4137-4151.

Jani S, **Da Eira D**, Hadday I, Bikopoulos G, Mohasses A, de Pinho RA, Ceddia RB. Distinct mechanisms involving diacylglycerol, ceramides, and inflammation underlie insulin resistance in oxidative and glycolytic muscles from high fat-fed rats. *Sci Rep*. 2021 Sep 27;11(1):19160.

Song E, **Da Eira D**, Jani S, Sepa-Kishi D, Vu V, Hunter H, Lai M, Wheeler MB, Ceddia RB, Sweeney G. Cardiac Autophagy Deficiency Attenuates ANP Production and Disrupts Myocardial-Adipose Cross Talk, Leading to Increased Fat Accumulation and Metabolic Dysfunction. *Diabetes*. 2021 Jan;70(1):51-61.

Sepa-Kishi DM, Jani S, **Da Eira D**, Ceddia RB. Cold acclimation enhances UCP1 content, lipolysis, and triacylglycerol resynthesis, but not mitochondrial uncoupling and fat oxidation, in rat white adipocytes. *Am J Physiol Cell Physiol*. 2019;316(3):C365-C376.